LOW ENRICHED URANIUM FUEL CYCLE IN HEAVY WATER REACTORS

By

JOHN VINCENT MARCZAK, B.Sc., M.Eng.

A Thesis
Submitted to the School of Graduate Studies
in Partial Fulfilment of the Requirements
for the Degree
Doctor of Philosophy

McMaster University
March, 1990

© Copyright by John Vincent Marczak, March 1990.

LOW ENRICHED URANIUM FUEL CYCLE

IN HEAVY WATER REACTORS

DOCTOR OF PHILOSOPHY (1990) McMASTER UNIVERSITY
(Nuclear Engineering) Hamilton, Ontario

TITLE: Low Enriched Uranium Fuel Cycle
in Heavy Water Reactors

AUTHOR: John Vincent Marczak, B.Sc. (University of Waterloo)
M.Eng. (McMaster University)

SUPERVISOR: Professor O.A. Trojan

NUMBER OF PAGES: xix, 461

ABSTRACT

Heavy water moderated thermal nuclear fission reactors have a greater inherent neutron economy than light water or graphite moderated reactor designs. Consequently, such units, operating on a variety of fuel cycles, may play an ever-increasing role in meeting future global energy demands. This thesis explores, analytically, the operational advantages and challenges associated with the use of a low enriched uranium (LEU) fuel cycle in advanced reactors based on the CANDU heavy water moderated, pressure tube design concept. The flexibility afforded through the use of LEU fuel is applied to enhance the operational and safety characteristics of reactors utilizing this fuel cycle. An investigation of factors influencing coolant void reactivity is conducted. Design modifications are introduced to reduce the coolant void reactivity, while maintaining the continued capability of high power operation. An enrichment and element radius graded fuel bundle design is developed with a central graphite core, an inner ring of 14 fuel elements, and an outer ring of 21 fuel elements. Fuel and lattice design perturbations are investigated to examine the effect of lattice pitch variations, capability of radioisotope production, the use of burnable poisons, and light water coolant. Xenon override requirements with LEU fuel are addressed. The efficacy of using modified two group (M-2) neutron diffusion theory for LEU fuel management studies is investigated. A modelling strategy is developed for the simulation of reactivity devices and fuel lattice properties using the M-2 methodology with a fixed energy cut-off. Detailed fuel management studies are conducted to examine the operational intricacies of LEU fuelling. Improved checkerboard type fuelling strategies are developed. Finally, the CANDU - Spectral Shift Advanced Thermal Reactor (CANDU-SSATR) is introduced and characterized. This multi-spectrum high burnup advanced reactor design utilizing simplified fuel management strategies holds great promise for the future.

ACKNOWLEDGEMENTS

The author gratefully acknowledges the support and guidance provided by his thesis supervisor, Professor O.A. Trojan, and the members of his supervisory committee: Professor A.A. Harms (1982-1990), Professor D.A. Smith (1982-1987), Professor J.S. Kirkaldy (1988), and Professor R.L. Judd (1989-1990).

This work was made possible through funding and computer resources provided by Atomic Energy of Canada Limited - Chalk River Nuclear Laboratories (AECL-CRNL). The author is indebted to Mr. J.B. Slater from AECL-CRNL for supporting this endeavour. Additional computer resources were provided by AECL-CANDU Operations, and Ontario Hydro, the author's current employer.

In dealing with a subject as complex and as far-reaching as the reactor physics and fuel management of low enriched uranium fuelled heavy water reactors, one cannot attempt to make definitive progress without consultation with experts in the field of CANDU reactor design. The author was very fortunate to have engaged in many an open dialogue with the members of the physics teams at AECL-CANDU Operations, AECL-CRNL and Ontario Hydro. The generous and helpful suggestions provided by these individuals, especially Mr. A.R. Dastur (AECL-CANDU Operations) is gratefully acknowledged.

The author extends his sincere gratitude to his parents, Helen and Eugene Marczak, for having provided him the opportunity to undertake this project and for their constant encouragement and support.

Finally, the author acknowledges the contributions to this work provided by his wife, Eva Marczak. A tireless word-processor, editor, illustrator, and slave-driver, Eva has given new meaning to the word, love. For all her support and efforts, the author will be forever grateful.

TABLE OF CONTENTS

		PAGE
	LIST OF TABLES	xi
	LIST OF ILLUSTRATIONS	xv
1.0	INTRODUCTION	1
	1.1 Energy Requirements	2
	1.2 The Global Supply of Energy	3
	1.3 Nuclear Energy Systems	8
	1.4 Purpose of This Thesis	9
2.0	HEAVY WATER MODERATED NUCLEAR REACTORS	12
	2.1 Introduction	12
	2.2 Pressure Tube Reactor Design	12
	2.3 CANDU-PHW Design Description	15
3.0	ADVANCED FUEL CYCLES IN CANDU REACTORS	21
	3.1 Introduction	21
	3.2 Once Through Natural Uranium Fuel Cycle	22
	3.3 Low Enriched Uranium Fuel Cycle	22
	3.4 Plutonium-Uranium Fuel Cycle	25
	3.5 Thorium Fuel Cycles	25
	3.6 Comparison of Resource Utilization	27
4.0	URANIUM ENRICHMENT: STRATEGIES AND FACILITIES	32
	4.1 Introduction	32
	4.2 Fuel Enrichment Techniques	32
	4.3 Nuclear Weapons Proliferation	37
	4.4 Enrichment Facilities: A Global Assessment	38
5.0	IMPROVING CANDU REACTOR OPERATING CHARACTERISTICS	40
	5.1 Introduction	40
	5.2 Reactivity, Point Kinetics, and Neutronic Transients	41

PAGE

5.3 System Response: Reactivity Feedback Effects 44
5.4 Power Coefficient of Reactivity 44
5.5 Acceptability of a Positive Coolant Void Reactivity Effect 45
5.6 Factors Influencing Coolant Void Reactivity 46
6.0 REDUCTION OF COOLANT VOID REACTIVITY IN CANDU REACTORS 50
6.1 Introduction 50
6.2 Methods of Reducing Void Reactivity 50
6.3 Analysis With the POWDERPUFS-V Lattice Physics Code 55
6.4 Analysis With the WIMS-CRNL Lattice Physics Code 72
6.5 Concluding Remarks 84
7.0 REDESIGN OF THE NUCLEAR FUEL BUNDLE 87
7.1 Introduction 87
7.2 CANDU 30(37) Fuel Bundle 87
7.3 POWDERPUFS-V Lattice Physics Analysis 89
7.4 WIMS-CRNL Modelling of 30(37) Element Fuel 97
7.5 Enriched Zirconium Pressure Tubes and Calandria Tubes 99
7.6 Comparison of 30(37) Element and 37 Element Bundle Designs 103
7.7 Characterization of the 30(37) Fuel Bundle Design and Variants 106
7.8 Perturbations to the 30(37) Fuel Bundle Design 115
7.9 Simulation Perturbations 130
7.10 Enrichment Grading in 30(37) Element Fuel 133
7.11 Fuel Element Radius and Enrichment Grading 136
7.12 Refinements to the Fuel Bundle Models 150
7.13 WIMS-CRNL Simulation Results 153
7.14 Kinetics Parameters 163

PAGE

8.0 STRATEGY FOR CORE CALCULATIONS 166
8.1 Introduction 166
8.2 Neutron Diffusion Equations 166
8.3 Energy Group Requirements 168
8.4 Core Calculations 169
8.5 Reactor Analysis 178
9.0 SPECIFICATION AND SIMULATION OF REACTIVITY DEVICES 194
9.1 Introduction 194
9.2 Adjuster Rod Requirements 195
9.3 Zone Controller System Requirements 199
9.4 Simulation of Reactivity Devices 199
9.5 Determination of Adjuster Rod Incremental Cross Section 207
9.6 Determination of Zone Controller Incremental Properties 210
9.7 Summary 212
10.0 REACTOR FUEL MANAGEMENT CALCULATIONS 213
10.1 Introduction 213
10.2 Fuel Management Requirements With Enriched Fuel 213
10.3 Fuel Management Philosophies 217
10.4 Data Handling and Interpretation 219
10.5 Continuous Bidirectional Fuel Management Studies 220
10.6 Time-Averaged Fuel Management Studies 237
10.7 Instantaneous Fuel Management Studies 250
10.8 Comment on Fuel Management With Enriched Fuel 253
11.0 CANDU HEAVY WATER SPECTRAL SHIFT ADVANCED THERMAL REACTORS 290
11.1 Introduction 290
11.2 Lattice Calculations: Reduced Lattice Pitch 296
11.3 Lattice Calculations: Increased Calandria Tube Diameter 302
11.4 Lattice Calculations: The Second Burnup Phase 308
11.5 Core Physics Calculations 319

PAGE

11.6 Concluding Remarks 330
12.0 SUMMARY, EXTENSIONS, AND CONCLUSIONS 332
12.1 Envisaged Nuclear Energy Development Strategy 332
12.2 Enhancement of CANDU Operating Characteristics: Coolant Void Reactivity Reduction 333
12.3 Redesign of the Nuclear Fuel Bundle 336
12.4 Additional Comparison of 14/21 and Nominal CANDU-600 Fuel Bundle Designs 344
12.5 Reactor Core Modelling and Fuel Management Simulation 346
12.6 CANDU - Spectral Shift Advanced Thermal Reactor 353
12.7 Extensions of the Analysis 357
12.8 Conclusions 364
12.9 Closing Remarks 367
A.0 CONTRIBUTION OF VARIOUS ISOTOPES TO THE VOID REACTIVITY EFFECT IN 37 AND 30(37) ELEMENT FUEL 368
A.1 Introduction 368
A.2 Analytical Methodology 368
A.3 Results 370
A.4 Data Interpretation 371
B.0 DETERMINATION OF THE REQUIRED ENERGY GROUP STRUCTURE 388
B.1 Introduction 388
B.2 Calculational Methodology 388
B.3 Lattice Physics Codes 389
B.4 3DDT Reactor Model 390
B.5 Results 394
B.6 Conclusions 401
C.0 CALCULATION OF ADJUSTER ROD INCREMENTAL PROPERTIES 405
C.1 Introduction 405

PAGE

C.2 Nominal Lattice Component Properties 405
C.3 Simulation of the Fuel Region 405
C.4 Fuel Annulus Region 408
C.5 Moderator Region 409
C.6 Material Properties for Nominal Lattice Cell Components 409
C.7 Neutronic Properties for Adjuster Rod Constituent Materials 409
C.8 Cobalt Adjuster Rod Boundary Conditions 414
C.9 MULTICELL Model 414
C.10 Incremental H and F Factors 420
D.0 CALCULATION OF ZONE CONTROLLER INCREMENTAL PROPERTIES 423
D.1 Introduction 423
D.2 Neutronic Properties for Constituent Materials 423
D.3 MULTICELL Model 425
D.4 Zone Controller Incremental Properties 430
E.0 DATA HANDLING: URANIUM AND SEPARATIVE WORK REQUIREMENTS 431
E.1 Introduction 431
E.2 Conversion and Fabrication Losses 431
E.3 Thermal Burnup to Electrical Energy Conversion Factor 431
E.4 Separative Work Requirements per Unit of Electrical Energy Produced 432
E.5 Uranium Requirement Calculations 432
E.6 Separative Work Requirements Calculations 437
E.7 Uranium and Separative Work Requirements for Specific Cases 438
E.8 Conversion of Burnup per Bundle to Burnup per MgU 439
F.0 WIMS-CRNL PROGRAM DESCRIPTION 440
F.1 SPECTROX Calculation 440

PAGE

F.2 DSN Calculation 441
F.3 PIJ Calculation 441
F.4 Leakage Routines 441
F.5 Burnup Calculation 442
F.6 WIMS-CRNL Energy Group Structure 442

BIBLIOGRAPHY 443

LIST OF TABLES

TABLE	TITLE	PAGE
1-1	Overview of the Total World Energy Potential	4
1-2	Practical World Energy Resource Picture	5
1-3	Uranium Resources	7
3-1	Approximate Equilibrium Fuel Consumption	29
3-2	Resource Consumption in CANDU-PHW Fuel Cycles	30
6-1a	POWDERPUFS-V Input Data for CANDU-600 37 Element Fuel	58
6-1b	POWDERPUFS-V Input Data for CANDU-600 37 Element Fuel (Continued)	59
6-2	Condensation of Energy Groups for WIMS-CRNL Simulations	74
6-3	CANDU-600 37 Element Fuel Lattice Properties	75
6-4	Material Properties for Initial WIMS-CRNL CANDU-600 37 Element Fuel Model	76
6-5	37 Element Fuel, Nominal Lattice Geometry: Effect of Fuel Enrichment	85
6-6	37 Element Fuel, 1.3 a/o U-235: Effect of Lattice Pitch Size	86
7-1	Fuel Flux and Power Distribution Across 37 Element Natural Uranium Fuel Bundle	88
7-2a	POWDERPUFS-V Input Data for CANDU-600 37 Element and 30(37) Element Fuel	90
7-2b	POWDERPUFS-V Input Data for CANDU-600 37 Element and 30(37) Element Fuel (Continued)	91
7-3	POWDERPUFS-V Analysis: 37 Element and 30(37) Element Fuel Four Factor Formula Data	93
7-4	POWDERPUFS-V Analysis: 37 Element and 30(37) Element Fuel Change in Four Factor Formula Components Upon Coolant Voiding	94
7-5	POWDERPUFS-V 30(37) Element Fuel Analysis	96
7-6	Enrichment Dependent Fuel Composition for WIMS-CRNL Simulations	98

TABLE	TITLE	PAGE
7-7	Effect of Enriched Zirconium and Lattice Pitch/Calandria Tube Size Variations	105
7-8	Effect of Fuel Enrichment on Burnup (Model 30(37)-XX-25-7-CC)	109
7-9	Effect of Fuel Enrichment on Burnup (Model 30(37)-XX-25-6.4478-CC)	109
7-10	Effect of Lattice Pitch on Burnup (Model 30(37)-1.3-XX-7-CC)	113
7-11	Effect of Lattice Pitch on Burnup (Model 30(37)-1.3-XX-6.4478-CC)	113
7-12	Effect of Poison in the Fuel Mix or Carbon Core	128
7-13	Effect of Varying Calandria Tube and Pressure Tube Wall Thicknesses (Model 30(37)-1.3-25-XX-CC)	131
7-14	Effect of Enrichment Grading (Model 30(37)-1.3/XX-25-6.4478-CC)	137
7-15	Basic Structure of Fuel Bundles: 12/21 and 14/21 Cases	139
7-16	Basic Dimensions of Fuel Elements 12/21 and 14/21 Cases	140
7-17	WIMS-CRNL Results: 12/21 and 14/21 Cases	143
7-18	Basic Structure of the Finalized 14/21 Fuel Lattice	152
7-19	WIMS-CRNL Results: NATNOM	157
7-20	WIMS-CRNL Results: 1421NAT	158
7-21	WIMS-CRNL Results: 14211312	159
7-22	WIMS-CRNL Results: 142117153	160
7-23	Spent Fuel Fissile Concentration	161
7-24	Kinetics Parameters for Equilibrium Conditions	165
8-1	Selected FMDP Fuel Table Data	180
8-2	FMDP Model: NATNOM x-Direction Mesh Sizes	185
8-3	FMDP Model: NATNOM y-Direction Mesh Sizes	185
8-4	FMDP Model: 14/21 x-Direction Mesh Sizes	186
8-5	FMDP Model: 14/21 y-Direction Mesh Sizes	186
8-6	FMDP Model: z-Direction Mesh Sizes	187
8-7	Zone Controller Light Water Fractional Fill	192

TABLE	TITLE	PAGE
9-1	Comparison of Adjuster Rod Requirements	197
9-2	Adjuster Rod Incremental Properties	209
9-3	Zone Controller Incremental Properties	211
10-1	Natural Uranium Requirements for Enriched Fuels	221
10-2	Separative Work Requirements for Enriched Fuels	222
10-3	CBDFA Cases - General Results	226
10-4	Adjuster Rod Configuration (CBDFA Cases)	227
10-5	Natural Uranium Requirements (CBDFA Cases)	231
10-6	Separative Work Unit Requirements (CBDFA Cases)	232
10-7	Resource Utilization Improvement (CBDFA Cases)	233
10-8	Uranium Plus Separative Work Costs (CBDFA Cases)	234
10-9	Time-Averaged Cases - General Results	256
10-10	Natural Uranium and Separative Work Requirements (Time-Averaged Cases)	257
10-11	Comparison of Adjuster Rod Worths: CBDFA vs TAA	258
10-12	Equilibrium Uranium Consumption: Comparison of Once Through Fuel Cycles	259
10-13	Instantaneous Results	260
11-1	30/37 Results: 15 cm Lattice Pitch	297
11-2	Summary of Spectral Shift Lattice Calculations (No Moderator, Zero Burnup Cases)	305
11-3	Summary of Spectral Shift Lattice Calculations (Increased Calandria Tube Diameter Cases)	307
11-4	Adjuster Loading: CANDU-SSATR	324
11-5	CANDU-SSATR Resource Utilization and Separative Work Requirements	329
A-1	WIMS-CRNL Results for 37 and 30(37) Element Fuel	369
B-1	Energy Group Structure: WIMS-CRNL Cases	391
B-2	Infinite Multiplication Factors	395

TABLE	TITLE	PAGE
B-3	NATNOM Fuel Properties: WIMS-CRNL 4 Group and 2 Group Structures	396
B-4	30/37 Fuel Properties: WIMS-CRNL 4 Group and 2 Group Structures	397
B-5	NATNOM and 30/37 Material Properties: WIMS-CRNL Modified 2 Group Format	398
B-6	NATNOM and 30/37 Material Properties: PPV and LATREP	399
B-7	3DDT Results: Effective Multiplication Factors	400
C-1	WIMS-CRNL Data for Approximation of Equilibrium Conditions	406
C-2	Material Properties for Nominal Lattice Cell Components	410
C-3	MULTICELL Fuel Region Boundary Conditions	411
C-4	MULTICELL Input Properties for Adjuster Rod Component Materials	415
C-5	MULTCFR Input Data for the Calculation of Cobalt Pencil Boundary Conditions	416
C-6	MULTICELL Cobalt Adjuster Boundary Conditions	417
C-7	MULTICELL Mesh Spacings: Cobalt Adjuster Simulations	419
C-8	Data Required for Determination of Incremental H Factors	422
D-1	MULTICELL Input Properties for Zone Controller Component Materials	426
D-2	MULTICELL Mesh Spacings: Zone Controller Simulations	429

LIST OF ILLUSTRATIONS

FIGURE	TITLE	PAGE
2-1	CANDU-PHW Reactor Assembly	17
2-2	CANDU-PHW 37-Element Fuel Bundle	19
2-3	CANDU-PHW Lattice Cell (Cross Section)	20
3-1	Once-Through Natural Uranium Fuel Cycle	23
3-2	Once-Through Slightly Enriched Uranium Fuel Cycle	24
3-3	Plutonium-Uranium Fuel Cycle	26
3-4	Thorium Fuel Cycle	28
5-1	Neutron Flux Transient Following Step Reactivity Insertion	43
6-1	Effect of Variation of Fuel U-235 Enrichment on Effective Multiplication Factor (37 Element Nominal Geometry PPV Results)	60
6-2	Effect of Variation of Fuel U-235 Enrichment on Void Reactivity (37 Element Nominal Geometry PPV Results)	61
6-3	Effect of Variation of Fuel U-235 Enrichment (Burnup vs Irradiation) (37 Element Nominal Geometry PPV Results)	62
6-4	Effect of Fuel Irradiation on k-Effective (37 Element Nominal Geometry PPV Results)	63
6-5	Effect of Irradiation on Void Reactivity (37 Element Nominal Geometry PPV Results)	64
6-6	Effect of Moderator Density on k-Effective for Various Fuel Enrichments (ω=0.0 neutrons/kilobarn) (37 Element Nominal Geometry PPV Results)	68
6-7	Effect of Moderator Density on k-Effective for Various Fuel Enrichments (ω=1.8 neutrons/kilobarn) (37 Element Nominal Geometry PPV Results)	69
6-8	Effect of Moderator Density on Void Reactivity for Various Fuel Enrichments (ω=0.0 neutrons/kilobarn) (37 Element Nominal Geometry PPV Results)	70

FIGURE	TITLE	PAGE
6-9	Effect of Moderator Density on Void Reactivity for Various Fuel Enrichments (ω=1.8 neutrons/kilobarn) (37 Element Nominal Geometry PPV Results)	71
6-10	Burnup Steps Used in WIMS-CRNL Calculations	78
6-11	Effect of Variation of U-235 Enrichment on Effective Multiplication Factor (37 Element, Nominal Geometry)	79
6-12	Effect of Variation of U-235 Enrichment on Coolant Void Reactivity (37 Element, Nominal Geometry)	80
6-13	Effect of Variation of Lattice Pitch on Effective Multiplication Factor (37 Element, 1.3 a/o U-235)	82
6-14	Effect of Variation of Lattice Pitch on Coolant Void Reactivity (37 Element, 1.3 a/o U-235)	83
7-1	Effect of Enriched Zirconium on k-eff Model: 30(37)-1.3-25-7-CC	101
7-2	Effect of Enriched Zirconium on Coolant Void Reactivity Model: 30(37)-1.3-25-7-CC	102
7-3	Effect of Fuel Enrichment on k-eff Model: 30(37)-XX-25-7-CC	107
7-4	Effect of Fuel Enrichment on Coolant Void Reactivity Model: 30(37)-XX-25-7-CC	108
7-5	Effect of Lattice Pitch on k-eff Model: 30(37)-1.3-XX-7-CC	111
7-6	Effect of Lattice Pitch on Coolant Void Reactivity Model: 30(37)-1.3-XX-7-CC	112
7-7	Effect of Bundle Configuration on k-eff Model: 1.3 a/o U-235, 25 cm LP, 7 cm CT	116
7-8	Effect of Bundle Configuration on Coolant Void Reactivity Model: 1.3 a/o U-235, 25 cm LP, 7 cm CT	117
7-9	Effect of Geometry and Composition (36/37 Element Fuel) on k-eff	120

FIGURE	TITLE	PAGE
7-10	Effect of Geometry and Composition on Void Reactivity (36/37 Element Fuel)	121
7-11	Effect of Light Water Coolant on k-eff Model: 30(37)-1.3-XX-7-CC	123
7-12	Effect of Light Water Coolant on Void Reactivity Model: 30(37)-1.3-XX-7-CC	124
7-13	Effect of Burnup on Pin Power Ratio Model: 30(37)-1.3/XX-25-6.4478-CC	135
7-14	Effect of Burnup on Pin Power Ratio (Inner/Outer) 14/21 Element Fuel Pin Size Grading	146
7-15	Burnup Dependence of k-eff	154
7-16	Burnup Dependence of Void Reactivity	155
7-17	Effect of Lattice Pitch Size Variation on Achievable Fuel Burnup	162
8-1	Continuous Bidirectional Fuelling Approximation	171
8-2	Time Averaged Fuelling Approximation (Eight Bundle Shift)	174
8-3	Instantaneous Channel Age Map	179
8-4	Reactor Model (x-y View)	182
8-5	Reactor Model (x-z View)	184
8-6	Burnup Regions	189
8-7	CPPF Region	191
10-1	Channel Power Distributions (CBDFA)	214
10-2	Bundle Power Distributions (CBDFA)	229
10-3	Fuelling Schemes	261
10-4	Channel Power Distributions (TAA)	262
10-5	Bundle Power Distributions (TAA)	266
10-6	Cell Flux Distributions (TAA)	272
10-7	Fuel Thermal Irradiation Distributions (TAA)	276
10-8	Fuel Burnup Distributions (TAA)	282
10-9	Fuelling Map: 142117153 Scheme A	288

FIGURE	TITLE	PAGE
10-10	Fuelling Map: 142117153 Schemes B1, B2, and B3	289
11-1	Effect of Fuel Enrichment on Effective Multiplication Factor Model: 30(37)-XX-15-6.4478-CC	298
11-2	Effect of Fuel Enrichment on Fast to Thermal Cell Flux Ratio Model: 30(37)-XX-15-6.4478-CC	299
11-3	Effect of Fuel Enrichment on Fissile Concentration Model: 30(37)-XX-15-6.4478	300
11-4	Burnup Dependence of Effective Multiplication Factor (Cases 333, 333A800, 333A1000)	310
11-5	Burnup Dependence of Time Integrated Average Infinite Multiplication Factor (Cases 333, 333A800, 333A1000)	311
11-6	Burnup Dependence of U-235 Concentration (Cases 333, 333A800, 333A1000)	312
11-7	Burnup Dependence of Pu-239 Concentration (Cases 333, 333A800, 333A1000)	313
11-8	Burnup Dependence of Pu-241 Concentration (Cases 333, 333A800, 333A1000)	314
11-9	Burnup Dependence of Relative Fissile Concentration (Cases 333, 333A800, 333A1000)	315
11-10	Burnup Dependence of Fast to Thermal Flux Ratio (Cases 333, 333A800, 333A1000)	316
11-11	Burnup Dependence of Fuel Thermal Irradiation (Cases 333, 333A800, 333A1000)	317
11-12	CANDU-SSATR Core Model (x-y View)	322
11-13	CANDU-SSATR Core Model (x-z View)	323
11-14	CANDU-SSATR Channel Power Distribution	326
11-15	CANDU-SSATR Bundle Power Distribution	327
A-1	37 Element NATNOM Production Effect	372
A-2	37 Element NATNOM Absorption Effect	373
A-3	37 Element NATNOM Fast Production Effect	374

FIGURE	TITLE	PAGE
A-4	37 Element NATNOM Thermal Production Effect	375
A-5	37 Element NATNOM Fast Absorption Effect	376
A-6	37 Element NATNOM Thermal Absorption Effect	377
A-7	37 Element NATNOM Total Reactivity Effect	378
A-8	30(37)-1.3-25-6.4478-CC Production Effect	379
A-9	30(37)-1.3-25-6.4478-CC Absorption Effect	380
A-10	30(37)-1.3-25-6.4478-CC Fast Production Effect	381
A-11	30(37)-1.3-25-6.4478-CC Thermal Production Effect	382
A-12	30(37)-1.3-25-6.4478-CC Fast Absorption Effect	383
A-13	30(37)-1.3-25-6.4478-CC Thermal Absorption Effect	384
A-14	30(37)-1.3-25-6.4478-CC Total Reactivity Effect	385
B-1	3DDT Model (x-y View)	392
B-2	3DDT Model (x-z View)	393
B-3	3DDT Results: Typical Power Distribution (NATNOM)	402
B-4	3DDT Results: Typical Power Distribution (30(37))	403
C-1	MULTICELL Cobalt Adjuster Model	418
D-1	MULTICELL Zone Controller Model	427

CHAPTER 1

INTRODUCTION

Energy, technology, and quality of life. These three facets of modern society have come to be a measure of one and the same. Technological developments require a strong and stable energy base, while facilitating the evolution of a "Value Society" (Melvin, 1979) (one that places a high value on the individual's time). This, in turn, offers the prospect of a stable population match to the capabilities of a finite environment.

It has been suggested that a consolidated energy conservation program and a drive toward more energy-efficient technologies may reduce the expected demand for energy (Foster, 1987). Indeed in Canada, the world's most energy intensive industrialized country, energy use per unit production has dropped by 14% over the period from 1973 to 1986 (Department of Energy Mines and Resources Canada (EMR), 1987). However, the continuing rapid growth of energy consumption in other parts of the world, and the increasing overall energy requirements in North America, make it imperative that solutions for the intermediate and longer-range future be more than passive ones (Stewart, 1981). Further, technology, no matter how energy efficient it becomes, will have to be applied to processing materials from a dwindling resource base. The recovery of low grade metals and heavy oils, and an increased emphasis on pollution control will lead to an eventual increase in energy use for the production of a unit quantity of a given commodity (Robertson, 1976).

The global implications of meeting the demands for energy are abundantly clear (Lewis, 1970), and the procurement of an adequate energy supply has become one of the most important problems facing our world today. As West German Chancellor Helmut Schmidt (as quoted by Donnelly, 1981) remarked when opening the 1980 World Energy Conference, "Energy is not only the central problem of human coexistence, but also of the future of mankind

itself".

To satisfy the future global energy demands in an era of heightened environmental awareness, existing technologies will be refined and optimized, technological innovation will become increasingly important, and novel energy forms will be pursued world-wide. This thesis, in keeping with the ever-increasing drive towards technological optimization, considers one potential facet of our future energy composite -- the low enriched uranium fuel cycle in heavy water moderated thermal nuclear fission reactors, one in a series of advanced fuel cycles for these inherently resource efficient units. The study begins with a demand-supply option evaluation, to gain a greater perspective on the global energy requirements, and to establish the potential role of current and advanced technology in meeting these needs.

1.1 ENERGY REQUIREMENTS

It is estimated (Lewis, 1972) that by the year 2200, the global population will level off to approximately 15 billion people, with an average per-person equivalent-thermal-power requirement of 20 kW. This represents a global power requirement of some 300 million megawatts (3×10^{14} Watts) or about 9 Q/annum (1 Q = 10^{18} BTU = 1.06×10^{21} J).

Note that power production in Canada currently runs at 12 kW per capita (EMR, 1987). Current global primary energy requirements amount to approximately 0.2 Q/annum (EMR, 1987).

Electricity is providing an ever-increasing proportion of the total energy demand. For example, electrical energy provided 22.3% of Canada's primary energy use in 1986, rising from 15.5% in 1975 (EMR, 1987). This trend is expected to continue and to be followed globally in the future (Krafft, 1987).

1.2 THE GLOBAL SUPPLY OF ENERGY

1.2.1 Global Energy Resources

The global energy potential is shown in Table 1-1. The potential of hydro power, tidal, geothermal, and wood sources are left as question marks in the table, since if every tree, stream, or water wave were tapped, or all of the heat from the core of the earth were extracted, these sources would represent a very large resource base. However, due to the impracticality of these schemes on such a scale, the actual potential has not been documented. It should also be noted that the potential for fusion based energy systems is limited here by the availability of lithium supplies for tritium production. In advanced fusion systems (Harms, 1983), this limitation will be lifted.

1.2.2 Practical Energy Resources

With a current global energy demand of 0.2 Q per year, it is evident from Table 1-1 that any one of the energy sources listed could provide the energy requirements of the world for some time to come. However, the question of resource practicality must be raised. For example, it is now generally considered that coal resources are practical only when they exist in seams over 36 cm thick and at depths above 1.2 km underground (Hart, 1977). Also current economic analyses indicate that fuel resources (uranium and thorium) for nuclear fission reactors should be considered practical only when they exist in concentrations of 100 parts per million or greater within 2.4 km of the surface (Hart, 1977). Clearly these definitions will change as the costs of energy alternatives change, but, as explained by Hart (1977), they are unlikely to change in the "near to medium" future.

Table 1-2 presents the practical world energy supply picture, from which it can be seen that coal and lignite could fuel a 0.2 Q society for 950 years, but could fuel a 9 Q society for only 21 years. Hydro-electricity could make a significant contribution to the energy needs of a 0.2 Q society, but in a 9 Q society, its contribution will fall far short of the total energy

Source	Total Energy Available
Fossil	10,000 Q
Nuclear Fission	10^9 Q(1)
Nuclear Fusion	10^9 Q(2)
Solar	5230 Q per year(3)
Wind	9 Q per year
Hydro	?
Tidal	?
Geothermal	?
Wood	?

Data from Hart (1977).

(1) Based on total uranium and thorium within a mile of the earth's land surface.

(2) Based on total lithium within a mile of the earth's land surface. (Lithium is required for the production of tritium which is "burned" in fusion reactors.)

(3) Based on total solar energy intercepted by the planet.

? Means all data purely speculative.

Table 1-1 Overview of the Total World Energy Potential

Source	Energy Content
Coal and Lignite[1]	190 Q
Petroleum[1]	11 Q
Natural Gas[1]	10 Q
Tar Sands[1]	1.7 Q
Shale Oil[1]	1.1 Q
Nuclear Fission[2]	10^6 to 10^8 Q
Nuclear Fusion[3]	10^6 to 10^8 Q
Solar[4]	15 Q per year
Wind	0.03 to 0.6 Q per year
Hydro	0.09 Q per year
Tidal	0.002 Q per year
Geothermal (Natural)[5]	0.002 Q per year
Wood	?

Data from Hart (1977).

(1) Based on distribution in known geologic formations and the assumption that similar distributions exist in similar geologic formations in the earth's crust.

(2) Based on an analytical method developed by Johan Brinck and tested on other metals. Uses concentration distribution in known mining areas and the average concentration in the earth's crust. Assumes use of all the uranium and thorium in breeder reactors. The lower number includes resources in large deposits only; the higher number includes small deposits.

(3) Assumes that the amount of energy is limited by availability of lithium and that the same fraction is recoverable as for fission fuel.

(4) Assumes that it is practical to use 1 percent of the land area.

(5) Excludes the as yet unknown potential from pumping water into areas where hot dry rocks exist close to the surface.

? Means all data purely speculative.

Table 1-2 Practical World Energy Resource Picture

requirements.

It should be noted that only a small percentage of the practical global energy resources have been geologically verified. However, it must be emphasized that the total fission reactor fuel resource is well defined by thermal flux and cosmic abundance methods (Hart, 1977), and it is only the distribution that is in doubt.

1.2.3 The Supply of Fuel for Fission Reactors

The crustal abundance of uranium averages 3 g/Mg of earth (Mooradian and Runnalls, 1974). In the entire crust of the earth there are more than 100 million million tonnes of uranium (Lewis, 1972). There are 2.5×10^{12} tonnes of uranium within one mile of the earth's surface under dry land (Lewis, 1972). If all of this were burned in fission reactors, the world would have one billion Q of energy at its disposal (Mooradian and Runnalls, 1974). Recovery of uranium from sea water will further increase this resource base (Best and Driscoll, 1986).

Future fuel cycles may use thorium as a fuel (Lewis, 1967). With a crustal abundance of 10 g/Mg (Mooradian and Runnalls, 1974), thorium holds much promise for application in advanced fuel cycles, though considerable research and development work must be pursued prior to large scale implementation of such schemes.

The current industry estimates of uranium resources are given in Table 1-3. From the table, it can be seen that the total OECD (Organization for Economic Cooperation and Development) uranium resource base is approximately 2000 GgU (i.e. 2×10^{12} gU). This is to be compared with the current OECD uranium requirements of 30 GgU/a, which in turn is expected to rise to over 40 GgU/a by the year 2000 (Cruickshank, 1988). Indeed, the world's current inefficient use of uranium resources could potentially lead to eventual shortages and a concomitant escalation in raw uranium prices.

Clearly then, it is prudent to adopt two approaches which can assure an adequate supply of nuclear fuel for the forseeable future:

Region	Reasonably Assured Resources (GgU)		Estimated Additional Resources (GgU)		Total
	<$80/kgU	$80-130/kgU	<$80/kgU	$80-130/kgU	
OECD America	277	370	112	99	858
OECD Europe	96	92	37	100	325
OECD Pacific	462	63	257	127	909
OECD Total	835	525	406	326	2092
Rest of WOCA	720	153	485	99	1457
WOCA	1555	678	891	425	3549

Data from Cruickshank (1988).
WOCA - World Outside Centrally Planned Economies Area
OECD - Organization for Economic Cooperation and Development

Table 1-3 Uranium Resources

(i) Confirmation of additional uranium resources through an expanded exploration program, and
(ii) Development of new nuclear fuel cycles which make more efficient use of uranium.

Both of these approaches are receiving great attention.

1.3 NUCLEAR ENERGY SYSTEMS

From the discussions presented in Section 1.2, it is evident that nuclear power can play an increasingly important role in meeting future global energy demands. Because of its advantages from an ecological and economic point of view, energy production via nuclear fission is expected to increase by 7% per year until at least the year 2000 (Zraket, 1987).

1.3.1 Current Technology

The world's nuclear power production capacity is primarily provided by pressurized light water (pressure vessel) reactors (PWRs) (57%), boiling light water (pressure vessel) reactors (BWRs) (26%), light water graphite reactors (LWGRs) (6%), pressurized heavy water reactors (PHWRs) (5%), gas cooled reactors (GCRs) (5%), and fast breeder reactors (FBRs) (0.5%) (Carle, 1987).

Nuclear technology is still quite young and has great scope for progress (Carle, 1987). Improved performance is considered vital to maintain and increase the competitive position of nuclear power, and to compensate for the expected increases in capital expenditure (Krafft, 1987). From a political perspective, it is essential to maintain a policy framework which stimulates efficiency in energy use and production as a means of optimizing, if not minimizing, investment requirements (Foster, 1987).

1.3.2 Future Technology

As time progresses, nuclear fusion systems (Harms, 1983) may become

increasingly important to our world energy supply. Before we arrive at that stage however, a development program along these lines can be envisaged:

(1) Deployment of thermal fission reactors with improved safety and efficiency and increased uranium utilization. This would include the introduction of advanced fuel cycles using plutonium, reprocessed uranium, or thorium (Hatcher, 1979; Slater, 1982).

(2) Implementation of ultimate resource efficient breeder reactor fission fuel cycles operating in either thermal (Critoph et al., 1976) or fast (Clarke and Main, 1983) neutron spectra. These in turn, may act as "fuel factories" for advanced converter reactors (Stewart, 1981). Accelerator-breeder technology may also be deployed at this time (Fraser et al., 1981).

(3) Development of fission-fusion synergetic systems (Harms and Haefele, 1981), combining "neutron rich" and "power poor" fusion systems with "neutron poor" and "power rich" fission reactors for a net overall system gain (Lidsky, 1975). These systems would operate either as hybrid units, or independently and linked via their fuel and energy chains (Harms and Heindler, 1982).

(4) Development of stand alone fusion systems (Harms, 1983), or more advanced and yet unknown energy systems.

1.4 PURPOSE OF THIS THESIS

While the proposed progression of technological development presented in Section 1.3.2 may be altered by the introduction of novel techniques or energy forms, it nevertheless provides a logical framework from which mankind and technology can proceed.

The purpose of this thesis is to aid in demonstrating the role that resource-efficient heavy water moderated nuclear fission reactors can play in

the world's energy future, and to illustrate how the continued advancement of heavy water reactor technology will enable an evolutionary development strategy which takes advantage of the design and operational experience gained from earlier generation systems.

This thesis begins by considering and comparing heavy water reactor options currently available. Because of its inherent design and operational advantages, enhanced resource utilization, and commercial availability and viability, the CANDU-PHW (Canada Deuterium Uranium-Pressurized Heavy Water) reactor technology (Atomic Energy of Canada Limited, 1974 and 1981) is considered for additional study.

The CANDU-PHW thermal reactor is nominally fuelled with natural uranium, though it is adaptable to a number of advanced fuel cycles (Hatcher, 1979), and can potentially hold a prominent position in development stages 1, 2, and 3 as outlined in Section 1.3.2.

This thesis briefly considers the range of possible CANDU-PHW fuel cycles as documented by other researchers, and then directs its study to the first in a series of advanced fuel cycles -- the low enriched uranium (LEU) fuel cycle (Archinoff, 1979). The implementation of this fuel cycle will conclusively demonstrate the flexibility of the CANDU-PHW design, will reduce the rate at which spent reactor fuel is generated, and will increase uranium utilization in comparison with the current CANDU-PHW once-through natural uranium fuel cycle. The LEU fuel cycle is novel for CANDU-PHW reactors, but is the norm for use with most other thermal reactor technologies (Cruickshank, 1988). This fact will simplify the introduction of the fuel cycle in CANDU-PHW reactors, since the additional processes required at the front end of the fuel cycle are already commercially available. LEU is therefore the logical first step for the next generation CANDU-PHW designs.

The additional fuel reactivity available when operating on a LEU fuel cycle affords the designer extra flexibility to improve system operational characteristics. To this end, core and fuel bundle design modifications are introduced in this thesis to reduce the increase in system reactivity upon coolant voiding in a CANDU-PHW reactor, and to flatten the power distribution across individual fuel bundles in the core.

Fuel management strategies with LEU fuel are also addressed. Novel and improved fuel management schemes are developed and characterized.

Finally, a new reactor design, the CANDU - Spectral Shift Advanced Thermal Reactor (CANDU-SSATR) is introduced in this thesis. The CANDU-SSATR yields high fuel burnup and improved uranium utilization, with minimal fuel management difficulties. Fuel in such reactors would be irradiated in a series of zones, each with a distinct neutron energy spectrum. This option holds great promise for the future.

The final chapter in this thesis summarizes the major results and conclusions from the analysis described in earlier sections. Extensions to this work are discussed with particular emphasis on the requirement for experimental verification of the theoretical analyses presented herein.

CHAPTER 2

HEAVY WATER MODERATED NUCLEAR REACTORS

2.1 INTRODUCTION

The World List of Nuclear Power Plants (Nuclear News, 1988) includes some 47 heavy water moderated reactors (HWRs), operable, under construction, or on order (30 MW(e) and over) as of June 30, 1988. Of this group, 29 are large CANDU-PHW pressure tube reactors (500 MW(e) or larger), located in Canada (22), Argentina (1), Korea (1), and Romania (5). India and Pakistan account for 13 of the 47 HWRs listed (though only 5 of these are in operation). The Indian and Pakistani designs are based on CANDU technology, as AECL was involved in the design and construction of the initial units in both countries.

Argentina has two additional HWRs included in the world list. These reactors, ATUCHA-1 and ATUCHA-2, are direct cycle boiling heavy water pressure vessel units.

Three additional HWRs are included in the world list. They are the Winfrith Steam Generating Heavy Water Reactor (SGHWR) in the UK, the FUGEN reactor in Japan, and the CIRENE reactor in Italy. These three pressure tube type units were designed independently and use boiling light water as coolant.

Other HWRs, not mentioned in the world list, include the Rolphton and Douglas Point CANDU-PHW reactors, the Gentilly-1 CANDU-BLW, and the CANDU-OCR (organic cooled reactor) at Whiteshell Nuclear Research Establishment (Pinawa). These older Canadian reactors are now retired.

2.2 PRESSURE TUBE REACTOR DESIGN

The pressure tube configuration of the CANDU, CIRENE, FUGEN and

SGHWR reactor designs offers several advantages over pressure vessel type reactors. The fabrication of massive pressure vessels requires the technological capabilities associated with a mature industrial base. Further, complex engineering studies are required each time it is necessary to design a larger vessel for a larger reactor unit. With a pressure tube configuration, designing a larger unit (within limits) is simply a matter of incorporating a larger number of pressure tube "building blocks" into the core -- a relatively straightforward process. From a safety perspective, control rod ejection from the relatively cool moderator environment is extremely improbable (Kugler, 1980). In addition, by maintaining separate coolant and moderator circuits, the flexibility of using separate fluids for both processes is available.

It is for these reasons that the pioneers of nuclear energy in Canada developed the CANDU-PHW pressure tube reactor design, and it is for these reasons also, that the advanced reactors to be considered later in this thesis will also maintain the pressure tube design.

In Sections 2.2.1 through 2.2.4 descriptions of the various heavy water moderated pressure tube reactor designs are provided. Design comparisons are also provided by Varley (1985).

2.2.1 CANDU-PHW

CANDU-PHW reactors are natural uranium fuelled, heavy water moderated, and pressurized heavy water cooled units utilizing the pressure tube concept (Pasanen, 1982).

An array of pressure tubes (380 in the standard CANDU-PHW 600 MW(e) design) containing the reactor fuel and coolant are distributed uniformly, passing through a large horizontal cylindrical vessel (the calandria) containing the heavy water moderator and the reflector. The pressure tubes are spaced 28.575 cm apart on an x-y grid. (This is referred to as a 28.575 cm lattice pitch (LP).) Each pressure tube is insulated from the cool depressurized moderator system by a concentric calandria tube.

Fuel for the CANDU reactors is in the form of short natural uranium dioxide fuel bundles (49.53 cm in length containing 37 fuel elements in the

CANDU-PHW 600 MW(e) design). This allows for both radial and axial fuel management schemes (Frescura and Wight, 1982). The reactor is fuelled bi-directionally (ie, alternating channels are fuelled from opposite ends of the core). Fuelling occurs at power. Fuel exit burnup is of the order of 7000 MWd/MgU.

Heat from the coolant is transferred to a light water secondary fluid in the steam generators. The steam from the secondary side is used to turn the turbines.

Reactivity control is effected by absorbing rods, light water zone control tubes, fuelling rate and dissolved moderator poisons. Further design information is provided in Section 2.3.

2.2.2 Steam Generating Heavy Water Reactor

The British SGHWR at Winfrith (commercial startup, 1968) is a 100 MW(e) prototype pressure tube reactor design. The reactor is a vertically oriented unit with 104 pressure tubes (26 cm LP). It is a direct cycle, heavy water moderated and boiling light water cooled reactor. Enriched uranium (2.3% U-235, 36-element) fuel bundles extend the full length of the core. Fuel exit burnup is of the order of 21000 MWd/MgU. The reactor is fuelled off-power.

Reactivity is controlled via adjustment to the moderator level and through the use of dissolved neutron poison (boron) in the moderator system.

Details on the SGHWR design can be found in Hicks et al. (1968), McMillan et al (1968), and O'Dell et al (1968).

2.2.3 CIRENE Reactor

The CIRENE reactor is a boiling light water cooled (exit quality 25%), heavy water moderated pressure tube reactor. There are 60 vertically oriented fuel channels in the reactor (27 cm LP), each containing 8-eighteen element power bundles (50 cm in length) and 2 graphite (reflecting) bundles (20-30 cm in length). A combination of natural fuel bundles (inner core) and

enriched fuel bundles (1.15 % U-235) (core periphery) are used in the core. The unit will be fuelled off-power.

The reactor is designed to operate on a direct steam cycle and produce 35 MW(e). A reactor startup date has not been finalized.

Reactivity control is effected via moderator level adjustment, and through the use of four vertically oriented two-phase control rods which extend the entire length of the core. (These rods consist of heavy water and borated light water filled tubes with several fine air bubbling mechanisms which can be operated at variable rates to adjust system reactivity.)

The CIRENE reactor is described in greater detail by Bonalumi et al. (1976).

2.2.4 FUGEN Reactor

The Japanese FUGEN reactor is a heavy water moderated and boiling light water cooled pressure tube unit operating on a direct cycle. The reactor began operation in 1979. The unit produces 165 MW(e) from its 224 vertically oriented fuel channels (24 cm LP).

Fuel for the FUGEN reactor is in the form of 28 element fuel assemblies containing mixed oxide fuel (1.5 and 1.9% U-235 enriched fuel and 0.6-1.3% Pu mixed oxide fuel). Fuel exit burnup is of the order of 17000 MWd/MgHE (heavy element). The reactor can be fuelled at power.

Reactivity control is effected via 4 control rods.

Additional details on the FUGEN reactor design can be found in Kato et al. (1984), and Akebi and Fujiki (1983).

2.3 CANDU-PHW DESIGN DESCRIPTION

Globally, the only heavy water moderated pressure tube reactor design to have achieved commercial success is the CANDU-PHW. In this section, a more detailed description of the CANDU-PHW design is provided. The CANDU-PHW 600 MW(e) design (or CANDU-600) (also known as the CANDU-6) is chosen as the standard design for illustrative purposes in this section, and adaptations of

the design are considered later in this thesis.

2.3.1 Reactor Description

As noted in Section 2.2.1, the CANDU-600 is comprised of 380 pressure tubes / calandria tubes passing horizontally through a heavy water filled calandria. The 28.575 cm lattice pitch is approximately optimal from a reactivity standpoint (Pasanen, 1982). The reactor is depicted in Fig. 2-1. Note that there are no fuel channels near the periphery of the calandria. This region is known as the reflector.

The pressure tube configuration results in the moderator system being operated independently of the high pressure coolant (approximately 9.5 MPa, 290 ^{o}C) in the pressure tubes. The moderator system operates at atmospheric pressure and at a relatively cool temperature of about 70 ^{o}C.

2.3.2 Reactor Control

In CANDU reactors, the power level and spatial distribution are controlled by a variety of mechanisms. The normal control mechanisms in the CANDU-600 consist of:

(a) Adjuster Rods: 21 cobalt or stainless steel absorbing rods vertically suspended in the mid-core region of the reactor (normally in-core).
(b) Zone Controllers: 14 light water compartments which can be filled to variable levels to control bulk and spatial power distributions.
(c) Mechanical Control Absorbers: 4 cadmium rods which can be introduced to quickly reduce reactor power.
(d) Moderator Poison: Boron or gadolinium can be dissolved in the moderator system. The poison is extracted using ion exchange columns.

(Note that some CANDU-PHW designs use enriched uranium booster rods as opposed

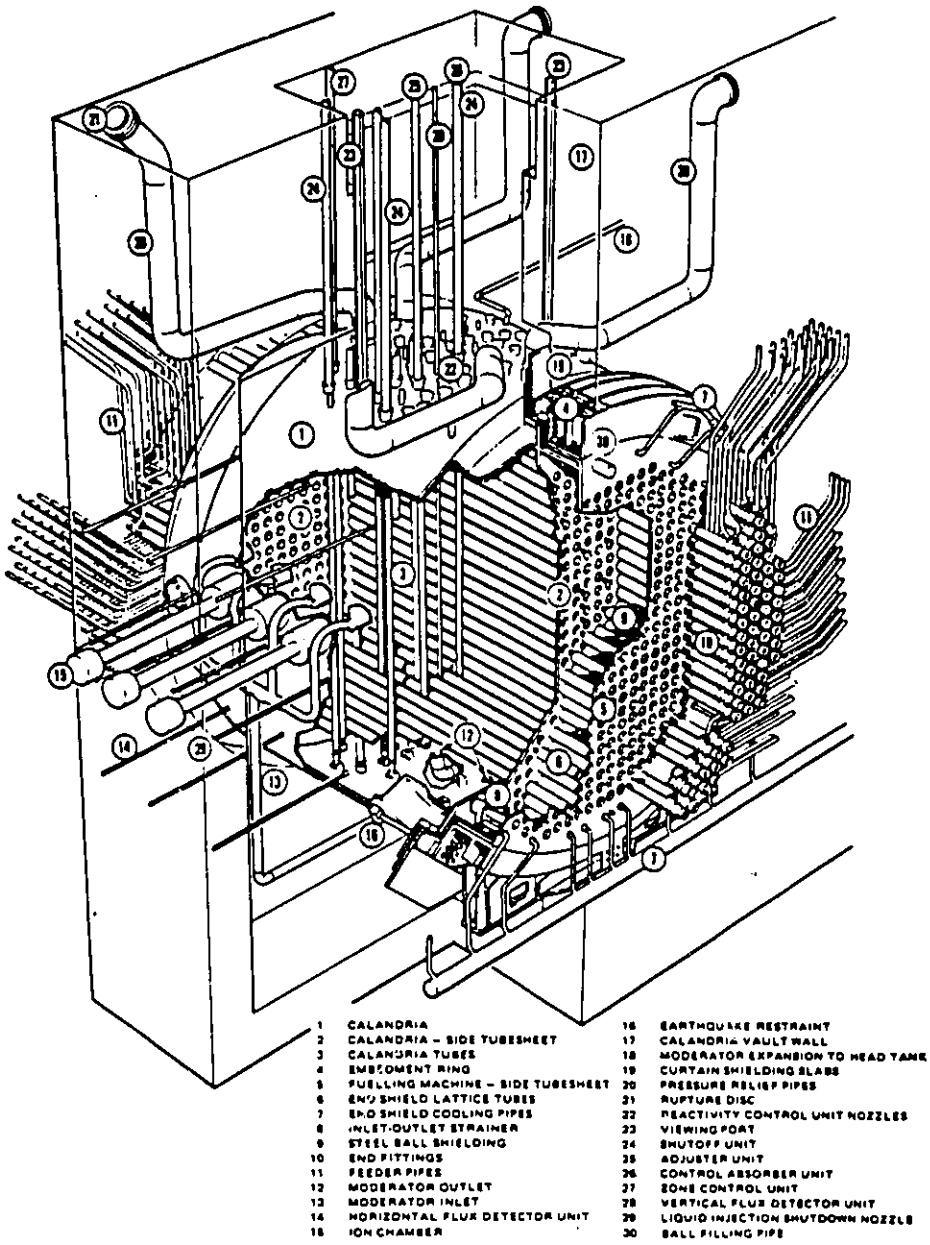

Figure 2-1 CANDU-PHW Reactor Assembly
(Figure courtesy of Atomic Energy of Canada Limited)

to absorbing adjuster rods (Trojan and Dastur, 1973).)

The CANDU-600 reactors employ two special shutdown systems (SDS):

SDS1: 28 cadmium shutoff rods,

SDS2: 6 nozzles for gadolinium injection into the moderator system.

All of the reactivity devices are located, or introduced into guide tubes positioned in the low pressure moderator environment. These vertically mounted guide tubes are located interstitially between columns of fuel channels (Kugler, 1980).

2.3.3 Reactor Fuelling

The CANDU-600 is fuelled at power. Two fuelling machines latch on to each end of a fuel channel, and new fuel bundles are inserted into one end of the fuel channel while the fuelling machine at the opposite end of the fuel channel accepts the spent fuel bundles (Frescura and Wight, 1982). A CANDU-600 fuel bundle is depicted in Fig. 2-2. A CANDU-PHW lattice cell, consisting of a fuel channel and surrounding moderator, is depicted in Fig. 2-3.

Further detailed descriptions of the CANDU-PHW design can be found in Pasanen (1982) and Atomic Energy of Canada Limited (1981).

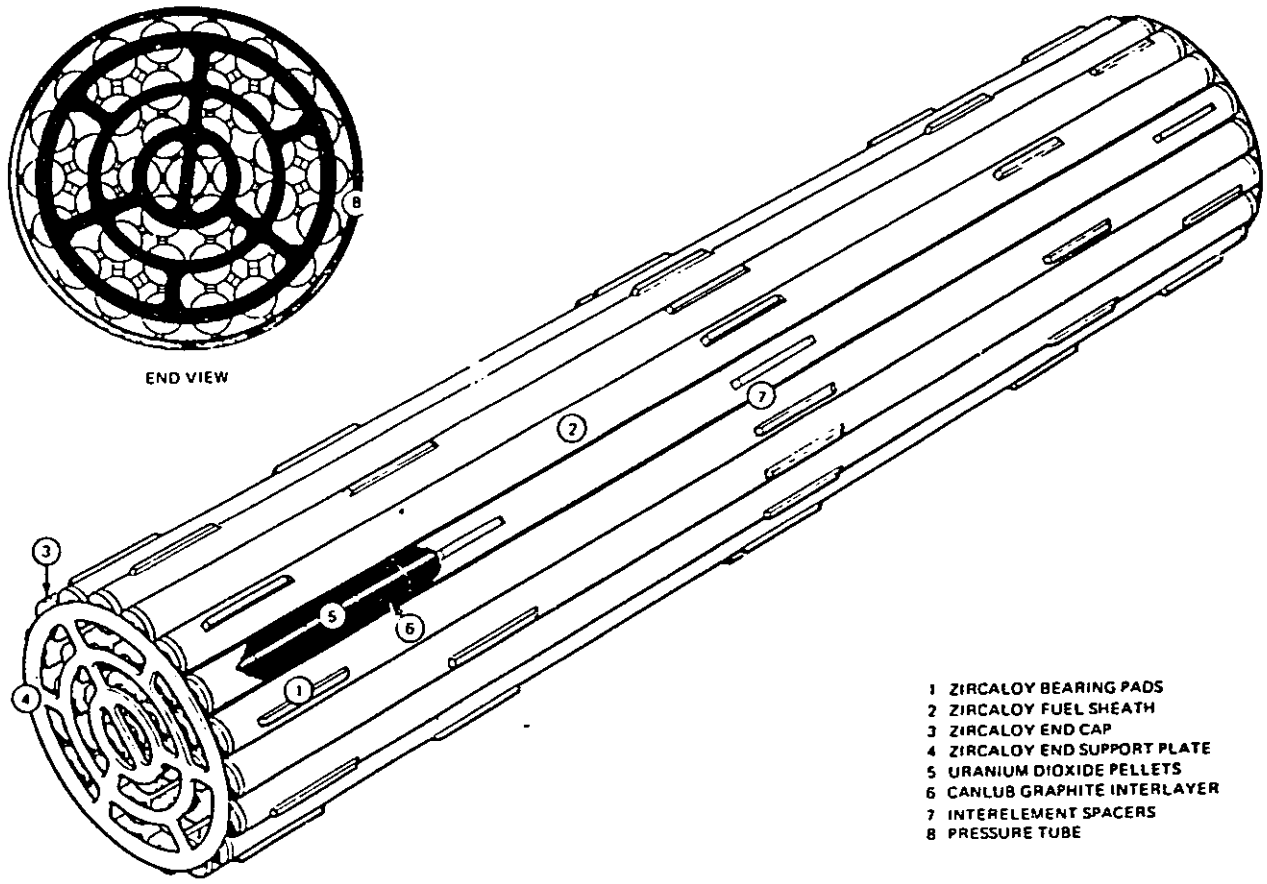

Figure 2-2 CANDU-PHW 37-Element Fuel Bundle
(Figure courtesy of Ontario Hydro)

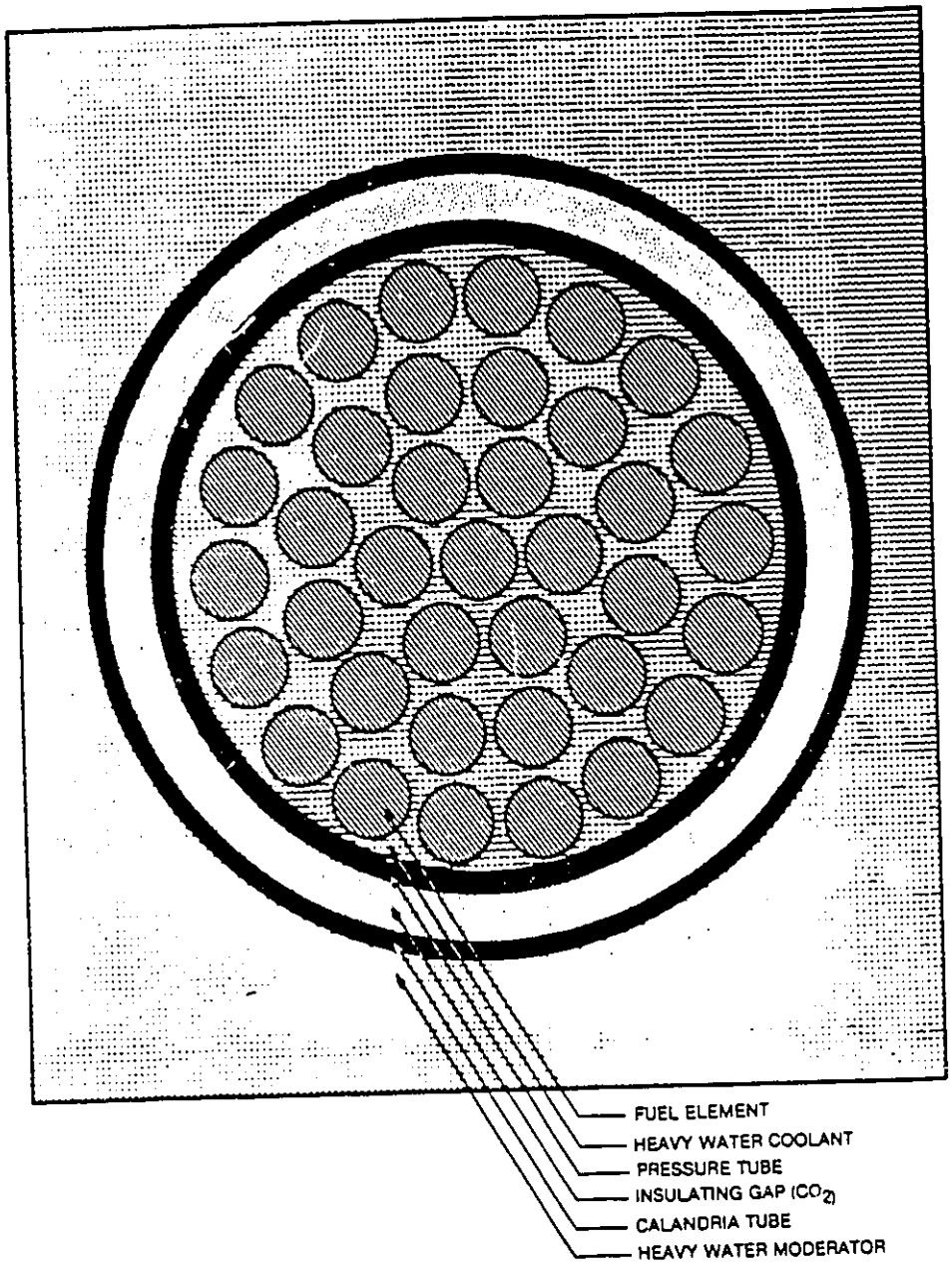

Figure 2-3 CANDU-PHW Lattice Cell (Cross Section)
(Figure courtesy of Ontario Hydro)

CHAPTER 3

ADVANCED FUEL CYCLES IN CANDU REACTORS

3.1 INTRODUCTION

As noted in Chapter 2, current generation CANDU-PHW reactors are designed to operate on a natural uranium fuel cycle. To maximize fuel burnup, strict attention has been paid to neutron economy in all aspects of the reactor design. This design philosophy allows the CANDU-PHW to be easily adapted to more advanced fuel cycles (Hatcher, 1979; Slater, 1981; Hawley, 1983), which can result in greater resource efficiency and improved economics (under future expected conditions (Slater, 1982)).

The International Nuclear Fuel Cycle Evaluation (INFCE) report (International Atomic Energy Agency, 1980 and 1980a) is the result of an exhaustive evaluation of all aspects of current and potential future nuclear fuel cycles. This study identified the important role that heavy water moderated nuclear reactors can play in energy production on a global scale. The potential for implementation of low enriched uranium fuel cycles, plutonium recycling, and thorium fuel cycles (Hatcher, 1979; Garvey, 1985), may indeed ensure the economic and technological viability of the CANDU-PHW concept far into the future.

The US Non-Proliferation Alternative Systems Assessment Program (NASAP) has identified heavy water reactor technology and in particular the CANDU-PHW design (Shapiro and Jesick, 1979) as a potential means of providing an economic alternative to light water reactors, while producing more energy per kilogram of uranium and per unit of separative work (see Chapter 4) expended, and posing an inherently low risk of nuclear weapons proliferation. The applicability of the CANDU-PHW design for US siting with some modifications for the use of advanced fuel cycles was studied by Combustion Engineering (Shapiro and Jesick, 1979).

On a global scale, a particular nuclear fuel cycle can be beneficial to an emerging nuclear program only if it meets the specific domestic needs of the developing nation. Thus, to support global non-proliferation policy objectives (Willrich, 1973), alternate fuel cycles should not only be identified on the basis of their enhanced proliferation resistance, but such fuel cycles must also be evaluated to determine if they are technically and economically sound, and are desirable from the perspective of long-term national energy security (Bagnal et al., 1981). The CANDU-PHW was identified as generally satisfying these requirements with a number of advanced fuel cycles (Bagnal et al., 1981). For all of these cycles, the main features of the CANDU-PHW reactor design can be retained (Garvey, 1985). Descriptions of various CANDU-PHW fuel cycles are given in Sections 3.2 through 3.5. Section 3.6 provides a comparison of various fuel cycles for CANDU reactors and other reactor variants.

3.2 ONCE-THROUGH NATURAL URANIUM FUEL CYCLE

The current fuel cycle employed in CANDU-PHW reactors is a once-through natural uranium cycle as depicted in Fig. 3-1. This is the simplest of all fuel cycles since it requires no uranium enrichment, no fuel reprocessing, and no fabrication of highly radioactive fuel. Uranium is mined, refined, fabricated into fuel, used in the reactor, and stored as spent fuel after use.

3.3 LOW ENRICHED URANIUM FUEL CYCLE

As noted in Chapter 2, most heavy water moderated reactor designs rely on the use of enriched uranium fuel. The CANDU-PHW reactor can be adapted to use a once-through low enriched uranium (LEU) fuel cycle. This fuel cycle is depicted in Fig. 3-2.

Studies have indicated that by enriching the uranium in the CANDU-PHW fuel to 1.2% U-235 (from the natural level of 0.7% U-235), uranium utilization would be increased by approximately one-third over the natural uranium fuel

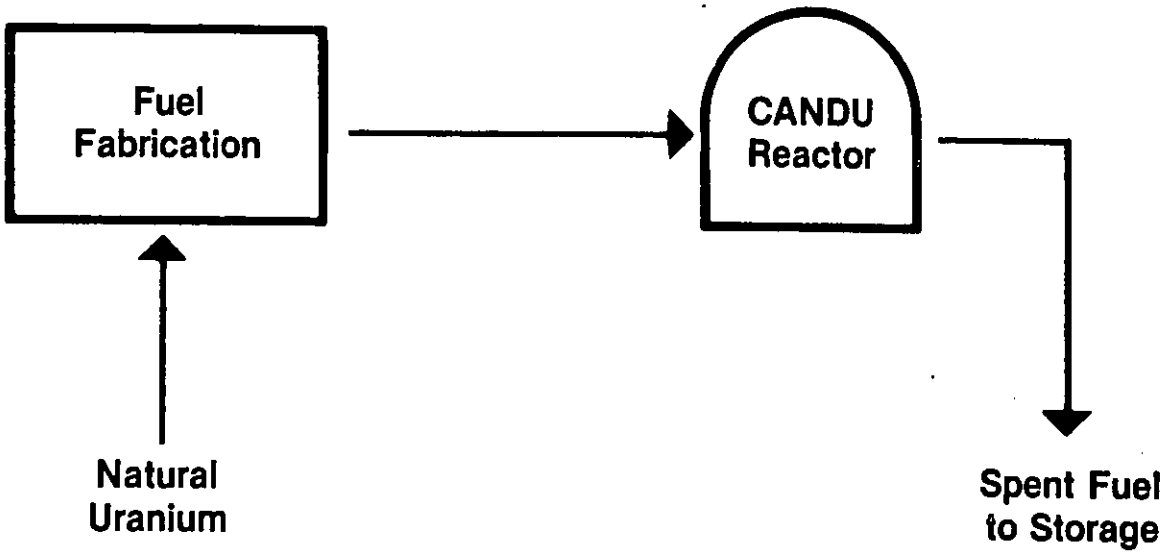

Figure 3-1 Once-Through Natural Uranium Fuel Cycle

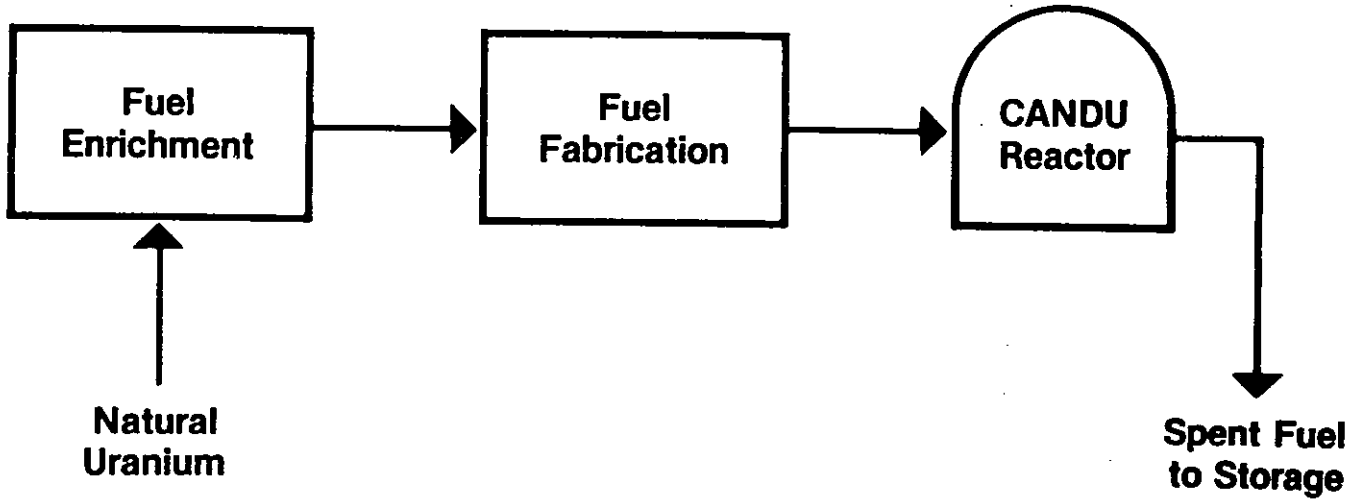

Figure 3-2 Once-Through Slightly Enriched Uranium Fuel Cycle

case (Archinoff, 1980). Fuel burnup would increase to approximately 21000 MWd/MgU (Atomic Energy of Canada Limited, 1979b).

It is anticipated that essentially no major changes would be required to the CANDU design to take advantage of the enriched uranium fuel cycle (Atomic Energy of Canada Limited, 1979b). Minor modifications in design may be required in the fuel storage and handling areas to accommodate the more reactive fresh fuel, and some modifications to the control and safety mechanisms may be required to preserve their performance.

Studies by Ontario Hydro (Archinoff, 1979; Archinoff, 1980), Combustion Engineering (Bagnal et al., 1981), and Atomic Energy of Canada Limited (Slater, 1982) suggest that optimally, the low enriched uranium fuel cycle should act as a transitional cycle prior to the introduction of plutonium recycling or thorium fuel cycles in CANDU-PHW reactors.

3.4 PLUTONIUM-URANIUM FUEL CYCLE

The spent fuel from a natural uranium CANDU-PHW reactor contains 3.8 grams of plutonium per kilogram of heavy elements (Archinoff, 1980). In a plutonium-uranium (or plutonium recycle) fuel cycle, the plutonium is extracted from the spent fuel in a reprocessing facility and mixed with uranium to create new mixed-oxide (MOX) reactor fuel.

The cycle, for natural uranium feed, is depicted in Fig. 3-3.

The Japanese FUGEN reactor (discussed in Chapter 2) uses a plutonium-uranium fuel cycle.

Plutonium for use in CANDU-PHW reactors can also be extracted from the stockpile of spent light water reactor fuel, or it can be created from fertile U-238 in the blanket region of a fast breeder reactor, an accelerator breeder, or a fusion reactor.

3.5 THORIUM FUEL CYCLES

Thorium, which is more than three times as abundant on earth as uranium (Mooradian and Runnalls, 1974), can be used to power CANDU-PHW

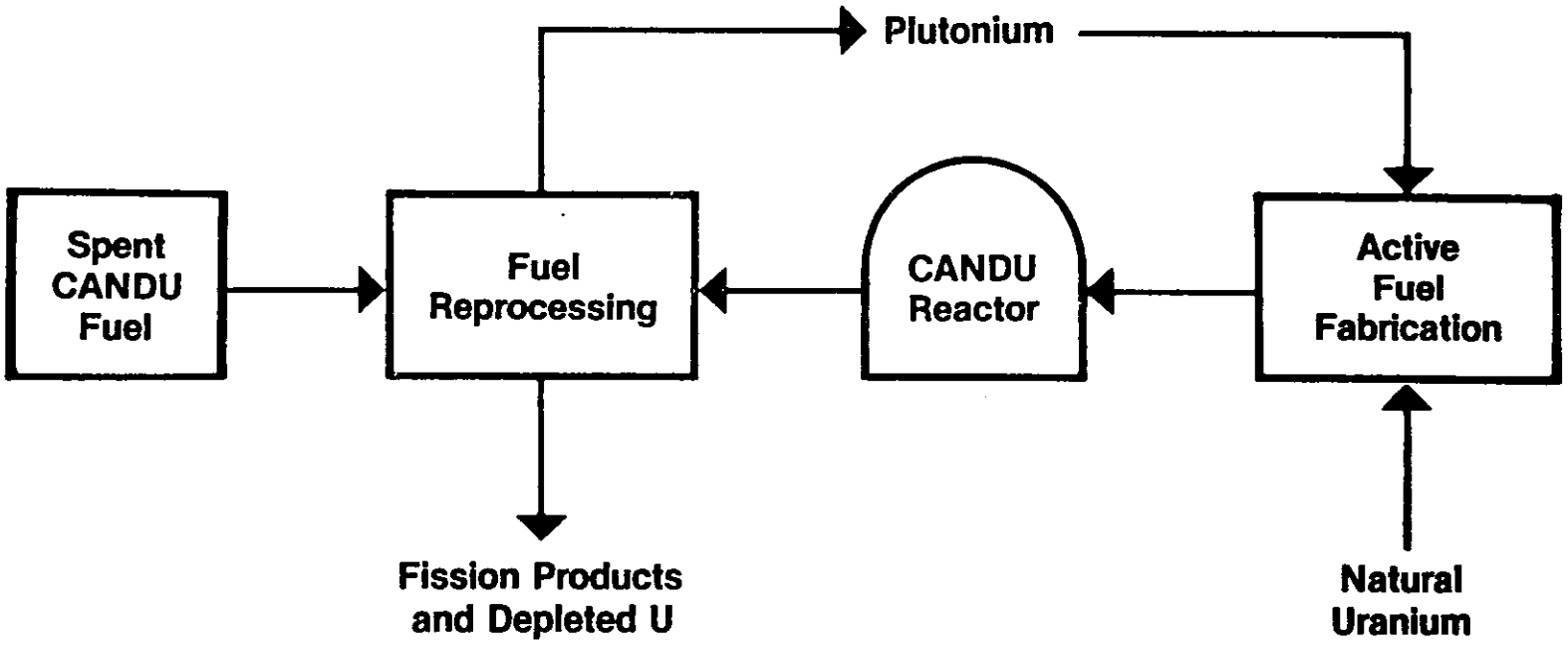

Figure 3-3 Plutonium-Uranium Fuel Cycle

reactors. Further, thorium is not in high demand in the world and hence it is expected that the price will remain relatively stable (Archinoff, 1980), thereby increasing the attractiveness of this fuel cycle in the future.

The basic thorium fuel cycle is illustrated in Fig. 3-4. Plutonium-239 or uranium-235 (and eventually U-233) can be used to provide the required initial fissile material. Depending on the burnup, and the time period between reprocessing, the thorium fuel cycle may require additional fissile isotopes to be added during fuel production (Slater, 1982) or a self-sufficient thorium cycle can be developed (Critoph et al., 1976), where, once an initial supply of fissile material has been introduced, the U-233 produced in the thorium can be reprocessed to satisfy all the fissile requirements of the reactor.

While most thorium fuel cycles include a reprocessing stage, Milgram (1982) has reported on the utility of a once-through thorium cycle in CANDU reactors, which combines the use of fertile thorium fuel bundles and enriched uranium driver bundles.

3.6 COMPARISON OF RESOURCE UTILIZATION

Table 3-1 shows the approximate raw material requirements for the fuel cycles considered in this chapter in comparison with light water reactors (LWRs) and liquid metal fast breeder reactors (LMFBRs). These data are representative of equilibrium operation.

Table 3-2 details the total fuel requirements including the amount of material required to initialize the reactor operation for several of the CANDU-PHW fuel cycles considered.

It can be seen that the resource utilization enhancements afforded through the use of enriched uranium fuel cycles in CANDU-PHW reactors pale in comparison with those achievable with advanced self-sufficient thorium fuel cycles. The LEU cycle does, however, represent an important first step -- to prove the flexibility and adaptability of the CANDU-PHW design, and thereby provide the means to progress effectively and expediently, through technological development in an evolutionary rather than revolutionary

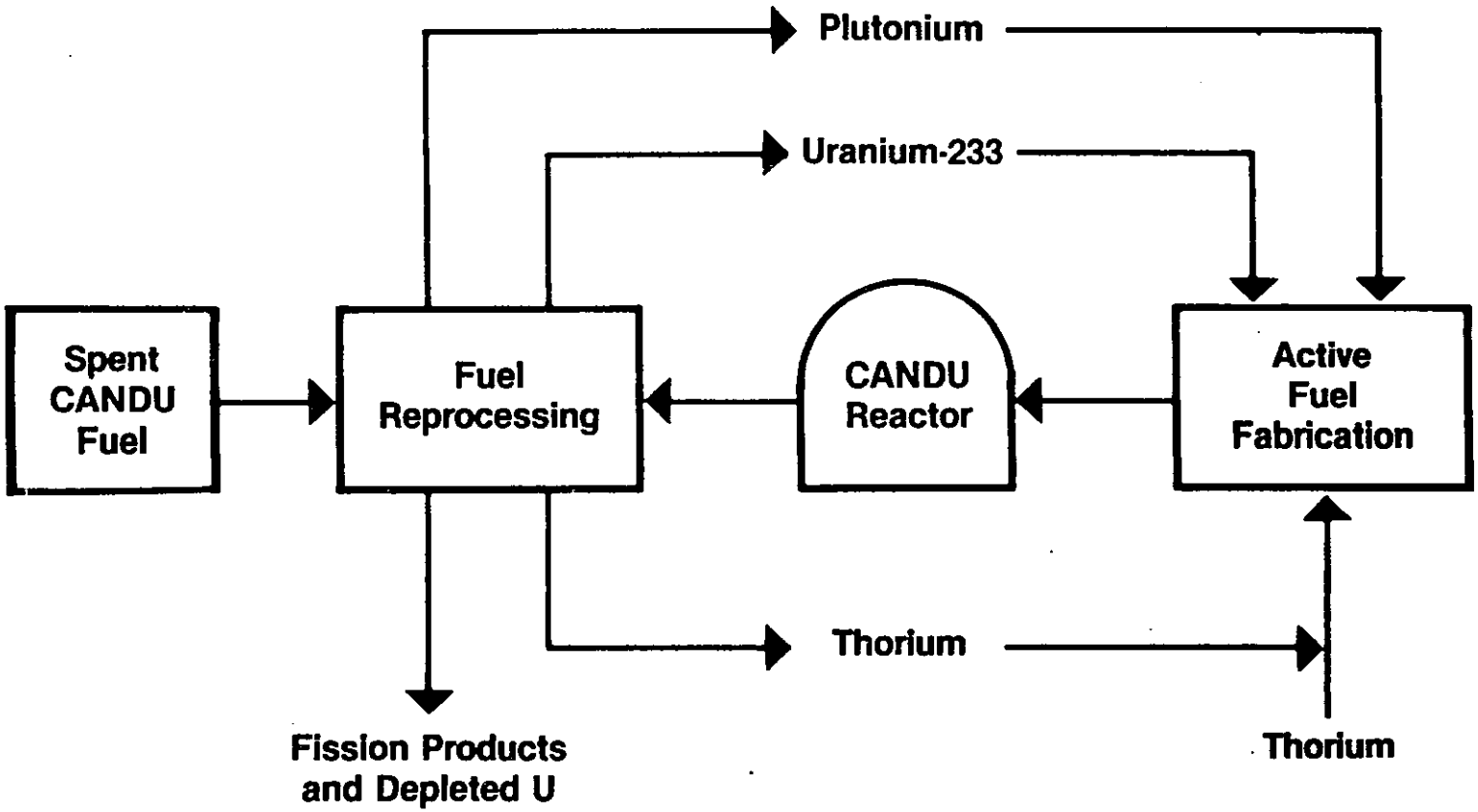

Figure 3-4 Thorium Fuel Cycle

Reactor	Fuel Cycle	Fuel Consumption (kg/MW-year)(e)	
		Uranium	Thorium
CANDU	Natural uranium once-through	167	-
	1.2% Enriched uranium once-through	118	-
	Plutonium/uranium	70	-
	Plutonium/thorium	45	1
	Uranium-235/thorium	32	1
	Thorium self-sufficient	-	2
LWR*	Enriched uranium once-through	200	-
	Uranium recycle	170	-
	Plutonium/uranium recycle	125	-
LMFBR**	Plutonium/uranium	2	-

Note: Data are from Hatcher (1979).

* Light water reactor fuelled with enriched uranium.
** Liquid metal fast breeder reactor fuelled with plutonium and uranium-238.

Table 3-1 Approximate Equilibrium Fuel Consumption

Fuel Cycle	Inventory[a] (MgU)	Equilibrium Feed		Burnup (MWd/kgHE)[c]
		kgU/(MW-a)(e)	MgU/a[b]	
Natural uranium once-through	144	166	133	7.5
1.2% U-235 once-through	190	118	94	20.8
Uranium/plutonium[d]	194	70	56	18.0
Thorium/uranium[e][f]	680	32	26	37.4
Thorium/uranium[e] self-sufficient[g]	871	0	0	10.0
Thorium/plutonium[f]	1385[h]	62[h]	50[h]	37.2
Thorium/plutonium self-sufficient[g]	1826[h]	0	0	10.0

Note: Data are from Hatcher (1978) and Critoph (1977).
Assuming electrical output of 1000 MW.

(a) Inventory is defined as the difference between actual requirements over a long time period and requirements determined from equilibrium feed rate applied from in-service date.

(b) Based on 80% capacity factor.

(c) Burnup per mass of Heavy Element, uranium or thorium.

(d) Plutonium from CANDU natural uranium; consumption is for combined cycle.

(e) Uranium-235 feed with 0.2% tails, uranium-233 recycle.

(f) High burnup fuel cycle optimized for cost.

(g) Low burnup fuel cycle for maximum uranium utilization.

(h) Uranium figures shown are the amount of spent natural uranium CANDU fuel required to provide fissile plutonium.

Table 3-2 Resource Consumption in CANDU-PHW Fuel Cycles

manner. It is the purpose of this thesis to provide additional analysis and understanding of the use of enriched uranium fuel cycles in CANDU-PHW reactors and thereby aid in the eventual realization of advanced fuel cycles in these or similar resource efficient reactors.

CHAPTER 4

URANIUM ENRICHMENT: STRATEGIES AND FACILITIES

4.1 INTRODUCTION

The introduction of a once-through low enriched uranium fuel cycle in CANDU-PHW reactors introduces the added complication of artificially increasing the concentration of U-235 in the feed fuel. Therefore, an examination of the technological feasibility of the LEU fuel cycle in such reactors would not be complete without considering the fuel enrichment stage of the cycle. This chapter has been provided to outline the process, to address the implications with respect to nuclear safeguards, and to comment on commercial availability.

4.2 FUEL ENRICHMENT TECHNIQUES

In this section, the following enrichment techniques are discussed: gas diffusion, gas centrifuge, separation nozzle, UCOR/helikon, chemical separation, and laser-based processes.

4.2.1 Gas Diffusion

In the gas diffusion enrichment technique (the primary enrichment technique in the US), uranium hexafluoride feed gas (UF_6) flows past a diffusion barrier made of a porous material. About half of the feed gas flows through the barrier to a lower pressure region. The gas passing through the barrier is slightly enriched in U-235.

The separation factor (S), per stage, is defined as the ratio of the U-235 to U-238 fraction in the enriched portion, divided by the same fraction in the depleted portion. For the diffusion process, S=1.00429, and is equal

to the square root of the ratio of the mass of $(U\text{-}238)F_6$ to $(U\text{-}235)F_6$.

Because there is only a small increase in enrichment per diffusion stage, it is necessary to use many stages in series in a countercurrent cascade. To separate natural uranium feed (0.711 weight percent (w/o) U-235) into product uranium containing 3 w/o U-235 (typical for light water reactors) and tailings containing 0.2 w/o U-235, requires 1272 stages (Benedict, 1977).

This enrichment technique is very energy intensive requiring the order of 2300-2500 kWh/kgSWU (International Atomic Energy Agency, 1980a), where a kilogram separative work unit (SWU) is a measure of the amount of enrichment performed. For a given process and quantity of feed fuel, the kgSWU expended is defined as the increase in total value of the product and tailings, taken together after enrichment, less the value of the feed. The value function is measured from an arbitrary base. To place this in perspective, at nominal capacity factors light water reactors require of the order of 100 kgSWU per year per installed MW(e) (International Atomic Energy Agency, 1980a). Details on the derivation of the definition of separative work are provided by Silvennoinen (1982). The pertinent equations are considered in Chapter 10 and Appendix E of this thesis.

4.2.2 Gas Centrifuge

A disadvantage of the gaseous diffusion process is the inherently large energy requirements as a consequence of irreversible flow through the diffusion barrier. The gas centrifuge has the advantage of a reversible separation mechanism with much lower power consumption than gaseous diffusion (Benedict, 1977).

In the centrifuge technique, UF_6 gas is introduced into a rapidly rotating cylindrical bowl. The pressure at the outside of the bowl is millions of times greater than at the axis due to centrifugal forces. This causes the concentration of U-238 to be appreciably higher at the outer radius. In addition, longitudinal countercurrent flow of UF_6 (induced by baffles and scoops) causes the gas enriched in U-235 to flow downward, and the gas enriched in U-238 to flow upward (Benedict, 1977).

The amount of separative work per unit time is proportional to the rotor length and to the fourth power of the peripheral velocity (Geston, 1983).

The separation factor for a centrifuge stage is approximately 1.055 (Edwards and Wilcox, 1988). Typically about 12 centrifuge stages are needed to achieve the enrichment levels required for light water reactor fuel (IAEA, 1980a), though in some machines, a U-235 concentration ratio of 2 can be set up between top and bottom, requiring only seven stages in an ideal cascade to span the range from 0.25% tailings to 3% product (Benedict, 1977). Energy requirements are approximately 100-400 kWh/kgSWU (International Atomic Energy Agency, 1980a).

The machines are subject to damage from vibration at resonant frequencies. This limits the length of the centrifuge. Even with a successful dampening system and operating at limiting peripheral velocities, a low enrichment plant with a capacity of 3 million kgSWU/a would need 60,000 fibreglass centrifuges 10 m long to do the work of 1200 gaseous diffusion stages (Benedict, 1977). This tends to increase construction and maintenance costs.

4.2.3 Separation Nozzle

The Becker separation nozzle enrichment method (Becker et al., 1981) is an aerodynamic process utilizing a combination of linear and centrifugal acceleration through a curved slit. UF_6 gas is diluted with hydrogen gas (4% UF_6, 96% H_2 (molecular percent)). The $(U\text{-}235)F_6$ accelerates through a tighter radius than the $(U\text{-}238)F_6$ and separation factors of about 1.015 are typical (Becker et al., 1981; Benedict, 1977).

Approximately 500 nozzles are required to produce 3% U-235. Power consumption is greater than in the diffusion process (approximately 4000 kWh/kgSWU) (Benedict, 1977).

Other aerodynamic separation techniques (Blahnik, 1979) include the vortex tube, separation probe, crossed beam, velocity slip, and the jet membrane method (which involves preferential penetration of $(U\text{-}235)F_6$

through an expending jet of easily compressible carrier gas).

4.2.4 UCOR/Helikon

The South African UCOR process is characterized as a fixed wall gas centrifuge, utilizing the helikon cascade technique. This technique is based on the principle that an axial flow compressor can simultaneously transmit several streams of different isotopic composition without resulting in significant mixing (Benedict, 1977). The process utilizes a gaseous UF_6 and H_2 mixture.

This enrichment technique has a separation factor of approximately 1.025 to 1.03 and requires 2000-2300 kWh/kgSWU (Blahnik, 1979; Becker et al., 1975). (Benedict (1977) quotes an energy requirement of 3500 kWh/kgSWU for the UCOR process.) 100 multistage modules would be needed to produce 5 million kgSWU/a at 3% U-235, 0.25% tailings (Benedict, 1977).

4.2.5 Chemical Separation

Chemical U-235 enrichment processes rely on an exchange between phases containing uranium of different valences (Blahnik, 1979). Redox chromatography in adsorption columns has been found to be one of the most efficient means of chemical enrichment of uranium (Sedo et al., 1980). The Japanese Asahi Chemical Enrichment (ACE) process is an example of this technique involving UO_2^{2+} and U^{4+} ions (Takeda, 1988). The construction of a pilot plant with a capacity of 1000 kgSWU/a was completed in 1985.

CEA in France has also developed a high separation factor, low energy consumption chemical enrichment technique known as CHEMEX (Coates et al., 1983). Exchange is achieved by means of two liquid phases, one organic, the other aqueous, which are allowed to interact in large pulsed columns. The columns are arranged in such a way as to constitute an enrichment cascade. The process involves the exchange of IV and VI valences (Coates et al., 1983).

4.2.6 Laser Based Processes

Laser based enrichment techniques can be divided into two separate categories: molecular laser isotope separation (MLIS) and atomic vapour laser isotope separation (AVLIS).

Laser isotope separation involves less capital expenditure than the diffusion or centrifuge technique, and uses only a fraction of the energy of a diffusion plant. Virtually complete separation can occur in a single pass (Palmer and Bolef, 1984).

4.2.6.1 Molecular Isotope Separation

The MLIS technique uses UF_6 gas with which the enrichment industry is quite familiar. In this process energetic tunable lasers preferentially excite the desired isotopic species (Forsen et al., 1975).

A supersonic nozzle expansion process is used to reduce the spread of molecular velocities (due to temperature). Infrared and ultraviolet laser photons are used to excite selectively and to dissociate the UF_6 molecules. The resulting UF_5, enriched in U-235 is a fine powder which can be removed from the UF_6 by gas filtration. However, under production conditions, British researchers expect the overall enrichment factors would prove too small for an economically viable single stage enrichment process to produce reactor fuel (Crocker and Roberts, 1987). The Japanese are more optimistic (Varley, 1988).

4.2.6.2 Atomic Vapour Laser Isotope Separation

The AVLIS technique involves the vapourization of (corrosive) uranium metal using tunable dye lasers in the visible spectrum (Forsen et al., 1975), taking advantage of small differences in absorption spectra between isotopic species. The atoms can be ionized and separated electrically or magnetically (Benedict, 1977; Blahnik, 1979).

Often several lasers of different energies are used. The first two

lasers in the visible range, bring the U-235 to an excited level just below the ionization potential. A third laser (in the infra-red range) ionizes the excited U-235 atoms (Blahnik, 1979; Crocker and Roberts, 1987).

In 1985, the US Department of Energy announced that the AVLIS technique had the best potential to meet the long term future separative work requirements and US research and development efforts are now concentrated on this process (Steyn, 1985).

4.3 NUCLEAR WEAPONS PROLIFERATION

Enrichment plants producing reactor grade uranium can be modified to produce weapons grade uranium. Safeguards (Kratzer, 1983) must be implemented to minimize the chance of this occurring. Some inherent characteristics of the facilities also deter diversion.

Diffusion plants operate using a series cascade arrangement. Any recycling of product for the purpose of obtaining highly enriched uranium would require long delays and pose serious criticality problems. For example, it takes approximately 25 days to achieve equilibrium for a 3% enrichment process, but more than 10 months for a 90% enrichment process (Blahnik, 1979).

Centrifuge plants operate a relatively small number of machines in a series cascade, but have many parallel units. These could be arranged in series to produce uranium at 90% enrichment in a matter of a few days (Blahnik, 1979).

In the separation nozzle process, proliferation concerns are less pronounced than for the gas centrifuge. The individual stages are already arranged in series. Nevertheless, by multiple recycle of the product stream, 90% enrichment can be achieved. The risk of inadvertent criticality limits the probability that the plant would be modified in this way (Blahnik, 1979).

The UCOR/helikon process has a high separative efficiency and low cascade equilibrium time. It is expected that it could easily be adapted to produce 90% enriched product (Blahnik, 1979).

Chemical exchange enrichment technology is the most attractive in terms of proliferation resistance. Large columns producing 3% U-235 are very

difficult to modify to produce weapons-grade material (Coates et al., 1983). Criticality concerns and a 3 to 30 year time period to reach equilibrium conditions at 90% enrichment greatly limit the attractiveness of this option for the production of material for nuclear weapons (Blahnik, 1979).

The laser separation technique indeed raises the issue of its potential use in the separation of material for weapons production as well as concerns over its general proliferation resistance (Steyn, 1985). The technological complexities inherent in the process may in fact minimize the proliferation concerns (Blahnik, 1979).

4.4 ENRICHMENT FACILITIES: A GLOBAL ASSESSMENT

The 1989 World Nuclear Industry Handbook (Cruickshank, 1988) notes that the global enrichment capacity is currently: 33 million kgSWU/a (operating), 250,000 kgSWU/a (under construction), 1.6 million kgSWU/a (planned), and 8.4 million kgSWU/a (shutdown or on standby).

The bulk of the world's enrichment supply is provided by the USA (Department of Energy diffusion plants), France (Comhurex and Eurodif diffusion plants), and the USSR (diffusion plants) (Varley, 1987b). The Eurodif facility in France is run by a consortium owned jointly by France, Italy, Belgium, Spain and Iran (Voigt et al., 1983).

The Urenco consortium (UK, West Germany and the Netherlands (equal partners), (Voigt et al., 1983)) operates centrifuge enrichment plants in each of the partner countries, with a total capacity of close to 2 million kgSWU (Varley, 1987b). These plants are becoming increasingly efficient (Edwards and Wilcox, 1988).

Japan has several centrifuge plants in operation and under construction (total 300,000 kgSWU/a). Argentina and China have small diffusion facilities. India has adopted centrifuge technology. South Africa has a 300,000 kgSWU/a UCOR/helikon facility in operation. Brazil and West Germany have small jet nozzle enrichment facilities.

As noted in Section 4.2.6.2, the USA is currently engaged in the development of the AVLIS process. A US development plan that would lead to

demonstration of the AVLIS process at full scale by 1992 is being implemented. Successful completion of the plan could lead to deployment of AVLIS by the mid-to-late 1990s (Sewell and Haberman, 1988).

Laser isotope separation techniques are also being studied in the UK (Crocker and Roberts, 1987), Japan (Varley, 1988), and France (Coates et al., 1988).

Of late, a buyers' market in the enrichment services industry has persisted, with a considerable world surplus of enriched uranium (Wolf and Blumenthal, 1987). Enrichment demand is expected to increase steadily to the year 2000. However, planned capacity should be sufficient to meet expected demand at least until the turn of the century (Cruickshank, 1988). The moth-balled diffusion capacity in the US could be brought back into service should the demand for enrichment services increase substantially (Wolf and Blumenthal, 1987).

Any country or utility embarking on an enriched uranium fuel cycle over the next decade can be assured that sufficient global capacity for enrichment services exists. Existing techniques are evolving and becoming more efficient. The cost of laser enrichment separative work is expected to be about three-quarters of that associated with advanced gas centrifuge technology (Steyn, 1985). This should result in a real cost reduction for all enrichment services.

The expected stability on the international market, the wide range of global suppliers, and the variety of enrichment techniques available, all tend to indicate that security of supply of enrichment services can be assured. This will allow a country, such as Canada, to experiment in the use of an enriched uranium fuel cycle in its CANDU-PHW reactors by initially purchasing enrichment services abroad. As the scope of the program is broadened, and a larger number of reactors begin operating on the enriched fuel cycle, indigenous fuel enrichment facilities can be developed. From the standpoint of assured source of supply, operational reliability, operational safety, and economics, this step of the nuclear fuel cycle can be depended on both for the short term and for the longer term future (Voigt et al., 1983).

CHAPTER 5

IMPROVING CANDU REACTOR OPERATING CHARACTERISTICS

5.1 INTRODUCTION

Future advancements in CANDU-PHW design must be geared towards:

(a) improved resource utilization,

(b) improved economics and marketability, and

(c) improved reactor operational and safety characteristics.

As global energy demands increase, and the percentage of these requirements met by nuclear fission reactors increases, the price of uranium will necessarily escalate to the point where advanced fuel cycles become economically viable. Consequently, improved resource utilization will generally lead to improved economics at some point in the future. Since neutron economy has always been stressed in the design of CANDU reactors, it is natural that this design variant will be at the forefront of the next generation of fission reactors.

There are several aspects of the current CANDU design which can be modified to improve the international acceptance of the reactor.

A first consideration is the relatively low burnup achievable with natural uranium fuel (approximately 7000 MWd/MgU (Pasanen, 1982) versus approximately 30000 MWd/MgU for enriched uranium fuelled LWRs (Sider et al., 1980)). Increasing burnup reduces the amount of spent fuel that must be disposed of or reprocessed. As discussed in Chapter 3, fuel burnup and resource utilization can be increased in CANDU reactors through the implementation of advanced fuel cycles. (Note that in current CANDU reactors, approximately 10% of the fuelling cost is to provide for spent fuel storage and disposal (Atomic Energy of Canada Limited, 1979a). Fuelling costs, in turn, represent approximately 13% of the total unit energy cost from a natural uranium fuelled CANDU reactor (Bartholomew et al., 1988).)

A second characteristic to be considered is the positive and relatively large coolant void reactivity effect in CANDU reactors (10-15 mk) (Pasanen, 1982) (see discussion in Section 5.2), which is deemed by many prominent reactor physicists to be an undesirable feature of any reactor design (e.g., Lamarsh, 1977; Untermyer, 1986; Thompson and Beckerley, 1964). A positive void coefficient is also in conflict with current US design criteria (discussed in Bagnal et al., 1981). Many countries have adopted similar safety design philosophies.

Finally, the nature of the primary pressure boundary within the CANDU reactor -- zirconium alloy pressure tubes connected to end fittings by rolled joints -- represents a somewhat foreign concept to many potential customers. It will be necessary to continue to document performance data and initiate appropriate standards for this type of pressure boundary to satisfy licencing requirements in nations such as the USA (Bagnal et al., 1981).

5.2 REACTIVITY, POINT KINETICS, AND NEUTRONIC TRANSIENTS

The issue of the positive void reactivity in CANDU reactors warrants further consideration.

The neutronic flux amplitude function, T(t), for a reactor undergoing a transient resulting from a step change in reactivity can be expressed by the point kinetic approximation (Henry, 1975) as:

$$T(t) = T_0(-\rho/(\beta-\rho)\exp(-(\beta-\rho)t/\Lambda) + \beta/(\beta-\rho)\exp(\lambda\rho t/(\beta-\rho))) \qquad (5.2\text{-}1)$$

where,

T_0 = the initial amplitude,

ρ = the system reactivity,

β = the delayed neutron fraction,

Λ = the prompt neutron lifetime, and

λ = the effective decay constant for the delayed neutron precursors.

Here only one delayed group is considered. The various parameters in Eq 5.2-1 are weighted averages taken over the core and over the entire energy

spectrum. The weighting function used is often the steady state adjoint flux distribution, also known as the neutronic importance function. Of particular importance to the discussion in the remainder of this thesis is the system reactivity, which is a measure of the deviation from a critical reactor state. The system reactivity can be expressed as [1-1/(k-eff)], where k-eff is the system effective multiplication factor (Henry, 1975). In this thesis, system reactivity is generally quoted in units of "milli-k" or mk, which is the nominal (dimensionless) reactivity multiplied by 1000.

For a CANDU reactor, typically (Kugler, 1975):

$$\beta \approx 0.0059$$

$$\Lambda \approx 0.001 \text{ s}$$

$$\lambda \approx 0.01 \text{ s}^{-1}$$

For an LWR (Henry, 1975):

$$\beta \approx 0.0075$$

$$\Lambda \approx 0.00006 \text{ s}$$

$$\lambda \approx 0.08 \text{ s}^{-1}$$

The curves shown in Fig. 5-1 were generated by substituting the above values into Eq 5.2-1, with step changes in system reactivity of 4 and 14 mk at time zero. (Note the logarithmic scale on the y axis of Fig. 5-1.) The curves for the 4 mk cases are approximately coincident in the figure, though as time progresses, the LWR case will increase at a faster rate than the CANDU case. However, because of the large difference in the prompt neutron lifetime between the two reactor variants, the superprompt critical transient (14 mk) in the LWR case results in the flux amplitude increasing at a much greater rate than for the CANDU reactor. (No feedback mechanisms were considered in these simulations.)

It is evident that due to the nature of the kinetics parameters, the degree of reactor run-away following a net increase in system reactivity is less in the case of a CANDU reactor than that which would result in a similar

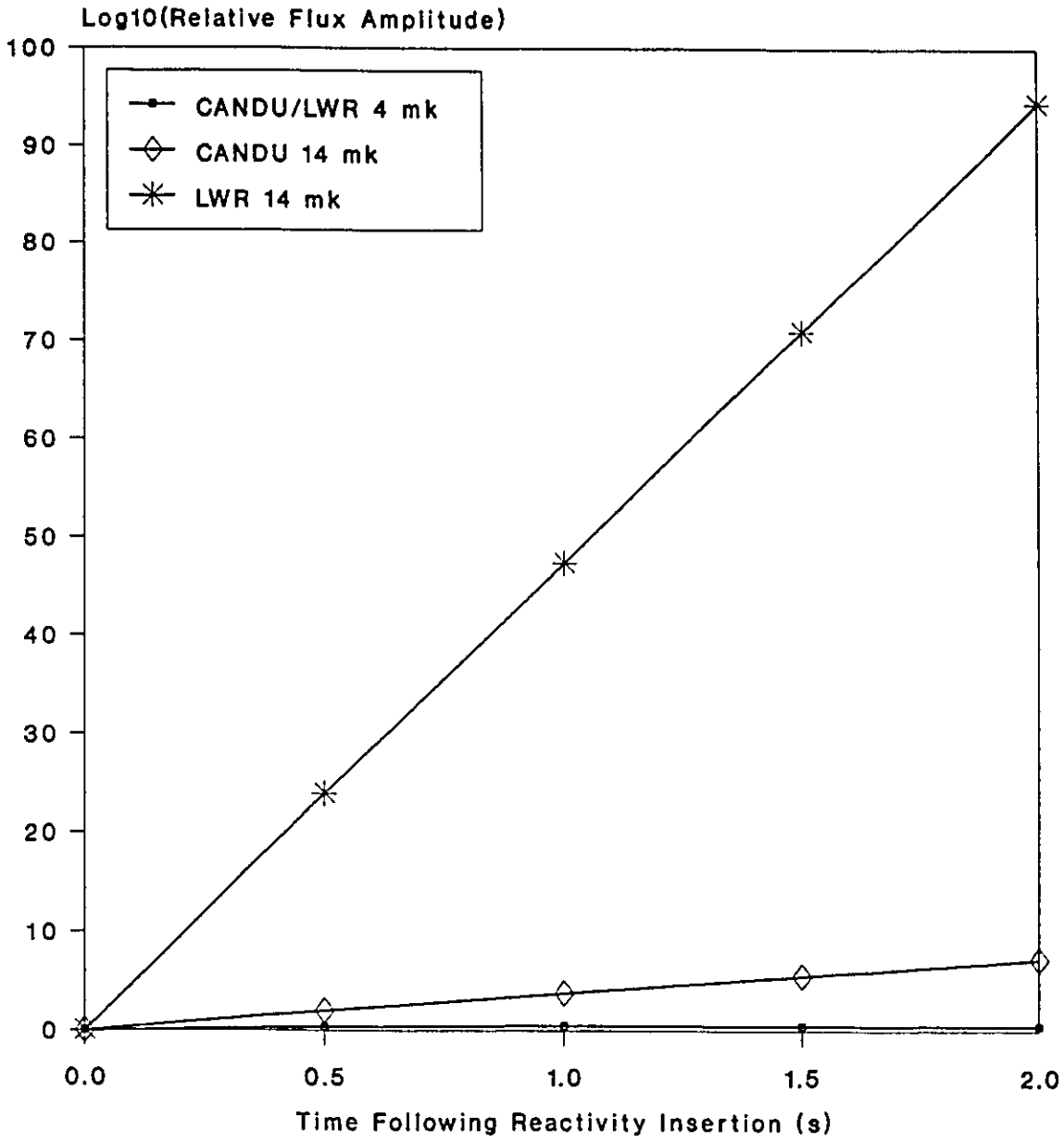

Figure 5-1 Neutron Flux Transient Following Step Reactivity Insertion

situation in an LWR. It is therefore important to emphasize that a particular intrinsic design characteristic (e.g., positive void reactivity) cannot be discussed in isolation of other, similarly intrinsic features (e.g., prompt neutron lifetime).

5.3 SYSTEM RESPONSE: REACTIVITY FEEDBACK EFFECTS

The positive coolant void reactivity in a CANDU reactor affects system behaviour following changes in reactor power and following loss-of-coolant accidents (LOCAs). As reactor power is raised, the coolant density reduction manifests itself as a positive reactivity contribution. Similarly, the reduction in system pressure following a LOCA causes the coolant to boil, and the positive void reactivity effect then results in a reactor power excursion which must be mitigated through control or shutdown system action.

Additional inherent system reactivity feedback mechanisms are also present during these events, one of the most important of which is the fuel temperature reactivity effect. The fuel temperature coefficient of reactivity is negative (approximately -0.006 mk/^{o}C (Pasanen, 1982)), and hence acts in opposition to the void reactivity effect when power is raised or a LOCA occurs. This effect must be included in determining the net system response.

5.4 POWER COEFFICIENT OF REACTIVITY

In CANDU physics, an important parameter is the power coefficient of reactivity which, to a good approximation, can be expressed as:

$$d\rho/dP \approx (\partial\rho/\partial T_F)(\partial T_F/\partial P) + (\partial\rho/\partial D_C)(\partial D_C/\partial P) + (\partial\rho/\partial T_C)(\partial T_C/\partial P) \qquad (5.4\text{-}1)$$

where:

ρ = the system reactivity,
P = the power,
T_F = the fuel temperature,
D_C = the coolant density, and
T_C = the coolant temperature.

All quantities are flux squared weighted core averaged properties. The third term in Eq 5.4-1 is positive but small, and hence the power coefficient is essentially the sum of two terms, approximately equal in magnitude but opposite in sign. In the range from 90-100% Full Power (FP), the power coefficient is small and negative (-0.02 mk/% FP) (Rouben, 1981). It becomes approximately zero at 110% FP and is positive above 120% FP (Rouben, 1981). As a consequence of the small magnitude of the power coefficient of reactivity, any reactivity perturbation introduced upon a change in reactor power will be insignificant in terms of reactor control.

5.5 ACCEPTABILITY OF A POSITIVE COOLANT VOID REACTIVITY EFFECT

In a CANDU-600, the positive coolant void reactivity is acceptable for a number of reasons:

(i) Combined with the fuel temperature reactivity effect, the power coefficient of reactivity becomes approximately zero.

(ii) The reactor is divided into two separate cooling loops, and as such, a LOCA can generally be expected to leave the cooling system in one half of the reactor intact, limiting the increase in system reactivity.

(iii) During a LOCA, the coolant voids at a slow enough rate to ensure effective shutdown system action with an acceptably small power pulse.

(iv) The long prompt neutron lifetime limits the rate of power increase following a LOCA.

(v) Two separate and independent shutdown systems are present, thereby increasing confidence in the ability of the shutdown systems to operate effectively.

In fact, a positive void coefficient can be seen as yielding several enhanced safety characteristics for a reactor system. First, it allows the crediting of neutronic shutdown system trip parameters (high neutron power, high rate of change of power) following a LOCA, rather than relying simply on process system trip parameters (low pressure, low pressurizer level, etc). The neutronic parameters are not subject to the lags inherent in the process system parameters and consequently allow the shutdown systems to act early in a transient, minimizing the negative ramifications of the accident.

A second important benefit of a positive coolant void reactivity effect is evident when considering the situation when reactor power is required to be reduced. With a positive void coefficient, the increase in coolant density accelerates the reduction in power, once initiated. With a negative coefficient, a void collapse will result in an increase in system reactivity which will oppose the desired reduction in reactor power.

From the above discussion it is clear that the coolant void reactivity effect in a CANDU reactor can be safely managed. Nevertheless, the design might be better received internationally if the coolant void reactivity were reduced somewhat. The objective should be to effect a system redesign such that the coolant void reactivity is positive (to enable the crediting of neutronic shutdown system trips on LOCAs or depressurization events) but less than the delayed neutron fraction.

5.6 FACTORS INFLUENCING COOLANT VOID REACTIVITY

Before examining measures to reduce the system void reactivity (Chapters 6 and 7) it is instructive to qualitatively examine the factors influencing the magnitude of this parameter.

In LWR pressure vessel reactors, the coolant and moderator fluids (light water) are one in the same. Hence a LOCA results in a severe reduction in the moderating capabilities of the reactor and the nuclear chain reaction can no longer be sustained. The coolant void coefficient of reactivity in these reactors is negative.

In pressure tube reactors the moderator remains intact when the coolant is lost, and consequently the void reactivity may be positive, as is the case in CANDU reactors.

Expressing the system multiplication factor (k-eff) as the product of the four-factor formula (Henry, 1975) times the non-leakage probability, yields:

$$\text{k-eff} = \varepsilon \eta f p \cdot P_{NL} \qquad (5.6\text{-}1)$$

where:

ε = the fast fission factor (ratio of the total number of fission neutrons produced by both fast and thermal fission to the number produced by thermal fission alone),
η = the number of neutrons emitted by thermal fission per thermal neutron absorbed in the fuel,
f = the thermal utilization (ratio of thermal neutron absorptions in the fuel to total thermal neutron absorptions),
p = the resonance escape probability (fraction of fission neutrons that slow down from fission to thermal energies without being absorbed), and
P_{NL} = the non-leakage probability.

Upon voiding the coolant in a CANDU reactor all of these factors change, thereby impacting on the magnitude of the void reactivity (Tin, 1981).

5.6.1 Change in the Fast Fission Factor

First consider the change in the fast fission factor. Fast neutrons are scattered to lower energies by the coolant. When the coolant is voided, the fast fission probability is enhanced and the fast fission factor is increased.

5.6.2 Change in the Eta Factor

When the coolant is voided, the thermal neutron spectrum in the vicinity of the fuel softens (neutron energies are reduced), since the rethermalization (heating up) of thermal neutrons passing from the cool moderator to the hot coolant no longer occurs. This results in the eta factor increasing for fresh fuel and decreasing for equilibrium fuel (where there is a considerable concentration of plutonium).

5.6.3 Change in the Thermal Utilization

When the coolant is voided it no longer absorbs neutrons. This causes an increase in the thermal utilization.

5.6.4 Change in the Resonance Escape Probability

When the coolant is voided there is a slight reduction in the slowing down power of the lattice cells, resulting in a small increase in the resonance absorption. This is more than compensated for by the much larger decrease in the resonance integral due to the increase in mutual self-shielding of the fuel elements when the coolant is voided. That is, in the absence of coolant, fewer fission neutrons are slowed to resonance energies in the vicinity of the fuel elements, resulting in an increase in the resonance escape probability.

5.6.5 Change in the Non-Leakage Probability

Neutronic leakage is higher in an air-cooled lattice, and hence removing the coolant will reduce the non-leakage probability. In large reactors, such as the CANDU-600, this change amounts to less than 1 mk and is of minor significance.

5.6.6 Magnitude of Individual Effects

The magnitude of the individual reactivity components will be considered more closely in Chapter 7. At this point it is noted that for equilibrium fuel conditions in the natural uranium fuelled CANDU-600, upon coolant voiding (Tin, 1981):

$$\Delta\rho = 10.1\ \text{mk} \tag{5.6.6-1}$$

$$\Delta\eta/\eta = -2.7\,E\text{-}3 \tag{5.6.6-2}$$

$$\Delta\varepsilon/\varepsilon = 5.0\,E\text{-}3 \tag{5.6.6-3}$$

$$\Delta p/p = 6.2\,E\text{-}3 \tag{5.6.6-4}$$

$$\Delta f/f = 2.4\,E\text{-}3 \tag{5.6.6-5}$$

$$\Delta P_{NL}/P_{NL} = -0.7\,E\text{-}3 \tag{5.6.6-6}$$

(Note that in this thesis, the expression "E -n" following a number is equivalent to "$x10^{-n}$".)

In this chapter, a basic conceptualization of the neutronic changes which occur when the coolant is voided has been developed. Chapters 6 and 7 delve deeper into the problem to devise a method of reducing the void reactivity to a more optimal value such that:

$$0 < \rho_v < \beta \tag{5.6.6-7}$$

where:

ρ_v = the coolant void reactivity, and

β = the delayed neutron fraction.

CHAPTER 6

REDUCTION OF COOLANT VOID REACTIVITY IN CANDU REACTORS

6.1 INTRODUCTION

In Chapter 5 it was determined that, optimally, the coolant void reactivity should be greater than zero but less than the delayed neutron fraction. In this chapter, methods of reducing the void reactivity which do not involve fuel bundle redesign are discussed. In Chapter 7, novel fuel bundle designs which yield reduced void reactivity and enhanced burnup characteristics are considered.

6.2 METHODS OF REDUCING VOID REACTIVITY

Inherent design features and innovative design modifications incorporated to reduce the void reactivity in other reactor designs may also be applicable to the CANDU case. Various schemes are examined in Sections 6.2.1 and 6.2.2. The application of similar techniques in CANDU reactor design is considered in Section 6.2.3.

6.2.1 Design Features of Fast Breeder Reactors

In liquid metal fast breeder reactors (LMFBRs), the sodium coolant void reactivity in many designs is positive.

Sodium itself does not absorb neutrons to any great extent. However, sodium slows down neutrons by inelastic scattering at high energy and by elastic scattering at the lower end of the spectrum. After a LOCA in a LMFBR, the loss of the sodium results in a reduction in this moderating effect, and the neutron spectrum becomes harder (more energetic). The number of fission

neutrons released per neutron absorbed in the fuel increases rapidly with incident neutron energy for all of the fissile nuclides at fast reactor energies (Lamarsh, 1977). Thus, as the sodium voids, system reactivity increases.

In addition to spectral modifications, the voiding of the sodium coolant also leads to an increase in neutronic leakage, which tends to reduce system reactivity (Duderstadt and Hamilton, 1976). Thus, there are two major opposing effects which are to be considered. In addition, Doppler and other feedback mechanisms also contribute to the net reactivity, though to a lesser degree (Bailey and Lu, 1977).

In homogeneous oxide LMFBRs, the void reactivity is directly proportional to the amount of sodium available for voiding (Turski et al., 1977). By increasing fuel pin size, increasing coolant velocity, derating the reactor, or increasing the coolant temperature, the void reactivity can be reduced by 10 to 20% (Turski et al., 1977). Given that a typical homogeneous cylindrical LMFBR may possess a sodium void reactivity of the order of 5$ (Bailey and Lu, 1977) (where 1$ is used to represent a reactivity level equal to the delayed neutron fraction), additional modifications are required to reduce the void reactivity to a more resonable level. (Studies have shown that the void reactivity must be reduced to <2$ to achieve acceptable core characteristics (Vitti et al., 1979). Bailey and Lu (1977) have suggested that the total of the void, Doppler, and other feedback mechanisms should be less than 1$ for acceptable transient energetics.)

One innovative method to reduce the void reactivity is to introduce a "spoiled geometry" configuration. Flattened cylindrical (pancake) shaped reactors (height to diameter ratio of 0.1) with enhanced axial leakage, or tall cylindrical reactors with enhanced radial leakage can reduce the void reactivity in LMFBRs to less than 2$, but the fuel doubling time increases from 13 to 30 years in the process (Bailey and Lu, 1977).

The introduction of heterogeneous cores can reduce the void worth to approximately 1.5$, with only a 10 - 30% increase in doubling time (Bailey and Lu, 1977). With heterogeneous LMFBRs, blanket regions can be dispersed throughout the core or arranged in "bullseye patterns" (Vitti et al., 1979).

Upon voiding, a large local leakage of neutrons occurs from the high importance fuel/driver regions to the lower importance internal blanket zones. In such reactors, the driver fuel fissile concentration must be higher than in homogeneous units since the inner blankets act as parasitic absorbers (Barthold and Beitel, 1979).

Modular LMFBRs consisting of several small decoupled reactors with blankets between them, promise even further reductions in void reactivity, ranging as low as 0.25$ (Bailey and Lu, 1977). Such reactors incur doubling time penalties of the order of 60%. Further, due to the decoupled nature of the reactors, each module requires a separate control system. The increased complexity will tend to limit the utility of such schemes in CANDU reactor design.

6.2.2 Design Features of Heavy Water Reactors

6.2.2.1 FUGEN Reactor

The Japanese have found that in the FUGEN BLW reactor, coolant void reactivity is largely improved to the negative side with the use of Pu fuel (Shiba et al., 1975). With Pu-MOX fuel in the central region and UO_2 on the periphery, a total void reactivity of approximately 2 mk results (Kato et al., 1974).

6.2.2.2 SGHWR Reactor

The SGHWR (heavy water moderated, boiling light water cooled reactor) in the UK had three main parameters which could be varied to influence reactor behaviour (Hicks et al., 1968):

(a) H_2O/UO_2 volume ratio,

(b) D_2O/UO_2 volume ratio, and

(c) enrichment level.

The objectives were mainly (Hicks et al., 1968):

(a) to achieve a design with a void coefficient of reactivity which

would be slightly negative, and

(b) to balance D_2O inventory charges against U-235 enrichment costs to give an acceptable compromise.

With 2% U-235 enriched fuel, and the following volume ratios:

$H_2O/UO_2 = 1$, and

$D_2O/UO_2 = 7$,

both criteria would be satisfied, and a fuel burnup of 20000 MWd/MgU would be achievable (Hicks et al., 1968). (Note that with a similar fuel enrichment, CANDU type reactors can achieve burnups greater than 50% higher than this.)

In the CANDU-600, by way of comparison, the coolant (D_2O) to fuel volume ratio is approximately 0.8, and the moderator to fuel volume ratio is approximately 16. The moderator to coolant volume ratio in the SGHWR is approximately 7, while in the CANDU, it is approximately 20. It is evident, therefore, that in the SGHWR, the degree of neutronic moderation is less than in the CANDU-600, and further, that the fraction of the moderation occuring in the coolant is substantially larger in the SGHWR than in the CANDU. Consequently, upon voiding the coolant, the fractional loss of moderation within a lattice cell will be greater in the SGHWR case. This effect is further enhanced by the fact that in the SGHWR, the coolant is H_2O, which has a larger slowing down cross section than D_2O. In the SGHWR approximately 30% of the moderation occurs in the coolant (Moore and Holmes, 1968). (In a CANDU-PHW lattice cell, lattice physics simulations conducted in this thesis indicate that less than 5% of the moderation occurs within the pressure tube boundaries.)

The Winfrith prototype SGHWR was designed and built before experimental confirmation of the theoretical methods was available. As a consequence, the core was equipped with additional interlattice moderator displacement tubes which enable the moderator to fuel ratio to be changed, giving some control of the void coefficient (McMillan et al., 1968). These, in fact, were later found to be unnecessary.

Note that the natural uranium fuelled commercial SGHWR design variant requires an increased lattice pitch and reduced coolant volume to provide acceptable burnup. These modifications result in the unit having a

substantially positive void coefficient (Cartwright, 1968).

6.2.2.3 ATUCHA Reactor

The Argentine ATUCHA reactor is a heavy water pressure vessel design (Markl, 1982). As such, the unit loses much of its moderating ability as the coolant voids, and a negative void coefficient of reactivity is achieved.

6.2.2.4 CIRENE Reactor

The CIRENE reactor in Italy is heavy water moderated and boiling light water cooled. It has a considerable positive coolant void coefficient of reactivity (Villani, 1968). This is due to the fact that it was originally conceived as a natural uranium fuelled reactor and hence the designers minimized the volume of light water to minimize parasitic absorption, but in so doing, also minimized the importance of the coolant to the slowing down power of the individual lattice cells.

Under certain circumstances the positive void coefficient has a stabilizing effect, in that as power increases, system pressure increases, the void fraction decreases, and power returns to its original setpoint (Villani, 1968). This stabilizing feature would not be available in the case of a major LOCA since system depressurization will occur.

Researchers at Atomic Energy of Canada (Dastur, 1988) have proposed to reduce the void reactivity in the CIRENE reactor by adding a parasitic absorber to the fuel mix. The change in the neutronic spectrum when the coolant voids would result in a substantial increase in the absorption rate in the parasitic material, thereby reducing the system void reactivity. This scheme does, however, carry with it a substantial burnup penalty.

6.2.3 Application to CANDU Reactors

The design features and innovations discussed in Sections 6.2.1 and 6.2.2 have some applicability to the CANDU reactor, as the use of an enriched

uranium fuel cycle introduces additional design flexibility.

By altering the shape of the CANDU reactor to a "spoiled geometry", as suggested for the LMFBR, the neutronic leakage effect upon coolant voiding would be enhanced. This would reduce the coolant void reactivity, though there would be a concomitant reduction in achievable fuel burnup. Burnup would also be reduced and control complications would be introduced in a modular-type CANDU reactor.

The use of plutonium mixed oxide fuel, as in the FUGEN reactor (Section 6.2.2.1) is expected to cause the void reactivity to be reduced in the CANDU reactor as well. As discussed in Chapter 3, this scheme is under consideration as an advanced CANDU fuel cycle.

The SGHWR design was not optimized to maximize burnup, but rather to achieve a small negative void reactivity. By reducing the amount of moderator in a CANDU reactor and increasing the importance of the coolant to the total cell moderation, the void reactivity can be reduced as in the SGHWR. This is examined in Section 6.3.

The use of parasitic absorbers in the fuel mix for control of void reactivity, as has been proposed for the CIRENE reactor, may also be applied to CANDU technology. However, the burnup penalty involved reduces the attractiveness of this option.

The remainder of this chapter deals with reducing the void reactivity in CANDU reactors by:

(i) increasing the fissile fuel content, and

(ii) reducing the amount of moderator D_2O per unit cell.

Two distinct lattice physics simulation methods were used in the analysis. The results are discussed in Sections 6.3 and 6.4.

6.3 ANALYSIS WITH THE POWDERPUFS-V LATTICE PHYSICS CODE

The POWDERPUFS-V (or PPV) computer code (Tin and Loken, 1979; Pasanen, 1982) is the standard lattice physics code for CANDU analysis. The code employs a simplified one dimensional annular cell model consisting of a homogenized fuel region, annulus, and moderator region. Because of the extent

to which empiricisms are used in the program, it is applicable only to heavy water moderated pressure tube type reactors.

The code provides neutronic properties as a function of fuel irradiation. (Irradiation in this case is the time integral of the fuel Westcott flux (Westcott, 1960).) With appropriate geometric buckling parameters (Henry, 1975) input to simulate leakage effects, the code can be used to estimate the effective multiplication factor and achievable fuel burnup for a given reactor variant.

Data output from the code can be "instantaneous" or "reaction rate averaged". In the former representation, cross sections, etc., provided at a given fuel irradiation, correspond to the reactor conditions at that particular point in the burnup history. In the latter representation, properties provided at a given fuel irradiation correspond to the average of the instantaneous properties from fresh fuel conditions to that irradiation level. That is:

$$\Sigma_R(r) = \int_0^r \Sigma(\omega)\, d\omega / r \qquad (6.3\text{-}1)$$

where

$\Sigma_R(r)$ = the reaction rate averaged cross section at irradiation r, and

$\Sigma(\omega)$ = the instantaneous cross section.

Fuel irradiation, ω, is quoted in terms of "neutrons per kilobarn" or n/kb. This procedure provides average system properties which are representative of a continuous bidirectionally fuelled reactor.

The code allows perturbation calculations to be performed to aid in analyzing the effect of modifying system conditions at any point in the burnup history. This option is used to calculate the effect of voiding the coolant, for example.

6.3.1 Effect of Fuel Enrichment

A series of PPV calculations were performed for the standard

CANDU-600 lattice cell with a 28.575 cm lattice pitch and 37 element fuel. The fuel enrichment was varied to study the effect of this parameter on the effective multiplication factor (k-eff) and coolant void reactivity. The salient features of the model are noted in Table 6-1.

In Fig. 6-1, the reaction rate averaged k-eff is plotted as a function of fuel irradiation for various fuel U-235 enrichments. (a/o refers to atomic percent.) The effect of increasing the U-235 concentration is to increase the reactivity of the fuel. This allows for greater fuel exit burnup.

In Fig. 6-2, the reaction rate averaged void reactivity is plotted as a function of fuel irradiation. The following observations can be made from the figure:

(i) The initial void reactivity drops substantially as the U-235 enrichment is increased.

(ii) In the natural uranium and 1.0 a/o U-235 cases, the void reactivity decreases with fuel irradiation. For the 1.3 a/o U-235 case, the void reactivity is relatively independent of the fuel irradiation.

(iii) Above 1.3 n/kb, the void reactivity in the natural uranium case is less than in the 1.3 a/o U-235 case. Given that the average fuel exit irradiation in the natural uranium case is approximately 1.8 n/kb, it is evident that, overall, the system void reactivity cannot be reduced simply by increasing the fuel enrichment.

It should be noted that, as shown in Fig. 6-3, there is not a one-to-one correspondence between fuel irradiation and burnup. As the U-235 concentration is increased, less fuel irradiation is required for a given burnup level.

The results from an additional series of reaction rate averaged PPV calculations in which the fuel enrichment in a standard 37 element fuel bundle was varied, are presented in Fig. 6-4 and 6-5. From Fig. 6-4, it can again be

Particulars	CANDU-600
Spectral Parameter *	0.0
Fuel Neutron Temperature (°C) *	225.0
Moderator Density (g/cm^3) *	0.0
Moderator Temperature (°C)	73.0
Coolant Density (g/cm^3)	0.80702
Fuel Density (g/cm^3)	10.6
Fuel Temperature (°C)	936.0
Annuli Neutron Temperature (°C) *	152.0
Moderator Neutron Temperature (°C) *	78.0
Sheath Absorption Factor	0.0
Rubber Band Perimeter (cm)	30.88967
Total Fuel Perimeter (cm)	141.27679
Coolant Thickness (cm)	0.4159343
Number of Annuli	4.0
Moderator Purity (atom %)	99.722
Sheath Material Code (Zircaloy-2)	40.0
Void Volume (cm^3/cm)	0.769273
Fuel Volume (cm^3/cm)	40.19070
Sheath Volume (cm^3/cm)	7.01865
Coolant Volume in Homogenized Zone (cm^3/cm)	27.80238
Radius of Homogenized Zone (cm)	4.94353
Outside Radius of First Annulus (cm)	5.1689
Outside Radius of Second Annulus (cm)	5.6032
Outside Radius of Third Annulus (cm)	6.4478
Outside Radius of Fourth Annulus (cm)	6.5875
Coolant Temperature (°C)	290.0
Total Coolant Volume (cm^3/cm)	34.96871
Flux Ratio C/F	1.059
Lattice Pitch (cm)	28.575
Coolant Material Code (D_2O)	0.0
Material Code of First Annulus (as above)	20.0
Material Code of Second Annulus (Zr-Nb)	70.0
Material Code of Third Annulus (Air)	0.0
Material Code of Fourth Annulus (Zircaloy-2)	50.0
Material Code of Fifth Annulus (D_2O)	0.0
Initial Flux Estimate ($n/cm^2/sec$) *	0.9E+14
U-238 Resonance Capture Fraction *	0.0

* Values for these parameters will be determined by the code. Values input are either flags or initial estimates.

Table 6-1a POWDERPUFS-V Input Data for CANDU-600 37 Element Fuel

Particulars	CANDU-600
Fast Neutron Yield Cross-Section (cm^2/g-fuel)	0.024
Fast Neutron Non-Escape Probability	0.0
Fuel Material Code (UO_2)	0.0
Fuel Heat Rating (kW/cm)	16.757
Power to Coolant Fraction	0.94332
Initial Exposure for a Perturbed Run (n/kb)	0.0
Neutron Temperature Convergence Criterion	0.001
Bundle Length (cm)	49.53
Pu-240 Self Shielding Factor *	0.0
Moderator Poison Concentration (mg/kg natural boron to heavy water by weight)	0.5
Nuclei per Mass of Fuel (g^{-1})	2.2303E+21
Exposure Increment (n/kb)	0.1
D_2O Coolant Purity (atom %)	99.722
DEEMS Convergence Criterion	0.01
Westcott Spectral Parameter Convergence Criterion	0.001
Maximum Exposure (n/kb)	2.9
Lattice Arrangement Indicator	0.0
Geometric Buckling (cm^{-2})	0.00007618
Xenon Absorption Cross Section (barns/atom) *	0.0
Pu-240 Convergence Criterion	0.001
Ratio of Flux Squared Weighted Mean Flux to Maximum Flux	0.764
Initial Th-232 Concentration	0.0
Initial U-233 Concentration	0.0
Initial U-234 Concentration	0.0
Initial U-235 Concentration	0.7204
Initial U-236 Concentration	0.0
Initial U-238 Concentration	99.2796
Initial Pu-239 Concentration	0.0
Initial Pu-240 Concentration	0.0
Initial Pu-241 Concentration	0.0
Initial Pu-242 Concentration	0.0
Isotopic Density Indicator (Reaction-Rate-Averaged)	1.0
Fuel Rods per Bundle	37.0
Perturbation Control (Normal)	0.0
Pu-239 Production Control	0.0
Saturating Fission Product Control (Include)	0.0
Printout Control	5.0
Central Radial Buckling for TUMULT (cm^{-2})	0.0
EXTERMINATOR Calculation Control	0.0
PERIGEE Calculation Control	0.0
Burn-Up Control (10 Equation Set)	2.0
Neutron Temperature Control	0.0
Extrapolated Reactor Length for TUMULT (cm)	0.0
Core Radius for TUMULT (cm)	314.27
Reactor Radius for TUMULT (cm)	379.73
Radial Form Factor for TUMULT	0.823
Total Fission Power for TUMULT (MW)	2173.0

* Values for these parameters will be determined by the code. Values input are either flags or initial estimates.

Note: TUMULT calculation is not part of the basic PPV lattice simulation.

Table 6-1b POWDERPUFS-V Input Data for CANDU-600 37 Element Fuel (Continued)

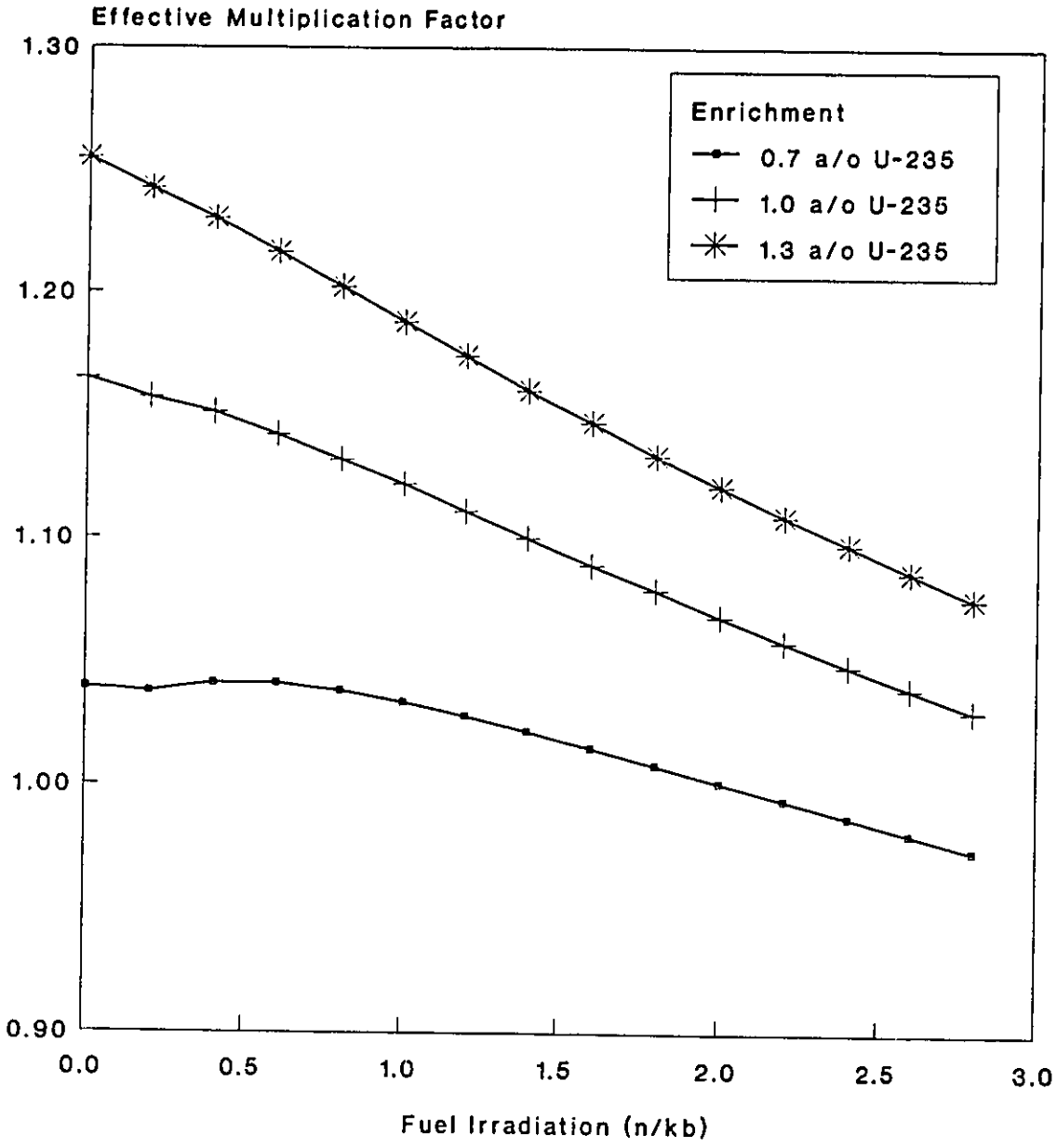

Figure 6-1 Effect of Variation of Fuel U-235 Enrichment on Effective Multiplication Factor
(37 Element Nominal Geometry PPV Results)

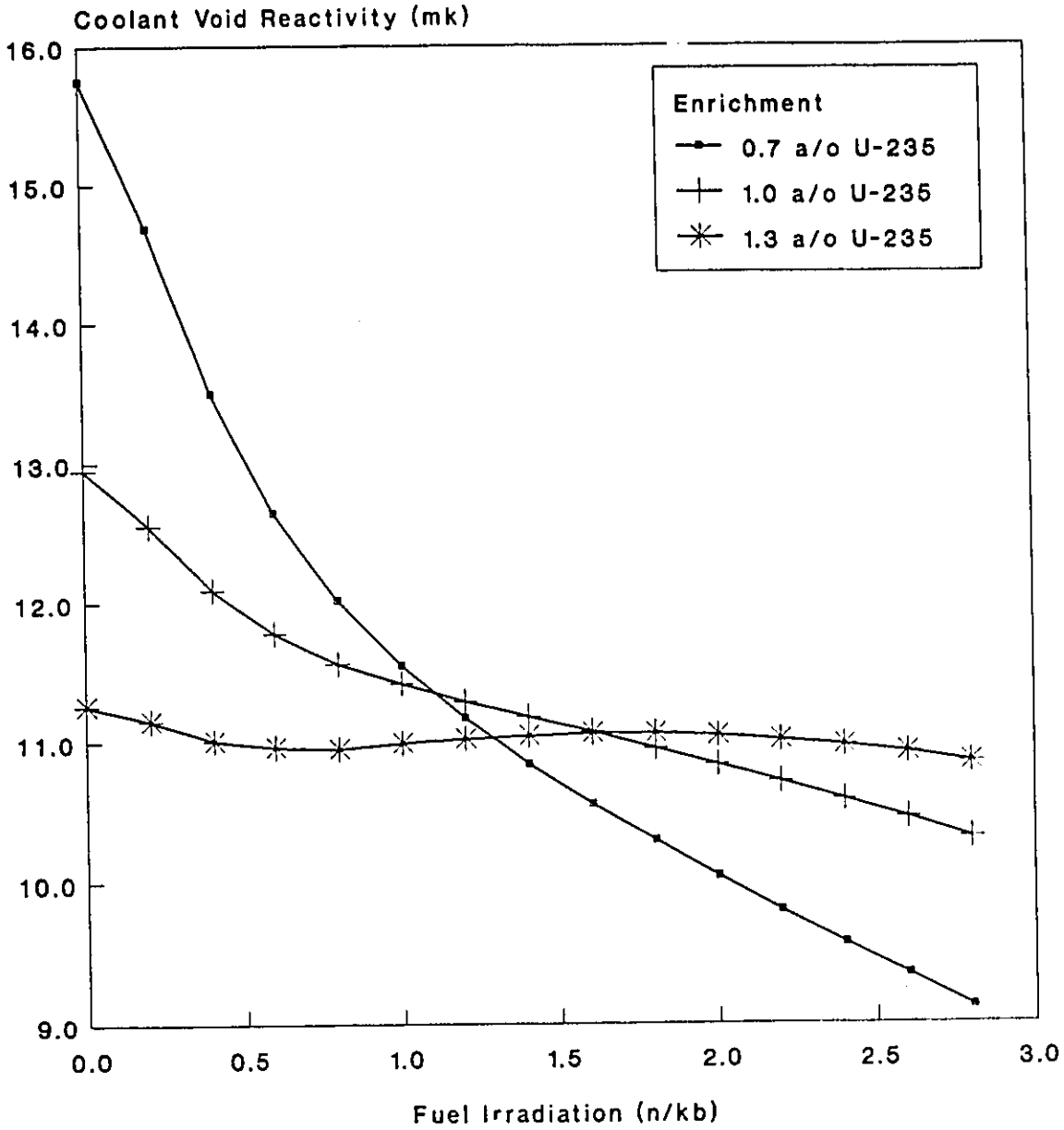

Figure 6-2 Effect of Variation of Fuel U-235 Enrichment on Void Reactivity (37 Element Nominal Geometry PPV Results)

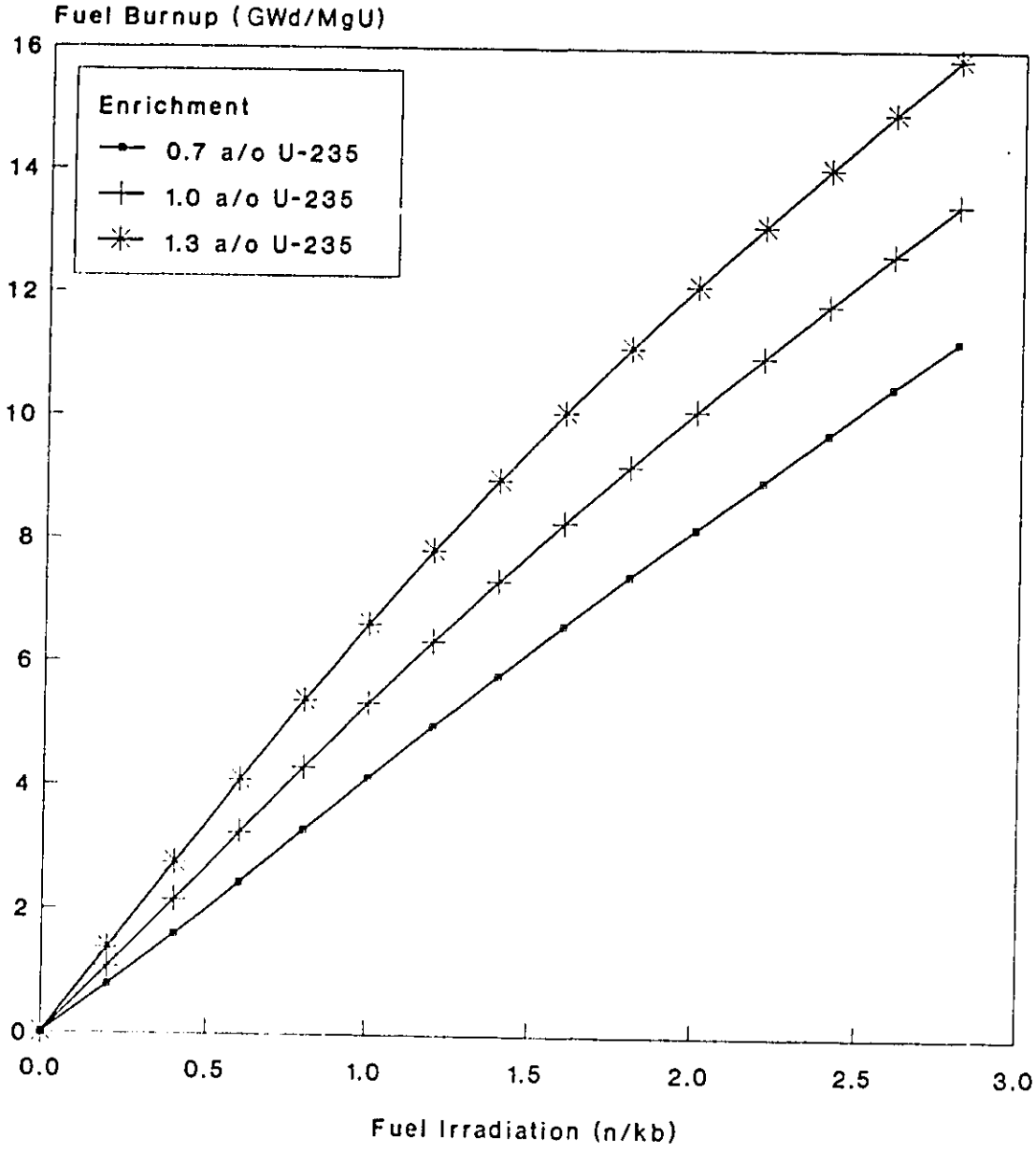

Figure 6-3 Effect of Variation of Fuel U-235 Enrichment
(Burnup vs Irradiation)
(37 Element Nominal Geometry PPV Results)

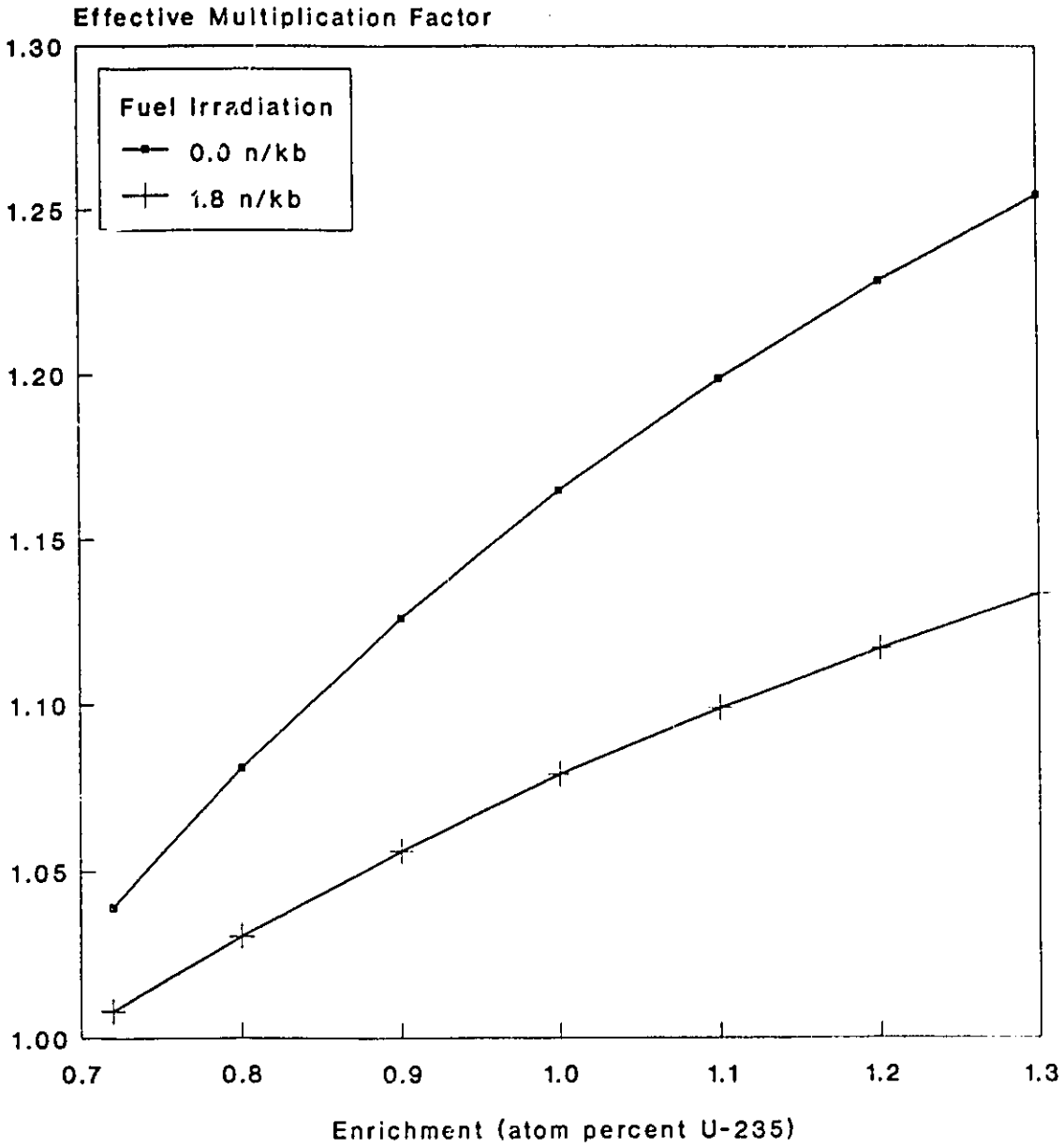

Figure 6-4 Effect of Fuel Irradiation on k-Effective
(37 Element Nominal Geometry PPV Results)

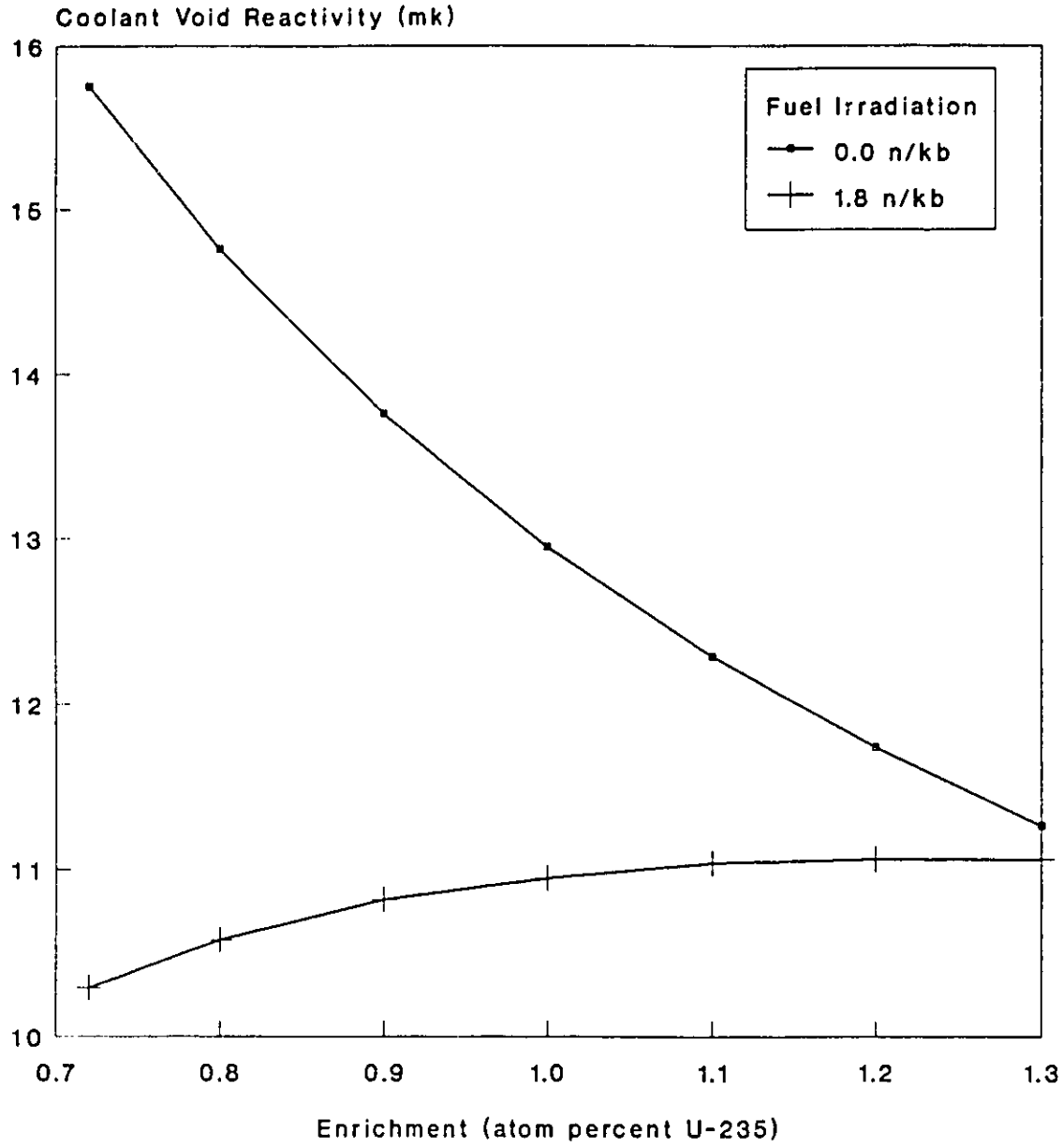

Figure 6-5 Effect of Irradiation on Void Reactivity
(37 Element Nominal Geometry PPV Results)

seen that for a given fuel irradiation, the value of k-eff increases as the fuel enrichment increases. The slope of the 1.8 n/kb curve in Fig. 6-4 is not as steep as the 0.0 n/kb case. Hence as irradiation is increased, k-eff becomes less dependent on the initial fuel enrichment.

In Fig. 6-5, note that as the fuel enrichment increases, the void reactivity at zero irradiation decreases. At an irradiation level of 1.8 n/kb, the void reactivity increases as fuel enrichment increases. The vertical distance between the two curves in Fig. 6-5 represents the change in void reactivity between 0 and 1.8 n/kb for a given fuel enrichment. Hence, as the fuel enrichment is increased, the void reactivity becomes less irradiation dependent. These characteristics were also noted in Fig. 6-2.

As the initial U-235 concentration is increased, the thermal absorption in the fuel region is increased. The relative change in the thermal utilization upon voiding is therefore reduced. This hardening of the spectrum in the fuel region also reduces the relative change in the eta factor when the coolant is voided, hence resulting in a reduced void reactivity.

At higher fuel burnups with enriched fuel, the importance of plutonium to the total fission source is reduced in comparison with the natural uranium case. This effect, coupled with the increased spectral hardening in the fuel region (reduced relative change in the eta factor), results in the void reactivity being less irradiation dependent with enriched uranium fuel. (See also the discussion in Section 7.3.1.) Adjustment of the fuel enrichment is therefore not effective in substantially reducing the coolant void reactivity over the entire burnup period. Section 6.3.2 examines the efficacy of reducing the moderator to fuel volume ratio to effect a reduction in void reactivity.

6.3.2 Effect of Adjusting Moderator Volume per Lattice Cell

In Section 6.2 it was identified that an effective method of reducing the system void reactivity was to harden the neutronic spectrum and increase the importance of the coolant to the total moderation in the lattice cell. In CANDU reactors this can be accomplished by decreasing the amount of moderator

fluid in the lattice cells. Several approaches could be adopted to effect this:

(a) The lattice pitch could be reduced,

(b) The calandria tube diameter could be increased,

(c) Moderator displacement rods (vertical or horizontal) could be introduced,

(d) Gases could be bubbled through the calandria, displacing the moderator to some extent and thereby effectively reducing the moderator density.

When the lattice pitch is reduced, it becomes increasingly difficult for reactivity devices to be placed at interstitial sites. In addition, fuelling machine clearances are reduced, and the end-shield structure is weakened.

Increasing the calandria tube diameter increases the amount of zirconium required in a lattice cell (circumference is increased and thickness is increased for maintenance of material strength). Also, during a serious process system failure, pressure tubes "slumping" against calandria tubes is a credited mechanism for transferring energy to the moderator system, which acts as a heat sink. With larger diameter calandria tubes, the pressure tubes would have to deform to a greater extent before effective heat transfer would occur. This could increase the probability of fuel failures during major reactor accidents. (The use of a non-concentric pressure tube / calandria tube arrangement would reduce this effect.)

The use of moderator displacement tubes (as in the SGHWR), would increase the complexity of the arrangement of the already densely packed devices on the reactivity mechanisms deck. If these tubes are removed from the core, they could increase system reactivity and lead to a reactor power excursion. If they are constructed as sealed hollow tubes, they could leak and thereby reduce their effectiveness in displacing the moderator. They will also contribute to increased parasitic absorption in the core.

Bubbling gases through the moderator has been proposed as a means of controlling the lattice moderating power in advanced CIRENE-type reactors

(Villani, 1968). This control mechanism affords considerable flexibility to fine tune the moderator density since the optimal value will vary with economics, enrichment level, etc. It also does not involve the introduction of additional parasitic materials to the cell, nor does it decrease the strength of the end-shield structure. However, should the bubbling system fail, a large increase in system reactivity could result. Therefore it would be prudent to install a passive shutdown system initiating mechanism which would automatically shut down the reactor in the event of a system failure.

These latter three options are considered in more detail in the next three sections (Sections 6.3.2.1 through 6.3.2.3).

6.3.2.1 Moderator Bubbler System

The moderator bubbler system was investigated using the PPV code, with the same 37 element fuel model as described in Section 6.3.1.

The effect of varying the bubbling rate was simulated by adjusting the moderator density. Calculations were performed with fuel enrichments of 0.7204 a/o U-235 (natural uranium) to 1.3 a/o U-235. Moderator density was varied from 0.1 g/cm^3 to 1.082 g/cm^3 (nominal value) in each case.

Results of the analysis are presented in Fig. 6-6 through 6-9. Figures 6-6 and 6-8 correspond to fresh fuel conditions. Figures 6-7 and 6-9 correspond to reaction-rate averaged properties up to 1.8 n/kb.

It is clear from these figures that while reducing moderator density will reduce the coolant void reactivity, the corresponding reduction in k-eff indicates that a substantial reduction in achievable fuel burnup will also result. For example, with the fuel enriched to 1.3 a/o U-235, and the effective moderator density reduced to 0.51 g/cm^3 (to yield a void reactivity coefficient very close to zero), a fuel burnup of less than 10000 MWd/MgU would be achievable. This is less than one half of the burnup expected in a CANDU reactor with 1.3 a/o U-235 fuel and the normal moderator density of 1.082 g/cm^3.

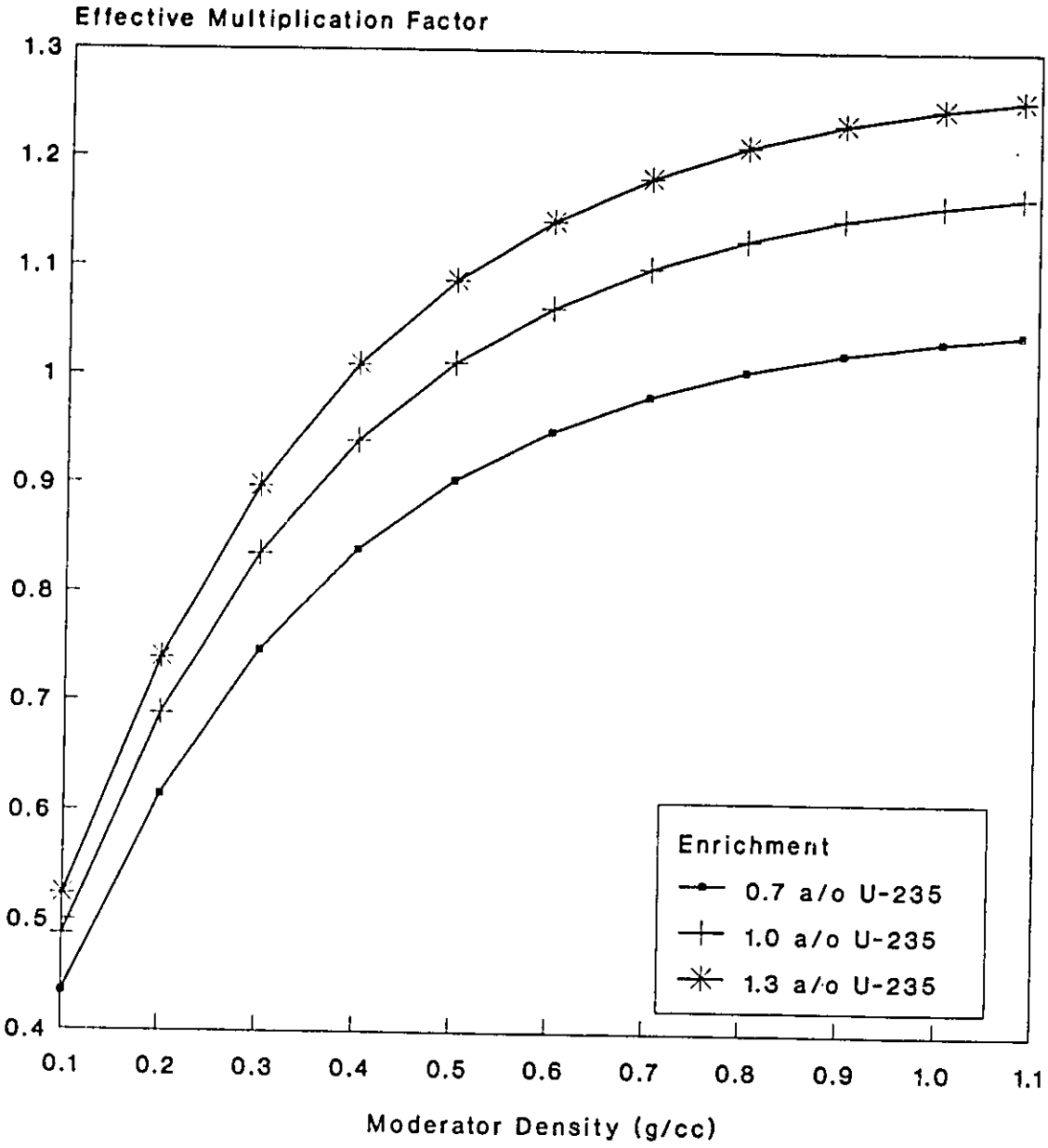

Figure 6-6 Effect of Moderator Density on k-Effective for Various Fuel Enrichments
(ω=0.0 neutrons/kilobarn)
(37 Element Nominal Geometry PPV Results)

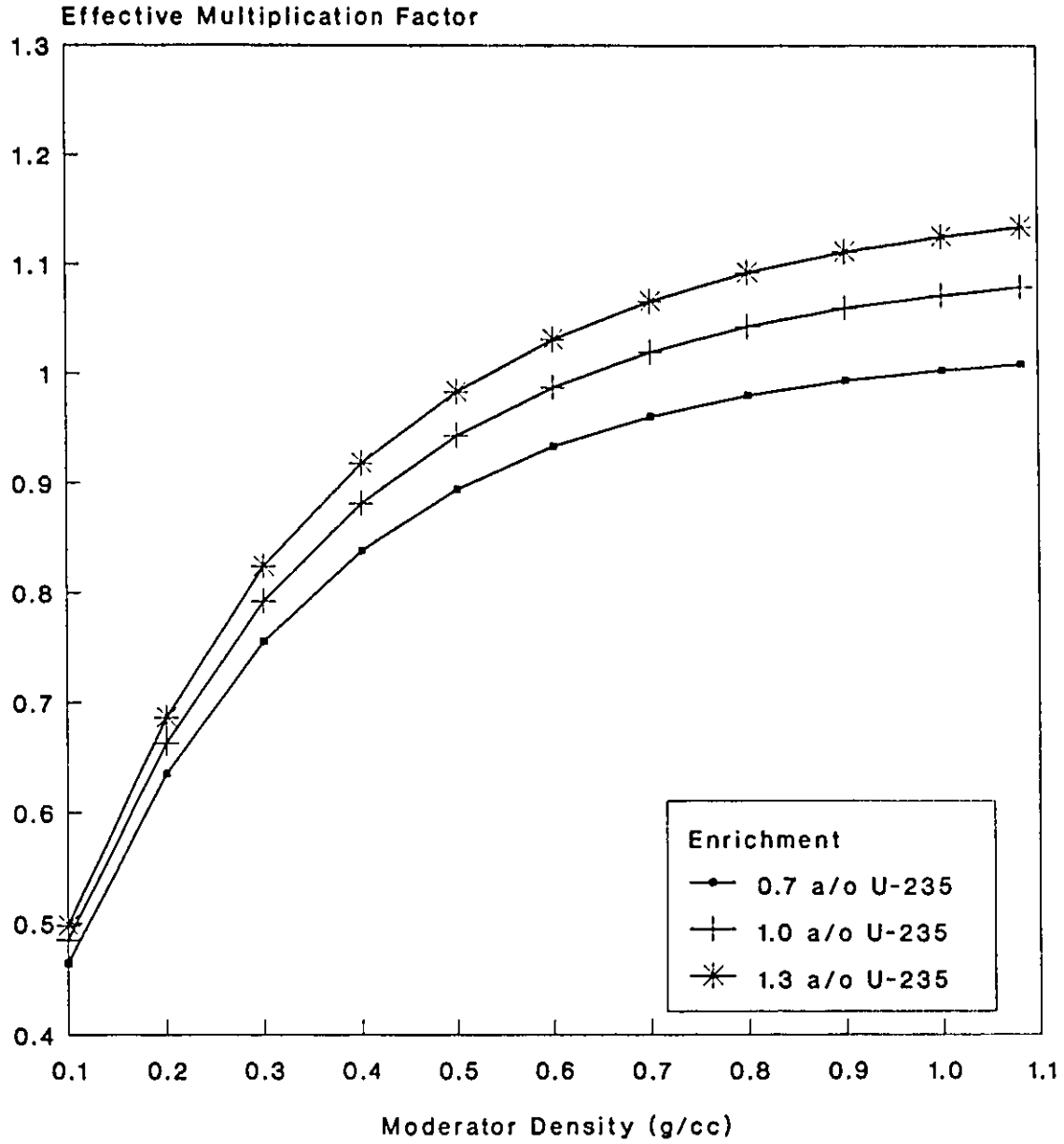

Figure 6-7 Effect of Moderator Density on k-Effective for Various Fuel Enrichments
(ω=1.8 neutrons/kilobarn)
(37 Element Nominal Geometry PPV Results)

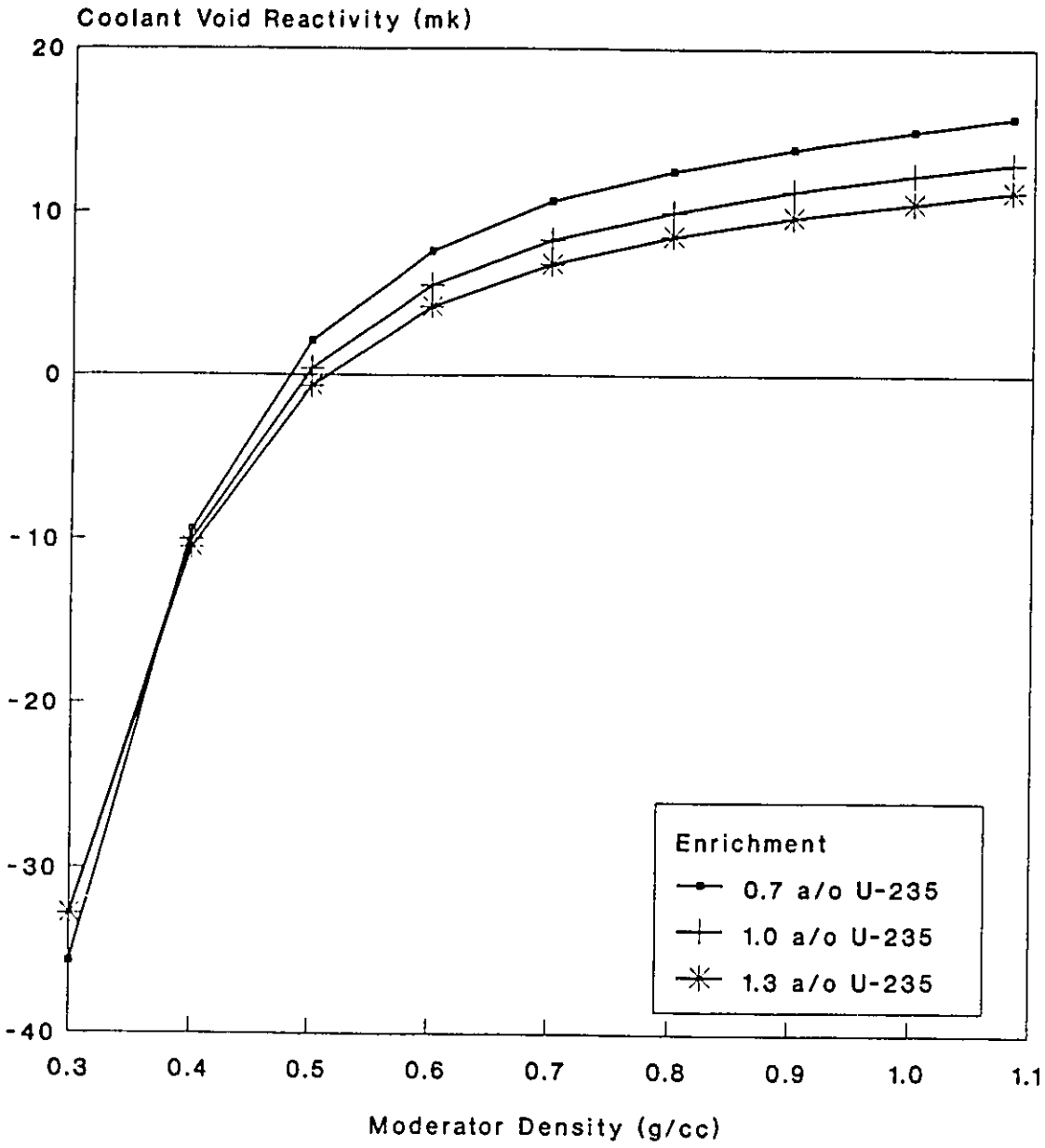

Figure 6-8 Effect of Moderator Density on Void Reactivity for Various Fuel Enrichments
(ω=0.0 neutrons/kilobarn)
(37 Element Nominal Geometry PPV Results)

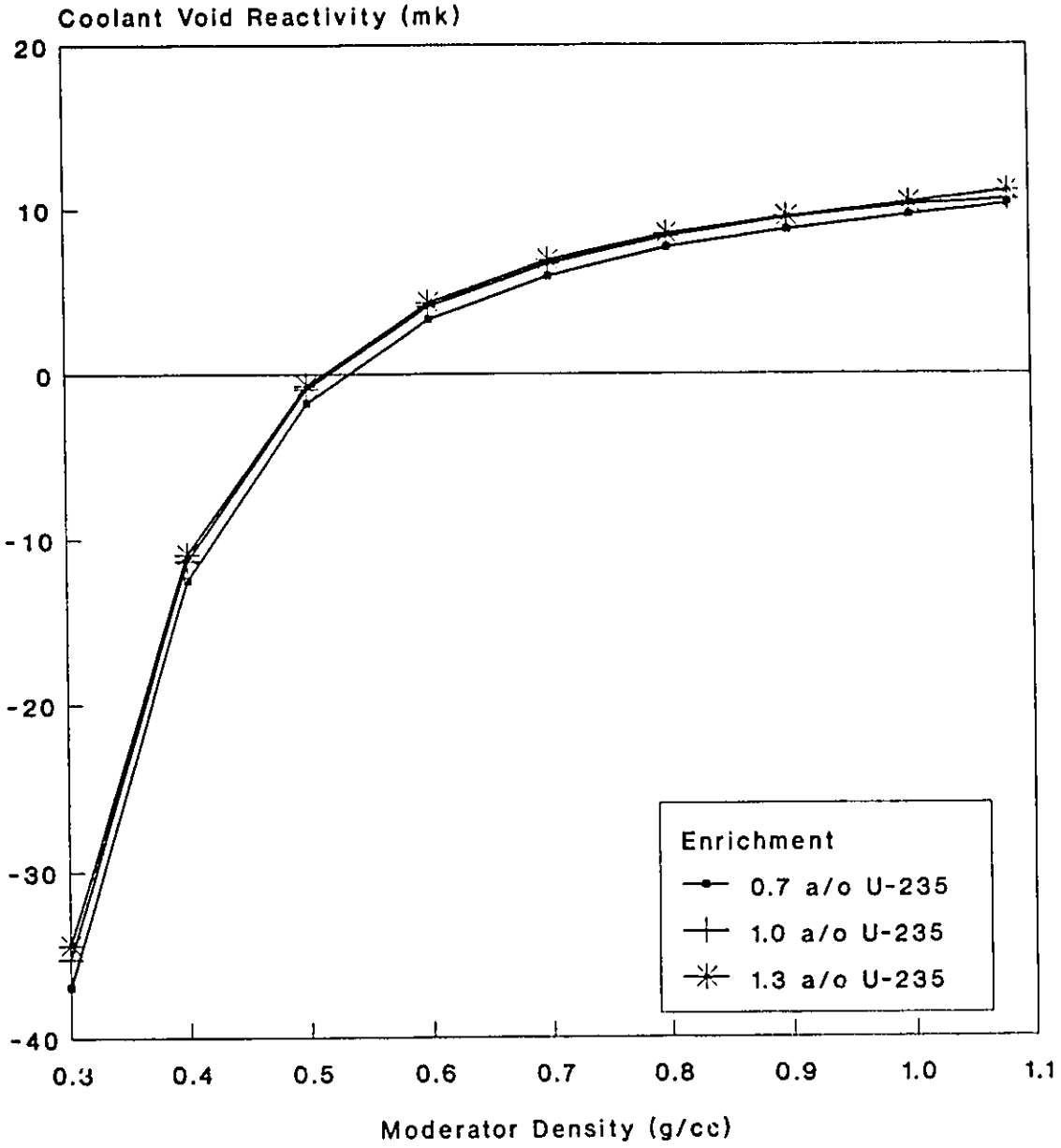

Figure 6-9 Effect of Moderator Density on Void Reactivity for Various Fuel Enrichments
(ω=1.8 neutrons/kilobarn)
(37 Element Nominal Geometry PPV Results)

6.3.2.2 Increasing the Calandria Tube Diameter

A series of PPV simulations were conducted to investigate the effect of reducing the moderator volume per lattice cell, by increasing the calandria tube diameter. A calandria tube outer radius of 12.5 cm was found to be sufficient to yield a void reactivity of zero. In comparison with the nominal calandria tube outer radius of 6.5875 cm, the altered calandria tube radius corresponded to an effective moderator density of 0.52 g/cm^3, very similar to the effective density required with the moderator bubbler system. The burnup was also reduced to less than 10000 MWd/MgU. The calandria tube mass was increased by a factor of 1.9 (assuming that the tube thickness was not altered).

6.3.2.3 Moderator Displacement Tubes

If the option of moderator displacement tubes were to be chosen, 52% of the moderator volume per lattice cell would have to be displaced to effect a void reactivity coefficient of zero. This would require approximately five 5 inch (outside diameter) tubes (standard CANDU-600 shutoff rod guide tube diameter) to be placed vertically within each lattice cell. In other words, approximately 1280 vertically mounted tubes would be required, each one running the entire vertical length of the reactor. This option appears particularly impractical.

6.4 ANALYSIS WITH THE WIMS-CRNL LATTICE PHYSICS CODE

Lattice cell calculations were also conducted with a more sophisticated program known as WIMS-CRNL (Donnelly, 1986).

6.4.1 Program Description

The WIMS-CRNL computer program is a multigroup two dimensional neutron transport code which can be applied to investigate a wide range of

lattice designs. Discrete ordinates (DSN) and collision probability (PIJ) calculational methodologies are available as solution options within the program (Askew et al., 1966). A more detailed description of the WIMS-CRNL code and structure is provided in Appendix F of this thesis.

6.4.2 WIMS-CRNL 37-Element Fuel Model

The 18 group WIMS-CRNL energy structure adopted is shown in Table 6-2. The standard CANDU-600 37 element fuel properties from which the WIMS-CRNL model was derived are provided in Table 6-3.

In these initial studies, the WIMS-CRNL discrete ordinates (DSN) calculational methodology was utilized (See Appendix F.2). Material properties are given in Table 6-4.

The effective cell radius in the model was 16.12171 cm. This provides a cell volume equal to that of a square lattice pitch, with each side 28.575 cm in length.

Annuli chosen in the model were calculated using the TESHOM code (Griffiths, 1978), with the recommended "AREA" annularization. With this option, the fuel elements in a given ring of a fuel cluster are homogenized such that there is an equal area of homogenized annulus on each side of the pitch circle. Further, the annulus volume per fuel pin is constant in all homogenized fuel annuli. In the model, the first annulus is chosen to be one-half of the distance between the first and second rings of fuel elements. This then defines the annulus volume per fuel pin to be used in each of the homogenized fuel annuli.

The standard geometric buckling of 0.7618 m^{-2} used in the PPV calculations (Section 6.3) was divided equally into axial and radial components for the leakage calculations.

The fuel bundle end cap regions were not modelled in this initial analysis. As a consequence the effective fuel density was reduced from the nominal density of 10.6 g/cm^3 to (nominal density) x (pellet stack length) / (bundle length) = 10.28 g/cm^3.

In the calandria tube, pressure tube, and fuel sheath, impurities were

Condensed Energy Structure Group Number	69 Group Energy Structure Group Numbers	High Energy Limit (eV)	Low Energy Limit (eV)
1	1 - 2	10.0E6	3.679E6
2	3 - 5	3.679E6	1.353E6
3	6 - 10	1.353E6	0.111E6
4	11 - 15	0.111E6	5530.0
5	16 - 23	5530.0	48.052
6	24 - 24	48.052	27.700
7	25 - 26	27.700	9.877
8	27 - 27	9.877	4.000
9	28 - 36	4.000	1.071
10	37 - 39	1.071	0.780
11	40 - 45	0.780	0.625
12	46 - 48	0.625	0.350
13	49 - 53	0.350	0.220
14	54 - 56	0.220	0.100
15	57 - 60	0.100	0.050
16	61 - 63	0.050	0.030
17	64 - 66	0.030	0.015
18	67 - 69	0.015	0.000

Note: In a two group condensation, thermal energies are generally taken to be all those less than 0.625 eV.

WIMS-CRNL standard 69 group energy structure
condensed to 18 groups for transport calculations.

Table 6-2 Condensation of Energy Groups for WIMS-CRNL Simulations

Lattice Cell / Fuel Bundle Property	Value
Lattice Pitch (cm)	28.575
Bundle Length (cm)	49.53
Number of Fuel Elements per Bundle	37.0
Pressure Tube (Zr-2.5% Nb) Inside Radius (cm)	5.1689
Pressure Tube Wall Thickness (cm)	0.4343
Calandria Tube (Zr-2) Inside Radius (cm)	6.4478
Calandria Tube Wall Thickness (cm)	0.1397
Coolant Temperature (average over channel) (°C)	290.0
Coolant D_2O Purity * (atomic percent)	98.8
Moderator Temperature (°C)	68.0
Moderator D_2O Purity * (atomic percent)	99.9
Fuel Element (sheath) Outside Radius (cm)	0.65405
Sheath (Zr-4) Wall Thickness (cm)	0.0419
UO_2 Pellet Outside Radius (cm)	0.6077
UO_2 Density (g/cm^3)	10.6
UO_2 Weight per Bundle (kg)	21.326
U Weight per Bundle (kg)	18.80
Stack Length of Pellets in Fuel Bundle (cm)	48.03
Radius of First Element Ring Containing 1 Fuel Element (cm)	0.0
Radius of Second Element Ring Containing 6 Fuel Element (cm)	1.48845
Radius of Third Element Ring Containing 12 Fuel Element (cm)	2.8753
Radius of Fourth Element Ring Containing 18 Fuel Element (cm)	4.3307
Angular Displacement of First Element Ring (radians)	0.0
Angular Displacement of Second Element Ring (radians)	0.0
Angular Displacement of Third Element Ring (radians)	0.2618
Angular Displacement of Fourth Element Ring (radians)	0.0

Note: Data from (Tin, 1981), except where indicated by asterisks.
* Values expected in practice.

Table 6-3 CANDU-600 37 Element Fuel Lattice Properties

Material	Temperature (K)	Density (g/cm^3)	Spectral Type	Constituent Material	Weight Percent*
Coolant	563.16	0.8034	Coolant	Deuterium	19.9004
				Hydrogen	0.1209
				Oxygen	79.9787
Moderator	341.16	1.0858	Moderator	Deuterium	20.0996
				Hydrogen	0.0101
				Oxygen	
Pressure Tube (Zr-Nb)	563.16	6.55	Moderator	Zirconium	97.5
				Boron	0.0003
				Niobium	2.5
Calandria Tube (Zr-2)	341.16	6.55	Moderator	Zirconium	99.71
				Iron	0.14
				Nickel	0.05
				Chromium	0.10
				Boron	0.0003
Gas Gap	341.16	0.0014	Moderator	Oxygen	100.0
Fuel	960.16	10.28	Fuel	U-235	0.6271
				U-238	87.5227
				Oxygen	11.8501
Sheath/Fuel Gap	563.16	0.0014	Sheath	Oxygen	100.0
Sheath (Zr-4)	563.16	6.55	Sheath	Zirconium	99.6897
				Iron	0.2100
				Chromium	0.1000
				Boron	0.0003

* Normalized internally to 100%.

Table 6-4 Material Properties for Initial WIMS-CRNL CANDU-600 37 Element Fuel Model

treated as 0.0003 weight percent (w/o) natural boron. The Zircaloy-2 calandria tube and Zircaloy-4 fuel sheaths contain 1.45 w/o tin. This material was not included in the WIMS-CRNL materials library and was therefore treated as zirconium.

A power density of 52.482 MW/MgU (initial) was chosen for the burnup calculations. (The significance of this value is explained in Section 7.5.1.1.) Main transport calculations were conducted after the burn times shown in Fig. 6-10.

6.4.3 Simulation Results

6.4.3.1 Effect of Fuel Enrichment

Figure 6-11 provides a graphical representation of the temporal variation in k-eff for fuel enrichments of 0.72 a/o (natural), 1.0 a/o, and 1.3 a/o U-235. The initial sudden drop in k-eff for all enrichments is due to the buildup of saturating fission products. Note that the curves here provide instantaneous results as opposed to the reaction rate averaged data given in the PPV study (Section 6.3).

The effect of increasing fuel enrichment is to increase the value of k-eff and hence increase the allowable burnup. If it is assumed that the reactor would be carrying a -15 mk adjuster rod load and a -3 mk liquid zone controller load (which are not considered in the lattice cell calculations), then the reactor burnup achievable would be approximately at the point where the burnup averaged k-eff is equal to 1.018 (i.e. 1.000 + 0.015 + 0.003). For the three cases shown in Fig. 6-11, this occurs at:

6230 MWd/MgU for 0.72 a/o U-235 (natural uranium)
15325 MWd/MgU for 1.00 a/o U-235
22405 MWd/MgU for 1.30 a/o U-235

These averages were calculated using the WIMS-CRNL code.

From Fig. 6-12, it can be seen that as the uranium enrichment is

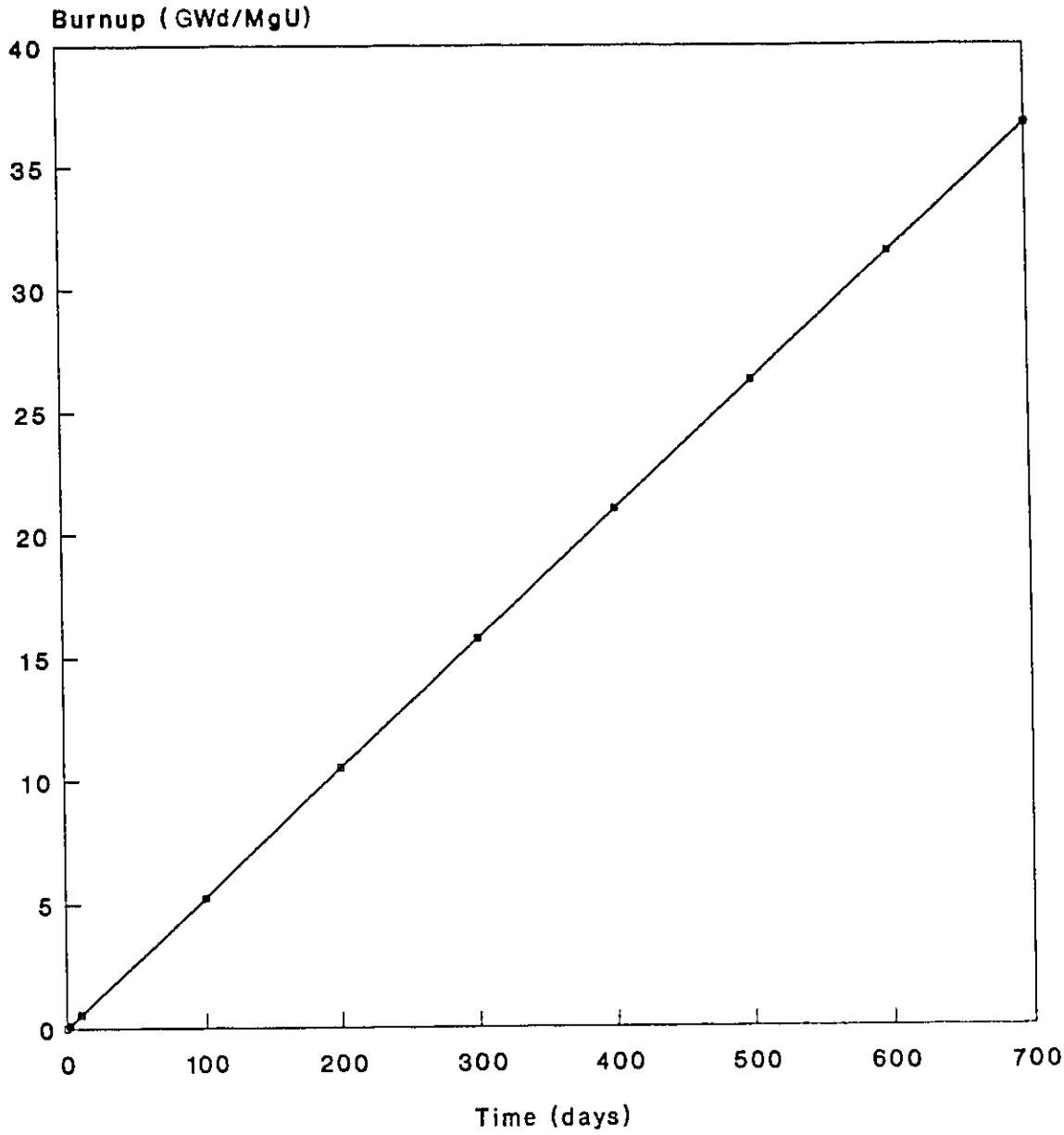

Figure 6-10 Burnup Steps Used in WIMS-CRNL Calculations

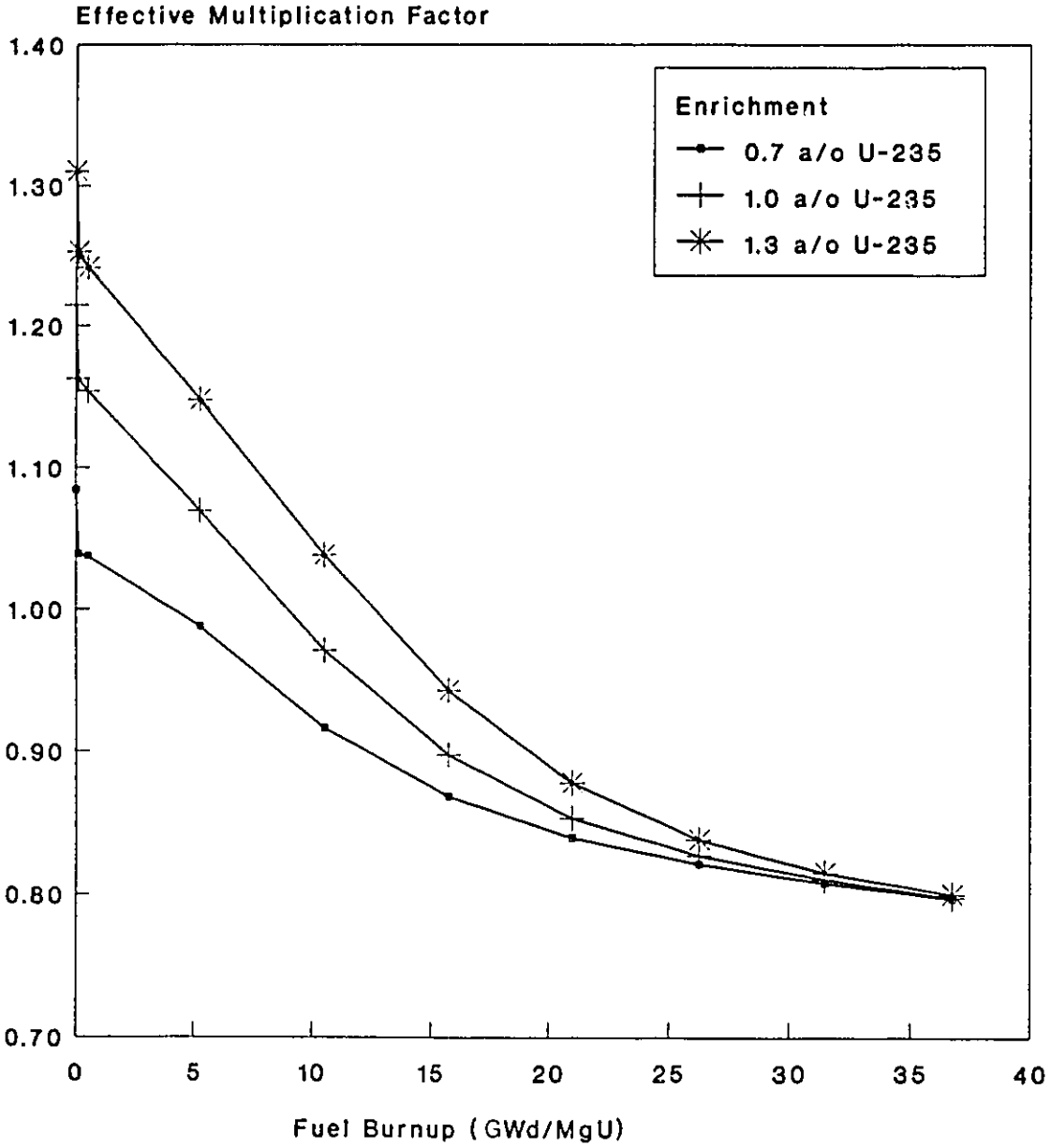

Figure 6-11 Effect of Variation of U-235 Enrichment on Effective Multiplication Factor
(37 Element, Nominal Geometry)

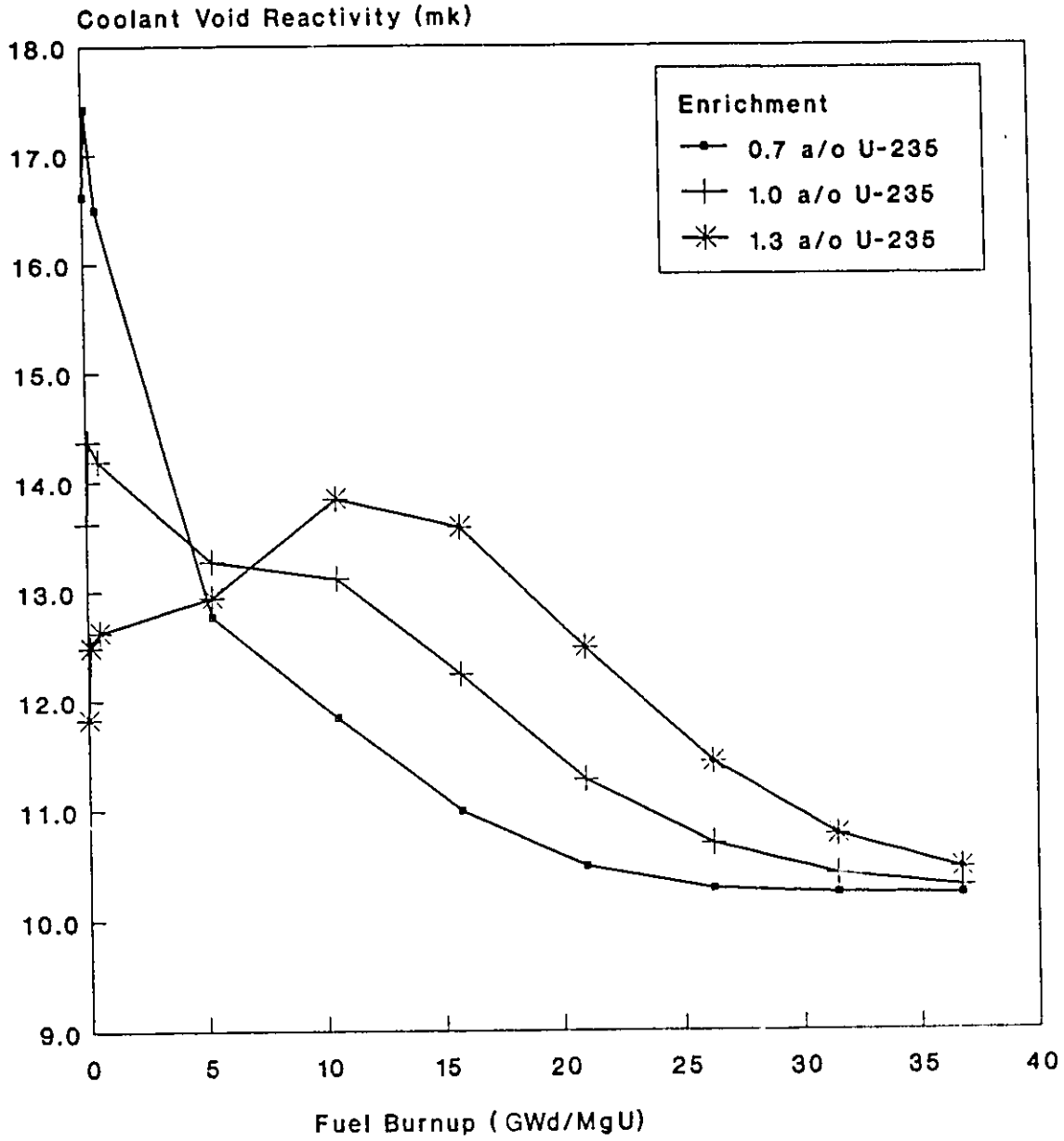

Figure 6-12 Effect of Variation of U-235 Enrichment on Coolant Void Reactivity
(37 Element, Nominal Geometry)

increased, the initial value of the void reactivity decreases. However, as burnup is increased, the fuel with the higher initial enrichment has a larger void reactivity. Overall, the trends are similar to those noted in the analysis conducted using the PPV code.

When interpreting the data, it is important to note the burnup limits listed above. For example, in Fig. 6-12 for the case of natural uranium, data points beyond 7000 MWd/MgU are not relevant, since the reactor cannot be made critical with a significant quantity of fuel having burnups greater than this.

Overall, the WIMS-CRNL code yields higher void reactivities and lower achievable burnups than the PPV data indicate. As noted earlier in this chapter, the methods of solution in the two codes are completely different. In CANDU safety analysis, the void reactivity calculated using PPV is usually increased by 1.5 mk to account for possible uncertainties (Dastur, 1984).

The underestimate of burnup using WIMS-CRNL can be attributed to the more general nature of the WIMS-CRNL code and its nuclear library. Phenomena such as the production of photo-neutrons are not treated by WIMS-CRNL, while they are implicit in the PPV data structure. It is noted that an updated nuclear library has been incorporated into a proprietary version of WIMS-CRNL. Reports indicate that the calculation of achievable burnup with the modified library yields results closer to those obtained using the PPV code (Donnelly, 1984). In any case, in this analysis, changes in neutronic properties are of a greater interest than absolute quantities. Further experimental analyses and subsequent fine tuning of the nuclear library data will be required to ensure the validity of the lattice cell simulations prior to implementation of any of the advanced fuel cycles.

6.4.3.2 Effect of Lattice Pitch Reduction

As noted in Section 6.2, the coolant void reactivity can be reduced by limiting the volume of moderator per lattice cell. This effect was investigated using the WIMS-CRNL code. A 37-element 1.3 a/o U-235 fuel lattice cell was simulated with various lattice pitch sizes. The results are depicted in Fig. 6-13 and 6-14.

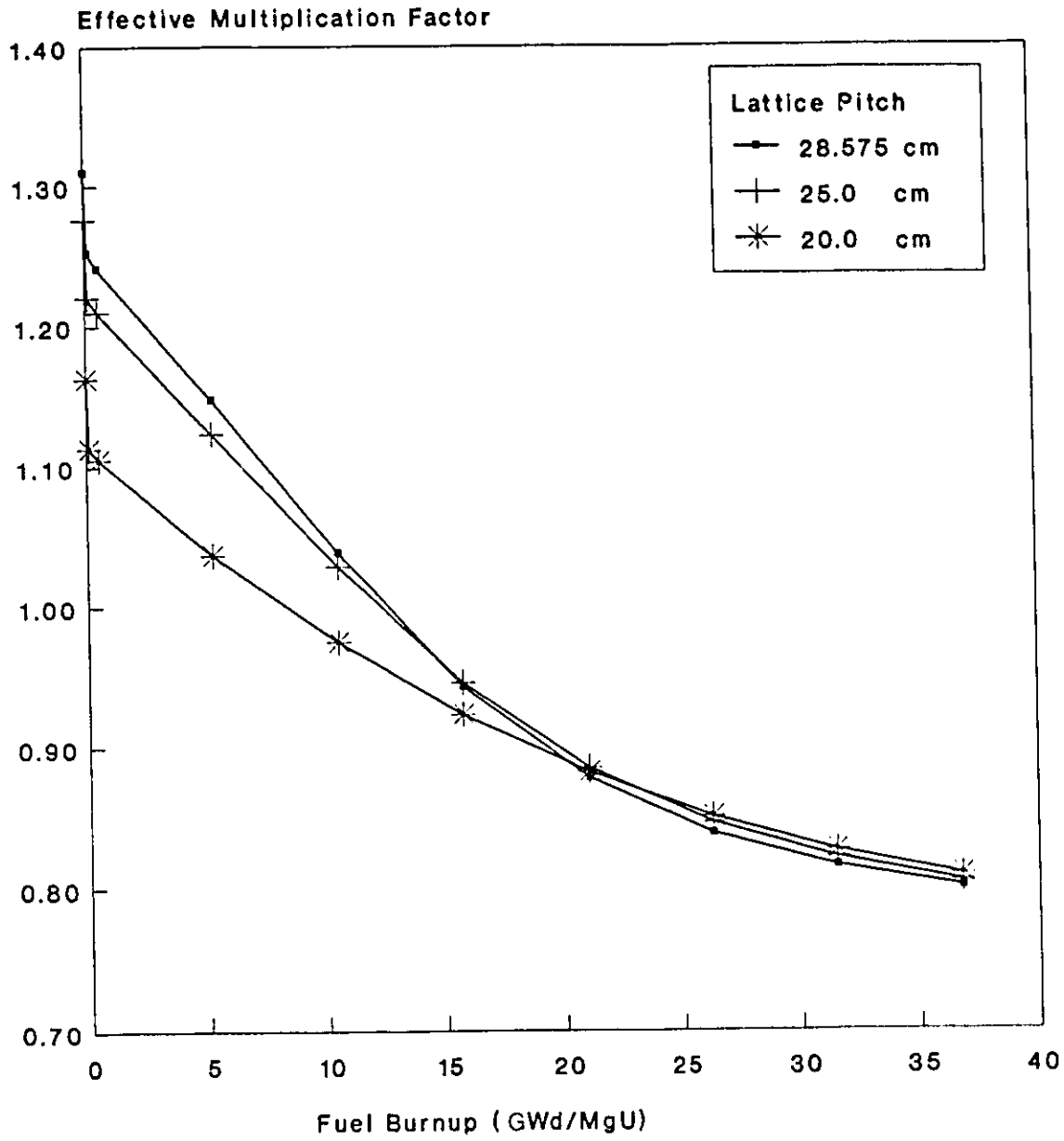

Figure 6-13 Effect of Variation of Lattice Pitch on Effective Multiplication Factor
(37 Element, 1.3 a/o U-235)

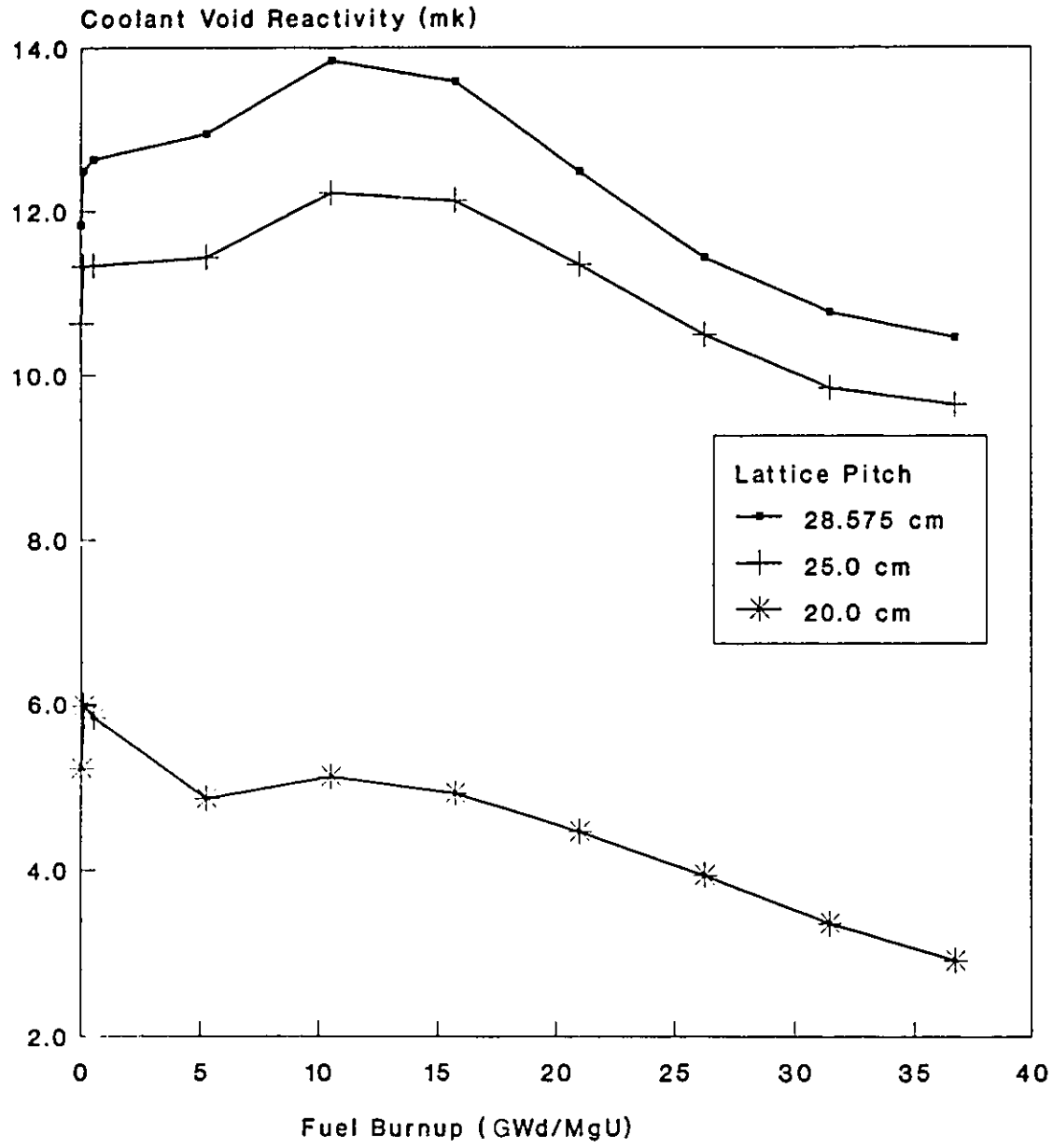

Figure 6-14 Effect of Variation of Lattice Pitch on Coolant Void Reactivity (37 Element, 1.3 a/o U-235)

The reduction in the lattice pitch reduces the achievable burnup. Using the same criteria adopted in Section 6.4.3.1 (burnup-averaged k-eff=1.018), achievable burnups are as follows:

28.575 cm LP	Burnup = 22405 MWd/MgU
25.000 cm LP	Burnup = 21539 MWd/MgU
20.000 cm LP	Burnup = 13220 MWd/MgU

The reduction in burnup is compensated for by a reduction in the void reactivity, as shown in Fig. 6-14. With a 20 cm lattice pitch the coolant void reactivity is reduced by approximately 60% in comparison with the 28.575 cm case. The corresponding burnup penalty is 40%. The 25 cm lattice pitch case exhibits a void reactivity reduction of greater than 10%, and a burnup penalty of approximately 4% when compared with the nominal 28.575 cm case.

Burnup and void reactivity data for a number of 37 element cases are summarized in Tables 6-5 and 6-6.

6.5 CONCLUDING REMARKS

In the development of the CANDU reactor system, neutron economy has always been stressed. While it is true that with the introduction of enriched uranium high burnup fuel cycles a given burnup penalty (in MWd/MgU) is of a lesser relative consequence, the penalties associated with the void reactivity reduction methods considered in this chapter may be too severe to merit implementation. In Chapter 7, the coolant void phenomenon is considered further, and novel fuel bundle designs coupled with lattice modifications are considered to reduce the void reactivity in CANDU type reactors and yet improve overall performance and fuel burnup.

Enrichment (a/o)	Fuel Burnup Achievable (MWd/MgU)	Coolant Void Reactivity (fresh fuel) (mk)
0.72	6230	16.6
0.8	9400	N/A
0.9	12590	N/A
1.0	15330	13.6
1.1	17859	N/A
1.2	20187	N/A
1.3	22410	11.8

Note: WIMS-CRNL results.

Table 6-5 37 Element Fuel, Nominal Lattice Geometry: Effect of Fuel Enrichment

Lattice Pitch Size (cm)	Fuel Burnup Achievable (MWd/MgU)	Coolant Void Reactivity (at 10500 MWd/MgU) (mk)
28.575	22410	13.8
27.0	22210	N/A
25.0	21540	12.2
23.0	19980	N/A
20.0	13220	5.1

Note: WIMS-CRNL results.

Table 6-6 37 Element Fuel, 1.3 a/o U-235: Effect of Lattice Pitch Size

CHAPTER 7

REDESIGN OF THE NUCLEAR FUEL BUNDLE

7.1 INTRODUCTION

The methods of reducing the coolant void reactivity that were considered in Chapter 6, could only be introduced at the expense of a substantial reduction in fuel burnup. Consequently, there is an incentive to devise more innovative ways to achieve this effect with minimal negative impact on achievable fuel utilization.

7.2 CANDU 30(37) FUEL BUNDLE

It has been found (Roshd et al., 1977) that the centre elements in a 37 element natural uranium fuel bundle have a proportionately larger contribution to the void reactivity than the outer elements. This is due to the fact that the fast neutron flux and hence fast fission rate peak at the centre of the bundle (see Table 7-1). Consequently the central elements produce most of the change in the fast fission rate when the coolant is lost. Further, the coolant acts as a source of resonance neutrons which are absorbed by the inner pins, and thus, upon voiding, the main change in resonance absorption is also produced by the central pins.

The central fuel pins in a 37 element bundle produce less power than those in the outer rings because of the thermal flux depression across the bundle (see Table 7-1). Hence, by removing the central fuel pins, one would expect a large change in void reactivity, with only a small reduction in operating power level (for a given peak pin power rating).

Roshd et al. (1977) proposed removing the central 7 pins (ring of 1 pin, ring of 6 pins) (see Fig. 2-3) from a 37 element natural uranium fuel bundle to form a 30(37) fuel bundle with the same outer dimensions, but with

Fuel Element Ring Number (from centre)	Fast Flux ($n/cm^2/s$)	Thermal Flux ($n/cm^2/s$)	Relative Power (% of bundle power)	Relative Power per Pin (% of bundle power)
1	2.30 E-1	9.96 E-2	2	2.0
2	2.26 E-1	1.06 E-1	13	2.2
3	2.16 E-1	1.21 E-1	30	2.5
4	1.96 E-1	1.50 E-1	55	3.1

Notes:
(1) Data obtained at fuel burnup of 5250 MWd/MgU using WIMS-CRNL model described in Chapter 6.
(2) Data normalized such that total cell absorption rate is 1 neutron/second.
(3) Division between fast and thermal energy groups is 0.625 eV.

Table 7-I Fuel Flux and Power Distribution Across 37 Element Natural Uranium Fuel Bundle

one ring of 12 pins and an outer ring of 18 pins. The space left after the removal of the central pins was to be filled with a large void tube or graphite (carbon) stringer. French and Jones (1976) conducted experiments with such fuel designs at the Atomic Energy of Canada Limited ZED-2 reactor. Replacement of the 37 element test bundles with 30(37) fuel (central pins replaced with an air filled aluminum tube) caused the cell coolant void reactivity to be reduced from 20 mk to 12 mk, while fission power was reduced by 13%.

The work in this thesis extends Roshd's analysis to enriched uranium fuel bundles, and further modifications are introduced to improve fuel performance.

7.3 POWDERPUFS-V LATTICE PHYSICS ANALYSIS

The POWDERPUFS-V (Tin and Loken, 1979) analysis in Chapter 6 used an early CANDU-600 37 element fuel reference model which contained 0.5 ppm of natural boron in the moderator (since adjuster rod shim was not allowed in CANDU-600 reactors at the time the model was set up). A modified reference CANDU-600 PPV data set is provided in Table 7-2 (a and b), which includes no moderator poison, and refinements to a number of other parameters. This refined model was used in the analysis conducted in this chapter. These changes in the basic model have only a relatively minor effect on the results.

A PPV 30(37) model was derived (Table 7-2) which includes all properties from the 37 element fuel model except for the required modifications to the:

(i) fuel perimeter,
(ii) coolant thickness,
(iii) void volume,
(iv) fuel volume,
(v) sheath volume,
(vi) coolant volume in homogenized zone,

Particulars	Standard CANDU-600	30/37** Fuel Design
Spectral Parameter *	0.0	
Fuel Neutron Temperature (°C) *	225.0	
Moderator Density (g/cm^3) *	0.0	
Moderator Temperature (°C)	68.0	
Coolant Density (g/cm^3)	0.804055	
Fuel Density (g/cm^3)	10.449747	
Fuel Temperature (°C)	687.0	
Annuli Neutron Temperature (°C) *	152.0	
Moderator Neutron Temperature (°C) *	78.0	
Sheath Absorption Factor	0.0	
Rubber Band Perimeter (cm)	30.88967	
Total Fuel Perimeter (cm)	141.27679	114.549
Coolant Thickness (cm)	0.4159343	0.4303
Number of Annuli	4.0	
Moderator Purity (atom %)	99.722	
Sheath Material Code (Zircaloy-2)	40.0	
Void Volume (cm^3/cm)	0.73975	15.190
Fuel Volume (cm^3/cm)	41.20616	32.587
Sheath Volume (cm^3/cm)	7.02746	5.691
Coolant Volume in Homogenized Zone (cm^3/cm)	27.80238	22.313
Radius of Homogenized Zone (cm)	4.94353	
Outside Radius of First Annulus (cm)	5.1689	
Outside Radius of Second Annulus (cm)	5.6032	
Outside Radius of Third Annulus (cm)	6.4478	
Outside Radius of Fourth Annulus (cm)	6.5875	
Coolant Temperature (°C)	290.0	
Total Coolant Volume (cm^3/cm)	34.96871	29.480
Flux Ratio C/F	1.059	
Lattice Pitch (cm)	28.575	
Coolant Material Code (D_2O)	0.0	
Material Code of First Annulus (as above)	20.0	
Material Code of Second Annulus (Zr-Nb)	70.0	
Material Code of Third Annulus (Air)	0.0	
Material Code of Fourth Annulus (Zircaloy-2)	50.0	
Material Code of Fifth Annulus (D_2O)	0.0	
Initial Flux Estimate ($n/cm^2/sec$) *	0.9E+14	
U-238 Resonance Capture Fraction *	0.0	

* Values for these parameters will be determined by the code. Values input are either flags or initial estimates.
** Only data which are altered for this design are indicated.

Table 7-2a POWDERPUFS-V Input Data for CANDU-600 37 Element and 30(37) Element Fuel

Particulars	Standard CANDU-600	30/37** Fuel Design
Fast Neutron Yield Cross-Section (cm^2/g-fuel)	0.024	
Fast Neutron Non-Escape Probability	0.0	
Fuel Material Code (UO_2)	0.0	
Fuel Heat Rating (kW/cm)	16.1518	
Power to Coolant Fraction	0.94332	
Initial Exposure for a Perturbed Run (n/kb)	0.0	
Neutron Temperature Convergence Criterion	0.001	
Bundle Length (cm)	49.53	
Pu-240 Self Shielding Factor *	0.0	
Moderator Poison Concentration (mg/kg natural boron to heavy water by weight)	0.0	
Nuclei per Mass of Fuel (g^{-1})	2.2303E+21	
Exposure Increment (n/kb)	0.1	
D_2O Coolant Purity (atom %)	99.722	
DEEMS Convergence Criterion	0.01	
Westcott Spectral Parameter Convergence Criterion	0.001	
Maximum Exposure (n/kb)	2.9	
Lattice Arrangement Indicator	0.0	
Geometric Buckling (cm^{-2})	0.00007618	
Xenon Absorption Cross Section (barns/atom) *	0.0	
Pu-240 Convergence Criterion	0.001	
Ratio of Flux Squared Weighted Mean Flux to Maximum Flux	0.764	
Initial Th-232 Concentration	0.0	
Initial U-233 Concentration	0.0	
Initial U-234 Concentration	0.0	
Initial U-235 Concentration	0.7204	
Initial U-236 Concentration	0.0	
Initial U-238 Concentration	99.2796	
Initial Pu-239 Concentration	0.0	
Initial Pu-240 Concentration	0.0	
Initial Pu-241 Concentration	0.0	
Initial Pu-242 Concentration	0.0	
Isotopic Density Indicator (Reaction-Rate-Averaged)	1.0	
Fuel Rods per Bundle	37.0	30.0
Perturbation Control (Normal)	0.0	
Pu-239 Production Control	0.0	
Saturating Fission Product Control (Include)	0.0	
Printout Control	5.0	
Central Radial Buckling for TUMULT (cm^{-2})	0.0	
EXTERMINATOR Calculation Control	0.0	
PERIGEE Calculation Control	0.0	
Burn-Up Control (10 Equation Set)	2.0	
Neutron Temperature Control	0.0	
Extrapolated Reactor Length for TUMULT (cm)	0.0	
Core Radius for TUMULT (cm)	314.27	
Reactor Radius for TUMULT (cm)	379.73	
Radial Form Factor for TUMULT	0.823	
Total Fission Power for TUMULT (MW)	2155.9	

* Values for these parameters will be determined by the code. Values input are either flags or initial estimates.
** Only data which are altered for this design are indicated.
Note: TUMULT calculation is not part of the basic PPV lattice simulation.

Table 7-2b POWDERPUFS-V Input Data for CANDU-600 37 Element and 30(37) Element Fuel (Continued)

(vii) total coolant volume, and

(viii) fuel rods per bundle.

Note that the Table 7-2 data correspond to the natural uranium case, though cases with 1.3 a/o U-235 were also considered.

For the purposes of this PPV study, it was assumed that the inner seven fuel pins were replaced by a void core 2.1425 cm in radius. (This corresponds to a void region extending from the centre of the fuel bundle to the outside edge of the second ring of fuel elements in a 37 element bundle.) No metallic tube was modelled around the void.

7.3.1 Comparison of 37 Element and 30(37) Element Fuel Bundle Designs

In Tables 7-3 and 7-4, a comparison is made of the reaction rate averaged PPV results for 37 and 30(37) element fuel. Table 7-3 shows the factoring of the effective multiplication factor into the four factor formula and the non-leakage probability (Eq 5.6-1) under conditions with coolant. Table 7-4 shows the relative change in each component in the four factor formula and non-leakage probability upon coolant voiding. (Note that the void reactivity is approximately equal to the sum of the relative individual changes in Table 7-4, divided by the value of k-eff from Table 7-3. This can be more rigorously shown to be true by examining the mathematical definition of reactivity change.)

From Table 7-3 it can be seen that for a given fuel enrichment, k-eff is higher with the 30(37) fuel than with 37 element fuel. In all cases, the effect of fuel enrichment on k-eff is primarily attributable to the change in the eta factor.

The PPV results in Table 7-4 indicate a reduction in void reactivity of less than 2 mk when the fuel design is changed from 37 element to the 30(37) configuration. The relative change in the fast fission factor upon coolant voiding is the most significantly reduced component when using the modified fuel bundle design.

In all four cases in Table 7-4, the void reactivity decreases when the

Case	Irradiation (n/kb)	Fast Fission Factor (ε)	Resonance Escape Probability (p)	Thermal Utilization (f)	Eta Factor (η)	Non-Leakage Probability (P_{NL})	Effective Multiplication (k-eff)
37 Element Natural	0.0	1.0261	0.9076	0.9337	1.2426	0.9697	1.0478
	1.8	1.0259	0.9079	0.9396	1.1944	0.9711	1.0151
37 Element 1.3 a/o U-235	0.0	1.0258	0.9081	0.9470	1.4715	0.9730	1.2631
	1.8	1.0257	0.9084	0.9480	1.3272	0.9732	1.1409
30(37) Element Natural	0.0	1.0222	0.9216	0.9261	1.2445	0.9670	1.0499
	1.8	1.0221	0.9218	0.9319	1.1848	0.9684	1.0074
30(37) Element 1.3 a/o U-235	0.0	1.0220	0.92219	0.94205	1.4746	0.9710	1.2710
	1.8	1.0219	0.92225	0.94212	1.3305	0.9710	1.1470

Table 7-3 POWDERPUFS-V Analysis: 37 Element and 30(37) Element Fuel Four Factor Formula Data

Case	Irradiation (n/kb)	Changes in 4-Factor Formula Components Upon Voiding					Void Reactivity (mk)
		$\Delta\varepsilon/\varepsilon$ ($\times10^3$)	$\Delta p/p$ ($\times10^3$)	$\Delta f/f$ ($\times10^3$)	$\Delta\eta/\eta$ ($\times10^3$)	$\Delta P_{NL}/P_{NL}$ ($\times10^3$)	
37 Element	0.0	5.05	6.04	3.21	2.49	-0.52	15.36
Natural	1.8	5.06	6.03	2.44	-2.43	-0.72	10.18
37 Element	0.0	5.06	6.04	2.43	1.02	-0.82	10.90
1.3 a/o U-235	1.8	4.96	6.04	2.21	-0.08	-0.82	10.80
30(37) Element	0.0	3.52	5.41	3.44	2.65	-0.31	13.90
Natural	1.8	3.42	5.41	2.57	-2.62	-0.52	8.20
30(37) Element	0.0	3.52	5.21	2.65	1.29	-0.51	9.70
1.3 a/o U-235	1.8	3.42	5.42	2.35	-0.22	-0.62	9.10

Table 7-4 POWDERPUFS-V Analysis: 37 Element and 30(37) Element Fuel Change in Four Factor Formula Components Upon Coolant Voiding

fuel irradiation is increased to 1.8 n/kb from 0.0 n/kb. This is primarily due to a reduction in the relative change in the eta factor as the importance of plutonium to the fission source increases. (See also the discussion in Section 5.6.2.)

The void reactivity in the enriched cases is considerably less sensitive to burnup than in the natural uranium cases.

Additional PPV analyses were conducted using the 30(37) 1.3 a/o U-235 fuel design, with modifications to the lattice pitch and calandria tube size, to reduce the system void reactivity. Results of the analysis at 0.0 and 1.8 n/kb are provided in Table 7-5.

From Table 7-5 it can be seen that reducing the lattice pitch and/or increasing the calandria tube radius results in a decrease in system void reactivity. However, even with the modified 30(37) fuel design, there is still a substantial burnup penalty involved in achieving a significant void reactivity reduction. For example, consider, in the fresh fuel case, a change from the 28.575 cm LP, 6.4478 cm calandria tube inner radius (CTIR) to a 25 cm LP and 10 cm CTIR. This yields a reduction in the system void reactivity from 10 mk to 3 mk, though at the expense of a 95 mk drop in initial fresh fuel reactivity, and a correspondingly large reduction in achievable burnup.

The results of the PPV analysis must be carefully considered. The relatively large reductions in void reactivity found in the experiments of French and Jones (1976), were not realized in the PPV simulations. The reason for this lies in the elementary geometric representation of the fuel bundle in the PPV model (Tin and Loken, 1979). The fuel region is modelled as a homogeneous zone consisting of the fuel bundle and enclosed coolant. Because there is no radial variation in the material properties across the fuel bundle, the PPV code cannot accurately model the effect of removing the central pins from a fuel element. Hence, it is clear that the more detailed treatment afforded with the WIMS-CRNL code (Donnelly, 1986) is required for analysis of these advanced fuel designs. The remainder of the lattice physics simulations considered in this chapter were conducted using the WIMS-CRNL computer code.

Lattice Pitch (cm)	Calandria Tube I.R. (cm)	Irradiation (n/kb)	Burnup (MWd/MgU)	k-eff (normal)	k-eff (void)	Void Reactivity (mk)
28.575	6.4478	0.0	0	1.2710	1.2868	9.66
28.575	6.4478	1.8	10683	1.1470	1.1590	9.06
28.575	7.0000	0.0	0	1.2672	1.2827	9.51
28.575	7.0000	1.8	10696	1.1432	1.1550	8.92
28.575	10.0000	0.0	0	1.2221	1.2340	7.89
28.575	10.0000	1.8	10883	1.1010	1.1101	7.45
25.000	6.4478	0.0	0	1.2447	1.2581	8.56
25.000	6.4478	1.8	10989	1.1227	1.1331	8.18
25.000	7.0000	0.0	0	1.2360	1.2487	8.23
25.000	7.0000	1.8	11032	1.1146	1.1245	7.90
25.000	10.0000	0.0	0	1.1342	1.1380	2.94
25.000	10.0000	1.8	11569	1.0243	1.0273	2.85
20.000	6.4478	0.0	0	1.1371	1.1404	2.54
20.000	6.4478	1.8	10595	1.0304	1.0333	2.72
20.000	7.0000	0.0	0	1.1090	1.1091	0.08
20.000	7.0000	1.8	12205	1.0075	1.0077	0.20
20.000	10.0000	0.0	0	0.6946	0.6396	-124.80
20.000	10.0000	1.8	14961	0.6903	0.6332	-130.60
15.000	6.4478	0.0	0	0.7517	0.6849	-129.75
15.000	6.4478	1.8	15866	0.7111	0.6482	-136.46
15.000	7.0000	0.0	0	0.6126	0.5193	-293.28
15.000	7.0000	1.8	16989	0.5361	0.4563	-326.20
15.000	10.0000	0.0	0	N/A	N/A	N/A
15.000	10.0000	1.8	N/A	N/A	N/A	N/A

Note: Fuel is enriched to 1.3 a/o U-235.

Table 7-5 POWDERPUFS-V 30(37) Element Fuel Analysis

7.4 WIMS-CRNL MODELLING OF 30(37) ELEMENT FUEL

The WIMS-CRNL code was used to simulate a 30(37) element fuel lattice. The DSN discrete ordinates solution option was utilized in the solution process (see Appendix F.2). The 18 group energy structure provided in Table 6-2 was employed. The enrichment dependent fuel composition is noted in Table 7-6.

Two additional materials were added to replace the inner two rings of fuel elements.

Initially, two core types were considered to replace the inner 7 fuel pins:

(1) air core (1.70825 cm in radius, 100% oxygen, 0.0014 g/cm^3) surrounded by a zircaloy tube (wall thickness 0.4343 cm). (This wall thickness is equal to that of the pressure tube.)
(2) graphite (carbon) core (2.10065 cm in radius, 100% carbon, 1.6 g/cm^3) surrounded by a zircaloy tube (wall thickness 0.0419 cm). (This wall thickness is equal to that of a fuel sheath.)

The heavier wall was deemed necessary in the air core case to minimize the possibility of deformation and/or leakage of D_2O into the hollow core.

Zero irradiation lattice physics simulations were performed for 1.3 a/o U-235 enriched fuel with the two core types described above. (The model also included a 7 cm calandria tube inside radius, 25 cm LP, 99.722 a/o D_2O coolant and moderator and 10.4497 g/cm^3 fuel density, similar to the PPV cases.) The results of the fresh fuel analysis conducted are summarized as follows:

Air Core:	Infinite Multiplication Factor = 1.31580
	Void Reactivity = 7.8 mk
Graphite Core:	Infinite Multiplication Factor = 1.31615
	Void Reactivity = 6.8 mk

With the graphite core, system reactivity is increased and void reactivity is decreased. Additional advantages of the graphite core include:

Initial U-235 Enrichment	U-235 (w/o)	U-238 (w/o)	Oxygen (w/o)
0.72046*	0.627	87.523	11.850
0.80	0.696	87.451	11.853
0.90	0.783	87.364	11.853
1.00	0.870	87.276	11.853
1.05	0.914	87.233	11.853
1.10	0.958	87.189	11.853
1.20	1.045	87.102	11.853
1.30	1.132	87.015	11.854
1.40	1.219	86.928	11.854
1.50	1.306	86.840	11.854
1.53	1.332	86.814	11.854
1.60	1.393	86.753	11.854
1.70	1.480	86.666	11.854
1.80	1.567	86.579	11.854
1.90	1.654	86.492	11.854
2.00	1.741	86.404	11.854
3.00	2.612	85.532	11.856

* Natural Uranium

Table 7-6 Enrichment Dependent Fuel Composition for WIMS-CRNL Simulations

(i) Reduced susceptibility to leakage and/or deformation,

(ii) Graphite core can act as a low-grade intermediate heat sink in event of a process system accident, and

(iii) Reduced axial neutronic streaming.

Because of these advantages, the graphite core design was chosen as the basis for further analysis.

7.5 ENRICHED ZIRCONIUM PRESSURE TUBES AND CALANDRIA TUBES

It has been found (Lone and Bartholomew, 1978; Lone, 1981) that the effective thermal neutron absorption cross section for Zr-90 is considerably less than previously published values would indicate (Mughabghab and Garber, 1973) (0.0174 barns vs 0.1 $\pm$ 0.07 barns). The effective cross section of natural zirconium is 0.205 barns, while that of natural Zr-2 is 0.244 barns, and natural Zr-2.5% Nb is 0.254 barns (including alloying impurities) (Townes, 1982). Hence, from a fuel economy perspective, there is an incentive to utilize zirconium enriched in the Zr-90 isotope. (Natural zirconium contains 51.5% Zr-90.)

The same technology used to produce uranium fuel enriched in the U-235 isotope can be employed to enrich the zirconium used in the reactor's pressure tubes and calandria tubes. Krishnan (1981) has established the OMEGA-P company to develop plasma centrifuge enrichment processes for a number of materials. Carty and other researchers at the University of Waterloo (Canada) are investigating laser isotope separation of Zr-90 (Nuclear Canada, 1986).

Using data from Townes (1982), the use of zirconium containing 99% Zr-90, 1% Zr-91, plus alloying impurities, will reduce the effective absorption cross section of Zr-2 by a factor of 3.5 and that of Zr-2.5%Nb by a factor of 3.04.

Townes (1982) noted that the use of such material in a CANDU-600 type reactor would be economically justified provided that the enriched zirconium could be produced for less than $2100/kg Zr. For enriched uranium fuelled reactors (with lower fuelling costs) the breakeven point was found to be of

the order of $600/kg Zr. (Townes (1984) also noted that the production of enriched zirconium was predicted to be of the order of $1000-$2000/kg Zr.)

The introduction of laser technology for isotope separation (see Chapter 4), could significantly reduce the cost of producing both enriched uranium and enriched zirconium. Further, the enriched zirconium could be re-used indefinitely, being recycled from one generation of reactors to the next. It is for these reasons that the next generation reactor designs may incorporate enriched zirconium in the pressure tubes and calandria tubes. It is noted that prior to implementation, a detailed investigative analysis would be required to demonstrate conclusively that the enriched zirconium would exhibit the predicted neutronic and mechanical characteristics.

7.5.1 Simulation of Enriched Zirconium With WIMS-CRNL

To simulate the presence of enriched zirconium in the pressure tube and calandria tube in a CANDU lattice cell, the density of the Zr-2 calandria tube was reduced from 6.55 g/cc to 6.55/3.50 = 1.87 g/cc. The density of the Zr-2.5%Nb pressure tube was reduced from 6.55 g/cc to 6.55/3.04 = 2.15 g/cc.

7.5.1.1 30(37) Element Fuel

The effect of using natural or enriched zirconium in a 30(37) element fuel bundle enriched to 1.3 a/o U-235 was simulated with the WIMS-CRNL code (DSN option). The results are shown in Fig. 7-1 and 7-2. The model included a 7 cm calandria tube (inside radius), 25 cm lattice pitch, and material properties as per Table 6-4. The inner 7 fuel elements (2 rings) were replaced by a carbon core (2.1 cm inside radius) surrounded by a Zr-4 sheath (0.04 cm in thickness). This model is identified with the code 30(37)-1.3-25-7-CC.

The standard CANDU-600 maximum time-averaged bundle power is 800 kW (Tin, 1981). This corresponds to a power density of 42.553 kW/kgU (assuming 18.8 kgU/bundle). If a 30(37) bundle is to operate at the same power as a 37 element bundle, the power density would have to increase to

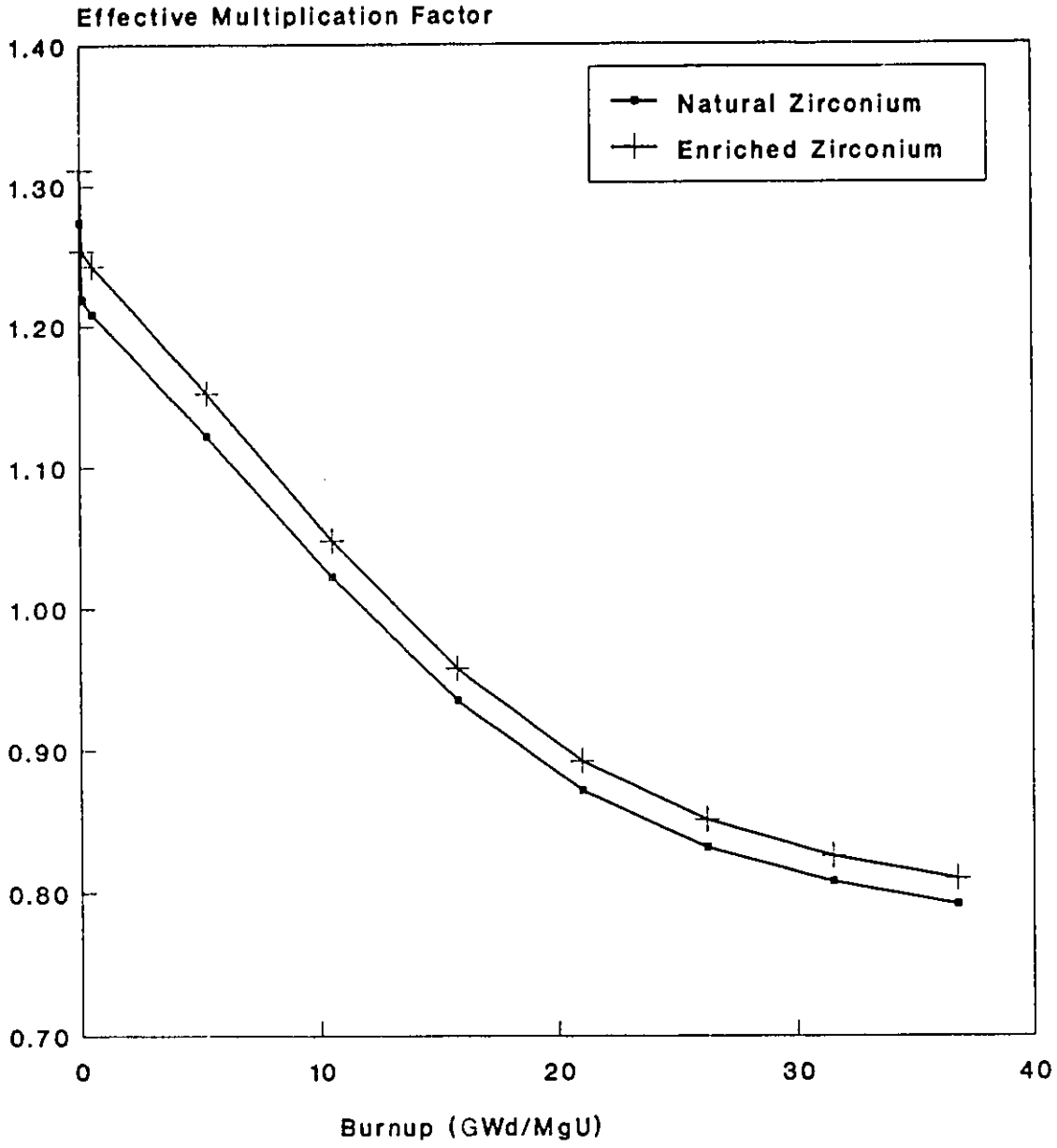

Figure 7-1 Effect of Enriched Zirconium on k-eff
Model: 30(37)-1.3-25-7-CC

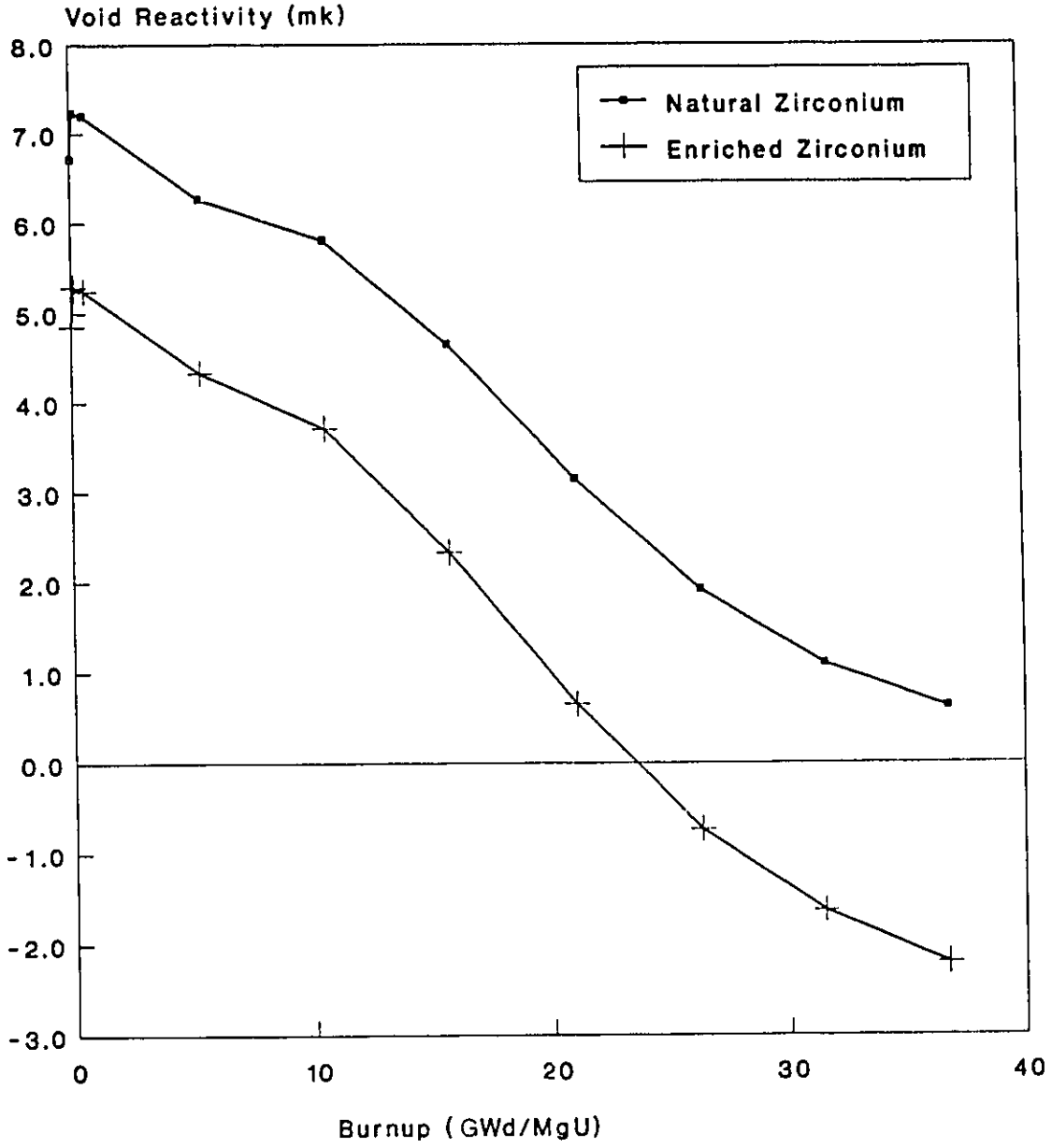

Figure 7-2 Effect of Enriched Zirconium on Coolant Void Reactivity
Model: 30(37)-1.3-25-7-CC

52.482 kW/kgU. This power density was assumed in the 30(37) fuel burnup cases.

From Fig. 7-1, it can be seen that enriched zirconium in the pressure tube and calandria tube increases the lattice cell reactivity by approximately 23 mk. This results in an increase in achievable burnup of approximately 15% (20650 MWd/MgU with natural Zr, vs 23760 MWd/MgU with enriched Zr, using the integrated k-eff = 1.018 criterion (Section 6.4.3.1)).

The system void reactivity (Fig. 7-2) is reduced by approximately 2 mk with enriched zirconium. This can be attributed to the increase in the importance of the region of the cell beyond the coolant zone to the entire system behaviour as the absorption in the zirconium alloy tubes is reduced. (A similar reduction in void reactivity can be found with natural zirconium by reducing the pressure tube wall thickness (Tin, 1981).)

7.5.1.2 37 Element Natural Nominal Fuel

The use of enriched zirconium in the pressure tube and calandria tube of natural uranium fuelled nominal CANDU-600 lattice, increases initial system reactivity by 29 mk and increases fuel burnup by approximately 3000 MWd/MgU (based on similar WIMS-CRNL calculations).

Because of the performance advantages achievable through the use of enriched zirconium, all subsequent analysis of advanced fuel designs considered in this study assumes the use of such material in the pressure tubes and calandria tubes. The only exception is the natural uranium, nominal CANDU-600 (NATNOM) calculations which provide the reference data, where natural zirconium is used throughout.

7.6 COMPARISON OF 30(37) ELEMENT AND 37 ELEMENT BUNDLE DESIGNS

Comparing the lattice physics results from Fig. 6-13/6-14 with those from Fig. 7-1/7-2, it is clear to see that the 30(37) element fuel design substantially reduces system void reactivity without incurring a significant burnup penalty. A reduction in the lattice pitch from 28.575 cm to 25 cm

reduces the void reactivity in a 37 element 1.3 a/o U-235 fuel lattice cell by approximately 1.5 mk. Increasing the calandria tube radius to 7 cm reduces the void reactivity by a further 0.3 mk. The transition from this stage to a 30(37) element design, reduces the void reactivity by 6 mk. The use of enriched zirconium reduces the void effect by an additional 2 mk.

Using the burnup-averaged k-eff = 1.018 criterion (see Section 6.4.3.1) to estimate achievable burnup, it was found that the transition from the 1.3 a/o U-235 37 element design with the nominal lattice pitch and calandria tube size (Model: 37-1.3-28.575-6.4478) to the 30(37)-1.3-25-7-CC design with natural zirconium, caused an 8% reduction in burnup (20650 MWd/MgU vs 22400 MWd/MgU). However, with enriched zirconium in the 30(37) lattice, achievable burnup rose to 23760 MWd/MgU, an increase of 6% over the 22400 MWd/MgU achievable with natural zirconium in the 1.3 a/o U-235 37 element design.

With enriched zirconium, 30(37), 1.3 a/o U-2355 enriched fuel, a 28.575 cm LP, and the nominal calandria tube radius of 6.4478 cm, (Model: 30(37)-1.3-28.575-6.4478-CC) a burnup of 24500 MWd/MgU is achievable, though the void reactivity is approximately 2 mk higher than in the 30(37)-1.3-25-7-CC enriched zirconium case.

The 30(37)-1.3-25-6.4478-CC enriched zirconium design yields a burnup of 24250 MWd/MgU, with a void reactivity approximately 0.5 mk higher than in the 30(37)-1.3-25-7-CC enriched zirconium case.

The results of the various simulations are summarized in Table 7-7.

The void reactivity reduction in the transition from the 37 element to the 30(37) element fuel bundle design can be attributed to the fact that in the 37 element bundle, the central fuel pins experience the largest changes in reaction rate upon coolant voiding. Removing these pins reduces the overall void effect (as discussed in Section 7.2). In Appendix A, a further characterization of the phenomenon is considered. In this appendix the contribution of changes in the neutron reaction rates in a number of fuel nuclides upon coolant voiding is examined. Nuclides investigated include: U-235, U-238, Np-239, Pu-239, Pu-240, Pu-241, and Pu-242. The analysis shows that the U-238 contribution to the void reactivity is the most substantially

Model Type*	Lattice Pitch (cm)	Calandria Tube Inner Radius (cm)	Enriched or Natural Zirconium	Achievable Fuel Burnup (MWd/MgU)	Coolant Void Reactivity at 10500 MWd/MgU (mk)
37	28.575	6.4478	NZ	22400	13.8
37	25.000	6.4478	NZ	21540	12.2
30(37)	25.000	7.0000	NZ	20650	5.8
30(37)	25.000	7.0000	EZ	23760	3.7
30(37)	28.575	6.4478	EZ	24500	5.9
30(37)	28.575	7.0000	EZ	24300	5.5
30(37)	25.000	6.4478	EZ	24250	4.2

* All cases are 1.3 a/o U-235. 30(37) cases have carbon cores.

Table 7-7 Effect of Enriched Zirconium and Lattice Pitch/Calandria Tube Size Variations

reduced parameter in comparing 37 and 30(37) element fuel. This is a consequence of the reduction in the fast production and fast absorption effects due to the removal of the central two element rings where the fast flux is at a maximum.

7.7 CHARACTERIZATION OF THE 30(37) FUEL BUNDLE DESIGN AND VARIANTS

7.7.1 Effect of Fuel Enrichment

The effect of fuel enrichment on the effective multiplication factor and the coolant void reactivity is depicted in Fig. 7-3 and 7-4, respectively (Model: 30(37)-XX-25-7-CC, where XX implies "variable").

The abrupt reduction in k-eff at the very early burnup stage (Fig. 7-3) is due to the initial build up of the saturating fission products. As the burnup approaches 40000 MWd/MgU, the k-eff curves tend to join together becoming relatively independent of the initial fuel enrichment. (At these high burnup stages, the remaining U-235 concentration is minimal for all of the cases considered.)

The initial void reactivity (Fig. 7-4) is reduced as the fuel U-235 enrichment is increased. However, similar to the situation with 37 element fuel (Fig. 6-12), the lower initial enrichment curves have a larger negative slope, resulting in a cross over of the curves as the burnup increases.

Table 7-8 provides a summary of the achievable burnup with this fuel design as a function of initial fuel enrichment. (The integrated k-eff = 1.018 criterion (Section 6.4.3.1) was used.) Also included for comparison purposes is the coolant void reactivity under fresh fuel conditions. Table 7-9 provides similar summary data for the same fuel design, though with a 6.4478 cm calandria tube inner radius (CTIR) (nominal CANDU-600 size) as opposed to the 7 cm variety. Comparing the results in the two tables, it can be seen that the larger calandria tube results in a reduction in achievable burnup of the order of 500 MWd/MgU while the void reactivity is only reduced by approximately 0.5 mk. These differences are

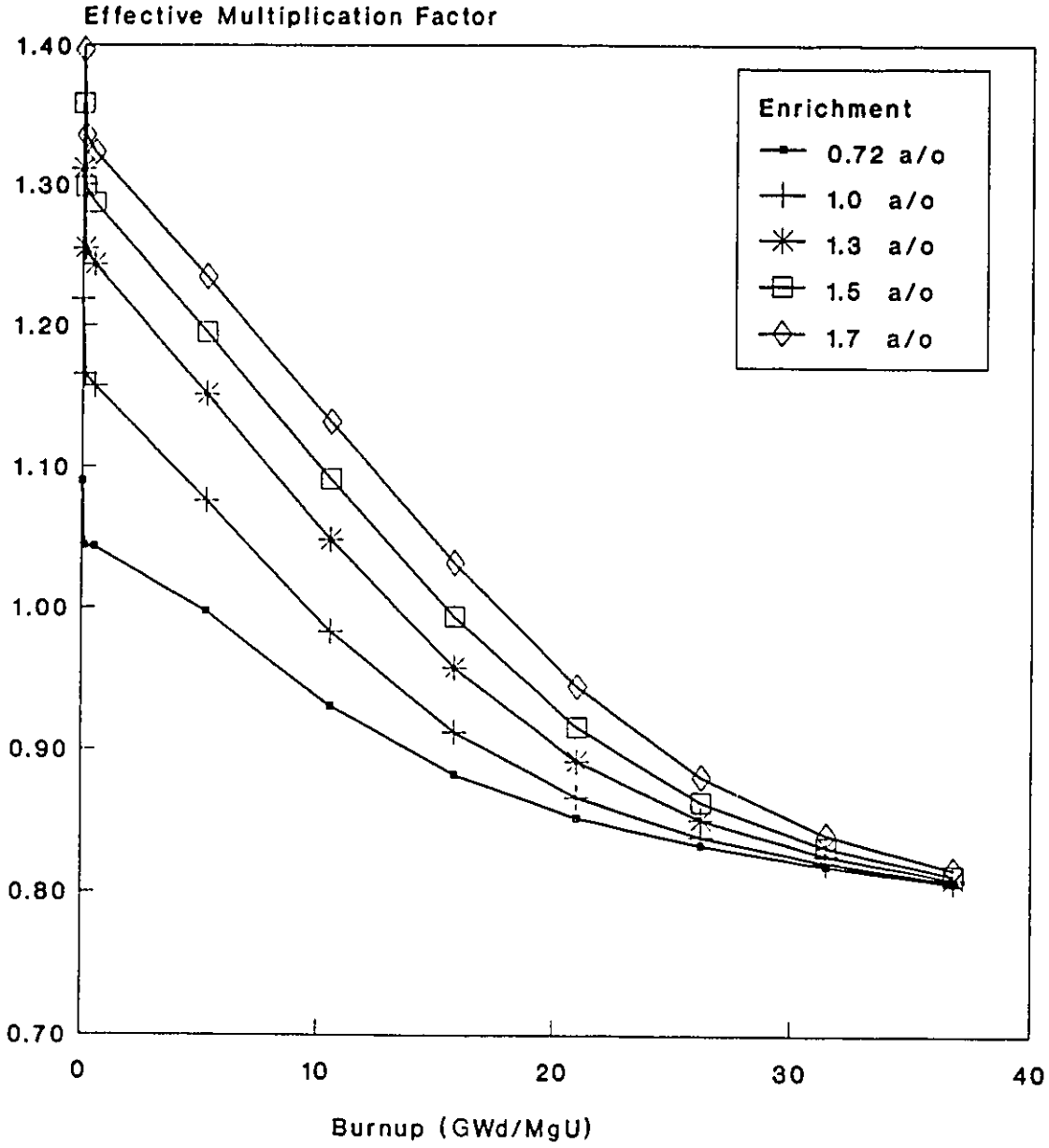

Figure 7-3 Effect of Fuel Enrichment on k-eff
Model: 30(37)-XX-25-7-CC

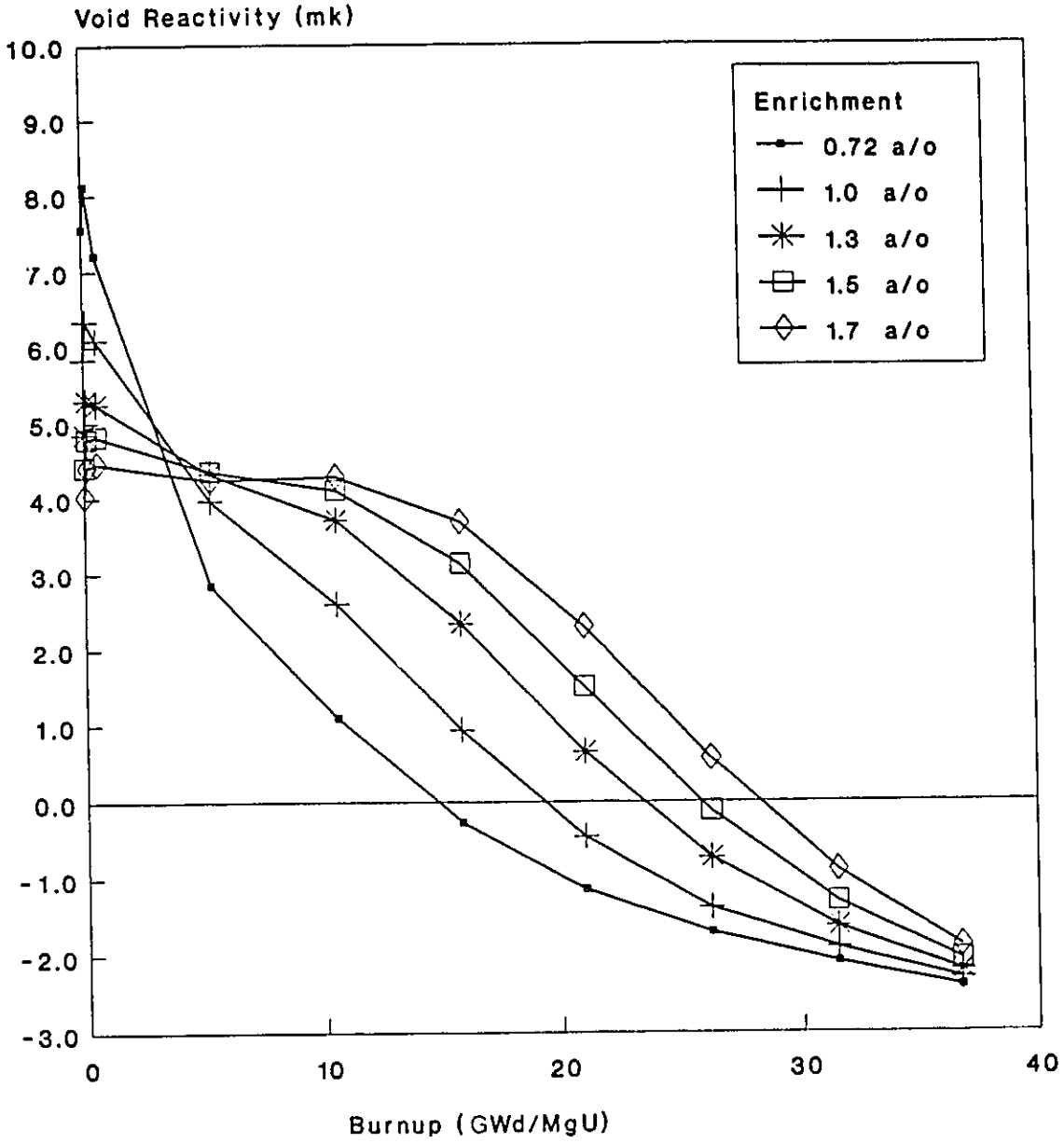

Figure 7-4 Effect of Fuel Enrichment on Coolant Void Reactivity
Model: 30(37)-XX-25-7-CC

Initial Fuel Enrichment (a/o U-235)	Fuel Burnup Achievable (MWd/MgU)	Coolant Void Reactivity (mk) (fresh fuel)
0.72	7148	7.56
1.00	16506	5.84
1.20	21486	5.11
1.30	23764	4.85
1.40	25895	4.62
1.50	27968	4.41
1.70	31935	4.03
3.00	51100	N/A

Table 7-8 Effect of Fuel Enrichment on Burnup (Model 30(37)-XX-25-7-CC)

Initial Fuel Enrichment (a/o U-235)	Fuel Burnup Achievable (MWd/MgU)	Coolant Void Reactivity (mk) (fresh fuel)
0.72	7936	8.01
0.90	14248	6.73
1.00	17068	6.27
1.10	19622	5.84
1.20	22008	5.52
1.30	24252	5.23
1.40	26379	4.99

Table 7-9 Effect of Fuel Enrichment on Burnup (Model 30(37)-XX-25-6.4478-CC)

slightly larger at lower initial fuel enrichments.

7.7.2 Effect of Lattice Pitch Size

The effect of the size of the lattice pitch on the effective multiplication factor and the coolant void reactivity is depicted in Fig. 7-5 and 7-6, respectively (Model: 30(37)-1.3-XX-7-CC). As the lattice pitch is reduced, the coolant becomes more important to the overall cell moderating power, and hence the void reactivity is reduced. The effect is similar to that noted in Fig. 6-14 for 37 element fuel. The data also indicates that the void reactivity reduction (in mk) per cm reduction in lattice pitch, increases as the lattice pitch size is reduced. Unfortunately, the burnup penalty also increases (Fig. 7-5).

Table 7-10 provides a summary of the achievable burnup with this fuel design as a function of lattice pitch size. Also included for comparison purposes, is the coolant void reactivity at 10500 MWd/MgU.

Table 7-11 provides similar information for the 30(37)-1.3-XX-6.4478-CC design (nominal CANDU-600 calandria tube size). The effect of altering the calandria tube radius is similar to that identified in Section 7.7.1. It is noted that as the lattice pitch size is reduced, the effect of the transition from a 6.4478 cm to a 7 cm calandria tube is enhanced. That is, the burnup penalty and void reactivity reduction associated with the change in calandria tube radius, is increased.

In the 7 cm calandria tube cases, the transition from a 27 cm lattice pitch to a 23 cm lattice pitch, results in a reduction in the void reactivity of 2.66 mk, and a burnup penalty of 1201 MWd/MgU, or a burnup penalty of 452 MWd/MgU per mk reduction in void reactivity. (Note that the corresponding value for the reduction in lattice pitch from 27 cm to 25 cm is 280 MWd/MgU per mk, and for the transition from 25 cm to 23 cm, the value is 562 MWd/MgU per mk.) In the transition from the 25 cm lattice pitch, 6.4478 cm calandria tube case, to the 25 cm lattice pitch, 7 cm calandria tube case, the corresponding figure is 946 MWd/MgU per mk. Hence, it is more economical to reduce the void reactivity by reducing the lattice pitch than by increasing

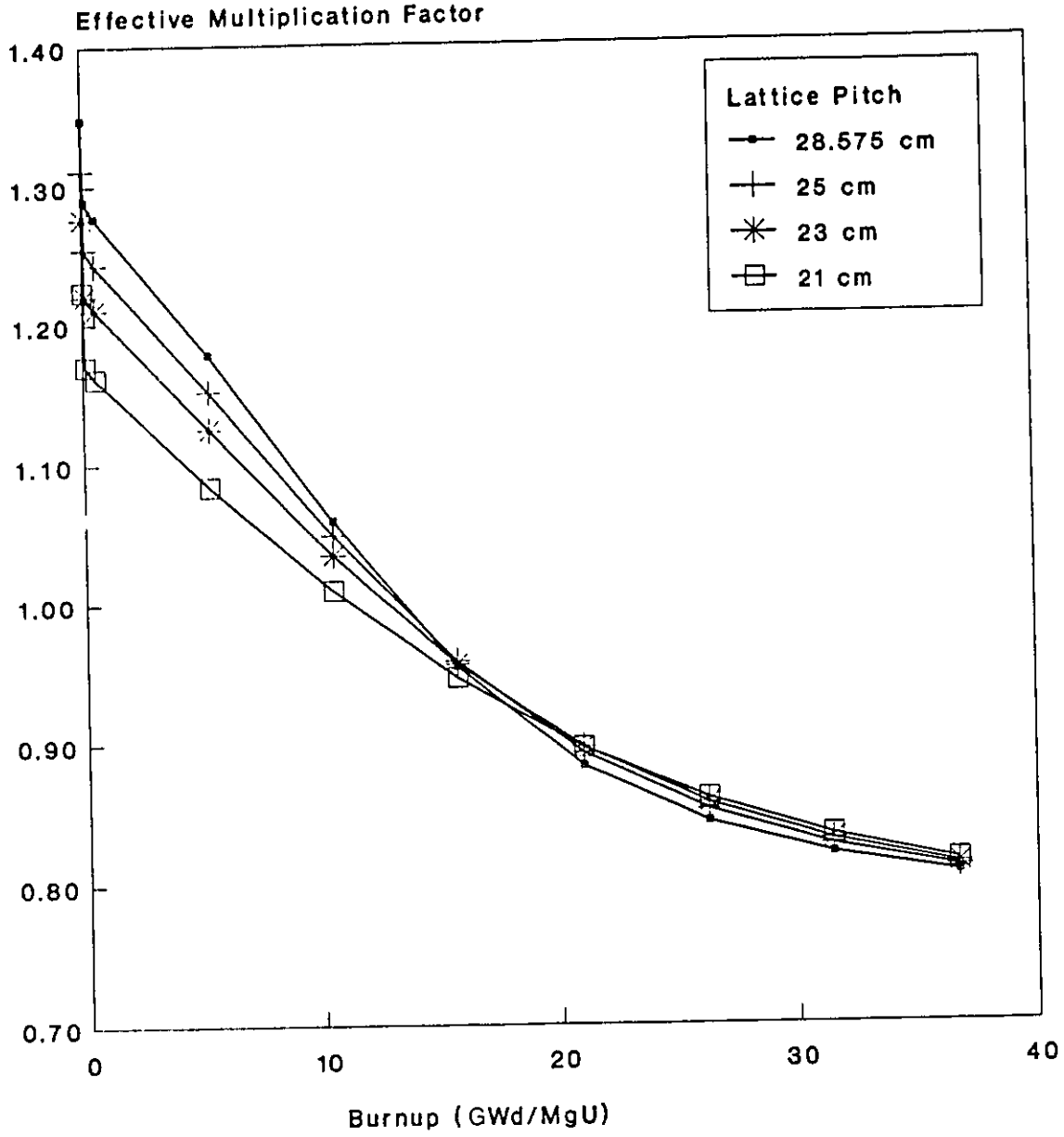

Figure 7-5 Effect of Lattice Pitch on k-eff
Model: 30(37)-1.3-XX-7-CC

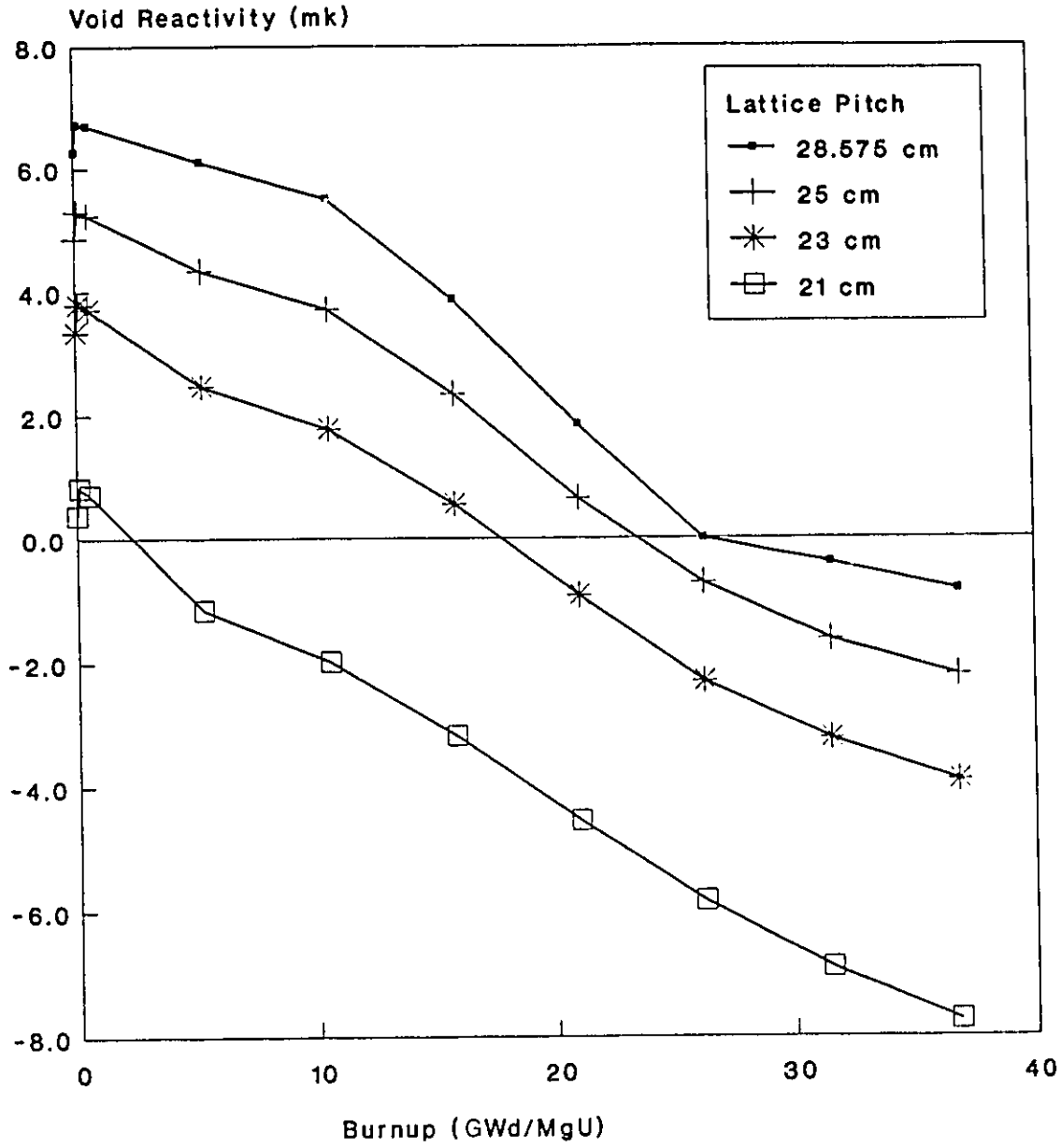

Figure 7-6 Effect of Lattice Pitch on Coolant Void Reactivity
Model: 30(37)-1.3-XX-7-CC

Lattice Pitch (cm)	Fuel Burnup Achievable (MWd/MgU)	Coolant Void Reactivity (mk) (at 10500 MWd/MgU)
28.575	24268	5.50
25.000	23764	3.71
23.000	22504	1.78
21.000	19277	-1.98
15.000	0*	N/A

* k-eff < 1.0 for all irradiations

Table 7-10 Effect of Lattice Pitch on Burnup (Model 30(37)-1.3-XX-7-CC)

Lattice Pitch (cm)	Fuel Burnup Achievable (MWd/MgU)	Coolant Void Reactivity (mk) (at 10500 MWd/MgU)
28.575	24526	5.87
28.000	24552	N/A
27.000	24543	5.27
26.000	24454	N/A
25.000	24252	4.23
24.000	23912	N/A
23.000	23342	2.61

Table 7-11 Effect of Lattice Pitch on Burnup (Model 30(37)-1.3-XX-6.4478-CC)

the calandria tube radius. The reason for this can be partially attributed to the increase in neutronic leakage due to streaming as well as the increase in parasitic absorption when the calandria tube (and gas gap) is enlarged. (For example in the 25 cm case at 10500 MWd/MgU, leakage (as calculated using WIMS-CRNL) is increased by 2.2 mk when the calandria tube inner radius is increased from 6.4478 cm to 7 cm.

7.7.3 Heavy Water Isotopic Purity Variations

The WIMS-CRNL simulations described in earlier sections were conducted assuming a coolant isotopic purity of 98.8 atomic percent (a/o) D_2O and a moderator isotopic purity of 99.9 a/o D_2O.

Increasing the coolant isotopic purity to 99.722 a/o D_2O in the 30(37)-1.3-25-6.4478-CC enriched zirconium lattice, results in the achievable burnup increasing from 24250 MWd/MgU to 24330 MWd/MgU, and the void reactivity at 10500 MWd/MgU decreases from 4.2 mk to 3.9 mk.

Reducing the moderator purity from 99.9 a/o to 99.722 a/o results in an achievable burnup of 23860 MWd/MgU and a coolant void reactivity of 4.48 mk at 10500 MWd/MgU.

Reducing the D_2O isotopic in the coolant or moderator increases the coolant void reactivity and decreases the burnup. The burnup coefficients as calculated for the above cases are:

86 MWd/MgU per a/o increase in coolant D_2O isotopic purity
2190 MWd/MgU per a/o increase in moderator D_2O isotopic purity.

The void reactivity coefficients are:

-0.4 mk per a/o increase in coolant D_2O isotopic purity
-1.4 mk per a/o increase in moderator D_2O isotopic purity.

Because of the influence of the coolant and moderator D_2O isotopic purities on the burnup achievable and the coolant void reactivity, strict

lower limits on isotopic purities must be imposed for both economic and safety reasons.

7.7.4 Moderator Temperature Coefficient

A WIMS-CRNL simulation was conducted for the 30(37)-1.3-25-7-CC fuel lattice with the moderator temperature increased to 90^{o}C (density 1.0707 g/cm^{3}) (from the reference value of 68^{o}C (density 1.0858 g/cm^{3})). This caused a reduction in system reactivity of approximately 2 mk and a reduction in void reactivity of approximately 0.2 mk at 10500 MWd/MgU. Achievable burnup was reduced by 1%. In the natural nominal CANDU-600, increasing the moderator temperature results in an increase in reactivity (approximately 0.08 mk/C^{o} (Tin, 1981)). The difference between the cases can be primarily attributed to the tighter lattice pitch considered in the enriched fuel study.

7.7.5 Effect of Degree of Coolant Voiding

Following a large loss of coolant accident, the hot coolant flashes to steam and much of it is ejected from the system. The degree of coolant voiding is a spatial and time dependent parameter and is a function of the heat transport system pipe break size and location.

To understand the relationship between system reactivity and the degree of coolant voiding, a series of lattice physics simulations were conducted with the 30(37)-1.3-25-6.4478-CC model, under fresh core conditions with various coolant densities. The system reactivity was found to increase linearly with decreasing coolant density.

7.8 PERTURBATIONS TO THE 30(37) FUEL BUNDLE DESIGN

7.8.1 Adjustments to the 30(37) Bundle Core

In Fig. 7-7 and 7-8, a number of different fuel bundle designs are

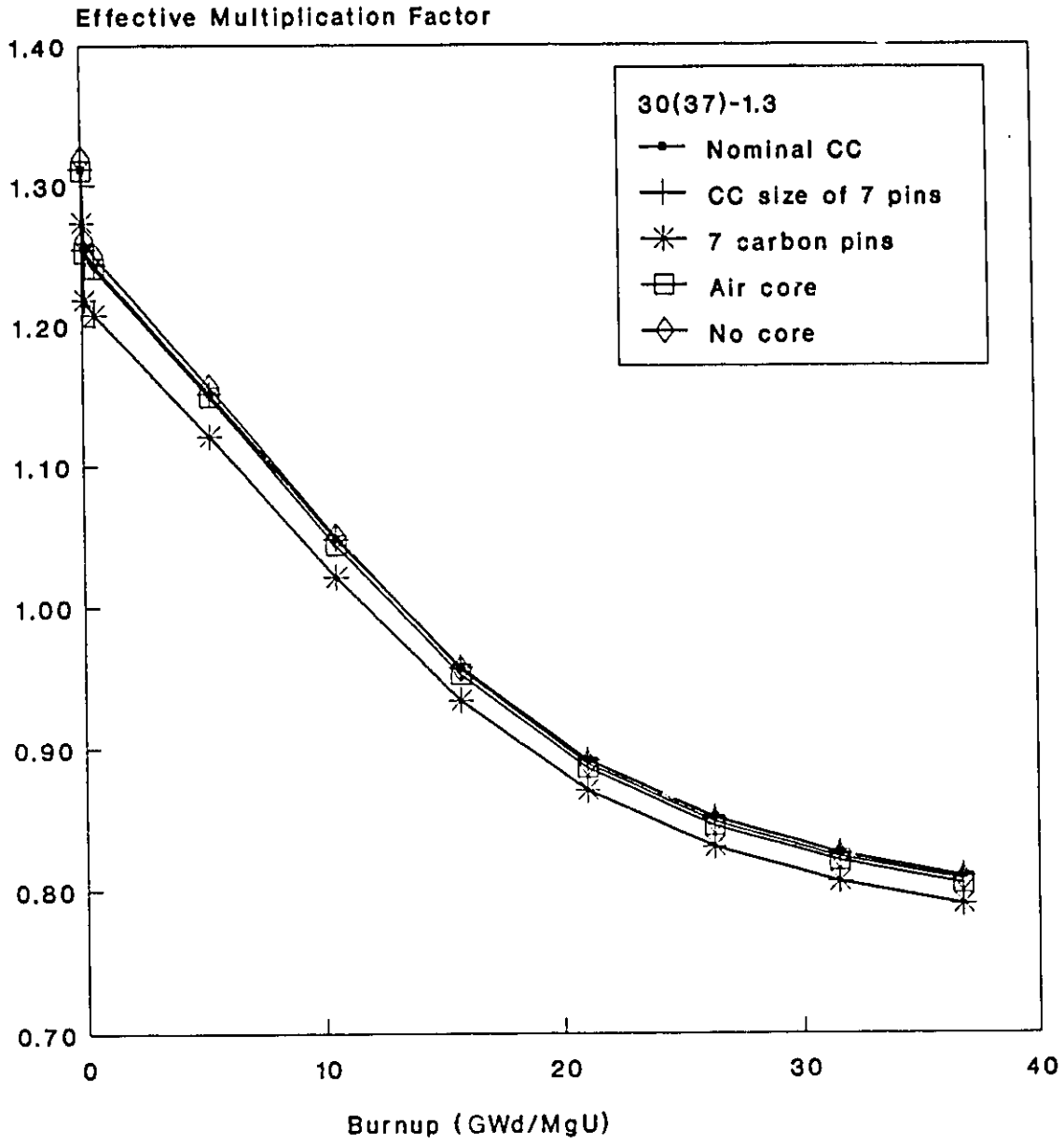

Figure 7-7 Effect of Bundle Configuration on k-eff
Model: 1.3 a/o U-235, 25 cm LP, 7 cm CT

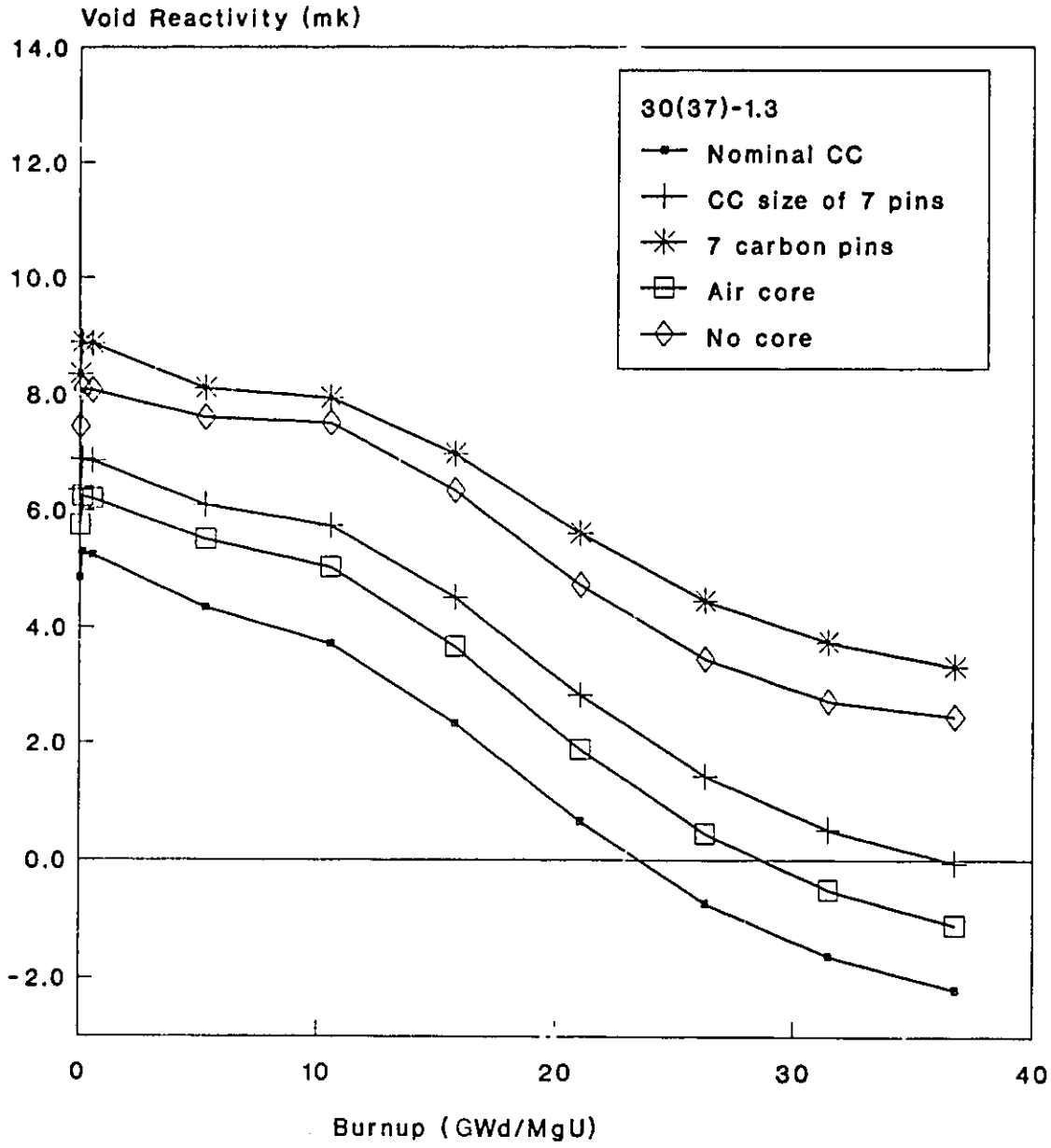

Figure 7-8 Effect of Bundle Configuration on Coolant Void Reactivity
Model: 1.3 a/o U-235, 25 cm LP, 7 cm CT

compared with the 30(37)-1.3-25-7-CC bundle introduced in Section 7.7. The modified bundle designs include:

(a) 30(37) design with a carbon core the same size as seven fuel elements. (This design has a carbon core of radius 1.68855 cm, surrounded by a Zr-4 sheath 0.0419 cm in thickness.) (Recall that the original 30(37) design has a carbon core of radius 2.10065 cm, surrounded by a similar sheath.)

(b) 30(37) design with a hollow air-filled core. (The core was assumed to be 1.70825 cm in radius, surrounded by a Zr-4 tube 0.4343 cm in thickness (see Section 7.4).)

(c) 30(37) design in which the 7 inner fuel elements of a 37 element bundle are replaced by 7 carbon elements of the same dimensions.

(d) 30(37) with no core at all. The inner two rings of fuel elements are replaced by coolant.

All designs considered maintained a 25 cm lattice pitch and 7 cm calandria tube radius.

Replacing the standard 30(37)-CC bundle by modified bundle designs a or b, above, does not substantially alter k-eff (Fig. 7-7). There is, however, a larger burnup penalty involved in modified design c. Achievable burnups for the various cases are as follows:

Standard 30(37)-CC:	23764 MWd/MgU
Modified Design a:	23706 MWd/MgU
Modified Design b:	23176 MWd/MgU
Modified Design c:	20510 MWd/MgU
Modified Design d:	23758 MWd/MgU

In Fig. 7-8, a greater distinction between the various cases can be

noted. Of the five designs considered in the figure, the standard 30(37) yields the lowest coolant void reactivity. Replacing the carbon core with an air core, reducing the size of the carbon core, or using no core at all, will cause the void reactivity to be increased. The largest increase in void reactivity results when the seven central fuel pins are replaced by seven carbon pins. (Note that the WIMS-CRNL DSN option homogenizes the carbon pins/coolant region prior to performing the main transport calculations (Donnelly, 1986).)

7.8.2 Isotope Production in the 30(37) Core

Additional simulations were conducted with the original 30(37) design, but with the carbon core replaced by either a lithium core (for the production of tritium) or a cobalt core (for Co-60 production). In both cases, the initial k-eff was substantially less than 1.0. With a central core consisting of 93.5% Li-7, and 6.5% Li-6, density 1.6 g/cm^3, the initial k-eff was 0.840. With a core consisting of natural cobalt (8.9 g/cm^3), the initial k-eff was 0.826. It would be possible to reduce the concentrations of Li or Co within the core and thereby increase the multiplication factors to more acceptable levels.

7.8.3 36(37) Element Fuel

If the central pin in a 37 element fuel bundle is replaced by a carbon core, a 36(37) element fuel bundle is formed. Figures 7-9 and 7-10 show the results of WIMS-CRNL simulations of such fuel designs.

Also included is a 36(37) bundle design with a central cobalt core. Because the core is much smaller in the 36(37) cobalt core case, the k-eff value is higher than with the 30(37) cobalt core case.

Achievable fuel burnups for the 3 cases considered are:

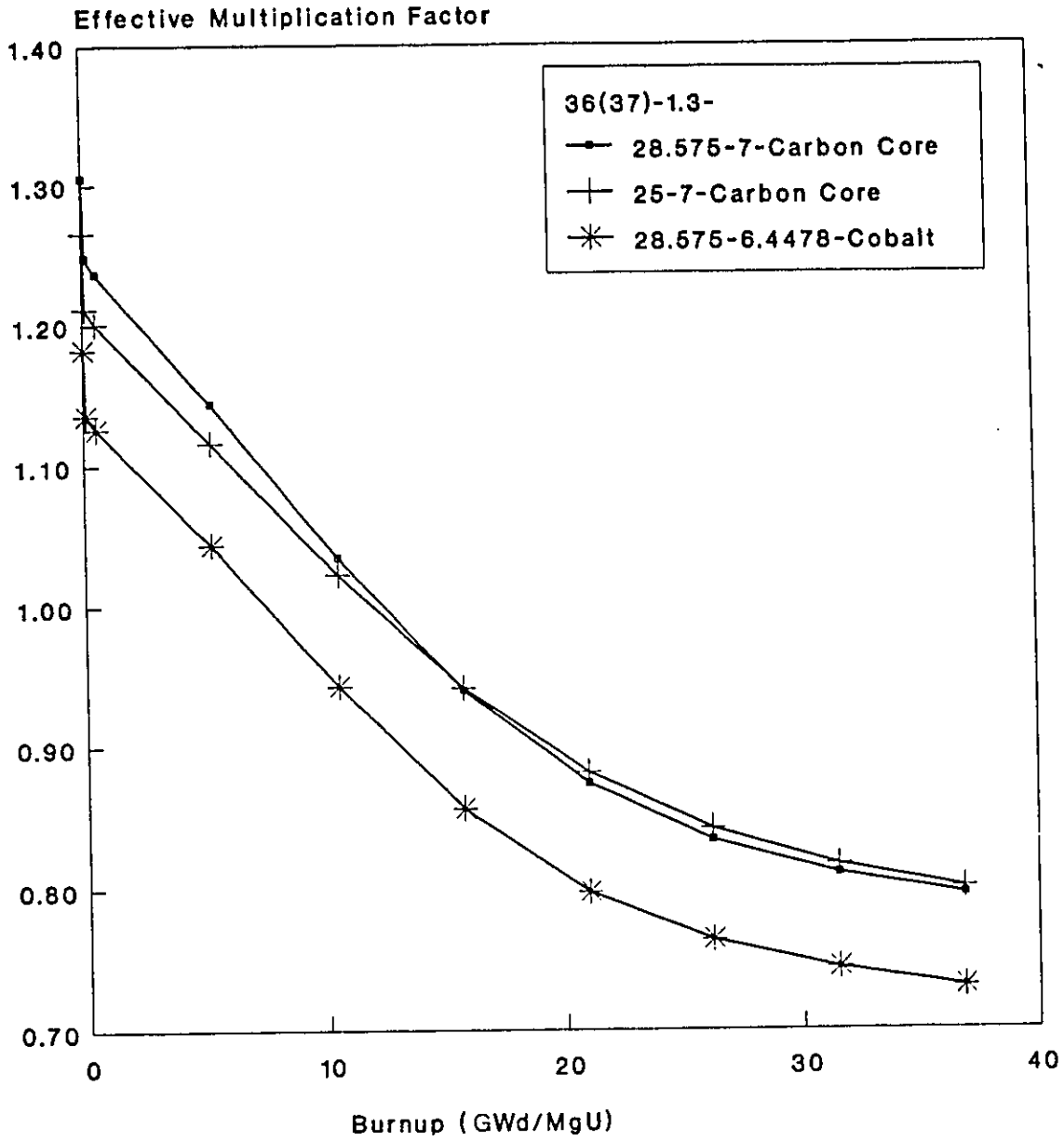

Figure 7-9 Effect of Geometry and Composition (36/37 Element Fuel) on k-eff

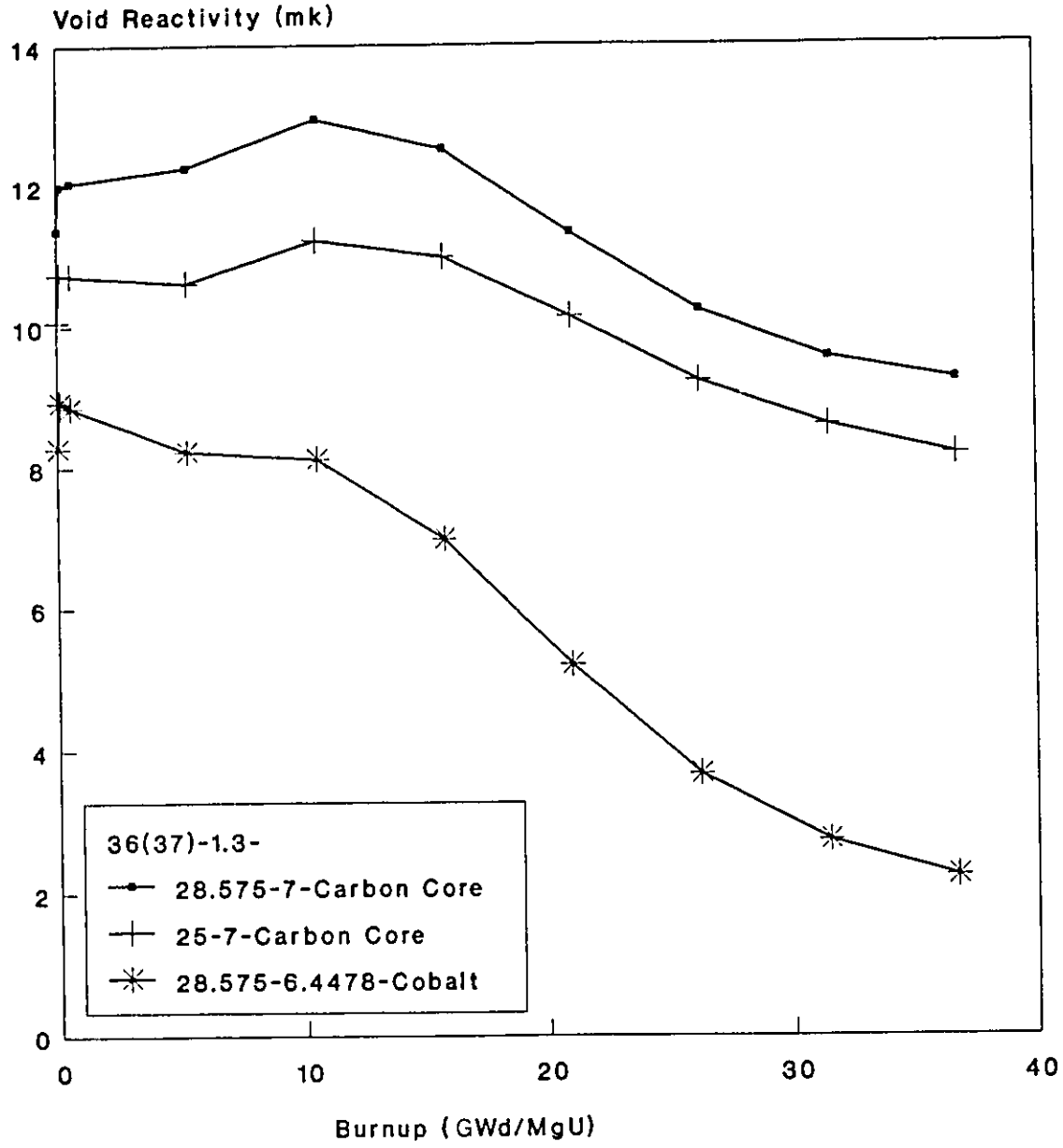

Figure 7-10 Effect of Geometry and Composition on Void Reactivity (36/37 Element Fuel)

Model: 36(37)-1.3-28.575-7-CC	Burnup = 21979 MWd/MgU
Model: 36(37)-1.3-25.000-7-CC	Burnup = 20841 MWd/MgU
Model: 36(37)-1.3-28.575-6.4478-Cobalt Core	Burnup = 12417 MWd/MgU

These are to be compared with the burnup of 23764 MWd/MgU with the 30(37)-1.3-25-7-CC design. The cobalt core imposes a very substantial burnup penalty. This economic penalty would have to be incorporated into the selling price of Co-60.

The coolant void reactivity in the 36(37) bundle is substantially greater than in the 30(37) element designs. The void reactivity effect is greatest in the central pins, and more of these are present in the 36(37) design than in the 30(37) bundle. Of the various 36(37) designs considered in Fig. 7-10, the void reactivity is the lowest in the cobalt core case. This can be attributed to the large depression in the neutron flux at the centre of the bundle due to the presence of the cobalt.

7.8.4 Light Water Coolant

A substantial amount of the radiation dose received by CANDU nuclear station operators and maintenance personnel results from activities involving repairs to the primary heat transport system. Tritium, produced in heavy water, is one of the most important isotopes contributing to the worker dose. Further, the use of heavy water coolant adds substantially to the capital cost of a nuclear station, and additional equipment must be installed to collect any and all leakage of this expensive material from the heat transport system. Consequently, there is an incentive to use other coolants, such as light water in the CANDU reactor. Heavy water would continue to be used in the moderator system.

Figures 7-11 and 7-12 show the results of WIMS-CRNL simulations conducted with the 30(37) element 1.3 a/o U-235 carbon core fuel bundle design, with a 7 cm calandria tube, light water coolant, and various lattice pitch (LP) sizes. Burnup achievable with the three LP sizes considered were:

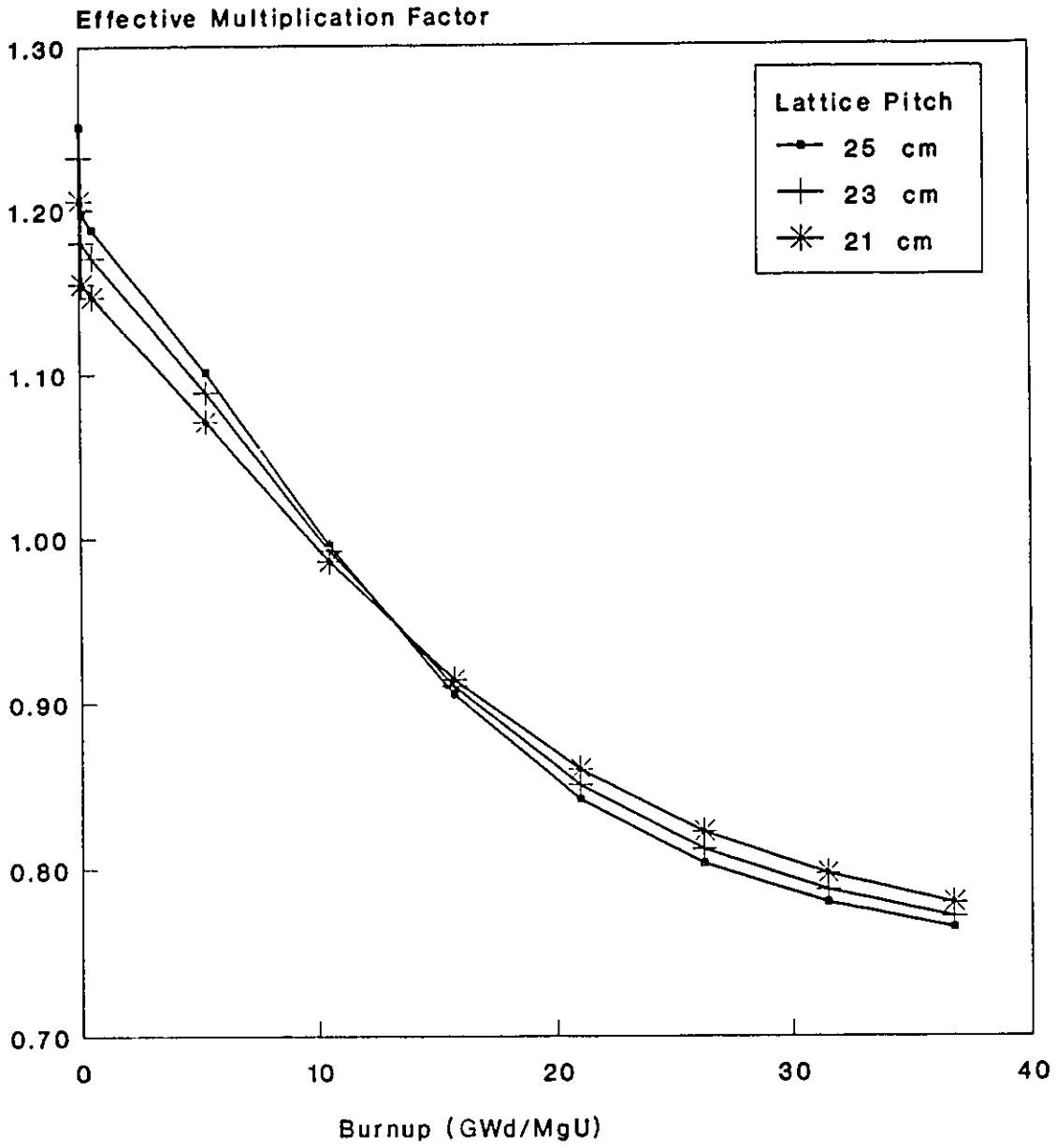

Figure 7-11 Effect of Light Water Coolant on k-eff
Model: 30(37)-1.3-XX-7-CC

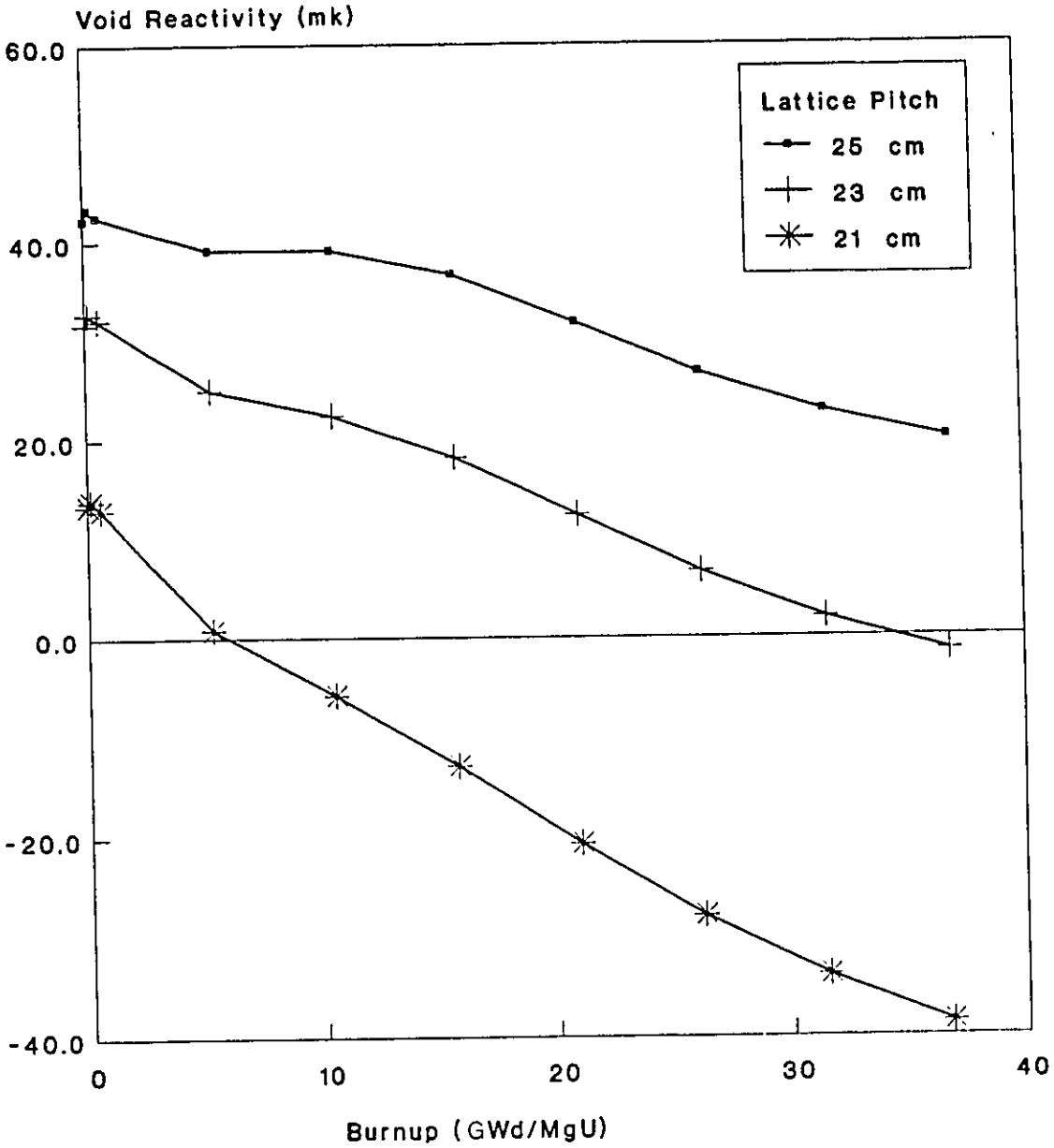

Figure 7-12 Effect of Light Water Coolant on Void Reactivity
Model: 30(37)-1.3-XX-7-CC

25 cm LP: 17854 MWd/MgU
23 cm LP: 17445 MWd/MgU
21 cm LP: 16431 MWd/MgU

These values are to be compared with the 23764 MWd/MgU achievable with heavy water coolant (25 cm LP, 7 cm calandria tube).

Note that in these light water cases, the "WIDTH" annularization option in the WIMS-CRNL model setup code, TESHOM, was chosen as recommended by Griffiths (1978) for this coolant type. With this option, fuel elements in a given ring of a fuel cluster are homogenized such that there is an equal width of homogenized annulus on each side of the pitch circle.

Comparing Fig. 7-6 and 7-12, it can be seen that the void reactivity is greatly increased when light water replaces heavy water coolant. The light water has a larger absorption cross section and moderation cross section than heavy water, and these parameters contribute to the overall void effect. With light water coolant, the void reactivity is much more dependent on fuel irradiation, and lattice pitch size.

Reducing the LP from 25 cm to 21 cm reduces the burnup by approximately 8%, and the void reactivity is reduced by more than 45 mk at 10500 MWd/MgU.

With light water coolant and a 21 cm LP, the average void reactivity in an equilibrium core can be very close to zero, and under fresh fuel conditions, the void reactivity would be comparable to the nominal CANDU-600 37 element natural fuel case. In comparison with the 30(37) element heavy water design with a 25 cm LP, there is a fuel burnup penalty of approximately 30%. The economic tradeoff would have to be considered.

Note that the use of boiling light water coolant (with its lower density) will result in a reduction of the void reactivity in comparison with the saturated light water coolant case. (Boiling light water coolant was used in the now retired Gentilly-1 CANDU-BLW prototype reactor in Quebec.)

7.8.5 Use of Neutron Poisons

7.8.5.1 Moderator Poison

In current generation CANDU reactors, neutron poisons (gadolinium or boron) are periodically added to the moderator to control reactivity. When restarting a reactor after a poison outage, Gd can be added for xenon simulation. Boron is often added during fuelling ahead or reactivity banking scenarios, where extra fuelling is done in anticipation of fuelling machine unavailability.

With the 30(37)-1.3-2.5-6.4478-CC fuel lattice model, the addition of 20 mg/kg (or 20 ppm) of natural boron to the moderator system (and maintaining that concentration with time) reduces the initial k-eff by 75 mk, reduces achievable fuel burnup by 39%, and causes the coolant void reactivity to increase by approximately 5 mk (based on WIMS-CRNL simulations). The use of moderator poison should therefore be carefully controlled. (When moderator poisons are no longer required they are removed via the moderator purification system (ion exchange columns).)

The reactivity worth of 1 ppm natural boron in the moderator of a CANDU-600 is approximately 8 mk. With the modified lattice and bundle design and the use of enriched fuel the reactivity worth is reduced by a factor of approximately two. This can be attributed to the reduced moderator volume and harder neutronic spectrum in the modified design.

7.8.5.2 Poisoned Fuel Bundles

It has been suggested that for extended burnups and fuel cycle lengths in light water reactors, 4-8% Gd_2O_3 can be added to the UO_2 fuel mix (Lang et al., 1983). The use of this burnable poison allows utilities the flexibility to practise more aggressive low leakage fuel management schemes (Krysinski et al., 1986).

The primary purpose of the poison added to the fuel mix is to reduce the initial local reactivity and thereby flatten the power distribution and

maximize reactor operating power without exceeding the licence channel and bundle power limits. As the fuel is irradiated, the reactivity decreases due to the reduction in the concentration of fissile material and the buildup of fission products. During this period, the poison concentration also becomes depleted as the poison atoms absorb neutrons. This reduction in poison concentration has a positive reactivity effect and the net result is that system reactivity changes more slowly with burnup than in the unpoisoned case.

The use of poison in the fuel mix in CANDU reactors can yield similar advantages. The poison can be added to the fuel pellets or to the carbon core. The following cases were studied with the WIMS-CRNL code:

(a) 30 ppm Gd-155 in the fuel mix,
(b) 30 ppm B-10 in the fuel mix,
(c) 3040 ppm Gd in the carbon core,
(d) 305 ppm Gd in the carbon core,
(e) 300 ppm B-10 in the carbon core,
(f) 3000 ppm B-10 in the carbon core.

All cases were modelled based on the 30(37)-1.3-25-6.4478-CC design with enriched zirconium pressure tubes and calandria tubes. The results are summarized in Table 7-12.

From the data presented in Table 7-12, it can be seen that the addition of Gd or B to the fuel mix or carbon core can reduce the peak k-eff and hence reduce local power peaking following refuelling. B-10 added to the fuel mix causes an increase in the void reactivity. B-10 in the carbon core reduces the void reactivity. The effect of B-10 on reducing k-eff extends over a longer burnup period than the effect of Gd, due to the slower burnout rate of B-10. Gd added to the fuel mix or the carbon core tends to reduce the void reactivity. Increasing the initial concentration of poison extends the effects to greater burnups.

In all cases, the addition of poison results in a burnup penalty. The added operational flexibility may justify this penalty. For example, the addition of 305 ppm Gd to the carbon core results in a 45 mk reduction in the

Poison Concentration (ppm)	Type of Poison	In Fuel or Core	Initial k-eff	k-eff at 10500 MWd/MgU	Initial Void Reactivity (mk)	Void Reactivity at 10500 MWd/MgU	Achievable Burnup (MWd/MgU)	Peak k-eff	Peak k-eff Occurs at (MWd/MgU)
0	--	--	1.32123	1.05337	5.23	4.23	24252	1.32123	0
30	Gd-155	fuel	1.12946	1.05354	3.73	4.24	24120	1.24538	800
30	B-10	fuel	1.05033	1.05560	7.16	4.23	22452	1.15551	3400
3040	Gd	core	0.97143	1.05453	--	--	23546	1.21823	1800
305	Gd	core	1.13976	1.05397	-3.19	4.20	24216	1.24688	800
300	B-10	core	1.17888	1.05462	1.74	4.23	23182	1.17093	2400
3000	B-10	core	0.92190	0.96114	--	--	0	0.98558	12600

Note: All cases are Model: 30(37)-1.3-25-6.4478-CC

Table 7-12 Effect of Poison in the Fuel Mix or Carbon Core

peak reactivity and only a 0.15% reduction in achievable burnup. (To put this in perspective, the variation in k-eff for natural nominal CANDU-600 fuel from fresh (with saturating fission products) to normal discharge burnup is approximately 45 mk.)

As the initial poison concentration is increased, there is a larger reduction in the initial k-eff. Eventually a point is reached where the fresh fuel can actually be less reactive than the spent fuel. With 3040 ppm Gd in the core, the initial k-eff is 0.971. It quickly increases, peaking at a value of 1.218 at 1800 MWd/MgU. Introducing such fuel into a region of the core may cause an initial reduction in local reactivity followed by a bolstering effect as the Gd burns away. Such temporal changes must be taken into consideration by the fuelling engineer. This delayed response may in fact prove operationally unacceptable. Further detailed fuelling studies would have to be undertaken to determine whether appropriate fuelling strategies could be developed for these poisoned fuel designs.

7.8.6 Increasing the Pressure Tube and Calandria Tube Wall Thicknesses

Increasing the thickness of the walls of the pressure tubes and calandria tubes (PT and CT) would allow operation at higher heat transport system pressures and temperatures, thereby increasing the overall efficiency of the steam cycle. Due to the nature of the materials and the system geometry, an increase in wall thickness of x% allows operation at x% higher pressure (Dalton, 1984).

The following cases were simulated using the WIMS-CRNL code:

(a) 30(37)-1.3-25-6.4478-CC,
(b) as above, but PT and CT wall thicknesses increased by 2%,
(c) as above, but PT and CT wall thicknesses increased by 10%,
(d) as above, but PT and CT wall thicknesses increased by 100%.

Enriched zirconium (see Section 7.5) was assumed in the composition of the PT and CT.

Results are summarized in Table 7-13. Increasing the PT and CT wall thicknesses reduces achievable burnup and increases the void reactivity (though the latter is only marginally affected). The use of enriched zirconium in the PT and CT minimizes the penalties associated with increasing the tube wall thickness.

7.9 SIMULATION PERTURBATIONS

In this section, a series of WIMS-CRNL simulations with various modelling perturbations are described.

7.9.1 Effect of Altering Time Steps

WIMS-CRNL main transport calculations (Donnelly, 1986) were normally conducted at burn times 0, 2, 10, 100, 200, ... days, at power densities of 52.482 MW/MgU(initial). A perturbation on this scheme was considered in which burn times for the 30(37)-1.3-25-6.4478-CC fuel model were altered such that main transport calculations were carried out at 0, 2, 10, 20, ... , 90, and 100 days. From the results at 100 days (5248 MWd/MgU), it was found that the finer time steps increased k-eff by 1 mk to 1.161, and the coolant void reactivity was reduced by 0.02 mk to 4.80 mk. The use of the larger time steps is therefore justified and is slightly conservative in terms of estimating burnup achievable and void reactivity.

7.9.2 Effect of Adjusting Number of Meshes in the Moderator

The TESHOM code (Griffiths, 1978) which was used to set up the WIMS-CRNL 30(37)-1.3-25-6.4478-CC model, divided the moderator annulus into six meshes for the main transport calculations. Increasing the number of meshes in the moderator region to seven, reduced the k-eff values by less than 0.01 mk.

Particulars	Nominal PT and CT	Nominal Plus 2%	Nominal Plus 10%	Nominal Times Two
PT Inner Radius (cm)	5.1689	5.1689	5.1689	5.1689
PT Outer Radius (cm)	5.6032	5.6119	5.6466	6.0375
CT Inner Radius (cm)	6.4478	6.4565	6.4912	6.8821
CT Outer Radius (cm)	6.5875	6.5990	6.6449	7.1615
PT Wall Thickness (cm)	0.4343	0.4430	0.4777	0.8686
CT Wall Thickness (cm)	0.1397	0.1425	0.1537	0.2794
Gas Gap Thickness (cm)	0.8446	0.8446	0.8446	0.8446
Burnup (MWd/MgU)	24252	24219	24059	22307
Void Reactivity (mk) at 10500 MWd/MgU	4.23	4.25	4.28	4.54

PT = Pressure Tube (Enriched Zr-2.5% Nb)
CT = Calandria Tube (Enriched Zr-2)

Table 7-13 Effect of Varying Calandria Tube and Pressure Tube Wall Thicknesses (Model 30(37)-1.3-25-XX-CC)

7.9.3 Effect of "WIDTH" Annularization

As in the 37 element WIMS-CRNL fuel model (see Section 6.4.2), the "AREA" annularization option in TESHOM was chosen for determining fuel region annulus sizes for the 30(37) cases (as recommended by Griffiths (1978)). This yielded an equal area of homogenized annulus on each side of the pitch circle in both fuel element rings. Choosing the "WIDTH" option instead, results in an annularization process in which the fuel elements and associated coolant are homogenized over an annular region having an equal width on each size of the pitch circles. A WIMS-CRNL DSN simulation with the 30(37)-1.3-25-6.4478-CC model, using the WIDTH option, resulted in k-eff being reduced by 0.3 mk and the void reactivity increasing by approximately 0.8 mk at 10500 MWd/MgU. Achievable burnup was not affected.

7.9.4 Effect of Critical Buckling

The WIMS-CRNL simulations were generally conducted assuming the standard CANDU-600 buckling of 0.7618 m^{-2}, divided equally into axial and radial components for leakage calculations. Additional calculations were conducted with the "critical buckling" option (Donnelly, 1986), in which the axial and radial buckling were uniformly adjusted after each burn step, modifying the neutronic leakage to maintain criticality in the lattice cell. This option, in fact, provides more appropriate lattice cell cross sections for use in large three dimensional core calculations (to be considered beginning in Chapter 8), since the fuel burns in a critical spectrum. However, calculating achievable burnup is not possible in this case using the methodology developed in Section 6.4.3.1.

The critical buckling option was used in a WIMS-CRNL simulation with the 30(37)-1.3-25-6.4478-CC model. This resulted in no change in the infinite multiplication factor for fresh fuel, but by 10500 MWd/MgU, the infinite multiplication factor was 7 mk higher than in the reference case. At 21000 MWd/MgU, the infinite multiplication factor in the critical buckling case was 2 mk lower than in the nominal case.

7.9.5 DSN vs PIJ Main Transport Calculations

The DSN (annularized, one dimensional transport calculation) option (see Appendix F.2) of WIMS-CRNL was used in the simulations discussed in this chapter. For the purposes of comparison, the more detailed two-dimensional collision probability PIJ option (see Appendix F.3) was used to simulate a 30(37)-1.3-25-6.4478-CC lattice. As recommended by Phillips (1982), 25 lines and 10 angles were chosen in the PIJ mesh. Six-fold symmetry was employed.

Compared to the DSN case, the PIJ case cost more than 3 times as much to run on the AECL-CRNL CYBER mainframe computer. The initial k-eff increased by 0.4 mk. The achievable burnup increased by 0.2%, and the coolant void reactivity decreased by 0.6 mk. The agreement between the two methodologies is excellent.

In this thesis, the DSN option was used for the initial scoping studies and sensitivity analyses. The final fuel bundle designs selected were analyzed using the more detailed WIMS-CRNL PIJ technique.

7.9.6 Modelling a Variation in Fuel Temperature

The standard fuel temperature used in the WIMS-CRNL simulations was 960 K. Because the outer fuel elements produce more power, they operate at higher temperatures than the inner elements. To bound the effect of this variation, two additional lattice physics simulations were performed with the 30(37)-1.3-25-6.4478-CC model. The first case included an inner fuel ring at 960.16 K and an outer fuel ring at 1100 K. In the second case, both rings of fuel elements were simulated at 1100 K. Achievable burnup was reduced by approximately 0.3% in both cases in comparison with the reference case.

7.10 ENRICHMENT GRADING IN 30(37) ELEMENT FUEL

In a 37 element natural nominal CANDU-600 fuel bundle, the power per

fuel pin is not uniform throughout the bundle, as noted in Table 7-1. The bundle power limits are derived such that fuel element centre-line melting or fuel sheath dryout will not occur. A more uniform power distribution across the bundle will allow operation at higher bundle powers without over-rating the highest powered fuel pins. As a figure of merit, the N_{eq} (N equivalent) parameter is often considered in fuel bundle performance analysis. This parameter is defined as:

$$N_{eq} = \sum_{i} p_i / p_m \qquad (7.10\text{-}1)$$

where the sum is over all elements, i,

p_i = the element power, and,

p_m = the maximum element power.

For fuel pencil diameters in the range of 1 to 2 cm, N_{eq} provides a good estimation of the relative fuel bundle power achievable (Orpen, 1984). For this range of element sizes, the tradeoff between a change in surface area as the element diameter is altered, is compensated for by a change in the distance from the surface to the element centre line, resulting in a fuel centreline temperature which is a function of element linear power (kW/m) only (Orpen, 1984).

For the natural nominal CANDU-600 37 element fuel bundle, N_{eq} is 32.6 at equilibrium conditions (based on WIMS-CRNL simulations). By increasing N_{eq}, the bundle can safely operate at higher powers.

In the 30(37)-1.3-25-6.4478-CC case, N_{eq} is approximately 28.2, on average. Enrichment grading (variation of initial fuel element enrichment) within the bundle can be employed to increase N_{eq} even further.

A series of lattice physics simulations were conducted with the 30(37)-1.3/XX-25-6.4478-CC model, in which the inner 12 fuel elements were enriched to 1.3 a/o U-235. The outer 18 elements were enriched from 0.72 to 1.3 a/o in the various cases. The inner pin to outer pin power ratio as a function of burnup is provided in Fig. 7-13 for a range of enrichment grading cases considered.

As can be seen in the figure, the effect of enrichment grading is

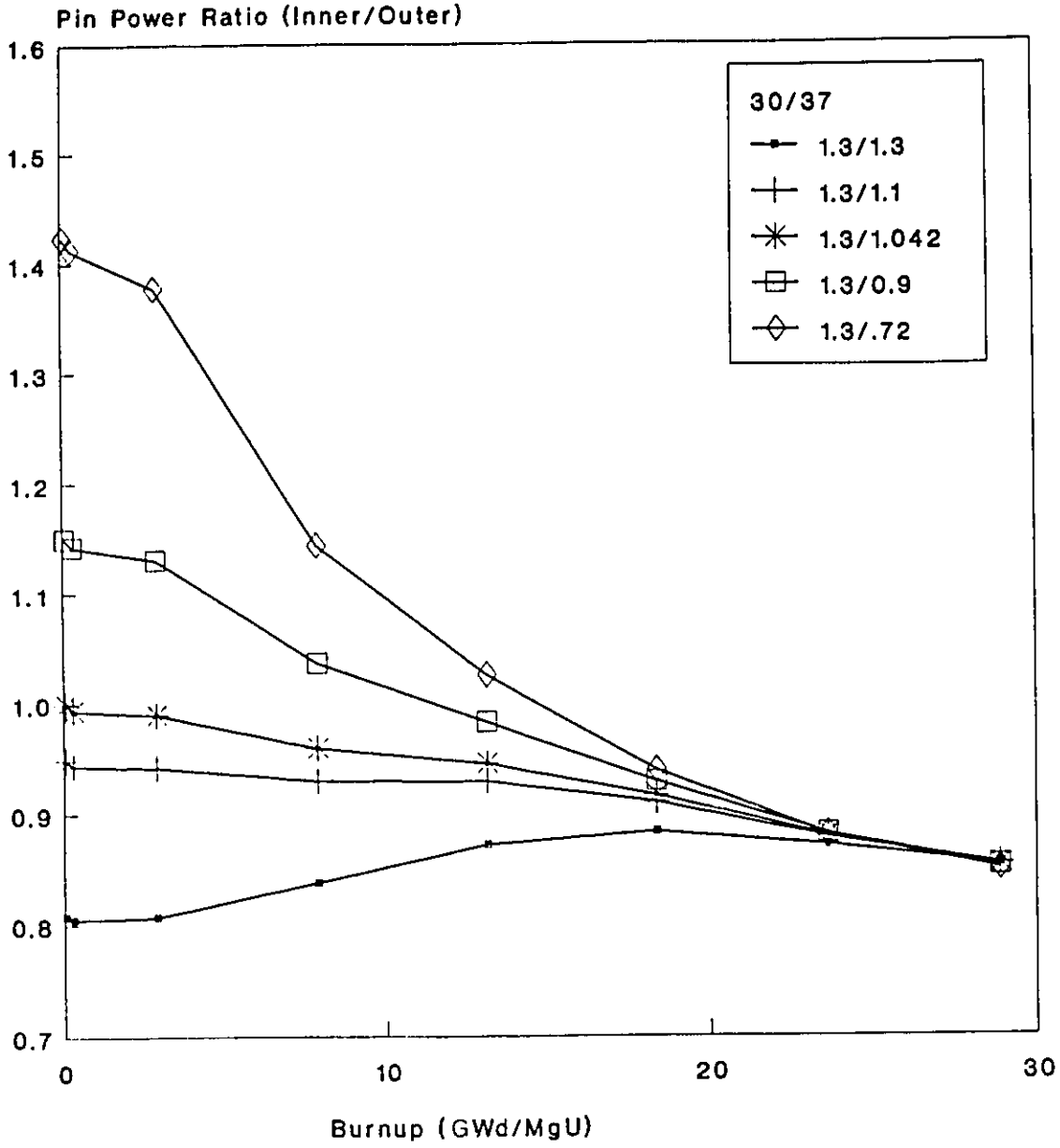

Figure 7-13 Effect of Burnup on Pin Power Ratio
Model: 30(37)-1.3/XX-25-6.4478-CC

largest at the initial burnup stages. As the burnup progresses, the U-235 concentration becomes diminished and the pin power ratio becomes independent of the initial enrichment grading.

Of the cases considered, the 1.3/0.9 enrichment grading case yielded the highest average N_{eq} (29.7). The 1.3/1.042 case yielded an initial N_{eq} of 30.0, but over the 21000 MWd/MgU burnup period, the average N_{eq} was only 29.4.

Achievable burnup and void reactivities calculated for a number of cases are given in Table 7-14. As is evident from the table, when the initial enrichment is decreased in the outer ring of fuel elements, the inner ring becomes increasingly important to the overall fuel behaviour and therefore the void reactivity effect (which is greatest in the inner fuel elements) is enhanced. As the burnup proceeds, the U-235 in the inner ring in the 1.3/NAT case burns out faster than in the 1.3/1.3 case. This, combined with the harder neutron spectrum in the 1.3/1.3 case, results in a void reactivity effect which is larger in the non-graded design at 10500 MWd/MgU and beyond.

7.11 FUEL ELEMENT RADIUS AND ENRICHMENT GRADING

As noted in Section 7.10, enrichment grading allows the flexibility to adjust the inner/outer pin power ratio under fresh fuel conditions. However, as the burnup proceeds, the pin power ratio tends to a value independent of the initial fuel enrichment.

Variation of the fuel element radii provides an additional means of influencing pin power ratios, and, as shall be demonstrated, the effect is evident over the entire fuel burnup range. Such element diameter variations have been considered by Gacesa et al. (1983) (33 element fuel) and Hatton and Barns (1980) (28 to 39 element fuel). Designs with up to 61 fuel elements and up to 3 separate element diameters have been evaluated (Barns, 1979). These designs were geared towards use with natural uranium fuel.

Inner Ring Fuel Enrichment (a/o U-235)	Outer Ring Fuel Enrichment (a/o U-235)	Achievable Burnup (MWd/MgU)	Void Reactivity at 0 MWd/MgU (mk)	Void Reactivity at 10500 MWd/MgU (mk)
1.3	0.720	15556	8.3	3.6
1.3	0.800	16952	-	-
1.3	0.900	18570	-	-
1.3	1.000	20077	6.5	4.0
1.3	1.042	20685	-	-
1.3	1.100	21523	-	-
1.3	1.200	22924	-	-
1.3	1.300	24252	5.2	4.2

Table 7-14 Effect of Enrichment Grading (Model 30(37)-1.3/XX-25-6.4478-CC)

7.11.1 Design Modifications

The basic structures of the modified fuel bundle designs considered in this section are given in Tables 7-15 and 7-16. All bundle designs were derived from the basic 30(37) model.

For bundle designs B1 through B6, the DSN (one-dimensional) transport scheme in WIMS-CRNL was used. For all other cases, the PIJ (two-dimensional) scheme was used (Donnelly, 1986).

The computer code, TESHOM (Griffiths, 1978), which is used to set up initial WIMS-CRNL models, assigns annuli according to the methodology discussed in Section 6.4.2 with the AREA annularization process. The annulus sizes are such that the annulus volume per fuel pin is the same in both fuel rings. While this is correct for equal sized elements, it is not acceptable for elements of different sizes, due to the nature of the SPECTROX calculations (Appendix F). A small FORTRAN computer code, TESHFIX, was written to modify the annulus radii within the fuel region such that the fuel/coolant volume ratio was constant in each fuel annulus. (Note that TESHFIX, and two additional codes, INTSPAC and ENRGRAD (discussed below), are undocumented computer codes prepared by the author specifically for the analysis conducted in support of this thesis.)

The TESHFIX code has two annularization options. The first, OPT1, yields annuli (proceeding radially outward from the bundle centre) of: carbon core; core sheath; fuel/coolant inner ring; coolant gap; fuel/coolant outer ring; and coolant gap (similar ordering as provided by TESHOM). The second option, OPT2, yields annuli of: carbon core; core sheath; coolant gap; fuel/coolant inner ring; fuel/coolant outer ring; and coolant gap. OPT1 was used for cases B1, B2 and B3. In all subsequent cases, OPT2 was used, since the OPT1 methodology resulted in overlapping annuli for the particular designs considered.

The imposed design requirements to maintain the amount of UO_2 constant in the fuel bundles (for design consistency) and to maintain a 1 mm minimum separation (Hatton and Barns, 1980) between fuel elements within a ring and between rings, were enforced through the application of the FORTRAN

Bundle Identifier	Enrichment (a/o U-235)		Number of Elements		Inner/Outer Ring Fuel Pencil Radius Ratio	Fuel Pencil Radius (cm)		Pitch Circle Radius (cm)	
	Inner Ring	Outer Ring	n_1 Inner Ring	n_2 Outer Ring		r_1 Inner Ring	r_2 Outer Ring	R_1 Inner Ring	R_2 Outer Ring
30(37)	1.3	1.3	12	18	1.00	0.6077	0.6077	2.8753	4.3307
B1	1.3	1.3	12	21	1.08	0.6077	0.5626	2.8753	4.3307
B2	1.3	1.3	12	21	1.08	0.6077	0.5626	2.8753	4.4000
B3	1.3	1.3	14	21	1.00	0.5626	0.5626	2.8753	4.4000
B4	1.3	1.3	14	21	1.00	0.5626	0.5626	3.0000	4.4000
B5	1.3	1.3	14	21	1.10	0.5944	0.5404	3.0800	4.4179
B6	1.3	1.3	14	21	1.21	0.6266	0.5188	3.1600	4.4409
B7*	1.3	1.3	14	21	1.10	0.5944	0.5404	3.0800	4.4179
B8*	1.3	1.3	14	21	1.07	0.5853	0.5470	3.0400	4.4100
B9*	1.3	1.2	14	21	1.07	0.5853	0.5470	3.0400	4.4100
B10*	1.3	1.3	14	21	1.07	0.5853	0.5470	3.0400	4.3600
B11*	1.3	1.3	14	21	1.07	0.5853	0.5470	3.0900	4.4100
B12*	1.6	1.5	14	21	1.07	0.5853	0.5470	3.0400	4.3600
B13*	1.7	1.5	14	21	1.07	0.5853	0.5470	3.0400	4.3600
B14*	1.7	1.53	14	21	1.07	0.5853	0.5470	3.0400	4.3600
B15*	1.6	1.6	14	21	1.07	0.5853	0.5470	3.0400	4.3600

* Cases identified with an asterisk were performed with the PIJ option in WIMS-CRNL. Other cases were performed with the DSN option.

Table 7-15 Basic Structure of Fuel Bundles: 12/21 and 14/21 Cases

Outer Radius of Fuel Pin (cm)	Outer Radius of Air Gap (cm)	Outer Radius of Element (cm)	Fuel Sheath Thickness (cm)
0.5188	0.5233	0.5591	0.0358
0.5404	0.5449	0.5821	0.0372
0.5470	0.5515	0.5892	0.0377
0.5626	0.5671	0.6059	0.0388
0.5853	0.5898	0.6301	0.0403
0.5944	0.5989	0.6399	0.0410
0.6077	0.6122	0.6541	0.0419
0.6266	0.6311	0.6700	0.0389*

* Except as noted with an asterisk, all fuel sheaths have (thickness/diameter) = constant.

Note: In all cases air gap is 0.0045 cm in width.
Refer to Table 7-15 for application in given fuel bundles.

Table 7-16 Basic Dimensions of Fuel Elements 12/21 and 14/21 Cases

computer code INTSPAC. With this code, the user inputs the number of elements in each ring and the radius ratio. The code then determines the appropriate fuel pin radii. The space between the fuel pin and sheath is maintained constant at 0.0045 cm (nominal CANDU-600 value) and the sheath thickness is adjusted such that sheath thickness / sheath radius is held constant at the nominal CANDU-600 value of 0.0641. Finally, based on geometric considerations, the code determines the separation between elements in each ring for a range of ring radii. Minimum ring radii are determined such that the interelement spacing is not less than 1 mm. Additional consideration must be given to the available radius choices such that adequate inter-ring spacing and carbon core and pressure tube clearances are maintained.

For the calculation of inner to outer pin power ratios a computer code ENRGRAD was prepared to manipulate the WIMS-CRNL output and provide these values as a function of irradiation.

Each of the fuel designs noted in Table 7-15 are considered in detail in Sections 7.11.2 and 7.11.3.

7.11.2 Increasing the Number of Fuel Elements

The 30(37) fuel bundle design can yield at best an N_{eq} of 30. However, as noted in Section 7.10, for natural nominal CANDU-600 37 element fuel, N_{eq} is 32.6 (based on WIMS-CRNL simulations). One way to increase N_{eq} is to increase the number of fuel pencils in a ring.

7.11.2.1 12/21 Fuel Bundle Design

The WIMS-CRNL code (Donnelly, 1986) was used to investigate the behaviour of a 12/21 fuel bundle, which is similar to the 30(37) design, except that the 18 outer elements are replaced by 21 elements of a smaller diameter. This yields an inner ring of 12 elements and an outer ring of 21 elements surrounding a graphite core.

The 21 elements in the outer ring of bundle design B1 in Table 7-15, were sized such that the total amount of uranium in the bundle was equal to

that in the 30(37) element design. Hence the outer ring fuel pin radii were reduced to 0.5626 cm, and the inner 12 pins were maintained with radii of 0.6077 cm. The ring pitch radii were not modified. From Table 7-17, it can be seen that the redesign resulted in a slight decrease in achievable burnup and a minimal increase in void reactivity.

The B1 design yielded an initial inner/outer pin power ratio (denoted as PR) of 0.943 (N_{eq} = 32.3). This increased to 1.02 at 24000 MWd/MgU (N_{eq} = 32.6).

For a given number of fuel elements in a bundle design, it is optimal to maintain a PR of 1.0. Hence the PR can also be used as a figure of merit.

In the B2 design, the elements were sized as in the B1 model, but the pitch radius of the outer ring of fuel elements was increased to 4.4 cm, yielding a bundle outer radius of approximately 5 cm (not including bearing pads). As can be seen in Table 7-17, the increased separation between element rings reduced the achievable burnup and increased the void reactivity. The PR was 0.939 initially, and 1.01 at 24000 MWd/MgU.

7.11.2.2 14/21 Fuel Bundle Design

To further increase N_{eq}, a 14/21 bundle design, B3, was considered. This yielded a PR of 0.80 initially, and 0.87 at 24000 MWd/MgU (N_{eq} = 32.2 and 33.2, respectively). As can be seen in Table 7-17, burnup and void reactivity were much more sensitive to the change in inter-ring spacing than to the change from a 12/21 to a 14/21 fuel bundle design.

Bundle design B4 was similar to B3, except that the inner ring pitch radius was increased to 3.0 cm, and the TESHFIX OPT2 annulus structure was chosen (see Section 7.11.1). This resulted in a small increase in achievable burnup and void reactivity in comparison with the B3 case (Table 7-17). The PR was initially 0.81, and at 24000 MWd/MgU it was 0.87, similar to the B3 case.

In bundle designs B1 through B4, the amount of fuel per fuel ring and per fuel bundle was the same as in the 30(37) case. In case B5, the total amount of fuel in the bundle was unchanged, but the distribution between rings

Bundle Identifier	Description**	Achievable Fuel Burnup (MWd/MgU)	Coolant Void Reactivity at 10500 MWd/MgU (mk)
30(37)	12/18 (1.00) 1.3/1.3	24305	4.2
B1	12/21 (1.08) 1.3/1.3	24250	4.4
B2	12/21 (1.08) 1.3/1.3	24198	5.1
B3	14/21 (1.00) 1.3/1.3	24194	5.2
B4	14/21 (1.00) 1.3/1.3	24225	5.4
B5	14/21 (1.10) 1.3/1.3	24247	4.9
B6	14/21 (1.21) 1.3/1.3	24313	4.6
B7*	14/21 (1.10) 1.3/1.3	24357	4.3
B8*	14/21 (1.07) 1.3/1.3	24352	4.4
B9*	14/21 (1.07) 1.3/1.2	23087	4.3
B10*	14/21 (1.07) 1.3/1.3	24395	3.8
B11*	14/21 (1.07) 1.3/1.3	24373	4.3
B12*	14/21 (1.07) 1.6/1.5	29301	-
B13*	14/21 (1.07) 1.7/1.5	30305	-
B14*	14/21 (1.07) 1.7/1.53	30633	-
B15*	14/21 (1.07) 1.6/1.6	30553	-

* PIJ cases.
** Data in the description column identify the number of elements in the inner and outer ring, the ratio of inner ring pellet diameter to the outer ring pellet diameter, and the inner and outer ring element fuel enrichment (in a/o U-235).

Table 7-17 WIMS-CRNL Results: 12/21 and 14/21 Cases

was altered. The inner/outer pin radius ratio (RR) was 1.1, as opposed to 1.0 in the B4 design. This redistribution of fuel was accompanied by an adjustment of the inner ring pitch radius to 3.08 cm which yielded an inter-element spacing of 1 mm. Further, the outer ring pitch radius was adjusted to 4.4179 cm, to yield a 5 cm radius bundle (not including bearing pads). The objective of these and subsequent modifications was to maintain the PR as close to 1.0 as possible and thereby maximize the value of N_{eq} in the 14/21 design.

From Table 7-17, it can be seen that in comparison with case B4, the B5 case has comparable burnup and a 0.5 mk reduction in void reactivity. The initial PR was 0.98, and at 24000 MWd/MgU, it was 1.05.

In bundle design B6, the RR was increased to 1.21. The outer pitch radius was adjusted to yield a 5 cm radius bundle. The inner element sheaths were reduced in thickness from the value required. The inter-pin spacing was reduced to 0.5 mm, which is considered unacceptable. Burnup was improved and the void reactivity was 0.8 mk lower than that calculated with the B4 design. The PR was initially 1.18 and increased to 1.26 at 24000 MWd/MgU. Clearly this design is unacceptable.

Design B7 is the same as B5, except that the PIJ option (Donnelly, 1986) in WIMS-CRNL was used in the simulation. Achievable burnup was increased by 0.5% and the coolant void reactivity at 10500 MWd/MgU was reduced by 0.6 mk. The inner/outer pin power ratio was not altered appreciably.

Designs B8, B10, and B11 are of the form 14/21 (1.07) 1.3/1.3 (inner ring contains 14 elements; outer ring contains 21 elements; inner/outer pin radius ratio is 1.07; inner and outer elements enriched to 1.3 a/o U-235). In design B8, the inner ring pitch radius was such that the spacing between elements was 1 mm. The outer ring pitch radius was chosen to yield a 5 cm radius bundle (not including bearing pads). With this design, the spacing between elements on the outer ring is 1.4 mm and the inter-ring spacing (distance between outside edge of inner ring elements and inside edge of outer ring elements) was 1.5 mm.

In design B10, the radius of the outer ring was reduced by 0.5 mm, to 4.36 cm and the radius of the inner ring was maintained at 3.04 cm. The

inter-ring spacing was reduced to 1 mm. The spacing between elements on the outer ring was 1.25 mm. Tightening the space between the element rings in this way reduced the void reactivity by approximately 0.6 mk, and increased achievable fuel burnup by 0.2% (in comparison with the B8 design).

In design B11, the 1 mm inter-ring spacing was maintained as in case B10, though both fuel ring pitch radii were increased by 0.5 mm, again yielding a 5 cm bundle. In this case, the spacing between elements on the inner ring was 1.24 mm, and on the outer ring, the spacing was 1.40 mm. The void reactivity was only reduced by 0.1 mk in comparison with design B8. Achievable burnup was comparable. Hence, the B10 case, which minimized the amount of coolant within the bundle structure was found to be optimal.

In all three cases, the PR varied with burnup in a similar fashion, starting at approximately 0.93, and approaching 1.00 at 24000 MWd/MgU.

7.11.3 Enrichment Grading in a 14/21 (1.07) Bundle

The 14/21 (1.07) 1.3/1.3 bundle design discussed in Section 7.11.2.2 yielded a PR of 1.00 only near the end of its burnup life, whereas initially, it was only 0.93. In order to increase the power flattening in the early burnup stages, enrichment grading can be implemented. As discussed in Section 7.10, enrichment grading increases the initial PR without substantially affecting the PR in high burnup bundles (due to the depletion to the initial U-235).

7.11.3.1 14/21 (1.07) 1.3/1.2 Fuel Bundle Design

By reducing the outer ring enrichment to 1.2 a/o U-235 and maintaining the inner ring enrichment at 1.3 a/o U-235 (design B9), the void reactivity is reduced by 0.1 mk (in comparison with the B8 case) and the achievable burnup is reduced by 5% (due to reduction in the average element enrichment).

The pin power distribution is improved with this design, as shown in Figure 7-14, which provides the PR for a number of pin size grading cases, and for the 14/21 (1.07) 1.3/1.2 (B9) case. The advantages of concurrent pin size and

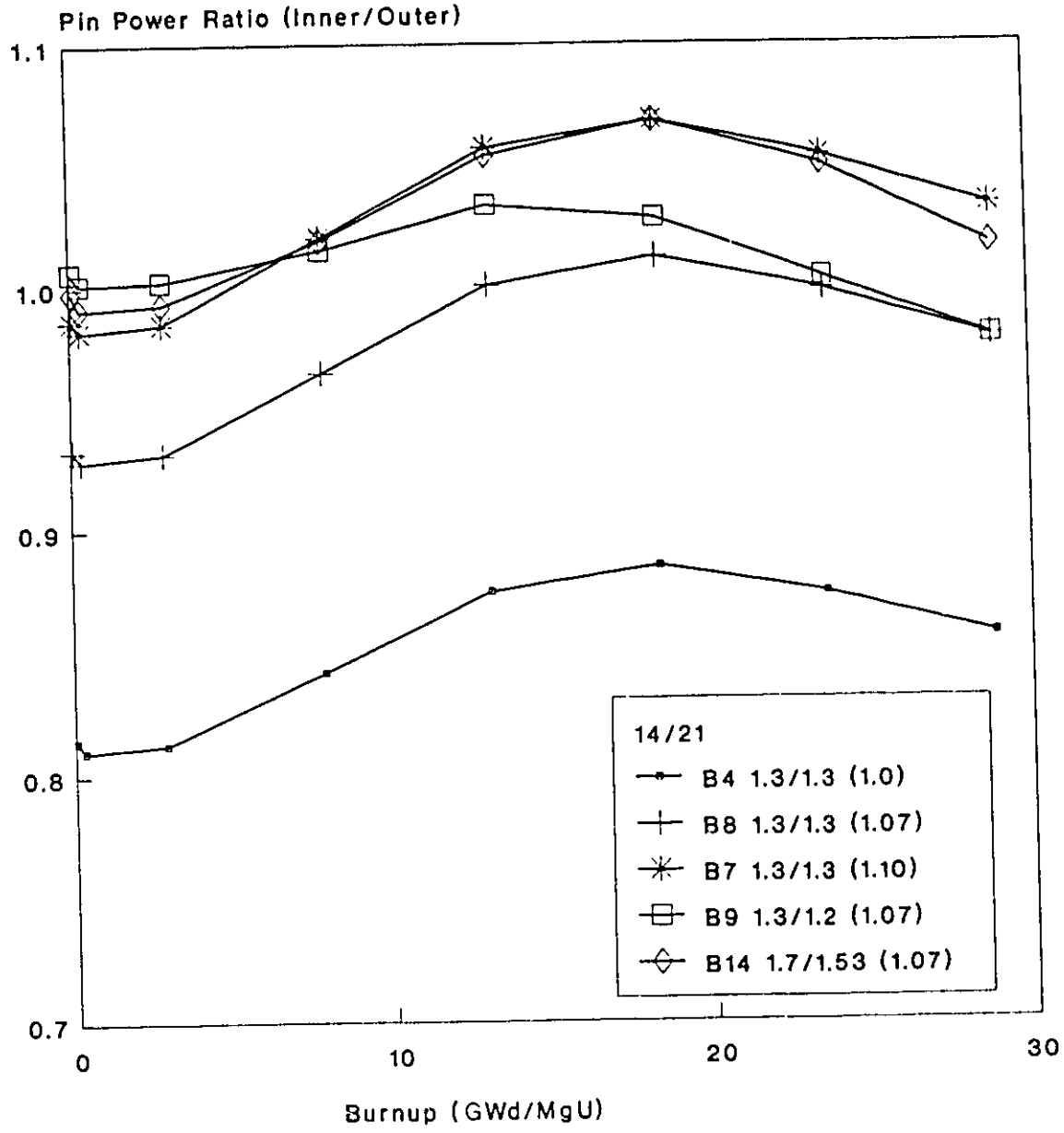

Figure 7-14 Effect of Burnup on Pin Power Ratio (Inner/Outer)
14/21 Element Fuel Pin Size Grading
(Note: xx/yy refers to enrichment graded bundle)

enrichment grading within a fuel bundle are evident in the figure. The PR for design B9 ranged from 1.00 initially, to a maximum of 1.034 (at 13000 MWd/MgU), and was reduced to 1.00 by the time the bundle reached its expected achievable burnup of 23000 MWd/MgU. The N_{eq} was at no time less than 34.3.

7.11.3.2 Higher Enrichments

For higher fuel burnups, higher initial fuel enrichments are required. A series of cases, B12 through B15 were considered, using the same basic 14/21 (1.07) bundle design. As can be seen from Figure 7-14, the 1.7/1.53 enrichment grading case (design B14) yields an initial PR of 1.00, though it peaked at 1.068 at 18000 MWd/MgU, and returned to 1.017 after 29000 MWd/MgU. At the PR peak, N_{eq} was reduced to 33.7, though initially, when fuel bundles are usually operating at their highest powers, the N_{eq} was 35. This is to be compared with the B15 design (enrichment 1.6 a/o U-235 no grading). In this case the initial PR was 0.91. It reached a maximum of 1.03, and returned to 1.00 at 29000 MWd/MgU.

It can be seen that as the enrichment is increased, the variation in PR throughout the burnup life of a bundle is also increased. Enrichment grading in the B14 design does not provide the same degree of pin power ratio flattening as in the B9 design (Section 7.11.3.1). Nevertheless, it represents an improvement over the non-graded design.

Similar WIMS-CRNL simulations were conducted to examine the 14/21 (1.07) design with natural uranium in both rings of elements. From fresh fuel to discharge, the PR ranged between 0.98 and 0.99.

At this stage one can envisage a reactor designed to accept bundles of various fuel enrichments, ranging for example, from natural to 1.3/1.2 to 1.7/1.53 enrichment graded designs. Economics and availability would dictate the fuelling option chosen. As conditions varied, so too could the feed fuel enrichment. To afford ease of implementation of the various options within a single reactor, there is an incentive to maintain a geometrically invariant bundle design (eg. 14/21 (1.07)), independent of the fuel enrichment. This would minimize the effect on the fuel channel thermohydraulics, and thereby

minimize the process system and secondary side modifications required when the fuel enrichment is altered. It is in the context of this scenario that this thesis continues to explore.

7.11.4 Heat Removal Capability and Maximum Operating Power

In comparison with the nominal CANDU-600 37 element natural uranium fuel bundle design (NATNOM), the 14/21 (1.07) designs considered in Section 7.11.3 have only 85.2% of the coolant flow area. The wetted perimeter (bundle and inner pressure tube surfaces) is reduced by 3%.

To remove the same amount of power in a channel fuelled with 14/21 bundles as in the case with NATNOM bundles, for a given set of reactor outlet header conditions, the flow velocity may have to increase, and/or the inlet temperatures may have to be reduced. Even without increasing the flow velocity, the pressure drop across the fuel channel would tend to be higher due to the additional constriction of the 14/21 bundle design.

While thermohydraulic analysis of the modified fuel bundle design is beyond the scope of this study, the following series of points are to be noted.

(a) Channel power in CANDU reactors is limited such that fuel centre line melting or fuel sheath dryout will not occur. This is known as the critical channel power. (Licence power limits are appreciably below these limits.)

(b) The limiting heat flux is referred to as the critical heat flux (or CHF). Upon reaching this condition, a small increase in the inlet temperature, or reduction in the flow rate results in an inordinate deterioration of the heat transfer rate in the system (Marinelli, 1977).

(c) At present, CHF correlations for various fuel bundle designs are obtained by empirical methods and are used to determine critical

channel powers (Wahba and Lorenc, 1984).

(d) It has been found that the CHF can be increased considerably in ribbed tubes above certain mass velocities for which swirling action (which promotes droplet formation) is enhanced (Marinelli, 1977).

(e) Groeneveld and Goel (1978), found that by decreasing the grid spacer pitch, the CHF could be increased more than 250%. These researchers also found that the CHF was enhanced by modifying bundle end plates to block the flow in larger subchannels, or through the use of twisted tape, lips, or mixing vanes. These modifications are generally accompanied by an increase in the pressure drop across the fuel channel. Macdonald (1985) found that the addition of four extra planes of spacer and bearing pads increased the critical channel power by up to 20%.

(f) By ensuring proper bundle alignment, and through the use of innovative end plate designs, the impact of the 14/21 design on channel pressure drop can be minimized. Strategic design of the carbon core surface can enhance mixing and therefore enhance the CHF. All elements in the graded 14/21 bundles will operate at approximately uniform power levels, with N_{eq} considerably greater than in the NATNOM case. This will tend to enhance the critical channel power.

(g) For a given set of reactor outlet header conditions, an increased pressure drop can be accomodated by an increase in the inlet header pressure. This would require an increased pressure tube wall thickness. As noted in Section 7.8.6, the use of enriched zirconium minimizes the economic penalty associated with such a modification.

Considerable experimental thermohydraulic analysis would be required to characterize and fine-tune the 14/21 bundle design prior to

implementation. For the purposes of this study, however, it is assumed that the 30(37) bundle can operate at powers comparable to those achievable with the NATNOM design.

7.12 REFINEMENTS TO THE FUEL BUNDLE MODELS

The WIMS-CRNL (Donnelly, 1986) models used in the previous sections did not include bundle end plates. Bundles were assumed to be operating at maximum power levels, and leakage and burnup calculations were conducted with the input nominal CANDU-600 buckling.

In this section, refinements to the lattice models are discussed. These modifications were included in the final lattice physics simulations of the NATNOM and 14/21 fuel designs (natural, 1.3/1.2, 1.7/1.53 enrichment graded). Model changes consisted of:

(a) Operating power level reduction to 611 kW/bundle.

(b) Modelling of bundle end plate and adjustment of fuel density.

(c) Use of critical buckling in burnup calculations.

(d) Use of PIJ transport calculation option.

7.12.1 Fuel Density and Operating Power Density

The maximum time-averaged CANDU-600 channel power is 800 kW, and the effective (flux-squared-weighted) to maximum thermal flux ratio is 0.764 (Tin, 1981). To more appropriately reflect average operating conditions, a bundle power of 800 x 0.764 = 611.2 kW was assumed in the refined models.

The NATNOM fuel bundle is 49.53 cm in length and contains 18.8 kgU or 21.326 kg UO_2 (Tin, 1981). With a fuel pin radius of 0.6077 cm, a stack length of 48.03 cm, and a total of 37 fuel elements (Tin, 1981), the effective density of the fuel along the stack length (including void spaces between pellets) is 10.3435 g/cm^3. Since the fuel bundle end plates were to be simulated explicitly (see Section 7.12.2) this fuel density was appropriate for the modified models.

With this same fuel density in the 14/21 (1.07) designs (inner ring

fuel pin radius 0.5853 cm, outer ring fuel pin radius 0.5470 cm) and assuming a 50 cm bundle length with a stack length of 50 x (48.03/49.53) = 48.49 cm, the total amount of UO_2 in a 14/21 (1.07) bundle is 17.456 kg (equivalent to 15.388 kgU).

The power density in the WIMS-CRNL NATNOM model was reduced to 611.2/18.8 = 32.51 MW/MgU (initial). In the 14/21 cases, it was adjusted to 611.2/15.388 = 39.719 MW/MgU (initial).

The basic structure of the finalized 14/21 fuel lattice is summarized in Table 7-18.

7.12.2 Fuel Bundle End Plates

Fuel bundle end plates (or end caps) were added to the final WIMS-CRNL bundle models. This modification introduces an additional material in the model which is added following the main transport calculations (Donnelly, 1986) in WIMS-CRNL.

The WIMS-CRNL ENDCAP option was used to effectively smear the endcap region zirconium/air/heavy water over 3.03% of the bundle length and extending radially from the bundle centreline to the pressure tube inside radius.

Using CANDU-600 bundle design data, the simulated endcap region composition was determined to be:

deuterium:	2.13 w/o
hydrogen:	0.01 w/o
oxygen:	8.56 w/o
iron:	0.19 w/o
zirconium:	89.01 w/o
boron:	0.0003 w/o
chromium:	0.09 w/o

The endcap region material was simulated as having an effective density of 3.478 g/cm^3, and a material temperature of 563 K.

The code internally multiplies the average flux in the fuel/coolant region by an input flux peaking factor, d, to determine the appropriate endcap

Lattice Cell / Fuel Bundle Property	Value
Lattice Pitch (cm)	25.0
Bundle Length (cm)	50.0
Number of Fuel Elements per Bundle	35.0
Pressure Tube (Zr-2.5% Nb)* Inside Radius (cm)	5.1689
Pressure Tube Wall Thickness (cm)	0.4343
Calandria Tube (Zr-2)* Inside Radius (cm)	6.4478
Calandria Tube Wall Thickness (cm)	0.1397
Coolant Temperature (average over channel) (°C)	290.0
Coolant D_2O Purity (atomic percent)	98.8
Moderator Temperature (°C)	68.0
Moderator D_2O Purity (atomic percent)	99.9
Fuel Element (sheath) Outside Radius (cm) (inner elements)	0.6301
Fuel Element (sheath) Outside Radius (cm) (outer elements)	0.5892
Sheath (Zr-4) Wall Thickness (cm) (inner elements)	0.0403
Sheath (Zr-4) Wall Thickness (cm) (outer elements)	0.0377
UO_2 Density (g/cm^3) (effective)	10.3435
UO_2 Weight per Bundle (kg)	17.456
U Weight per Bundle (kg)	15.388
Stack Length of Pellets in Fuel Bundle (cm)	48.49
Radius of First Element Ring Containing 14 Elements (cm)	3.04
Radius of Second Element Ring Containing 21 Elements (cm)	4.36
Angular Displacement of First Element Ring (radians)	0.2244
Angular Displacement of Second Element Ring (radians)	0.0
Carbon Core Radius (cm)	2.10065
Core Sheath Outer Radius (cm)	2.14255
Operating Power Density (MW/MgU initial)	39.719

* Enriched zirconium.

Table 7-18 Basic Structure of the Finalized 14/21 Fuel Lattice

region neutron flux for the reaction rate edits. A peaking factor of approximately 1.15 is appropriate for the natural nominal CANDU-600 37 element fuel bundle (NATNOM) (Chow, 1984), though based on WIMS-CRNL simulations, increasing this value to 1.30 only results in a 0.3 mk reduction in the initial effective multiplication factor and a 0.6% reduction in achievable burnup. A peaking factor of 1.15 was used for the NATNOM and 14/21 natural uranium designs. A peaking factor of 1.30 was assumed for the enriched fuel cases, due to the larger relative absorption in the fuel region in these cases.

7.12.3 Critical Buckling

As noted in Section 7.9.4, the use of the critical buckling option in the WIMS-CRNL burnup calculations yields cell averaged properties which are more appropriate for use in a three dimensional full core fuel management simulation (which will be considered beginning in Chapter 8). As such, the critical buckling option was used in the final WIMS-CRNL simulations.

7.12.4 PIJ Option

Because of the inherent increased accuracy afforded with the two dimensional PIJ transport calculation in WIMS-CRNL (Donnelly, 1986), this option was chosen for the final model simulations.

7.13 WIMS-CRNL SIMULATION RESULTS

7.13.1 General

Results of the lattice physics simulations conducted with the refined simulation models (Section 7.12) are depicted in Fig. 7-15 and 7-16, where k-eff and coolant void reactivity are plotted as a function of burnup for the various cases. Model names in the figures correspond to the element numbers and enrichments. That is, the 14/21, natural uranium fuel bundle is denoted

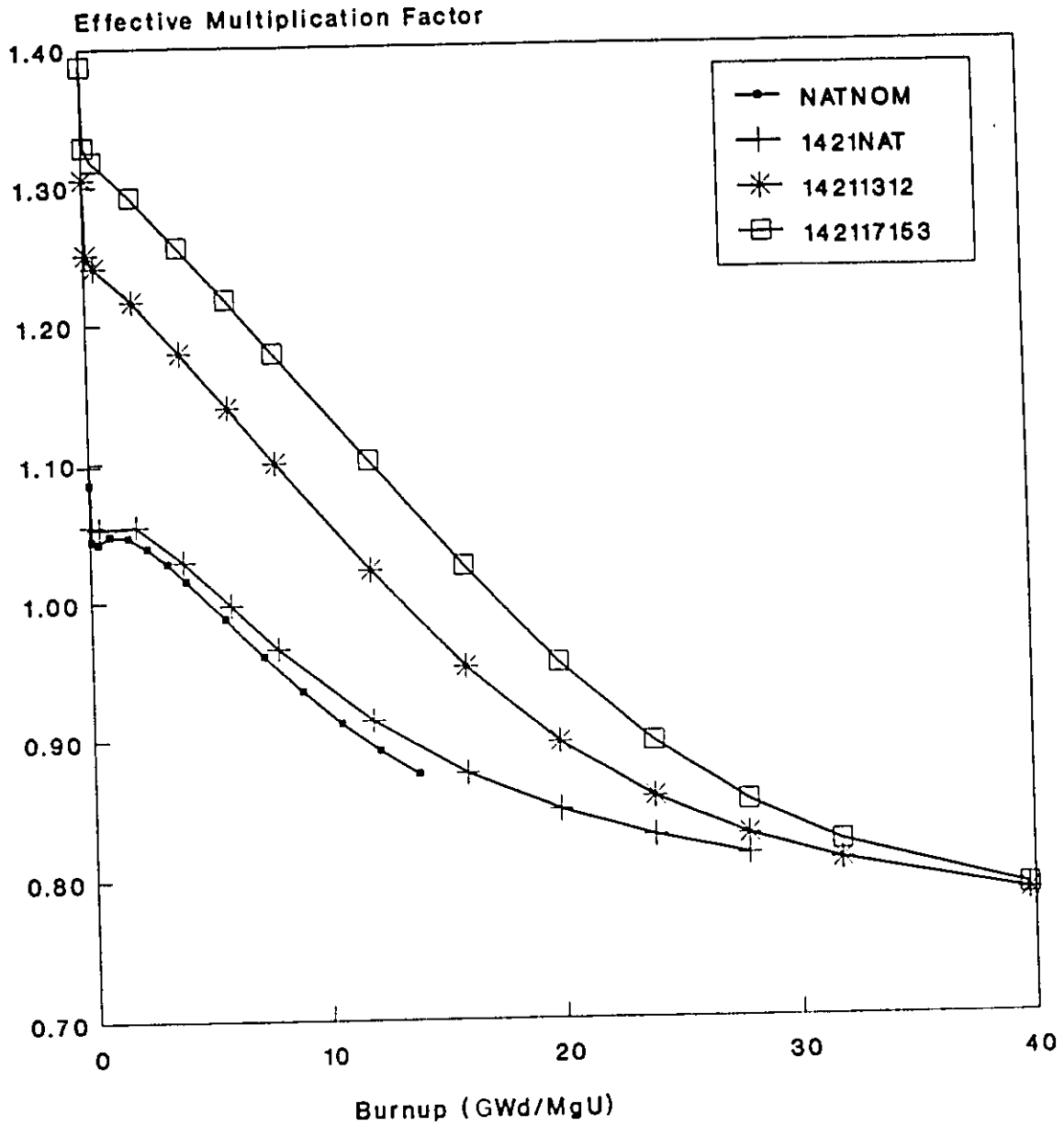

Figure 7-15 Burnup Dependence of k-eff

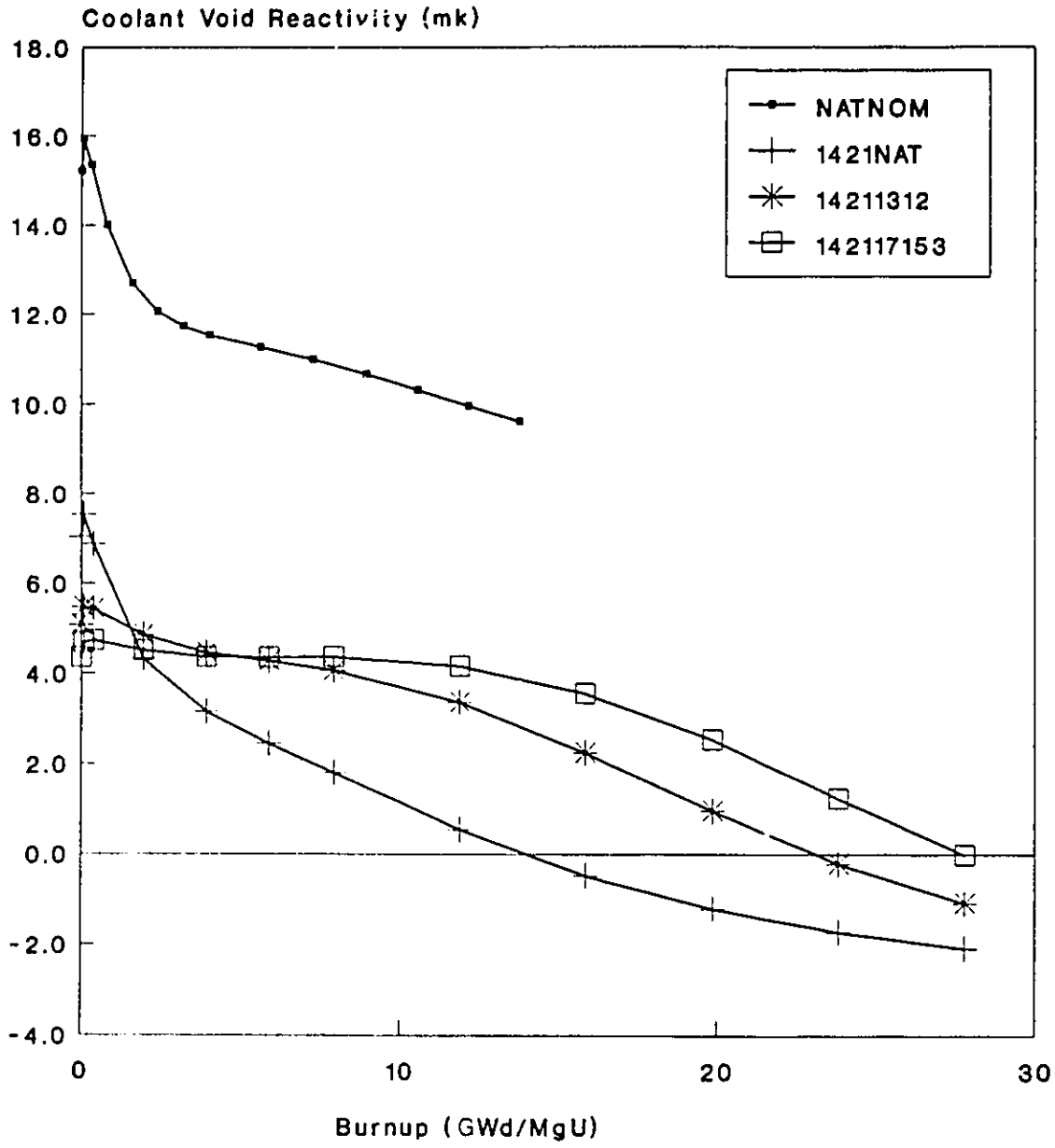

Figure 7-16 Burnup Dependence of Void Reactivity

"1421NAT", the 14/21 enrichment graded designs are denoted "14211312" and "142117153" for the 1.3/1.2 and 1.7/1.53 enrichment cases, respectively. The natural nominal CANDU-600 37 element model is denoted "NATNOM".

In Tables 7-19 through 7-22, fuel properties at various stages through the burnup period are provided. Isotope concentrations are quoted in terms of grams of material per centimeter of bundle length. (The natural nominal 37 element bundle is 49.53 cm in length. The 14/21 bundles are 50 cm in length.)

7.13.2 Fissile Composition of Spent Fuel

In Table 7-23, the fissile isotope concentration (taken as U-235, Pu-239, and Pu-241) in the spent fuel is compared for the four cases. As can be seen, the use of enriched fuel reduces the fissile concentration in the spent fuel on a per mass of spent fuel and a per unit energy production basis. This reduction in fissile concentration increases the expense involved in spent fuel fissile isotope recycling, but also increases the weapons proliferation resistance (Willrich, 1973) of the fuel cycle.

7.13.3 Effect of Lattice Pitch Variation

The effect on achievable fuel burnup of varying the lattice pitch for the various bundle designs from 24 cm to 28.575 cm is depicted in Fig. 7-17. These data are based on the results of a series of WIMS-CRNL simulations performed with the refined models discussed in Section 7.12, though the critical buckling option was not selected.

From Fig. 7-17, it can be seen that the achievable burnup is less sensitive to LP size as the enrichment is increased. Further the optimal LP size decreases as the U-235 concentration is increased. This is due to the fact that sufficient initial excess reactivity is available in the enriched cases to take advantage of the greater production and utilization of plutonium with a reduced LP (harder neutron spectrum).

Time (days)	Fuel Thermal Irradiation (n/kb)	Burnup (MWd/MgU)	Fast to Thermal Flux Ratio	Concentration of Isotopes (grams per cm of bundle length)				Fissile Concentration [U-235]+[Pu-239]+[Pu-241]	
				U-235	U-238	Pu-239	Pu-241	g/cm	Relative to Initial
0	0.0	0	0.420	2.70	376.77	0.00	0.00 E-0	2.70	1.00
50	0.6	1626	0.455	2.08	376.17	0.41	3.43 E-3	2.50	0.93
100	1.2	3251	0.470	1.63	375.57	0.67	1.76 E-2	2.31	0.86
125	1.5	4064	0.474	1.44	375.27	0.75	2.75 E-2	2.21	0.82
175	2.0	5689	0.480	1.12	374.66	0.87	5.10 E-2	2.04	0.75
225	2.6	7315	0.483	0.87	374.03	0.93	7.56 E-2	1.88	0.70
275	3.2	8940	0.486	0.67	373.40	0.97	9.97 E-2	1.74	0.65

Table 7-19 WIMS-CRNL Results: NATNOM

Time (days)	Fuel Thermal Irradiation (n/kb)	Burnup (MWd/MgU)	Fast to Thermal Flux Ratio	Concentration of Isotopes (grams per cm of bundle length)				Fissile Concentration [U-235]+[Pu-239]+[Pu-241]	
				U-235	U-238	Pu-239	Pu-241	g/cm	Relative to Initial
0	0.0	0	0.545	2.19	305.50	0.00	0.00 E-0	2.19	1.00
50	0.7	1986	0.611	1.59	304.89	0.40	5.17 E-3	2.00	0.91
100	1.4	3972	0.638	1.18	304.28	0.62	2.47 E-2	1.83	0.83
150	2.1	5958	0.652	0.87	303.66	0.74	5.09 E-2	1.66	0.76
200	2.8	7944	0.661	0.64	303.04	0.80	7.77 E-2	1.52	0.69
300	4.2	11916	0.673	0.34	301.74	0.85	1.28 E-1	1.31	0.60

Table 7-20 WIMS-CRNL Results: 1421NAT

Time (days)	Fuel Thermal Irradiation (n/kb)	Burnup (MWd/MgU)	Fast to Thermal Flux Ratio	Concentration of Isotopes (grams per cm of bundle length)				Fissile Concentration [U-235]+[Pu-239]+[Pu-241]	
				U-235	U-238	Pu-239	Pu-241	g/cm	Relative to Initial
0	0.0	0	0.680	3.78	303.91	0.00	0.00 E-0	3.78	1.00
50	0.5	1986	0.720	3.12	303.46	0.32	2.18 E-3	3.43	0.91
100	0.9	3972	0.732	2.56	303.01	0.54	1.28 E-2	3.11	0.82
200	1.9	7944	0.735	1.69	302.06	0.78	5.19 E-2	2.52	0.67
400	4.2	15888	0.719	0.63	299.90	0.89	1.38 E-1	1.66	0.44
600	6.8	23831	0.712	0.19	297.41	0.87	1.90 E-1	1.25	0.33

Table 7-21 WIMS-CRNL Results: 14211312

Time (days)	Fuel Thermal Irradiation (n/kb)	Burnup (MWd/MgU)	Fast to Thermal Flux Ratio	Concentration of Isotopes (grams per cm of bundle length)				Fissile Concentration [U-235]+[Pu-239]+[Pu-241]	
				U-235	U-238	Pu-239	Pu-241	g/cm	Relative to Initial
0	0.0	0	0.756	4.87	302.81	0.00	0.00 E-0	4.87	1.00
50	0.4	1986	0.788	4.19	302.43	0.28	1.43 E-3	4.47	0.92
100	0.8	3972	0.794	3.59	302.04	0.50	9.06 E-3	4.10	0.84
200	1.6	7944	0.792	2.58	301.21	0.76	4.08 E-2	3.38	0.69
400	3.4	15888	0.760	1.17	299.35	0.92	1.22 E-1	2.20	0.45
600	5.7	23831	0.732	0.42	297.12	0.90	1.79 E-1	1.49	0.31
800	8.4	31775	0.725	0.12	294.58	0.86	2.10 E-1	1.20	0.25

Table 7-22 WIMS-CRNL Results: 142117153

Fuel Type	Fuel Exit Burnup (MWd/MgU)	Fissile Material Concentration in Spent Fuel	
		($g/kgU_{initial}$)	(g/MWd)
NATNOM	6921	5.05	0.73
1421NAT	8379	4.87	0.58
14211312	23129	4.15	0.18
142117153	30568	3.99	0.13

Table 7-23 Spent Fuel Fissile Concentration

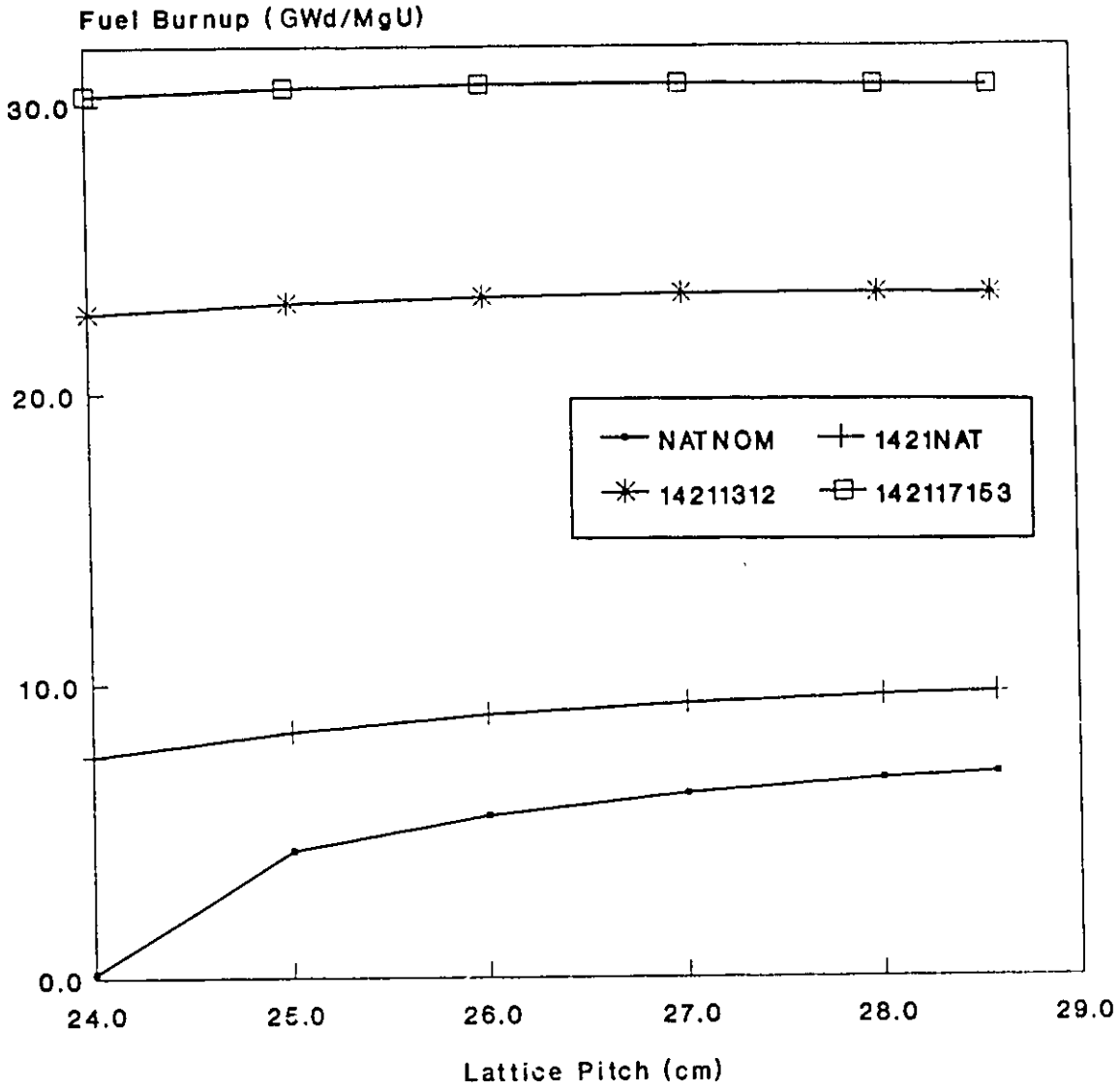

Figure 7-17 Effect of Lattice Pitch Size Variation on Achievable Fuel Burnup

7.13.4 Effect of Altering Operating Power Density: NATNOM

As noted in Section 7.12.1, the NATNOM bundle was simulated as operating at a power density of 32.51 MW/MgU. For comparison purposes, this was increased to 39.719 MW/MgU (the value used in the 14/21 cases). This had no effect on the infinite multiplication factor at zero burnup, but at 3500 MWd/MgU (one-half the nominal exit burnup), the infinite multiplication factor was reduced by 2 mk. This can be attributed to the slightly higher xenon reactivity load and neptunium hold-up (Np-239 decays to Pu-239) at higher power densities.

7.13.5 Effect of Flooding the Gas Gap

One type of accident which can occur in a CANDU reactor is the flooding of the gas gap between the pressure and calandria tubes with D_2O. In a CANDU-600 NATNOM fuel lattice, this causes an increase in local reactivity of 0.3 mk (based on WIMS-CRNL simulations at 0 burnup). In the 14211312 design, due to the harder neutronic spectrum, flooding the gas gap causes a 5.0 mk increase in local reactivity under fresh fuel conditions, rising to 10.7 mk at 28000 MWd/MgU. Such accidents are limited in scope when they occur, usually affecting only a single channel, and hence the global reactivity insertion is much smaller than the delayed neutron fraction. However, the potential for this type of accident occuring provides an incentive to use passive safety systems and potentially a non-conducting inert solid annulus between the pressure tube and calandria tube to eliminate such reactivity excursions. These proposals are considered again in Chapter 11.

7.14 KINETICS PARAMETERS

The computer code KINETIC (van Dyk, 1983) was used to determine appropriate kinetics parameters for the various bundle/lattice designs. This code extracts data from the WIMS-CRNL simulations and determines instantaneous and/or time-averaged kinetics properties.

The photoneutron yield per fission (KINETIC input parameter) defaults to a value of 8.53E-4 (appropriate for the NATNOM case). In the 14/21 cases, this was adjusted such that the photoneutron yield per fission was proportional to the lattice cell heavy water volume per effective volume of fuel operating at the maximum rating within a fuel bundle.

The burnup averaged kinetics properties are provided in Table 7-24. The prompt neutron lifetime data have been modified to account for the effect of the reflector, which is not included in the basic KINETIC calculations.

As can be seen, the average delayed neutron fraction decreases as enrichment increases. This can be attributed to the larger overall proportion of fissions in plutonium isotopes in the enriched cases. (The plutonium isotopes have a smaller delayed neutron fraction than U-235.) The equilibrium coolant void reactivity effect (Fig. 7-16) is less than the delayed neutron fraction for all of the 14/21 cases.

The smaller lattice pitch and harder neutron spectrum in the 14/21 cases results in a reduction in the prompt neutron lifetime. Increasing the enrichment also reduces this parameter. Note that the prompt neutron lifetime in all of the cases is considerably larger than the 6.0E-5 s value applicable in Light Water Reactors (see Chapter 5).

Having examined the lattice properties for the NATNOM and 14/21 fuel bundle designs, the next stage in the study is to analyze reactor operation and fuel management with these fuel designs. The ground work and full core model development are detailed in Chapters 8 and 9, and comprehensive fuel management studies are provided in Chapter 10.

Case*	Delayed Neutron Fraction	Decay Constant (s^{-1})	Prompt Neutron Lifetime** (s)
NATNOM	5.8 E-3	1.1 E-2	9.0 E-4
1421NAT	5.5 E-3	1.2 E-2	7.2 E-4
14211312	5.2 E-3	1.2 E-2	6.5 E-4
142117153	5.2 E-3	1.2 E-2	6.3 E-4

* Properties averaged from fresh to discharge burnup.
** Adjusted for reflector effects.

Table 7-24 Kinetics Parameters for Equilibrium Conditions

CHAPTER 8

STRATEGY FOR CORE CALCULATIONS

8.1 INTRODUCTION

To this point in the analysis, consideration has only been given to the neutronic characteristics of individual lattice cells. Fuel management calculations require an extension of the study to full reactor core three dimensional (3-D) simulations. In this chapter, discussion will focus on identifying the requirements for the simulation of enriched fuel reactor cores, and describing the detailed reactor models used in the fuel management studies.

8.2 NEUTRON DIFFUSION EQUATIONS

8.2.1 Multigroup Representation

The diffusion approximation to the neutron balance equation for a discretized neutron energy group, g, can be expressed as:

$$- \text{div } D_g \text{ grad } \phi_g + \Sigma_{ag} \phi_g + \sum_h (\Sigma_{gh} \phi_g - \Sigma_{hg} \phi_h) = \sum_h (\chi_{hg} \nu\Sigma_{fh} \phi_h) / k \qquad (8.2.1\text{-}1)$$

where:

D_g = the diffusion coefficient,
ϕ_g = the group g neutron flux,
Σ_{ag} = the group g absorption cross section,
Σ_{gh} = the scattering cross section from group g to group h,
Σ_{hg} = the scattering cross section from group h to group g,

χ_{hg} = the fraction of fissions induced by neutrons of energy group h, which yield neutrons born in energy group g,

$\nu\Sigma_{fh}$ = the production cross section for energy group h (product of the number of neutrons released per fission times the fission cross section), and

k = the effective multiplication factor.

The summations are over all energy groups, h, from 0 up to approximately 10 MeV. Further information on the derivation of the diffusion approximation can be found, for example, in Harms (1987), Henry (1975), and Lamarsh (1977).

The neutronic properties used in the diffusion equations are usually homogenized cell-averaged properties from lattice physics codes, such as those discussed in the previous chapters (See also Appendix B.).

8.2.2 Modified Two Group Representation

For most thermal reactor calculations it is often sufficient to consider only a modified two-energy group (M-2) representation:

$$\begin{aligned} -\text{div}\, D_1 \,\text{grad}\,\phi_1 + \Sigma_{a1}\phi_1 + \Sigma_m \phi_1 &= \nu\Sigma_f \phi_2 / k \\ -\text{div}\, D_2 \,\text{grad}\,\phi_2 + \Sigma_{a2}\phi_2 &= \Sigma_m \phi_1 \end{aligned} \qquad (8.2.2\text{-}1)$$

where:

subscripts 1 and 2 refer to the fast and thermal groups, respectively,

D = the diffusion coefficient,

Σ_a = the absorption cross section,

Σ_m = the moderation cross section (net slowing down, fast to thermal),

$\nu\Sigma_f$ = the production cross section, and

k = the effective multiplication factor.

It is noted that in Eq 8.2.2-1 all fissions are assumed to be induced by thermal neutrons, and the spectrum of the fission neutrons is entirely in the fast group. For the usual cutoff energies between the two groups

(e.g. 0.625 eV as in WIMS-CRNL (Donnelly, 1986)), the latter assumption is quite valid (see Duderstadt and Hamilton (1976)). The former assumption, however, is not valid unless the modified production cross section is obtained from the true two group cross sections via:

$$\nu\Sigma_f = \nu\Sigma_{f2} + \nu\Sigma_{f1}\,\phi_1/\phi_2 \qquad (8.2.2\text{-}2)$$

All data on the right hand side of Eq 8.2.2-2 are cell averaged properties obtained from an appropriate lattice code. The effects of fast neutron induced fissions are therefore incorporated directly into the production cross section.

Similarly, the fast moderation cross section is derived according to:

$$\Sigma_m = \Sigma_{12} - \Sigma_{21}\,\phi_2/\phi_1 \qquad (8.2.2\text{-}3)$$

8.3 ENERGY GROUP REQUIREMENTS

The choice of the energy group structure for use in reactor core analysis is determined by examining the increased accuracy afforded through the use of a large number of energy groups, and weighing this against the reduced computation time and expense associated with, for example, the modified two-group (M-2) representation. Indeed, the accuracy of the nuclear data will impose an upper limit on the number of energy groups to be considered.

Experience has shown that there is no advantage to simulating natural uranium fuelled CANDU reactor cores in more than two energy groups (Roshd, 1976). However for the purposes of fuel management analysis of heavy water moderated reactors fuelled with enriched uranium, it was necessary to determine whether the two group approximation would continue to be appropriate.

In Appendix B, details of the analysis conducted to address this question are provided. From a comparison of a three dimensional reactor core

simulation performed using four neutron energy groups, two neutron energy groups and the M-2 representation, it was found that the WIMS-CRNL generated M-2 approach would be sufficient for the fuel management calculations required in this analysis.

8.4 CORE CALCULATIONS

8.4.1 Introduction

The computer code FMDP (Wight and Sibley, 1977; Wight, Gold, and Marczak, 1979), the current standard code for CANDU fuel management calculations, was chosen for use in this analysis. (The Ontario Hydro version of the code is known as OHRFSP (Wight, 1987).) The FMDP code utilizes the M-2 energy group structure. The basic theory of the code is described in Section 8.4.2. (See also Frescura and Wight, 1982.)

8.4.2 Fuel Management Design Program - FMDP

The core of an on-power fuelled nuclear reactor which has been operating for a sufficient period such that all channels have been refuelled once, will contain fuel with different burnups ranging from fresh to discharge. It is an important aspect of reactor design to be able to calculate the core burnup and power distribution to ensure that safety and economic criteria are met.

For three dimensional diffusion theory calculations, it is often not practical to directly simulate the operating history of a reactor with a given fuel type for the length of time required to determine such parameters as discharge burnup, residence time, fuelling rates, and reference power distributions. Instead, approximate solutions and averaging techniques are utilized.

The difficulty lies in the fact that the cross sections used in the diffusion equations directly depend on the burnup, B, and since B depends on the neutron flux history of a bundle, the neutron flux and fuel burnup must be

solved in a manner to yield consistency between the parameters if true "average" values are to be calculated.

8.4.2.1 The Continuous Bidirectional Fuelling Approximation

The simplest approximation in fuel management calculations is to ignore the burnup variation axially in a fuel channel. This approach is known as the Continuous BiDirectional Fuelling Approximation (CBDFA).

With a continuous bidirectional fuelling scheme in a reactor, the average irradiation, ω, (neutron flux integrated over time) averaged over two adjacent channels is just one half of the exit irradiation. Due to the neutronic coupling between adjacent fuel channels, and the near monotonic variation in fuel properties as a function of irradiation, the approximation of uniform axial irradiation produces reasonably accurate power distributions and fuelling related information (exit burnup, etc.). The CBDFA is detailed further in Fig. 8-1.

In Fig. 8-1, the fuelling rate is constant at r cm/s in a fuel channel of length L cm. The exit irradiation, $\omega(L)$ is a pre-defined input quantity for both channel 1 (subscripted 1) and channel 2 (subscripted 2).

The CBDFA does not allow one to examine the axial variation in flux and power that results when various fuel management schemes are used. It does, however, allow one to determine approximate fuelling rates and overall power distributions.

In this thesis, the CBDFA option in FMDP is used primarily for scoping studies. Since it is not necessary to iterate between fluxes and irradiations when using this methodology, the CBDFA is the least expensive calculational algorithm available for this purpose in FMDP.

8.4.2.2 The Time-Averaged Approximation

A more sophisticated fuel management tool is the Time Averaged Approximation (TAA). With this approximation it is assumed that the power distribution calculated by cross sections averaged over the fuel's residence

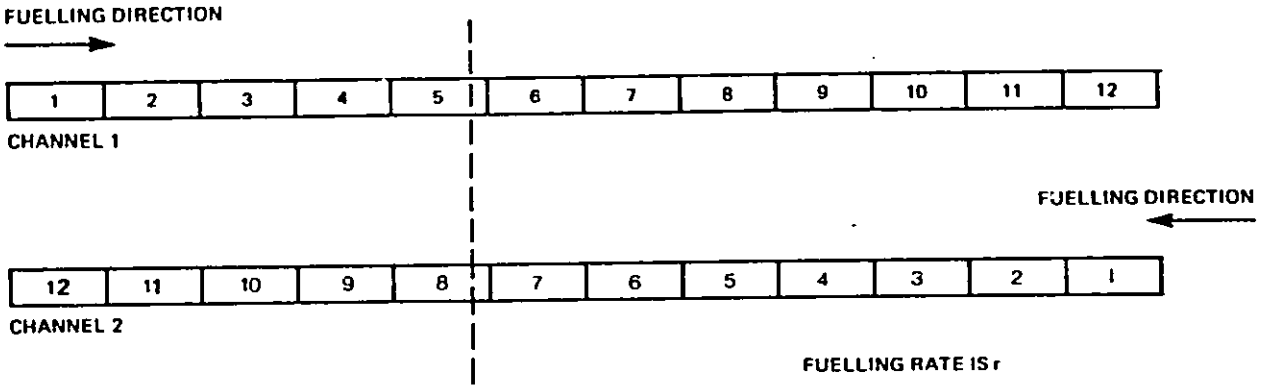

CONTINUOUS FUELLING APPROXIMATION

$$\omega_1(x) = \int_0^x \frac{\phi(x)}{r}\, dx$$

$$\omega_2(x) = \int_x^L \frac{\phi(x)}{r}\, dx$$

$$\bar{\omega}(x) = \frac{1}{2}(\omega_1(x) + \omega_2(x)) = \frac{1}{2}\int_0^L \frac{\phi}{r}\, dx = \frac{1}{2}\omega(L), \text{ a constant}$$

$$\bar{\Sigma} = \frac{1}{\omega(L)}\int_0^{\omega(L)} \Sigma(\omega)d\omega$$

Figure 8-1 Continuous Bidirectional Fuelling Approximation
(Figure courtesy of Atomic Energy of Canada Limited)

time is approximately the time-averaged power (Wight and Sibley, 1977). That is, the power distrubution is calculated using cross sections obtained from:

$$\Sigma = \int_{\omega_i}^{\omega_f} \Sigma(\omega)\, d\omega / \Delta\omega \qquad (8.4.2\text{-}1)$$

where ω_i is the irradiation at the beginning of the dwell time and ω_f at the end. Dwell time is defined as the time between fuel channel visits. These cross sections vary with axial position since the beginning and end of dwell time irradiations are axially varying parameters.

To obtain the initial and final irradiation for each axial position, one starts with an assumed axial flux distribution, and a specified average exit irradiation.

Consider a channel with M bundles in it, fuelled with an N bundle shift, push-through fuelling scheme. That is, when refueled, N fresh bundles are placed in one end of the channel and N spent bundles are withdrawn from the other end. (For the nominal CANDU-600 design, M=12 and N=8.) Then, the average exit irradiation is given by:

$$\omega_{out} = \sum_{i=1}^{N} \omega_i / N \qquad (8.4.2\text{-}2)$$

where the summation is taken over all discharged bundles. But:

$$\omega_i = \sum_{j} \Delta\omega_j \qquad (8.4.2\text{-}3)$$

where the summation is over all positions occupied by the bundle during its core residence. Thus:

$$\omega_{out} = (1/N) \sum_{i=1}^{N} \sum_{j} \Delta\omega_j = (1/N) \sum_{k=1}^{M} \Delta\omega_k = T\,S/N \qquad (8.4.2\text{-}4)$$

where

$$S = \sum_{k=1}^{M} \phi_k \qquad (8.4.2\text{-}5)$$

The double sum in Eq 8.4.2-4 includes all positions in the channel, and hence the summation in Eq 8.4.2-5 is over all bundles in the channel. This is made more clear by reference to Fig. 8-2.

The dwell time can be determined given an axial flux shape by rearranging Eq 8.4.2-4. Thus:

$$T = N\omega_{out}/S \qquad (8.4.2\text{-}6)$$

Then $\Delta\omega_j$, the incremental irradiation at bundle position j, is given by:

$$\Delta\omega_j = T\phi_j = \phi_j N \omega_{out}/S \qquad (8.4.2\text{-}7)$$

The fluxes to be used in Eq 8.4.2-7 are the time-averaged fluxes that are to be calculated. Thus, an iterative procedure must be set up to ensure consistency between the time averaged cross sections and the time-averaged neutronic flux. It should be noted that the fluxes referred to in Eq 8.4.2-7 are related to the thermal cell flux calculated in the M-2 group neutron diffusion equations by a factor, F, which in itself is irradiation dependent and is derived from a lattice code calculation.

The following steps summarize the time-averaged calculational procedure, which begins with an input first guess flux distribution, channel exit irradiation, and tables of neutronic cross sections as a function of irradiation.

(i) An initial guess of ϕ_{2k} (the thermal cell flux for position, k) and F_k are made.

(ii) Axially integrated fuel fluxes are calculated according to Eq 8.4.2-5.

(iii) The starting and ending irradiations (ω_i and ω_f respectively)

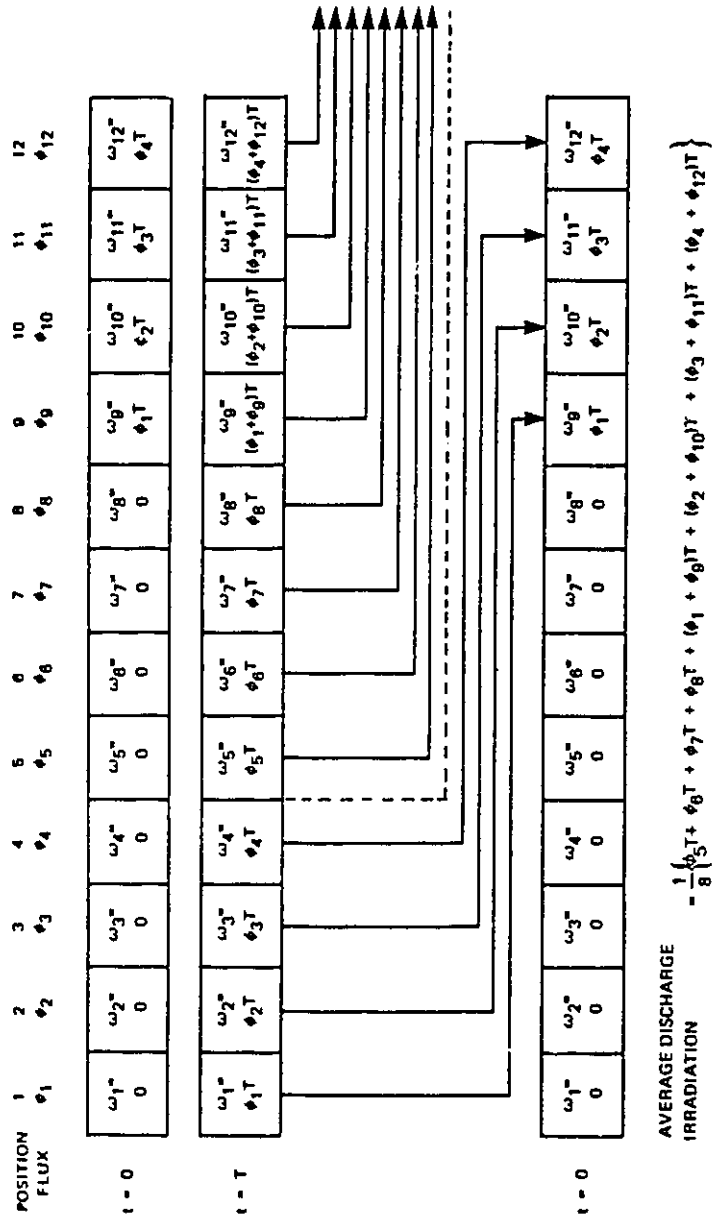

Figure 8-2 Time Averaged Fuelling Approximation (Eight Bundle Shift)
(Figure courtesy of Atomic Energy of Canada Limited)

are then determined using Eq 8.4.2-7 and accounting for the nature of the fuelling scheme. For an N bundle shift scheme:

$$\omega_i(j) = 0 \qquad \text{for } j \leq N \qquad (8.4.2\text{-}8)$$

$$\omega_i(j) = \omega_f(j\text{-}N) \qquad \text{for } j > N \qquad (8.4.2\text{-}9)$$

$$\omega_f(j) = \omega_i(j) + \Delta\omega_j \qquad (8.4.2\text{-}10)$$

(iv) The newly determined irradiation ranges allow for a new calculation of F_k with ϕ_{2k} remaining fixed, averaging in a fashion similar to Eq 8.4.2-1.
(v) Steps (ii) through (iv) are repeated until self-consistent sets of $\Delta\omega_j$ and S are found for each channel.
(vi) Time averaged cross sections for each bundle are determined from Eq 8.4.2-1.
(vii) With these cross sections, the flux distribution, eigenvalue, and power distribution are calculated. (See Eq 8.2.2-1.)
(viii) Steps (ii) through (vii) are repeated until the flux shape, eigenvalue, and irradiation distribution have converged.

At this point, adjustments are made to the input channel exit irradiations and to parameters such as adjuster loading to influence system reactivity and to ensure acceptable power distributions. This is done external to the code by the user. With these changes the code performs steps (ii) through (viii) again. The entire process is complete when the reactor is critical, flux and irradiation distributions are converged, reactor bundle and channel power limits are acceptable and the desired radial power distribution is achieved.

For fuelling schemes involving more complex bundle rearrangements a similar approach can be employed. Properties for a given bundle position are calculated by averaging the irradiation history of all bundles which reside in that position, for the period of time while they are at that position.

8.4.2.3 Instantaneous Approximation Cases

The TAA methodology allows a fuelling engineer to investigate various fuelling strategies. However, since the power distribution calculated in this manner is generated using a set of time-averaged cross sections, additional analyses must be conducted to ensure the viability of a given scheme. It is necessary to show that not only will bundle and channel powers not exceed specified limits on an average sense, but at all times throughout the operating life of a unit.

To better characterize a proposed fuelling strategy without performing detailed on-going fuelling simulations, the FMDP code is fitted with a module to perform calculations based on "snapshots" of a reactor history. These snapshots are obtained by assigning "ages" to fuel channels (either randomly or in a prespecified pattern) and deriving properties for the particular channels based on the given ages. The properties are obtained by determining the effective irradiation for a bundle location by assuming a linear variation of irradiation with time:

$$\omega = \omega_i + r\,(\omega_f - \omega_i) \qquad (8.4.2\text{-}11)$$

where:

ω = the effective irradiation,
r = the channel age (individual values are applied to each channel),
ω_f = the irradiation at the end of a dwell time, and
ω_i = the irradiation at the beginning of a dwell time. (These latter two parameters are obtained from TAA calculations.)

It is noted that for more complex fuelling schemes, the channel dwell time is defined as the time period between which a particular component of a fuelling strategy repeats itself. (For example, if a fuelling strategy involves a combination of two and four bundle shifts evenly spaced, the dwell time is the

time between successive two (or four) bundle shifts.) In these cases, to calculate the effective irradiation at a given bundle position, it is necessary to determine the stage (or cycle) in the fuelling sequence the channel age refers to, and the fraction of time, f, passed within that cycle. The FMDP maintains data files containing the time-averaged beginning and end of cycle irradiations for every fuel bundle in each fuel cycle, and the appropriate instantaneous fuel properties are obtained using Eq 8.4.2-11 with r replaced by f.

Channel ages can be determined using a variety of techniques. One way is to have the code select ages randomly over the interval (0,1). Several initiating seeds can be used to derive a set of age maps and corresponding power distributions, to allow the evaluation of a given fuelling strategy. However, given that reactor fuelling is not performed using a random channel selection process, the random age approximation tends to over-estimate expected power peaking. Consequently, even with natural uranium fuel, the data is often post-processed to remove effects resulting from the clustering of refuelling operations. With enriched fuel, the random age selection process becomes quite unworkable, as it is recognized that extreme care on the part of the fuelling engineer is required to ensure that fuel and fuel channels are not overrated.

Alternatively, channel ages can be generated according to a pattern arrangement rather than being randomly distributed. The "knight's-move" pattern is often the basis for the channel age distribution. Consider a selection of 16 fuel channels fuelled in order according to the sequence:

2	15	6	13
9	4	11	16
12	1	14	7
5	8	3	10

The reactor is divided into groups of 16 channels, and each channel within the group is assigned a primary sequence number as above. These second order groups are also numbered according to the sequence above. Finally the

second order groups are collected into several third order groups, each of which contains 16 second order groups. These also are numbered in a similar fashion. Finally each channel is assigned a real number to it:

aa.bbcc

where:

aa is the two digit primary sequence number,

bb is the second order group number, and

cc is the third order group number.

These numbers are then sorted into ascending order and ages are assigned starting from 0 and ending at (n-1)/n where n is the number of fuel channels (380). The age map, so generated, is shown in Fig. 8-3. This patterned distribution was used in the instantaneous studies discussed in Chapter 10.

The FMDP code performs a number of additional types of calculations, though these are outside the scope of this study.

8.5 REACTOR ANALYSIS

8.5.1 Creation of Fuel Tables

The transition from lattice physics analysis to core physics analysis requires the lattice properties to be transferred to the reactor code. The computer code, WIMS-FMDP (Donnelly and van Dyk, 1983) was used to extract the 18 energy group data from the WIMS-CRNL lattice physics calculations (see Chapter 7) and convert these to the M-2 group structure (Eq 8.2.2-1) required for use in FMDP. The WIMS-FMDP code provides properties as a function of fuel thermal irradiation. Collectively, these data are known as "fuel tables". The cross sections extracted using WIMS-FMDP were those corresponding to a critical buckling spectrum. Benoist diffusion coefficients were also used. (See Donnelly, 1986.) Selected data from these fuel tables are given in Table 8-1.

	1	2	3	4	5	6	7	8	9	10	11	12
A									.0816	.8921	.3368	.7711
B						.2421	.6789	.9921	.5211	.2053	.6421	.9553
C					.7421	.0553	.8632	.4289	.7079	.0211	.8289	.3947
D				.5684	.3079	.4921	.1789	.6158	.2737	.4579	.1447	.5816
E			.3474	.7816	.0737	.8816	.3263	.7605	.1026	.9105	.3553	.7895
F			.6526	.9658	.5132	.1974	.6342	.9474	.5395	.2237	.6605	.9737
G		.0316	.8395	.4053	.7000	.0132	.8211	.3868	.7263	.0395	.8474	.4132
H		.4684	.1553	.5921	.2658	.4500	.1368	.5737	.2921	.4763	.1632	.6000
J	.1079	.9158	.3605	.7947	.0632	.8711	.3158	.7500	.1184	.9263	.3684	.8026
K	.5447	.2289	.6658	.9789	.5000	.1868	.6237	.9368	.5553	.2395	.6763	.9895
L	.7289	.0421	.8500	.4158	.6868	0.0000	.8132	.3789	.7395	.0526	.8605	.4263
M	.2947	.4789	.1658	.6026	.2526	.4368	.1289	.5658	.3053	.4895	.1763	.6132
N	.0763	.8868	.3316	.7658	.0895	.9000	.3447	.7789	.0711	.8789	.3237	.7579
O	.5158	.2000	.6368	.9500	.5289	.2132	.6500	.9632	.5105	.1947	.6316	.9447
P		.0158	.8237	.3895	.7158	.0289	.8368	.4026	.6974	.0105	.8184	.3842
Q		.4526	.1395	.5763	.2816	.4658	.1526	.5895	.2632	.4474	.1342	.5711
R			.3211	.7553	.1211	.9289	.3711	.8053	.0842	.8947	.3395	.7737
S			.6289	.9421	.5579	.2447	.6816	.9947	.5237	.2079	.6447	.9579
T				.3816	.7447	.0579	.8650	.4316	.7105	.0237	.8316	.3974
U					.3105	.4947	.1816	.6184	.2763	.4605	.1474	.5842
V						.8842	.3289	.7632	.1053	.9132	.3579	.7921
W									.5421	.2263	.6632	.9763

	13	14	15	16	17	18	19	20	21	22
A	.1132	.9211								
B	.5500	.2342	.6711	.9842	.5079					
C	.7342	.0474	.8553	.4211	.6947	.0079				
D	.3000	.4842	.1711	.6079	.2605	.4447	.1316			
E	.1237	.9316	.3737	.8079	.0974	.9053	.3500	.7842		
F	.5605	.2474	.6842	.9974	.5342	.2184	.6553	.9684		
G	.7474	.0605	.8684	.4342	.7211	.0342	.8421	.4079	.7026	
H	.3132	.4974	.1842	.6211	.2868	.4711	.1579	.5947	.2684	
J	.0868	.8974	.3421	.7763	.1105	.9184	.3632	.7974	.0658	.8737
K	.5263	.2105	.6474	.9605	.5474	.2316	.6684	.9816	.5026	.1895
L	.7132	.0263	.8342	.4000	.7316	.0447	.8526	.4184	.6895	.0026
M	.2789	.4632	.1500	.5868	.2974	.4816	.1684	.6053	.2553	.4395
N	.1000	.9079	.3526	.7868	.0789	.8895	.3342	.7684	.0921	.9026
O	.5368	.2211	.6579	.9711	.5184	.2026	.6395	.9526	.5316	.2158
P	.7237	.0368	.8447	.4105	.7053	.0184	.8263	.3921	.7184	
Q	.2895	.4737	.1605	.5974	.2711	.4553	.1421	.5789	.2842	
R	.1158	.9237	.3658	.8000	.0684	.8763	.3184	.7526		
S	.5526	.2368	.6737	.9868	.5053	.1921	.6263	.9395		
T	.7368	.0500	.8579	.4237	.6921	.0053	.8158			
U	.3026	.4868	.1737	.6105	.2579	.4421				
V	.1263	.9342	.3763	.8105	.0947					
W	.5632	.2500								

Figure 8-3 Instantaneous Channel Age Map

Fuel Type	Fuel Thermal Irradiation (n/kb)	Fast Transport Cross Section (cm^{-1})	Thermal Transport Cross Section (cm^{-1})	Thermal Absorption Cross Section (cm^{-1})	Moderation Cross Section (cm^{-1})	Fast Absorption Cross Section (cm^{-1})	Production Cross Section (cm^{-1})	Fuel to Cell Thermal Flux Ratio	Bundle Power to Cell Thermal Flux Ratio (1E-11 kW cm^2 s)
NATNOM	0.0	0.2400	0.3509	3.522 E-3	8.468 E-3	1.611 E-3	4.710 E-3	0.583	0.251
	1.0	0.2401	0.3518	3.892 E-3	8.454 E-3	1.696 E-3	4.986 E-3	0.540	0.253
	2.0	0.2402	0.3521	3.973 E-3	8.454 E-3	1.768 E-3	4.887 E-3	0.529	0.242
	3.0	0.2403	0.3523	4.000 E-3	8.478 E-3	1.817 E-3	4.694 E-3	0.525	0.229
	Reflector	0.2457	0.3693	4.520 E-5	9.510 E-3	0.0	0.0	0.000	0.000
1421NAT	0.0	0.2275	0.3291	4.454 E-3	8.094 E-3	1.659 E-3	5.839 E-3	0.690	0.241
	1.0	0.2275	0.3300	4.962 E-3	8.015 E-3	1.760 E-3	6.474 E-3	0.656	0.254
	2.0	0.2277	0.3304	5.125 E-3	7.996 E-3	1.860 E-3	6.495 E-3	0.644	0.248
	3.0	0.2278	0.3307	5.189 E-3	8.009 E-3	1.929 E-3	6.305 E-3	0.639	0.237
	Reflector	0.2452	0.3664	4.432 E-5	9.410 E-3	0.0	0.0	0.000	0.000
14211312	0.0	0.2267	0.3296	5.537 E-3	7.752 E-3	1.745 E-3	8.797 E-3	0.610	0.363
	2.0	0.2218	0.3307	5.757 E-3	7.809 E-3	1.928 E-3	8.061 E-3	0.597	0.313
	4.0	0.2276	0.3310	50581 E-3	7.923 E-3	2.032 E-3	6.894 E-3	0.609	0.259
	6.0	0.2279	0.3312	5.484 E-3	8.001 E-3	2.106 E-3	6.200 E-3	0.616	0.229
	Reflector	0.2449	0.3654	4.403 E-5	9.200 E-3	0.0	0.0	0.000	0.000
142117153	0.0	0.2263	0.3300	6.120 E-3	7.594 E-3	1.804 E-3	1.045 E-2	0.567	0.432
	2.0	0.2269	0.3310	6.137 E-3	7.707 E-3	1.972 E-3	9.028 E-3	0.568	0.352
	4.0	0.2275	0.3312	5.810 E-3	7.860 E-3	2.066 E-3	7.407 E-3	0.592	0.280
	6.0	0.2278	0.3313	5.612 E-3	7.970 E-3	2.136 E-3	6.418 E-3	0.606	0.238
	8.0	0.2280	0.3314	5.542 E-3	8.023 E-3	2.189 E-3	5.956 E-3	0.611	0.219
	Reflector	0.2447	0.3649	4.388 E-5	9.091 E-3	0.0	0.0	0.000	0.000

Note: Reflector properties are not a function of irradiation.

Table 8-1 Selected FMDP Fuel Table Data

8.5.2 Numerical Techniques

The numerical solution of the M-2 group neutron diffusion equations in FMDP requires that the reactor be divided into mesh cells. Neutronic properties are assigned to each of the cells. A first order finite difference approximation to the flux gradient is used.

The neutron diffusion equations are solved iteratively, with over-relaxation techniques employed (Wight, 1987).

8.5.3 Treatment of Reactivity Devices

The neutronic properties for mesh cells containing or contained within lattice cells are obtained from the WIMS-FMDP generated fuel tables (appropriate fuel bundle irradiations must be defined). Reflector properties for mesh cells in the reflector region are also obtained from WIMS-FMDP, though they are not assumed to be irradiation dependent. The properties for mesh cells containing reactivity devices (adjuster rods, zone controllers, etc.) are obtained from the fuel tables but with additional "incremental" cross sections added to simulate the presence of the devices. This is discussed in greater detail in Chapter 9.

8.5.4 Reactor Model

8.5.4.1 Mesh Sizes

The reactor model used in the fuel management analysis is depicted in Fig. 8-4 and 8-5. Adjuster rod types/numbers and zone controller numbers are also identified in these figures. Mesh spaces are given in Tables 8-2 through 8-6. In each case, the first and last mesh cells have dimensions of zero. Mesh lines were placed to delineate lattice cells and reactivity devices where practicable. (In the NATNOM case, each lattice pitch is 28.575 cm in length. For the 14/21 fuel bundle design, the lattice pitch size was 25 cm.)

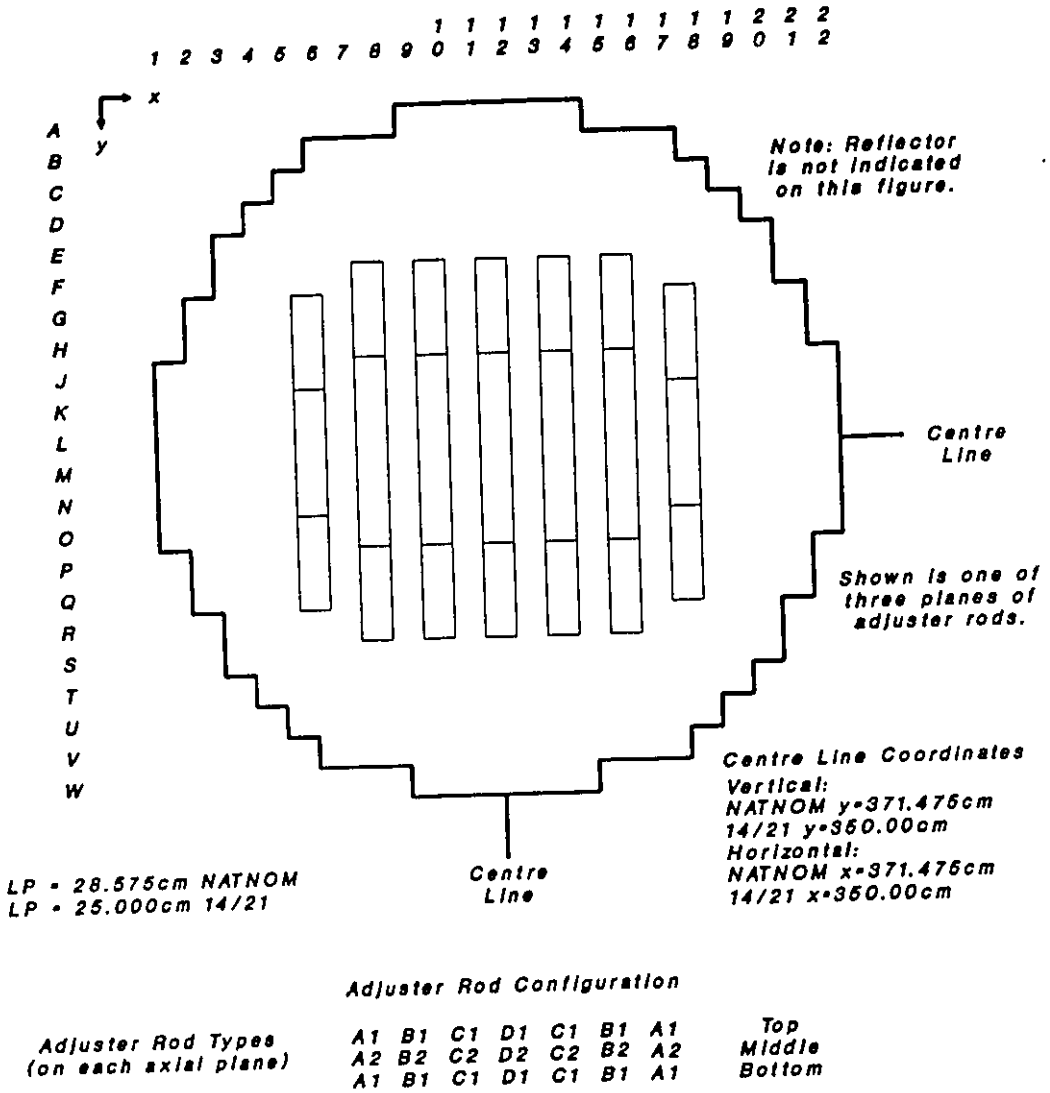

Figure 8-4a Reactor Model (x-y View)

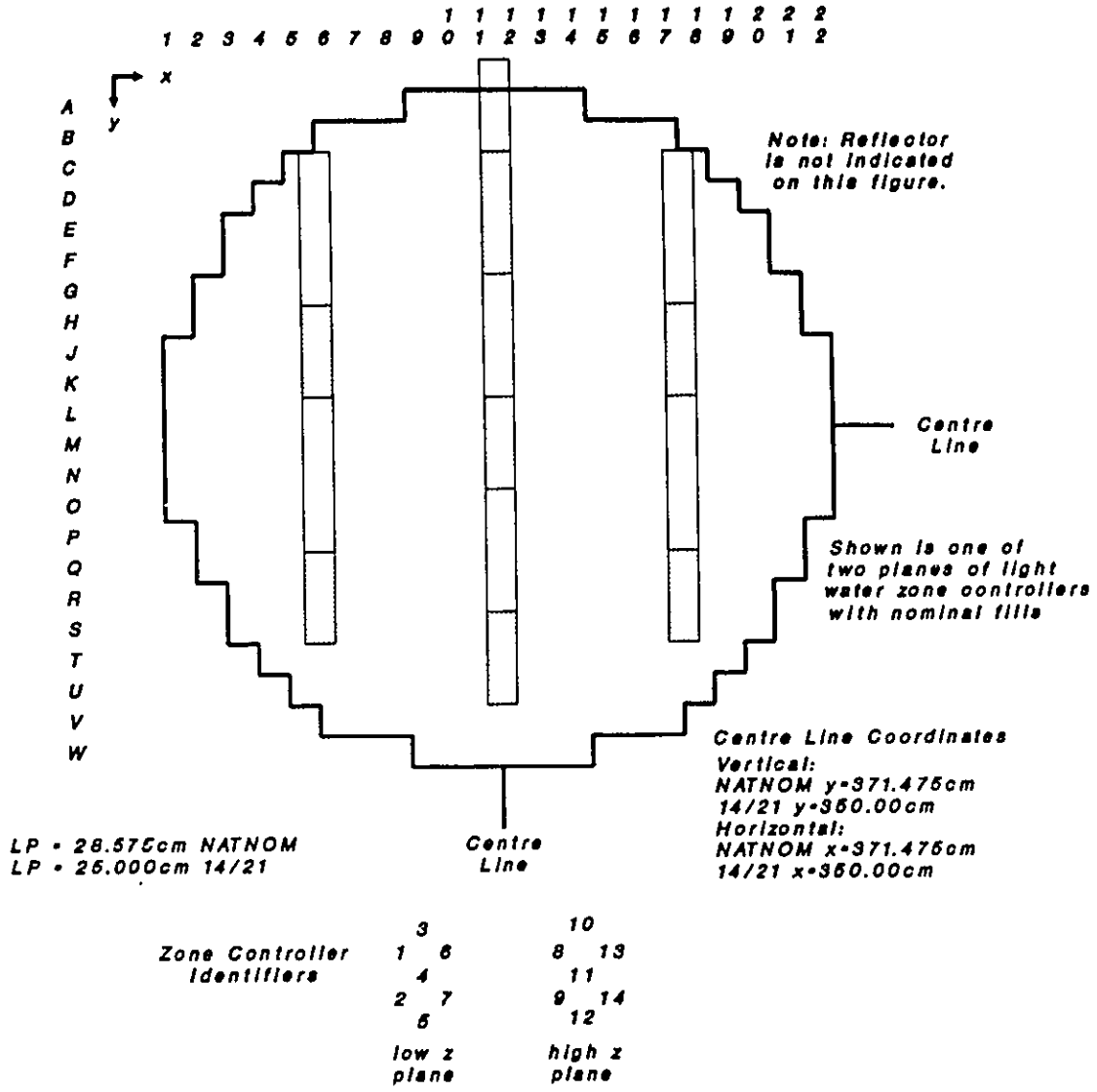

Figure 8-4b Reactor Model (x-y View)

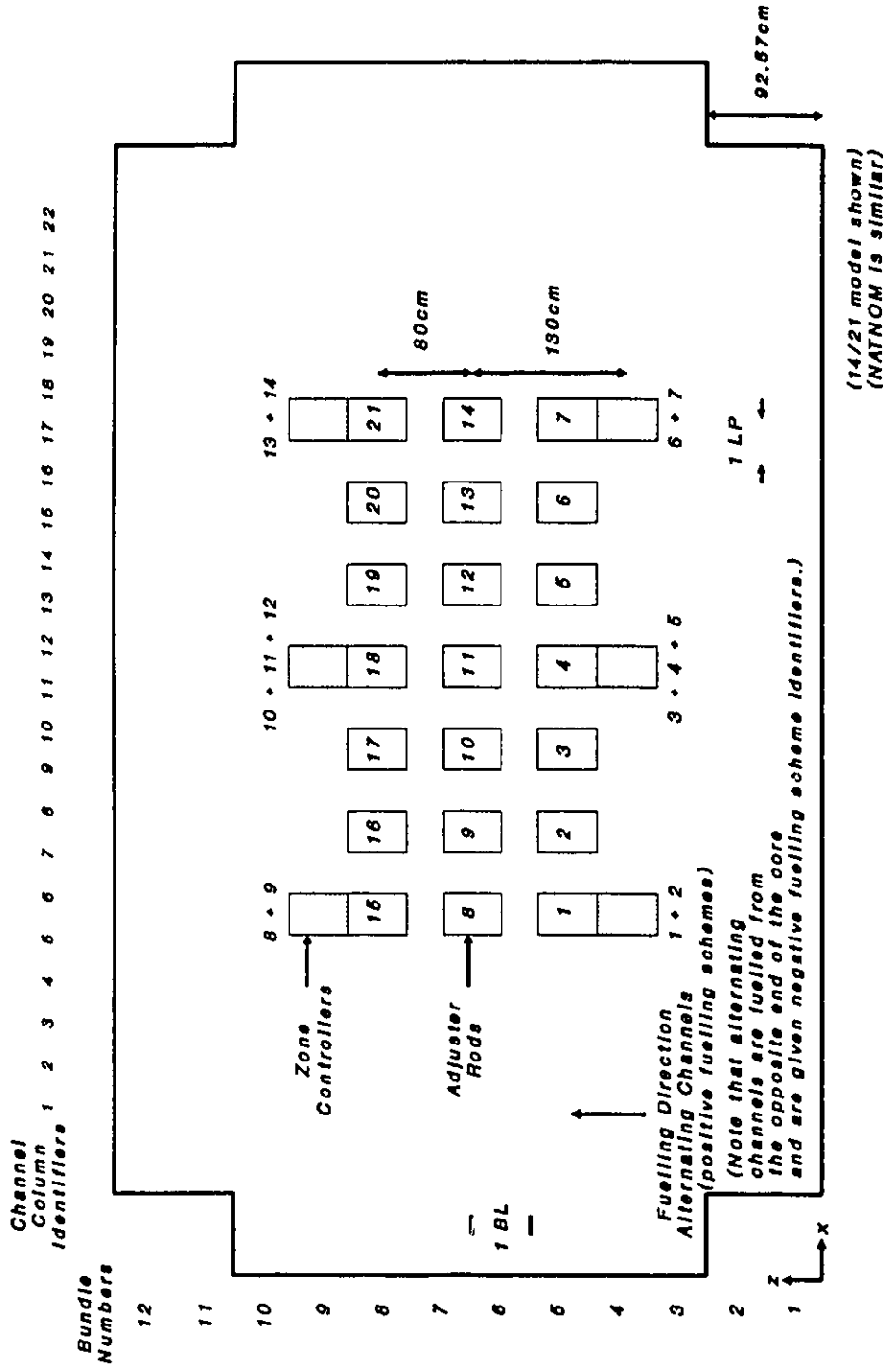

Figure 8-5 Reactor Model (x-z View)

Mesh Number (x-direction)	Mesh Size (cm)
1	0.0000
2 to 7	28.5750
8 to 35	14.2875
36 to 41	28.5750
42	0.0000

Table 8-2 FMDP Model: NATNOM x-Direction Mesh Sizes

Mesh Number (y-direction)	Mesh Size (cm)
1	0.0000
2 to 27	28.5750
28	0.0000

Table 8-3 FMDP Model: NATNOM y-Direction Mesh Sizes

Mesh Number (x-direction)	Mesh Size (cm)
1	0.0
2 to 8	25.0
9 to 36	12.5
37 to 44	25.0
45	0.0

Table 8-4 FMDP Model: 14/21 x-Direction Mesh Sizes

Mesh Number (y-direction)	Mesh Size (cm)
1	0.0
2 to 29	25.0
30	0.0

Table 8-5 FMDP Model: 14/21 y-Direction Mesh Sizes

Mesh Number (z-direction)	Mesh Size	
	NATNOM Cases	14/21 Cases
1	0.000	0.00
2	49.530	50.00
3	43.040	42.57
4	6.490	7.43
5	43.355	45.00
6	6.175	5.00
7	43.355	45.00
8	0.470	5.00
9	5.705	45.00
10	43.825	5.00
11	5.705	25.00
12	24.765	25.00
13	24.765	25.00
14	24.765	25.00
15	24.765	5.00
16	5.705	45.00
17	43.825	5.00
18	5.705	45.00
19	0.470	5.00
20	43.355	45.00
21	6.175	7.43
22	43.355	42.57
23	6.490	50.00
24	43.040	0.00
25	49.530	---
26	0.000	---

Table 8-6 FMDP Model: z-Direction Mesh Sizes

8.5.4.2 Reflector Volume

The nominal CANDU-600 design (NATNOM) has a main reflector radius of 379.7 cm. The ends of the reactor, being less neutronically important, have a reduced reflector radius (337.8 cm). This "notch" region has an axial dimension of 92.57 cm at each end of the reactor.

In the 14/21 cases, the lattice pitch was reduced to 25 cm and the bundle length was increased to 50 cm. To maintain the reflector volume (outside the lattice cells) constant, the reflector radii were adjusted to 346.97 cm (main reflector region), and 301.6 cm (notch) in the 14/21 cases. The notch axial depth was maintained at 92.57 cm as in the NATNOM case.

The size of the reflector in an actual application will be dependent on the relative cost of the heavy water and uranium (larger reflectors yield higher burnups).

8.5.4.3 Burnup Regions

The CANDU-600 reactor utilizes adjuster rods and differential burnup to achieve flux and power radial flattening. Fuel burnup is increased in the central region of the core to depress the flux in this region. For the purposes of this study, a two burnup zone reactor was considered. The boundary between the inner and outer fuelling zones is depicted in Fig. 8-6.

8.5.4.4 CPPF Region

The high power region of the core (channels with power greater than 85% of maximum power for a reference power distribution) is known as the CPPF region (where CPPF is a contraction of Channel Power Peaking Factor). This factor is defined for the purpose of calculating in-core neutron overpower detector calibration factors. The CPPF is equal to:

$$CPPF = (CP(i,t)/CP(i,0)) \quad \max \text{ in CPPF region} \qquad (8.5.4\text{-}1)$$

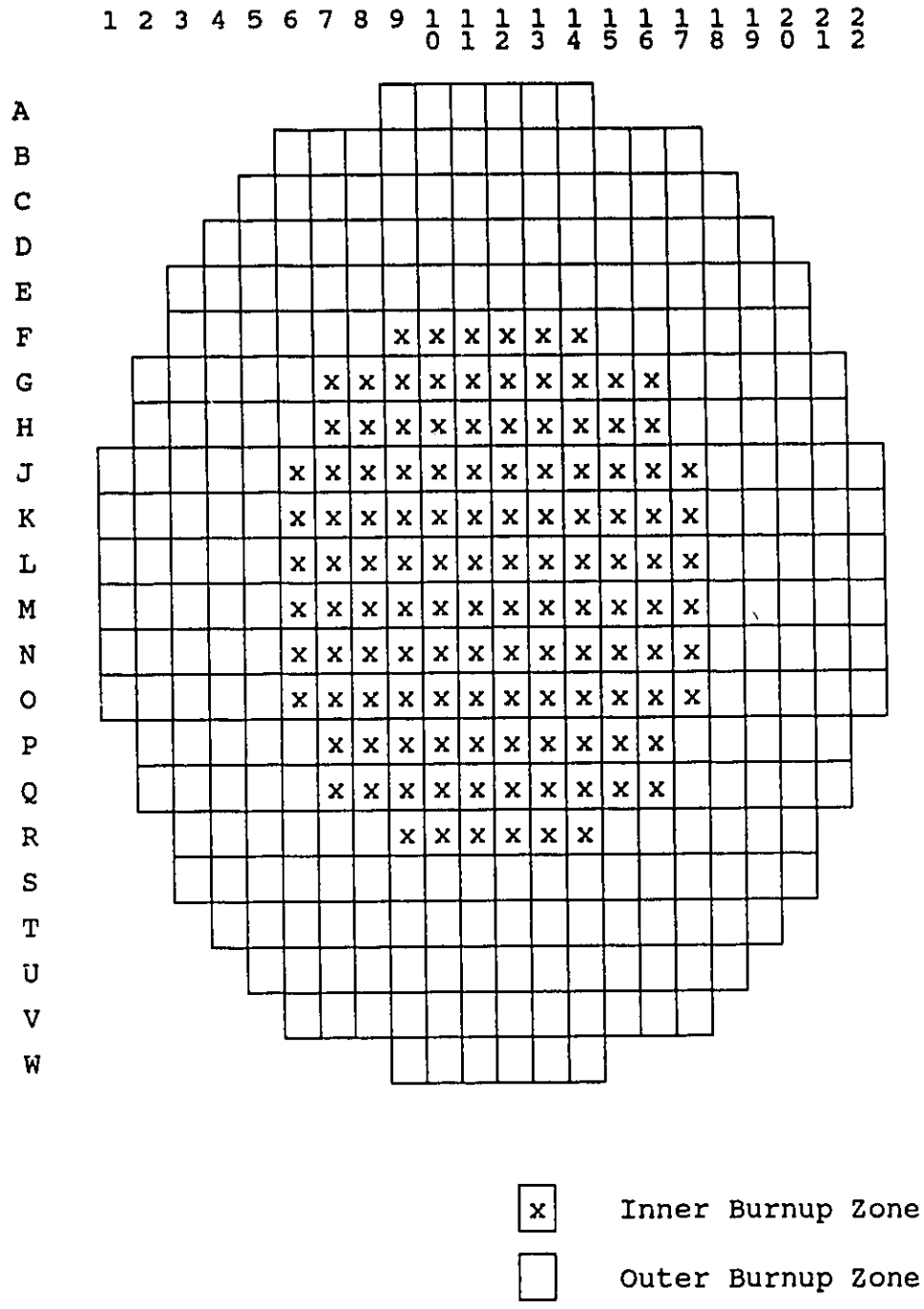

Figure 8-6 Burnup Regions

where:

CP(i,t) = the instantaneous power in channel i, and

CP(i,0) = the pre-defined reference power in channel i.

The CPPF region is depicted in Fig. 8-7, and is referred to in Section 10.7.

8.5.4.5 Reactivity Device Positions/Levels

In the fuel management calculations to be considered in Chapter 10, the adjuster rods were assumed to be in-core (Fig. 8-4a). The zone controllers were filled with light water to the levels given in Table 8-7 (average zone level 40.8%) and shown in Fig. 8-4b (where the shaded zone represents the nominal fill level). Any deviations from this configuration are noted explicitly in the text.

8.5.4.6 Boundary Conditions

To enable the diffusion approximation to provide a reasonable representation of the actual reactor flux distribution, appropriate boundary conditions are applied at the model perimeter. These boundary conditions are extrapolation distances (Henry, 1975), at which the flux is arbitrarily set equal to zero. The computer code, FMDP, requires extrapolation factors as boundary condition input parameters. These factors, when multiplied by the transport mean free path, are equal to twice the extrapolation distance.

A radial extrapolation factor of 3.06 cm and an axial extrapolation factor of 3.67 cm were used in the models. These are based on empirical values of 6 cm for the extrapolation distance into the endshield, and 5 cm for the radial extrapolation distance. The corresponding value for the effective mean free path (0.306 cm) was obtained by averaging the reflector mean free path for the NATNOM and 14211312 cases (both fast and thermal data).

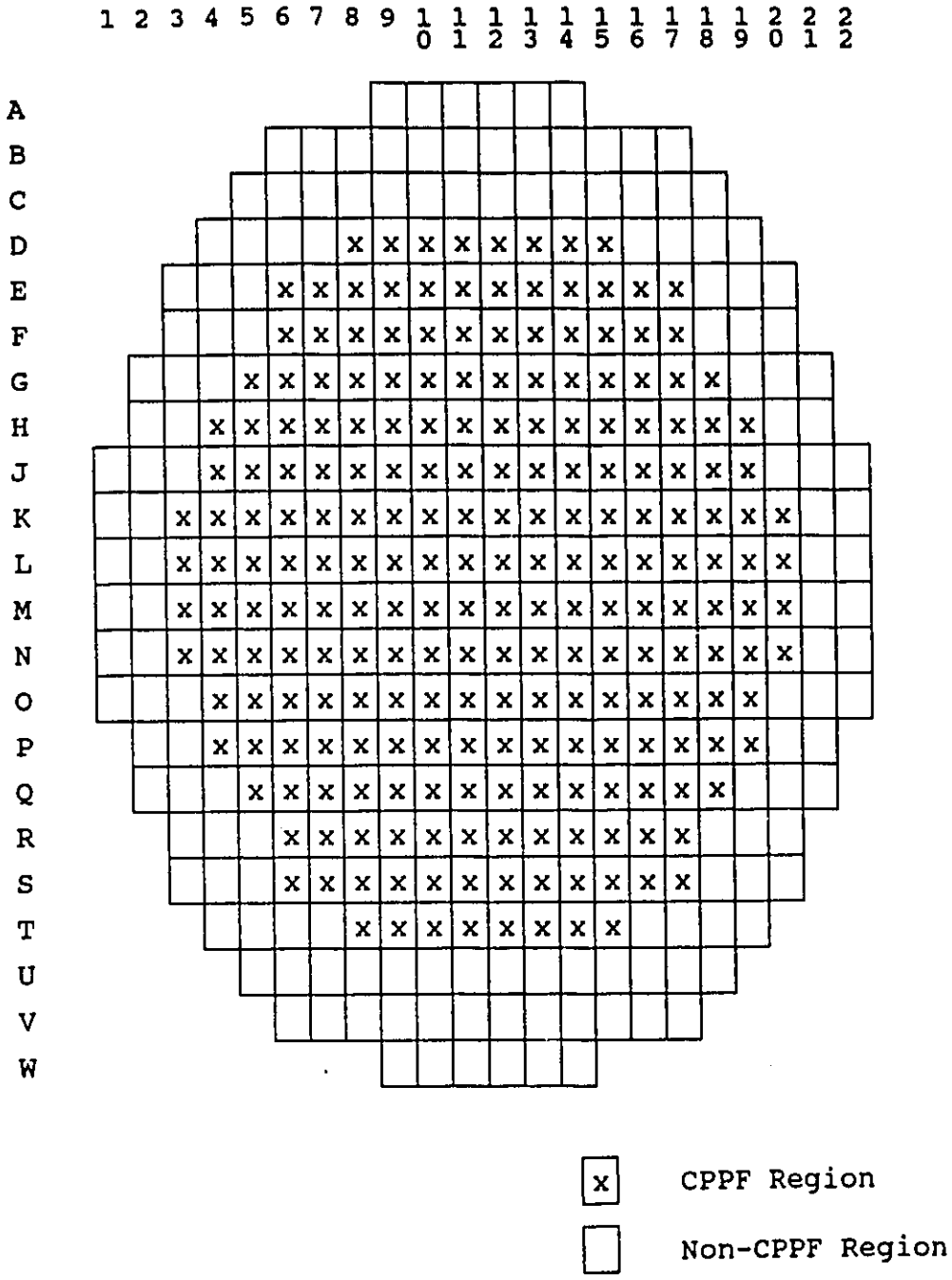

Figure 8-7 CPPF Region

Zone Controller Number	Zone Fractional Fill
1	0.3750
2	0.3750
3	0.5000
4	0.4286
5	0.4286
6	0.3750
7	0.3750
8	0.3750
9	0.3750
10	0.5000
11	0.4286
12	0.4286
13	0.3750
14	0.3750

Table 8-7 Zone Controller Light Water Fractional Fill

8.5.4.7 Power Normalization

The power calculated for the reactor models was normalized to a total fission power of 2155900 kW. This corresponds to a reactor thermal power (total reactor power delivered to the coolant and leaving the core) equal to 2058400 kW. These values are appropriate to the Pt. Lepreau CANDU-600 station (Jenkins, 1985). In Chapter 10, all powers are quoted in terms of thermal power, as is standard practice in this type of analysis.

CHAPTER 9

SPECIFICATION AND SIMULATION OF REACTIVITY DEVICES

9.1 INTRODUCTION

On power fuelling in pressure tube type reactors minimizes the requirements for bulk reactivity reserves. Nevertheless, in-core reactivity devices are necessary to provide adequate control of the bulk and spatial power distribution.

The reactivity devicesare required to compensate for bulk reactivity perturbations (resulting from, for example, xenon transients, inability to refuel, inadvertent downgrading of heavy water, and various reactivity feedback effects following a change in reactor power, etc.). These devices must be capable of both fine and coarse reactivity control, and must operate on a much finer time scale than is available with semi-continuous refuelling.

In CANDU nuclear reactors, region-wise neutronic decoupling places an additional spatial reactivity control requirement on the units, to guard against xenon-induced spatial power oscillations (Akhtar and Trojan, 1975; Akhtar and Trojan, 1976) and to offset non-symmetries in fuelling and burnup.

CANDU-600 reactors utilize automatic moderator poison addition systems, mechanical control absorbers, and adjuster absorber rods for bulk reactivity control. The light-water zone controller system provides both bulk and spatial reactivity control (AECL, 1981). Similar control systems are expected to be used in the advanced CANDU designs.

For the purposes of control mechanism specification and simulation in fuel management studies, only two of these systems need be considered:

(i) Adjuster Absorber Rods (AAs)

(ii) Light Water Zone Controllers (ZCRs).

These devices are normally in-core, and therefore it is important to

model their presence when analyzing the behaviour of heavy water reactors with various fuel types.

Adjuster rod and zone controller requirements are addressed in Sections 9.2 and 9.3, respectively. Sections 9.4 through 9.6 deal with the simulation of such devices in reactor core models. The results of the analysis are summarized in Section 9.7.

9.2 ADJUSTER ROD REQUIREMENTS

As noted in Chapter 2, adjuster rods provide radial and axial power flattening. They are withdrawn from the core in banks as necessary to provide additional positive reactivity when fuelling machines are unavailable. In addition, they can be withdrawn to override xenon transients during trip recoveries (Akhtar and Trojan, 1977; Trojan and Dastur, 1973), while undergoing generation maneuvering (Akhtar and Trojan, 1971), and following regulating system-induced reactor power setbacks and stepbacks.

The adjuster rod system must provide sufficient positive reactivity to allow up to one full-power-week of operation without refuelling. In addition, it must provide approximately 30 minutes of xenon override time following a trip of the reactor's first shutdown system (shutoff absorber rods drop in core). During this 30 minute period, operating personnel must assess the reasons for the reactor trip, ensure the system has stabilized, remove the shutoff rods, control absorbers and adjuster banks, and raise reactor power to a sufficient level (approximately 60% FP) such that the xenon burnout rate is greater than the xenon production rate. If reactor power is not at or above 60% FP within the xenon override time, the reactor will poison out, with a forced down time of approximately 40 hours before the unit can be restarted. This forced down time carries with it considerable economic consequences.

Of the basic requirements noted above, the 30 minute xenon override time places the greatest requirement on the adjuster rod system reactivity.

9.2.1 Simulation of Post-Reactor Trip Conditions

After a reactor trip, the xenon burnout via neutron absorption ceases, though xenon production via iodine decay continues, resulting in an initial decrease in system reactivity. Eventually as the iodine concentration decreases, xenon decay exceeds xenon production and the xenon concentration gradually reduces to zero.

The WIMS-CRNL code (PIJ option) (Donnelly, 1986) was used to simulate the xenon transient during the 30 minutes following a reactor trip from full power. The initial burnstep from which the xenon transients began was chosen to be the mid-point main transport calculation burnup for the various fuel types. Results are given in Table 9-1. Note that the change in reactivity data quoted reflects primarily the effect of xenon buildup over the 30 minutes after shutdown. The small contributions of other fission products, and actinide concentration changes over this period were not factored out. Fuel and coolant temperature reactivity feedback was not simulated.

The simulation results indicate that for a 30 minute xenon override time, the adjuster rod worth must be 11.79 mk for NATNOM fuel. It has been found, generally, that simulations such as these underestimate the required adjuster rod reactivity for a given xenon override time, and that in the NATNOM study an adjuster loading of 15 mk would be a more appropriate value. (Note that to allow one full power week without refuelling would require a considerably smaller adjuster loading of only 3 to 4 mk.)

Sensitivity studies were conducted to ascertain the dependence of the Table 9-1 results on the system burnup at the time of the transient. Increasing burnup by 25% decreased the change in xenon reactivity over a 30 minute period by less than 0.1 mk.

The results were found, as expected, to be very sensitive to the equilibrium flux level (see, for example, Henry, 1975). The flux squared weighted average fuel flux should be used in determining the initial xenon and iodine concentrations. This weighted flux value is a function of the reactor core power distribution, and most appropriately determined after the core design and fuel management schemes have been fully specified. For the

Case Identifier	Pre-Trip Burn Time (days)	Pre-Trip Burnup (MWd/MgU)	Pre-Trip Power Density (MW/MgU)	Change in Reactivity 30 Minutes After Trip (mk)	Ratio of Change in Reactivity with Respect to NATNOM
NATNOM	100	3251.0	32.510	-11.79	1.00
1421NAT	100	3971.9	39.719	-14.06	1.19
14211312	300	11915.7	39.719	-11.44	0.97
142117153	400	15887.6	39.719	-10.56	0.90

Table 9-1 Comparison of Adjuster Rod Requirements

purposes of ascertaining relative adjuster rod worth requirements, however, the approach taken here is adequate.

9.2.2 Data Interpretation

The data in Table 9-1 indicate that the 1421NAT case requires approximately 19% greater adjuster rod reactivity than in the NATNOM case for a given xenon override time. Repeating the NATNOM case at the same power density as in the 1421NAT case yielded comparable reactivity worth requirements for both of the fuel variants. Nevertheless, given the expected higher flux level in the 1421NAT case due to the reduction in the amount of uranium per bundle, it is expected that the adjuster rod reactivity worth in the 1421NAT case would be greater than in the NATNOM case, as these simulations indicate.

As the uranium enrichment increases, the results in Table 9-1 indicate a reduction in the required adjuster rod worth for a 30 minute xenon override time. This can be attributed to the increase in the fuel absorption cross section as the fuel enrichment rises, which reduces the thermal flux in the fuel region. This, in turn, causes a given change in the fuel absorption cross section to have a smaller effect on the cell reactivity due to self shielding. In addition, the increased fuel fission cross section requires a larger change in absorption rate to effect a given change in reactivity. (See further discussion in Section 10.5.5.5.)

For a given adjuster rod system reactivity worth, a reactor fuelled with 142117153 type fuel will have a xenon override time which is approximately 33% larger than for the same reactor fuelled with 1421NAT type fuel. Operationally, this increased time could be used to advantage in that following a reactor trip, operators would have an extended period of time to ascertain the cause of the trip, correct the fault, and raise reactor power before poisoning out. This feature would be of greatest use to inexperienced utilities, where trips may be more frequent. As an alternative, the worth of the adjuster loading could be decreased as the fuel enrichment is increased, thereby maintaining the required 30 minute xenon override time, and in the

process, realizing an increase in achievable fuel burnup, due to a decrease in parasitic absorption. Note that with a reduced adjuster rod system worth, unit operators would have to rely more heavily on burnup grading to provide necessary power flattening.

9.3 ZONE CONTROLLER SYSTEM REQUIREMENTS

The liquid zone control absorbers are the primary devices for controlling reactivity within the reactor during normal operation. The change in system reactivity when all zone compartments drain from full should be +6 mk (nominal CANDU-600 value) to provide adequate depth of control. Normally zone compartments are approximately 40% full. Draining from this state contributes 2 to 3 mk to system reactivity.

9.4 SIMULATION OF REACTIVITY DEVICES

9.4.1 Alternatives

The available methods for simulating reactivity devices in core calculations can be divided into two distinct classes (Dastur and Buss, 1983). In one class of methods, the fuel and reactivity devices are treated as line sources and line sinks in a full core simulation model. Due to the high cost of such simulations, this class of methods has not been used extensively for power reactor applications.

The alternate methodology involves simulating the effect of reactivity devices in a reactor by modifying the lattice macroscopic neutronic cross sections in the regions affected by the devices. In this second approach, the effect of the neutronic interaction between the fuel and reactivity devices is precalculated for representative lattice cells. In the full core simulation, therefore, it is not necessary to reevaluate these interactions for each device and each fuel channel. Consequently this class of simulation methodology is much less computationally demanding, and hence substantially more cost-effective.

A number of computational tools have been developed for determining the effect of reactivity devices on lattice cell cross sections. These codes simulate a lattice cell with and without the reactivity device present. The cell averaged cross sections for the two cases are compared. The difference represents the device incremental cross sections which are to be used in the core simulations.

The GETRANS two dimensional integral transport code (Roshd and Chow, 1978), and SHETAN, its three-dimensional counterpart (Chow and Roshd, 1980), have been successfully applied in the determination of device incrementals.

An alternative method, more widely applied, involves the use of a computer code, MULTICELL (Dastur, Marczak, Piva, and Donnelly, 1979; Dastur and Buss, 1983) which combines aspects of transport theory and diffusion theory to provide a relatively inexpensive technique to determine device incremental cross sections. The MULTICELL approach was adopted for this study. The methodology is described in more detail in Section 9.4.2, and in the code literature (Dastur et al., 1979; Dastur and Buss, 1983). Results have been found to agree well with the SHETAN transport code and with experiments (Dastur and Buss, 1983).

9.4.2 The MULTICELL Methodology

9.4.2.1 Geometrical Considerations

The MULTICELL code solves the two-energy group three-dimensional neutron diffusion equations using a first-order finite difference approximation to the flux derivative. Iterative methods are used to obtain the solution. Neutronic leakage is adjusted at each iteration to achieve convergence. Boundary conditions in terms of current to flux ratios (CFRs) are applies at the surface of the fuel and strongly absorbing reactivity devices (since diffusion theory is not valid in these regions). Reflection boundaries are assumed on all sides of the modelled lattice cell.

The code uses rectangular geometry, and hence all devices are approximated by rectangular shapes. The fuel region is rectangularized in the

MULTICELL model such that the actual surface area is conserved. Similarly, the surface area of cobalt adjuster pencils, etc, is conserved since CFR boundary conditions are applied to such regions.

Recognizing the importance of the moderator region to the cell neutronics, the volume of the moderator region is conserved in the MULTICELL model. The volume of the fuel annulus region (including pressure and calandria tubes) is modified to provide the adjustments to the modelled moderator region as required. Annulus region cross sections are also adjusted to conserve reaction rates.

9.4.2.2 Simulation of the Fuel Region

The treatment of the fuel region is dependent on the MULTICELL code energy group structure chosen. The code is generally applied using fuel properties from the POWDERPUFS-V lattice physics code (Tin and Loken, 1979) with the Westcott cross section structure (Westcott, 1970). With some modifications to the procedure, it was successfully applied here using the WIMS two group structure, with a cut-off between groups 1 and 2 at 0.625 eV.

When using the WIMS two energy group structure, it was found that the flat fast flux (uniform source) option in MULTICELL was not appropriate, even for devices that did not appreciably alter the neutronic spectrum. The full two group option in the MULTICELL code proved to be optimal.

With the two-energy group structure in MULTICELL, the fuel source is treated as a thin region (10^{-7} cm in width) at the periphery of the fuel region. Current to flux ratio boundary conditions are used to model the neutronic sink component of the nuclear fuel. The 2 group neutron diffusion equations are solved in the fuel source region and beyond.

9.4.2.2.1 Calculation of the Source Region Production Cross Section

The neutron production cross section for the source region is obtained by forcing the reaction rate in the MULTICELL thin source region to be equal to that in the WIMS-CRNL total fuel region:

$$\nu\Sigma_{f2s}\,\phi_{2s}\,2\pi r_s\,t = (\nu\Sigma_{f1}\,\phi_1 + \nu\Sigma_{f2}\,\phi_2)\,\pi r_s^2 \qquad (9.4.2\text{-}1)$$

where:

$\nu\Sigma_{f2s}$ = the MULTICELL source region production cross section,
r_s = the source region radius (in this case, taken to be the inner radius of the pressure tube),
t = the thickness for the source region in the MULTICELL model (10^{-7} cm),
ϕ_{2s} = the thermal flux at the surface of the fuel region (in this case, taken to be the thermal flux in the coolant region in the WIMS-CRNL model between the fuel bundle outer radius and the pressure tube inner radius, and
$(\nu\Sigma_{f1}\,\phi_1 + \nu\Sigma_{f2}\,\phi_2)$ = the total production rate per unit volume in the WIMS-CRNL source region (from WIMS-SHETAN output (Donnelly, 1985)).

9.4.2.2.2 Calculation of Fuel Region Boundary Conditions

Current to flux ratio (CFR) boundary conditions were calculated for the fuel region by considering the neutron balance equations:

$$\Delta J_1 A - \nu\Sigma_f\,\phi_2\,V + \Sigma_m\,\phi_1\,V + \Sigma_{a1}\,\phi_1\,V = 0 \qquad (9.4.2\text{-}2)$$

$$\Delta J_2 A + \Sigma_{a2}\,\phi_2\,V - \Sigma_m\,\phi_1\,V = 0 \qquad (9.4.2\text{-}3)$$

where:

ΔJ = the neutron leakage per unit surface area,
$\nu\Sigma_f$ = the production cross section,
Σ_m = the moderation cross section,
Σ_a = the absorption cross section,
A = the surface area,

V = the fuel region volume, and,

ϕ = the neutron flux.

Rearranging these equations gives:

$$CFR_1 = \Delta J_1 / \phi_{1s} = (\nu\Sigma_f \phi_2 V - \Sigma_m \phi_1 V - \Sigma_{a1} \phi_1 V)/(\phi_{1s} A) \qquad (9.4.2\text{-}4)$$

$$CFR_2 = \Delta J_2 / \phi_{2s} = (\Sigma_m \phi_1 V - \Sigma_{a2} \phi_2 V)/(\phi_{2s} A) \qquad (9.4.2\text{-}5)$$

However, since the fuel region source is treated separately, the first term on the right hand side of Eq 9.4.2-4 is neglected, yielding:

$$CFR_1 = \Delta J_1 / \phi_{1s} = (- \Sigma_m \phi_1 V - \Sigma_{a1} \phi_1 V)/(\phi_{1s} A) \qquad (9.4.2\text{-}6)$$

The terms on the right hand side of Eq 9.4.2-5 and 9.4.2-6 are obtained from the WIMS-CRNL output and the WIMS-SHETAN post-processer code.

9.4.2.2.3 Calculation of Fuel Region Properties

After the neutron flux is determined in the region of solution, the MULTICELL code calculates cell-averaged cross sections. It is therefore necessary to provide cross sections for the fuel and reactivity device regions even though the neutron diffusion equations are not solved there. The fuel region cross sections are determined using the WIMS-SHETAN code to compress the 18 group WIMS-CRNL energy structure to 2 groups and to flux and volume weight the cross sections for all materials enclosed by the pressure tube in the WIMS-CRNL simulations. This includes fuel, fuel sheath, and coolant regions. These data are then transferred to the MULTICELL code. A special flag is set in the code input to denote the material as a rectangularized cylinder. The code internally multiplies the input cross sections for this region by $4/\pi$ to conserve reaction rates.

9.4.2.3 Simulation of Fuel Annulus Region

As noted in Section 9.4.2.1, the fuel annulus region is simulated as a rectangularized zone surrounding the source region. The annulus properties are obtained by volume and flux weighting the pressure tube, gas gap, and calandria tube cross sections. The WIMS-SHETAN code is used to homogenize the WIMS-CRNL results and condense the 18 group energy structure to 2 groups.

The dimensions of the annulus region are adjusted so that the volume of material inside the annulus plus fuel region is equal to the actual volume enclosed by the calandria tube. To ensure conservation of reaction rates, the annulus cross sections input to MULTICELL are multiplied by the factor V_A/V_M where V_A is the actual annulus volume and V_M is the modelled annulus volume.

9.4.2.4 Simulation of Moderator Region

The importance of the moderator as the chief scattering material in the cell is recognized by preventing any change in the moderator volume in the specification of the MULTICELL model material distribution. Properties are obtained from the WIMS-CRNL/WIMS-SHETAN lattice cell simulations.

9.4.2.5 Simulation of Reactivity Devices

The use of diffusion theory in the calculation of the neutron flux distribution, requires that all materials in the region of solution be only weakly absorbing. Hence, materials such as air, light water, and zirconium can be included in the region of solution, while materials such as cobalt and cadmium must be treated with appropriate boundary conditions. In both cases material properties are required as input to the MULTICELL code.

9.4.2.5.1 Neutronic Properties for Reactivity Device Constituent Materials

Neutronic properties for the reactivity device constituent materials

can be obtained in a number of ways. Tables of neutronic cross sections are published by various sources and in various forms (e.g. Westcott, 1970; Mughabghab and Barber, 1973; Lamarsh, 1977; Walker et al., 1977). Such tabular data can be modified to correct for neutron temperature (Westcott, 1970). This is the usual approach taken in CANDU applications.

Alternatively, and often more appropriately, cross sections can be obtained from the nuclide libraries in the lattice physics codes. In this way, consistence in neutronic energy grouping between the fuel and lattice structural materials and reactivity device materials can be attained.

Chan and Dastur (Chan, 1981) devised a strategy of coupling POWDERPUFS-V (Tin and Loken, 1979), MULTICELL (Dastur and Buss, 1983), and WIMS-CRNL (Donnelly, 1986) in an effort to obtain incremental cross sections for rod-in-tube type stainless steel adjusters using the Westcott cross section convention (Westcott, 1970). A two dimensional WIMS-CRNL model was devised with the adjuster rod surrounded by an annulus of fuel located 1.414 times half a lattice pitch from the centre of the device. This allowed boundary conditions and neutronic properties to be obtained by post-processing the WIMS-CRNL results. A modified one-group version of MULTICELL was devised. The thermal source was derived from down-scattering of an assumed flat fast flux across the MULTICELL model. Incremental cross sections consistent with the POWDERPUFS-V lattice physics properties were then determined, with quite successful results.

There are several differences between the rod-in-tube type problem, above, and the calculation of incremental cross sections for cobalt adjusters in the current study. First, the homogeneity of the cobalt pencils allowed for a more simplified approach. Secondly, the complexities introduced to couple WIMS-CRNL and PPV data were not necessary in this case since WIMS-CRNL data were used throughout.

The modelling of a device using the WIMS-CRNL code to calculate neutronic properties and boundary conditions for subsequent input to MULTICELL holds much merit since the self-shielding effects and neutronic spectral variation through component materials can be explicitly modelled. However, since the WIMS-CRNL code is only two-dimensional, some error is introduced in

the transition from the true configuration with the device perpendicular to the fuel to the situation with a fuel annulus surrounding the reactivity device. Further, the expense and effort involved in setting up and running the required WIMS-CRNL simulations would have to be weighed against the achievable increase in accuracy. Given that in previous applications the use of simple tabular data for obtaining device constituent material properties (e.g. Jenkins, 1984) has provided accurate agreement with station measurements, the additional complexities with the WIMS-CRNL simulations did not seem justified for the purposes of this study. Instead the following approach was taken.

It was recognized that the devices would be placed interstitially between the fuel channels in the moderator region. Two group cross sections for each constituent material of each device were calculated using a number of simplified WIMS-CRNL fuel lattice simulations (taking advantage of the models developed for the calculation of the fuel properties), with a modified region added at the periphery of the cell. This modified region consisted of a ring of the constituent material for which cross sections were to be determined. The thickness of the ring was chosen such that the volume of the material in the annular ring per bundle length matched the actual amount of the constituent material in a lattice cell with the device. The WIMS-SHETAN code was then used to post-process the WIMS-CRNL data to obtain the constituent material two group properties under spectral conditions very close to those which the material would be subjected to in the true reactor environment. Sensitivity studies were conducted to examine the effect of varying fuel enrichment, fuel irradiation and the constituent material ring radius.

9.4.2.5.2 Calculation of Boundary Conditions on Reactivity Devices

In the MULTICELL simulations performed in this study, it was necessary to model the cobalt adjuster pencils with boundary conditions. The appropriate two group current to flux ratio (CFR) boundary conditions were calculated using the cobalt material properties (obtained in Section 9.4.2.5.1) as input to the MULTCFR code (Marczak, 1981). This code

was written to automate the calculation of boundary conditions on cylindrical devices based on the Kushneriuk methodology (Kushneriuk, 1959). The Kushneriuk method uses an analytical approach to determine neutronic properties for homogeneous cylindrical devices surrounded by predominantly scattering media. The MULTCFR code calculates the CFRs for each energy group according to the following equation (Dastur and Buss, 1983):

$$CFR = -(4/\beta - 3g)^{-1} \qquad (9.4.2\text{-}7)$$

where β, the blackness, is a function of the device properties and radius. The parameter, g, is a complex function defined in (Kushneriuk, 1959), and is dependent on the product of the radius of the absorbing cylinder and the macroscopic transport cross section of the surrounding medium. The MULTCFR code interpolates tabular data for the g function as presented by Kushneriuk (1959). The CFRs defined in this manner are appropriate to be used as device boundary conditions in the MULTICELL diffusion theory calculations.

9.5 DETERMINATION OF ADJUSTER ROD INCREMENTAL CROSS SECTIONS

9.5.1 Device Description

The cobalt adjuster rod design chosen for use in the advanced CANDU designs was that proposed for the Gentilly-2 cobalt conversion project (Jenkins, 1984). Each cobalt adjuster rod is comprised of a number of cobalt bundles, 21.0388 cm in length. The adjuster bundles are capable of holding up to 6 zirconium sheathed cobalt pencils on a two inch pitch circle. Each cobalt pencil is comprised of 8 cobalt slugs, 0.6223 cm in diameter and 2.5273 cm in length. The zirconium sheaths are 0.8001 cm in outside diameter (OD), 0.0635 cm in width, and 20.9550 cm in length. The bundle has two additional support tubes (each 0.8001 cm OD, thichness 0.0635 cm), on a 2.6924 cm pitch circle, and a central support rod of solid zirconium (0.9195 cm OD). Top and bottom end plates containing 50.05 g and 53.07 g of zirconium, respectively, complete the structure.

Adjuster rods travel through stationary Zircaloy-2 guide tubes with OD 8.89 cm, and thickness 0.127 cm. Circular holes are drilled through the tubes in a repeating pattern, removing 40% of the Zircaloy-2 material.

9.5.2 Simulation Results

The MULTICELL model used in the simulations, and all associated calculations are detailed in Appendix C.

Sensitivity studies were conducted which showed that the device incremental properties were not appreciably affected by either fuel enrichment or fuel burnup. The analysis did indicate a dependence on the lattice geometry, due to altered cell sizes, differences in the moderating capabilities of the cells, and the difference in the amount of fuel per lattice cell and per unit length of reactivity device. Hence two sets of adjuster rod incremental properties were developed -- one set for the NATNOM case, and a second set for all of the 14/21 cases (based on the 14211312 data). The incremental properties are provided in Table 9-2. These incremental cross sections are to be applied over a volume of 1 LP by 1 LP by 1 bundle length (BL).

The adjuster rod guide tubes are in core regardless of the position of the adjuster rods. The FMDP core model (Chapter 8) incorporated materials with the incremental guide tube cross sections from Table 9-2 for the simulation of these devices. To simulate an adjuster rod in core, an additional material was overlapped on top of the guide tube in the adjuster region. Because of this overlapping in the core model, the incremental adjuster rod properties quoted in Table 9-2 were obtained by taking the difference between the MULTICELL cross sections with the guide tube and the adjuster inserted, minus the MULTICELL cross sections with the guide tube present and no adjuster inserted. Incremental properties for the guide tube were calculated with respect to the case with no devices in the cell.

Fuel Model Type	Device Description	Incremental Fast Transport Cross Section (cm^{-1})	Incremental Thermal Transport Cross Section (cm^{-1})	Incremental Fast Absorption Cross Section (cm^{-1})	Incremental Thermal Absorption Cross Section (cm^{-1})	Incremental Moderation Cross Section (cm^{-1})	Incremental Production Cross Section (cm^{-1})	Incremental Bundle Power to Cell Thermal Flux Ratio (1E-11 $kWcm^2s$)	Incremental Fuel to Cell Thermal Flux Ratio
NATNOM	Guide Tube	4.140 E-5	-1.260 E-4	2.210 E-6	1.319 E-5	-1.132 E-5	1.388 E-6	7.014 E-5	0.0002
	1 Co Pencil	1.083 E-4	1.235 E-4	6.325 E-5	2.488 E-4	-5.105 E-6	2.112 E-5	1.067 E-3	0.0026
	2 Co Pencils	2.165 E-4	2.470 E-4	1.265 E-4	4.975 E-4	-1.021 E-5	4.223 E-5	2.134 E-3	0.0051
	3 Co Pencils	3.003 E-4	3.694 E-4	1.812 E-4	6.950 E-4	-8.420 E-6	6.462 E-5	3.266 E-3	0.0079
	4 Co Pencils	3.840 E-4	4.917 E-4	2.358 E-4	8.924 E-4	-6.630 E-6	8.701 E-5	4.397 E-3	0.0106
	5 Co Pencils	4.674 E-4	6.008 E-4	2.903 E-4	1.042 E-3	-5.810 E-6	9.943 E-5	4.980 E-3	0.0122
	6 Co Pencils	5.508 E-4	7.098 E-4	3.449 E-4	1.191 E-3	-4.990 E-6	1.119 E-4	5.562 E-3	0.0137
14/21	Guide Tube	5.320 E-5	-1.353 E-4	3.481 E-6	1.452 E-5	-1.428 E-5	1.260 E-6	4.803 E-5	0.0001
	1 Co Pencil	1.507 E-4	1.510 E-4	7.248 E-5	2.843 E-4	-3.910 E-6	2.017 E-5	7.689 E-4	0.0022
	2 Co Pencils	3.014 E-4	3.020 E-4	1.450 E-4	5.686 E-4	-7.820 E-6	4.034 E-5	1.538 E-3	0.0043
	3 Co Pencils	4.159 E-4	4.410 E-4	2.113 E-4	8.046 E-4	-7.695 E-6	6.676 E-5	2.545 E-3	0.0069
	4 Co Pencils	5.304 E-4	5.800 E-4	2.776 E-4	1.041 E-3	-7.570 E-6	9.318 E-5	3.552 E-3	0.0095
	5 Co Pencils	6.419 E-4	7.185 E-4	3.444 E-4	1.222 E-3	-8.215 E-6	1.054 E-4	4.017 E-3	0.0108
	6 Co Pencils	7.534 E-4	8.570 E-4	4.111 E-4	1.403 E-3	-8.860 E-6	1.176 E-4	4.483 E-3	0.0121

Table 9-2 Adjuster Rod Incremental Properties

9.6 DETERMINATION OF ZONE CONTROLLER INCREMENTAL PROPERTIES

9.6.1 Device Description

The light water zone controller design and layout was chosen to be the same as the nominal CANDU-600 design (Atomic Energy of Canada Limited, 1981). The device consists of a Zircaloy-2 tube (11.684 cm OD, 0.127 cm thickness). The tube can be filled to a variable level with light water. 4.7% of the interior compartment is occupied by bubbler tubes, etc., composed of Zircaloy-2.

9.6.2 Simulation Results

The MULTICELL model used in the simulations, and all associated calculations, are detailed in Appendix D.

Sensitivity studies conducted showed that the device incremental cross sections were not appreciably affected by either fuel burnup or enrichment. As in the adjuster cases two sets of incremental properties were found -- one set for the NATNOM case and one set for all of the 14/21 cases (based on the 14211312 data). The incremental properties are provided in Table 9-3. These incremental cross sections are to be applied over a volume of 1 LP by 1 LP by 1 BL.

The incremental cross sections for the empty zone controller were calculated by taking the difference between the MULTICELL cross sections with the empty zone controller in the cell and the results with no devices. In the core model, these incremental properties are added over the entire zone controller length, independent of the fill level. The incremental cross sections for the zone controllers with water were found by taking the difference between the MULTICELL cross sections with the zone controller full and the MULTICELL cross sections with the zone controller empty. In the core model a full zone controller is simulated as a combination of two devices. Empty zone controller incrementals (Table 9-3) are added to the full zone controller incrementals (Table 9-3) to provide the appropriate total effect.

Fuel Model Type	Zone Controller Status	Incremental Fast Transport Cross Section (cm^{-1})	Incremental Thermal Transport Cross Section (cm^{-1})	Incremental Fast Absorption Cross Section (cm^{-1})	Incremental Thermal Absorption Cross Section (cm^{-1})	Incremental Moderation Cross Section (cm^{-1})	Incremental Production Cross Section (cm^{-1})	Incremental Bundle Power to Cell Thermal Flux Ratio (1E-11 kW/cm^2s)	Incremental Fuel to Cell Thermal Flux Ratio
NATNOM	Drained	-1.657 E-2	-2.794 E-2	-4.053 E-5	1.052 E-4	-6.914 E-4	6.664 E-5	3.368 E-3	0.0085
	Full	2.284 E-2	1.573 E-1	1.810 E-4	1.135 E-3	2.929 E-3	-3.505 E-5	-1.771 E-3	-0.0063
14/21	Drained	-1.969 E-2	-3.054 E-2	-3.051 E-5	1.679 E-4	-8.194 E-4	1.334 E-4	5.085 E-3	0.0132
	Full	2.737 E-2	2.034 E-1	1.789 E-4	1.369 E-3	3.652 E-3	-2.060 E-4	-7.852 E-3	-0.0227

Table 9-3 Zone Controller Incremental Properties

A mesh cell in the core model which contains an interface between the filled and empty portion of a zone controller, uses appropriately prorated incremental cross sections.

9.7 SUMMARY

In core reactivity devices are required for both spatial and bulk control of the reactor power distribution. Analyses were conducted to determine the differences in reactivity device requirements when the advanced 14/21 fuel designs are introduced.

Reactivity device incremental cross sections for cobalt adjuster rods and light water zone controllers were determined for the NATNOM and 14/21 fuel designs. Incremental properties were found to be relatively insensitive to fuel burnup or fuel enrichment.

The incremental properties are provided in Tables 9-2 and 9-3. These properties were used in the core calculations detailed in Chapter 10.

CHAPTER 10

REACTOR FUEL MANAGEMENT CALCULATIONS

10.1 INTRODUCTION

The nominal fuelling scheme for a CANDU reactor is an 8 bundle shift bidirectional scheme (Atomic Energy of Canada Limited, 1981). This fuelling scheme is depicted in Fig. 10-1. Fuelling is conducted at power. This scheme provides sufficient reactivity gain per channel fuelled without exceeding licence bundle and channel power limits. To avoid exceeding these power limits and improve operational flexibility, some stations fuel the centre region of the reactor with a 2 or 4 bundle shift scheme. This, however, places extra duty requirements on the fuelling machines. The benefits often outweigh the drawbacks.

10.2 FUEL MANAGEMENT REQUIREMENTS WITH ENRICHED FUEL

As the fuel enrichment is increased, the positive reactivity insertion upon refuelling is also increased. The increased fission cross section of the fresh fuel results in localized flux and power peaking in the vicinity of the freshly inserted fuel. Careful fuel management techniques with innovative fuelling schemes and/or design modifications are required to ensure that bundle and channel power limits are not exceeded.

Studies of fuel management requirements with enriched fuel have been conducted in the past at Ontario Hydro (Bonalumi and Lau, 1979). For push-through bidirectional fuelling, these studies concluded that maximum enrichments of 0.9 weight percent (w/o) U-235 would be feasible in the Bruce NGS-B CANDU reactors. These researchers recommended the use of a 2 bundle shift scheme in the inner core region and a 4 bundle shift in the outer core. For higher enrichments, localized power peaking would cause several

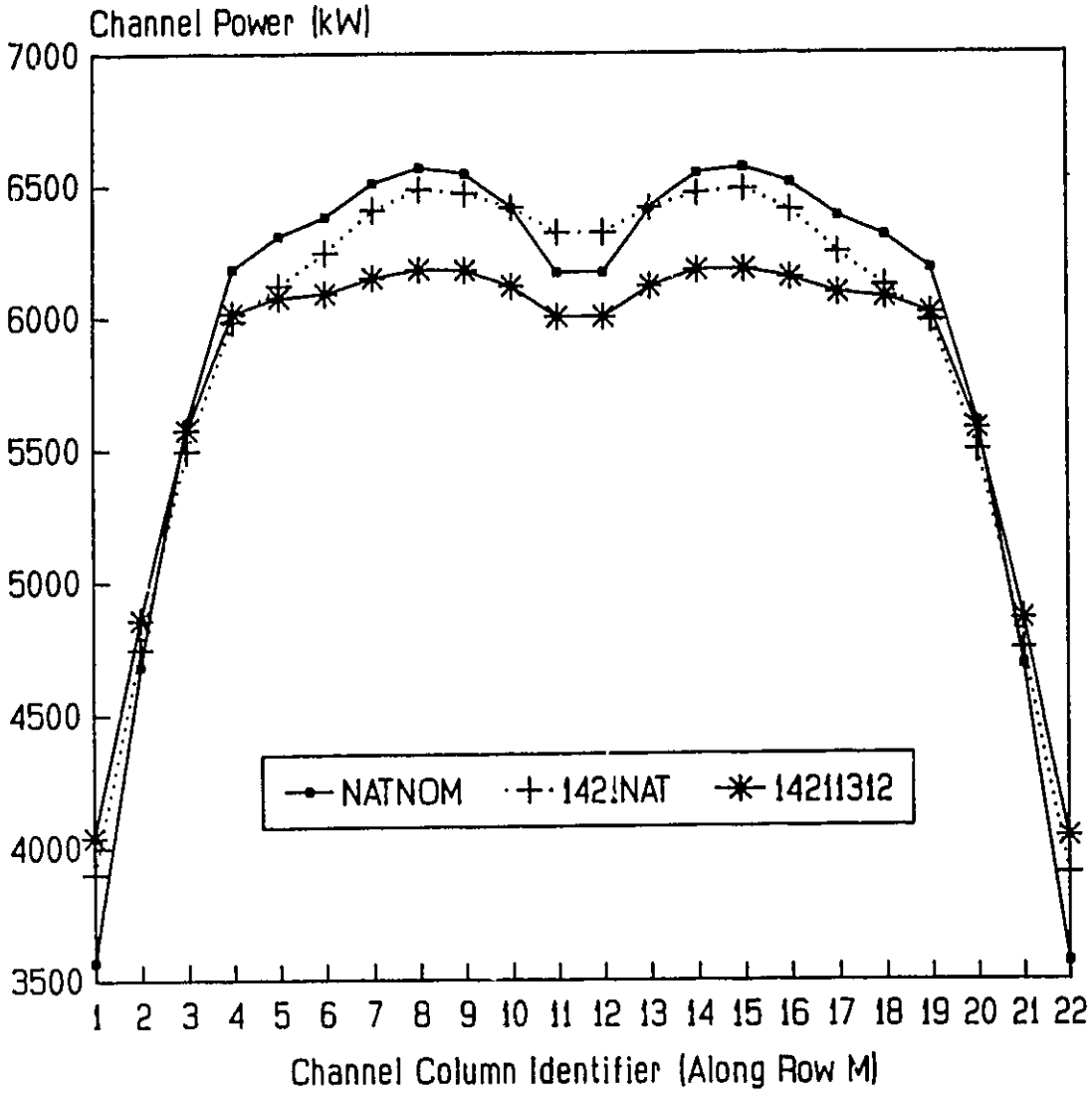

Figure 10-1a Channel Power Distributions (CBDFA)

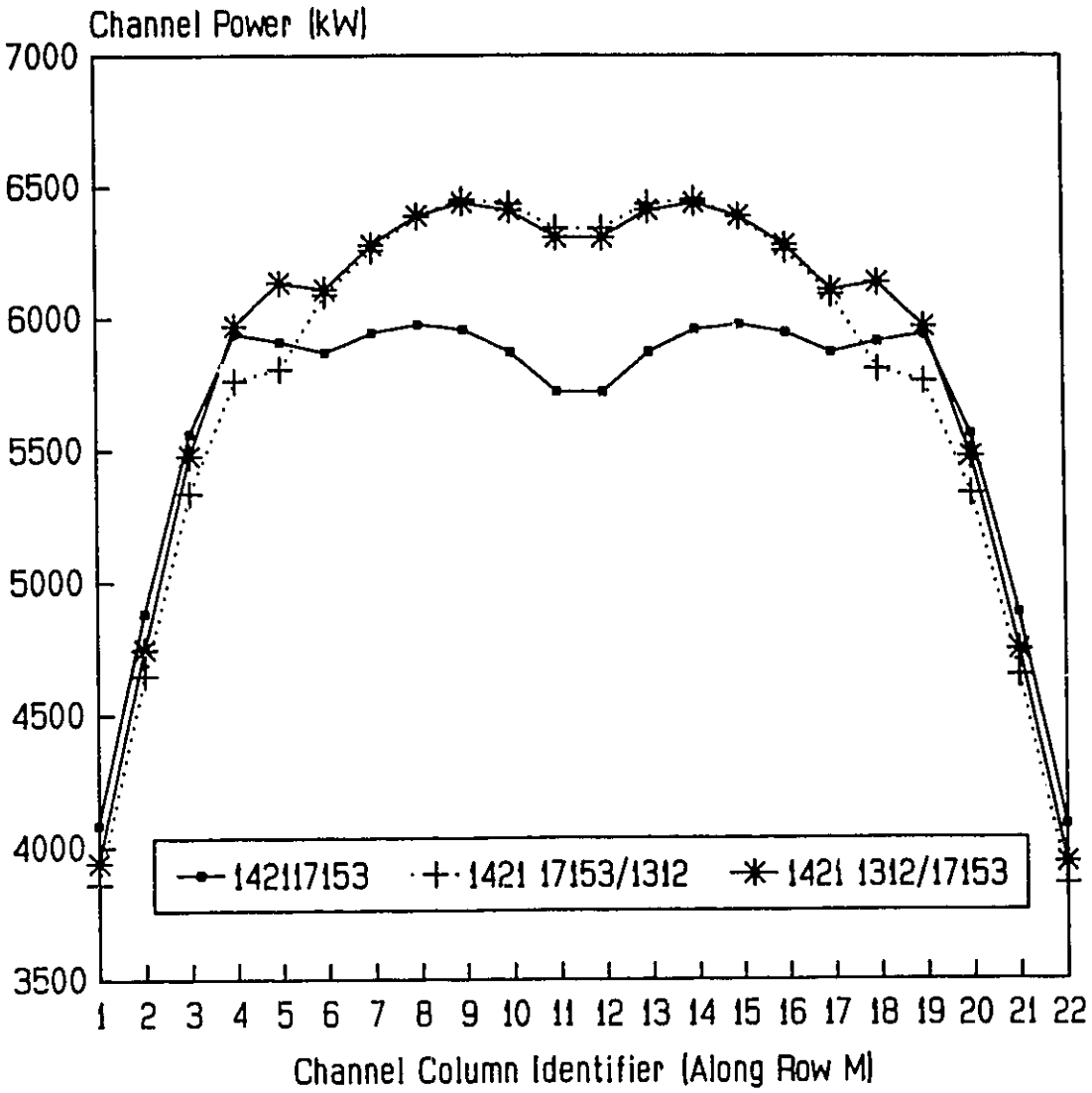

Figure 10-1b Channel Power Distributions (CBDFA)

channels to exceed their critical channel power, resulting in dryout, and possible failure of the fuel bundles.

Bagnal et al. (1981), in a Combustion Engineering study, recommended the use of a 2 bundle shift scheme with 1.2 w/o U-235.

Recent and on-going fuel management studies at AECL in Chalk River, Ontario (Boczar and van Dyk, 1986), have demonstrated that by employing a 1 or 2 bundle shift bidirectional fuelling scheme and repositioning the adjuster absorber rods (for flux and power shaping) towards the ends of the channels (as opposed to the central portion of the reactor), fuel enrichments of at least 1.7 w/o are feasible. A disadvantage with this scheme is that the placement of fresh fuel at the ends of the reactor increases leakage and burnup is therefore not optimized.

The efforts at AECL-CANDU Operations at Mississauga, Ontario, have been concentrated on an alternative and novel fuel management scheme which would not require the redeployment of reactivity devices (Chan and Dastur, 1985). These schemes, generically referred to as "checkerboard fuel management" (Younis et al., 1986), involve the use of distinct fuelling schemes in alternating zones of channels which are neutronically coupled. This methodology forms the analytical basis from which this thesis extends.

Indeed these checkerboard fuelling schemes, while novel for CANDU on-power fuelling applications, bear underlying features in common with current off-power fuelled light water reactor fuelling schemes (Levine, 1982), those suggested for Britain's SGHWR (O'Dell et al., 1968), and for LMFBR fuel management (Dickson and Arnold, 1983). Before delving further into the CANDU checkerboard fuelling, it is prudent at this point to examine the rationale behind these similar schemes employed in this entire range of reactor variants, all of which utilize off-power batch refuelling and enriched fuels. (Enrichment in this context can be in terms of fissile uranium or plutonium).

10.3 FUEL MANAGEMENT PHILOSOPHIES

10.3.1 SGHWR

Britain's SGHWR reactor uses fuel assemblies which extend the entire length of the core. Hence, only radial fuel management is possible.

The two main fuel management principles employed involve feeding the outer channels of the reactor with a higher fuel enrichment, and moving partially irradiated fuel from the outer zone inwards (O'Dell et al., 1968). The former method is used for fresh conditions. The latter is used at equilibrium.

A 3-cycle "roundelay" fuelling pattern (O'Dell et al., 1968) was found to be most effective for the SGHWR during equilibrium operation with yearly fuelling outages. This scheme achieves flux flattening by means of an inward radial fuel move. During a shutdown, fuel is discharged from the, for example, "white" squares of the checkerboard region in the reactor core inner zone. These fuel assemblies are replaced by partially irradiated fuel from the outer region. Fresh fuel is then loaded into the outer region of the core. On the next shutdown, a similar scheme is followed, except the "black" squares of the inner zone checkerboard region are refuelled (O'Dell et al., 1968).

For commercially-sized units based on the SGHWR concept, a nine cycle dual-feed enrichment scheme is preferred (O'Dell et al., 1968). In such schemes, the reactor is divided into an array of 9 channel (3 by 3) supercells. One channel per supercell is refuelled at each 6-month fuelling outage. Power flattening is achieved by using higher enrichment fuel in the outer zone supercells.

10.3.2 Pressurized Water Reactors

In pressurized water reactors (PWRs), radial fuel management also consists of a combination of enrichment and average irradiation zonal variations. Power flattening and low leakage fuelling objectives are often at

odds (Levine, 1982).

The conventional PWR core loading pattern is known as the "out-in" scheme (Killmar et al., 1988). The highest enriched fuel asemblies are positioned at the boundary of the core to flatten the power distribution. These are moved towards the central region at the next fuelling outage. Power flattening objectives are therefore maintained.

The "out-in" scheme is suitable to operations in which yearly fuelling outages are provided. This has been the development path chosen in the FR Germany (Killmar et al., 1988). In terms of burnup optimization, the use of shorter cycles is preferred (Silvennoinen, 1976).

In the USA, utilities have generally opted to use fuelling strategies which require fuelling outages every 18 to 24 months (Ardrews and Lobre, 1988). To achieve these extended operating cycles, new core management and loading pattern technologies have been developed (Keller and Shank, 1987). Low leakage patterns ("in-out" schemes), have contributed significantly towards achieving these operating goals, through reduced neutron losses from the core, and through the use of fresh fuel to drive previously irradiated fuel to even higher burnups. The use of checkerboard-type or similar scatter loading patterns aids neutronic coupling of fuel of varying burnup in both low leakage and power flattening schemes (Levine, 1982; Silvennoinen, 1976).

10.3.3 Fast Breeder Reactors

Most early Fast Breeder Reactor (FBR) designs were conceived to operate with homogeneous cores surrounded by fertile blankets (Dickson and Arnold, 1983). However, so called heterogeneous designs first conceived by French designers, offer improvements in both safety and economics (Till, 1979). In such heterogeneous designs, the flux is flattened across the core by scatter-loading (Silvennoinen, 1976; Till, 1979; Dickson and Arnold, 1983) or bullseye loading schemes (Vitti et al., 1979) in which driver and blanket assemblies are distributed within the central core region. The fuel doubling time is increased (Bailey and Lu, 1977) and the sodium void reactivity is reduced (Dickson and Arnold, 1983) in comparison with the homogeneous

designs.

10.3.4 On-Power Fuelling

On-power fuelling in nuclear reactors (such as CANDU) is complex, though it offers several advantages over off-power refuelling (Bartholomew et al., 1988):

(a) Enables the unit to have a lifetime capacity factor advantage of typically 5-10% over off-power fuelling.

(b) Permits major outages independent of fuelling operations.

(c) Allows higher average burnup and therefore lower fuelling costs.

(d) Allows on-power removal of defective fuel.

In addition, on-power fuelling minimizes the bulk reactivity control requirements and minimizes variations in the reactor characteristics throughout its operating lifetime.

Using a simplified calculational algorithm, Silvennoinen (1976) demonstrated that fuel utilization can be almost doubled by utilizing continuous on-power refuelling as opposed to yearly fuelling outages.

Because of the operational advantages afforded through the use of on-power fuelling, this strategy was adopted for application in the fuel management studies of the advanced reactor designs considered in this thesis.

Before discussing the results of the fuel management simulations conducted in support of this study (beginning in Section 10.5), a background discussion on the data handling methods used in the presentation and interpretation of the results is provided (Section 10.4 and Appendix E).

10.4 DATA HANDLING AND INTERPRETATION

For a comparison of reactor burnup and SWU requirements with other published data, it is necessary to convert the results of the core physics analysis (fuel bundles required per full power day (FPD)) into units of kgU_{mined}/MW(e)-a and kgSWU/MW(e)-a.

Details on the assumptions involved, and the derivation of the

appropriate governing equations and conversion factors are presented in Appendix E.

The results of the analysis in Appendix E indicate that the natural uranium requirements are not affected if fuel of the desired enrichment is produced directly, or if it is produced by dilution of quantities of uranium enriched to other (higher) standard U-235 concentrations. However, separative work requirements are increased in the latter case. It is also shown in Appendix E, that the natural uranium requirements as a function of the tailings concentration increase faster as the product enrichment increases.

Tables 10-1 and 10-2 show the natural uranium and separative work requirements (respectively) to produce 14211312 and 142117153 fuel. The entries in these tables were obtained using the equations and data provided in Appendix E. Note that it would be necessary to expend an infinite amount of kgSWU to produce uranium with no tailings. To produce 1 kg of natural uranium fuel product, 1.01 kg of natural uranium feed are required (accounting for fabrication and conversion losses (see Appendix E)). No separative work is required in this case.

Having considered the natural uranium and separative work requirements for the various fuel types, attention is now focussed on the results of the core simulations. The CBDFA, TAA, and Instantaneous Approximation analyses are considered in Sections 10.5, 10.6, and 10.7 respectively.

10.5 CONTINUOUS BIDIRECTIONAL FUEL MANAGEMENT STUDIES

10.5.1 Cases Considered

The CBDFA fuel management calculational approach was utilized to study reactor operation with six fuel variants:

(i) NATNOM: Natural uranium fuelled, nominal CANDU-600 reactor.
(ii) 1421NAT: Natural uranium, 14/21(1.07), 25 cm lattice pitch, nominal calandria tube.
(iii) 14211312: 14/21(1.07) fuel bundle design, inner ring 1.3 a/o U-235,

Product Enrichment (a/o U-235)	Tailings U-235 Concentration (a/o U-235)	Natural Uranium Requirements per kg Product (kg)
1.3/1.2	0	1.744
	0.1	1.863
	0.2	2.027
	0.3	2.269
	0.4	2.662
	0.5	3.413
1.7/1.53	0	2.250
	0.1	2.450
	0.2	2.727
	0.3	3.135
	0.4	3.800
	0.5	5.067

Table 10-1 Natural Uranium Requirements for Enriched Fuels

Product Enrichment (a/o U-235)	Feed Enrichment (a/o U-235)	Tailings U-235 Concentration (a/o U-235)	kg SWU per kg Product	
			Mix Feed with Natural Uranium	Mix Feed with Uranium Tailings
1.3/1.2	1.3/1.2	0.2	0.76	0.76
		0.3	0.56	0.56
	2.0	0.2	0.89	1.27
		0.3	0.69	0.94
	3.0	0.2	0.99	1.60
		0.3	0.78	1.19
	4.0	0.2	1.04	1.79
		0.3	0.84	1.34
1.7/1.53	1.7/1.53	0.2	1.41	1.41
		0.3	1.07	1.07
	2.0	0.2	1.51	1.70
		0.3	1.17	1.30
	3.0	0.2	1.66	2.15
		0.3	1.32	1.65
	4.0	0.2	1.76	2.42
		0.3	1.42	1.85

Table 10-2 Separative Work Requirements for Enriched Fuels

outer ring 1.2 a/o U-235, 25 cm lattice pitch, nominal calandria tube
(iv) 142117153: 14/21(1.07) fuel bundle design, inner ring 1.7 a/o U-235, outer ring 1.53 a/o U-235, 25 cm lattice pitch, nominal calandria tube.
(v) 1421 17153/1312: A reactor fuelled with 142117153 type fuel in the inner 124 channels and 14211312 type fuel in the outer 256 channels.
(vi) 1421 1312/17153: A reactor fuelled with 14211312 type fuel in the inner 124 channels and 142117153 type fuel in the outer 256 channels.

The object of the CBDFA studies was to examine the reactor characteristics (burnup, device requirements for reactivity control and power distributions) and to draw conclusions from the trends so determined.

Variants (v) and (vi) above were examined to study the effect of low leakage fuel management versus power shaping objectives via enrichment zoning. In variant (v), fuel with a lower enrichment is placed in the outer radial zone of the reactor (outer burnup zone in Fig. 8-6). Higher enrichment fuel is placed in the central zone. Neutrons leaking from the high enrichment central region can interact with the fuel in the outer zone before leaking from the core. By placing lower enrichment fuel in the outer zone fewer neutrons from the fissioning of the fresh fuel are lost from the reactor. However by placing the highest enrichment fuel in the high importance central region, there will be an increase in the power peaking in the central region. Special care must be taken to ensure that maximum bundle and channel power limits are not violated.

Variant (vi), where the enrichment zones are reversed (high enrichment outer zone, low enrichment inner zone), nominally allows for a flatter power profile, by placing the higher reactivity fresh fuel near the outer edge of the reactor to compensate for the increased neutronic leakage in this area.

Upon implementation however, the effectiveness of these latter two variants will not be as substantial as one may have initially suspected. The primary reason for this is that local reactivity is easily controlled by altering the exit burnup of the fuel. That is, the same local average reactivity can be achieved with low enriched fuel in a given lattice location for a short period of time, or with fuel of greater initial enrichment in the

location for a correspondingly longer time period.

10.5.2 Inherent Assumptions in CBDFA Cases

For these fuel management studies, the inner/outer burnup zone boundary was as in the standard CANDU-600 (Fig. 8-6). This boundary was not optimized for the different fuel variants. Optimizing the boundaries could improve burnup by several percent in each case (Wight and Girouard, 1978). Further, the flexibility to achieve the CBDFA power distributions using actual fuel management schemes is dependent on the fuel enrichment. Consequently the CBDFA results must be viewed as a first approximation, though for initial scoping studies they will provide important information on fuel management and fuelling requirements for the various fuel designs.

The adjuster rod layout was as per the nominal CANDU-600 design (Fig. 8-4a and 8-5), though the actual grading of the adjusters was treated as a variable parameter in the study.

The inner and outer core exit irradiations and the adjuster rod gradings were determined in an iterative fashion. The objective was to maintain criticality (effective multiplication factor, k-eff=1), to provide an adjuster rod worth of approximately 15 mk, to maintain channel powers less than 6.5 MW, and to ensure that maximum bundle powers did not exceed 800 kW. These requirements are similar to those in place for the nominal CANDU-600 design for this type of analysis. It is noted that the CBDFA studies do not consider the fact that bundles in an actual reactor range in age from freshly refuelled to end of cycle burnup. This results in a perturbation to the individual channel powers and is known as "fuelling ripple".

10.5.3 CBDFA Analysis Methodology

10.5.3.1 Reactivity Correction

The iterative process of converging on irradiation distributions and adjuster grading was ended before complete convergence was attained. It was

therefore necessary to correct the burnup results for the various cases for this non-convergence. The results were corrected specifically for the variation of k-eff from unity, the variation in adjuster worth from 15 mk, and the variation in zone controller worth from 3 mk at the nominal levels in the models (see Table 8-7).

The correction factor was obtained individually for each case by calculating the change in reactivity and uncorrected exit burnup resulting from a slight variation in zonal exit irradiation, as part of the iteration process.

Adjuster rod worths were obtained by comparing system eigenvalues with and without devices inserted. Zone controller worths at the nominal level were obtained by comparing the eigenvalue for the nominal case to the corresponding value with zones drained.

10.5.3.2 Calculations for Mixed Fuel Types

The 14/21 mixed fuel type cases, 17153/1312 and 1312/17153, required additional analyses to determine such parameters as uranium and separative work requirements per unit of electrical production. In these cases, the quantity, z, from Appendix E (Sections E.3 and E.4) must be a weighted average of the "z" for each fuel type. That is:

$$z = f_{1312}\, z_{1312} + f_{17153}\, z_{17153} \qquad (10.5.3\text{-}1)$$

where f_x is the fraction of the bundles of type x which are replaced daily in the reactor.

10.5.4 CBDFA Results

The results of the final iteration of the CBDFA cases are given in Table 10-3. The burnup results quoted are not corrected for system and device reactivity. The adjuster rod configurations for the converged cases are given in Table 10-4. Adjuster rod types are as per Fig. 8-4 and 8-5.

Particulars	Reactor Fuel Type					
	NATHOM	1421NAT	14211312	142117153	1421 17153/1312	1421 1312/17153
k-eff	1.00019	1.00011	0.999931	0.999906	0.999969	1.00032
Outer Core Exit Irradiation (n/kb)	2.40	2.80	7.00	8.50	6.70	8.26
Inner Core Exit Irradiation (n/kb)	2.78	3.10	6.70	8.10	8.40	6.86
Average Exit Irradiation (n/kb)	2.53	2.91	6.81	8.24	7.24	7.64
Outer Core Burnup (MWh/bundle)	3056	2959	8698	11370	8698	11525
Inner Core Burnup (MWh/bundle)	3525	3269	8994	11752	11656	8855
Average Burnup (MWh/bundle)	3221	3069	8805	11503	9630	10351
Adjuster Worth (mk)	14.92	14.97	14.94	15.39	15.71	15.36
Zone Controller Worth - Nominal Fill (mk)	3.15	3.05	2.54	2.39	2.51	2.46
Refueling Rate (bundles/FPD)	16.0	16.9	5.9	4.5	5.4	5.0
Burnup Correction Factor (MWh/bundle/mk)	35.4	52.4	42.4	36.3	42.9	42.8
Maximum Channel Power (kW)	6568	6486	6292	6381	6488	6440
Maximum Bundle Power (kW)	762	722	728	742	727	722

Table 10-3 CBDFA Cases - General Results

Adjuster Rod Type	Cobalt Pins in Adjuster Rods (CBDFA Cases)					
	NATNOM	1421NAT	14211312	142117153	1421 17153/1312	1421 1312/17153
A1	1	2	2	3	3	2
A2	2	2	2	3	3	2
B1	2	2	3	3	3	3
B2	2	2	3	3	3	3
C1	2	3	3	3	3	3
C2	2	3	3	3	3	3
D1	3	3	3	4	3	3
D2	3	2	3	4	3	3
Worth (mk)	14.92	14.97	14.94	15.39	15.71	15.36

Table 10-4 Adjuster Rod Configuration (CBDFA Cases)

In Fig. 10-1, channel power distributions along row M are shown for the various cases. Figure 10-2 is a plot of the bundle power profile along channel M-12 (in the middle of the adjuster region) for each of the cases.

In Table 10-5 the data from Table 10-3 are modified to account for system and device reactivity, and presented in terms of natural uranium requirements per unit electrical production. The mathematical procedure was as developed in Appendix E. For the mixed fuel cases the following fractional contributions were derived from the simulations:

17153/1312: $f_{17153} = 0.315$; $f_{1312} = 0.685$

1312/17153: $f_{17153} = 0.560$; $f_{1312} = 0.440$

(Refer to Section 10.5.3.2 for an explanation of these parameters.)

In a similar manner, separative work requirements for the various cases were calculated. These data are provided in Table 10-6. (See also Section E.4). SWU requirement calculations assumed production of enriched uranium at the required enrichment level (no dilution).

In Table 10-7, the resource utilization improvement for each fuelling scheme (compared to the NATNOM case) is presented.

Finally, in Table 10-8, a fuelling cost scenario is investigated, in which fuel cycle costs are calculated based on $100/kgU, and $100/kg SWU. These data do not include fuel fabrication or waste management costs, the latter of which may, in future, play an increasingly important role in fuel management economics.

10.5.5 Interpretation of CBDFA Results

The results in Table 10-5 indicate that burnup increases as fuel enrichment increases. For the case with a U-235 tailings concentration of 0.0 a/o U-235, natural uranium utilization also is increased as the U-235 concentration increases. For the higher tailings U-235 concentrations considered, the natural uranium utilization is highest for the 14211312 type

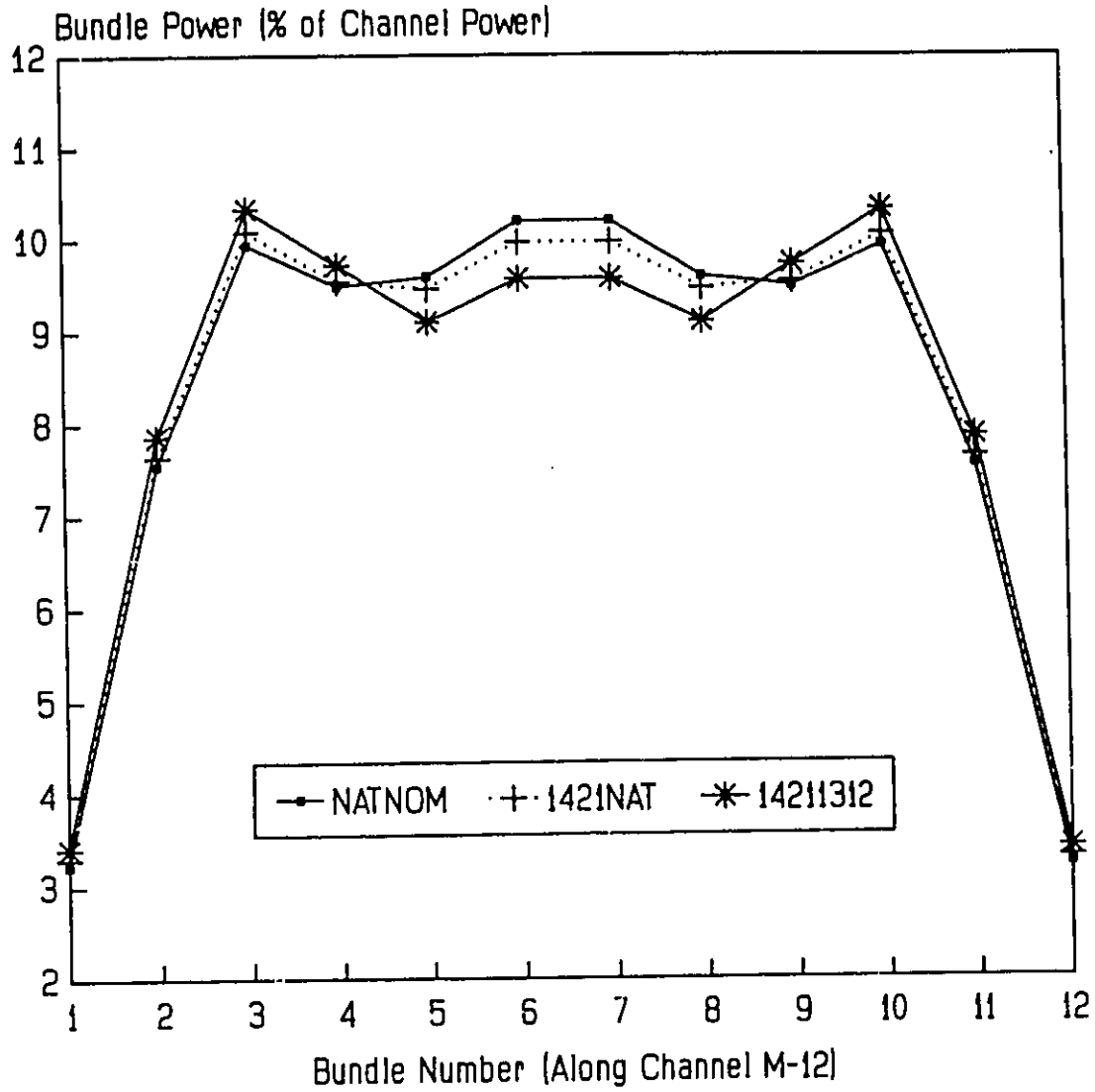

Figure 10-2a Bundle Power Distributions (CBDFA)

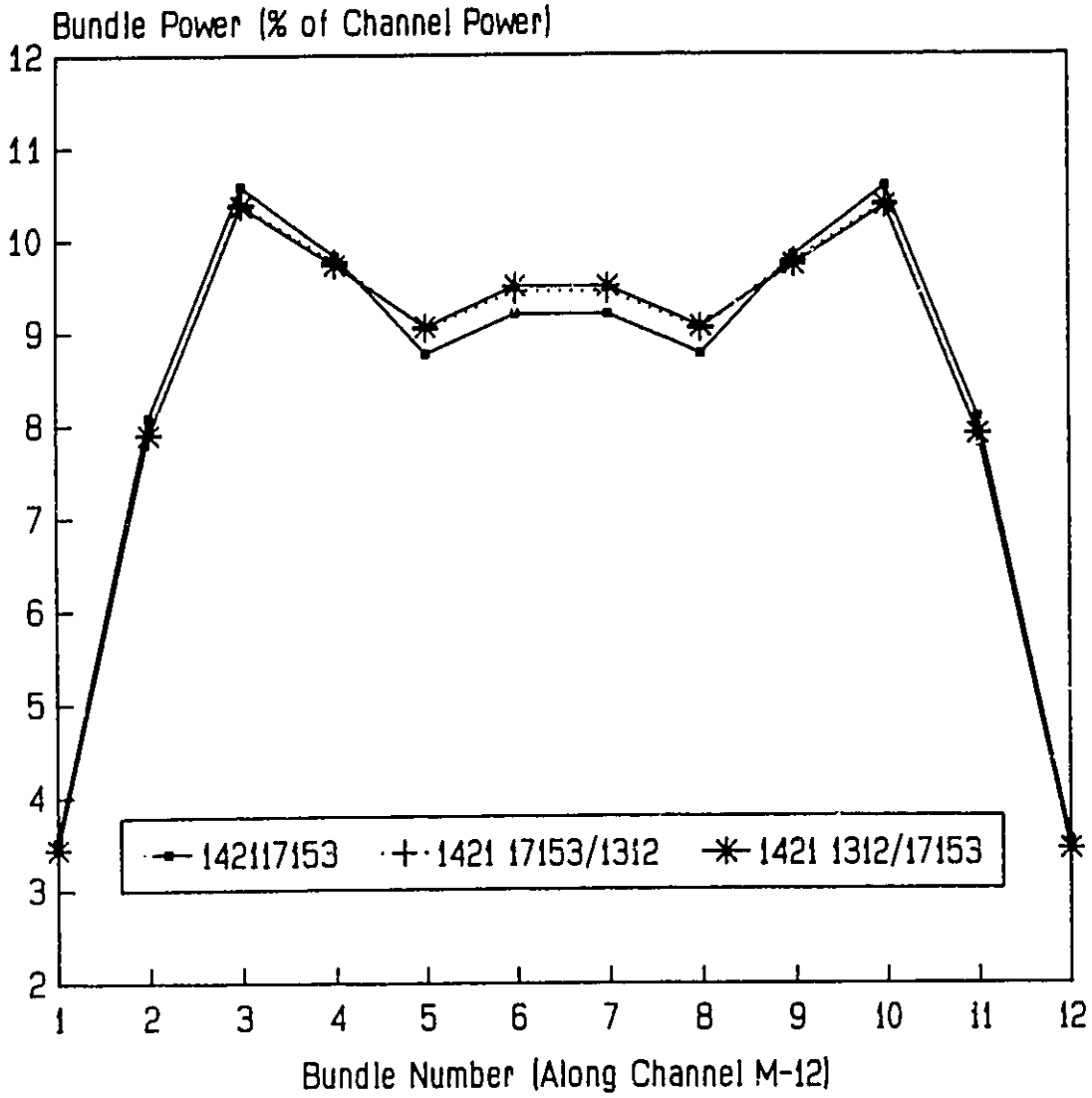

Figure 10-2b Bundle Power Distributions (CBDFA)

Tailings U-235 Concentration (a/o U-235)	Natural Uranium Requirements (kgU_{mined}/MW(e)-a)					
	NATNOM	1421NAT	14211312	142117153	1421 17153/1312	1421 1312/17153
0.0	166.2	142.8	86.4	85.1	85.9	85.1
0.2	166.2	142.8	100.4	103.2	101.4	101.6
0.3	166.2	142.8	112.4	118.6	114.7	115.6
Burnup *	7159	8333	23786	31134	26111	28059

* Burnup units are (MWd/MgU) (corrected)

Table 10-5 Natural Uranium Requirements (CBDFA Cases)

Tailings U-235 Concentration (a/o U-235)	Separative Work Requirements * (kg SWU/MW(e)-a)					
	NATNOM	1421NAT	14211312	142117153	1421 17153/1312	1421 1312/17153
0.0	0.0	0.0	∞	∞	∞	∞
0.2	0.0	0.0	37.7	53.4	43.6	47.2
0.3	0.0	0.0	27.6	40.4	32.4	35.4

* Enriched to product enrichment

Table 10-6 Separative Work Unit Requirements (CBDFA Cases)

Tailings U-235 Concentration (a/o U-235)	Resource Utilization Improvement Over NATNOM (%)					
	NATNOM	1421NAT	14211312	142117153	1421 17153/1312	1421 1312/17153
0.0	0.0	14.1	48.0	48.8	48.3	48.8
0.2	0.0	14.1	39.6	37.9	39.0	38.9
0.3	0.0	14.1	32.3	28.6	30.9	30.4

Table 10-7 Resource Utilization Improvement (CBDFA Cases)

Tailings U-235 Concentration (a/o U-235)	Uranium Plus Separative Work Costs* ('00$/MW(e)-a)					
	NATNOM	1421NAT	14211312	142117153	1421 17153/1312	1421 1312/17153
0.0	166.2	142.8	∞	∞	∞	∞
0.2	166.2	142.8	138.1	156.6	145.0	148.8
0.3	166.2	142.8	140.0	159.0	147.1	151.0

* Based on costs of $100/kg Uranium mined and $100/kg SWU.
Does not include fabrication or waste disposal costs.

Table 10-8 Uranium Plus Separative Work Costs (CBDFA Cases)

fuel. The reason for this change as the tailings concentration increases is as discussed in Section E.5.3, where it was shown that natural uranium requirements, as a function of the tailings concentration, increase faster as the product enrichment increases.

10.5.5.1 1421NAT Fuel Design

From the data in Tables 10-5 and 10-7 it is clear that the 1421NAT fuel design results in both increased burnup and natural uranium utilization (NUU) as compared with the NATNOM 37 element fuel design. The improved burnup is a consequence of both the modified bundle design and the use of enriched zirconium in the pressure and calandria tubes. This 14% increase in fuel burnup is realized without the requirement for enriched fuel. Additional costs associated with the production of enriched zirconium structural components would have to be weighed against the reduction in fuel requirements (and hence the reduction in waste management costs) associated with the 1421NAT design to evaluate the cost effectiveness of such a proposal.

10.5.5.2 14211312 Fuel Design

The 14211312 fuel design results in a fuel burnup increase of 232% over the NATNOM design, and a substantial improvement in NUU (32-48% depending on the tailings concentration). Spent fuel inventories and fuel fabrication costs are reduced compared with the NATNOM design. Separative work requirements, however, add additional expense to the fuel bundle cost. The fuel burnup (23786 MWd/MgU), is somewhat less than the approximately 30000 MWd/MgU burnups regularly reached in LWRs. As a consequence, there is an incentive to further increase the feed fuel enrichment to maximize bundle burnup and hence minimize the spent fuel volume and fuel fabrication costs.

10.5.5.3 142117153 Fuel Design

The 142117153 fuel design allows CANDU fuel to achieve burnups

comparable to LWR designs with a considerably lower feed fuel enrichment. To achieve this burnup, there are penalties to be paid both in terms of separative work costs and (except for the 0.0 w/o U-235 tailings case) in terms of NUU. The extra costs for natural uranium and separative work may be more than compensated for by the 31% increase in fuel burnup achievable with the 142117153 design over the 14211312 case. The 31134 MWd/MgU burnup represents a 335% increase over the NATNOM design. Specific economic and political scenarios will dictate the viability of this scheme.

10.5.5.4 Mixed Enrichment Fuel Designs

The mixed enrichment 14/21 fuel designs, 17153/1312 and 1312/17153, allow the examination of low leakage fuelling and radial power flattening in CANDU via enrichment zoning. The simulations indicate that the resultant burnup and NUU for the two variants are in a range between the results for the 14211312 and 142117153 cases. From this preliminary study, it is evident that adjustment of exit irradiation gives sufficient flexibility in shaping the power distribution and controlling burnup. The increased complication in fuelling with two separate types of fuel would not be justified for fuel utilization optimization purposes. It is noted that fuel management strategies geared towards minimizing the peak bundle power upon refuelling may benefit from the 14/21 mixed enrichment 1312/17153 design, where lower enrichment (lower reactivity) fresh fuel is placed in the hotter central core region.

10.5.5.5 Adjuster Loading Requirements as a Function of Fuel Enrichment

In Table 10-4 it is evident that the adjuster rod loading (number of cobalt pencils per bundle) must be increased as fuel enrichment is increased, for the same net reactivity effect. The reason for this becomes clear when one considers a one-energy-group neutron balance equation for an infinite reactor:

$$\Sigma_a\phi = \nu\Sigma_f\phi / k_\infty \qquad (10.5.5\text{-}1)$$

Then, by introducing an absorber to the system which causes:

$$\Sigma_a \rightarrow \Sigma_a + \Delta\Sigma_a \qquad (10.5.5\text{-}2)$$

one can easily show that the change in system reactivity is:

$$\Delta\rho = \Delta\Sigma_a / \nu\Sigma_f \qquad (10.5.5\text{-}3)$$

Hence a larger change in the absorption cross section is required to effect an equivalent change in reactivity as the fission cross section (and hence fuel enrichment) is increased.

10.6 TIME-AVERAGED FUEL MANAGEMENT STUDIES

To further examine the feasibility of fuelling a CANDU reactor with enriched uranium fuel, a time-averaged approximation (TAA) fuel management study was conducted using the 142117153 fuel design. This design yielded burnups similar to LWRs in the CBDFA studies. It remained to be shown that an actual fuelling scheme could be developed for this fuel variant, which was the highest enrichment design considered in this study, and hence the most limiting with respect to fuelling strategy development.

10.6.1 Cases Considered

The nominal fuelling scheme in a CANDU-600 is the 8 bundle shift bidirectional refuelling scheme. (Various schemes are shown in Fig. 10-3 (see end of chapter).) This scheme provides an acceptable axial bundle power distribution without over-extending the fuelling machine load (approximately 2 channels refuelled per full power day).

As a first attempt to devise an acceptable fuelling strategy for the

142117153 fuel design, simple push through fuelling schemes were experimented with. The current generation of CANDU fuelling machines are constructed to accomodate push through schemes involving even numbers of bundles. Consequently, in this study 2, 4, 6 and 8 bundle push through bidirectional fuelling schemes were considered.

Following an examination of these push through schemes, various checkerboard fuelling strategies were considered, beginning with a scheme similar to that developed at AECL (Chan and Dastur, 1985). This development was then extended to more advanced schemes which would be required for this high enrichment fuel. In the following subsections the results of the analyses are presented in a heuristic manner, to convey an understanding of the processes involved in developing an appropriate fuelling strategy for use with 142117153 fuel. The tables and figures for the remainder of Chapter 10 are grouped at the end of the chapter to ease comparisons of the various schemes considered.

10.6.2 Inherent Assumptions in the TAA Cases

Where possible, inner and outer burnup zones were maintained as in the nominal CANDU-600 design. The adjuster rod configuration was not altered from the CBDFA analysis. (Details regarding adjuster grading can be found in Table 10-4).

The target maximum bundle and channel powers were as in the reference CBDFA analysis:

Maximum Channel Power: 6500 kW

Maximum Bundle Power: 800 kW

This then allowed for additional margin for the effects of fuelling ripple, which would bring the maximum channel and bundle powers closer to their design limits.

Burnup data obtained from the simulations were corrected for deviation of the system eigenvalue from unity using a flux-squared weighted reactivity/burnup relationship. Burnup data were not corrected for adjuster worth variation from -15 mk as was done in the CBDFA cases. Since changes in the reactor flux/power distribution resulting from changes to the fuelling scheme affect both adjuster rod reactivity and xenon worth, xenon override

times will not be substantially altered as a consequence.

10.6.3 NATNOM Reference Fuelling Study

The first time-averaged fuel management strategy examined in this analysis was the 8 bundle shift (8BS) fuelling scheme for the CANDU-600 NATNOM 37 element natural uranium fuel design. The general results of the analysis are summarized in Table 10-9. (Other entries in this table will be discussed in subsequent sections). The dwell times quoted in Table 10-9 are the mean times between channel fuelling visits. The fewer number of bundles replaced per visit, the smaller the dwell time. The dwell time for the NATNOM case with its reference 8BS fuelling scheme is about 190 full power days (FPDs). To maintain reactor criticality, it is necessary to refuel approximately 2 channels per day using an 8BS fuelling scheme. Current fuelling machine designs are sufficient to accomodate this refuelling rate.

Channel powers along row M of the reactor are shown in Fig. 10-4. The bundle power distribution along channel M-12 is shown in Fig. 10-5. (With the bidirectional push-through fuelling schemes considered in this thesis, Channel M-12 is fuelled such that fresh bundles are inserted into the end of the channel with high bundle numbers. Channel M-12 is therefore referred to as being fuelled with a negative fuelling scheme. Channel M-11, adjacent to M-12, is fuelled with a positive fuelling scheme. In this case, fresh fuel enters from the opposite end of the core.)

The cell-averaged thermal flux distribution along channel M-12 is displayed in Fig. 10-6. In Fig. 10-7, the channel M-12 beginning and end of cycle thermal irradiation distributions are plotted. These data represent the channel conditions just after refuelling and just prior to refuelling, respectively. Fig. 10-8 provides similar information, though this time for beginning and end of cycle fuel burnup. (Note that these figures also include the results for the other TAA schemes considered later in this chapter.)

Table 10-10 shows that the burnup achievable with a NATNOM 8BS fuel shifting scheme is 7141 MWd/MgU. This is within 0.25% of the value determined using the CBDFA approach (see Table 10-5), hence verifying the effectiveness

of the CBDFA for analysis of this fuel variant.

No separative work is required when using natural uranium fuel.

10.6.4 Simple Push-Through Fuelling Schemes With 142117153 Fuel

The 142117153 CBDFA simulation was used as a starting point in the development of a fuelling scheme appropriate for this fuel variant. Inner and outer fuelling zone exit irradiations were maintained at the CBDFA values, with burnups subsequently corrected for eigenvalue variations from unity, as in the NATNOM case. In the next four subsections, simple push through fuelling schemes involving 2, 4, 6 and 8 bundles are discussed. The drawbacks of these schemes for 142117153 fuel will soon become evident. Results of the analyses are provided in Tables 10-9 and 10-10, as well as in Fig. 10-4 through 10-8.

10.6.4.1 Two Bundle Shift Fuelling Scheme

The 2BS fuelling scheme yields an unacceptable axial power profile as is evident in Fig. 10-5. Because of the small number of bundles entering the channel on each refuelling, bundles remain in core for two dwell times before reaching the centre of the channel. Since adjacent channels are fuelled with the same scheme, though from opposite ends of the core, there is not a great deal of neutronic leakage from adjacent channels to boost the central bundle powers. As a consequence, there is a dished axial power distribution. (Note also the similar though much more symmetric effect on the cell flux axial profile (Fig. 10-6).) Fresh bundles at the inlet end boost the power considerably in that region. At the outlet end, increased neutronic leakage from the fresh bundles in adjacent channels increases the bundle power. Because of the depressed power in the centre of the core, maximum bundle powers are large, and occur at the ends of the reactor where leakage from the active fuel region is maximized. (It is noted that the use of fertile axial blankets may improve the natural uranium utilization of the 2 BS fuelling scheme by utilizing the leakage flux for the production of fissile isotopes.)

The maximum bundle power for the 2BS TAA case was calculated to be 1124 kW, well above the 800 kW target. Even if the maximum channel power was lowered from the 6708 kW calculated, to 6500 kW, and the maximum bundle power was reduced proportionately, the limiting bundle power would exceed the target by 36%. Fuel melting concerns would be escalated using this scheme.

Repositioning of the adjuster rods towards the ends of the channels will reduce the flux peaking (Boczar and van Dyk, 1986).

One advantage of the 2BS scheme is that the number of channels to be refuelled each day is approximately the same as in the NATNOM case (about 2 channels per day). Consequently the reactivity increase upon refuelling is expected to be kept to a minimum. It should be noted that the reactivity decay rate is approximately 38% larger in the enriched cases than in the NATNOM case (see Table 10-9). Consequently, the reactivity increase per channel refuelled will be somewhat larger for the 2BS 142117153 fuelling strategy than for the NATNOM 8BS scheme. Extra demands will be placed on the reactor regulating system as a result, and careful selection of channels for refuelling will be a requirement.

10.6.4.2 Four Bundle Shift Fuelling Scheme

The 4BS TAA simulation resulted in a maximum bundle power of 915 kW. This value is 14% higher than the target of 800 kW. The reason, once again, is that the axial power distribution is depressed at the centre of the core due to the absence of fresh fuel in that region. The central region only receives fuel bundles that have already spent a complete dwell time in another position in the channel. The problem is magnified because adjacent channels have a similar absence of high (relative) reactivity fuel in the central channel region.

The axial power and flux distributions are shown in Fig. 10-5 and 10-6, respectively. The depression is not as great as with the 2BS scheme since bundle positions 3 and 4 receive fresh fuel in the 4BS scheme and once-irradiated fuel in the 2BS strategy. The axial power profile is more greatly skewed towards the channel inlet end (where fresh bundles are placed)

than the flux distribution. The reason for this is evident when examining Fig. 10-7 and 10-8. Because the fuel towards the outlet end is considerably more irradiated than the inlet end, a given flux level will produce less fissions and hence less power, resulting in the power profile being skewed towards the inlet end.

The fuel channel visits per day are about half those required with the 2BS scheme, since twice as many bundles are replaced each time (Table 10-9). However the reactivity associated with the replacement of four fuel bundles will cause large core flux and power tilts, which will have to be mitigated through the action of a powerful reactor regulating system.

10.6.4.3 Six Bundle Shift Fuelling Scheme

A reactor fuelled with a 6BS 142117153 scheme would require three channels to be refuelled every four days. The maximum bundle power of 841 kW is only 5% higher than the 800 kW target. This may be acceptable, provided the fuelling ripples are kept within strict limits. (This possibility is considered in detail in Section 10.7.)

The axial power distribution is not depressed in the central region with this scenario (Fig. 10-5). In fact, since fresh bundles are placed in the central positions of the channels as well as at the ends, the flux and hence powers peak at the channel central region and fall towards the edges due to neutronic leakage effects. The peaking of the axial power distribution in the adjuster region increases the effect of the adjuster rods on controlling radial power peaking. As can be seen in Fig. 10-4, as the number of bundles added per fuelling visit increases, the axial power profile becomes more flattened.

10.6.4.4 Eight Bundle Shift Fuelling Scheme

In a time averaged sense, the 8BS fuelling scheme would seem ideal. Channel refuelling visits are minimized (one channel refuelled every two days (approximately)). Maximum bundle powers do not exceed 800 kW. Bundles reside

in the core an average of 1016 full power days (FPD) (3/2 x 677). Flux and power profiles appear very acceptable.

The TAA does not allow an appreciation of the large power perturbation associated with a channel refuelling involving the placement of eight enriched fuel bundles in one channel at one visit. Each refuelling operation would add an average of more than 1 mk to core reactivity. The local effects of this would (under normal conditions) lead to fuel melting in the central core region with the reactor operating at full power. The TAA approximation indicates that "on average" the power distribution is acceptable. Properties for the fuel bundles are averaged from the beginning to the end of the cycle (see Fig. 10-7 and 10-8). As the irradiation or burnup increment between channel visits is increased, the variation in the channel power distribution from the beginning to the end of the dwell time is increased (the fuelling ripple effect). In the TAA, therefore, deep power depressions at the end of a dwell time can mask the massive power surges that can occur following a channel refuelling. This can result in an acceptable TAA average power distribution, with quite unacceptable results at the beginning and end of cycle scenarios. This effect will be addressed further in Section 10.7 when "instantaneous" cases are considered in an effort to quantify the fuelling ripple that would result with the various fuelling strategies. At this point, however, one can envisage that an acceptable fuelling strategy would require a minimum number of bundles replaced per visit thereby minimizing the fuelling ripple associated with the scheme. Various strategies of this nature are considered in Sections 10.6.5 and 10.6.6.

10.6.5 Checkerboard Fuelling: Case A

Comparing the axial bundle power distributions for the 2BS and 6BS 142117153 cases (see Fig. 10-5), it can be seen that while the former scheme yields unacceptably high maximum bundle powers near the ends of the channels, the latter scheme has higher bundle powers at the centre of the channels. In an attempt to find an acceptable fuelling strategy for enriched fuels in CANDU reactors, Chan and Dastur (1985) proposed a scheme involving 2 bundle shifts

in all of the outer fuel channels, in combination with an inner region fuelling scheme made up of alternating pairs of channels, one pair of channels being fuelled with a 2BS fuelling scheme (bidirectional pair) and the adjacent fuel channel pair being fuelled with a 6BS fuelling scheme. Inter-pair neutronic leakage tended to flatten the resultant flux shape. This scheme was shown to be acceptable for fuel enrichments up to 1.3 w/o U-235 (Chan and Dastur, 1985). However, as enrichment is increased fuel management complications are also increased, and a fuel management study performed by Younis et al. (1986) using 1.5 w/o U-235, required that the 6BS fuelling scheme in the checkerboard format be modified such that it consisted of three 2BS schemes with unequal irradiation periods between each shift. This was required to overcome the large fuelling ripple resulting from a 6BS scheme with high enrichment, and still allow high reactivity fuel to boost the power in the centre of the channel.

The checkerboard fuelling scheme of Chan and Dastur (1985) was used to study fuel management with 142117153 fuel. With such high fuel enrichment even more rigorous controls over fuel channel refuelling selection would have to be maintained in order to limit maximum bundle and channel powers to acceptable levels.

The fuelling map for the "A" series of fuel management calculations is shown in Fig. 10-9. The inner fuelling zone boundary was modified somewhat from the nominal CANDU-600 design to allow front to back fuelling symmetry (pair-wise bidirectional grouping maintained). The modified 6BS fuelling region was expanded over a larger core region than suggested by Younis et al. (1986) since the higher enrichment required a larger region of pair-wise coupling between 2BS and 6BS schemes for sufficient flux flattening and power shaping.

The modified 6BS fuelling scheme was identified as multicycle fuelling scheme 50, consisting of three 2BS fuelling schemes with an unequal irradiation time between each 2BS. The scheme is depicted in Fig. 10-3. Pairs of channels fuelled bidirectionally with fuelling scheme 50 were surrounded by channel pairs fueled bidirectionally with a simple 2BS scheme.

It was found that in order to provide an acceptably flattened axial

power distribution in a time-averaged sense, the irradiation time between the first and second, and second and third 2BS components of fuelling scheme 50 must be minimized. That is, it should be as much like a 6BS scheme as possible to increase the power in the central part of the core. The fractional dwell time for each of the 2BS components was chosen as 0.05, 0.05 and 0.9, respectively.

By viewing the fuelling diagrams in Fig. 10-3 it can by seen that after the third 2BS fuelling operation, there is a relatively long burnup period and then the cycles begin repeating themselves. The total time for the three 2BS components is identified as the dwell time, T. After the first and second 2BS fuelling operations, the channel burns for a period 0.05 T. Following the third 2BS fuelling operation the channel burns for a period 0.90 T.

The results of the fuel management study using this fuelling strategy are shown in Tables 10-9 and 10-10 (variant 142117153:A). The inner and outer zone fuel exit irradiations were chosen to provide an acceptable radial power distribution (see Fig. 10-4) and to maintain criticality.

Figures 10-5 through 10-8 provide representative bundle power, flux, irradiation and burnup distributions respectively for this fuelling scheme. By comparing the cell flux distribution from the 2BS and 6BS time-averaged fuelling schemes to that resulting from the 142117153:A fuelling strategy, it can be seen that the combination of the two strategies combine favorably to achieve a more flattened axial power distribution (Fig. 10-6).

The maximum bundle power of 909 kW exceeds the target maximum by 14%. The location of this maximum powered fuel bundle is position 2 of central channel L-12 which is fuelled with a 2BS fuelling scheme. In order to reduce this value, it would be necessary to modify the fuelling strategy, perhaps also by adjusting the burnup times between refuelling the 2BS channels, thereby reducing the peaking at the channel inlet end.

The timing between fuellings must be carefully monitored with such a fuelling strategy. Further, the interchannel coupling is not optimized since channels are grouped in bidirectional pairs rather than individually. In Section 10.6.6 an alternative innovative fuelling scheme is suggested which

may be more attractive for application with 142117153 fuel.

10.6.6 Checkerboard Fuelling: Case B

The fuelling strategy developed in Section 10.6.5 required channels to be paired bidirectionally to achieve a front-to-back power symmetry. By choosing a fuelling scheme that is symmetric in itself, the fuel channel pairing is not necessary. This would allow the introduction of a checkerboard fuelling strategy in which a given fuel channel can be surrounded completely by channels fuelled with an alternate fuelling scheme, thereby maximizing the inter-channel power coupling via neutronic leakage. Such a strategy is investigated in this section.

Consider the fuelling map as shown in Fig. 10-10. In this strategy, symmetric fuelling schemes with bundle powers which peak near the central region of the core are surrounded by channels with bundle powers peaking near both ends of the channels. Inter-channel leakage effects will minimize the extent of bundle power peaking.

10.6.6.1 Strategy 142117153:B1

As a first fuelling variant, channels identified as INNER1 and OUTER1 in Fig. 10-10 were fuelled with generalized fuelling scheme 19, while the INNER2 and OUTER2 type fuel channels were fuelled with generalized fuelling scheme 16. These schemes are depicted in Fig. 10-3.

Fuelling scheme 19 is a symmetric fuelling scheme in which a fresh bundle is placed at each end of the core, the two centre bundles (6 and 7) are removed, and the remaining bundles move one position towards the centre of the channel following each refuelling. This scheme, on its own, would tend to maximize bundle powers at the ends of the channels.

Fuelling scheme 16 is an inversion of scheme 19, in that two fresh bundles are placed at the centre of the core and a bundle is removed from each end, with all other bundles shifting one position away from the channel centre. On its own, this scheme would yield bundle powers which peak at the

centre of the channel.

Results of the analysis of the fuelling strategy (142117153:B1) are given in Tables 10-9 and 10-10. The maximum bundle power with such a scheme is 1268 kW, which is 59% higher than the target of 800 kW for the time-averaged maximum. It is clear that insufficient channel coupling is present to counter the large local reactivity perturbation resulting from the placement of two fresh bundles adjacent to each other at the centre of a channel.

Channel and bundle power distributions for this case are shown in Fig. 10-4 and 10-5, respectively. The power peaking at the centre of the channels fuelled with generalized scheme 16 is to be noted.

10.6.6.2 Strategy 142117153:B2

In fuelling strategy B2, the same checkerboard pattern of fuelling is used as with strategy B1, however channels are fuelled with multicycle fuelling scheme 54 (INNER2 and OUTER2 channels), alternating with channels fuelled with generalized fuelling scheme 19 (INNER1 and OUTER1 channels). Generalized scheme 19 is unchanged from case B1 (see Fig. 10-3). Multicycle scheme 54 is a weighted combination of generalized schemes 22 and 23. A weighting of 0.3 is placed on scheme 22. A weighting of 0.7 is placed on scheme 23. These schemes are depicted in Fig. 10-3.

In strategy 54, fresh fuel is placed at positions 4 and 9 and subsequently shifted towards the centre of the channel. The scheme is designed such that fresh fuel bundles are not placed side by side in adjacent channels or in the same channel. After a short irradiation period, the slightly irradiated bundles are then shifted towards the channel centre, to boost power in that region.

The results of the analysis for the 142117153:B2 fuelling strategy are given in Tables 10-9 and 10-10. Typical channel and bundle power distributions for this fuelling strategy are shown in Fig. 10-4 and 10-5, respectively. This strategy yields a maximum bundle power of 870 kW, which is 9% over the target value of 800 kW. By weighting scheme 22 more heavily, the

maximum could be reduced, however it would be at the expense of increasing the power in positions 4 and 9. Further, since scheme 23 entails a fuelling operation in which only fuel shuffling rather than fuel replacement was performed, it seemed prudent to modify the strategy to introduce one fresh bundle at each of the two stages, thereby minimizing fuelling ripple.

The scheme finally devised is discussed in Section 10.6.6.3.

10.6.6.3 Strategy 142117153:B3

Strategy 142117153:B3 is similar to the B2 variant, except scheme 54 is replaced by scheme 55 in the INNER2 and OUTER2 fuel channels (Fig. 10-10). Scheme 55 consists of equal weightings of generalized fuelling schemes 24 and 25. These schemes are depicted in Fig. 10-3. The strategy mixes new bundle placements between both component schemes, while utilizing a similar shuffling scheme to that developed for strategy 54.

Alternating channels (INNER1 and OUTER1 channels in Fig. 10-10) are fuelled with scheme 19, which places a fresh bundle at each end of the core.

It is instructive to follow a bundle from fresh to discharge with scheme 55. Since the scheme is symmetric, it is necessary only to follow a fresh bundle placed at position 4 in scheme 24. The bundle placed in position 9 in scheme 25 follows a mirror image of fresh bundle 4, though it is one fuelling visit out of step.

The fresh bundle introduced at position 4 is irradiated for 0.5 T, and then shifted to position 6 where it stays for time, T. It is then shifted to position 5 for time T, position 4 for time 0.5 T, and finally positions 3, 2, and 1, residing at each of these positions for time, T. The bundle is then discharged. From this discussion it can be seen that all bundles reside at every position in one half of the channel for a period of time equal to one dwell time, T. For positions 4 and 9, the irradiation time of a bundle in these positions is divided into two 0.5 T intervals. The time between the intervals is 2 T.

The results of the 142117153:B3 fuelling study are given in Tables 10-9 and 10-10. The maximum time-averaged bundle power was 808 kW, an

acceptable 1% higher than the target of 800 kW.

In this fuelling strategy the inner fuelling region was expanded slightly to provide improved power flattening. The inner/outer fuelling zone boundary for this strategy is depicted in Fig. 10-10.

A radial channel power profile for this strategy is depicted in Fig. 10-4. Axial bundle and cell flux distributions are provided in Fig. 10-5 and 10-6, respectively. Beginning and end of cycle irradiations are depicted for representative channels in Fig. 10-7 and 10-8 respectively.

The 142117153:B3 fuelling strategy requires an average of 3.36 fuelling visits per full power day. This represents a 67% increase in fuel channel visits per day over the NATNOM case. However, the number of bundles replaced each day averages 4.48, representing a decrease of approximately 72% over the NATNOM value of 16.08.

The increased number of fuelling visits with this scheme is expected to be operationally acceptable, this rate often being met by present-day Ontario Hydro fuelling machines, at reactors utilizing 4BS and even 2BS fuelling schemes in the central region of the core (Bruce NGS-B and Bruce NGS-A, respectively).

The data in Table 10-10 indicate that all of the 142117153 fuelling strategies achieve approximately the same burnup. The mean value of 31279 MWd/MgU for all 8 schemes reported, is within 0.5% of the CBDFA value (31134). The population standard deviation was calculated to be 92 MWd/MgU (0.3% of the mean). From this analysis, it is clear that the fuel shuffling scheme used will not have a significant impact on uranium utilization. The data does, however, indicate that the 2BS and 142117153:A fuelling strategies, in which all fresh bundles are placed at the ends of the channels, do yield the lowest fuel burnup of all cases considered. The burnup in the 2BS case was 0.3% lower than in the 142117153:B3 case. The burnup in the 142117153:A case was 0.8% lower than in the 142117153:B3 case. Over the lifetime of a reactor, these small variations can translate into a substantial amount of fuelling dollars.

10.6.7 Effect of Fuelling Schemes on Adjuster Worth

In Table 10-11 adjuster rod worths for the NATNOM:8BS and 142117153:A and B3 cases are compared with their respective CBDFA values. The flux shape dependence of rod reactivity is noted. To assess the effectiveness of the assigned adjuster loading for xenon override it would be necessary to also examine the xenon reactivity worth with these flux shapes. This effect was not studied further.

10.6.8 Comparison With Other Once Through Fuel Cycles

In Table 10-12 the fuel consumption rates with the advanced CANDU fuel designs considered in this analysis are compared with data for the once through cycle in LWRs and the natural and 1.2% enriched uranium fuelled CANDU. The advantages of the modified design are evident from the table. Uranium consumption rates are reduced by 14% in the 1421NAT natural uranium case in comparison with the CANDU 37 element natural uranium design. Uranium consumption is reduced by 13 to 15% for the enriched cases (142117153 and 14211312) in comparison with the 37 element 1.2% enriched CANDU fuel bundle design.

The separative work requirements in the CANDU-PHW LEU fuel cycle (Tables 10-6 and 10-10) can also be compared with those for a typical LWR cycle. Assuming 0.2 a/o U-235 tailings, an LWR requires approximately 160 kgSWU/MW(e)-a (using data from Hatcher (1978) and Shapiro and Jesick (1979)), which is considerably greater than the CANDU requirements.

10.7 INSTANTANEOUS FUEL MANAGEMENT STUDIES

The time-averaged fuel management studies in Section 10.6 provide much useful information required in the development of fuelling strategies. The TAA analysis is, however, based on the assumption that fuelling ripple can be maintained at manageable levels. Fuelling strategies were deemed acceptable provided that the time-averaged maximum channel and bundle powers were within

specified limits, and with a further proviso that the reactivity insertion per fuelling operation was maintained at a value approximately equal to that in the NATNOM case. This latter condition assured channel ripples would be of the same order as that in the NATNOM study. However, since the reactivity insertion with the 142117153 fuel was concentrated in only a very few bundles, the effects on local bundle powers after refuelling was not adequately assessed in the TAA studies. Consequently, it was necessary to perform Instantaneous Approximation calculations to verify the operational acceptability of the fuel management strategies developed.

Maximum bundle and channel licenced operating powers at Ontario Hydro's Bruce NGS-B reactors (Ontario's most modern operating reactors) are 1035 kW and 7200 kW respectively, using natural uranium fuel (AECB, 1986). For the purposes of this analysis it was assumed that these limits would be similarly applicable in the 142117153 fuel design cases. It is recognized that the bundle design and axial power differences will affect critical heat flux and hence licence power limits, however, these values were nevertheless used to identify an appropriate limiting operating environment.

As discussed in Chapter 8, the instantaneous module of FMDP provides a "snap-shot" representation of a reactor at a particular instant in its irradiation history. Channel ages were chosen using the patterned age distribution described in Chapter 8.

10.7.1 Instantaneous Simulation Results and Interpretations

Instantaneous simulations were performed for the NATNOM, 142117153:6BS, A and B3 cases. The results are summarized in Table 10-13. In this table, "overpower" is defined as the ratio of instantaneous to time-averaged power.

It can be seen that the 142117153 cases yield considerably higher bundle and channel overpowers than the reference NATNOM case.

The 142117153:6BS case results clearly indicate that it is unacceptable to use such a fuelling scheme with 142117153 fuel. Maximum bundle and channel powers exceed their limits by 33% and 27%, respectively.

Comparing the 142117153:A and B3 cases, it can be seen that in terms of minimizing CPPF, the B3 case is superior. This is to be expected given the smaller number of fuel bundles replaced per visit, on average, with the 142117153:B3 fuelling strategy.

The 142117153:A instantaneous study yielded a lower maximum bundle power than the B3 case, which is the opposite of the TAA results.

The B3 fuelling strategy yielded a maximum bundle power of 1069 kW, which is 3% over the target limit of 1035 kW. It is expected that fuel bundles based on the enhanced 1421 design will be able to operate at such powers without adverse effects.

It should be noted that it is only bundles with low irradiation that operate at elevated powers. In the event of an accident (such as a major loss of reactivity control (LORC)), high powered bundles have an increased susceptibility to failure. However, due to the ductility of the sheaths and the low fission product load in the fresher fuel bundles, the resultant release of radioactivity would be less than might otherwise be expected.

The patterned age distribution used in the instantaneous calculations can easily bias the results of one fuelling strategy over another, especially when multicycle fuelling schemes are involved. With these schemes, channel ages then represent the fraction of time between the beginning of the first cycle and the end of the last cycle, rather than representing the time between fuel channel visits. The patterned distribution can therefore concentrate channels together that have recently been refuelled, resulting in excess channel ripples. In practice, with proper fuelling controls the ripples can be reduced from those obtained using the patterned age distribution.

A more complete assessment of a given fuelling strategy would require a full core burnup history to be simulated, from fresh core to well into equilibrium conditions. Each channel refuelling would be simulated to ensure that the scheme is operationally acceptable. Such a study is very costly and time consuming, though it would be required to demonstrate the feasibility of any novel fuelling strategy. Younis et al. (1986) successfully performed such a study for 1.5 w/o U-235 enriched 37 element fuel using a scheme from which the 142117153:A strategy evolved.

10.8 COMMENT ON FUEL MANAGEMENT WITH ENRICHED FUEL

The fuelling schemes showing the most promise for implementation in enriched-uranium-fuelled CANDU reactors involve complex push through and/or reshuffling schemes in order to maintain acceptable bundle and channel powers. The timing between successive refuellings becomes crucial for controlling the axial power profile. Since fuel bundles remain in-core for many cycles (6-12 refuellings as opposed to 1-2 refuellings in the NATNOM case), the fuelling strategies in the enriched cases are much less forgiving. A fuelling error can lead to consequences both large in magnitude and long in duration. Fuelling of such reactors would be necessarily under the control of a fuelling computer which could assess all possible alternatives and anticipate current and future optimal fuelling strategies.

The question of fuel bundle integrity under a range of power histories and over much greater irradiation periods than current generation fuel must be addressed. The outcome of these studies may place additional restrictions on acceptable fuel management strategies in future.

Additional complexities arise with the replacement of failed fuel. Given the strong influence that inter-channel neutronic leakage plays in determining axial channel power distributions, it becomes imperative to replace defective fuel with fuel of approximately the same reactivity. This could be achieved either by maintaining a selection of fuels of varying enrichment from which to choose a replacement bundle, or to employ strategic fuel redeployment to avoid operation with an unacceptable power distribution upon replacement of a defective bundle.

The transition from a fresh core to equilibrium will pose even greater challenges, and will take a longer period than in current NATNOM reactors. The use of depleted fuels, moderator poison, poisoned fuel, or transition from equilibrium operation at lower enrichment levels will have to be investigated. Such studies have been conducted for enrichment levels up to 1.2% U-235 by Combustion Engineering (Bagnal et al., 1981).

The 1421 fuel design and adjuster loading does provide a wide

flexibility in achieving the transition to enrichments up to the 142117153 design by starting first with 1421NAT fuel and gradually converting to 14211312 bundles and finally to the 142117153 design. The gradual transition process would result in a greater time requirement to achieve a final equilibrium state, though it would be operationally more manageable than starting with an initial core of 142117153 fuel and suppressing the large initial excess reactivity.

It should also be noted that the 1421 bundle design and the corresponding advanced reactor design discussed in this chapter would also allow utilities the flexibility of converting from a high enrichment fuel to a lower enrichment or even a natural uranium fuelled core if economic or political conditions dictate such a requirement. The transition again can be gradual, in this case, towards a reduced fuel enrichment. As the transition between enrichments occurs, adjuster grading would be altered to maintain an appropriate adjuster rod reactivity worth. Adjuster penetrations and banking would not have to be altered. The reactor regulating system feedback controls would also be modified to account for the altered dynamic response of the reactor as these changes occurred. These feedback mechanisms and optimized control schemes have yet to be fully characterized.

The great flexibility in fuel enrichment afforded with the 1421 fuel bundle design in conjunction with the slightly modified calandria proposed in this chapter indeed holds promise for application in next generation CANDU reactors (1421NAT through 142117153). Even higher fuel enrichments could be attained through the use of smaller fuel bundles, where the reactivity gain per bundle refuelled would be less. This, however, would be over-shadowed somewhat by the even greater change in fresh to discharge fuel reactivity, resulting from the higher burnups achieved with fuel of greater enrichment.

As an alternative to smaller fuel bundles, higher enrichments could be attained through the use of poison in the fuel mix (see Section 7.8.5.2 and Lang et al., 1983), or by switching to off-power batch fuel reloading and using moderator poison and/or control rods for reactivity shim. These alternatives bring with them negative economic aspects in terms of uranium utilization (unless the control rods are fertile uranium (Barre et al., 1988))

and operational control complexities with reactivity suppression requirements and the necessity of dealing with a reactor which is constantly in a changing state.

If the political and economic forces dictate a trend towards higher burnups than achieveable with the 142117153 fuel design, it may be prudent to look toward even more advanced CANDU designs. The 142117153 fuel design provides burnups of approximately 30000 MWd/MgU, which is comparable to current LWR burnups (Sherpereel and Frank, 1982; Keller and Shank, 1987). The current trend in LWR technology is towards burnups of the order of 50000 MWd/MgU (Keller and Shank, 1987), primarily to extend times between batch refuellings, and hence increase capacity factors, but also to reduce the quantity of spent fuel generated per MWh of electricity produced. In Chapter 11, an advanced CANDU reactor is introduced which will be capable of meeting or exceeding these burnup levels without the use of moderator poisons or fuel poisons and without having to deal with excessive fuelling ripple. This novel reactor concept represents a departure from current CANDU technology and is to be known as the CANDU Spectral Shift Advanced Thermal Reactor.

Time-Averaged Case Identifier	Maximum Channel Power (kW)	Maximum Bundle Power (kW)	Exit Irradiation (n/kb)			k-eff***	Refuelling Rate		Dwell Time (FPD)	Reactivity Decay Rate (mk/FPD)	Fuel*** Exit Burnup (MWh/bundle)
			Outer Core	Inner Core	Average		Bundles per FPD	Channels per FPD			
NATNOM: 88S	6452 (S-10)*	803 (E-10,6)*	2.40 (256)**	2.78 (124)**	2.53	1.00019	16.08	2.01	189	-0.414	3217
142117153:2BS	6708 (M-9)	1124 (L-12,2)	8.10 (256)	8.50 (124)	8.25	0.995932	4.46	2.23	170	-0.572	11603
142117153:4BS	6432 (M-9)	915 (M-9,3)	8.10 (256)	8.50 (124)	8.25	0.999457	4.46	1.12	341	-0.547	11593
142117153:6BS	6406 (S-10)	841 (S-12,7)	8.10 (256)	8.50 (124)	8.24	1.00009	4.48	0.75	509	-0.570	11560
142117153:8BS	6407 (S-10)	800 (S-10,7)	8.10 (256)	8.50 (124)	8.24	0.999647	4.49	0.56	677	-0.603	11526
142117153:A	6386 (S-10)	909 (L-12,2)	8.00 (252)	8.37 (128)	8.14	0.999652	4.51	2.25	224	-0.520	11483
142117153:B1	6659 (E-9)	1268 (D-10,6)	8.10 (256)	8.50 (124)	8.24	1.00060	4.47	2.24	170	-0.563	11566
142117153:B2	6474 (S-13)	870 (D-10,7)	8.10 (256)	8.50 (124)	8.24	0.999075	4.47	3.35	170	-0.537	11576
142117153:B3	6342 (N-14)	808 (N-15,7)	8.05 (244)	8.45 (136)	8.21	1.00041	4.48	3.36	170	-0.545	11558

* Location (Row-Column) or (Row-Column,Bundle)
** Number of channels
*** Data in this table are not corrected to account for k-eff ≠ 1.0

Table 10-9 Time-Averaged Cases - General Results

Time-Averaged Case Identifier	Burnup (corrected for k-eff)	Separative Work Requirements* (kg SWU/MW(e)-a)			Natural Uranium Requirements (kg U_{mined}/MW(e)-a)		
		0.0**	0.2**	0.3**	0.0**	0.2**	0.3**
NATNOM :88S	7141	0.0	0.0	0.0	166.6	166.6	166.6
142117153:2BS	31225	∞	53.2	40.3	84.9	102.9	118.3
142117153:4BS	31378	∞	52.9	40.1	84.5	102.4	117.7
142117153:6BS	31322	∞	53.0	40.2	84.6	102.6	117.9
142117153:8BS	31208	∞	53.2	40.3	84.9	103.0	118.4
142117153:A	31089	∞	53.4	40.5	85.3	103.3	118.8
142117153:B1	31365	∞	53.0	40.1	84.5	102.4	117.8
142117153:B2	31310	∞	53.1	40.2	84.6	102.6	118.0
142117153:B3	31334	∞	53.0	40.2	84.6	102.5	117.9

* Enriched to product enrichment
** Tailings concentration (a/o U-235)

Table 10-10 Natural Uranium and Separative Work Requirements (Time-Averaged Cases)

Case Identifier	Adjuster Rod Worth (mk)		Percent Change
	CBDFA	TAA	
NATNOM :88S	14.92	16.38	+9.8
142117153:A	15.39	11.99	-22.1
142117153:B3	15.39	12.01	-22.0

Table 10-11 Comparison of Adjuster Rod Worths: CBDFA vs TAA

Reactor	Fuel Cycle	Uranium Consumption (kgU/MW-year)(e)
LWR	Enriched uranium	200*
CANDU	37 element Natural uranium	167*
	1.2% Enriched uranium	118*
CANDU (advanced)	1421NAT Natural uranium	143
	14211312 Enriched uranium	100
	142117153 Enriched uranium	103

Note: All data corresponds to once through uranium based fuel cycles. 0.2% uranium tailings in enriched cases.
*Data from Hatcher (1979). Data for NATNOM case is consistent with this analysis.

Table 10-12 Equilibrium Uranium Consumption: Comparison of Once Through Fuel Cycles

Case Identifier	Effective Multiplication Factor	Maximum Channel Power (kW)	Maximum Bundle Power (kW)	Maximum Channel Overpower in the CPPF Region	Maximum Bundle Overpower in the CPPF Region	Standard Deviation of Channel Overpower in the CPPF Region
NATNOM	1.00050	6863 (M-7)*	850 (S-10,7)**	1.079	1.131	0.039
142117153:6BS	1.00307	9177 (L-6)	1375 (L-2,6)	1.588	1.882	0.186
142117153:A	0.990444	7055 (E-9)	985 (P-10,2)	1.188	1.265	0.089
142117153:B3	1.00149	6938 (P-10)	1069 (M-8,9)	1.133	1.373	0.045

* Location (Row-Column)
** Location (Row-Column,Bundle)

Table 10-13 Instantaneous Results

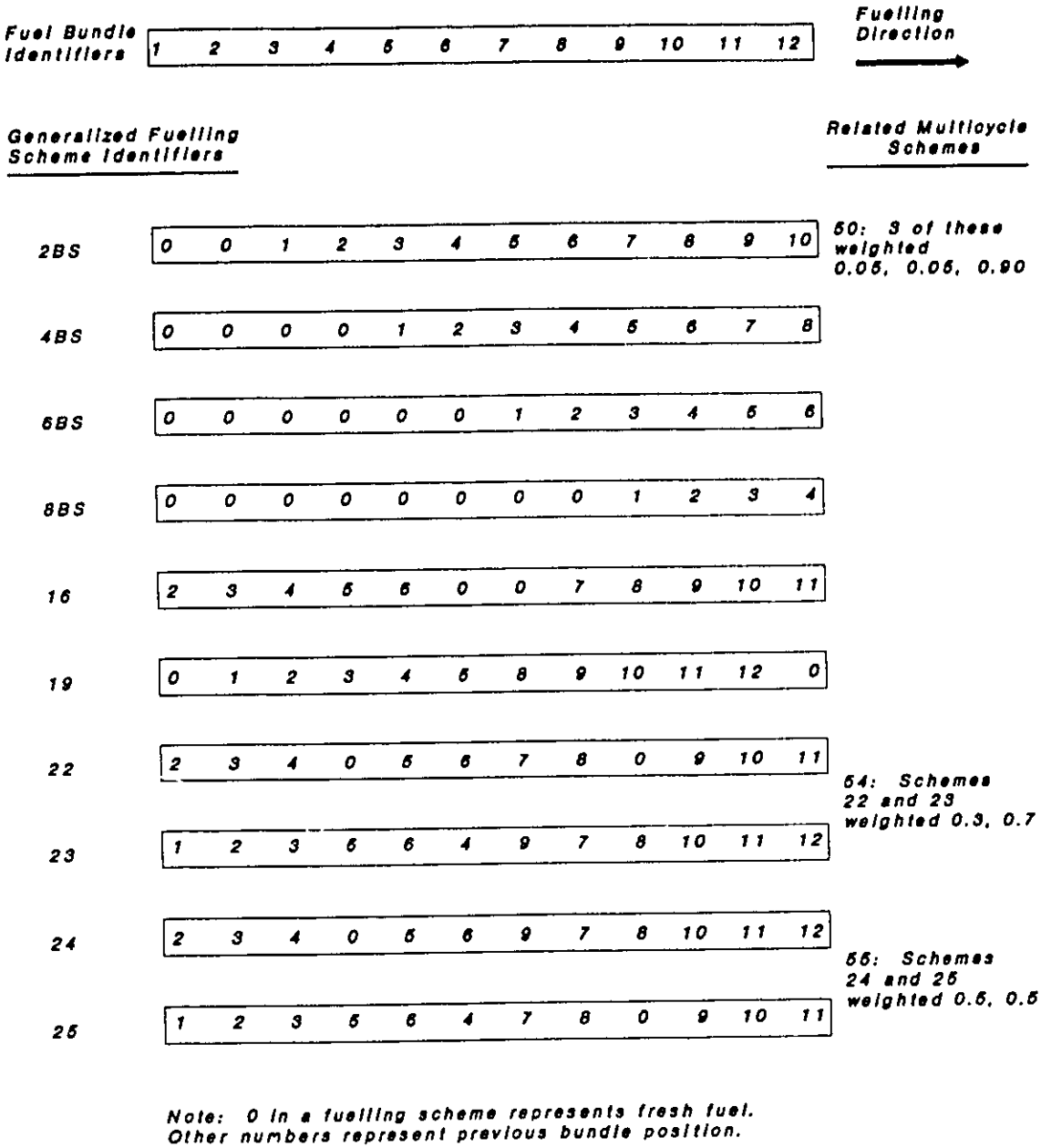

Figure 10-3 Fuelling Schemes

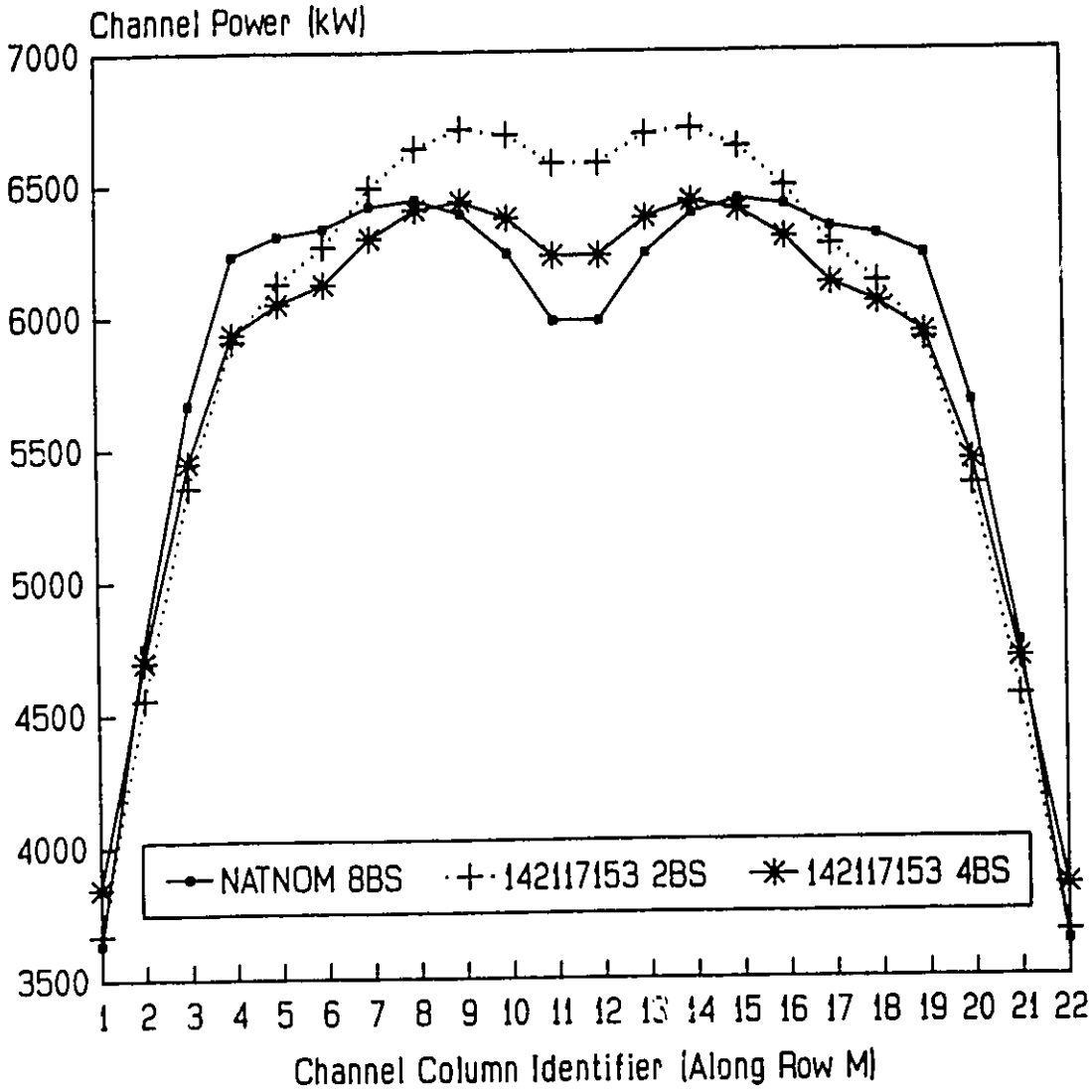

Figure 10-4a Channel Power Distributions (TAA)

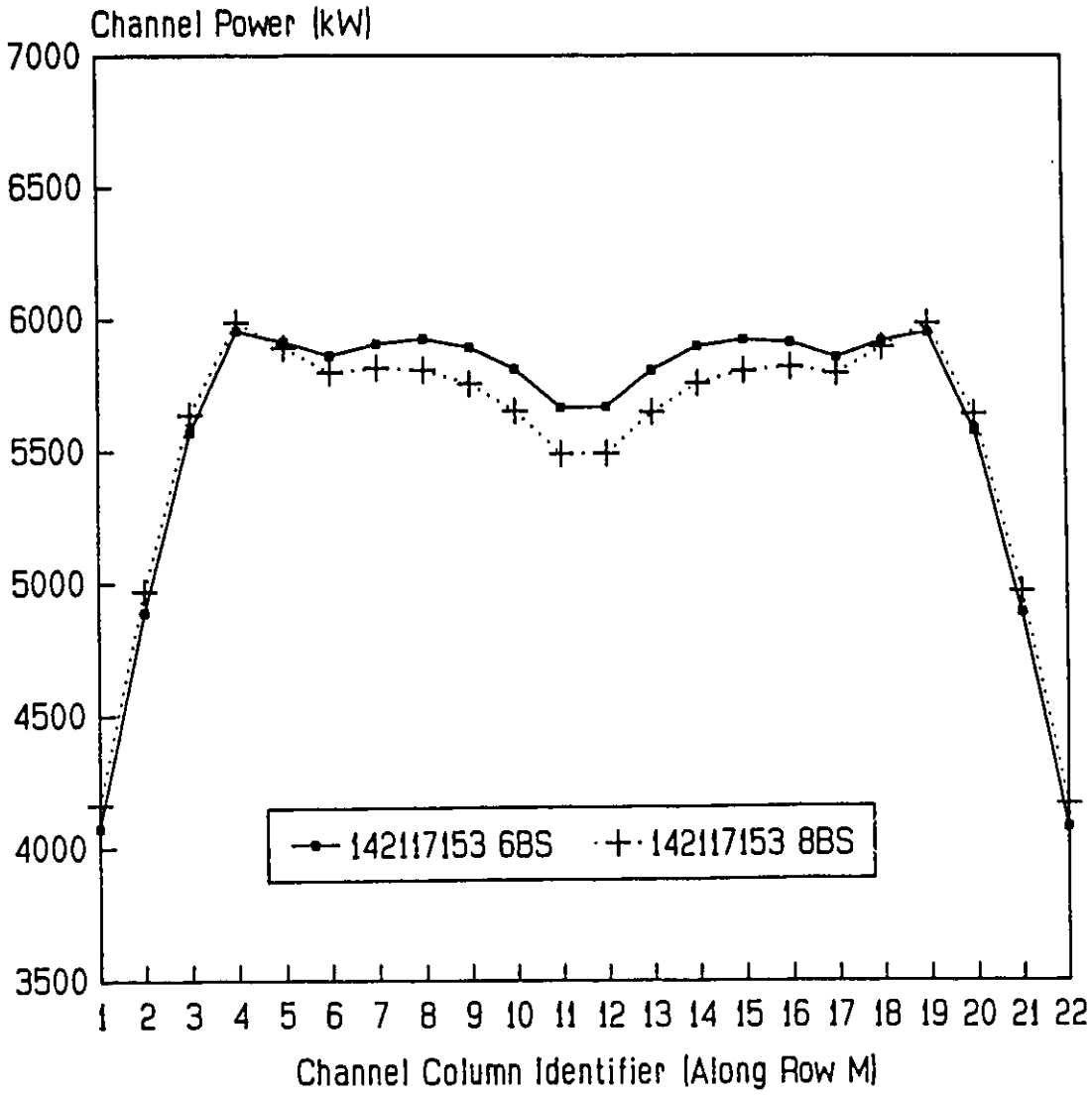

Figure 10-4b Channel Power Distributions (TAA)

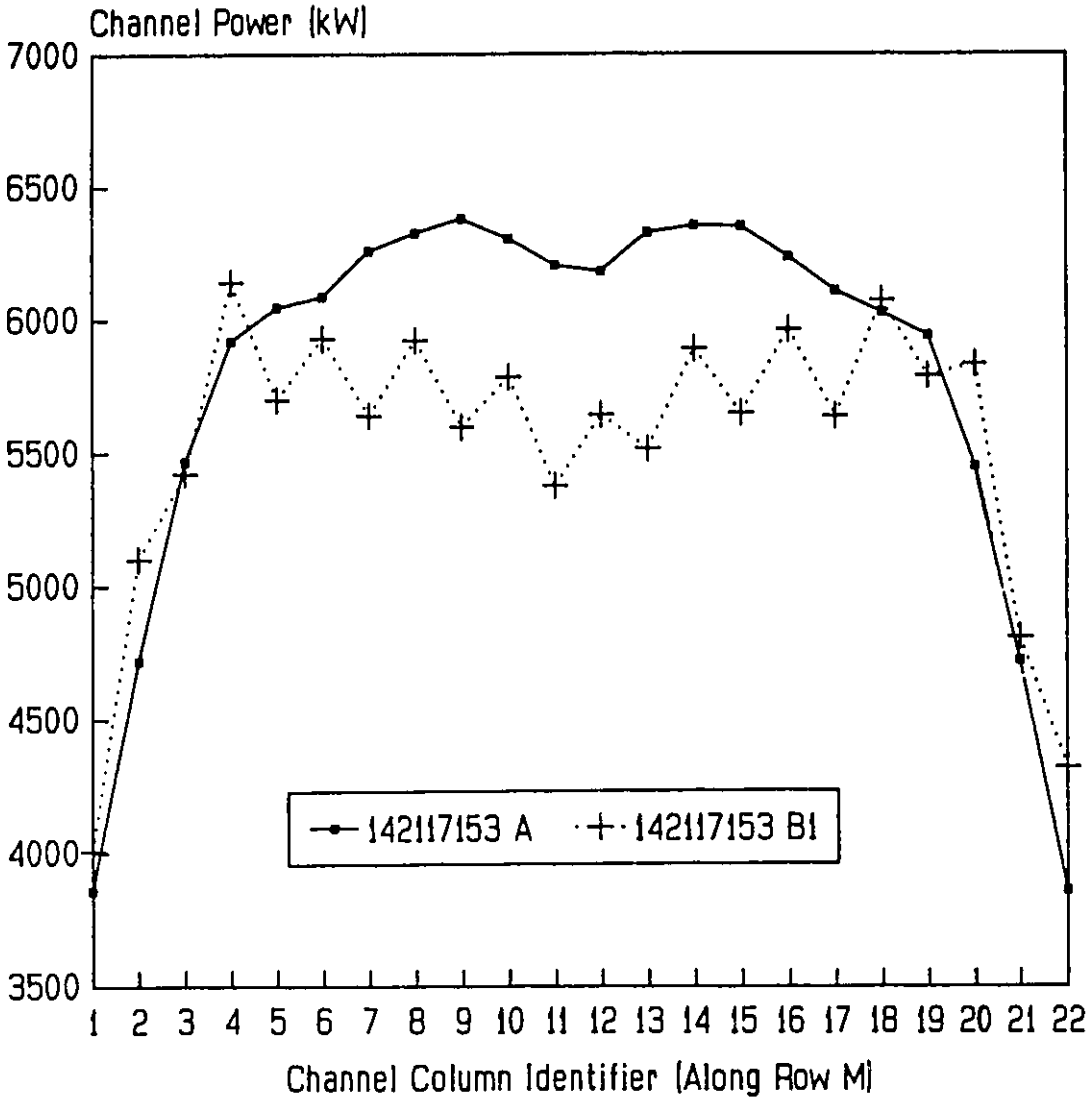

Figure 10-4c Channel Power Distributions (TAA)

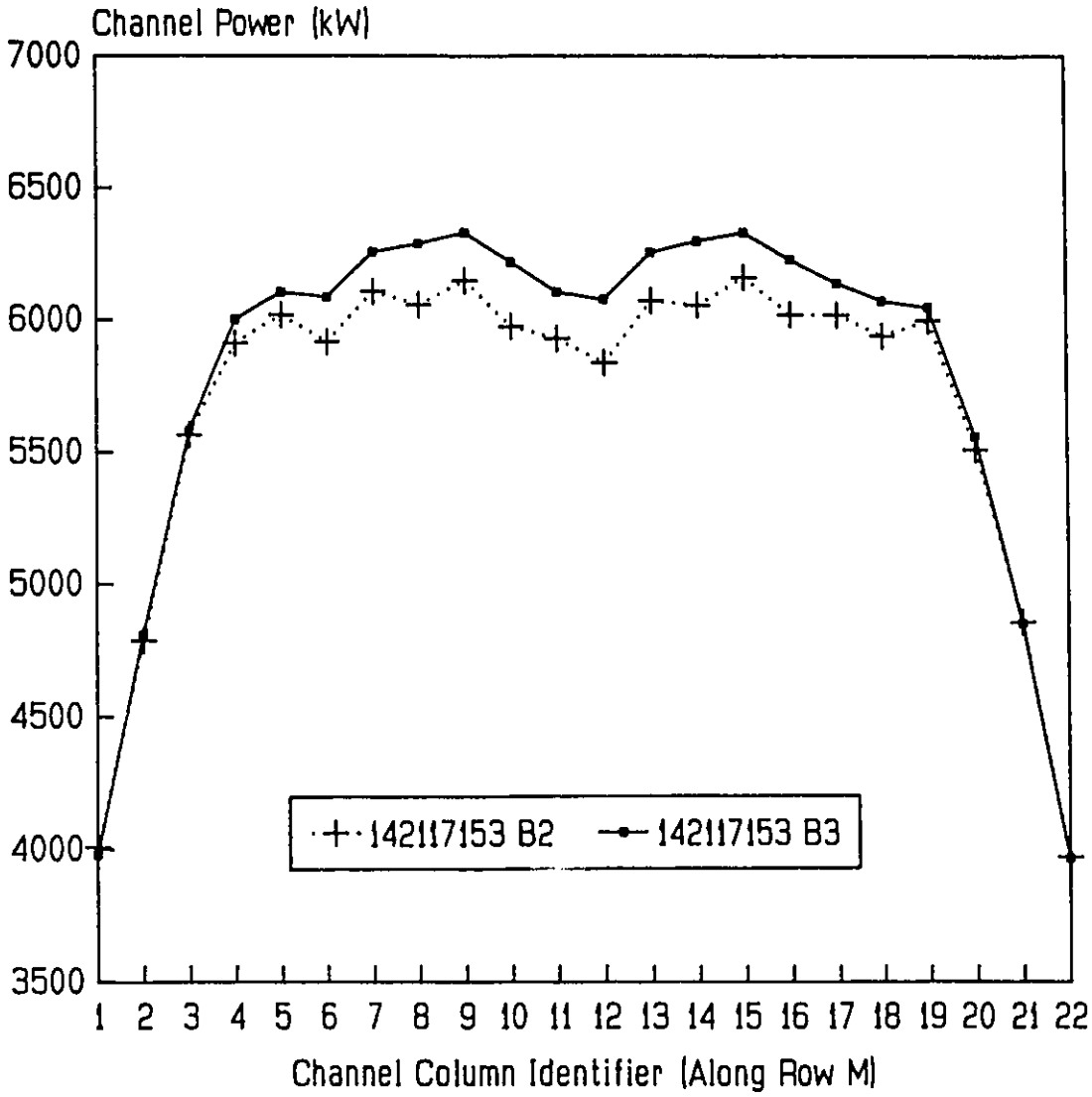

Figure 10-4d Channel Power Distributions (TAA)

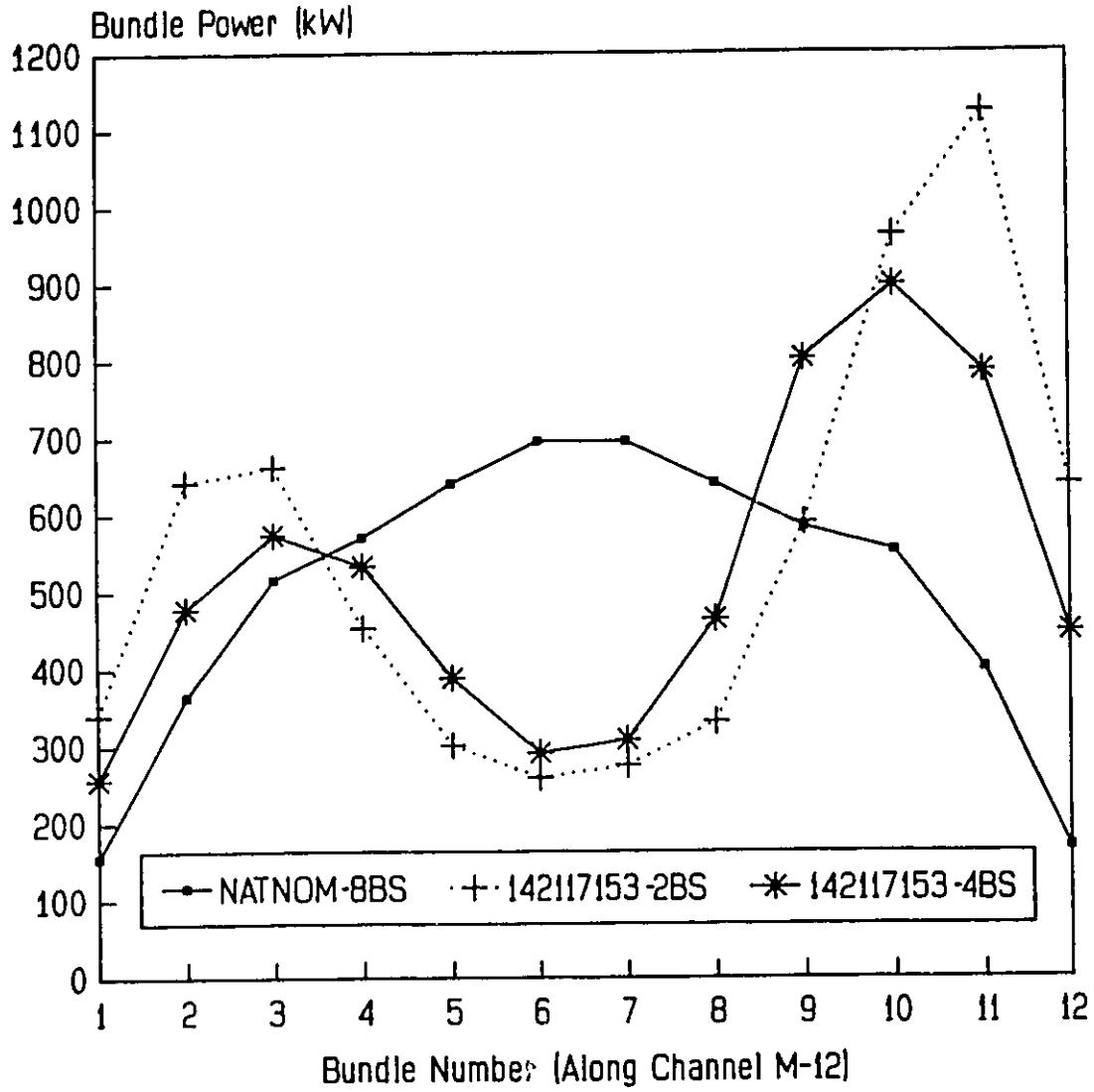

Figure 10-5a Bundle Power Distributions (TAA)

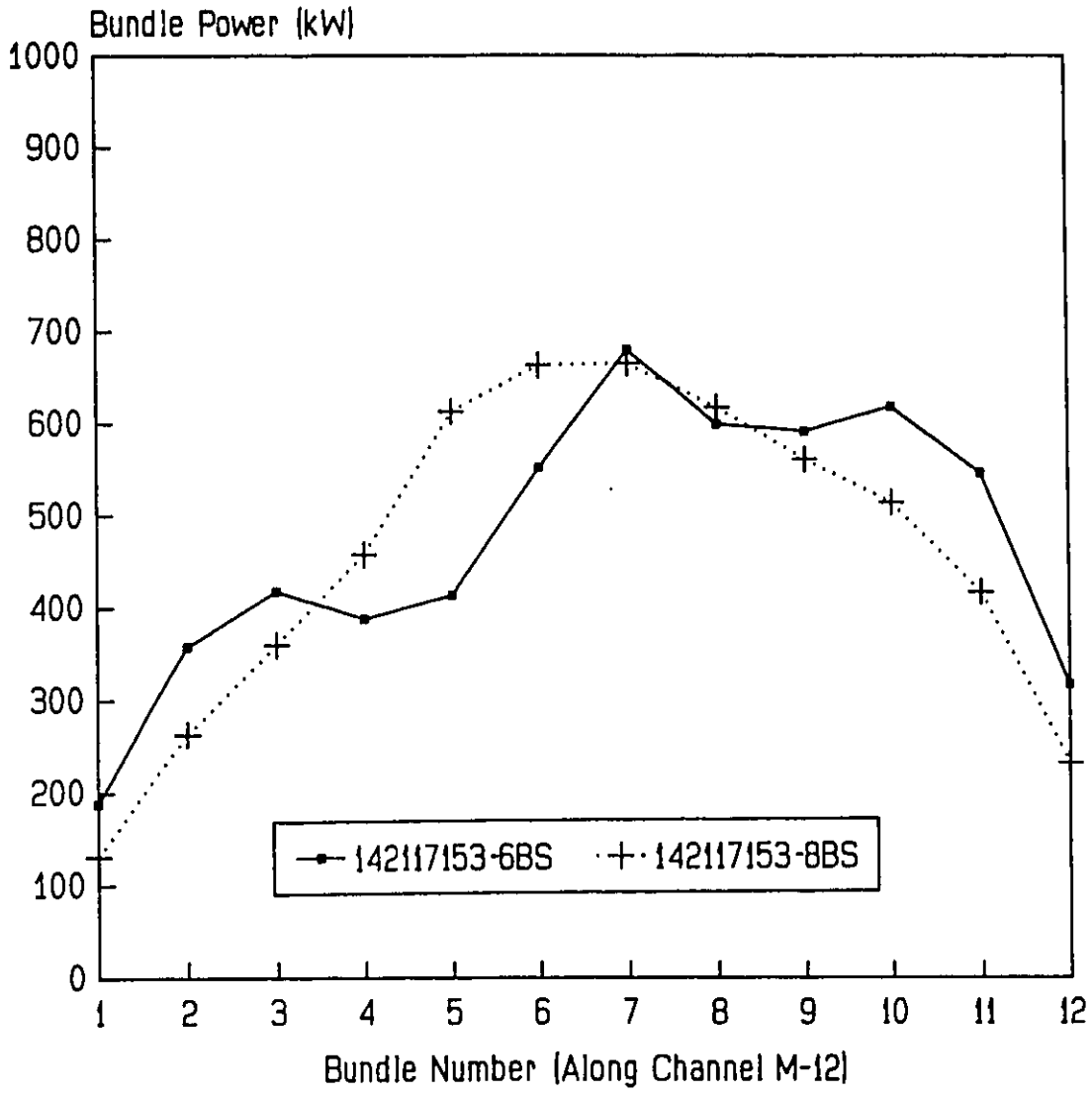

Figure 10-5b Bundle Power Distributions (TAA)

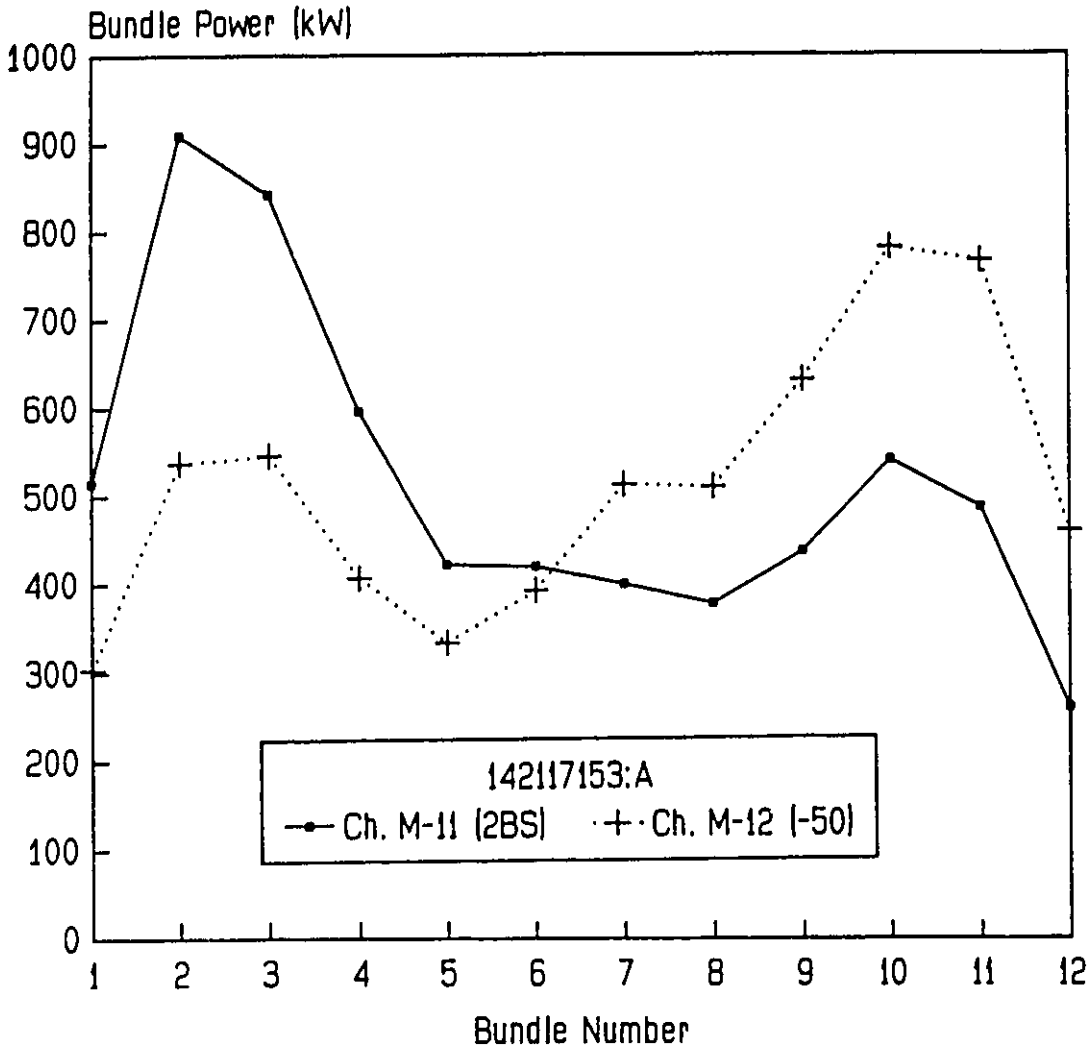

Figure 10-5c Bundle Power Distributions (TAA)

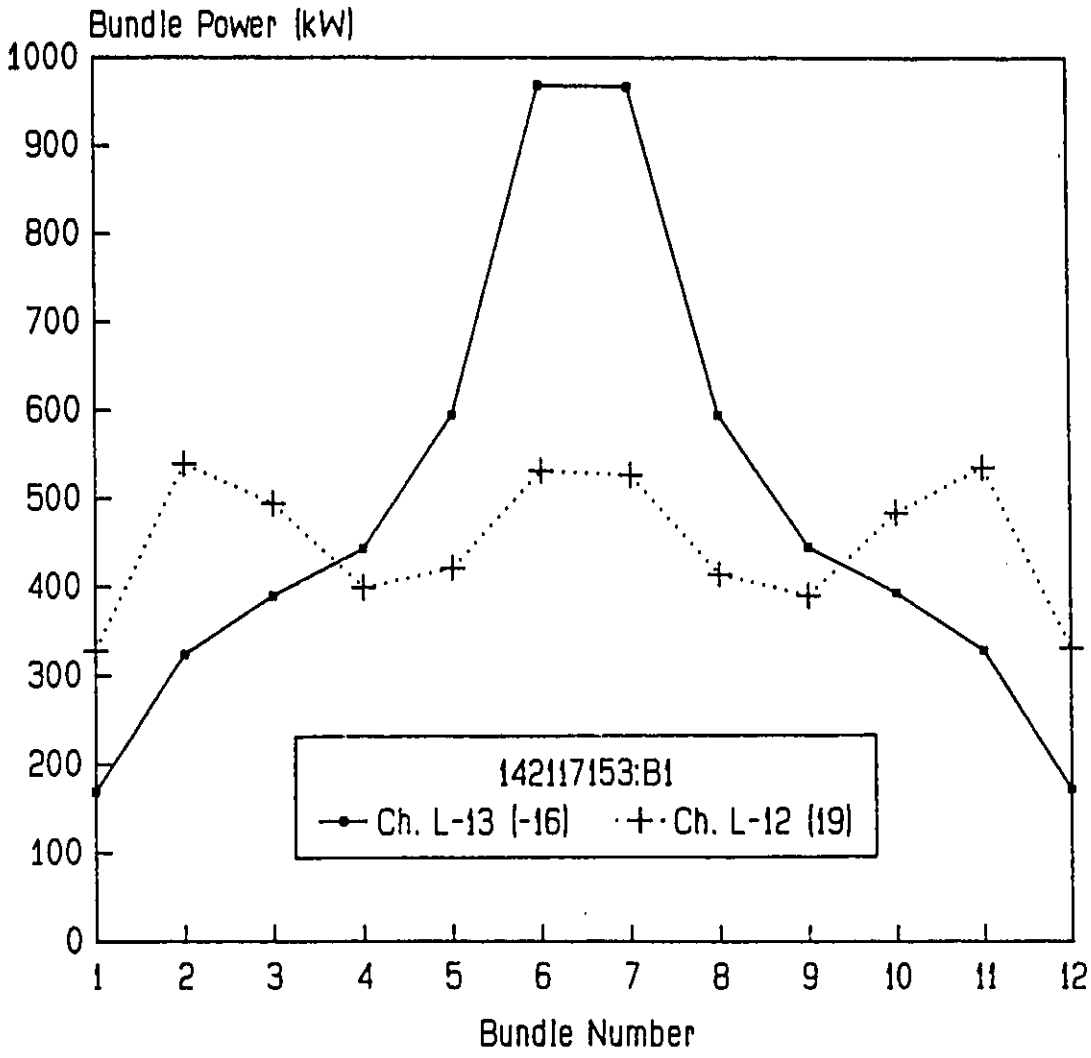

Figure 10-5d Bundle Power Distributions (TAA)

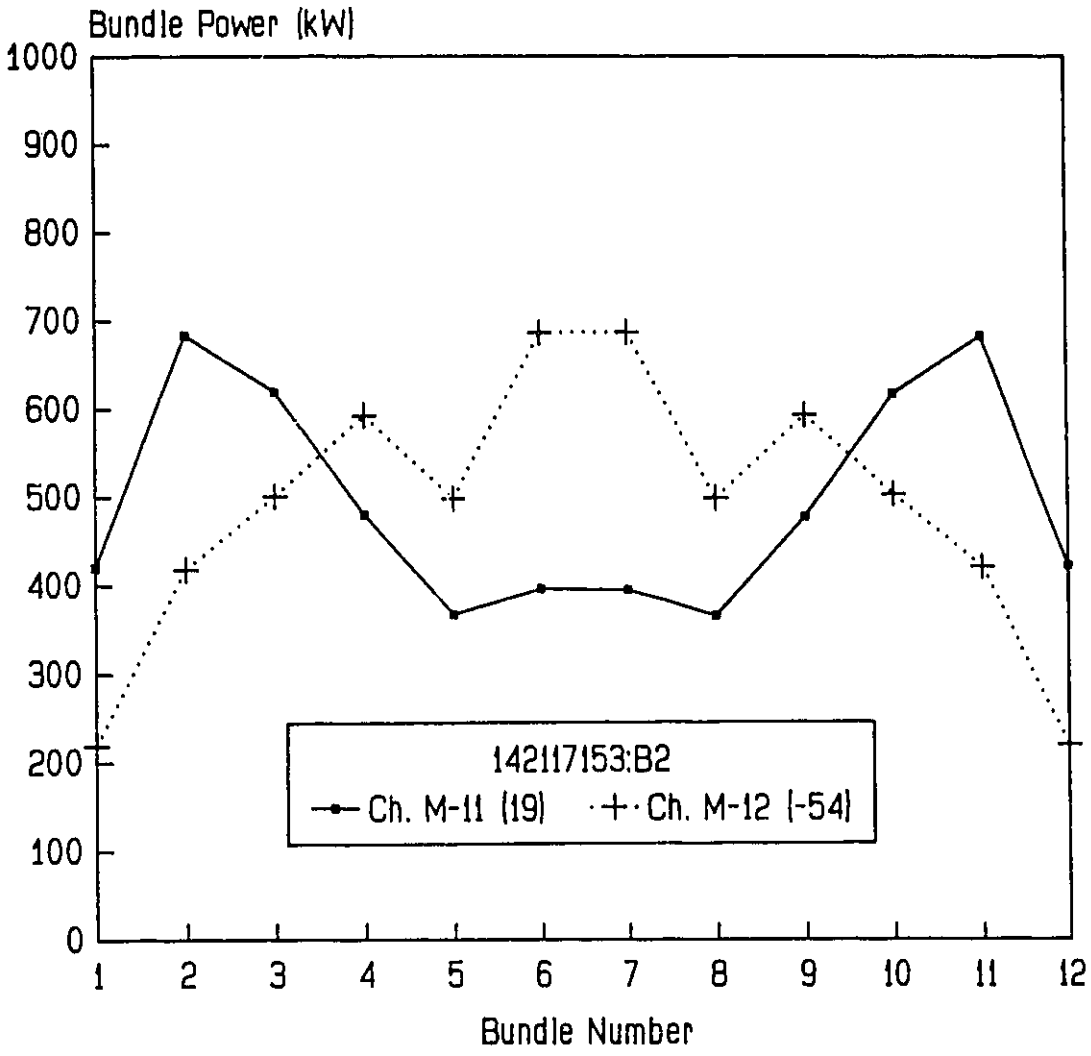

Figure 10-5c Bundle Power Distributions (TAA)

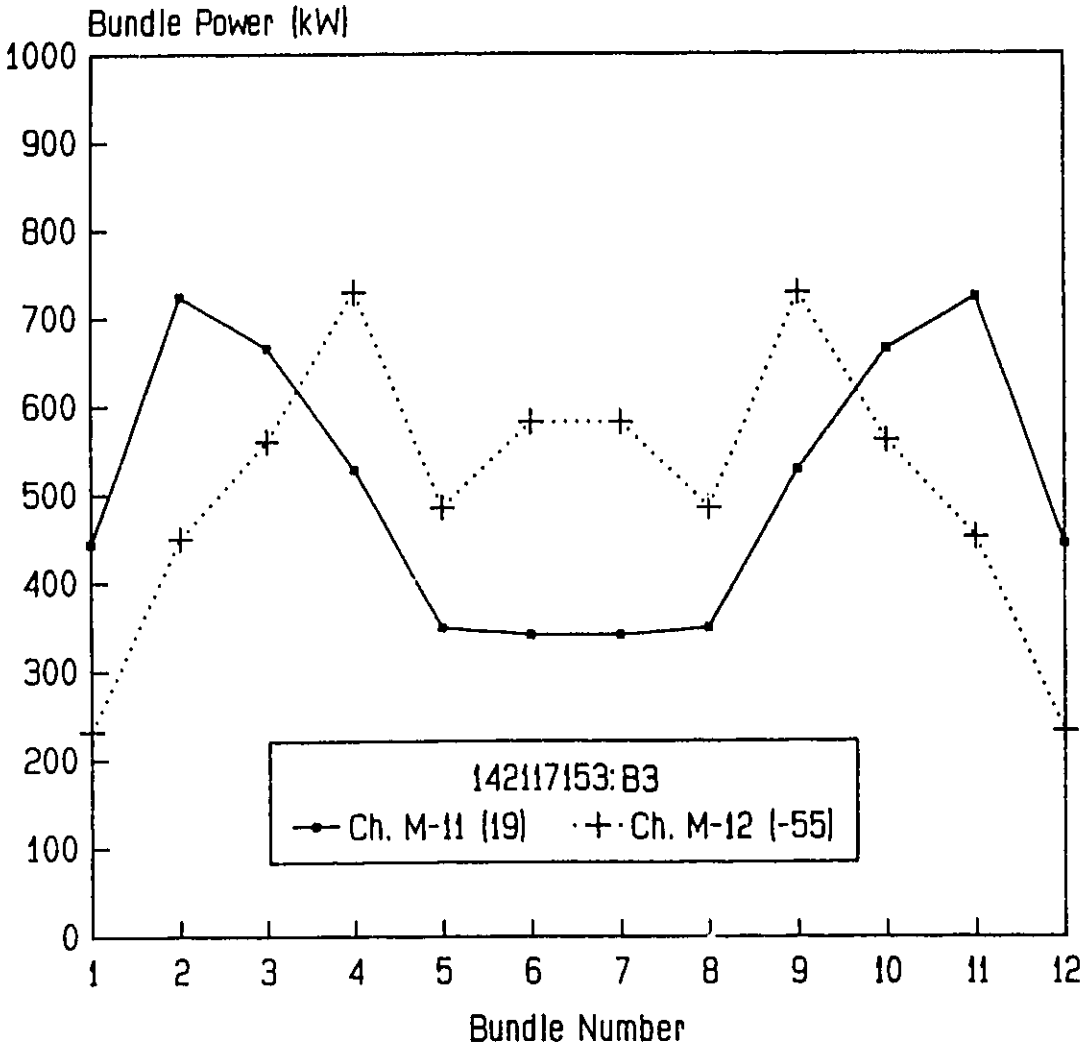

Figure 10-5f Bundle Power Distributions (TAA)

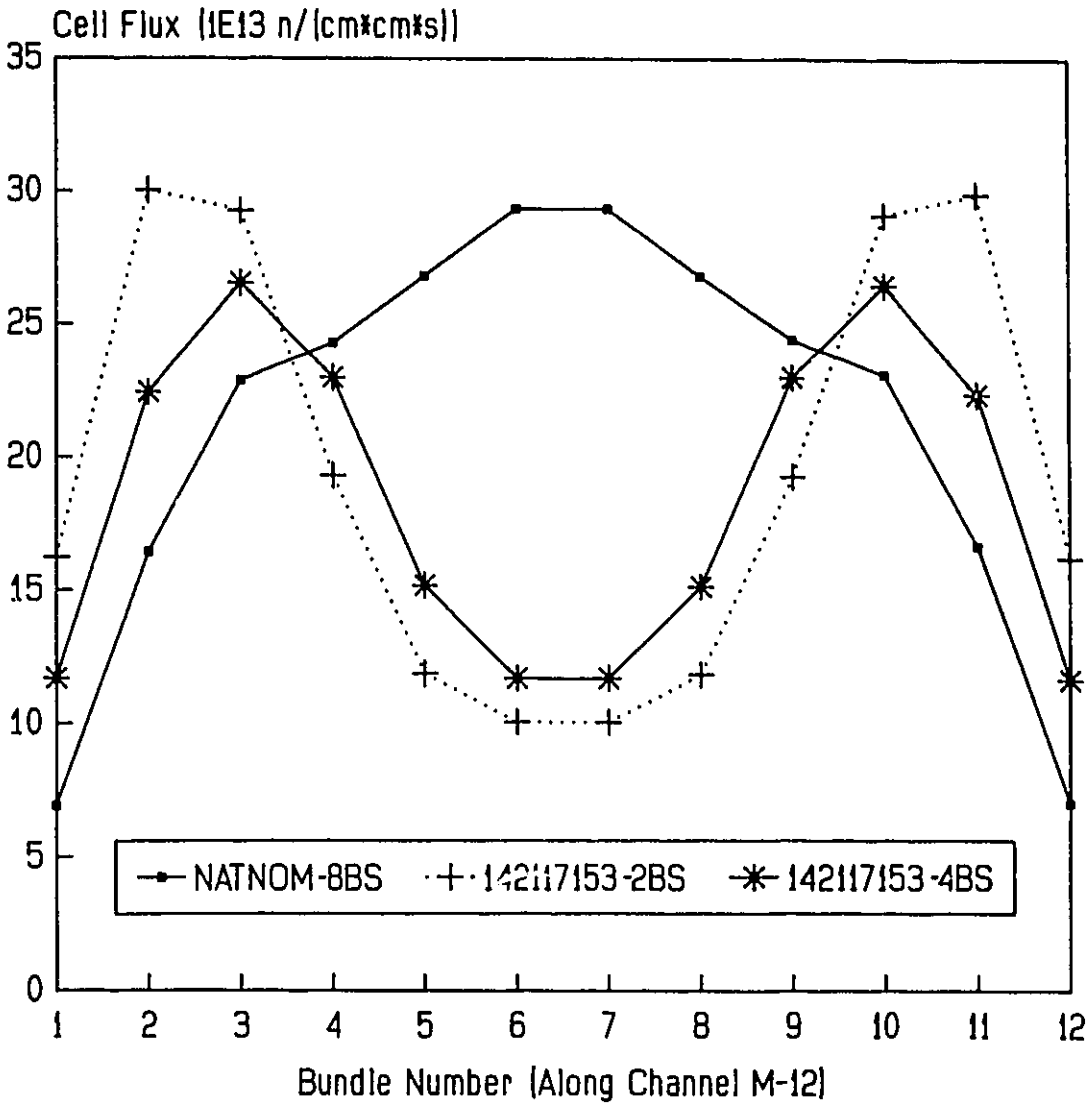

Figure 10-6a Cell Flux Distributions (TAA)

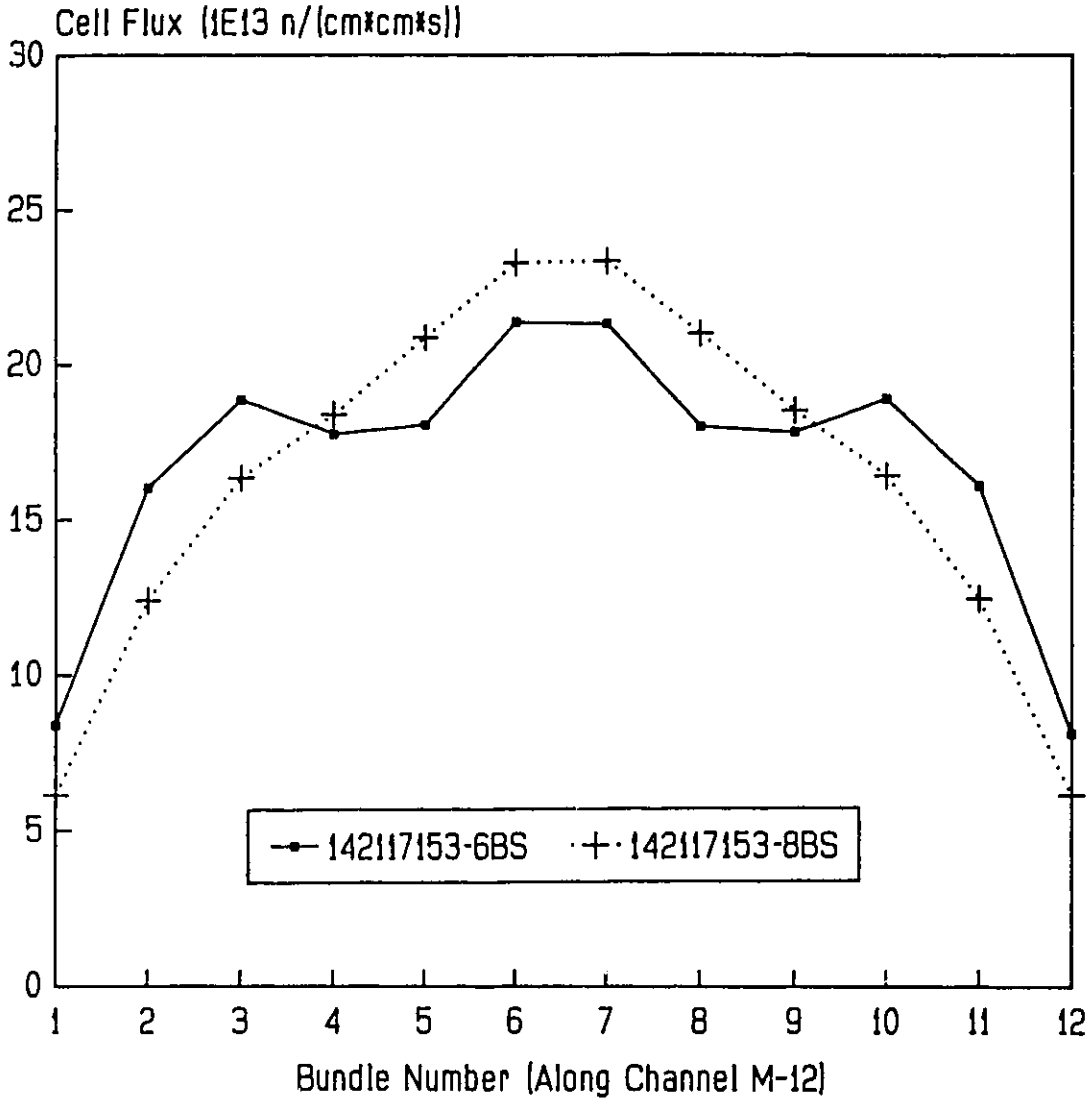

Figure 10-6b Cell Flux Distributions (TAA)

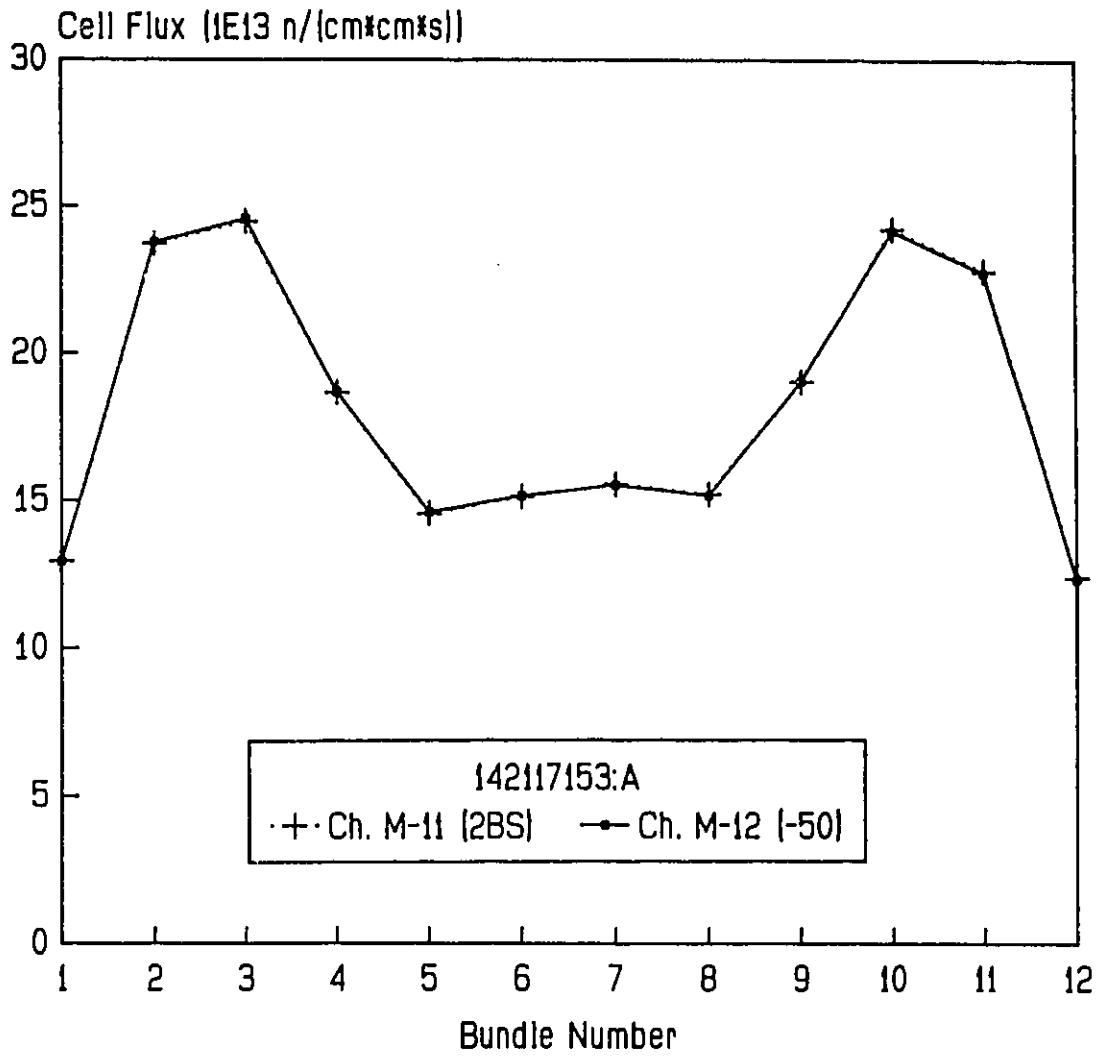

Figure 10-6c Cell Flux Distributions (TAA)

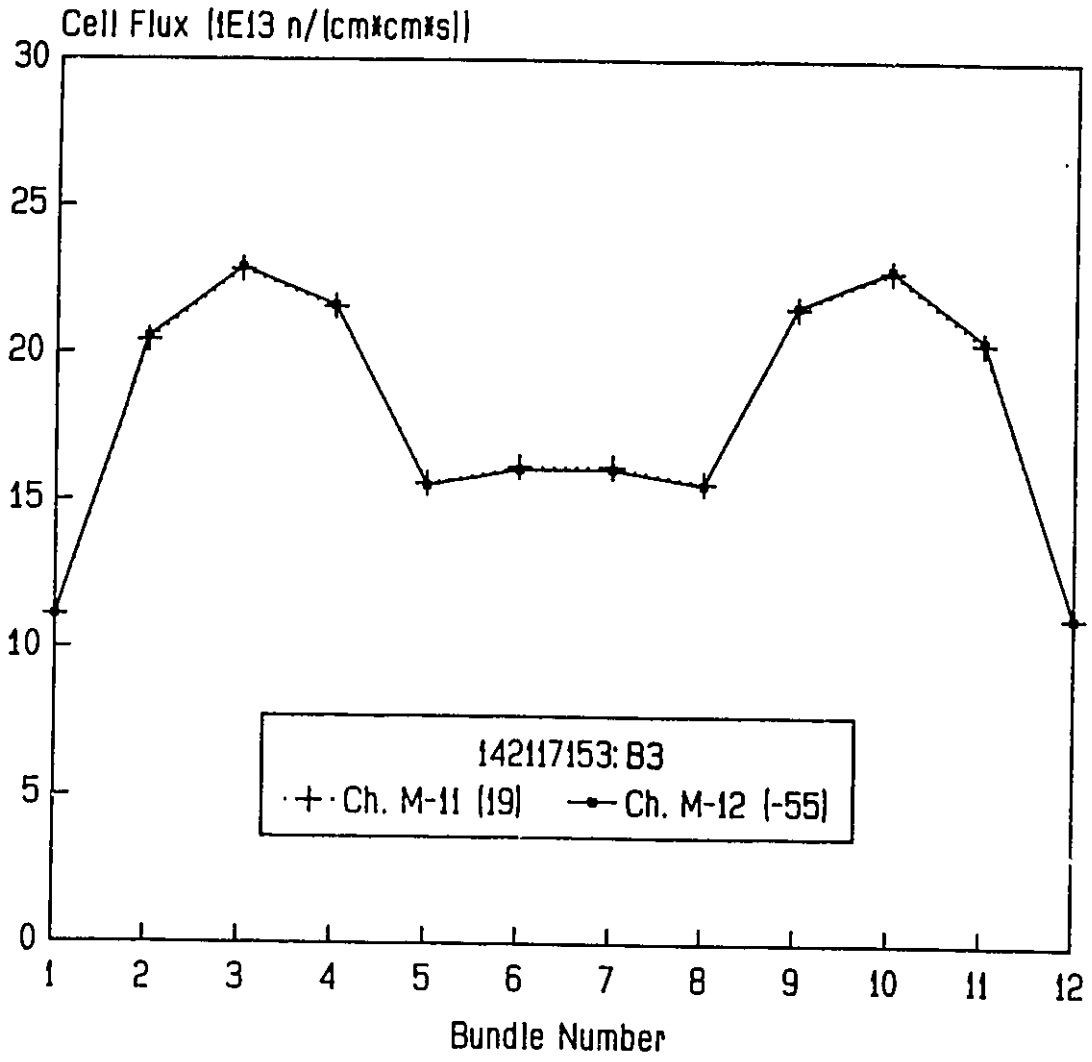

Figure 10-6d Cell Flux Distributions (TAA)

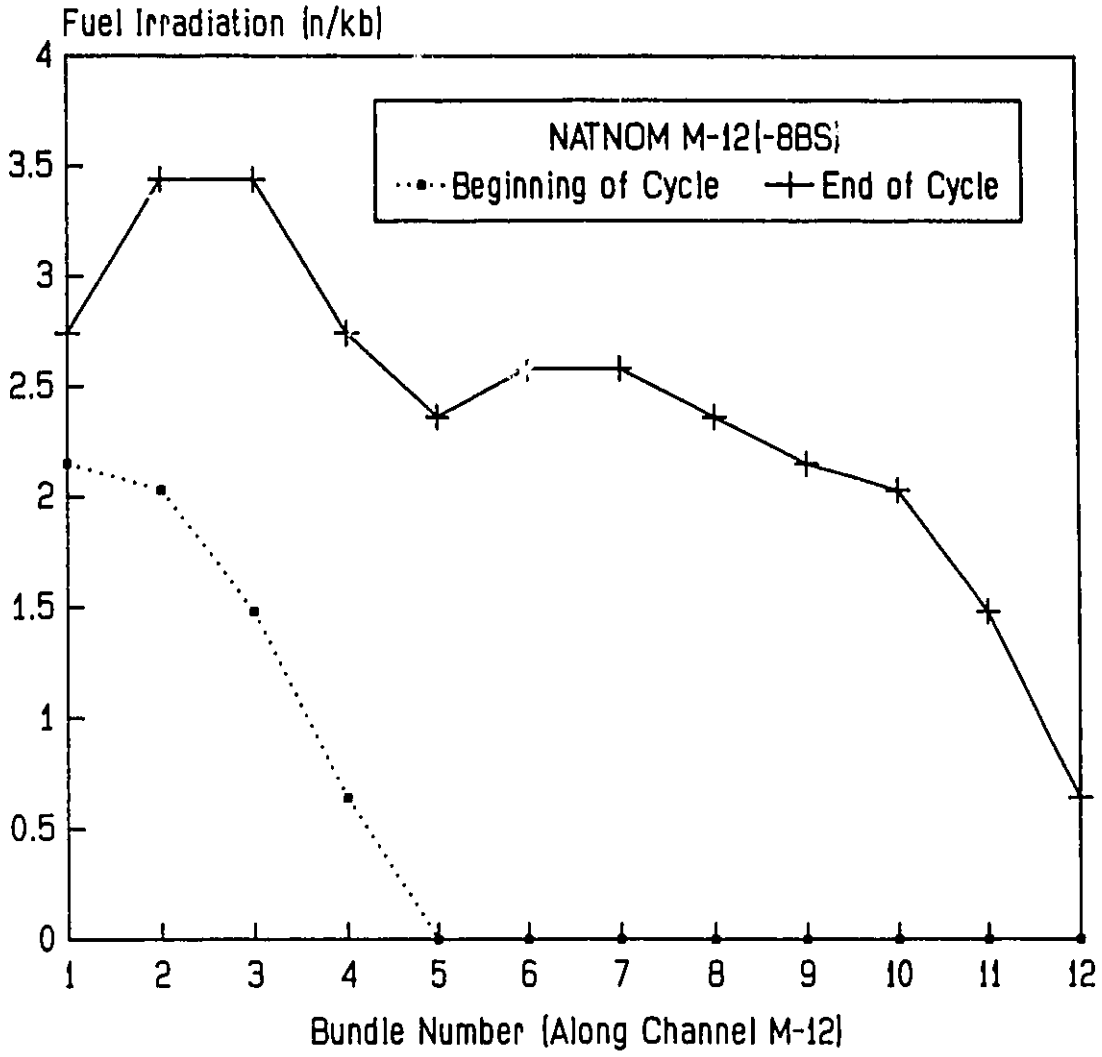

Figure 10-7a Fuel Thermal Irradiation Distributions (TAA)

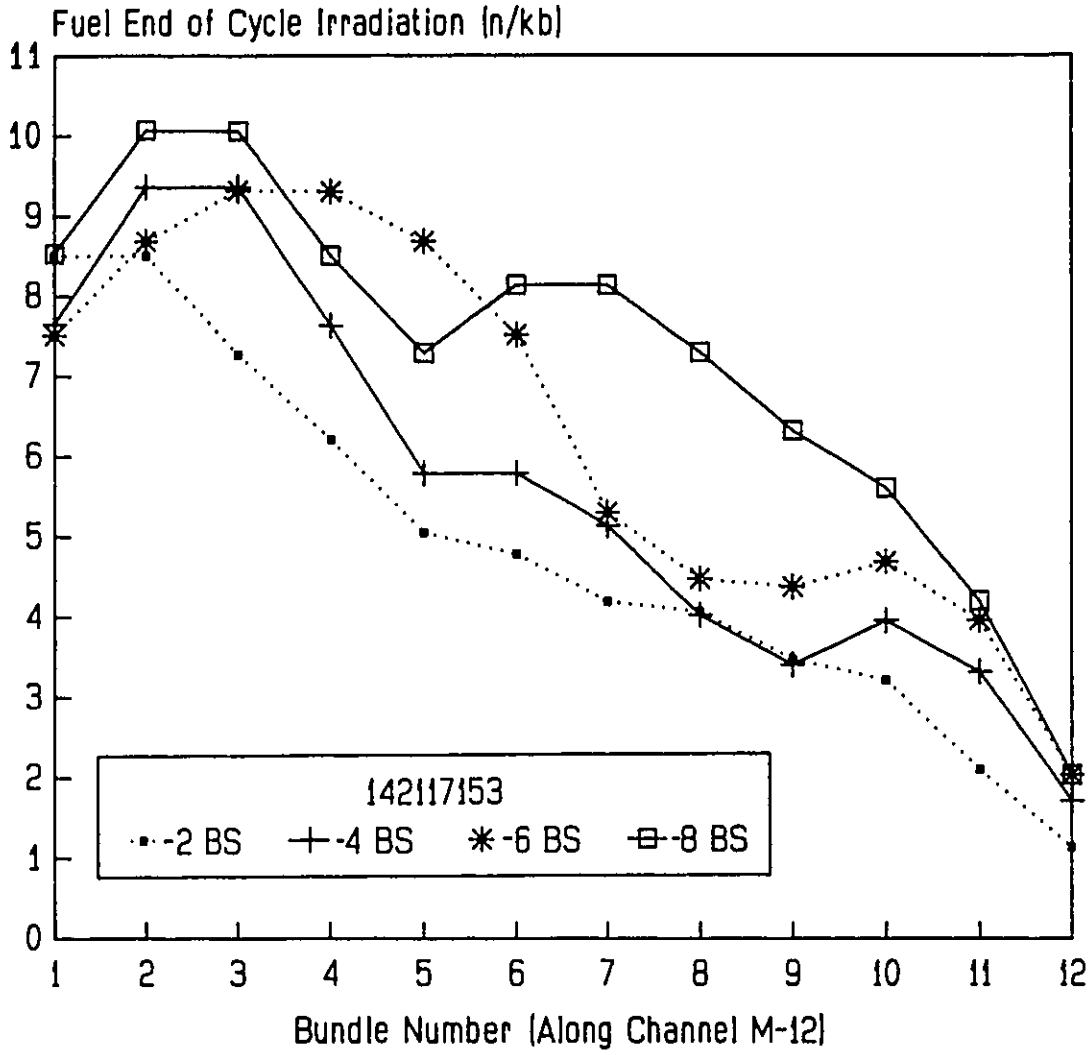

Figure 10-7b Fuel Thermal Irradiation Distributions (TAA)

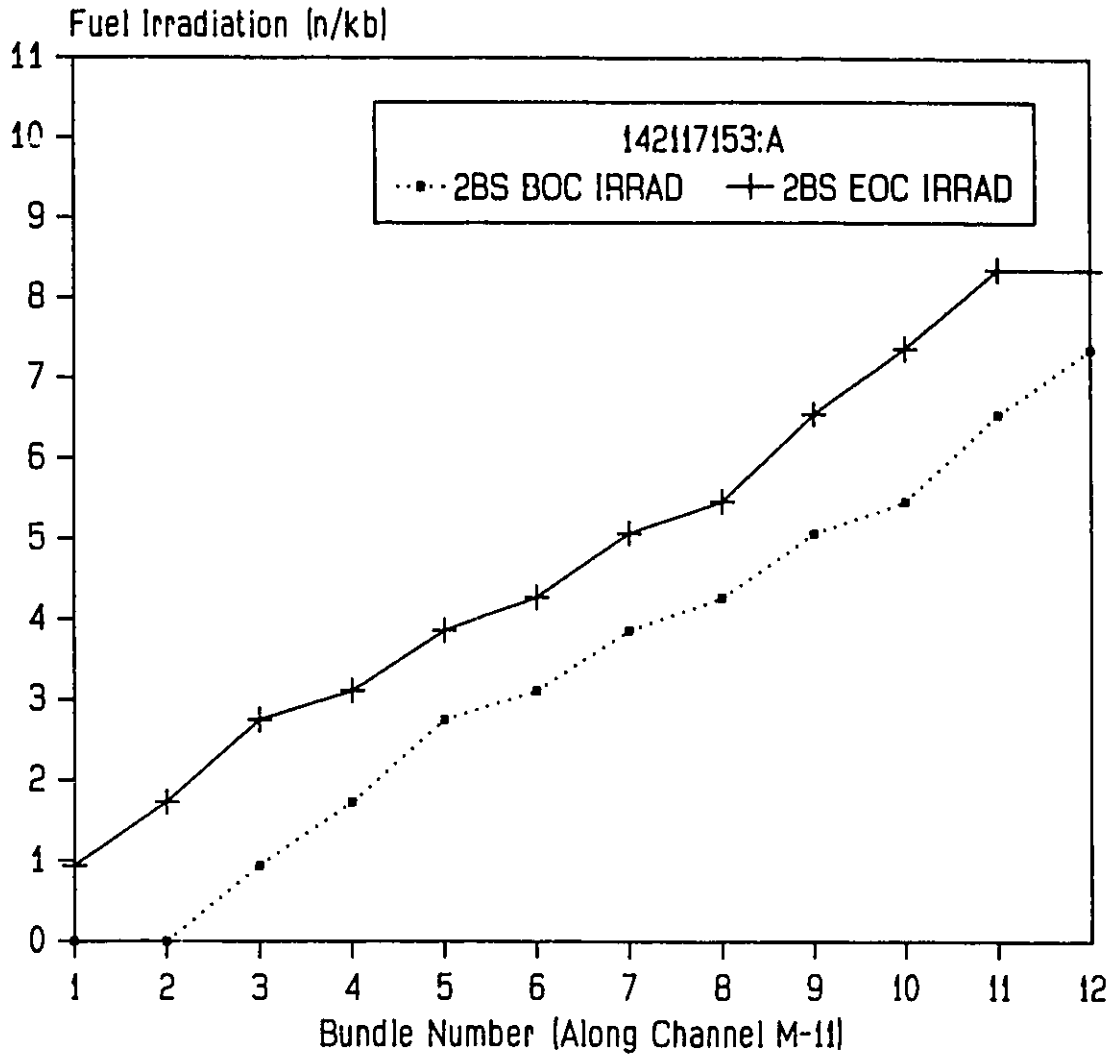

Figure 10-7c Fuel Thermal Irradiation Distributions (TAA)

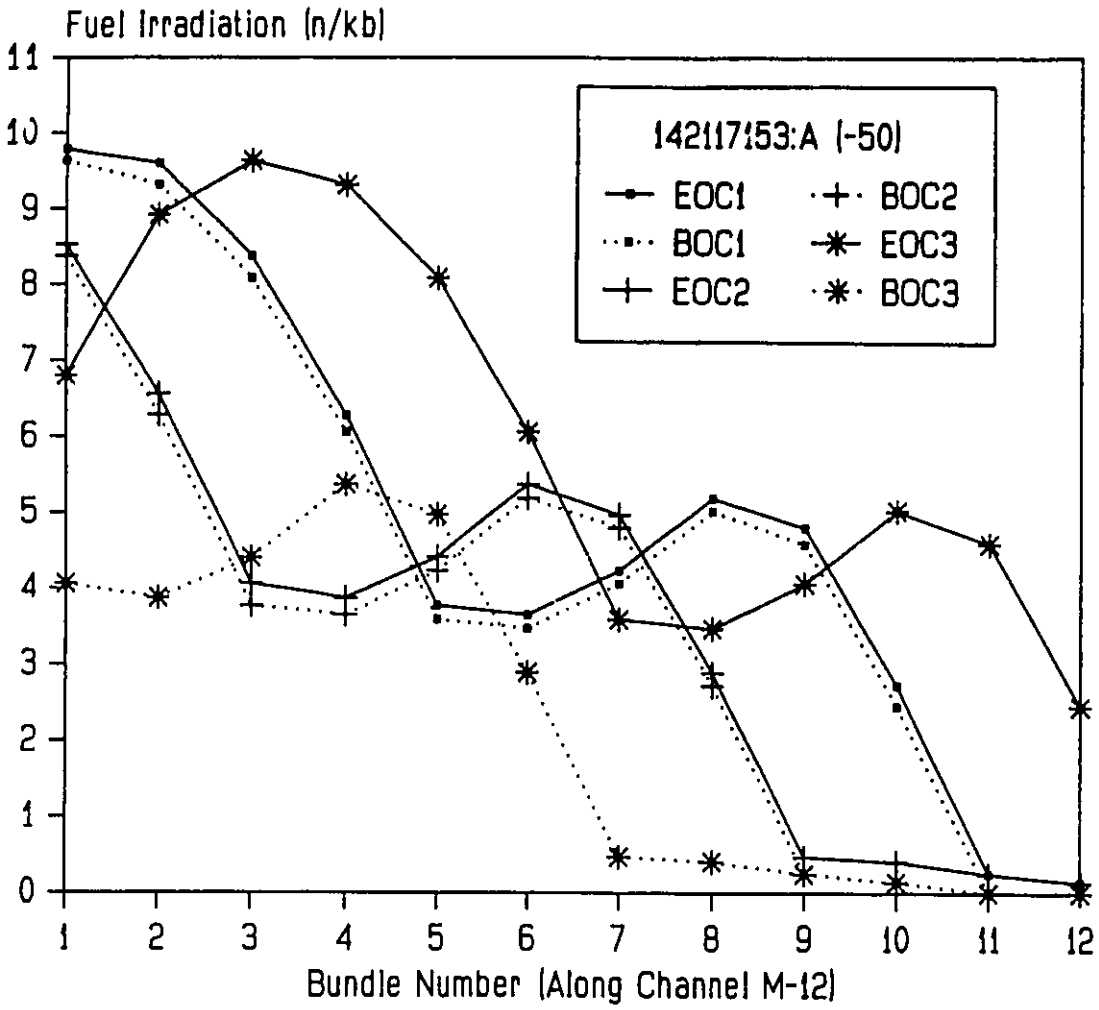

Figure 10-7d Fuel Thermal Irradiation Distributions (TAA)

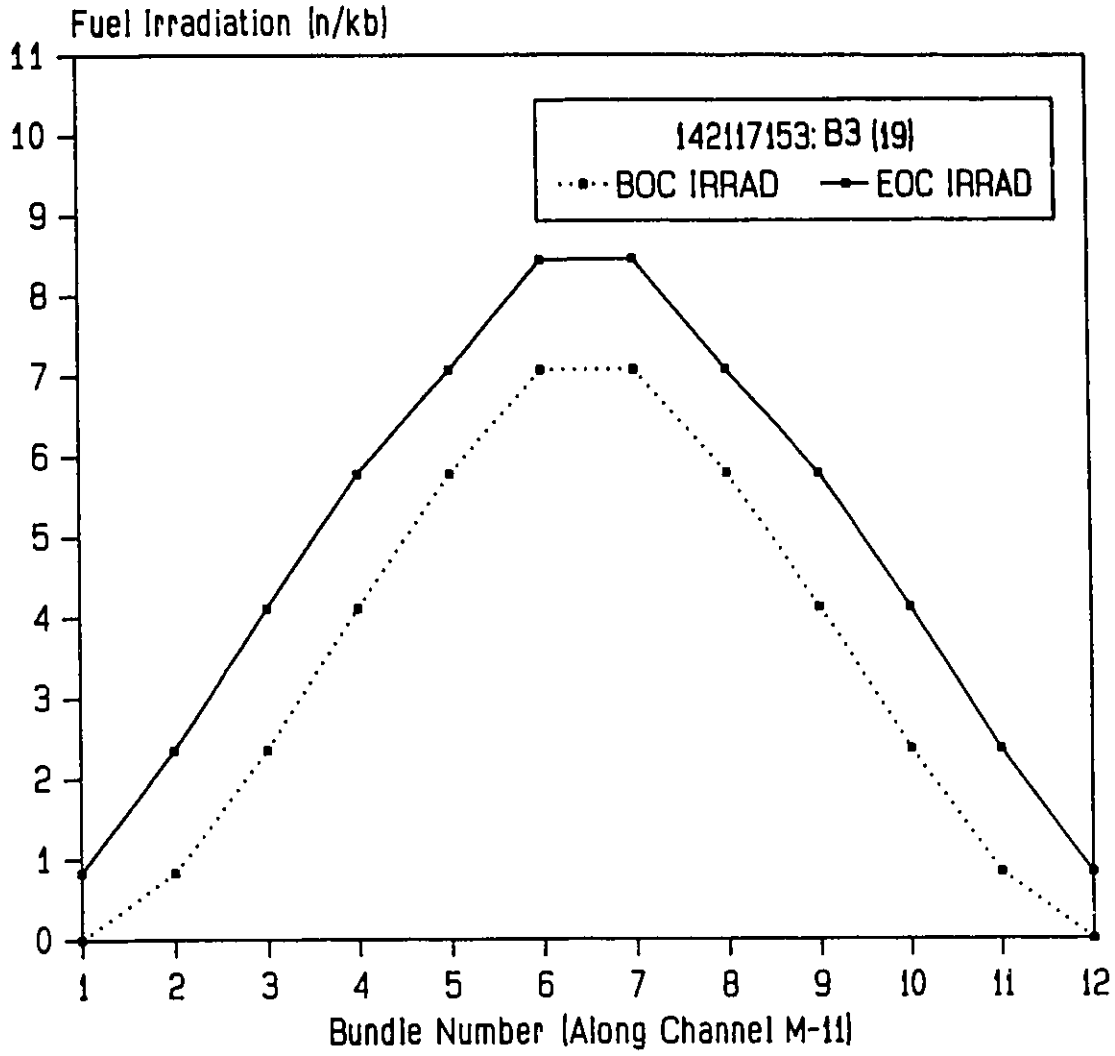

Figure 10-7c Fuel Thermal Irradiation Distributions (TAA)

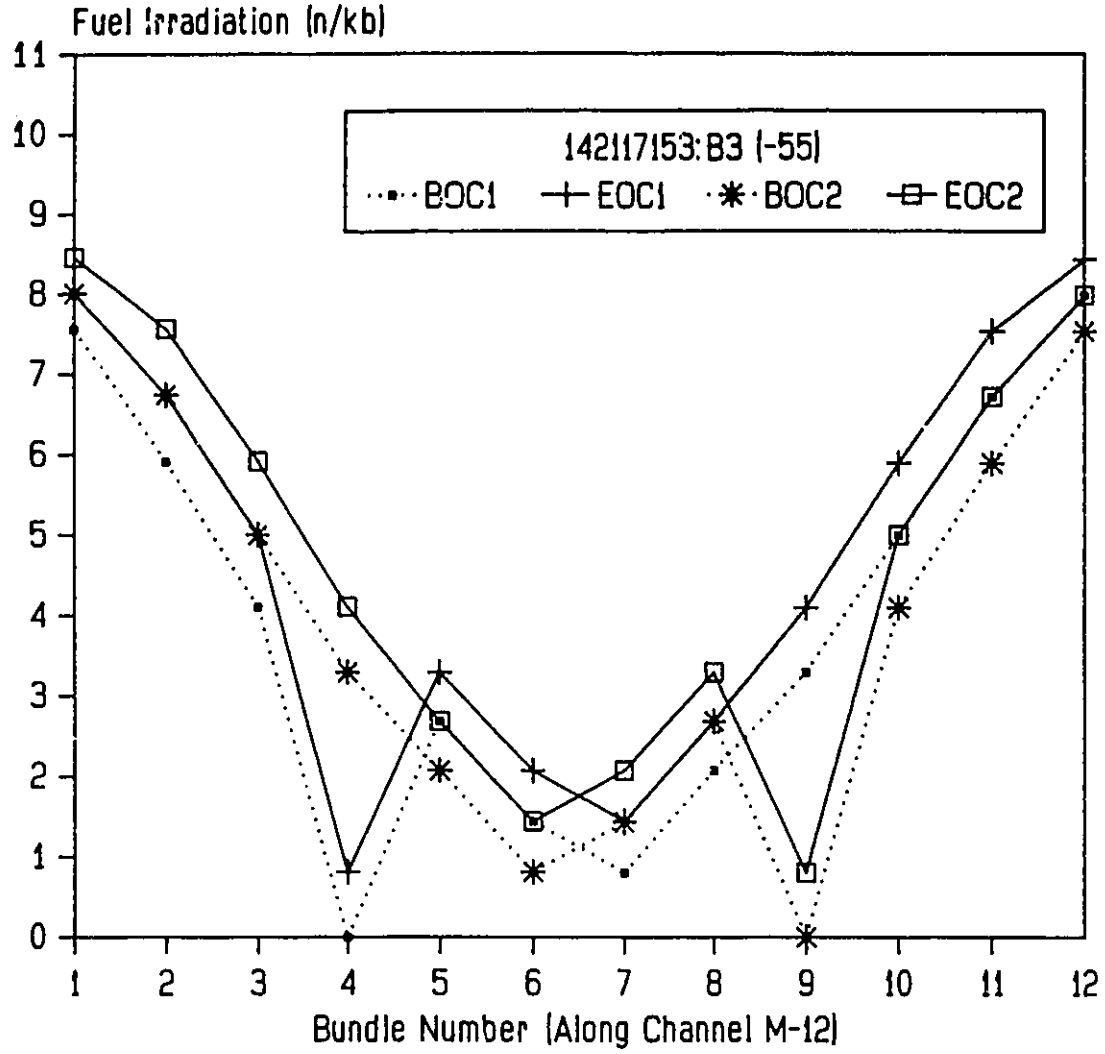

Figure 10-7f Fuel Thermal Irradiation Distributions (TAA)

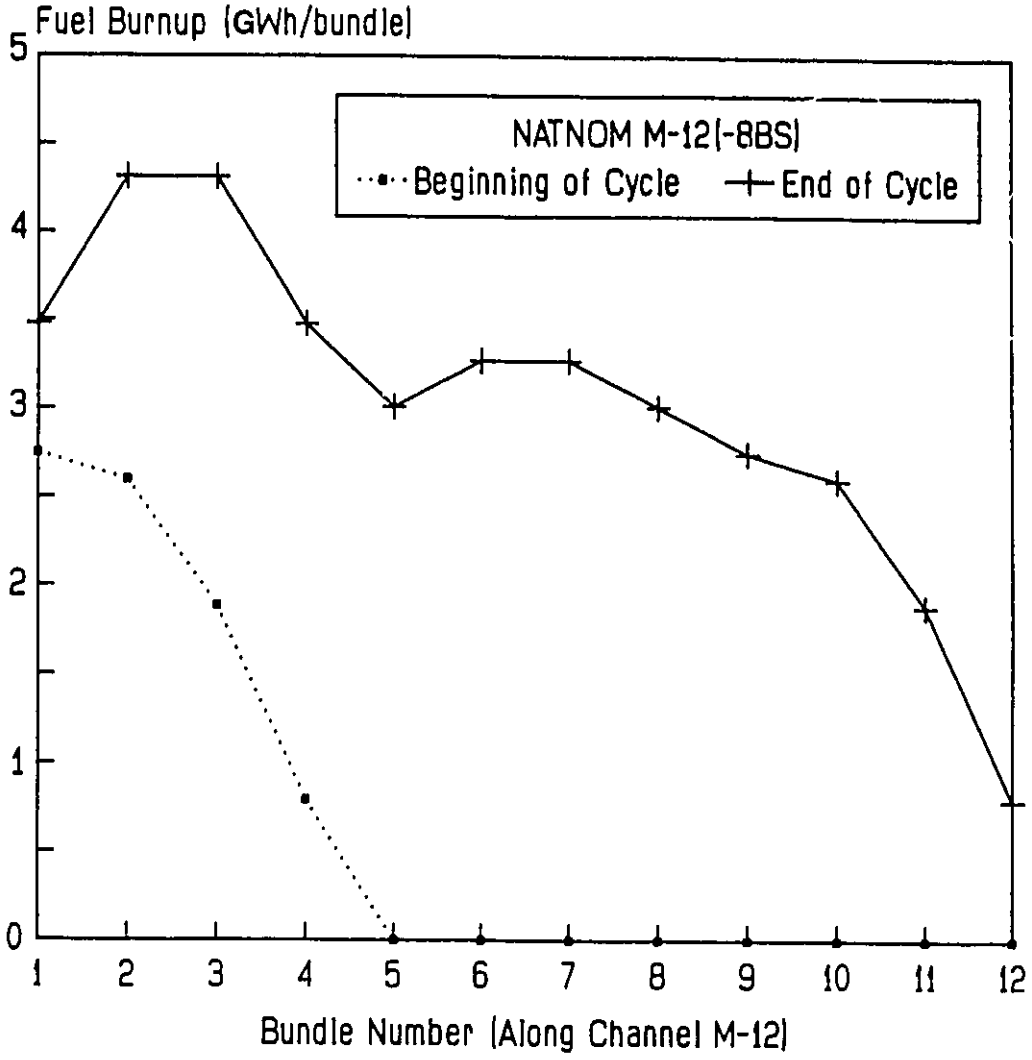

Figure 10-8a Fuel Burnup Distributions (TAA)

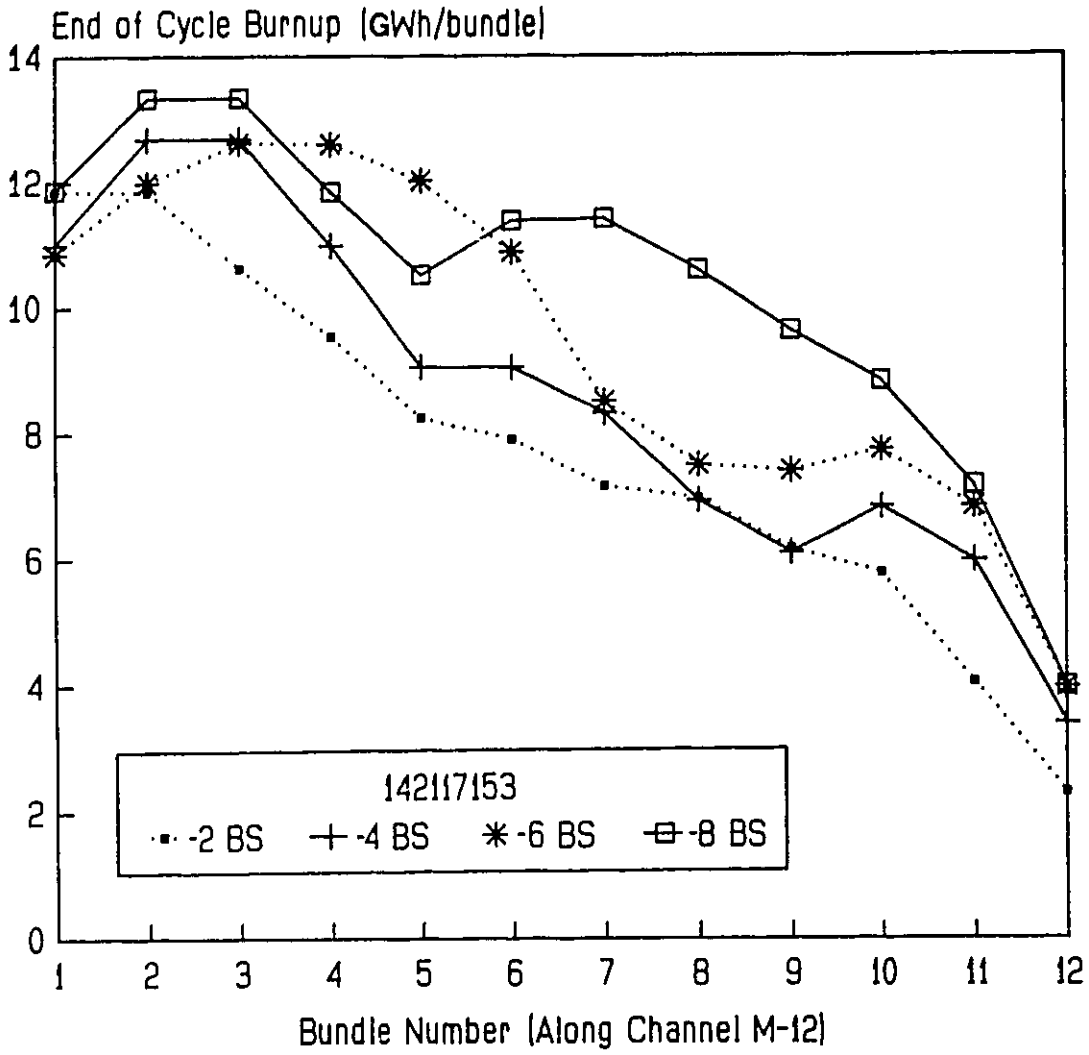

Figure 10-8b Fuel Burnup Distributions (TAA)

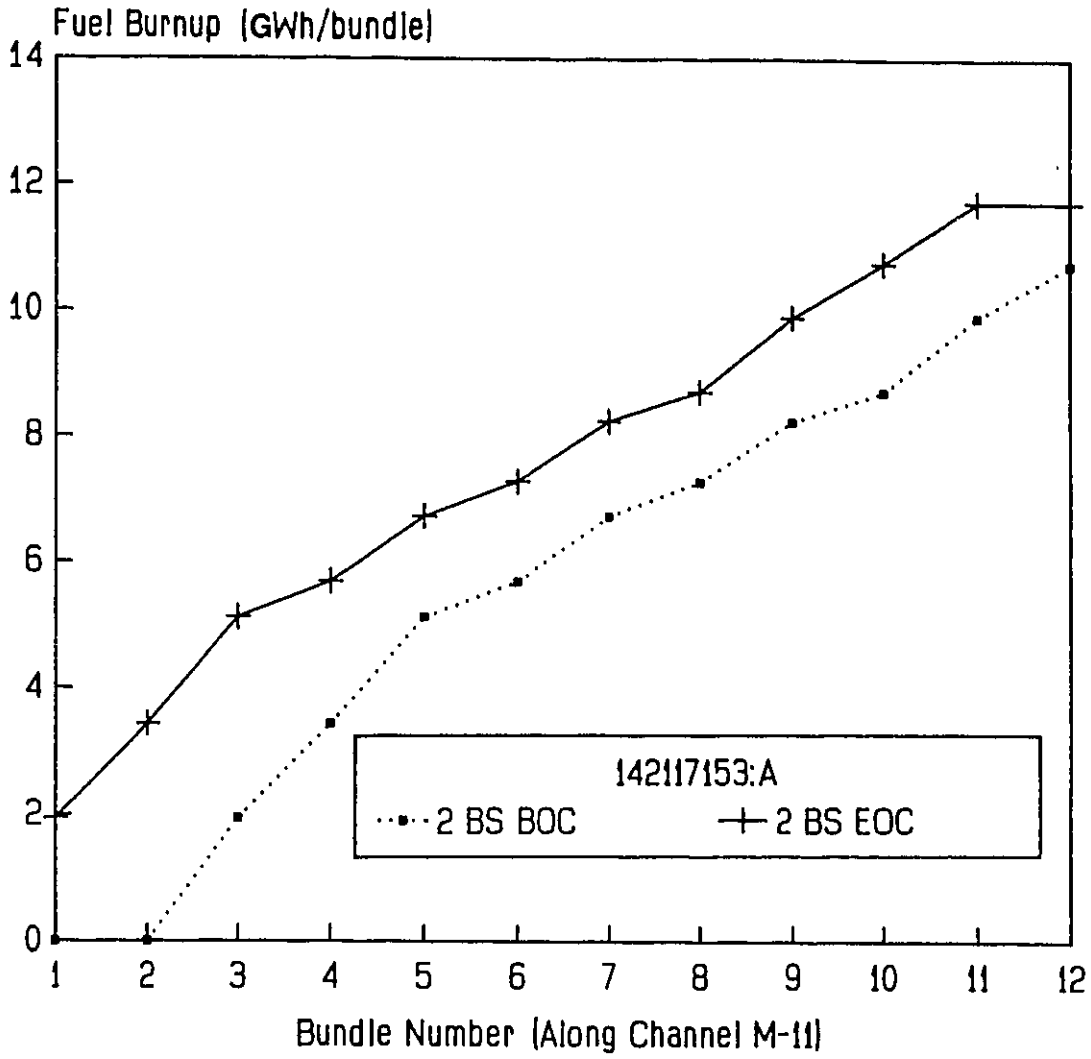

Figure 10-8c Fuel Burnup Distributions (TAA)

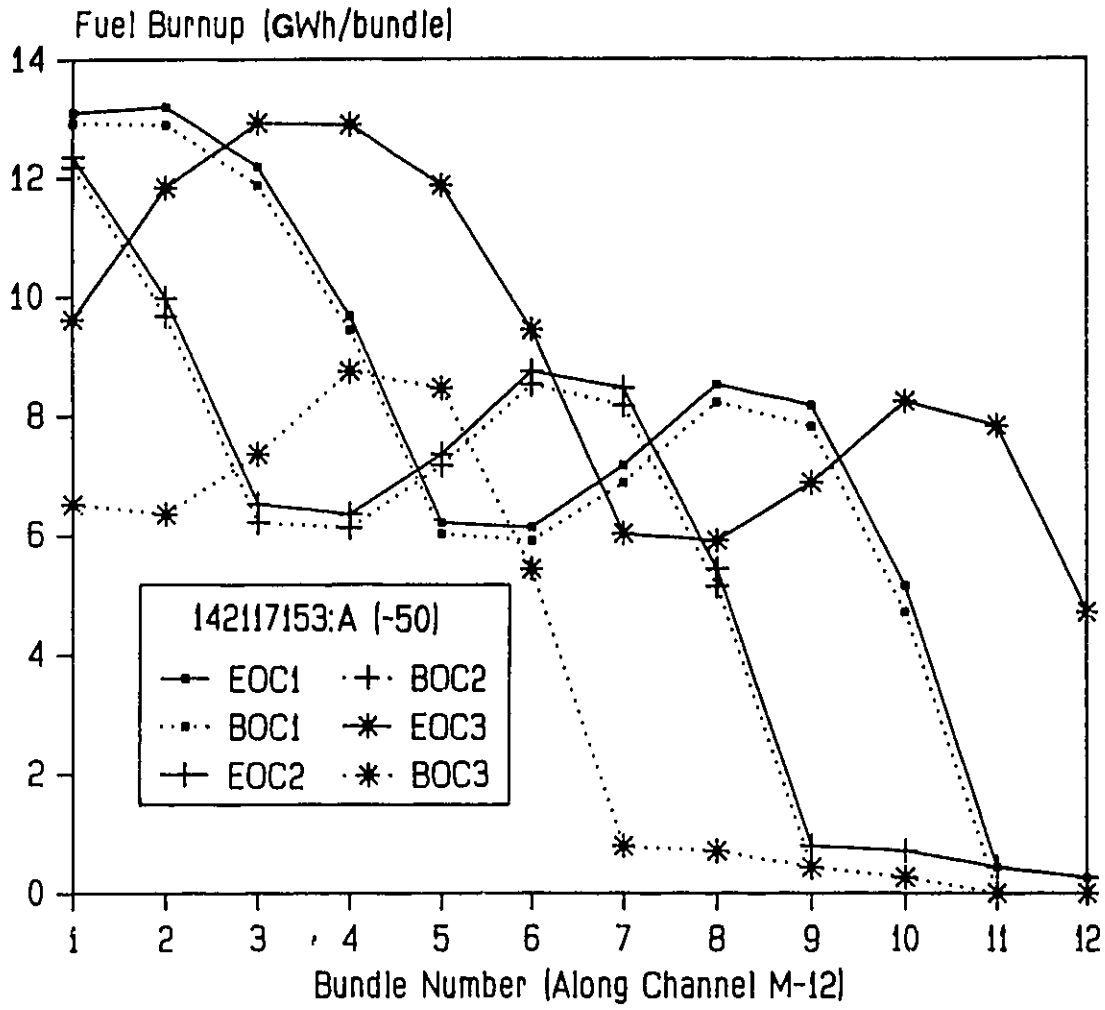

Figure 10-8d Fuel Burnup Distributions (TAA)

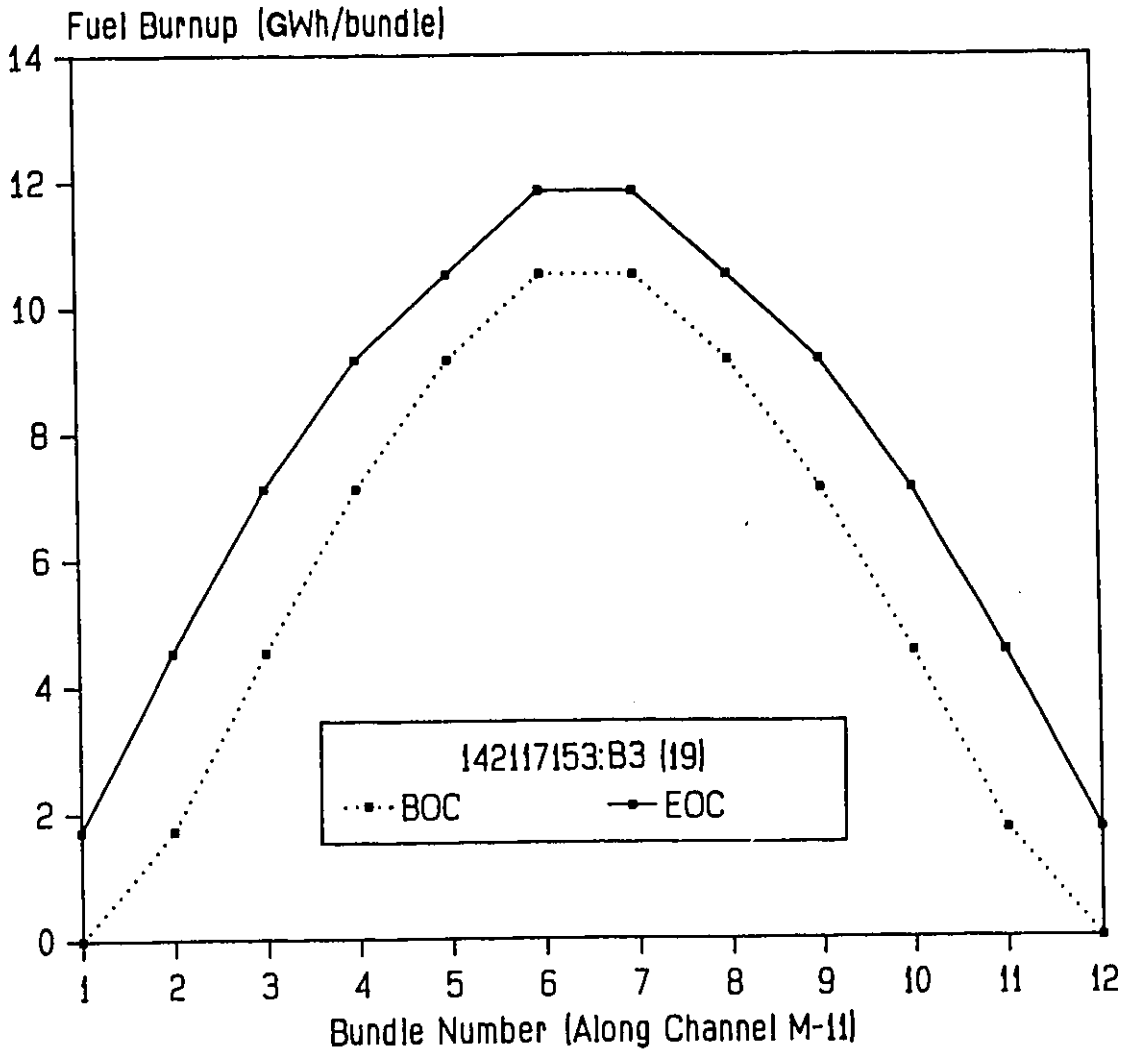

Figure 10-8c Fuel Burnup Distributions (TAA)

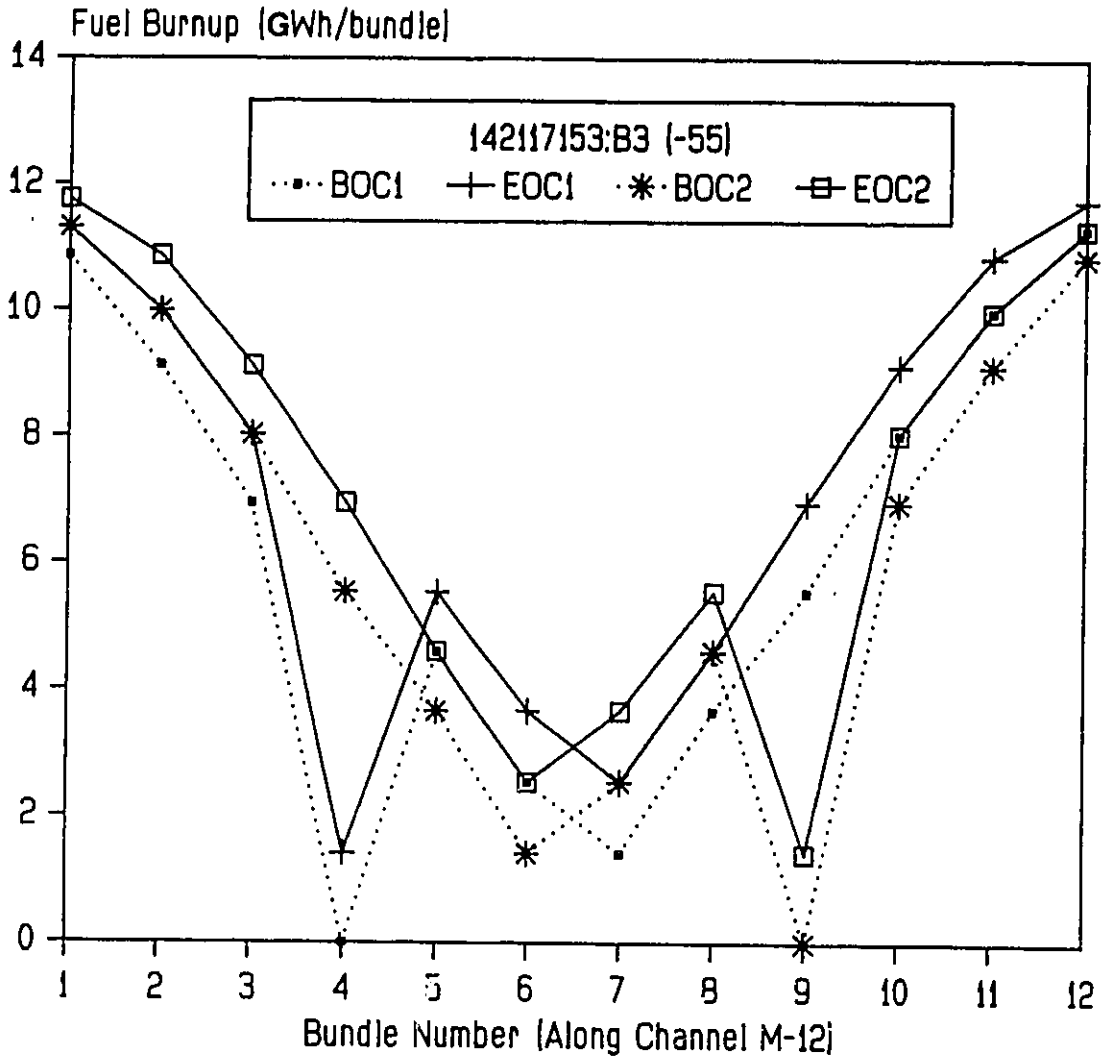

Figure 10-8f Fuel Burnup Distributions (TAA)

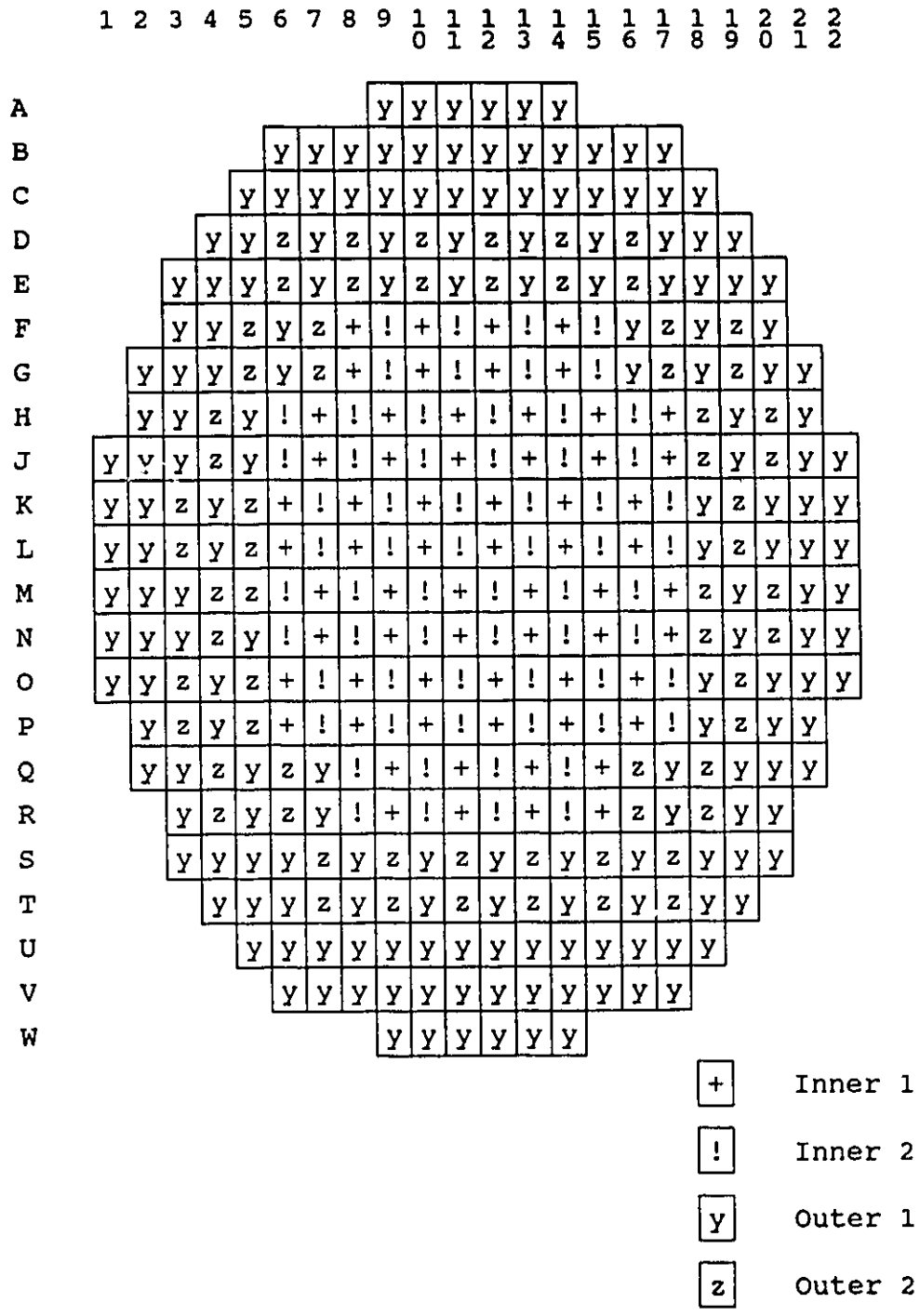

Figure 10-9 Fuelling Map: 142117153 Scheme A

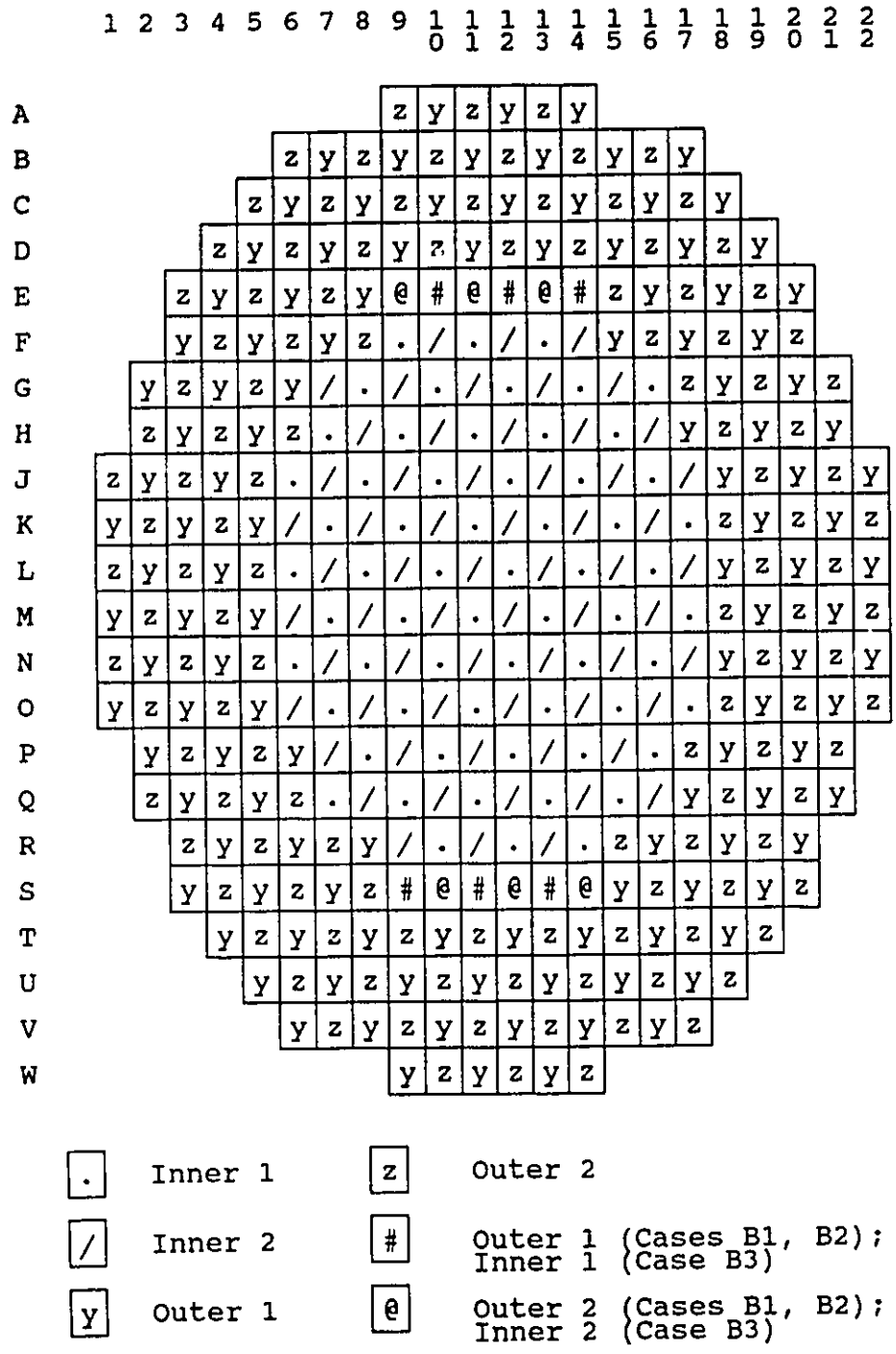

Figure 10-10 Fuelling Map: 142117153 Schemes B1, B2, and B3

CHAPTER 11

CANDU HEAVY WATER SPECTRAL SHIFT ADVANCED THERMAL REACTORS

11.1 INTRODUCTION

Reactors employing off-power refuelling rely on the use of burnable poisons and control rods to suppress the initial reactivity of a newly reloaded core. The parasitic neutron absorption in these materials results in a burnup penalty and hence an increase in the cost of the product electricity.

Higher fuel burnups (of the order of 50000 MWd/MgU (Coleman et al., 1981)) can be obtained via control of the neutron spectrum in the reactor (i.e., varying the spectral characteristics through the fuel burn cycle). Fresh fuel is subjected to a hard (high energy) spectrum, where the fission cross sections are smaller than in a soft spectrum (reduced initial power peaking) and U-238 conversion to Pu-239 is enhanced. Gradually, with burnup, the spectrum is softened to increase the fission cross sections and utilize the store of bred plutonium.

In BWRs the spectral shift is accomplished by varying the core pressure and hence water/steam density. Initially the pressure is low to reduce the coolant to fuel mass ratio, and as burnup increases, pressure is increased (Lang et al., 1983).

In PWRs a more complicated scheme has to be implemented to achieve the required shifting of the neutron spectrum. The coolant initially is a combination of D_2O and H_2O. The D_2O, with its smaller moderation cross section, reduces the slowing down power of the coolant. As a result the neutron spectrum is harder than in the situation with all H_2O coolant. As burnup increases the D_2O is gradually extracted from the coolant and the spectrum softens (Hellens et al., 1978; Sider and Matzie, 1980).

More recently, the use of water displacement rods, made of inert

material (USA) or fertile material (France) have been suggested for initial spectral hardening (Barre et al., 1988; Hittner, et al., 1988).

All of these spectral shift mechanisms rely on changing the characteristics of the core through a burn cycle. Operationally, this will further complicate the reactor control procedures which, nominally, would be required to accomodate the wide ranging system reactivity and compensatory reactivity control materials. By altering the neutron spectrum the reactor response characteristics are substantially altered. The control systems and operator actions must account for these variations. As a consequence, operator ability to intuitively predict reactor response to system perturbations is inhibited, thereby increasing operator response time. This could have a detrimental effect on operational safety.

In CANDU reactors, on-power semi-continuous fuelling is employed for optimum resource utilization. CANDU reactors operate in an equilibrium state from about one full-power year to the end of life (approximately 40 years). During this equilibrium period the reactor behaviour is relatively time-independent. While this eases the requirements on the control systems and enables operators to develop excellent predictive intuition, it eliminates the option of varying the entire reactor spectrum over a burn cycle as in units with batch refuelling.

An alternative solution can be implemented which would allow:

(a) on-power fuelling,
(b) maintenance of a standard equilibrium operating state, and relatively invariant flux and power distributions,
(c) fresh fuel irradiation in a hard neutron spectrum, and,
(d) partially irradiated fuel burnup in a more thermalized neutron spectrum.

This could be accomplished by dividing the reactor into a number of spectral zones. Fuel would be irradiated in a spectrum which is increasingly thermalized. In a CANDU reactor this spectral zoning could be achieved in a number of ways.

(a) Moderator displacement rods could be placed between fuel channels in the central core region creating a harder spectrum at the centre of the core and a softer spectrum at the core periphery. Fuel would be shuffled from the inner to outer reactor zones.

(b) The lattice pitch (inter-channel spacing) could be reduced for the channels in the central region of the reactor, thereby reducing the fuel to heavy water ratio and consequently decreasing the neutronic thermalization in this region.

(c) The calandria could be modified to keep moderator fluid completely isolated from the central core region. A zone of lattice cells with moderator would surround an unmoderated central core region.

(d) The calandria tube radius could be varied either radially (central core channels have large calandria tubes, outer channels do not), or axially (calandria tubes wide at channel centre (hard spectrum), and narrow at channel axial ends (increased thermalization)).

Each of these approaches poses additional operational and/or safety concerns which must be addressed in the design and development stages.

In Case (a) the moderator displacement rods would have to be positioned in a calandria which in the current design is essentially lacking in open space given the multitude of instrumentation already in-core. Further, if the rods were removed or simply shifted, system reactivity could increase substantially, possibly resulting in channel and/or core damage. Neutronic losses by the displacement tubes must also be considered. Further, if the tubes are hollow (to minimize parasitic neutron absorption) D_2O ingress through small leaks in the tube walls could cause large increases in reactivity.

In Case (b), the reduced lattice pitch would structurally weaken the calandria tube sheet (which supports individual fuel channels). A hexagonal lattice arrangement may alleviate some potential problems. In addition, fuelling machine clearances would be reduced. The channel endfittings are

wider than the channels themselves and the fuelling machines must latch over the end-fittings. Hence reductions in lattice pitch may require an end-fitting/fuelling machine redesign as well. It may be possible to have one endfitting opening to two channels with a toggle to direct fuel to the required channel. The feeder layout must also be considered in such a design.

From a reactor safety perspective, void reactivity would be reduced with the tighter lattice pitch (due to the increased reliance on the coolant for neutron moderation). There is also the concern that if an accident resulted in pressure and calandria tube displacement (due to structural melting), a local increase in fuel channel separation could greatly increase reactivity, further aggravating the situation.

In Case (c), the shell of thermalized channels surrounding the unmoderated central core region does not lend itself easily to spectral tuning of the central reactor zone. Further, leaks at the inner/outer calandria boundary could lead to a rapid increase in system reactivity.

In Case (d), spectral tuning (at the construction stage) is easily accomodated by simply varying the calandria tube diameter. The increased pressure tube diameter results in an increase in the amount of zirconium and hence absorption in the calandria tube. There is a potential for leakage from the calandria or pressure tube to the gas gap, which could result in a very large reactivity excursion, if, in a very unlikely event, several tubes leak simultaneously. To minimize the consequence of this potential accident, passive safety systems would necessarily be required in addition to enginneered protection. For example, the gas gap could operate at a higher pressure than the moderator. If the pressure dropped below a prescribed value a pressure balance upset would result in the gas gap system being flushed with heavily poisoned water to mitigate the potential neutronic effects should the gas gap fill with unpoisoned D_2O. A similar pressure balanced system would flood the core with heavily poisoned water should the pressure in the gas gap increase (due to D_2O ingress from the primary heat transport system). The required speed of response of these protective systems would be directly related to the calandria tube diameter. Such passive systems have been incorporated into the new PIUS reactor concept (Office of Technology

Assessment, 1984).

An alternative to a gas gap would be a solid region between the calandria and pressure tubes. This region would be constructed of a low heat conductivity, neutronically transparent material. One can envisage that at elevated temperatures (accident conditions) such a material could be designed to undergo a phase change which would increase its heat conductivity, thereby increasing the efficacy of the moderator as a heat sink in large loss of coolant accidents in conjunction with a failure of the emergency core cooling system. If it is deemed necessary to maintain a gas flow through the gap region, the intertube space could be filled with small fused solid spheres of inert material, This would allow gas flow and yet minimize the inflow of heavy water in the event of a pressure tube or calandria tube leak.

A further benefit of operating with enlarged calandria tubes is that the heat transfer to the moderator from the pressure tube is reduced. Hence electrical efficiency is increased. A drawback during severe accident scenarios is that a greater amount of pressure tube sag would be required to allow contact with the calandria tube (to utilize the moderator as a heat sink).

The radial variation spectral shift option would be superior to the axial calandria tube variation option for a number of reasons:

(a) Calandria tubes would be uniform along a given channel avoiding the requirements for welds and reducing stresses.
(b) The zonal structure can be more well-defined and the number of bundles at zone boundaries (which are influenced by the neutron spectrum in both adjacent zones) are kept to a minimum.
(c) Operationally, it would be easier for operators to manage radial rather than axial zones.

The effect of neutronic streaming from the core would be minimized with the axial zoning option, however (reduced calandria tube diameter at axial ends of channels).

The options mentioned thus far result in a reactor which is

essentially a hybrid unit. Another option would be to have an undermoderated reactor feeding one or more reactors with a softer neutronic spectrum. These units could be grouped in an "energy park" (Gordon and Harms, 1977), where all aspects of the fuel cycle could be managed within one location. This type of synergetic relationship between reactor units has been suggested for the fast breeder program and for other advanced reactor variants (Harms and Haefele, 1981).

A cost/benefit analysis of any of these options would be required prior to development and implementation.

For the purposes of this study, emphasis has been placed on the neutronics of what now shall be referred to as the CANDU Spectral Shift Advanced Thermal Reactor (CANDU-SSATR). In this analysis, lattice calculations for cells with reduced lattice pitches and cells with enlarged calandria tubes were examined separately to investigate their possible application. Re-irradiation of a bundle in a more thermalized spectrum was studied only for initial irradiations from the enlarged calandria tube cases. For core calculations, as an elementary example, the case of a two-radial-zone reactor was considered. The inner region of the core is a hard spectrum zone, created by increasing the fuel to moderator ratio. The outer region is a soft spectrum zone with a reduced fuel to moderator ratio. Unirradiated fuel is placed in the inner region. By optimizing the characteristics of the neutron spectrum, the initial reactivity of the fresh fuel can be controlled, thereby keeping fuelling ripple within manageable limits.

Irradiated fuel from the inner zone is transferred to the outer zone after an optimized irradiation period. In the outer zone the plutonium bred in the inner region is fissioned. The U-235 reactivity is also increased in the softer spectrum. There is, however, a penalty to pay in terms of increased fission product negative reactivity in the softer spectrum outer region. A reprocessing step to remove fission products between burn steps or the use of in-situ rejuvenation (Harms, 1978) would increase fuel utilization, though questions of technical and economic viability would have to be addressed. For the purposes of this illustrative example, a reprocessing/rejuvenation step was not considered.

In the following subsections, results of the lattice and core analysis pertinent to the CANDU-SSATR development are described.

11.2 LATTICE CALCULATIONS: REDUCED LATTICE PITCH

To investigate the characteristics of a reactor operating with a reduced lattice pitch and increased U-235 enrichment, WIMS-CRNL (DSN option) (Donnelly, 1986) calculations were performed for a cell with a 15 cm lattice pitch (LP) and fuel enrichments of 8, 5, 3, and 1.3 a/o U-235.

The 30(37) element carbon (graphite) core fuel design of Chapter 7 was employed in this analysis. A buckling term of 0.7618 m^{-2} (nominal CANDU-600 value) was divided evenly between axial and radial components. Enriched zirconium was assumed in the pressure and calandria tubes. The nominal CANDU-600 calandria tube radius was maintained.

Results of the analysis are summarized in Table 11-1. In Fig. 11-1, the variation in k-eff as a function of burnup is shown for each case. In Fig. 11-2, the fast to thermal flux ratio is plotted as a function of burnup for each case. The cut-off between the fast (group 1) and thermal (group 2) flux is 0.625 eV. In Fig. 11-3, the variation in fissile nuclide concentrations (U-235 + Pu-239 + Pu-241) relative to the initial values are plotted as a function of burnup.

The results indicate that the reduction in lattice pitch substantially reduces the effective multiplication factor of the system. Even with an enrichment of 8 a/o U-235, the initial value of k-eff is 56 mk less than that obtained in the 1.3 a/o U-235 case using a 25 cm LP (Chapter 7). This would reduce the fuelling ripple and hence simplify reactor fuel management.

From Table 11-1 and Fig. 11-2 it is clear that an increase in the initial U-235 concentration causes an increase in the fast to thermal flux ratio. The reason for this is that while the fast flux is dictated primarily by the fission rate and the cell moderation capability (approximately constant in each case), the large U-235 production cross section tends to reduce the required thermal neutron flux for a given power level as the U-235 enrichment is increased. As the fuel burns, the spectrum hardens, due to the absorption

Parameter	Units	Fuel Identifier 30/37 (15 cm LP)			
		8 a/o U-235	5 a/o U-235	3 a/o U-235	1.3 a/o U-235
Initial k-eff	-----	1.23042	1.15637	1.07496	0.91029
Burnup *	MWd/MgU	45012	16023	2158	**
Initial ϕ_1/ϕ_2	-----	15.3	10.9	7.7	4.6

* Point where $\int$k-eff = 1.018
** k-eff < 1 at all burnups

Table 11-1 30/37 Results: 15 cm Lattice Pitch

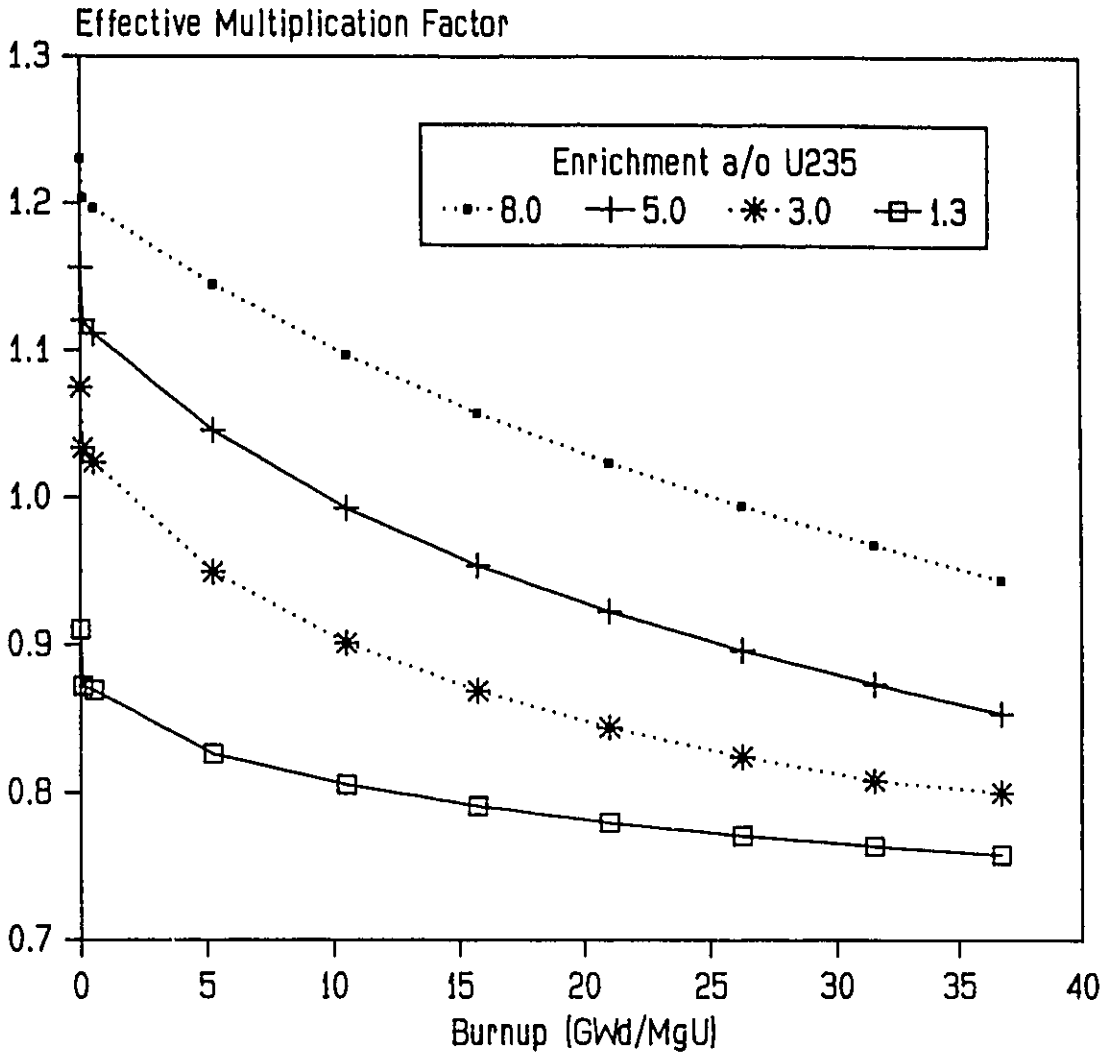

Figure 11-1 Effect of Fuel Enrichment on Effective Multiplication Factor
Model: 30(37)-XX-15-6.4478-CC

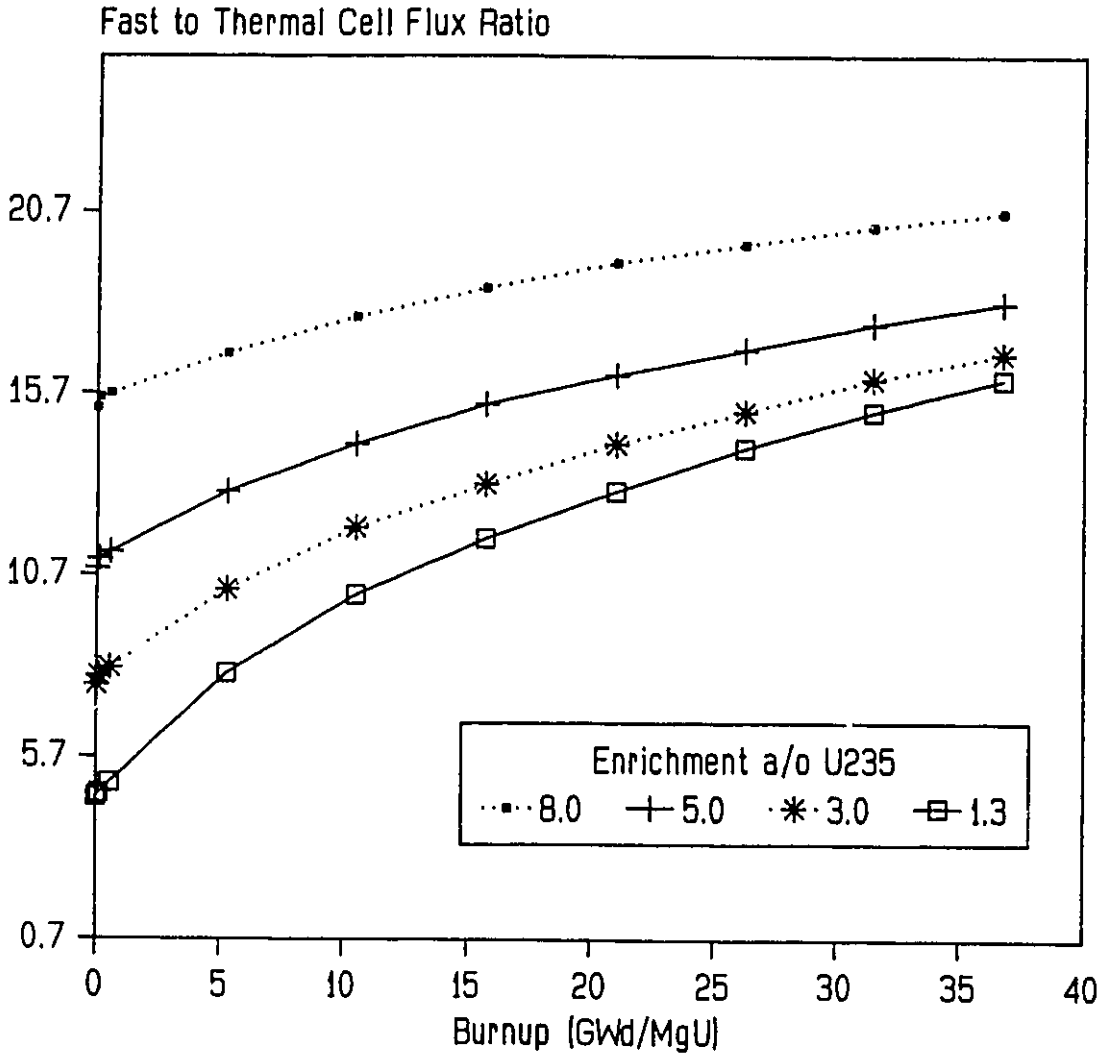

Figure 11-2 Effect of Fuel Enrichment on Fast to Thermal Cell Flux Ratio
Model: 30(37)-XX-15-6.4478-CC

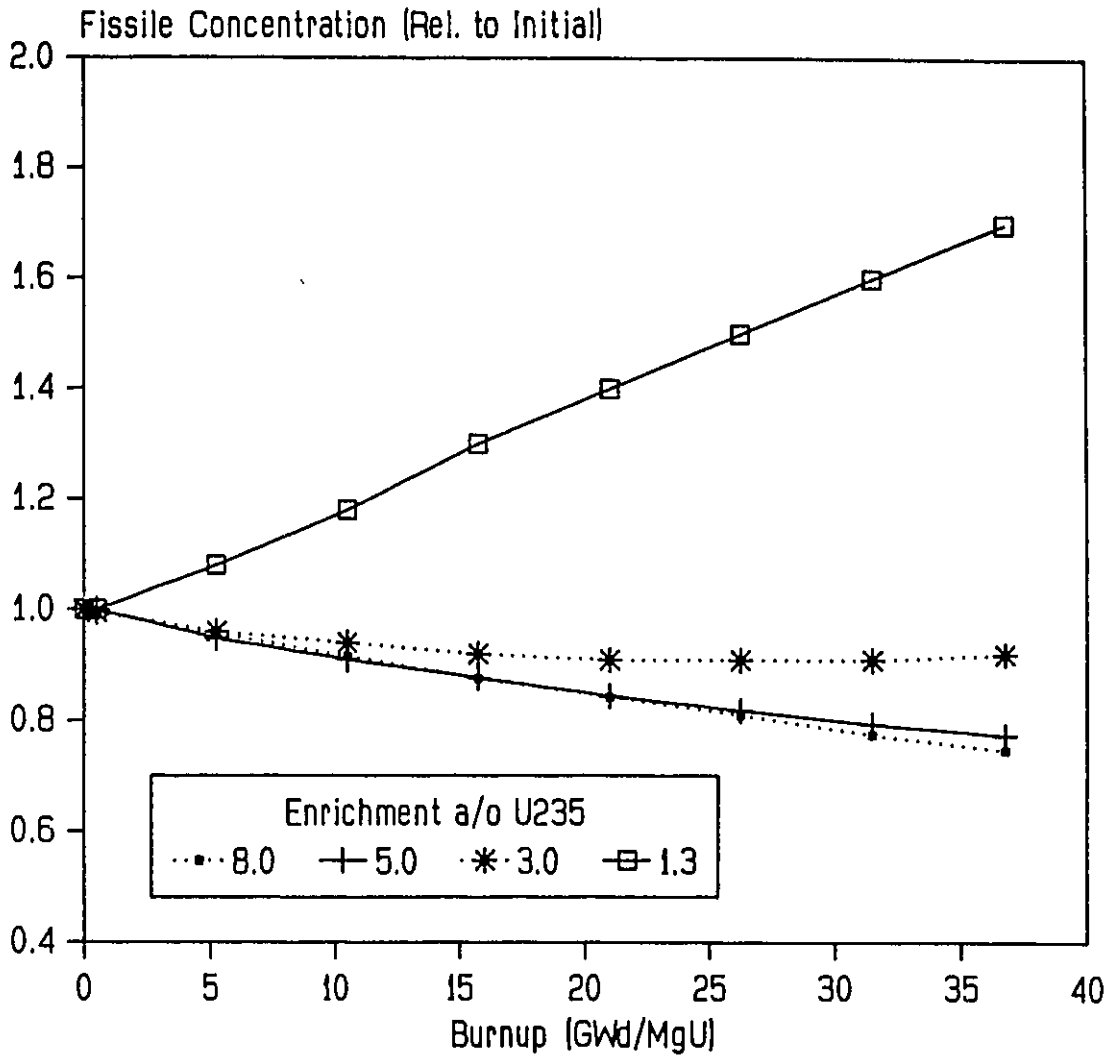

Figure 11-3 Effect of Fuel Enrichment on Fissile Concentration
Model: 30(37)-XX-15-6.4478

of thermal neutrons by the growing fission product concentration, and a larger power contribution results from higher-energy-neutron-induced fissions in the fissile plutonium isotopes, which are increasing in concentration.

For the purposes of comparison with the data in Table 11-1, it is noted that with fresh fuel, the fast to thermal cell flux ratio in the 30(37)-1.3-25-6.4478-CC case (Chapter 7) was 0.7. Reducing the LP to 15 cm resulted in this ratio increasing by a factor of almost 7.

From Fig. 11-3, it can be seen that the fissile concentration decreases as burnup increases for all except the 1.3 a/o U-235 case which has a breeding ratio (BR) of greater than unity. However, in this case the value of k-eff is less than unity for all burnups. Consequently the buildup of fissile nuclides is relying on neutronic leakage from adjacent cells to maintain criticality. The breeding ratio of the system (rather than the cell) must be considered. This fuel type could prove useful in a breeding blanket or at a inter-spectral zone boundary.

For all cases, there is a decrease in k-eff as burnup increases. This is due to a combination of a buildup of fission products and (except for the 1.3 a/o U-235 case) a reduction in the total fissile nuclide concentration.

The high enrichments required for these fuels do not seem justified given the low burnup potential indicated in Table 11-1. However, one must consider that this would only be the first stage in the bundle burnup history. After being irradiated in this hard neutron spectrum, the bundles would be transferred to a region with a more thermalized flux distribution for re-irradiation. This would increase total achievable burnup to more acceptable levels.

In Table 11-1 it is very important to note how rapidly self-sustaining burnup increases with enrichment. In changing from 3 a/o to 5 a/o U-235, burnup increased by 6933 MWd/MgU per atom percent increase. In changing from 5 a/o to 8 a/o U-235, burnup increased by 9663 MWd/MgU per atom percent increase. Further gains could be made by increasing the initial fuel enrichment even further. Such studies are indeed warranted. It is to be noted that as enrichment is increased, safeguards concerns and inadvertent criticality considerations are also intensified, thereby reducing potential

overall benefits.

In these cases, bundle pin enrichment and radius grading were not investigated. As overall enrichment is increased, bundle grading becomes more important to optimizing burnup, and hence additional studies in this area would be required before a fuel design was finalized.

11.3 LATTICE CALCULATIONS: INCREASED CALANDRIA TUBE DIAMETER

The reduced LP option of Section 11.2 poses fewer reactor safety concerns than the increased calandria tube diameter (ICTD) option, though designing endfittings and fuelling machines for this reduced space environment would require significant engineering effort. The enlarged calandria tube option introduces additional operational safety concerns from potential pressure tube or calandria tube leaks. As noted, these concerns would best be mitigated through the introduction of passive safety features -- also representing a significant engineering undertaking -- or by replacing the gas gap with a neutronically transparent, thermally insulating solid medium.

The ICTD scheme was chosen for further lattice and core physics analysis of the CANDU-SSATR since:

(a) the option allows for significant flexibility in spectral control,

(b) the lattice pitch remains constant in all spectral zones, simplifying the core and allowing for ease of reactor modelling.

For this initial survey, the nominal 37 element CANDU-600 fuel bundle and a 28.575 cm LP was used as the design basis. U-235 enrichments of 3, 5, and 8 a/o were considered. Fuel pencil enrichment grading and element size grading were not investigated, though burnup would be considerably improved with such modifications.

The DSN option of WIMS-CRNL (Donnelly, 1986) was used for these lattice calculations. Cases considered for the initial irradiation period included:

(a) no moderator (nominal calandria tube radius, but all moderator removed),

(b) 1/2 nominal moderator volume (enlarged calandria tube),

(c) 1/3 nominal moderator volume (enlarged calandria tube).

In all cases, a 0.1397 cm calandria tube wall thickness was maintained. Note, therefore, that as the calandria tube radius is increased, the mass of zirconium per unit length is increased, thereby reducing neutron economy. Further, by increasing the calandria tube radius while maintaining a fixed wall thickness, the ability of the tube to withstand a pressure tube rupture is reduced.

Endcaps were included in the WIMS-CRNL calculations. A power level of 32.510 MW/Mg Initial Heavy Elements was used for the burnup studies.

All of the cases considered were identified with a three digit code. The first digit refers to the atomic percent U-235 in the initial fuel, and the last two digits identify the volume of moderator as a percentage of the nominal case.

Leakage from the cell was simulated by specifying a reactor buckling of 0.7618 m^{-2} and assuming an equal division between axial and radial components. In most cases Benoist diffusion coefficients were calculated and used in the leakage analysis (Benoist, 1968). This methodology allows a more accurate treatment of the streaming effect of neutrons in the gas gap between the pressure and calandria tubes.

In all cases, the gas gap region was given the neutronic properties of air. Enriched zirconium was not used in the pressure and calandria tubes.

11.3.1 No Moderator Cases

Prior to investigating the cases with enlarged calandria tubes, a limiting set of no moderator cases was studied with the nominal calandria tube diameter, but with all of the moderator removed.

The three no moderator cases considered (800, 500, and 300, corresponding to 8, 5, and 3 a/o U-235,respectively), failed when the Benoist

diffusion coefficient option (Benoist, 1968) in WIMS-CRNL was chosen. This was due to the mismatch between the expected and actual geometry used in the lattice physics model (see Donnelly, 1986). The transport-averaged diffusion coefficient option was selected and the 800 case was run successfully. The 500 and 300 runs failed in the burnup cases due to extremely low system eigenvalues.

The results for the initial (zero burnup) lattice calculations for the three fuel enrichments with no moderator, are summarized in Table 11-2.

From Table 11-2, it is clear that the absence of any moderator causes the lattice cells to be extremely subcritical. The unit would have to rely strongly on the leakage of neutrons from the more thermalized part of the core to maintain reactor criticality. Such a coupling could be engineered, though overall, the resultant neutronic spectrum in the zone with no moderator would tend to become more thermalized, and hence such a design may not prove optimal.

It is interesting to note that while the initial system eigenvalues are quite low, they do not change rapidly with burnup. It was found that the infinite multiplication factor for the 800 case decreased by only 46 mk after a burnup of 32510 MWd/MgU. This is to be compared with a 92 mk reduction in the infinite multiplication factor for NATNOM fuel over a burnup of 7315 MWd/MgU. Hence, on average, the NATNOM fuel lattice eigenvalue drops approximately 9 times faster with burnup than in the 800 case. The effect of spectrum hardening is indeed evident. (It is noted that the actual variation will be dependent on the spectrum of the leakage from the adjacent lattice cells. Further analysis will be required to better characterize this behaviour.)

From Table 11-2, it can also be seen that spectral control can also be achieved by adjusting the fuel enrichment in the cell. The fast to thermal flux ratio for the 800 case is approximately 5.7 times larger than in the 300 case, while the fuel enrichments differ by a factor of approximately 1.7.

Parameter	Case Identifier		
	800	500	300
Infinite Multiplication Factor	0.95699	0.78411	0.63446
Effective Multiplication Factor	0.59616	0.47712	0.37796
ϕ_1/ϕ_2	2047.8	793.2	358.6

Table 11-2 Summary of Spectral Shift Lattice Calculations (No Moderator, Zero Burnup Cases)

11.3.2 Increased Calandria Tube Diameter Cases

Variants studied with increased calandria tube diameters included cases with 33% and 50% nominal moderator volumes. The 33% moderator volume cases incorporated a calandria tube with a 13.7 cm outer radius. The calandria tube outer radius in the 50% moderator cases was 12.315 cm. (These values are to be compared to the nominal calandria tube outer radius of 6.5875 cm.) In all cases, the lattice pitch retained its nominal value of 28.575 cm.

It is noted that the coolant takes on an ever-increasing role in the neutron thermalization process as the calandria tube diameter is increased. Hence the 33% and 50% factors must not be taken as a percentage (with respect to nominal) of the cell's ability to moderate neutrons.

The results of the increased calandria tube diameter lattice physics simulations are shown in Table 11-3. For completeness, data for the 800 no-moderator case are also included in the table. The fissile concentration data in Table 11-3 include the contributions of U-235, Pu-239 and Pu-241 only. It is noted that the contribution of fast fissions in U-238 to the total fission rate is greater as the calandria tube diameter is increased.

From Table 11-3 it can be seen that only in the 800 case does the relative fissile concentration increase with burnup. Note that in this case, the effective multiplication factor nevertheless decreases with burnup, since the negative reactivity effect of the growing fission product concentration surpasses the increase in system reactivity associated with the breeding of fissile material.

Table 11-3 again identifies the very important role that fuel enrichment has on controlling the neutron spectrum. While very large spectral shifts are attainable by adjusting the calandria tube diameter, fuel enrichment will play an important role in spectral fine-tuning to achieve on-going system optimization. This fine-tuning would also be extended to controlling relative burnup periods in the various reactor spectral zones.

The initial k-eff value for the 142117153 case from Chapter 10 was 1.38736. The 333, 350, 533, 800, and 833 cases all had initial k-eff values

Case	Time (days)	Burnup (MWd/MgU)	Effective Multiplication Factor	Fast to Thermal Flux Ratio	Fissile Concentration	
					(g/cm)	Relative to Initial Value
333	0	0	1.20154	2.63	11.25	1.00
	500	16255	0.97400	2.94	7.79	0.69
	1000	32510	0.84023	2.90	5.20	0.46
350	0	0	1.35457	1.65	11.25	1.00
	500	16255	1.09396	1.70	7.12	0.63
	1000	32510	0.90574	1.59	4.00	0.36
533	0	0	1.28800	3.19	18.75	1.00
	500	16255	1.08705	3.39	14.39	0.77
	1000	32510	0.96655	3.22	10.57	0.56
550	0	0	1.44331	1.96	18.75	1.00
	500	16255	1.22912	1.98	13.81	0.74
	1000	32510	1.08176	1.88	9.39	0.05
800	0	0	0.59616	2049.65	30.01	1.00
	500	16255	0.57906	4714.60	30.03	1.00
	1000	32510	0.56824	7114.00	30.23	1.01
833	0	0	1.35436	3.71	30.01	1.00
	500	16255	1.18882	3.81	24.90	0.83
	1000	32510	1.08843	3.83	20.13	0.67
850	0	0	1.50602	2.24	30.01	1.00
	500	16255	1.33534	2.25	24.44	0.81
	1000	32510	1.22696	2.18	19.18	0.64

Table 11-3 Summary of Spectral Shift Lattice Calculations (Increased Calandria Tube Diameter Cases)

less than this (see Table 11-3). Consequently, on-power fuel management with any of these fuels would be expected to be more easily conducted than in the 142117153 case.

All of these cases represent only the first phase in a bundle's burnup history. After being irradiated for an initial burnup period in the hard spectral zone, the bundles are transferred to a softer spectral zone with the nominal 6.5875 cm outside radius calandria tube. This second phase is considered in Section 11.4.

11.4 LATTICE CALCULATIONS: THE SECOND BURNUP PHASE

After a burnup period of 1000 days (32510 MWd/MgU), the time-averaged infinite multiplication factor for the 333 case was 1.08889 as determined using WIMS-CRNL. (This is to be compared to the 1.045 value (equivalent to burnup-averaged k-eff=1.018) nominally used in identifying expected burnup in the NATNOM analysis (Chapter 6).) All other designs considered (except the no moderator cases) yielded even higher time-averaged infinite multiplication factors after 1000 days. These other cases would require additional burnup in the hard spectrum zone before being transferred to the softer spectral zone in order to reduce local reactivity. For the purposes of this study, where a burnup of 50000 MWd/MgU was the target, only the 333 case was considered further for subsequent transfer to the more thermalized outer core region.

The transfer of fuel from a hard spectral zone to a softer spectral zone at a specific point during the burnup period was effected with WIMS-CRNL as follows:

(1) A second lattice physics model was created with all material names and numbers as in the initial model. This new model was the same as the first, except the calandria tube diameter was set at its nominal value rather than the enlarged value.

(2) The number of mesh subdivisions in the moderator region was increased to 10 from 6 used in the first model. (See Donnelly, 1986,

and Phillips, 1982 for WIMS-CRNL technical specifications.)

(3) Individual element and isotopic constituents of the materials in the first model were stored on WIMS-CRNL internal file 50 as a function of burnup.

(4) File 50 was read into the second model to modify the constituent materials to correspond to the first model components at a specific point during the burnup. Since the material numbers in both models coincided, the effect was to transfer the exact material components from one geometry to another.

(5) Fuel burnup was then allowed to continue in this modified geometry and altered flux spectrum.

The second burnup stage was initiated after burn periods of 800 days and 1000 days in the 333 geometry. These two separate cases were conducted to examine the sensitivity of the fuel properties to the fractional split in burnup phases. The cases were given the identifiers 333A800 and 333A1000, respectively.

The results of the 333, 333A800, and 333A1000 lattice cell calculations are presented in Fig. 11-4 through 11-11.

Fig. 11-4 is a plot of effective multiplication factor versus burnup for the three cases. It is to be noted here that the burnup plotted in these figures for the 333A800 and 333A1000 cases is taken to begin at 0 MWd/MgU, even though the fuel had been subjected to burnups of 26008 and 32510 MWd/MgU respectively, during the first burnup stage in the harder neutronic spectrum. The accumulated burnup difference at "0" MWd/MgU for the two second burnup phase cases is therefore 6502 MWd/MgU. This difference must be considered when comparing case results.

In Fig. 11-5, the time-averaged infinite multiplication factor is plotted for each of the cases as a function of fuel burnup. These data were obtained using the spectrum corresponding to the situation with critical

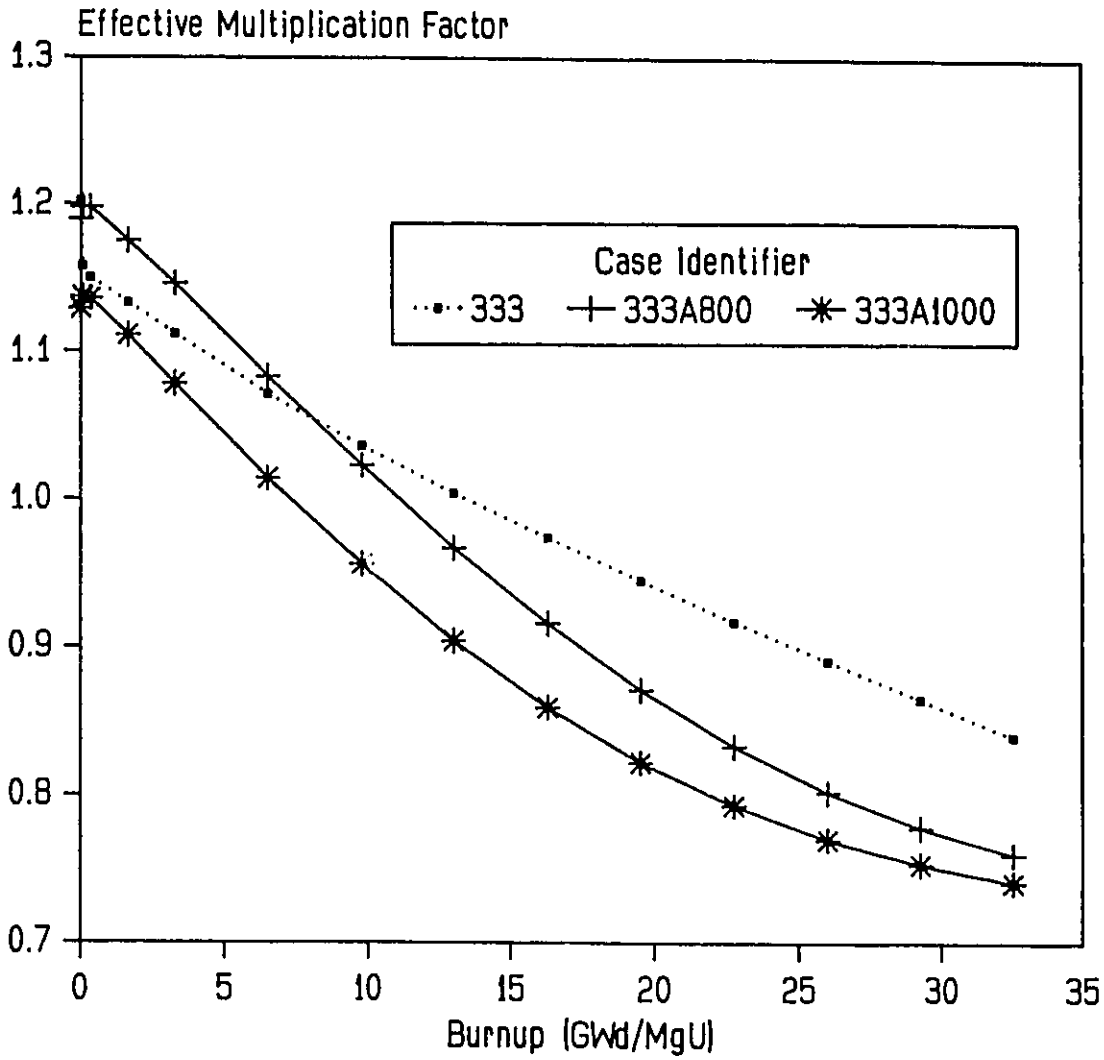

Figure 11-4 Burnup Dependence of Effective Multiplication Factor (Cases 333, 333A800, 333A1000)

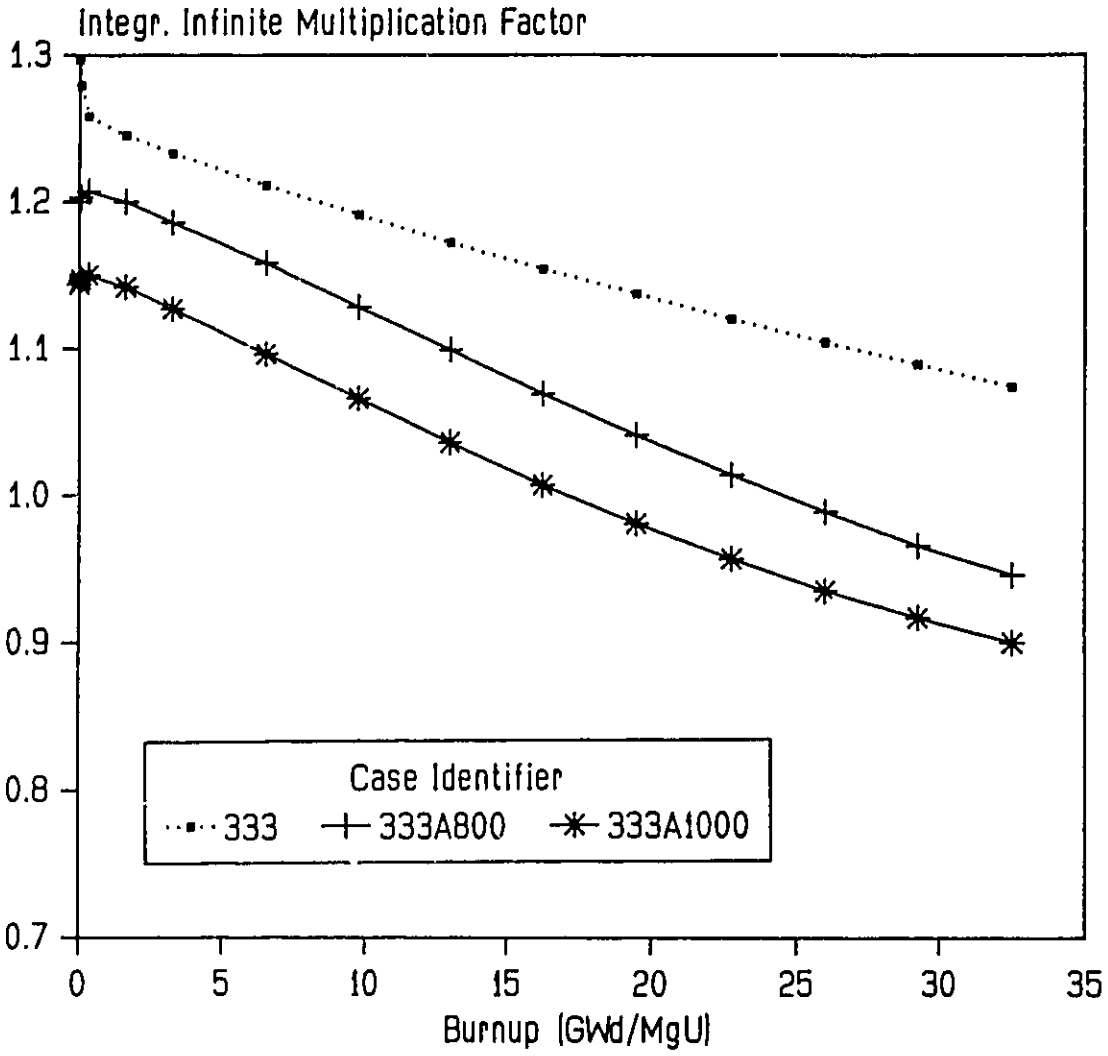

Figure 11-5 Burnup Dependence of Time Integrated Average Infinite Multiplication Factor
(Cases 333, 333A800, 333A1000)

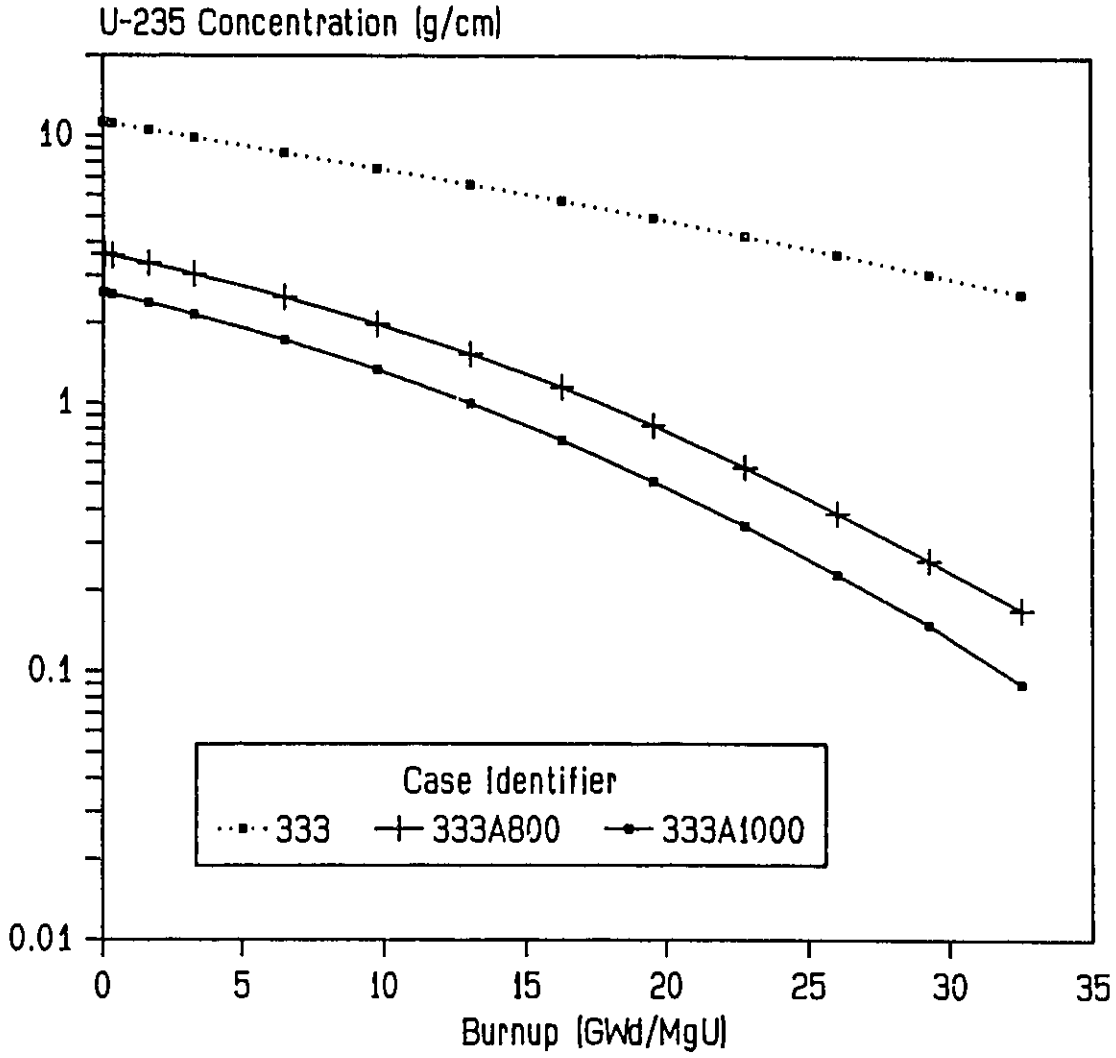

Figure 11-6 Burnup Dependence of U-235 Concentration (Cases 333, 333A800, 333A1000)

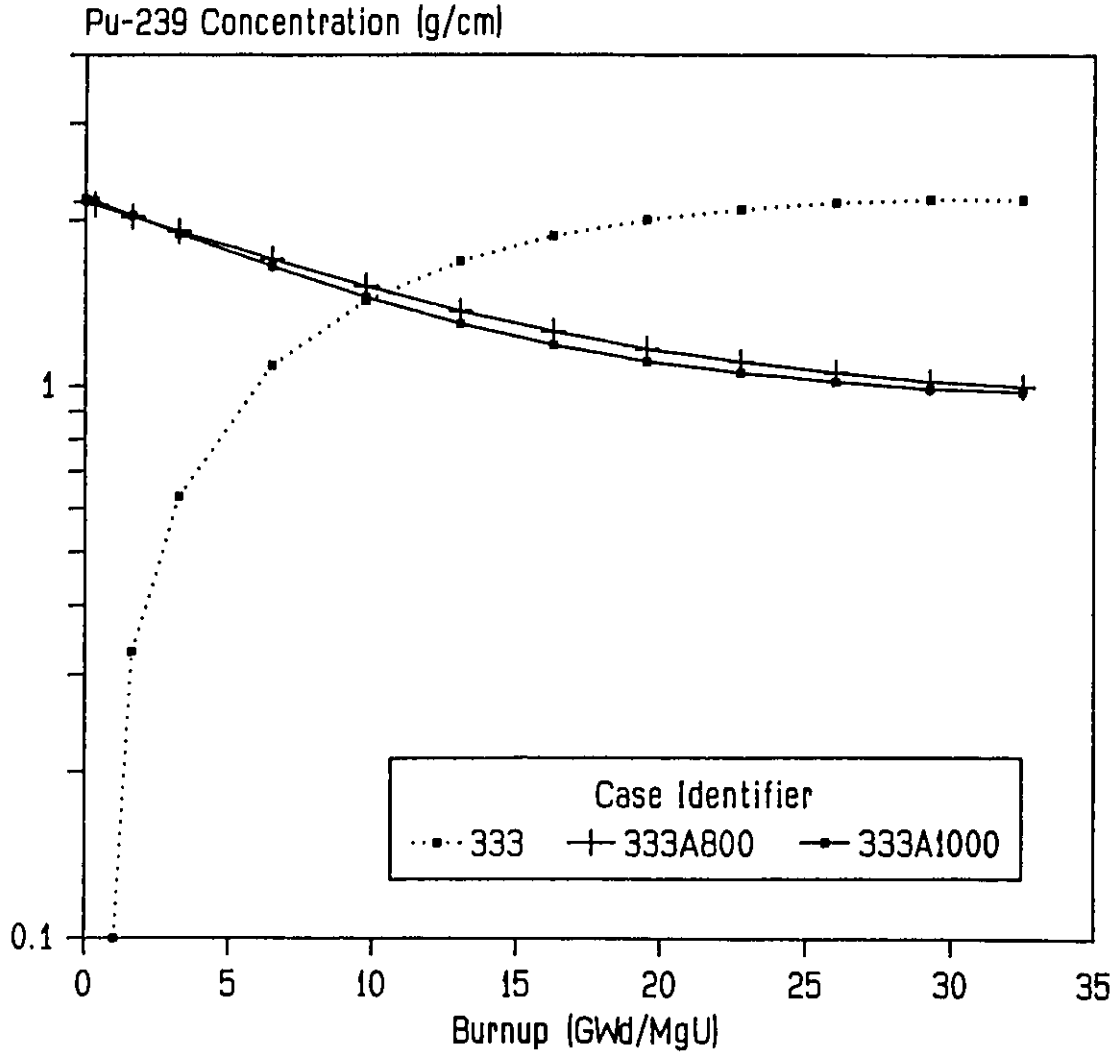

Figure 11-7 Burnup Dependence of Pu-239 Concentration (Cases 333, 333A800, 333A1000)

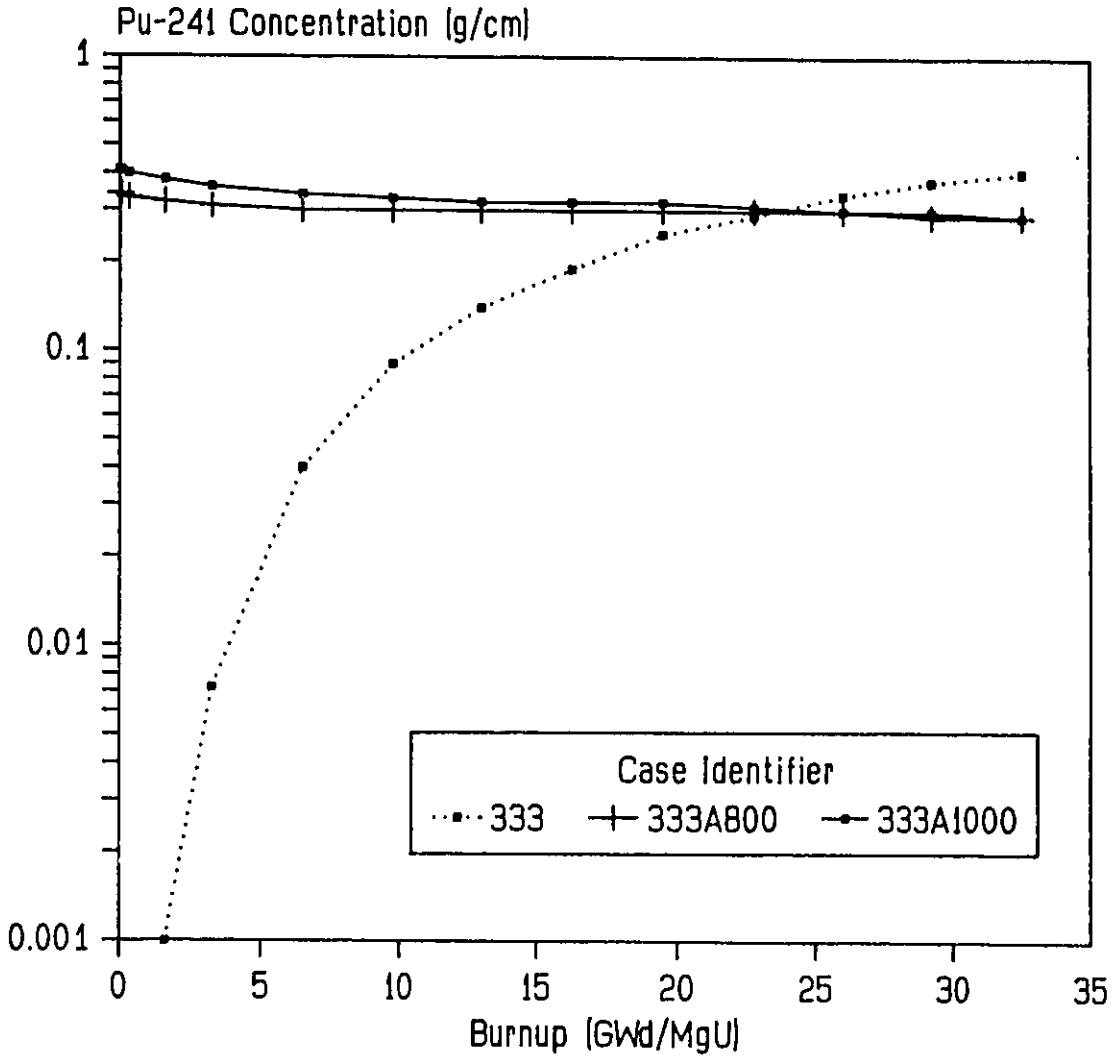

Figure 11-8 Burnup Dependence of Pu-241 Concentration (Cases 333, 333A800, 333A1000)

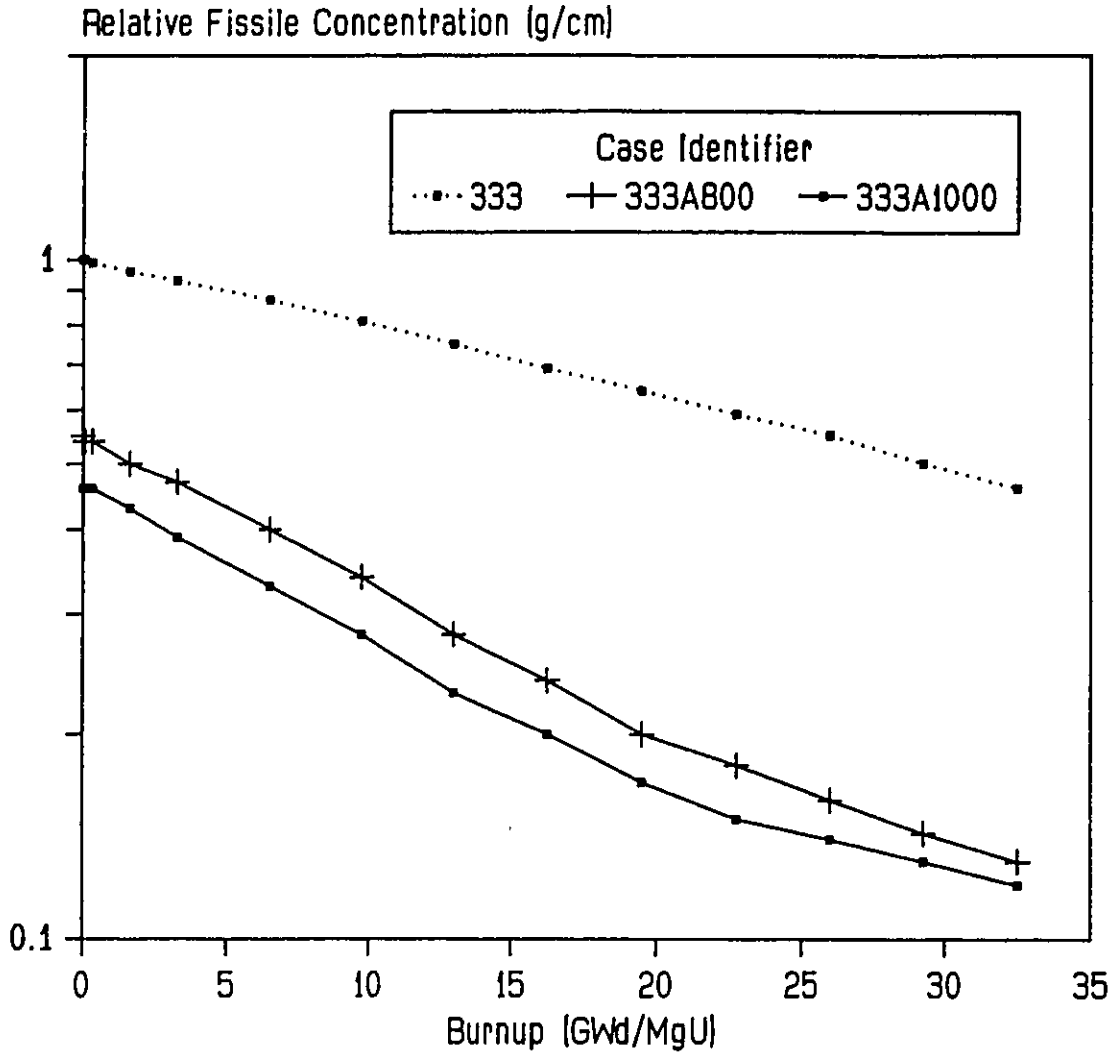

Figure 11-9 Burnup Dependence of Relative Fissile Concentration (Cases 333, 333A800, 333A1000)

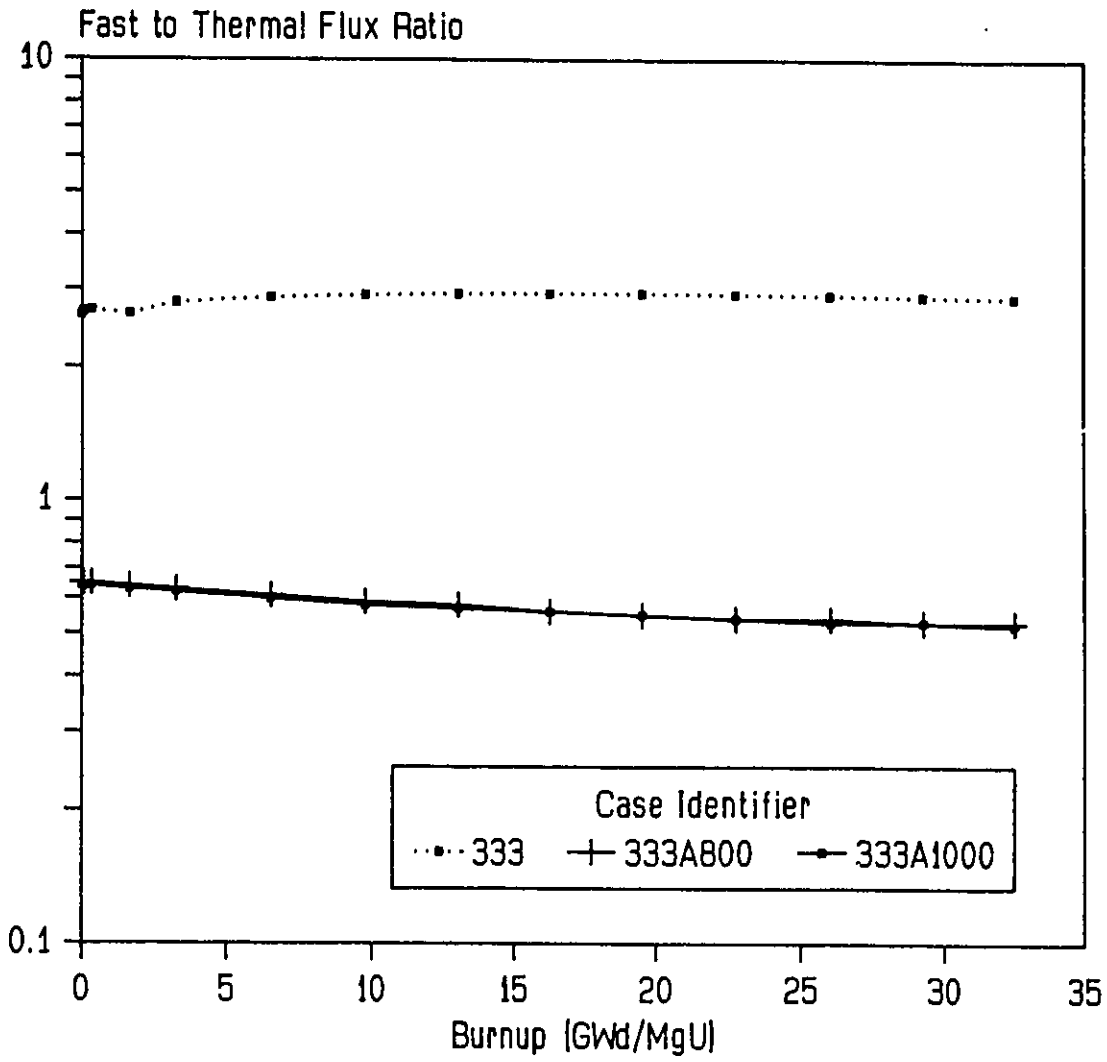

Figure 11-10 Burnup Dependence of Fast to Thermal Flux Ratio (Cases 333, 333A800, 333A1000)

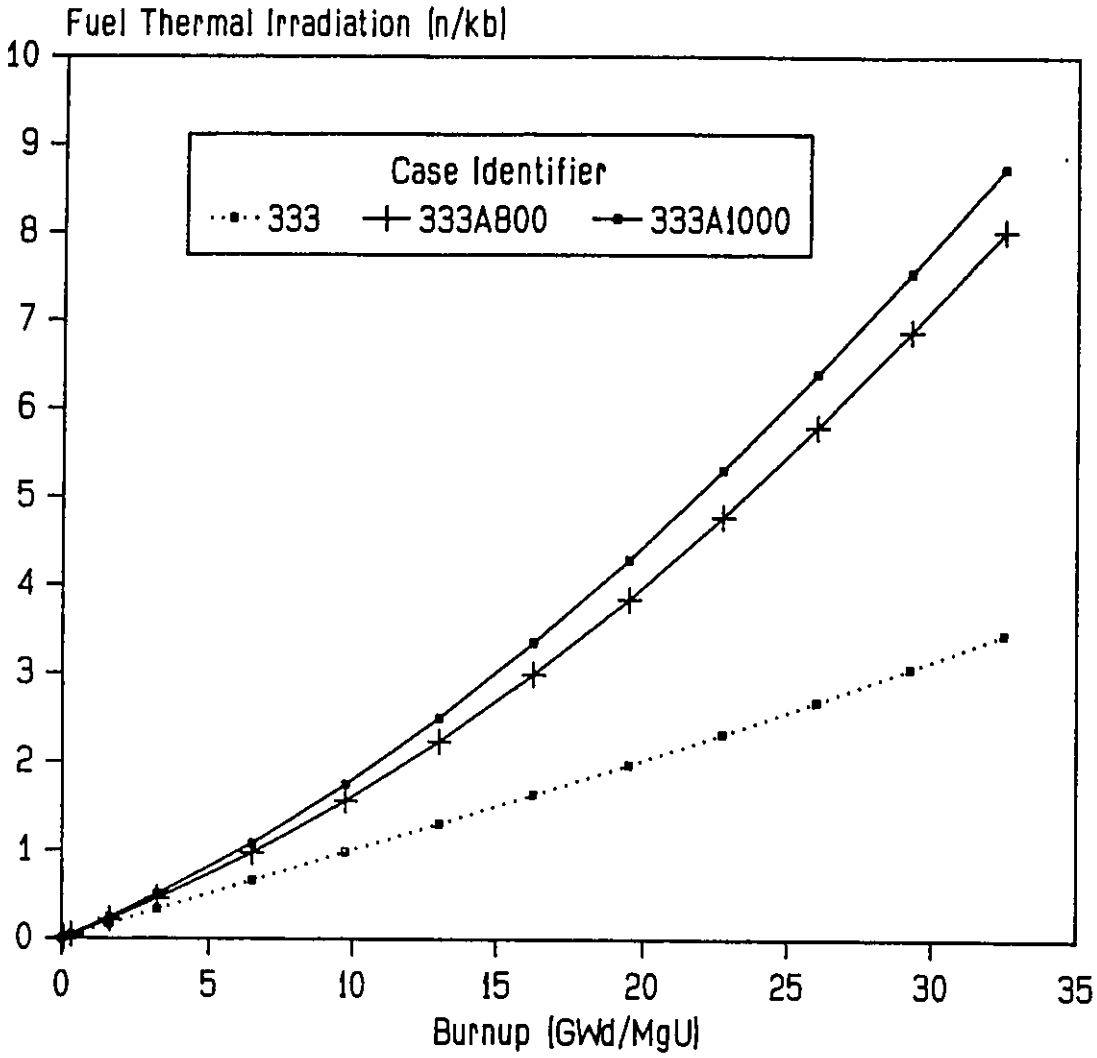

Figure 11-11 Burnup Dependence of Fuel Thermal Irradiation (Cases 333, 333A800, 333A1000)

buckling. Data for the 333A800 and 333A1000 cases apply only to the second irradiation period. In comparing the curves in Fig. 11-4 and 11-5, the effect of the increased leakage in the 333 case is evident.

Figures 11-6 through 11-9 deal with the variation of fissile composition for the various cases. Figure 11-6 provides a plot of the variation of U-235, Pu-239, Pu-241 and the sum of these isotopes as a function of burnup for the 333 case. The isotope densities are in terms of g/cm of bundle length with proper accounting of the effect of the bundle end-cap. Figures 11-7 and 11-8 provide similar data for the 333A800 and 333A1000 cases. It is instructive to note that in all three cases, the U-235 concentration decreases as a function of burnup. The plutonium concentrations, on the other hand, increase during the first burnup phase (harder spectrum) and decrease during the second burnup phase (more thermalized spectrum).

In Fig. 11-9 the relative fissile concentration is plotted as a function of burnup for the three cases. The initial fissile concentration (11.25 g/cm) is normalized to unity in this figure. It should also be noted that in deriving the fissile concentration data for this figure, only contributions from U-235, Pu-239 and Pu-241 were considered. No attempt has been made to weight the concentrations according to their $\nu\sigma_f$ values. Figure 11-9 clearly indicates that the fissile concentration of the fuel decreases much more slowly as a function of burnup in the hard spectral region (first burnup phase, case 333).

In Fig. 11-10, the fast to thermal flux ratio for the three cases is plotted as a function of burnup for the 333, 333A800 and 333A1000 cases. The cutoff between fast and thermal regions was again chosen as 0.625 eV. It can be seen that cell geometry has a significant influence on the flux spectrum. Over the burnup history, the fast to thermal flux ratio in the 333 case rises initially from 2.63, peaking at 2.94 after approximately 18000 MWd/MgU, and then slowly decreases to 2.89 after 32510 MWd/MgU (1000 days). In the 333A800 and 333A1000 cases, the fast to thermal flux ratio starts off at 0.64 and slowly decreases to 0.52 after 32510 MWd/MgU in the second burnup phase.

To relate burnup to fuel thermal irradiation for core calculation purposes, a conversion as per Fig. 11-11 was used. In this figure, fuel thermal irradiation is plotted as a function of burnup for the three cases. As is evident in the figure, fuel thermal irradiation as a function of burnup is dependent on the cell geometry (related to fast to thermal flux ratio), and it is also influenced by the fissile concentration. Note that in Fig. 11-11, the burnup data implicitly includes the effect of fast and thermal irradiation, though it is plotted as a function of thermal irradiation only. Neutronic fuel tables for core calculations are presented as a function of fuel thermal irradiation. There is an inferred relationship between fast and thermal irradiation based on the lattice physics simulations conducted to generate the fuel tables.

The next stage in the analysis of the spectral shift CANDU reactor was to carry out core physics calculations to demonstrate the feasibility of such a plan. This is discussed in Section 11.5.

11.5 CORE PHYSICS CALCULATIONS

The lattice physics calculations from Section 11.4 indicate that the fuel should burn for at least 1000 days in the hard spectral region before being transferred to the outer zone, in order to allow the time-averaged multiplication factor to be sufficiently low such that adjuster rod requirements for excess reactivity control and flux flattening are minimized. Hence for core calculations, the 333/333A1000 case was chosen for study.

It is noted that in the 333 study (Fig. 11-5) the time-averaged multiplication factor is larger at 800 days than at 1000 days. It is further noted that the time-averaged multiplication factor after 700 days in the 333A800 case is larger than the corresponding value at 500 days in the 333A1000 case (these latter values averaged only over the second burnup phase). This would indicate that an optimization of the initial enrichment for this case would yield a lower U-235 concentration, allowing an earlier transfer to the softer spectral zone to take better advantage of the available U-235 and bred plutonium. Again, it is stressed that this work is an initial

study to address the feasibility of the CANDU-SSATR. Optimization of the zonal enrichment, spectrum, etc., would be required prior to implementation.

11.5.1 Reactor Core Model

The WIMS-FMDP computer code (Donnelly and van Dyk, 1983) was utilized to calculate lattice cell properties as a function of irradiation using the WIMS-CRNL output data. Cross sections were obtained for the fuel cells using the critical buckling spectrum. Benoist diffusion coefficients were also used. The modified two-group diffusion theory representation (see Section 8.2.2) was utilized in this initial analysis. It is expected that the use of a greater number of energy groups may be more appropriate for subsequent detailed analysis in this area.

The geometry chosen for the FMDP reactor core analyses consisted of a quarter-face, full axial length model. The mesh spaces were chosen uniformly as 28.575 cm (nominal lattice pitch) in the x and y directions, and as 49.53 cm in the z direction.

A reflector radius of 379.7 cm and a notch radius of 337.8 cm was chosen, consistent with the nominal CANDU-600 design. The notch length was chosen as two bundle lengths (99.06 cm as opposed to the CANDU-600 notch length of 96.52 cm) to simplify the model.

An adjuster region was modelled as extending over the entire central core region and axially from 198.12 cm to 396.24 cm (i.e. over the central four axial bundles).

"Bidirectional" reflective boundary conditions were chosen at the planes corresponding to channel row L and also at the plane corresponding to channel column 12. This boundary condition is similar to a regular reflection boundary condition but with the added feature that the neutron flux at, for example, the bundle 1 position in the reflection plane is set equal to the flux at the bundle 12 position at the boundary of the reactor model. This modification thereby allows for the simulation of the effect of bidirectional fuelling.

The core was divided into an inner fuelling zone and an outer fuelling

zone. The inner zone was fueled with 333 type fuel. The outer zone was fueled with 333A1000 type fuel. The inner zone fuel thermal exit irradiation was fixed at 3.450 n/kb. This value corresponds to a burnup of 1000 days or 32510 MWd/MgU. The exit irradiation of the outer zone was not fixed.

Adjuster rods were modelled using incremental fast and thermal absorption cross sections in the lattice cells of the adjuster region. The value of the ratio of the fast to thermal absorption cross section was maintained at 0.26 as was calculated for the 3-pin cobalt adjuster in the NATNOM case (see Chapter 9).

The continuous bidirectional fuelling approximation (CBDFA) methodology was used in the analysis (see Chapter 8).

The adjuster grading, inner/outer zone boundary and the outer zone exit irradiation were treated as variable parameters. These parameters were iterated upon until the following conditions were met:

(a) The reactor was critical.
(b) The number of bundles per day required in the outer zone matched the number of bundles per day being discharged from the inner zone.
(c) The maximum channel power was less than 6500 kW.
(d) The maximum bundle power was less than 800 kW.

These conditions were met by choosing an outer zone exit irradiation of 2.750 n/kb, an inner/outer zone boundary as shown in Fig. 11-12, and an adjuster loading as per Fig. 11-12 and 11-13 and Table 11-4.

11.5.2 Results of the CANDU-SSATR Core Calculations

With the reactor model defined as in Section 11.5.1, the resultant total fuel burnup attainable through both burnup phases was found to be:

Burnup Phase 1: Burnup = 33050 MWd/MgU
Burnup Phase 2: Burnup = 13493 MWd/MgU
Total: Burnup = 46543 MWd/MgU (uncorrected)

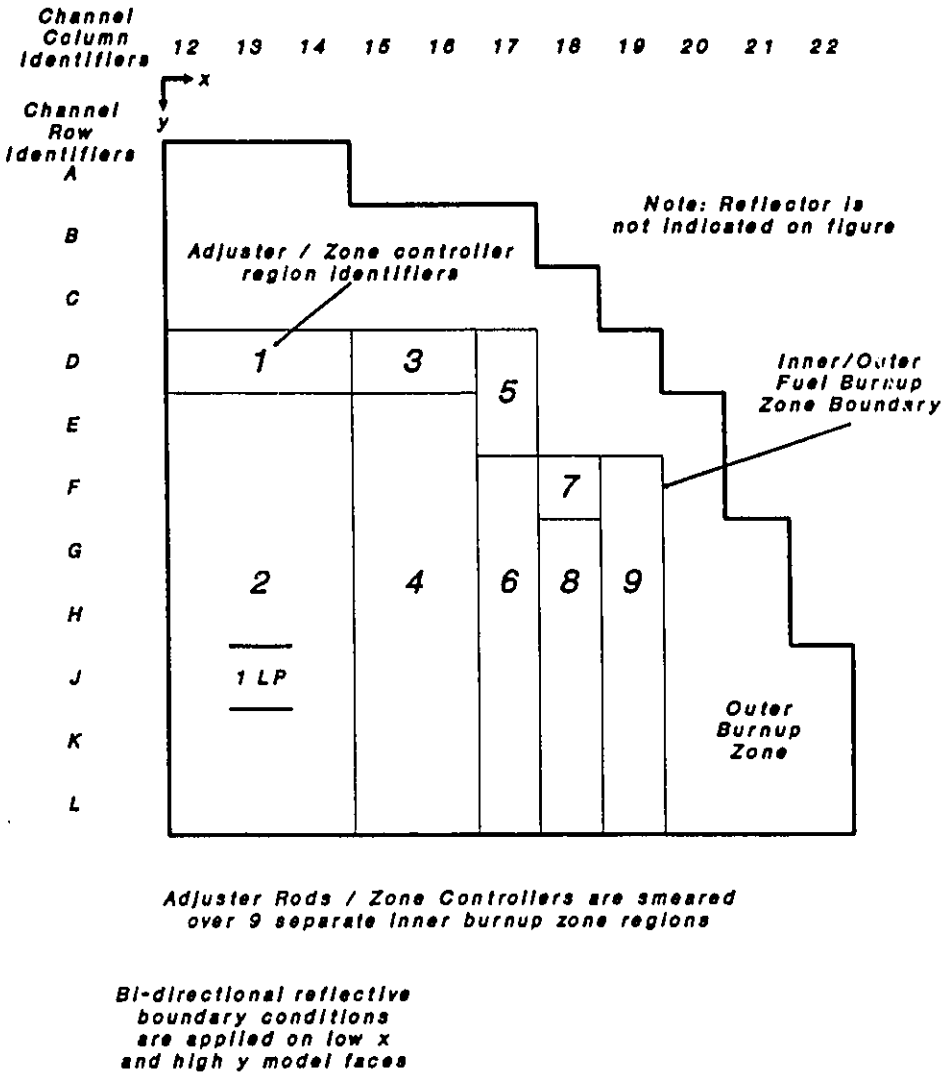

Figure 11-12 CANDU-SSATR Core Model (x-y View)

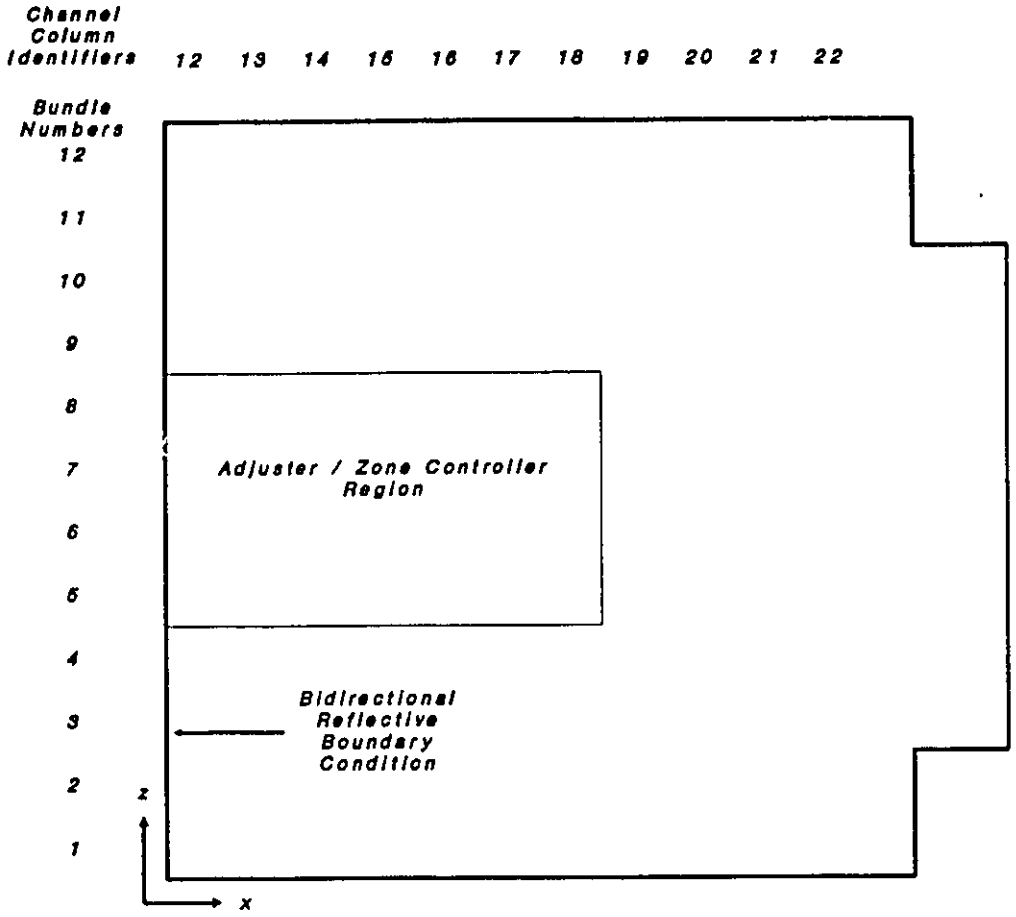

Figure 11-13 CANDU-SSATR Core Model (x-z View)

Adjuster Region*	Adjuster Type	Incremental Fast Absorption Cross Section (cm^{-1})	Incremental Thermal Absorption Cross Section (cm^{-1})
AA01	ADJ03	25.4E-5	9.7E-4
AA02	ADJ02	8.2E-5	3.1E-4
AA03	ADJ03	25.4E-5	9.7E-4
AA04	ADJ02	8.2E-5	3.1E-4
AA05	ADJ03	25.4E-5	9.7E-4
AA06	ADJ01	3.2E-5	1.2E-4
AA07	ADJ03	25.4E-5	9.7E-4
AA08	ADJ01	3.2E-5	1.2E-4
AA09	ADJ03	25.4E-5	9.7E-4

* See Figures 11-12 and 11-13
Total Adjuster Rod Worth 31.1 mk

Table 11-4 Adjuster Loading: CANDU-SSATR

The effective multiplication factor was 1.00001. The maximum channel power was 6488 kW (Channel L-12), and the maximum bundle power was 684 kW (Bundle L-19,9). Power distributions are provided in Fig. 11-14 and 11-15.

The inner zone (240 channels) would be fueled with a total of 2.46 fresh fuel bundles per day on average. The outer zone (140 channels) would require 2.46 bundles per day transferred from the inner zone.

The reactivity worth of the adjuster rods was found to be -31.1 mk. Attributing -15 mk for a required adjuster loading, and -3 mk for the worth of a bulk and spatial zone controller system, the reactor, as modelled carried an excess negative reactivity load of 31.1 - 15 - 3 = 13.1 mk.

The excess negative reactivity of 13.1 mk would normally be compensated for by increasing the system burnup. A sensitivity study conducted by varying the outer core exit irradiation and comparing the change in average core burnup and system reactivity, yielded a burnup reactivity coefficient of -347 MWd/MgU/mk. Applying this to the uncorrected burnup yields an expected burnup achievable of 51089 MWd/MgU. Additional sensitivity studies conducted using only the WIMS-CRNL data yielded similar expected total corrected burnups.

It is noted that the burnup in Phase 1 reached 33050 MWd/MgU in the reactor core calculations. The burnup in the corresponding lattice physics simulation was 32510 MWd/MgU. The 1.6% difference can be attributed to the fact that in the core calculations, the H factors (power to flux ratios) were obtained via quadratic interpolation of the H factors from the WIMS-FMDP output. These values, in turn, were obtained via a high order interpolation routine, which interpolated the H factors from the WIMS-CRNL main transport calculations (performed approximately every 100 FPD). The burnup in the lattice physics simulations, on the other hand, was determined using H factors obtained with the flux spectra associated with each of the main transport calculations in combination with a succession of burnup steps (approximately 10 FPD). These burnup steps explicitly included the change in fissile content of the fuel and hence the fine variation in H factors between main transport calculations.

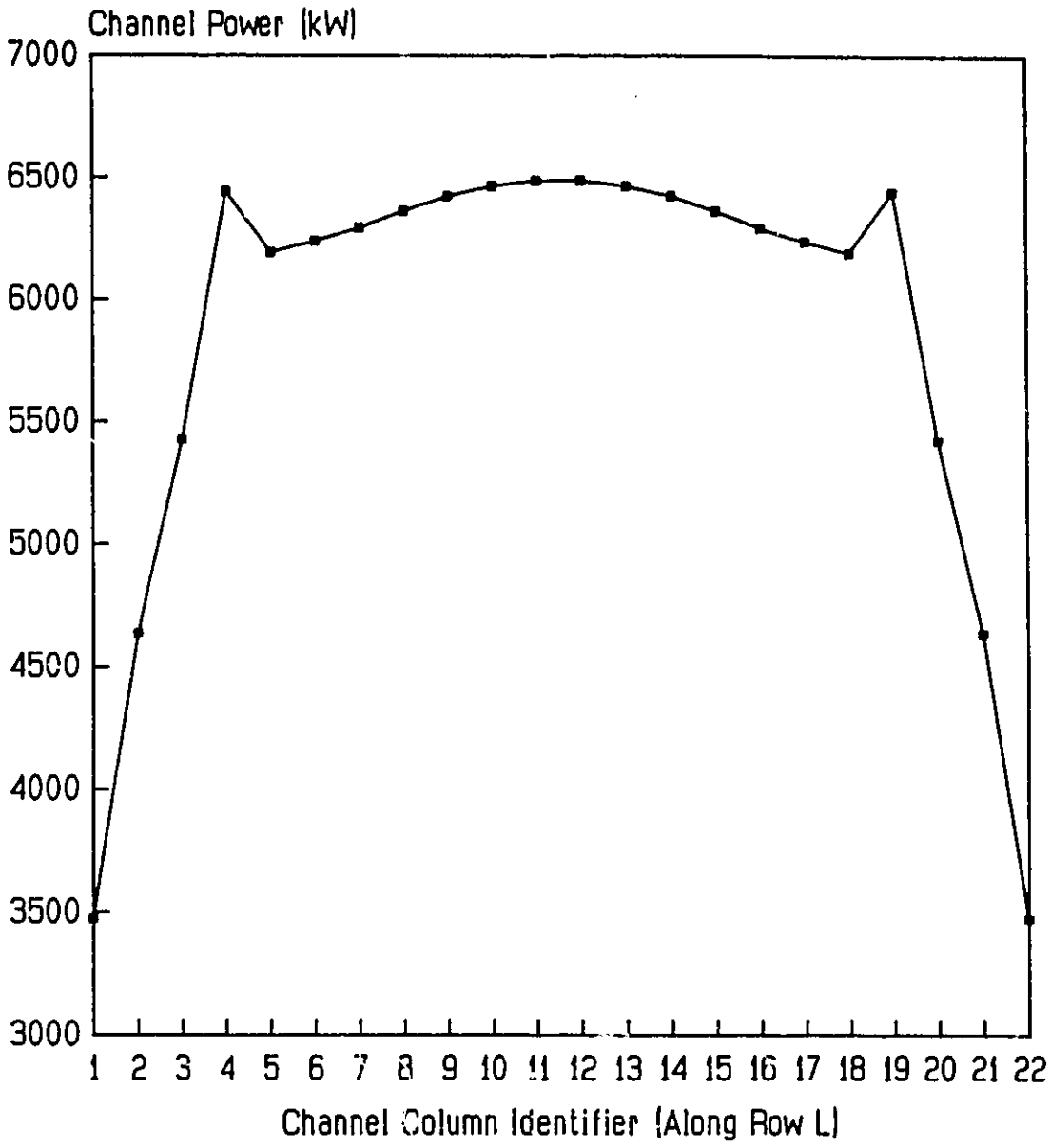

Figure 11-14 CANDU-SSATR Channel Power Distribution

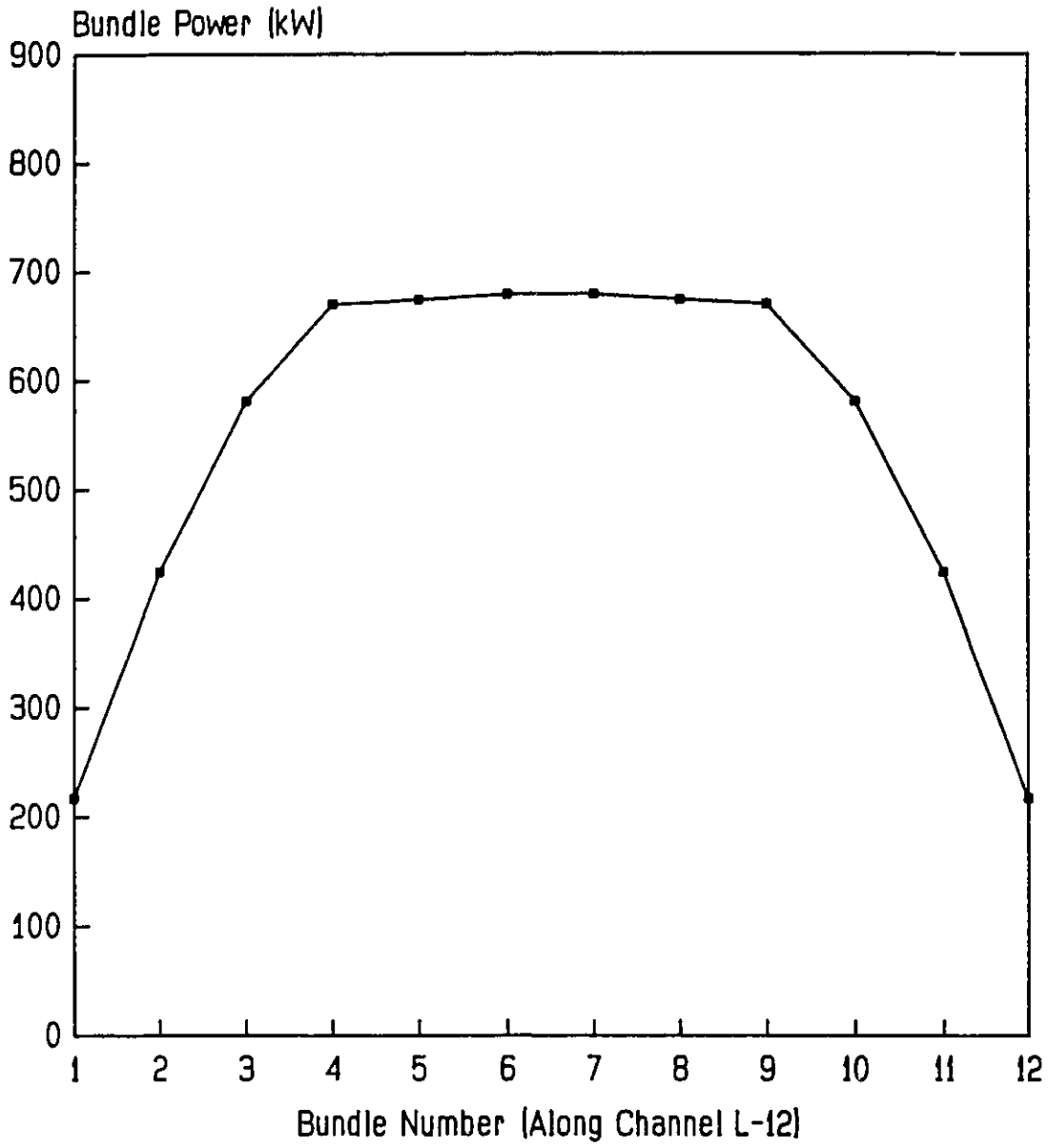

Figure 11-15 CANDU-SSATR Bundle Power Distribution

11.5.3 Comparison of CANDU-SSATR Fuel Burnup With Other CANDU Variants

The CANDU-SSATR fuel bundle design considered in this first investigation consisted of 3 a/o U-235 in a nominal 37-element configuration. Burnup across the bundle rings was skewed towards the outer pins, since no compensatory enrichment or element-size grading was incorporated into this initial bundle design. After burning the 333 fuel for 1000 days (32510 MWd/MgU), the ring burnups ranged from 21318 MWd/MgU to 38978 MWd/MgU, with the inner ring having attained a burnup equaling 55% of that attained in the outer ring. After 600 days in the second burnup stage (with a nominal calandria tube diameter) (52016 MWd/MgU total), the inner ring burnup was 38781 MWd/MgU and the outer ring burnup was 59604 MWd/MgU. The inner ring, therefore, had attained a burnup of only 65% of that attained in the outer ring. It is noted that the relative difference between the burnups in the fuel element rings decreases with time, due to the equalizing effects of the varying fuel burnout rates.

If, for the purposes of resource analysis, we assume that the fuel can yield approximately 50000 MWd/MgU (see Section 11.5.2), then proceeding as in Chapter 10, the natural uranium and separative work requirements per unit energy production can be calculated. These data are presented in Table 11-5, where comparisons are also provided with the NATNOM case.

From Table 11-5 it can be seen that the non-optimized CANDU-SSATR can provide a uranium resource utilization improvement over the NATNOM case for scenarios with tailings concentrations of 0.3 a/o U-235 or less. The scheme would only be economical if the savings achievable with the CANDU-SSATR in terms of fabrication and disposal costs (resulting from the increased uranium utilization), could offset the cost of producing fuel at the required enrichment. The cost data in the last column of Table 11-5 are to be compared with the 166.2 '00$/MW(e)-a quoted in Chapter 10 for the NATNOM fuel case.

In comparison with the 1421 fuel designs discussed in Chapter 10, the non-optimized CANDU-SSATR is less resource efficient than the enriched 1421 variants, though more resource efficient than the 1421NAT design. For example, with a tailings concentration of 0.2 a/o U-235, the CANDU-SSATR

Tailings U-235 Concentration (a/o U-235)	Uranium Requirements (kgU_{mined}/ MW(e)-a)	Separative Work Requirements (kgSWU/ MW(e)-a)	Percentage Improvement in Resource Utilization Over NATNOM Case	Uranium Plus Separative Work Costs* ('00$/ MW(e)-a)
0.0	99.2	∞	40.3	∞
0.1	111.3	140.6	33.0	252.0
0.2	128.2	101.3	22.9	222.5
0.3	153.0	80.6	7.9	233.6
0.4	193.4	66.9	-16.4	260.3
0.5	270.5	57.1	-62.7	327.6

*Based on costs of $100/kg Uranium mined and $100/kg SWU.
Does not include fabrication or waste disposal costs.

Table 11-5 CANDU-SSATR Resource Utilization and Separative Work Requirements

requires 28% more uranium and 2.7 times more separative work than the 14211312 design per unit energy production. The CANDU-SSATR provides 2.1 times greater burnup than the 14211312 variant and hence spent fuel volumes are reduced correspondingly.

In comparison with the 1421NAT design, the CANDU-SSATR with 0.2 a/o U-235 tailings provides 6 times greater fuel burnup (hence 1/6 of the spent fuel volume) and achieves an 11% improvement in resource utilization.

With additional modifications including the use of enriched zirconium in the pressure tubes and calandria tubes, and the application of advanced uranium enrichment techniques which yield close to 0.0 a/o U-235 tailings concentration, the CANDU-SSATR would be expected to yield a natural uranium utilization which is comparable, if not surpassing that obtained with the 14211312 design under similar conditions.

11.6 CONCLUDING REMARKS

The CANDU-SSATR concept introduced in this chapter has provided an alternative path of development in the evolution of the CANDU design. Utilizing the same basic principles inherent in the nominal CANDU-600 reactor design, though with the introduction of a novel spectral shift feature, the CANDU-SSATR holds much promise for the future.

The design represents an evolutionary development building upon the proven CANDU concept. Optimization of the CANDU-SSATR will allow:

(a) Improved natural uranium utilization,

(b) Ease of on-power fuelling due to limited initial fuel local excess reactivity,

(c) Reduction in spent fuel volumes (comparable to that achievable with proposed LWR designs), and

(d) Additional flexibility in design with "replaceable" calandria tubes, to alter the neutronic spectrum if economics necessitate such changes during the life of the reactor.

Further conceptual studies can be envisaged which will include detailed evaluations of hybrid reactor units (range of spectral zones within a single unit, as considered here) and compare these to synergetic/symbiotic systems in which a series of reactors operate independently, each in a certain spectral region. (In such systems fuel is initially loaded in a hard spectrum reactor and transferred, after irradiation, to a series of softer spectrum units.) The effect of increasing inter-zonal leakage can be investigated. (With a chequerboard-type spectral zone layout this effect will be maximized.) There also exists the possibility of a fuel cleanup operation between burnup steps -- possibly involving in-situ rejuvenation of spent nuclear reactor fuel (Harms and Hartmann, 1978). The entire operation can take place at a single site -- a nuclear energy park (Gordon and Harms, 1977), a self-contained facility which will deal with all aspects of the nuclear fuel cycle.

CHAPTER 12

SUMMARY, EXTENSIONS, AND CONCLUSIONS

12.1 ENVISAGED NUCLEAR ENERGY DEVELOPMENT STRATEGY

The global demand for energy is continuing to escalate as developing countries become increasingly industrialized. An examination of the global energy resources (Section 1.2) indicates that nuclear generated power has the potential to satisfy the predicted demand for many generations to come, provided that efficient use is made of the available resources.

Nuclear power has advantages over its alternatives from both an ecological and economic point of view (Zraket, 1987), and subsequently it has become the near term energy option of choice. However, nuclear technology is still quite young and has great scope for progress (Carle, 1987). Much of this progress will be geared towards increased safety characteristics, improved reliability, enhanced resource utilization, and reduced costs.

Because of the inherent neutron economy of heavy water moderated nuclear fission reactor systems in general (International Atomic Energy Agency, 1980 and 1980a; Shapiro and Jesick, 1979), and the design and operational advantages (Kugler, 1980), system reliability (Bartholomew et al., 1988), enhanced resource utilization (Hatcher, 1979), and commercial availability and viability (Atomic Energy of Canada Limited, 1981) of the CANDU-PHW reactor design in particular, such systems have the potential to form the design basis for the next generation of thermal fission reactors.

This thesis explores the use of a low enriched uranium (LEU) fuel cycle in advanced CANDU-PHW reactors. The LEU cycle has been identified as an optimal transitional fuel cycle for use in such reactors prior to the introduction of plutonium recycling or thorium-based schemes (see Chapter 3).

12.2 ENHANCEMENT OF CANDU OPERATING CHARACTERISTICS: COOLANT VOID REACTIVITY REDUCTION

The implementation of an LEU fuel cycle in CANDU reactors will result in:

(a) Increased resource utilization,
(b) Increased fuel burnup,
(c) Reduction in spent fuel volumes and disposal costs,
(d) Increased flexibility of reactor design.

The increased flexibility of design is a consequence of the increased reactivity of the fresh nuclear fuel in the enriched case. To a certain extent the designer can trade neutron economy for improved safety and operational characteristics without adversely affecting system economics.

Operational safety and international acceptance of the CANDU-PHW concept could be improved if the coolant void reactivity were reduced. Studies were undertaken in this thesis to reduce the coolant void reactivity to a value less than the delayed neutron fraction, but greater than zero (to enable the continued crediting of neutronic shutdown system trips on LOCAs, for example). Adjustment of the fuel enrichment (Section 12.2.1), reduction of the moderator to fuel volume ratio (Section 12.2.2), and modifications to the fuel bundle design (Section 12.3) were considered to effect this operational enhancement.

12.2.1 Effect of Increasing Fuel Enrichment

From lattice physics simulations conducted in this thesis using a standard 37 element CANDU-600 fuel model with various fuel enrichments, the following conclusions can be drawn (Sections 6.3 and 6.4):

(i) The use of enriched uranium yields higher fresh fuel reactivities. This is primarily due to an increase in the eta

factor. In the transition from natural to 1.3 a/o U-235, simulations showed that burnup increased by a factor of 3.6.

(ii) As fuel irradiation is increased, the effective multiplication factor becomes less dependent on the initial fuel enrichment.

(iii) In the natural uranium and 1.0 a/o U-235 cases, the void reactivity decreases with fuel burnup. For the 1.3 a/o U-235 case, the void reactivity is relatively independent of fuel irradiation.

(iv) At low burnups, the enriched fuel cases have a lower coolant void reactivity than the natural uranium fuel case. The reverse is true at high burnups. For the cases considered, the transition occurs between 5000 and 9000 MWd/MgU.

(v) As the initial U-235 concentration is increased, the thermal absorption in the fuel region is increased. The relative change in the thermal utilization upon voiding is therefore reduced. This hardening of the spectrum in the fuel region also reduces the relative change in the eta factor when the coolant is voided, hence resulting in a reduced void reactivity.

(vi) At higher fuel burnups with enriched fuel, the importance of plutonium to the total fission source is reduced in comparison with the natural uranium case. This effect, coupled with the increased spectral hardening in the fuel region, results in the void reactivity being less irradiation dependent with enriched uranium fuel (primarily due to a reduction in the change in the eta factor).

Therefore, increasing the fuel enrichment will increase the achievable burnup, though it does not provide a particularly effective means for reducing the coolant void reactivity.

12.2.2 Effect of Reducing the Moderator Volume per Lattice Cell

In Chapter 6 of this thesis, in an effort to reduce the coolant void reactivity, a number of methods of reducing the moderator volume per lattice cell were identified and critically evaluated. Alternatives considered included:

(a) Reduction in lattice pitch (LP),
(b) Increased calandria tube diameter,
(c) Use of gas bubblers to reduce the effective moderator density,
(d) Use of moderator displacement rods.

Lattice cell simulations were conducted (Section 6.3 and 6.4) to investigate these options. From the results of the simulations, the following conclusions can be drawn with respect to moderator volume reduction:

(i) To effect a zero value for the coolant void reactivity with a standard CANDU-600 fuel bundle and 1.3 a/o U-235 enriched uranium, it would be necessary to either:
  (a) Reduce the effective moderator density to 0.51 g/cm^3 (from its nominal value of 1.082 g/cm^3), or
  (b) Increase the calandria tube outer radius to 12.5 cm, or
  (c) Position 1280 vertically mounted 5" OD tubes interstitially between the fuel channels throughout the core, each tube running the entire vertical length of the reactor.

(ii) The burnup achievable under the conditions noted in (i) above, is less than half of that achievable with the nominal CANDU-600 core configuration using 37 element 1.3 a/o U-235 fuel.

(iii) With a fuel enrichment of 1.3 a/o U-235, a 25 cm LP reduces the void reactivity by 10% while incurring a 4% burnup penalty (with respect to the nominal 28.575 cm LP case). A 60% reduction in void

reactivity is achievable with a 20 cm LP. The burnup penalty is increased in this case to 40%.

12.3 REDESIGN OF THE NUCLEAR FUEL BUNDLE

Reducing the void reactivity by modifying the moderator to fuel volume ratio or through the use of spoiled geometries, will result in substantial burnup penalties, as evidenced above. Since one of the major features of the CANDU design is its inherent neutron economy, such schemes are not particularly attractive from a basic philosophical standpoint, nor are they expected to be economical in the long or short term. However, redesigning the nuclear fuel bundles used in a CANDU reactor can result in a significant coolant void reactivity reduction without adversely affecting achievable burnup.

Roshd et al. (1977) conducted an investigation in which the inner 7 fuel pins in a 37 element natural uranium fuel bundle were replaced by a large void tube or graphite stringer creating a 30(37) fuel bundle. The objective of this design modification was to reduce the coolant void reactivity while maintaining high bundle operating powers. Experiments by French and Jones (1976) confirmed this behaviour.

The work in this thesis has extended Roshd's analysis to enriched uranium fuel bundles, and additional modifications have been introduced to further improve fuel performance. The results of this work are outlined below.

12.3.1 Analysis of the 30(37) Bundle Design

Based on initial lattice physics simulations and engineering considerations, a central graphite core was found to be superior to an air or gas filled core (Section 7.4).

The transition from the 37-1.3-28.575-6.4478-CC fuel bundle design (nominal CANDU-600 enriched to 1.3 a/o; code description provided in Section 7.5.1.1), to the 30(37)-1.3-25-7-CC design with natural zirconium caused an 8%

reduction in achievable burnup (20650 MWd/MgU vs 22400 MWd/MgU). However, with enriched zirconium in the 30(37) lattice, achievable burnup rose to 23760 MWd/MgU, and increase of 6% over that achievable with natural zirconium in the 1.3 a/o U-235 37 element design.

The following changes to the coolant void reactivity (VR) result from each component of the lattice transition from the 37 element design:

LP reduced 28.575 to 25 cm:	VR down 1.5 mk
Calandria tube radius increased to 7 cm:	VR down 0.3 mk
30(37) element design:	VR down 6 mk
Use of enriched zirconium:	VR down 2 mk

Adoption of the 30(37) design proved to be the most effective means of reducing the void reactivity, though the other modifications introduced also play an important role in controlling this parameter.

The 30(37)-1.3-25-6.4478-CC enriched zirconium design was found to yield a burnup of 24250 MWd/MgU with a void reactivity 0.5 mk higher than in the 30(37)-1.3-25-7-CC enriched zirconium case.

The results of the various cases considered are summarized in Table 7-7 of this thesis.

Appendix A provides a further characterization of the void reactivity reduction phenomenon arising in the transition from a 37 element natural CANDU-600 lattice to a 30(37)-1.3-25-7-CC design. In this appendix, the contribution of changes in reaction rates in U-235, U-238, Np-239, Pu-239, Pu-240, Pu-241, and Pu-242 upon coolant voiding were examined. The analysis shows that the U-238 contribution to the void reactivity is the most substantially reduced parameter in comparing 37 and 30(37) element fuel bundle designs. This is a consequence of the reduction in the fast production and fast absorption effects due to the removal of the central two element rings where the fast flux is a maximum.

12.3.2 Characterization of the 30(37) Element Bundle Design

In Section 7.7 the 30(37) element enriched uranium fuel bundle design and variants thereof were more fully characterized. Some of the more general findings include:

(a) As the fuel enrichment increases, the initial k-eff increases, though as the burnup approaches 40000 MWd/MgU, the k-eff curves tend to join together. (At this latter stage the remaining U-235 concentration is minimal in all cases (Section 7.7.1).)

(b) The initial void reactivity (Fig. 7-4) is reduced as the U-235 enrichment is increased. However, as with the 37 element cases, the higher enrichment fuel is less sensitive to burnup, resulting in a cross over of the curves as the burnup increases (Section 7.7.1).

(c) As the lattice pitch size is reduced, the effect of the transition from a 6.4478 cm to a 7 cm calandria tube is enhanced. That is, the burnup penalty and void reactivity reduction associated with the change is enhanced (Section 7.7.2).

(d) It is more economical to reduce the void reactivity by reducing the lattice pitch than by increasing the calandria tube radius. This can be attributed to both the increased parasitic absorption and increased neutronic leakage (streaming) in the enlarged calandria tube cases (Section 7.7.2). (In the finalized fuel bundle/lattice designs developed in this thesis, the nominal CANDU-600 calandria tube diameter was used.)

(e) The coolant void reactivity was found to increase if either the moderator or coolant D_2O isotopic purities are reduced. These changes are also accompanied by a burnup reduction (Section 7.7.3). Careful monitoring and control of these parameters is required for

both economic and safety reasons.

(f) The moderator temperature coefficient of reactivity was found to be negative in the 30(37)-1.3-25-7-CC design under steady state unpoisoned equilibrium conditions. It is positive under similar conditions in the natural nominal CANDU-600. The difference between the cases can be attributed to the tighter lattice pitch in the enriched lattice analysis.

(g) System reactivity was found to increase linearly as coolant density is decreased.

12.3.3 Perturbations to the 30(37) Fuel Bundle Design

In Section 7.8.1, adjustments to the central core in the 30(37) element bundle design were investigated. Perturbations included:

(a) Graphite core the same size as seven fuel elements (1.69 cm radius).
(b) Hollow air filled core.
(c) 7 separate carbon elements to replace the 7 inner fuel elements.
(d) No core at all.

All of these designs yielded lower achievable burnups and higher void reactivities than with the standard 30(37), 2.1 cm radius graphite core. Perturbation (c) yielded the lowest burnup and highest void reactivity of the four perturbation cases considered. Such designs need not be considered further due to their less than optimal performance characteristics.

Replacing the carbon core with a lithium or cobalt core for isotope production, yielded extremely reduced k-eff values (Section 7.8.2).

A 36(37) design with either a graphite core or cobalt core resulted in reduced achievable burnup and higher void reactivities. Of the 36(37) designs considered, the void reactivity was least in the cobalt core case as a result

of the depression of the neutron flux at the centre of the bundle due to the presence of the cobalt (Section 7.8.3).

The use of these modified bundles for increased tritium or cobalt production is technically viable, though restrictions will be necessary to ensure that reactor criticality can be maintained and that the system coolant void reactivity will remain within specified limits.

12.3.4 Use of Light Water Coolant

As discussed in Section 7.8.4, the use of light water coolant can reduce the plant capital cost and worker radiation dose. With a 25 cm LP and a 1.3 a/o U-235 30(37) element fuel bundle design, analysis conducted in this thesis has demonstrated that the use of light water coolant reduces burnup by 25% in comparison with the heavy water case. The coolant void reactivity is of the order of 40 mk in this case. Reducing the LP from 25 to 21 cm, reduces the burnup by a further 8%, but the void reactivity is reduced by more than 45 mk at 10500 MWd/MgU.

With light water coolant, the void reactivity is considerably more burnup sensitive than in the heavy water case.

With light water coolant and a 21 cm LP, the initial void reactivity is comparable to that in the current CANDU-600. The equilibrium core void reactivity is very close to zero, and the achievable burnup (16431 MWd/MgU) is approximately 30% less than in the 30(37)-1.3-25-7-CC heavy water cooled case.

Note that boiling light water coolant would yield a higher burnup and lower void reactivity than the saturated cases considered.

The use of an LEU fuel cycle will indeed reopen the possibility of introducing a boiling or saturated light water cooled, heavy water moderated CANDU reactor.

12.3.5 Neutron Poisons

As discussed in Section 7.8.5.1, the addition of neutron poison to the moderator system increases the coolant void reactivity, and decreases

achievable fuel burnup. The reactivity worth of moderator poison in the 30(37)-1.3-25-6.4478-CC fuel lattice was found to be approximately one-half of the worth of the same concentration of poison in the natural nominal 37 element CANDU-600 case. This can be attributed to the reduced moderator volume, increased fission cross section, and harder neutronic spectrum in the modified design.

To reduce the reactivity of fresh fuel bundles, neutron poison can be added to the fuel mix. A number of cases were investigated (Section 7.8.5.2). Poison was added to either the carbon core or the fuel elements themselves.

In all cases, the addition of poison results in a burnup penalty. The added operational flexibility may justify this penalty. For example, 305 ppm Gd added to the carbon core in the 30(37)-1.3-25-6.4478-CC lattice, results in a 45 mk reduction in the peak reactivity and only a 0.15% reduction in achievable burnup.

B-10 added to the carbon core reduces the void reactivity. B-10 added to the fuel elements increases the void reactivity. Gd added to the fuel mix or the carbon core tends to reduce the void reactivity.

The effect of B-10 on reducing k-eff extends over a longer burnup period than the effect of Gd.

The addition of larger quantities of poison to the fuel mix can reduce the initial k-eff value to less than 1. As the poison burns away k-eff will increase. This delayed behaviour may cause operational difficulties.

12.3.6 Increasing the Pressure Tube and Calandria Tube Wall Thicknesses

To operate at higher pressures and temperatures (for increased secondary side efficiency), it will be necessary to increase the thickness of the pressure and calandria tubes. Studies conducted in Section 7.8.6 of this thesis have demonstrated that this reduces achievable burnup and increases the void reactivity. The use of enriched zirconium minimizes these negative effects.

12.3.7 Enrichment Grading

For fuel pencil diameters in the range of 1 to 2 cm, the parameter "N-equivalent" (N_{eq}) (Section 7.10) provides a good basis for comparison of the relative fuel bundle power achievable.

For natural nominal CANDU-600 37 element fuel bundle, lattice physics simulations indicate that N_{eq} is approximately 32.6 at equilibrium conditions.

In the 30(37)-1.3-25-6.4478-CC case, N_{eq} was found to be approximately 28.2, on average. Enrichment grading (variation of the initial fuel element enrichment between rings of fuel elements) can be employed to increase N_{eq} even further, though for the 30(37) design it cannot be increased beyond 30, the total number of elements in the bundle.

The effect of enrichment grading was examined in this thesis. The impact on N_{eq} was found to be largest at the initial burnup stages. As the burnup progresses, the U-235 concentration becomes depleted and, as shown in this analysis, the inner to outer ring pin power ratio becomes independent of the initial enrichment grading. It is concluded therefore, that enrichment grading alone will only be partially effective in maximizing N_{eq}.

Of the cases considered in Section 7.10, the inner/outer a/o U-235 enrichment grading case 1.3/0.9, was found to yield the highest average N_{eq} (29.7). The 1.3/1.042 case yielded an initial N_{eq} of 30.0, but over the 21000 MWd/MgU burnup period, the average N_{eq} was only 29.4.

When the initial enrichment is decreased in the outer ring of fuel elements, the inner ring becomes increasingly important to the overall fuel behaviour and therefore the void reactivity effect (which is greatest in the inner fuel elements) is enhanced. As burnup proceeds, the U-235 in the inner ring in the cases with low outer ring enrichment burns out faster than in the 1.3/1.3 case. This, combined with the harder neutron spectrum in the 1.3/1.3 case, results in a coolant void reactivity effect which is larger in the non-graded design at higher burnups.

12.3.8 Fuel Element Radius and Enrichment Grading

In Section 7.11, a number of bundle design modifications were introduced to increase N_{eq} above the NATNOM value of 32.6. Efforts were primarily concentrated on the development of various 14/21 fuel bundle designs.

The (inner pin power to outer pin power ratio) (denoted PR) was used as a figure of merit in evaluating the 14/21 fuel bundle designs considered.

It was found that the coolant void reactivity was minimized and burnup was optimized, by minimizing the amount of coolant within the bundle structure. A minimum separation of 1 mm was maintained between fuel elements within an element ring and between element rings in all cases considered.

Adjustments to the pin sizes were found to have an impact on the PR. The 14/21 design which included fuel pins enriched to 1.3 a/o U-235 with an inner pin / outer pin radius ratio of 1.07, was found to yield a PR of 1.00 at 24000 MWd/MgU (i.e. near the end of its burnup cycle), but initially, the PR was only 0.93. Recalling from the 30(37) element enrichment grading cases, that such enrichment modifications primarily affect the beginning of life PR only, it became apparent that a combination of enrichment and element radius grading (a novel concept in CANDU bundle design) could allow operation over the entire burnup range with a PR of approximately 1.00. This led to the development of a 14/21 (1.07) 1.3/1.2 optimized bundle design. The PR for this case (B9 in Section 7.11) ranged from 1.00 initially, to a maximum of 1.034 (at 13000 MWd/MgU) and was reduced to 1.00 by the time the bundle reached its expected achievable burnup of 23000 MWd/MgU. The N_{eq} was at no time less than 34.3.

This same 14/21 (1.07) design was considered for higher enrichment cases. The 14/21 (1.07) 1.7/1.53 bundle was found to have an initial PR of 1.00. However, the variation was larger over the burnup period than in the 14/21 (1.07) 1.3/1.2 case. In this case, N_{eq} was no lower than 33.7. With this design, during the early burnup stages when fuel bundles are generally operating at their highest powers, the N_{eq} was 35.

For a 14/21 (1.07) natural uranium bundle, similar lattice physics

simulations were conducted which indicated that the PR ranges between 0.98 and 0.99. N_{eq} is always greater than 34.7.

The 14/21 (1.07) fuel design was found to be near optimal for use with the 1.7/1.53 and 1.3/1.2 enrichment graded cases and for use with natural uranium fuel. Economics and the availability of enriched uranium would dictate the fuelling option chosen, but at this stage a reactor concept can be envisaged which can accept any of these bundle designs as conditions require. By maintaining a constant bundle geometry, system thermohydraulics will not be a function of the enrichment option chosen.

12.4 ADDITIONAL COMPARISON OF 14/21 AND NOMINAL CANDU-600 FUEL BUNDLE DESIGNS

The natural nominal CANDU-600 37 element fuel bundle design (NATNOM) was compared with the range of optimized 1421 (1.07) designs: 1421NAT, 14211312, and 142117153.

12.4.1 Fissile Composition of Spent Fuel

The use of the enriched fuel 1421 design reduces the fissile concentration in the spent fuel on a per mass of spent fuel and on a per unit energy production basis (Section 7.13.2). Reprocessing becomes more expensive (should this option be pursued in the future) but nuclear weapons proliferation resistance is enhanced.

12.4.2 Effect of Lattice Pitch Variation

The effect of varying the lattice pitch in the various cases was investigated. It was found (Section 7.13.3) that achievable burnup is less sensitive to LP size as enrichment is increased. Further, the optimal LP size decreases as enrichment is increased. This is due to the fact that sufficient initial excess reactivity is available in the enriched cases to take advantage of the greater production and utilization of plutonium with a reduced LP

(harder neutron spectrum). Economic benefits can be attained by reducing reactor D_2O requirements as fuel enrichment is increased.

12.4.3 Effect of Flooding the Gas Gap

The flooding of the gas gap between the pressure tube and calandria tube was found to yield a local reactivity of 0.3 mk in the NATNOM case (Section 7.13.5). However, in the 14211312 design, due to the harder neutron spectrum, a local reactivity increase of between 5.0 and 10.7 mk (depending on the burnup) could result in the event of a gas gap flooding. Such accidents are limited in scope, usually affecting only a single fuel channel and hence the global core reactivity insertion under such conditions will be much less than the delayed neutron fraction. Such events, however, must be considered in the safety analysis conducted prior to licensing this reactor design.

12.4.4 Kinetics Parameters

Kinetics parameters for the various lattice and bundle designs were considered in Section 7.14. The average (over the burnup range) delayed neutron fraction was found to decrease as fuel enrichment increases. This can be attributed to the larger overall proportion of fissions in plutonium isotopes in the enriched cases. The equilibrium coolant void reactivity effect was found to be less than the delayed neutron fraction for all of the 14/21 cases. This was the desired feature of the modified bundle/lattice design.

The smaller lattice pitch and harder neutron spectrum in the 14/21 cases results in a reduction in the prompt neutron lifetime. Increasing the enrichment also reduces this parameter. Nevertheless, the prompt neutron lifetime in the 142117153 case remains more than ten times larger than the corresponding value for a typical light water reactor. Reactivity excursions will be correspondingly less severe.

12.4.5 Xenon Override

Adjuster rods in a CANDU reactor can be removed to provide positive reactivity to override the negative reactivity effects of the xenon transient following a reactor shutdown. Generally, the removal of the adjuster rods should provide sufficient positive reactivity to allow a return to reactor power within 30 minutes of a reactor trip from steady state full power conditions.

Lattice physics analyses were conducted to simulate the xenon transient for 30 minutes following a reactor trip for each of the fuel designs of interest.

The results of the simulation (Section 9.2), indicate that as enrichment increases, the required adjuster rod worth for a 30 minute xenon override time decreases. This can be attributed to a harder spectrum in the enriched fuel cases, and also to the fact that with an increased fuel fission cross section, a larger change in absorption rate is required to effect a given change in reactivity.

The 1421NAT case was found to require a 19% larger adjuster rod worth than in the NATNOM case to provide a 30 minute xenon override time. This is due to the increased flux level in the 14/21 cases. The 14211312 and 142117153 cases have adjuster rod reactivity requirements which are only 97% and 90% (respectively) of that required for the NATNOM case. For the enriched fuel cases, one can either reduce the adjuster rod reactivity worth, or xenon override times can be extended in relation to the NATNOM case.

12.5 REACTOR CORE MODELLING AND FUEL MANAGEMENT SIMULATION

Having examined the lattice physics of the NATNOM and 14/21 bundle designs, comprehensive fuel management studies were required to fully characterize reactor operation with these fuel types.

12.5.1 Strategy for Fuel Management Calculations

In Chapter 8, the multigroup diffusion theory representation of the neutron balance equation was introduced. From past experience it was known that for the NATNOM case, the modified two energy group representation (M-2, Section 8.2.2) provided sufficient accuracy for three dimensional full reactor core simulations. However, for the purposes of fuel management analysis of heavy water reactors fuelled with enriched uranium, it was necessary to determine if the M-2 approximation would continue to be appropriate. From a comparison of three dimensional reactor core simulations (Appendix B) performed using four neutron energy groups, two energy groups, and the M-2 representation, with properties derived from a series of lattice physics codes, it was found that the WIMS-CRNL generated M-2 approach would provide sufficient accuracy for the fuel management calculations required in this analysis. A core simulation strategy consistent with the M-2 approach was developed and applied as explained in Chapters 8 and 9 of this thesis.

Several types of fuel management calculations were conducted in support of the analysis (see Section 8.4.2):

(a) Continuous Bidirectional Fuelling Approximation: CBDFA

(b) Time Averaged Approximation: TAA

(c) Instantaneous Approximation

For the analysis in this thesis, initial scoping studies were conducted using the CBDFA methodology. The TAA was used for detailed fuel management scheme characterization and evaluation. The Instantaneous Approximation was then used to determine sample fuelling ripple (power perturbation) effects with several of the fuelling schemes.

12.5.2 Simulation of Reactivity Devices

In the FMDP core model, reactivity devices (e.g. adjuster rods and liquid zone controllers) are simulated by adding incremental cross sections to the lattice cell properties in the regions in which the devices are situated (Section 9.4.2).

The modelling of the reactivity devices is detailed in Chapter 9 and Appendices C and D.

Sensitivity studies were conducted which showed that the device incremental properties were not appreciably affected by either fuel enrichment or fuel burnup. The analysis did indicate a dependence on the lattice cell geometry due to the altered cell sizes and the differences in the amount of fuel per lattice cell and per unit length of reactivity device. Hence two sets of adjuster rod and zone controller properties were developed -- one set for the NATNOM case, and a second set for all of the 14/21 cases (based on the 14211312 data).

12.5.3 Governing Equations

In Section 10.4 and Appendix E, the analytical formulation of the equations governing natural uranium and separative work requirements are considered. These equations are required for the interpretation of the results of the fuel management simulations.

From the analysis conducted in Appendix E, several conclusions of a general nature can be drawn.

First, if it is necessary to produce uranium product of a given U-235 enrichment by dilution of a more enriched feed material, the amount of natural uranium equivalent required per kilogram of product is independent of the feed material enrichment (Section E.5.2).

Second, the amount of separative work required is increased if enriched feed dilution is necessary (as opposed to producing material at the product enrichment directly). (Section E.6).

Third, it was determined that natural uranium requirements as a function of the tailings concentration increase faster as the product enrichment increases. This affects the natural uranium utilization statistics.

12.5.4 Continuous Bidirectional Fuel Management Studies

The CBDFA fuel management calculational approach was used to analyze reactor operation with six fuel variants:

(a) NATNOM
(b) 1421NAT
(c) 14211312
(d) 142117153
(e) 1421:17153/1312 (low leakage)
(f) 1421:1312/17153 (power shaping)

The latter two cases involve the use of differential feed fuel enrichment in the inner and outer radial zones of the reactor core. The cases are described in more detail in Section 10.5.1.

The CBDFA simulation results (Section 10.5.4) indicate that for a tailings concentration of 0.0 a/o U-235, natural uranium utilization (NUU) is increased as the U-235 concentration increases. For the higher tailings concentrations considered, the natural uranium utilization is highest for the 14211312 type fuel.

By examination of the one energy group neutron balance equation, one can demonstrate analytically (Section 10.5.5.5) that, as also found in the CBDFA analysis, an increased adjuster rod absorption cross section is required to effect an equivalent change in reactivity as the fission cross section (i.e. fuel enrichment) is increased.

The use of enriched zirconium and a modified bundle and lattice design result in the 1421NAT case yielding a fuel burnup 14% in excess of the NATNOM case. The 14211312 case has an achievable burnup (23786 MWd/MgU) which is 232% above the NATNOM design and NUU is increased by 32 - 48% (depending on the tailings concentration). The fuel burnup with the 142117153 fuel design (31134 MWd/MgU) represents a 335% increase over the NATNOM design. Extra separative work costs and reductions in NUU in comparison with the 14211312 case are associated with this scheme.

The 1421 mixed radial enrichment studies yield burnup and NUU results which lie between the 14211312 and 142117153 cases. The flexibility available through radial adjustment of fuel exit burnup would indicate that the added complications involved with two fuel types would not be justified for NUU optimization purposes. It is noted that fuel management strategies geared towards minimizing the peak bundle power upon refuelling may benefit from the 1421:131217153 design, where lower enrichment (lower reactivity) fresh fuel is placed in the hotter central core region.

12.5.5 Time Averaged Studies

The CBDFA analysis provides an indication of achievable burnup, natural uranium utilization, adjuster rod requirements, and possible power distributions. The TAA and Instantaneous simulations enable further characterization of particular fuelling schemes for viability assessment.

In this thesis, fuel management with 142117153 type fuel was considered, and was compared with the NATNOM case. The 142117153 fuel yields burnups comparable to current light water pressure vessel reactors, though with considerably improved resource utilization. The 142117153 fuel was the most enriched fuel type considered in Chapter 7 of this work (and higher than that considered by other researchers), and therefore poses the greatest challenges in terms of fuel management to maintain acceptable power distributions and to maximize fuel burnup.

12.5.5.1 Push-Through Fuelling Schemes

As a first fuel management strategy, the use of simple push-through fuelling schemes was investigated using the TAA methodology.

A two bundle shift (2BS) fuelling scheme was found to yield excessively high bundle powers near the axial ends of the core with 142117153 fuel, thereby increasing neutronic leakage and also forcing unit derating to meet bundle and channel power limits. One advantage of this scheme is that the number of channels refuelled each day is comparable to that in the NATNOM

8BS scenario. Acceptable local reactivity increases per channel refuelled could be expected. Note however that the reactivity increase is more localized (2BS vs 8BS), and that the reactivity decay rate in the 142117153 case is 38% larger than with NATNOM fuel.

The 4BS fuelling scheme also yielded a dished time-averaged axial power distribution. 6BS and 8BS provide more acceptable time-averaged power distributions since fresh fuel is added to the central area of the core, reducing flux and power depressions in that area.

The TAA methodology does not allow an appreciation of the effects of a fuelling scheme immediately after refuelling. A deep power depression at the end of a dwell time can mask the extreme power surges which can occur following a refuelling operation. This may occur even if a particular fuelling scheme has an acceptable time-averaged power distribution. It is intuitively evident, therefore, that fuelling schemes such as the 142117153 8BS strategy, which requires a channel to be refuelled every two days, and which adds 1 mk to system reactivity at each refuelling, will be unacceptable. Operational power limits cannot be maintained with such schemes without considerably derating the reactor. More acceptable fuelling strategies would minimize the number of bundles replaced per channel visit and take advantage of the neutronic coupling between adjacent fuel channels and fuel bundles to minimize local peaking upon refuelling and thereby maximize control of the reactor power distribution. Checkerboard fuelling provides the key to the on-power fuelling of enriched CANDU-PHW reactors.

12.5.5.2 Checkerboard Fuelling: 142117153:A

2BS fuelling schemes yield power distributions which are peaked at the axial ends of the core. 6BS schemes yield higher powers near the centre of the core. A checkerboard strategy consisting of bidirectionally fuelled alternating channel pairs, one pair fuelled using the 2BS scheme, the next using a 6BS scheme, was devised by Chan and Dastur (1985). Younis et al. (1986) found that if the six bundle shifts were broken down into three sets of 2BS with short burn steps after the first and second sets of 2 BS fuellings,

and an extended burnup period after the third set, that enrichments of up to 1.5 w/o U-235 could be successfully employed in a CANDU reactor.

This same checkerboard strategy was applied in this thesis using higher enrichment 142117153 fuel (Section 10.6.5). Zone boundaries were modified to maximize pairwise neutronic coupling. It was found that to provide an acceptably flattened time-averaged power distribution, the burnstep between successive 2BS steps in the 6BS schemes should be minimized. The timing between refuellings with such a scheme must be carefully monitored. Further, it was noted that interchannel coupling is not optimized with this scheme since channels are grouped in bidirectional pairs rather than individually.

12.5.5.3 Checkerboard Fuelling: 142117153:B

The checkerboard strategy discussed in Section 10.6.5 and summarized in Section 12.5.5.2 required channels to be paired bidirectionally to achieve front-to-back axial symmetry. Modified checkerboard schemes were devised in this thesis (Section 10.6.6) which were axially symmetric in themselves, allowing individual channels to be surrounded completely by channels fuelled with an alternate fuelling scheme, to maximize the effects of inter-channel neutronic coupling. Several strategies were investigated (B1, B2, and B3 in Section 10.6.6). Strategy B3 (Fig. 10-3) was found to be optimal.

In the B3 fuelling strategy, alternating channels are fuelled by either fuelling scheme 19 or scheme 54. Scheme 19 places a fresh bundle at each end of the fuel channel. Scheme 54 involves alternating between placing a fresh fuel bundle at position 4 and position 9. The bundles are then transferred to the centre of the core and gradually pushed towards the ends of the channels.

The B3 fuelling strategy requires an average of 3.36 channel visits per full power day (FPD), with a total of 4.48 bundles replaced per FPD. This represents a 67% increase in channel visits and a 72% reduction in daily bundle replacements in comparison with the NATNOM case.

All of the 142117153 fuelling schemes investigated yielded

approximately the same burnup. The mean burnup of the TAA cases was within 0.5% of the CBDFA value. The B3 checkerboard scheme yielded an average exit burnup of 31334 MWd/MgU. The 2BS and checkerboard A schemes, in which fresh fuel is placed at the channel ends in all channels, yielded burnups which were 0.3% and 0.8% (respectively) lower than in the B3 case.

12.5.6 Instantaneous Analysis

Instantaneous calculations were conducted in this thesis to examine the operational acceptability of the various fuel management strategies considered. The results of this analysis (Section 10.7) indicate that very careful selection of channels for refuelling is required when enriched uranium bundles are used. This is due to the large power perturbations associated with the refuelling operations in these cases. Errors (or less than optimal choices) made in fuelling tend to have longer term ramifications due to the extended burnups in the enriched fuel cases. Computer assisted fuel channel selection would be a necessity.

12.5.7 Comparison With Other Once-Through Cycles

In comparison with light water reactor once-through fuel cycles, the 14211312 and 142117153 CANDU-PHW fuel cycles require approximately one-half of the amount of natural uranium and one-quarter to one-third of the separative work per unit electrical energy output. Natural uranium requirements for the 14211312 and 142117153 strategies are reduced by approximately 40% in comparison with the NATNOM case.

12.6 CANDU - SPECTRAL SHIFT ADVANCED THERMAL REACTOR

On-power fuelling with 142117153 fuel poses significant operational challenges. To increase burnup even further (up to 50000 MWd/MgU) may require excessive use of poison in the fuel bundles (Section 7.8.5.2) to suppress initial reactivity to a more manageable level. Alternatively, a CANDU -

Spectral Shift Advanced Thermal Reactor (CANDU-SSATR), a novel reactor design which was introduced and developed in Chapter 11 of this thesis, could be employed to more easily satisfy the requirements for greatly extended burnups without the serious fuel management complications inherent in a single thermal spectrum reactor.

As noted in Chapter 11, such schemes have been suggested for use in extended burnup light water reactors. This thesis, however, represents the first attempt to apply this strategy to CANDU reactors. Fresh fuel is subjected to a harder neutronic spectrum to maximize conversion of U-238 to Pu-239, and to minimize the fresh fuel reactivity, thereby enabling more simplified fuel management. The fuel is subsequently transferred to a more thermalized region to burn the bred plutonium.

In Chapter 11, novel CANDU-specific spectral hardening techniques including lattice pitch reduction and calandria tube enlargement were investigated. Reactor core simulations were conducted for the case of two spectral zones. The conclusions drawn from the analysis are provided in Sections 12.6.1 - 12.6.3.

12.6.1 Operation With a 15 cm Lattice Pitch

Utilizing the 30(37) fuel bundle design introduced in Chapter 7, maintaining the nominal calandria tube radius, and reducing the lattice pitch (LP) to 15 cm from 25 cm, causes the fast to thermal flux ratio to increase by a factor of almost 7 for 1.3 a/o U-235. The fresh fuel reactivity is substantially reduced because of the LP reduction (Section 11.2).

An increase in fuel enrichment was found to further increase the fast to thermal flux ratio. For example, in the transition from 1.3 a/o U-235 fuel to 8 a/o U-235, the fast to thermal flux ratio in the fresh fuel case increases by a factor of 3.3. Consequently, in these spectral shift designs, adjustments to the initial fuel enrichment can be introduced to fine tune the neutronic spectrum.

The breeding ratio in the 15 cm LP, 1.3 a/o U-235 case was found to be greater than unity. However, the initial k-eff in this case was less than

unity. This fuel would require additional neutronic in-leakage for sustained operation. It could be used in a blanket-type region of the core or at an interspectral boundary.

12.6.2 Increased Calandria Tube Diameter

The increased calandria tube diameter (ICTD) option allows for considerable flexibility in spectral control. To characterize operation with the utilization of this option, the nominal CANDU-600 37 element fuel bundle design with a 28.575 cm LP was used as the design basis. Enrichment and calandria tube diameter were considered to be variable. Fuel enrichments of 3, 5, and 8 a/o U-235 were examined. Calandria tube diameters to effect 33% and 50% of the nominal moderator volume were considered. Cases with no moderator were also evaluated.

The no moderator cases were found to be extremely subcritical (Section 11.3.1), though the fuel reactivity was considerably less dependent on burnup in the harder spectrum than in the nominal CANDU-600 lattice.

The ICTD cases also illustrated the effect that reducing the moderator volume and increasing fuel enrichment has on spectral hardening (Section 11.3.2).

Due to the lower initial fuel reactivities, fuel management in the 333, 350, 533, 800 and 833 cases (see Section 11.3) would be less restrictive than with 142117153 fuel (considered in Chapter 10).

Lattice physics simulations were conducted with the 333 fuel transferred after 800 and 1000 full power days in the hard spectral zone (burnup 26008 and 32510 MWd/MgU, respectively), to another lattice position with a nominal CANDU-600 calandria tube diameter, for continued irradiation (Section 11.4). These cases were identified as 333A800 and 333A1000, respectively.

The plutonium concentration which increased during operation in the hard spectral zone was burnt off during the softer spectrum second irradiation period. Overall, the fissile fuel concentration was found to decrease much more rapidly in the soft spectrum burnup period.

12.6.3 Core Physics Calculations

For the purposes of characterizing the CANDU-SSATR, a simple two-spectral zone core model was considered, incorporating the 333 and 333A1000 fuel lattices.

The adjuster grading, zone boundaries, and outer zone exit irradiation were iterated upon until the following criteria were met:

(a) The reactor was critical.

(b) The number of fuel bundles per day required in the outer zone matched the number of bundles per day being discharged from the inner zone.

(c) The maximum channel power was less than 6500 kW.

(d) The maximum bundle power was less than 800 kW.

A converged solution yielded an inner zone burnup of 33050 MWd/MgU and an outer zone burnup of 13493 MWd/MgU, for a total of 46543 MWd/MgU, with an adjuster/zone controller load of -31.1 mk. Reducing the adjuster/zone controller load to -18 mk would increase total burnup to approximately 51000 MWd/MgU.

For the purposes of resource analysis, a burnup of 50000 MWd/MgU was assumed for this reactor (Section 11.5.3). For tailings concentrations of less than 0.3 a/o U-235, the CANDU-SSATR yields a natural uranium utilization improvement over the CANDU-600 NATNOM case.

With a tailings concentration of 0.2% U-235, the CANDU-SSATR requires 28% more uranium and 2.7 times more separative work than the 14211312 design of Chapters 7 and 10. The CANDU-SSATR provides 2.1 times greater exit burnup than the 14211312 design and hence spent fuel volumes are reduced correspondingly. With additional modifications including the use of enriched zirconium in the pressure and calandria tubes, and the application of advanced uranium enrichment techniques which yield close to 0.0 a/o U-235 tailings concentrations, the CANDU-SSATR would be expected to yield a natural uranium

utilization which is comparable, if not surpassing that obtainable with the 14211312 design under similar conditions.

12.7 EXTENSIONS OF THE ANALYSIS

The analysis in this thesis has attempted to provide further details on the use of the LEU fuel cycle in CANDU or other related heavy water reactors. There are many areas of study identified through the course of this work which require additional investigation prior to the implementation of such schemes.

12.7.1 Physics Analysis

From an analytical methods and modelling perspective, further experimental investigations and fine tuning of the lattice physics code nuclear library data are required to ensure the validity of the results of the lattice cell simulations for enriched fuel (Chapter 6), for modified fuel bundles (Chapter 7), and for the spectral shift cases (Chapter 11).

The validity of the M-2 group approximation in the simulation of the CANDU-SSATR reactor core should be analyzed. The effect on the lattice properties of the change in neutronic leakage at the inter-zonal boundaries in the CANDU-SSATR should be considered by modifying the leakage spectrum in the lattice cell simulations for these fuel regions to more accurately reflect the true conditions. Also, a more detailed characterization of the leakage phenomenon through the enlarged gas gap in these cases is required.

Experimental analysis is required to identify critical channel powers (CCPs) in the enriched fuel cases. Enhancements to the CCP (as identified in Section 7.11.4), modifications to the shape of the carbon core in the 14/21 designs, and other methods such as partial channel bypassing of the coolant (Garland, 1985) require further study.

Additional studies should be undertaken to examine the control aspect of LEU fuelled CANDU reactors. Investigation of harmonic subcriticality, xenon stability, and the requirements to prevent xenon oscillations (Akhtar

and Trojan, 1976) in these modified reactors must be considered.

In the 1421 fuel management studies (Section 10.6), the effect of modifications to the flux distribution on xenon worth, adjuster rod worth, and adjuster rod requirements, requires further investigation (see Section 10.6.7).

Reactivity feedback effects (fuel temperature, moderator temperature, coolant temperature, etc.) should be more fully investigated.

Prior to implementation of any advanced fuel cycles, a full safety analysis and licencing study will be necessary. This will address issues such as worker safety, public safety, and environmental protection. Such studies will also be required to address the fuel enrichment process at the front end of the LEU fuel cycle.

Investigations are required to analyze the effect of filling the gas gap with D_2O in the CANDU-SSATR designs. The use of passive safety systems or alternate gap materials may be necessary (Section 11.1).

12.7.2 Fuel Performance

The ability of the fuel to withstand the high fuel burnups expected with the use of LEU fuel requires an analytical and experimental research and development program to add to our existing data base (Hastings et al., 1985). Since fission gas release is primarily dictated by operating temperature and is only weakly dependent on burnup (Bairot, 1983), the more flattened radial power distribution in the 14211312 and 142117153 fuel bundle designs (Chapter 7) may tend to improve fuel performance. Modifications to the thin graphite or siloxane "CANLUB" coating between the fuel sheath and UO_2 (MacEwan et al., 1983) which protects the sheath from fission product attack may be required. Experimental investigation of fuel performance, pellet-clad interaction, fuel sheath water-side corrosion resistance over extended burnup periods, irradiation damage, and dimensional stability is required before such schemes can be implemented.

To collect fission product gases, plenums may be required at the ends

of the fuel bundles to accomodate the higher fuel burnups. The use of annular fuel pellets (Badruzzaman, 1980), in which the hot central region of each fuel pellet is removed, will reduce the average fuel temperature, limit fission gas releases, and provide a zone for fission gas buildup. Hastings and MacDonald (1984) found that the use of interpellet graphite spacers could reduce the amount of fission gases formed, by providing a conductive medium to lower the average fuel temperature and by providing additional voidage for the fission product gases in the graphite porosity. Continued investigation into these areas is warranted.

Properties of the graphite core in the 1421 bundle design (Chapter 7) under in-service conditions should also be considered.

If poison is to be used in the fuel or graphite mix (Chapter 7), the effect on fuel performance must also be studied.

Fuel performance with the various 14/21 checkerboard fuelling schemes (Chapter 10) should be considered. The power ramps upon refuelling and reactivity device movement should be evaluated.

Optimization of the CANDU-SSATR fuel bundle design (Chapter 11) is necessary. Enrichment and pin size grading becomes increasingly important for higher enrichment fuel bundles.

12.7.3 Fuel Management

Full core simulations of extended periods of reactor operation explicitly including the effects of refuelling individual fuel channels will provide additional confidence in the fuelling schemes developed. This is an expensive and laborious but necessary task.

Fuel management schemes in the transition from fresh core to equilibrium conditions must be developed and optimized.

The use of optimization techniques such as those proposed by Wight and Girouard (1978) and Rozon et al. (1981) to maximize fuel burnup by adjusting the radial variation in channel average exit irradiation, can be applied to the LEU fuelled CANDU-PHW as well.

The derivation of optimized yet flexible fuelling rules and the

development of a computer program which expresses these rules as computer logic is necessary to ensure that channel fuelling does not result in excess bundle or channel powers, and that fuel exit burnup is maximized. The program must be able to accomodate day-to-day situations which can affect fuelling capability (e.g. fuelling machine(s) unavailable, damaged closure plugs, fuel failures, etc.). Many researchers have applied optimization techniques to light water reactor fuelling. (See for example Wall and Fenech, 1965 (dynamic programming); Tzanos, 1978 (linear programming); Ahn and Levine, 1985.) The optimization process will involve a trade-off between power shape flattening and high fuel burnup.

A strategy for the replacement of failed fuel (with fuel of the same initial enrichment or depleted uranium) would have to be considered in CANDU-PHW LEU fuelling.

Fuel management schemes and optimized spectral zones (number of zones; arrangement within core; spectral hardening within zones) in the CANDU-SSATR are yet to be developed. Due to the lower initial fuel reactivity, fuelling schemes for the CANDU-SSATR will be more easily devised than in the 142117153 case (Chapter 10).

Fuel management concerns and fission gas accommodation may be best addressed with the use of shorter fuel bundles.

Fuel management with poisoned fuel bundles should be investigated (Section 7.8.5.2).

12.7.4 Economics

The work in this thesis has only marginally addressed fuel cycle economics (Chapters 10 and 11). The total economic costs of any reactor system are comprised of capital costs (interest, depreciation and decommissioning), fuel charges, operation, maintenance, and administrative expenses, and waste disposal.

Fuelling costs in the latest current generation CANDU-PHW reactors are only about 13% of the total unit energy cost (TUEC) (Bartholomew et al., 1988). In addition, as the balance of plant becomes more complex, the reactor

and fuel components of the cost equation are expected to become less significant in relative terms. Therefore, improvements which reduce reactor or fuelling costs will be tempered by these effects.

Interest, depreciation and decommissioning charges account for approximately 75% of the latest current generation CANDU-PHW TUEC (Bartholomew et al., 1988). These charges apply whether or not the unit is operating. Hence, efforts to improve performance and capacity factor will have a marked effect on TUEC, and consequently design modifications which address this objective will necessarily be included in all future reactor concepts.

The flexibility of the CANDU-PHW operating with 14/21 variable enrichment fuel (introduced in this thesis) will make this an attractive design choice for a wide range of economic scenarios.

Ontario Hydro (James, 1978; Archinoff, 1980) has conducted preliminary economic studies of potential future CANDU-PHW fuel cycles. These analyses would have to be updated and considered in much greater detail prior to the implementation of such schemes.

12.7.5 Nuclear Safeguards

The facilities constructed for the production of nuclear generated electricity, can also be used to produce material for nuclear weapons. Nuclear safeguards (Willrich, 1973) are the procedures and equipment employed by nations to ensure, confirm, and provide verification that materials and processes used for the production of nuclear energy are not diverted to the production of nuclear weapons. Safeguards act primarily as an institutional deterrent.

While some argue (Holdren, 1982), that nuclear power lowers the barriers to nuclear weapons production by bringing the required resources and technical personnel together, others contend (Spinrad, 1982) that there are no effective technical barriers to nuclear weapons production, only institutional ones, and that nuclear power presents more discouraging than encouraging factors as a route to proliferation. This is particularly so due to the

nature of the materials produced in nuclear fuel (considerable concentrations of even-numbered Pu isotopes), the relative openness of parts of the industry, and the fact that many countries have had nuclear power instituted as a trade-off against nuclear weapons by agreeing to the Non-Proliferation Treaty and implementing the safeguards specified by the International Atomic Energy Agency. (For a description of the historical development of these agreements, see, for example, Willrich (1973).)

Nuclear weapons proliferation is a very serious concern in today's society. But the denial of civilian nuclear power as a potential energy resource to the newly-developing industrial nations could be equally as threatening to world stability (Stewart, 1981). The continued development of more stringent safeguards measures to be applied in all power reactor systems and fuel enrichment and production facilities may ensure that this route to weapons proliferation is effectively nullified. Efforts in this regard may take the form of pre-irradiation of fuel bundles to deter diversion, increased use of monitoring equipment such as bundle counters (Knox, 1984), or a rearrangement of nuclear facility siting to utilize secure energy parks, thereby limiting the handling and transport of bred nuclear fuel (Stewart, 1981).

12.7.6 Waste Management

Several options for disposing of nuclear wastes exist. Methods under consideration include surface storage in canisters (Dyne, 1975), underground waste disposal in stable crustal formations (Tammemagi, 1976), glacial storage (Boulton, 1978), ocean storage (Boulton, 1978), outer space disposal (Dyne, 1975), or radionuclide transmutation using neutrons from an accelerator-spallation device or a reactor (Dyne, 1975). All of the options contain distinct advantages and disadvantages over the alternatives.

The barriers to establishing a disposal facility today are primarily political, though research and development of novel disposal techniques should be continued. It is noted that the CANDU LEU fuel cycle produces considerably less spent fuel waste than the NATNOM fuel cycle.

12.7.7 Innovative Design Features

The use of alternative coolants such as saturated or boiling light water, gases, or organic fluids warrants continued study.

The use of thicker pressure tubes (especially with enriched zirconium) will allow operation at higher pressures and temperatures for improved secondary side efficiency.

In-situ rejuvenation of spent reactor fuel (using the fast neutron spectrum from a fusion reactor or spallation device) can greatly improve fuel utilization in any fission reactor system without the need for reprocessing (Harms and Hartmann, 1978). Such schemes warrant further in-depth study.

The use of axial and/or radial fertile fuel blankets will also enhance neutron economy, and therefore may be useful in advanced heavy water reactors.

In Chapter 11, the CANDU spectral shift reactor was considered. It would be prudent to extend this study to a high conversion reactor design (Edlund, 1988). Such units would begin with higher initial enrichments and operate in a harder neutron spectrum for the entire burnup period. For light water reactor high conversion units (upon which the heavy water pressure tube version could be based), enrichments of 7 to 8% U-235 and fuel to water ratios to 1 to 2 have been proposed to achieve a conversion ratio of 0.9 (Brogli et al., 1988).

Passive safety and inherent safety features in advanced fission reactors may herald the coming of a second nuclear era (Weinberg, 1984). Sweden's PIUS reactor concept (Office of Technology Assessment, 1984), for example, is designed to ensure safe shutdown and adequate decay heat removal under any credible circumstances. Passive protective features in the design are independent of operator intervention and require no mechanical or electrical/electronic components. The core is situated at the bottom of a large pool of borated water. Under upset conditions, the water from the pool will quench the core.

General Electric (GE) is developing a new boiling water reactor design with enhanced natural circulation, and Westinghouse is considering the

implementation of advanced features in pressurized water reactors to improve inherent safety (Office of Technology Assessment, 1984). GE is also incorporating inherent safety features (shutdown, containment, decay heat removal, etc.) in its PRISM liquid metal reactor design (Varley, 1987a).

Passive safety and inherent safety features should also be considered for application in advanced heavy water reactor designs. (Note that the CANDU-PHW reactor already has many passive safety features including the capability of decay heat removal by natural circulation, a negative fuel temperature reactivity coefficient, and a large independent moderator system which can be used for heat removal under severe accident conditions.)

Additional improvements to the heavy water reactor design will include (Dunn et al., 1986):

(a) maximizing output from components,
(b) minimizing the number of components,
(c) simplifying installation of equipment,
(d) maximizing construction access through modular design,
(e) maximizing shop fabrication,
(f) improving construction and installation schedules,
(g) extending plant lifetime, and
(h) using advanced technology to its fullest.

Studies geared toward the development and implementation of these features in next generation heavy water reactors will result in improved system economics, increased performance, and enhanced reactor safety.

12.8 CONCLUSIONS

This thesis has considered the first stage in the advancement of heavy water reactor technology -- the use of the low enriched uranium fuel cycle. The CANDU-PHW reactor was chosen as the design basis from which the development would extend.

The LEU fuel cycle in CANDU-PHW reactors has been shown, in this

thesis, to provide improved uranium utilization over the natural uranium counterpart. It is concluded that the additional design flexibility afforded with the use of LEU fuel can be successfully applied to the improvement of the reactor operating characteristics. An optimized 14/21 fuel bundle design with a graphite core was devised, which, in a modified CANDU-PHW lattice, will yield a coolant void reactivity which is greater than zero but less than the delayed neutron fraction, thereby enhancing reactor safety. To maximize operating power, the 14/21 bundle design employs both enrichment and element size grading to maximize pin power uniformity at all burnup stages. The simultaneous use of both of these power flattening techniques is novel for CANDU fuel bundle development. A range of bundle enrichments was developed in this thesis for the 14/21 design: 1421NAT, 14211312, 142117153.

It has been demonstrated in this thesis, that a detailed lattice physics model, which explicitly treats the radial variation in the bundle geometry, is required to properly model the modified fuel bundles. Further, it is concluded that in the modified bundle designs, the largest contributing factor to the reduction in coolant void reactivity is the reduction in the U-238 fast production and fast absorption effects. This is a direct result of the removal of the two central element rings where the fast flux is at a maximum.

Fuel management schemes with LEU fuel are more complex than for the natural uranium counterpart. The benefits of on-power fuelling can be retained with the use of checkerboard fuelling schemes in advanced CANDU-PHW LEU reactors. These schemes take advantage of the neutronic coupling between fuel channels to obtain optimal flux and power distributions. The unique operational implications of such schemes were considered in this thesis.

It is concluded that the checkerboard scheme, B3 (developed in Chapter 10 of this thesis), represents an operational improvement over earlier checkerboard fuelling strategies. The fuelling schemes in the B3 strategy are axially symmetric to fully utilize inter-channel neutronic coupling effects. With this fuelling strategy, every second channel is fuelled by a scheme which places fresh fuel at the ends of the channel and withdraws spent fuel from the middle. These channels alternate with others in which the fresh fuel is

loaded closer to the centre of the channel and is eventually shifted to the ends of the channel and withdrawn. The B3 strategy was applied to a CANDU reactor fuelled with 142117153 fuel. This strategy yielded a fuel burnup comparable to that achievable in current light water reactors requiring 3 to 4% U-235. (CANDU fuel management with enrichment levels as high as 142117153 has not previously been addressed in published literature.)

The analysis in this thesis has demonstrated that fuelling ripple is greatly enhanced with LEU fuel due to the large reactivity difference between fresh and spent fuel. It is concluded that computerized and optimized selection of channels for refuelling is required. Poisoning of fresh fuel to reduce initial reactivity may be necessary.

Sensitivity studies conducted in this thesis have demonstrated that the modified two energy group (M-2) diffusion theory representation of the reactor core provides sufficiently accurate results for CANDU fuel management calculations with LEU fuel. A self-consistent M-2 methodology was developed to incorporate lattice physics results and reactivity device incremental properties into the fuel management calculational routines.

It is concluded that, in the longer term, the CANDU - Spectral Shift Advanced Thermal Reactor (CANDU-SSATR introduced as a novel reactor design in Chapter 11 of this thesis) will hold the greatest promise for high burnup LEU fuelled CANDU reactors. In such reactors, fuel enriched to 3% U-235 can achieve burnups of at least 50000 MWd/MgU with initial effective multiplication factors (k-eff) comparable to those in the 14211312 case. By placing the fresh fuel in a hard neutron spectrum at the centre of the reactor, the initial k-eff is greatly reduced, and the plutonium concentration increases (due to transmutation of U-238). Subsequently, the fuel is transferred to a lower energy neutron spectrum, where the bred plutonium is burned.

The CANDU-SSATR devised and studied in this thesis was a simple two zone design consisting of 333 and 333A1000 fuel lattices (see Chapter 11), with a fuel burnup of approximately 50000 MWd/MgU (comparable to the expected high burnup in advanced light water off-power fuelled reactors). The analysis has demonstrated the operational feasibility of the CANDU-SSATR concept.

Design optimization is expected to yield a CANDU-SSATR resource utilization comparable to the best achievable with the 14/21 fuel types.

12.9 CLOSING REMARKS

Heavy water reactor technology has been developed with an emphasis on neutron economy to maximize resource utilization. Given the finite global quantities of nuclear fuel, recent trends in all reactor designs have been geared towards this same goal. The neutron economy of the heavy water reactor concept, coupled with the technological, operational, and safety advantages of on-power fuelling and a pressure-tube type design, will make units such as the advanced CANDU-PHW reactors considered in this thesis attractive to utilities world-wide.

The world deserves the best that technology has to offer. It is hoped that the work presented in this thesis will bring us a small step closer towards achieving an improved reactor design for future application. It is one step of many, but God willing, we shall succeed.

APPENDIX A

CONTRIBUTION OF VARIOUS ISOTOPES TO THE VOID REACTIVITY EFFECT IN 37 AND 30(37) ELEMENT FUEL

A.1 INTRODUCTION

The 30(37) element, carbon core, enriched fuel bundle exhibits a markedly reduced coolant void reactivity in comparison with the natural nominal CANDU-600 37 element fuel bundle. This difference in behaviour is evident in the data shown in Table A-1, in which results of the WIMS-CRNL (Donnelly, 1986) simulations conducted for the two fuel designs are compared. The two WIMS-CRNL models considered were 37-0.72-28.575-6.4478 and 30(37)-1.3-25-6.4478-CC-EZ. (Refer to Chapter 7 for the naming convention.)

In order to characterize the contribution of various nuclides to the void reactivity phenomenon, and thereby determine the reasons for the burnup dependence of this system parameter, the void effect due, individually, to a number of nuclear species within the reactor fuel was investigated using the WIMS-CRNL code.

A.2 ANALYTICAL METHODOLOGY

The infinite multiplication factor can be expressed as:

$$k_\infty = P/L \qquad \text{(A.2-1)}$$

where P is the neutron production rate and L, the loss rate due to absorption.

The reactivity is given by:

$$\rho = (k_\infty - 1)/k_\infty = (P - L)/P \qquad \text{(A.2-2)}$$

Fuel Burnup (MWd/MgU)	Effective Multiplication Factor		Void Reactivity (mk)	
	37-NATNOM*	30(37)-1.3**	37-NATNOM*	30(37)-1.3**
0	1.08401	1.32123	16.61	5.23
105	1.03937	1.26335	17.42	5.68
525	1.03753	1.25211	16.49	5.64
5248	0.98804	1.15931	12.77	4.82
10496	0.91634	1.05337	11.84	4.23
15745	0.86792	0.96038	10.99	2.38
20993	0.83969	0.89334	10.49	1.30
26241	0.82166	0.85237	10.28	-0.19
31489	0.80827	0.82782	10.24	-1.05
36737	0.79721	0.81171	10.23	-1.60

* Model: 37-0.72-28.575-6.4478 (NATNOM)
** Model: 30(37)-1.3-25-6.4478-CC-EZ (30(37), 1.3 a/o U-235)

Table A-1 WIMS-CRNL Results for 37 and 30(37) Element Fuel

and hence the change in system reactivity upon voiding is given by:

$$\Delta\rho = (P\text{-}L)/P - (P_o - L_o)/P_o \qquad \text{(A.2-3)}$$

where the subscript "o" refers to the situation with coolant and the unsubscripted parameters refer to the situation after voiding.

If only one of the many nuclear species present is considered, then its contribution to the entire system void reactivity is given by:

$$\Delta\rho_i = (P_i/P - P_{io}/P_o) + (-L_i/P + L_{io}/P_o) \qquad \text{(A.2-4)}$$

where P_i is the neutron production rate due to fissioning of species i, and L_i is the neutron absorption rate in species i. Again, the subscript "o" refers to the unvoided case.

The two bracketed quantities on the right hand side of Eq. A.2-4 are referred to as the production effect and the absorption effect, respectively. The components can be further divided into two neutron energy groups (group 1, with energies above 0.625 eV, and group 2 with energies below 0.625 eV). That is:

$$\begin{aligned}\Delta\rho_i = {} & (P_{i1}/P - P_{i1o}/P_o) + (P_{i2}/P - P_{i2o}/P_o) \\ & + (-L_{i1}/P + L_{i1o}/P_o) + (-L_{i2}/P + L_{i2o}/P_o)\end{aligned} \qquad \text{(A.2-5)}$$

where the subdivision between groups 1 and 2 is evident. The four sets of bracketed quantities on the right hand side of Eq. A.2-5 are identified as the fast production, thermal production, fast absorption, and thermal absorption effects, respectively.

A.3 RESULTS

Reaction rate edits (Donnelly, 1986) from WIMS-CRNL simulations were conducted for the following nuclides:

U-235, U-238, Np-239, Pu-239, Pu-240, Pu-241, and Pu-242.

A FORTRAN computer program, RHOVOID, was prepared to process the data according to Eq. A.2-4 and A.2-5.

The results are displayed graphically in Fig. A-1 through A-14, where for both fuel designs, the individual reactivity contributions for five of the seven nuclides considered are presented. To minimize confusion, data for Np-239 and Pu-242 are not included in the plots since their contribution to the void reactivity was found to be relatively minimal at all burnups. Fig. A-7 and A-14 depict the total reactivity contribution, $\Delta\rho_i$, due to each of the other five nuclear species considered.

A.4 DATA INTERPRETATION

The data presented in Fig. A-1 through A-14 are for five nuclides only. In the WIMS-CRNL model, the fuel itself contains 48 separate materials (fission products, actinides, etc.). Further, changes in the absorption rate in the fission products, coolant, moderator, and other lattice cell materials also contribute to the void effect. There is also a neutronic leakage component to the void effect.

The results of this analysis (Fig. A-1 to A-14) indicate that indeed there exists a complex interaction between the various materials present in the fuel mix with respect to the void reactivity effect. No one component can be considered in isolation. As the nuclide mix and distribution changes in the bundle with burnup, the flux spectrum and distribution is affected, and the contribution to the void reactivity of individual nuclear species is altered.

Despite the differences in the magnitude of the various contributing effects noted in comparing the two fuel designs, several clear trends are evident in both of the fuel lattices. From Fig. A-7 and A-14, it can be seen that in both designs the largest contribution to the void reactivity effect is due to U-238. The fast production effects (Fig. A-3, A-10) and fast absorption effects (Fig. A-5, A-12) in U-238 are positive and relatively burnup independent in both cases. (Recall that the fast fission rate in U-238 is enhanced when the slowing down effect of the coolant is removed.) The

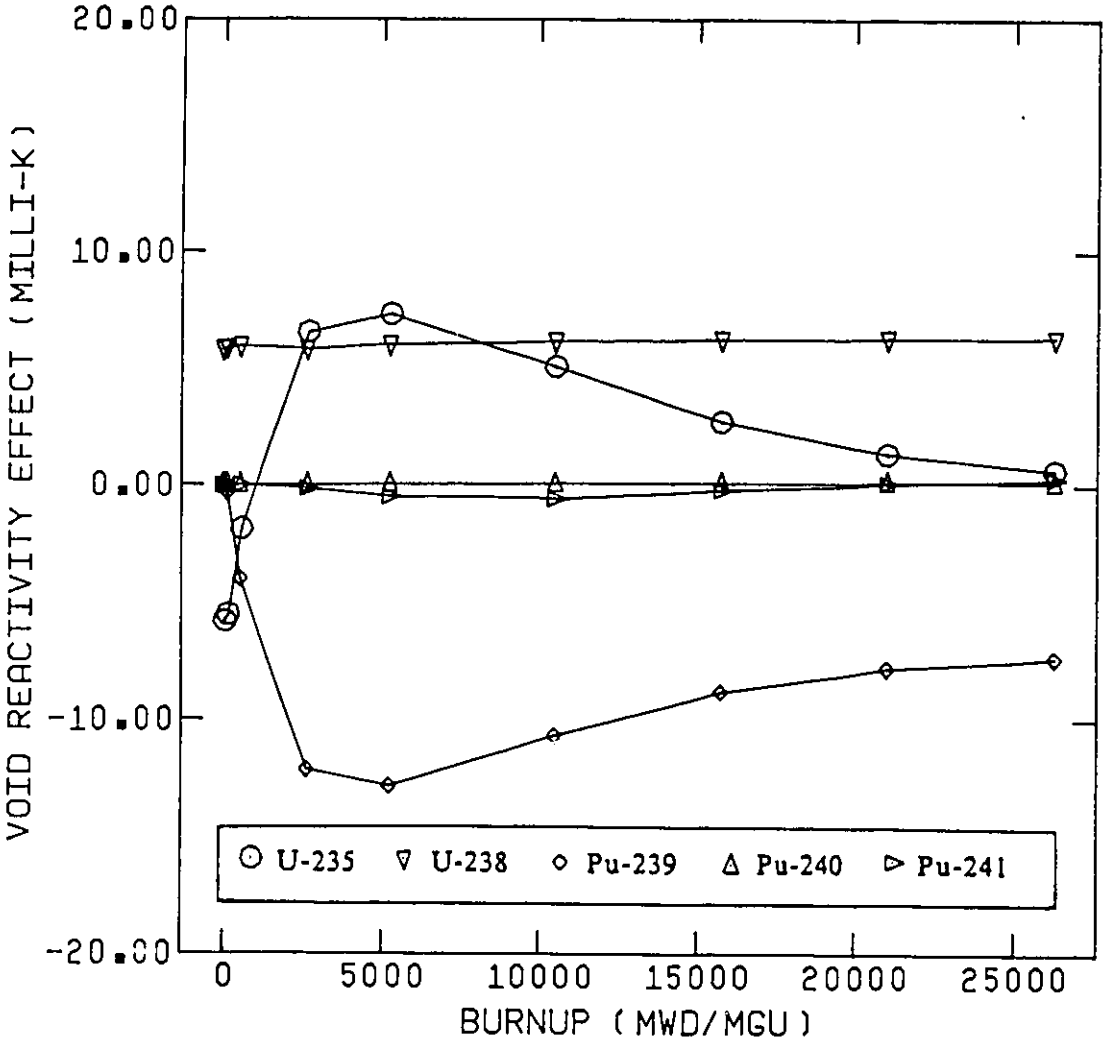

Figure A-1 37 Element NATNOM Production Effect

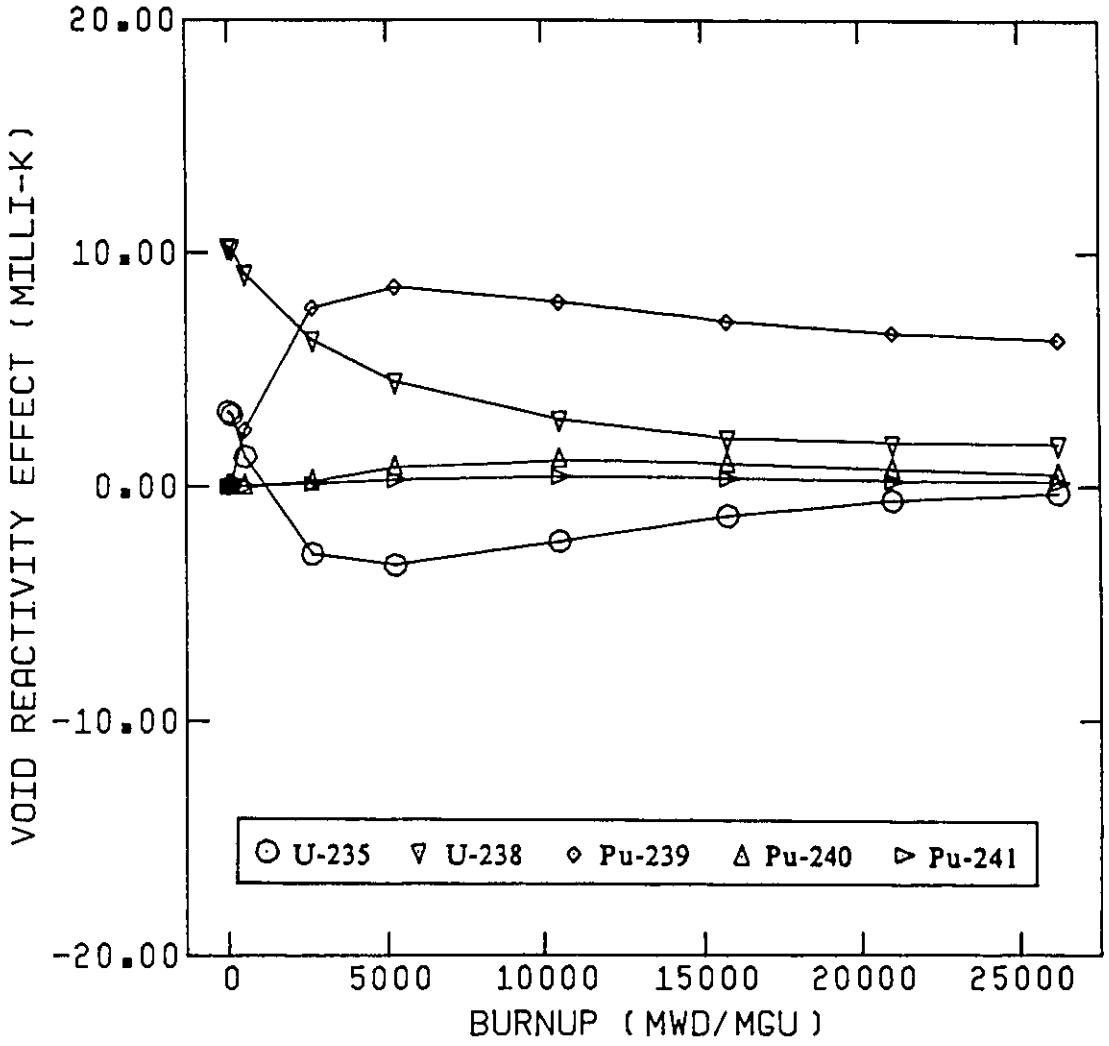

Figure A-2 37 Element NATNOM Absorption Effect

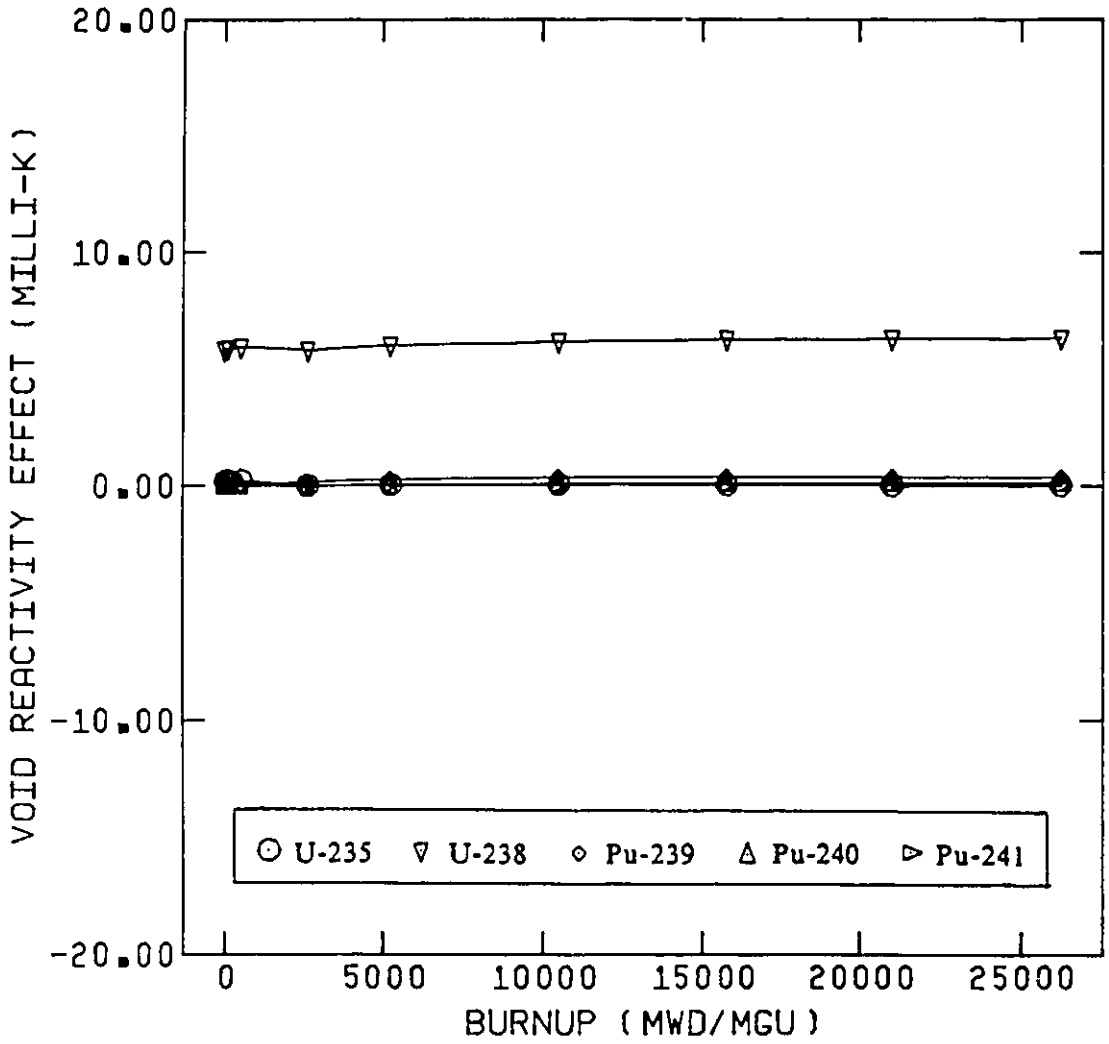

Figure A-3 37 Element NATNOM Fast Production Effect

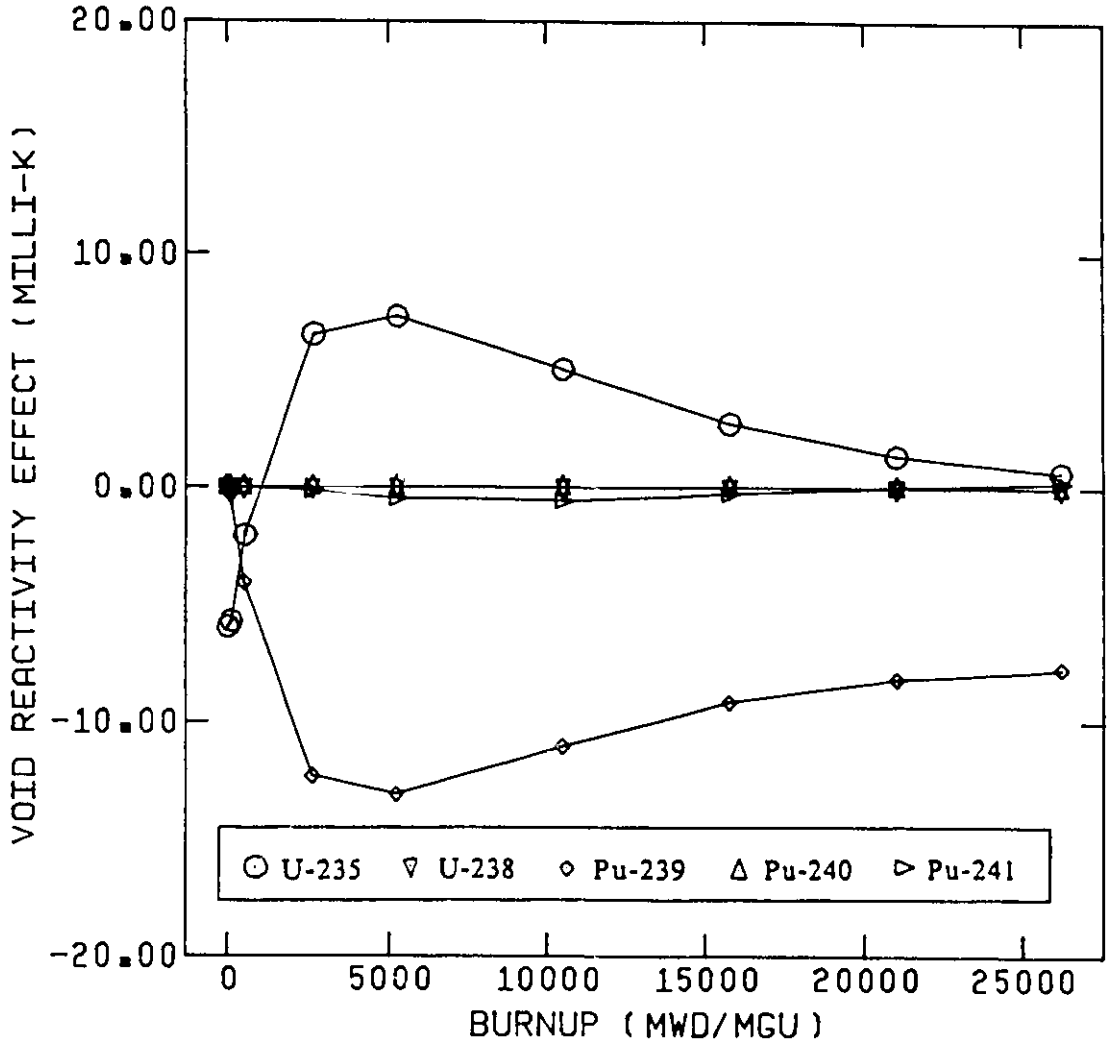

Figure A-4 37 Element NATNOM Thermal Production Effect

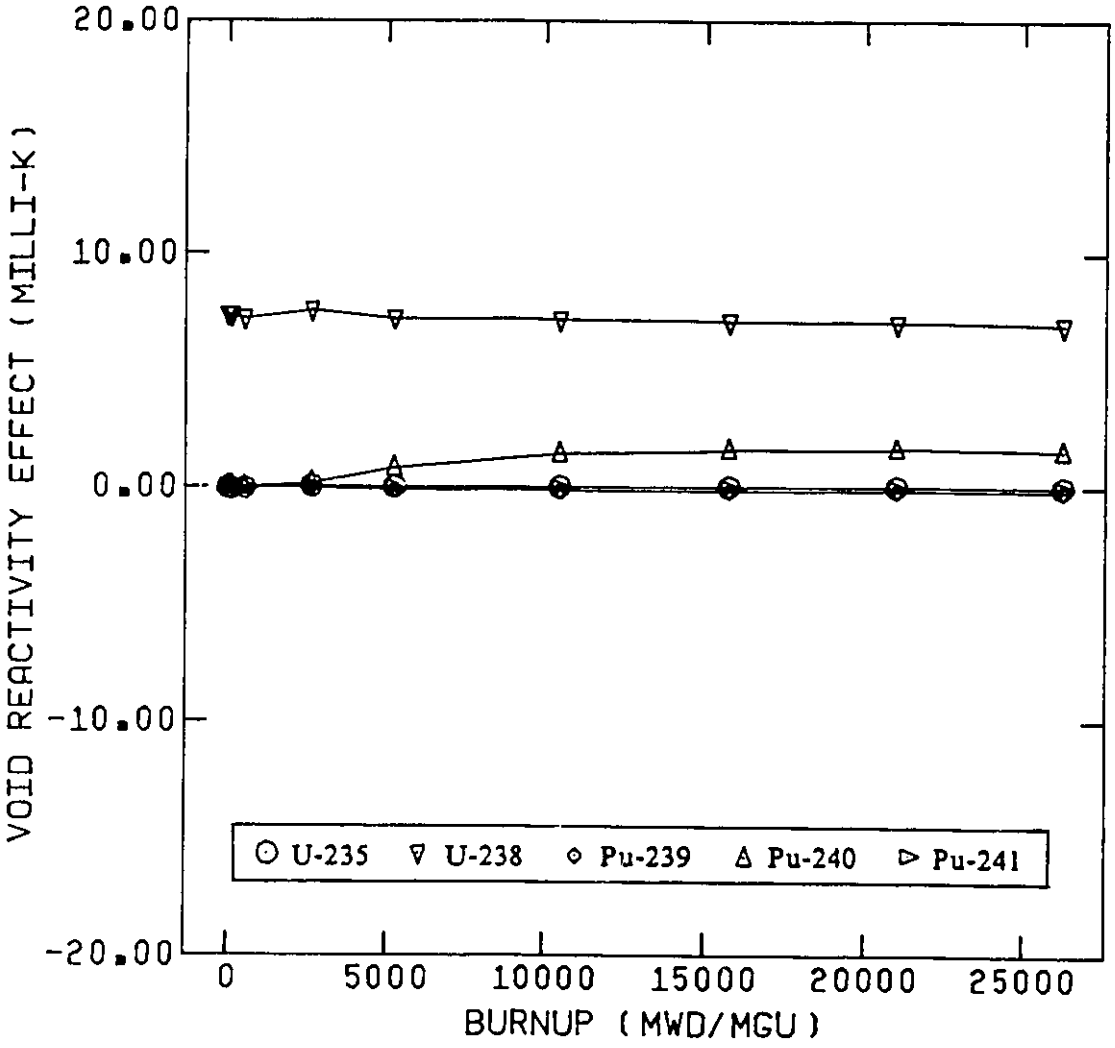

Figure A-5 37 Element NATNOM Fast Absorption Effect

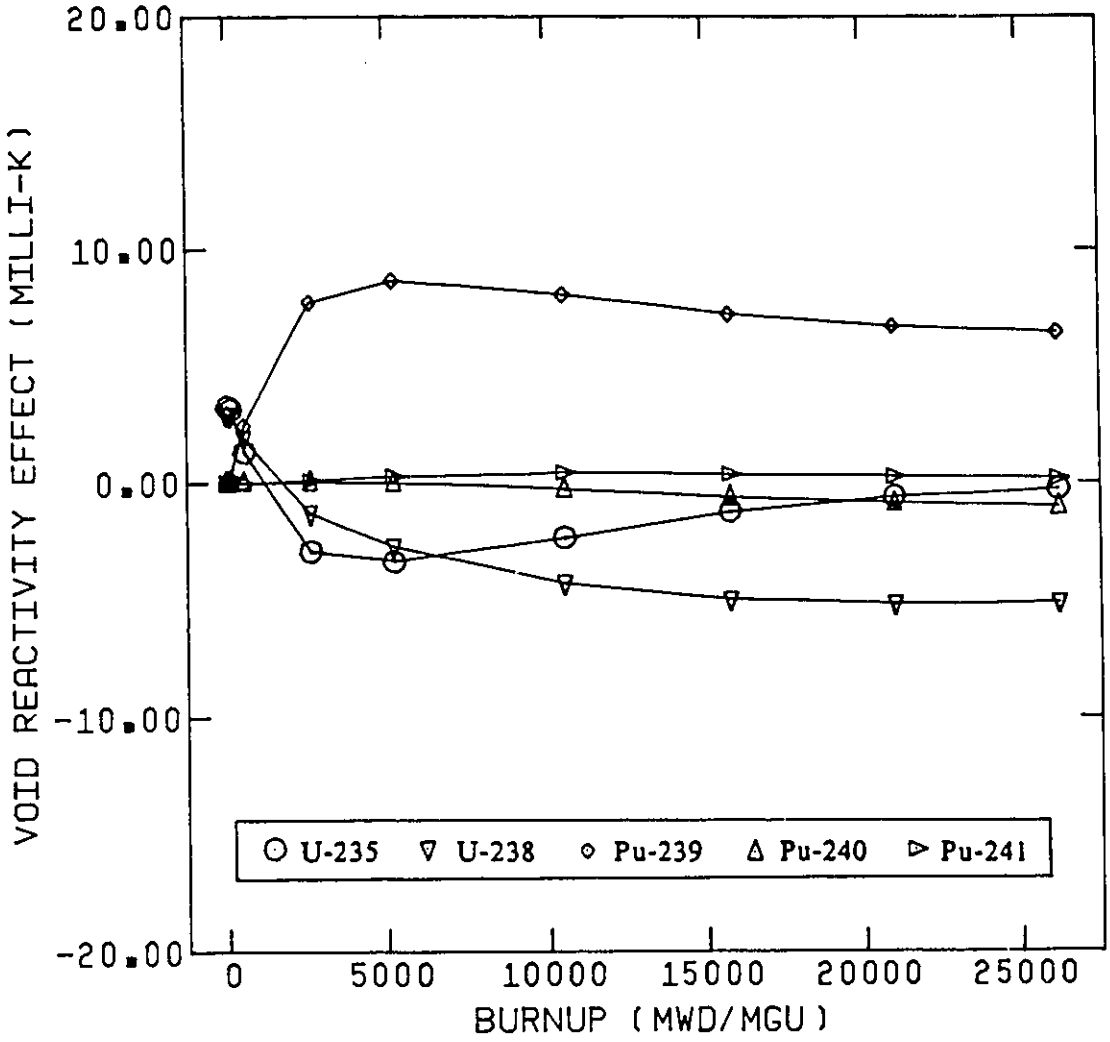

Figure A-6 37 Element NATNOM Thermal Absorption Effect

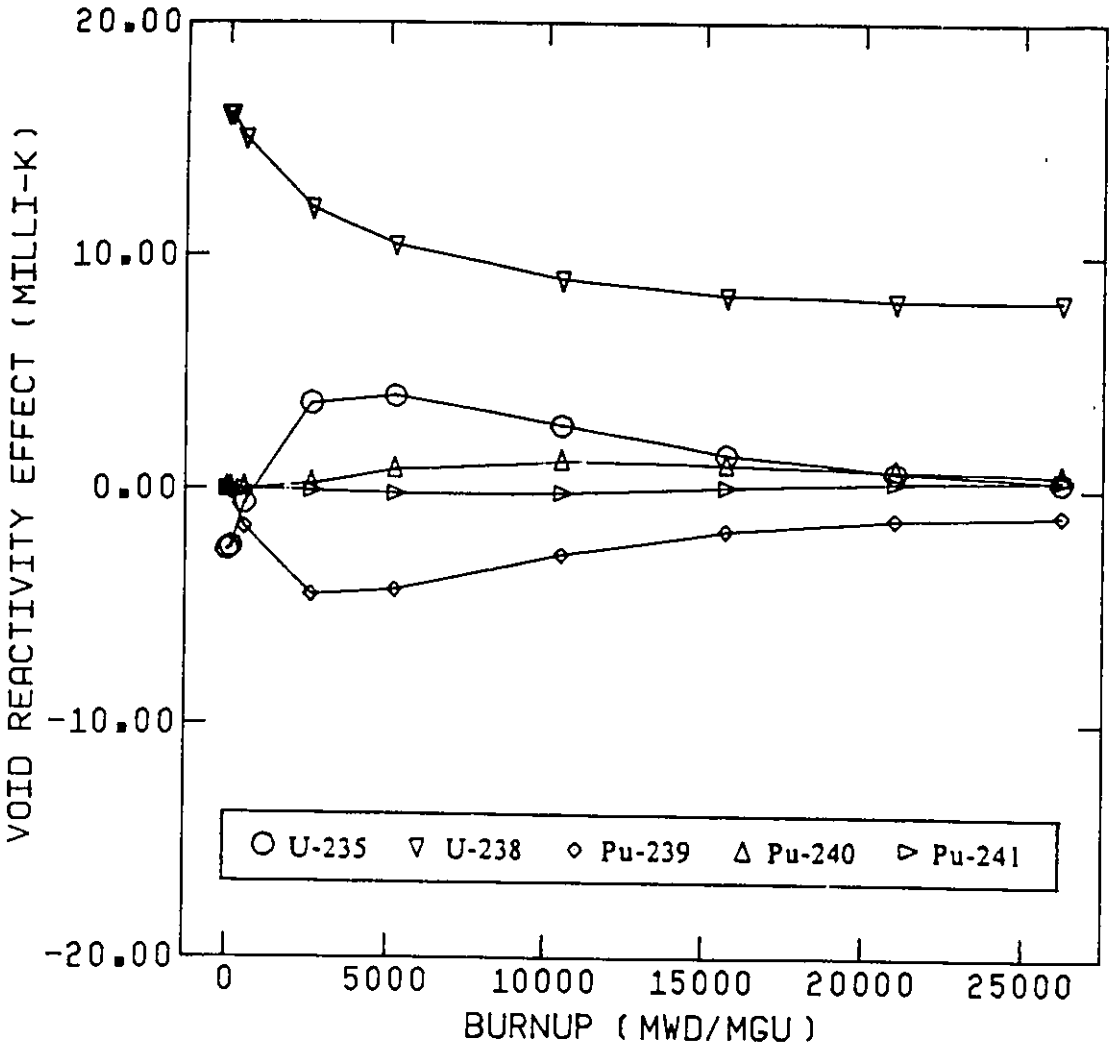

Figure A-7 37 Element NATNOM Total Reactivity Effect

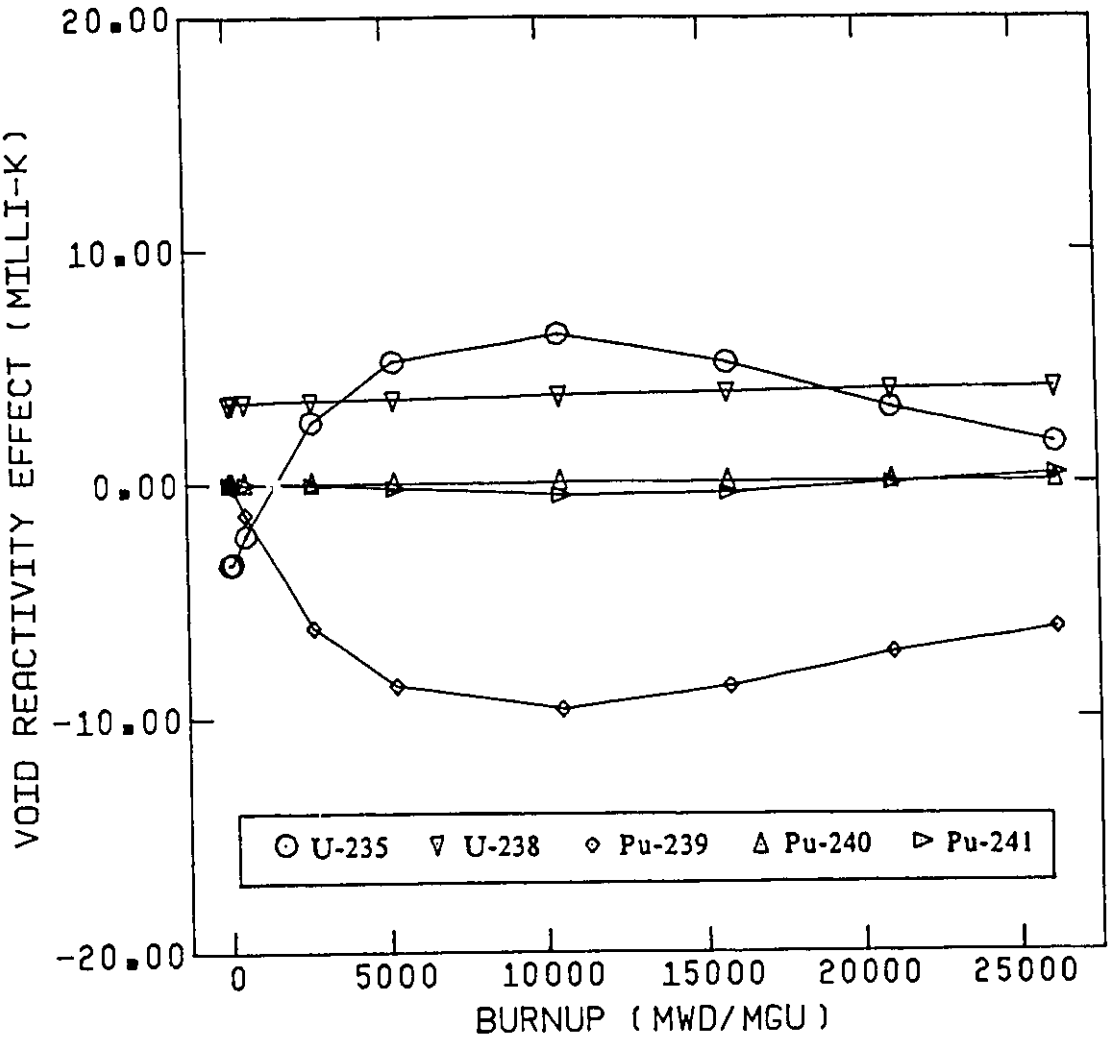

Figure A-8 30(37)-1.3-25-6.4478-CC Production Effect

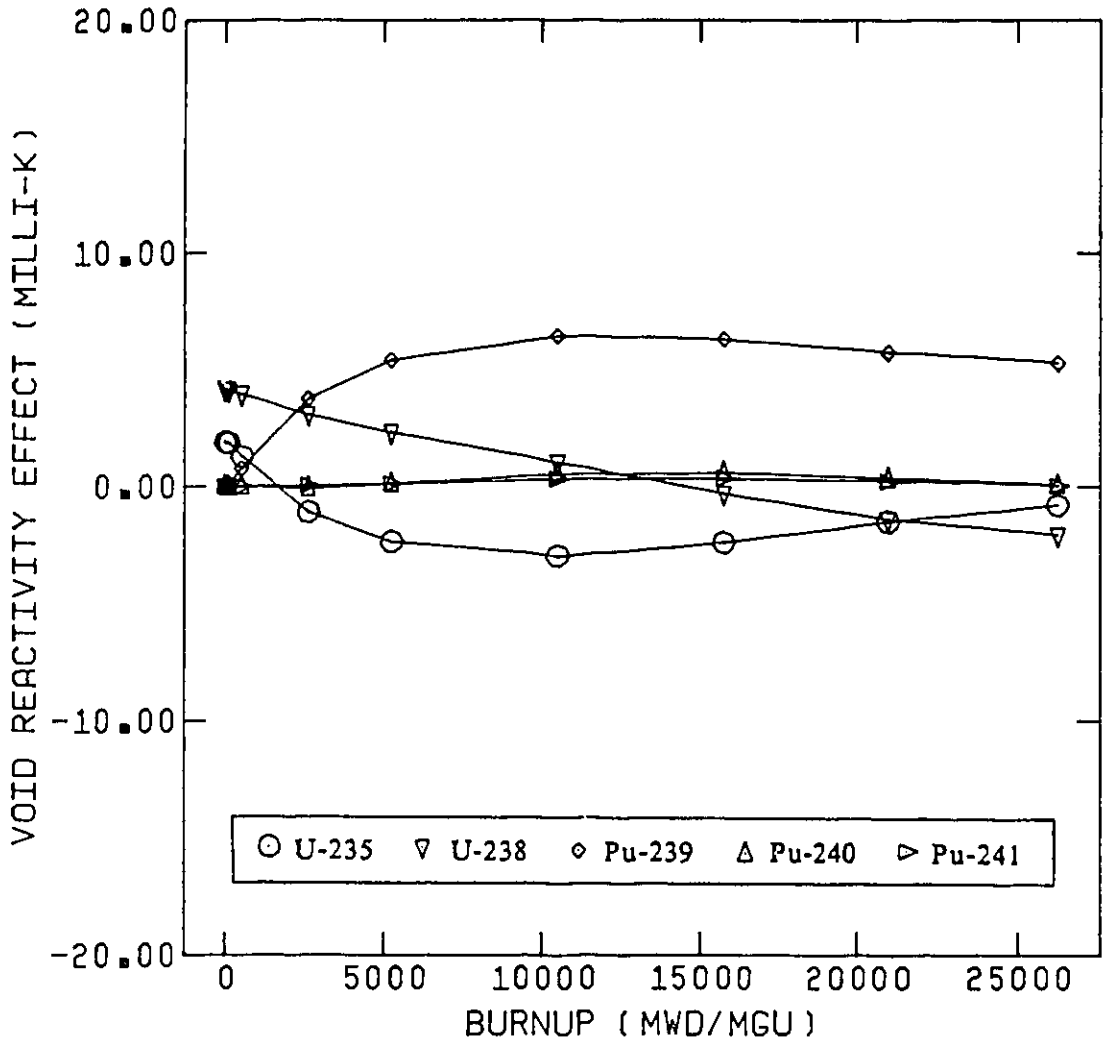

Figure A-9 30(37)-1.3-25-6.4478-CC Absorption Effect

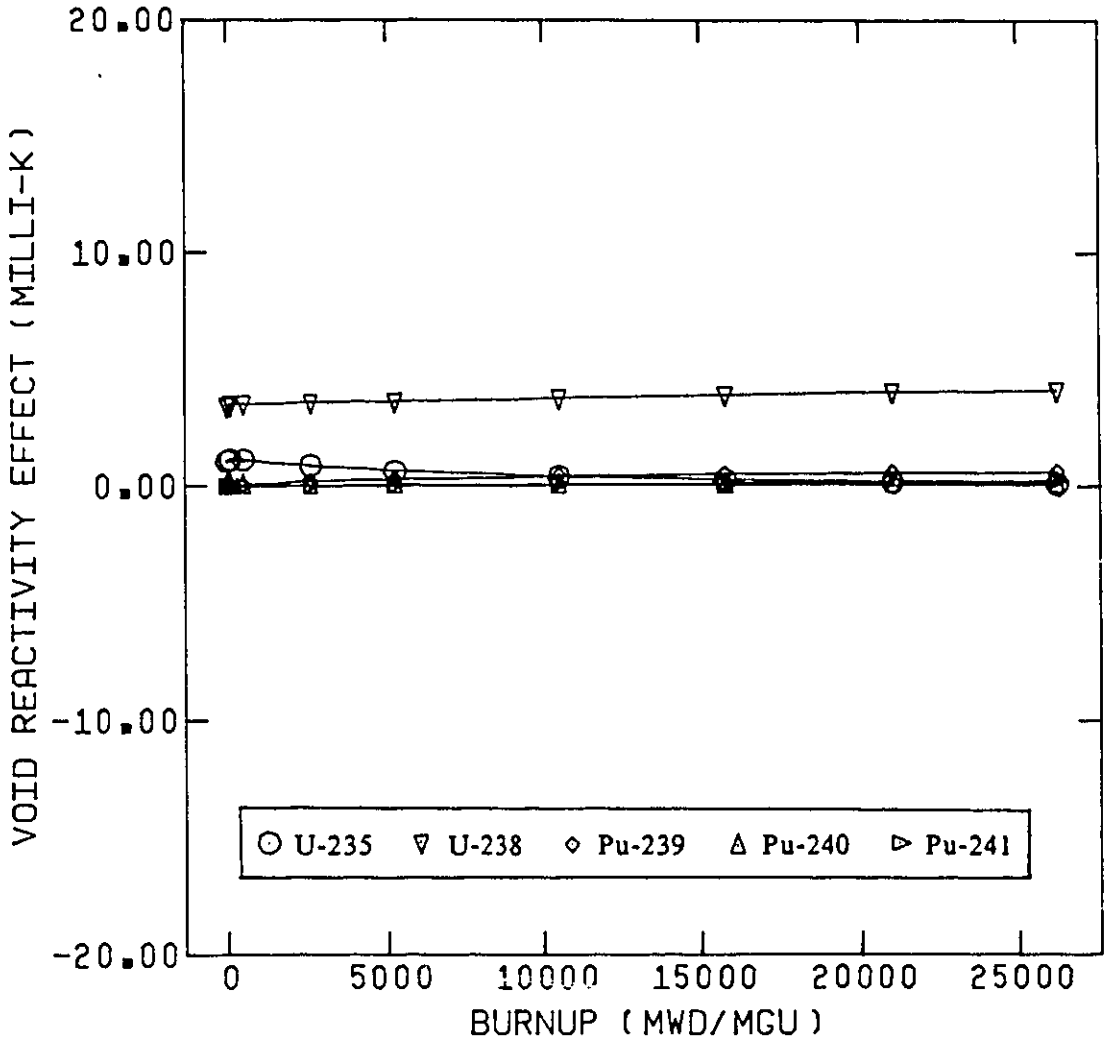

Figure A-10 30(37)-1.3-25-6.4478-CC Fast Production Effect

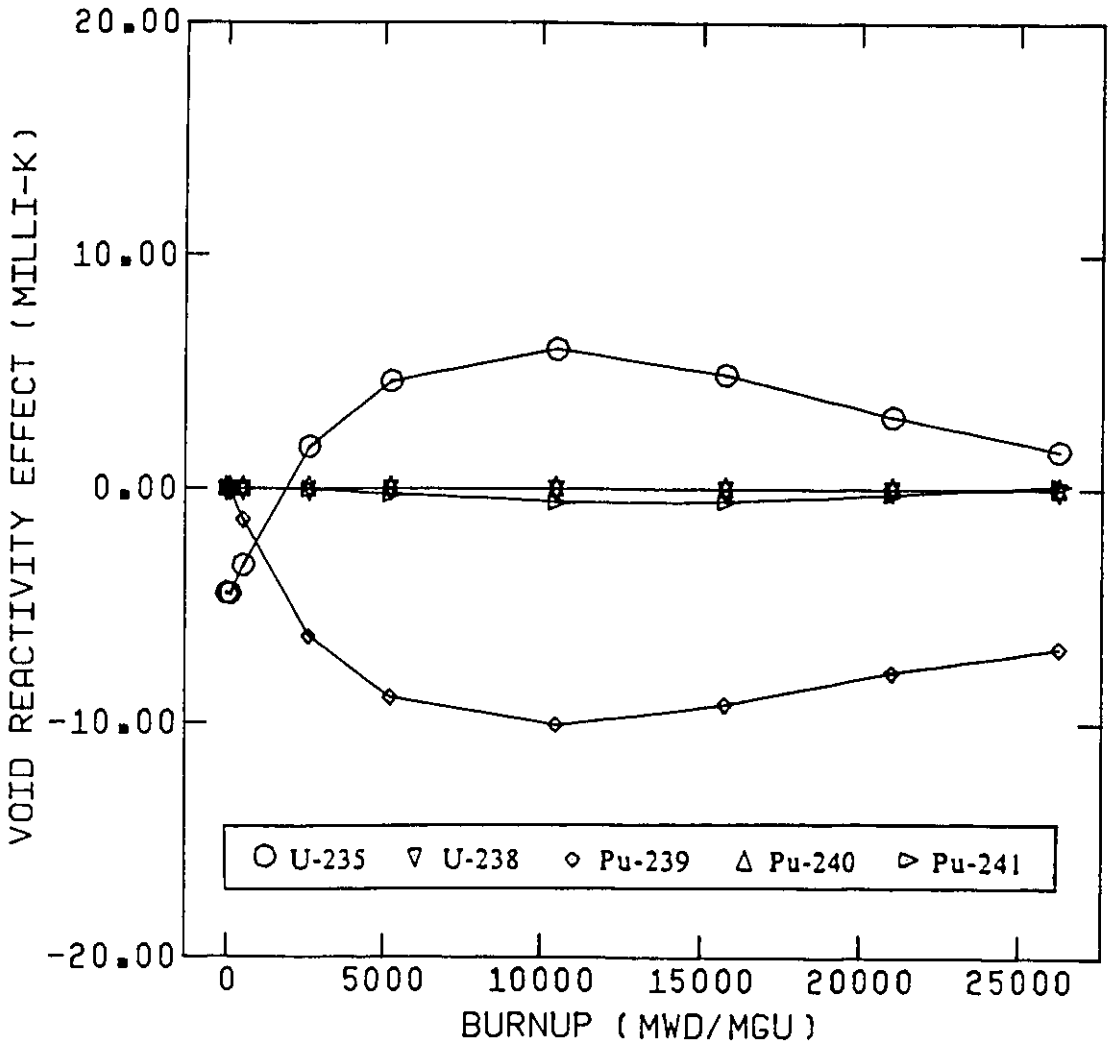

Figure A-11 30(37)-1.3-25-6.4478-CC Thermal Production Effect

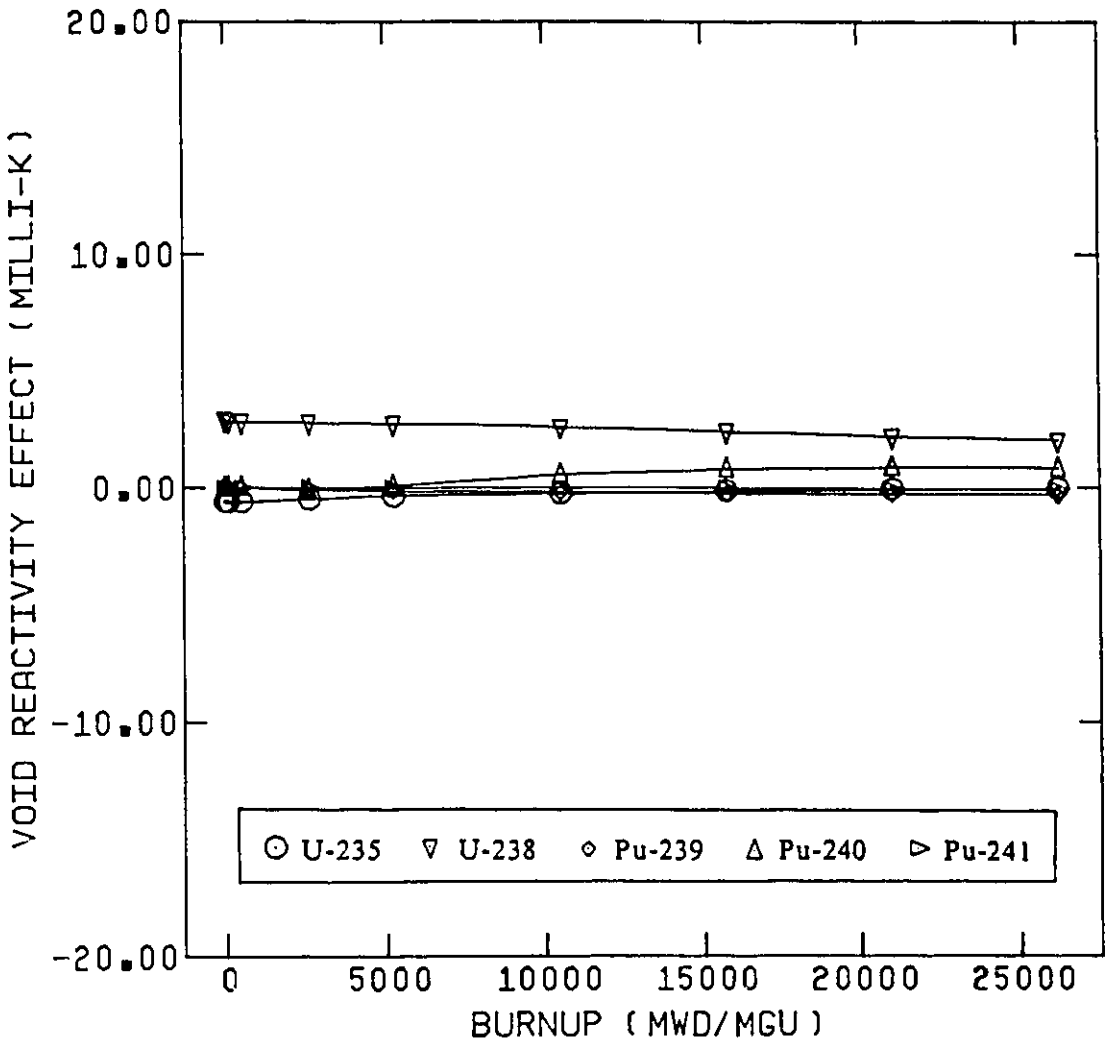

Figure A-12 30(37)-1.3-25-6.4478-CC Fast Absorption Effect

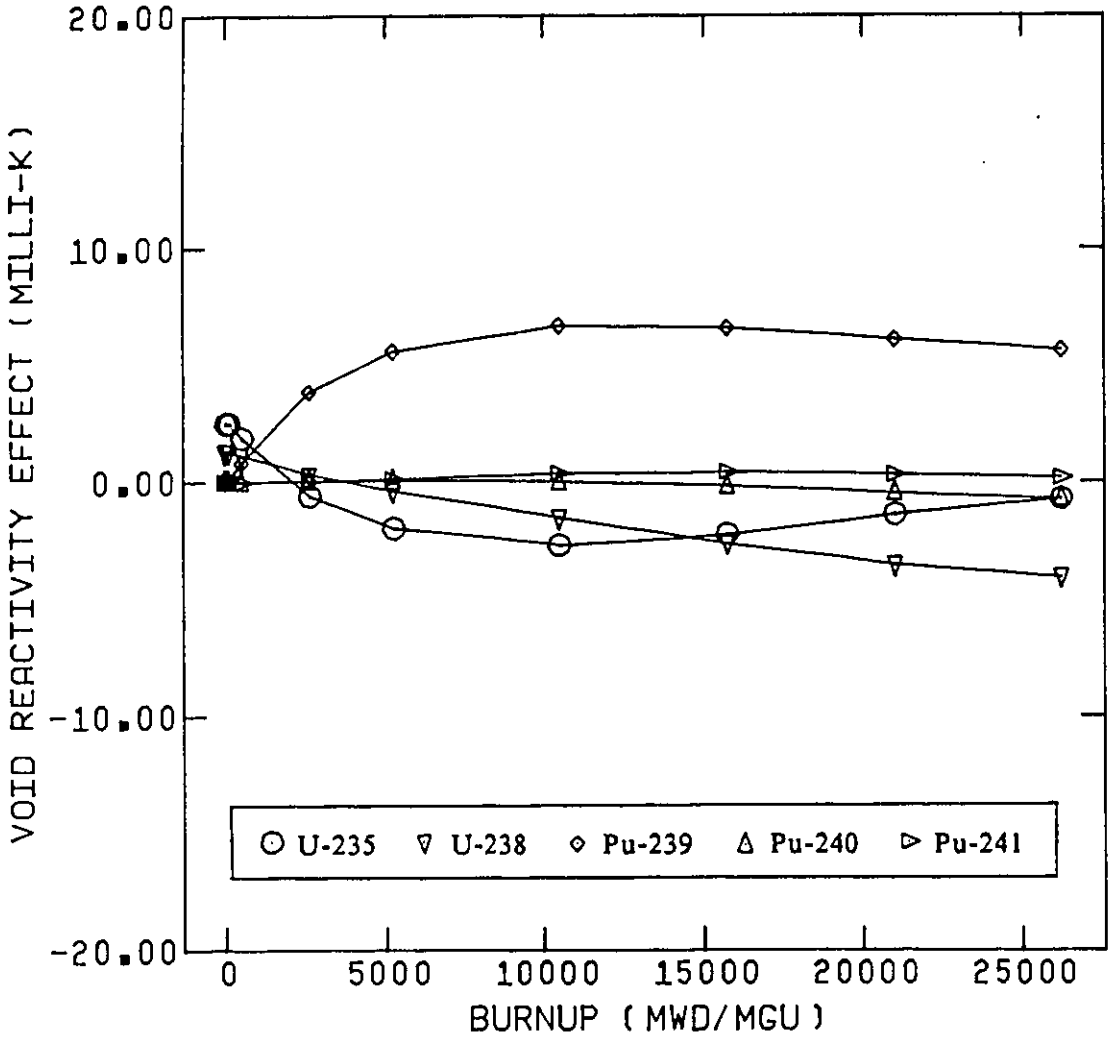

Figure A-13 30(37)-1.3-25-6.4478-CC Thermal Absorption Effect

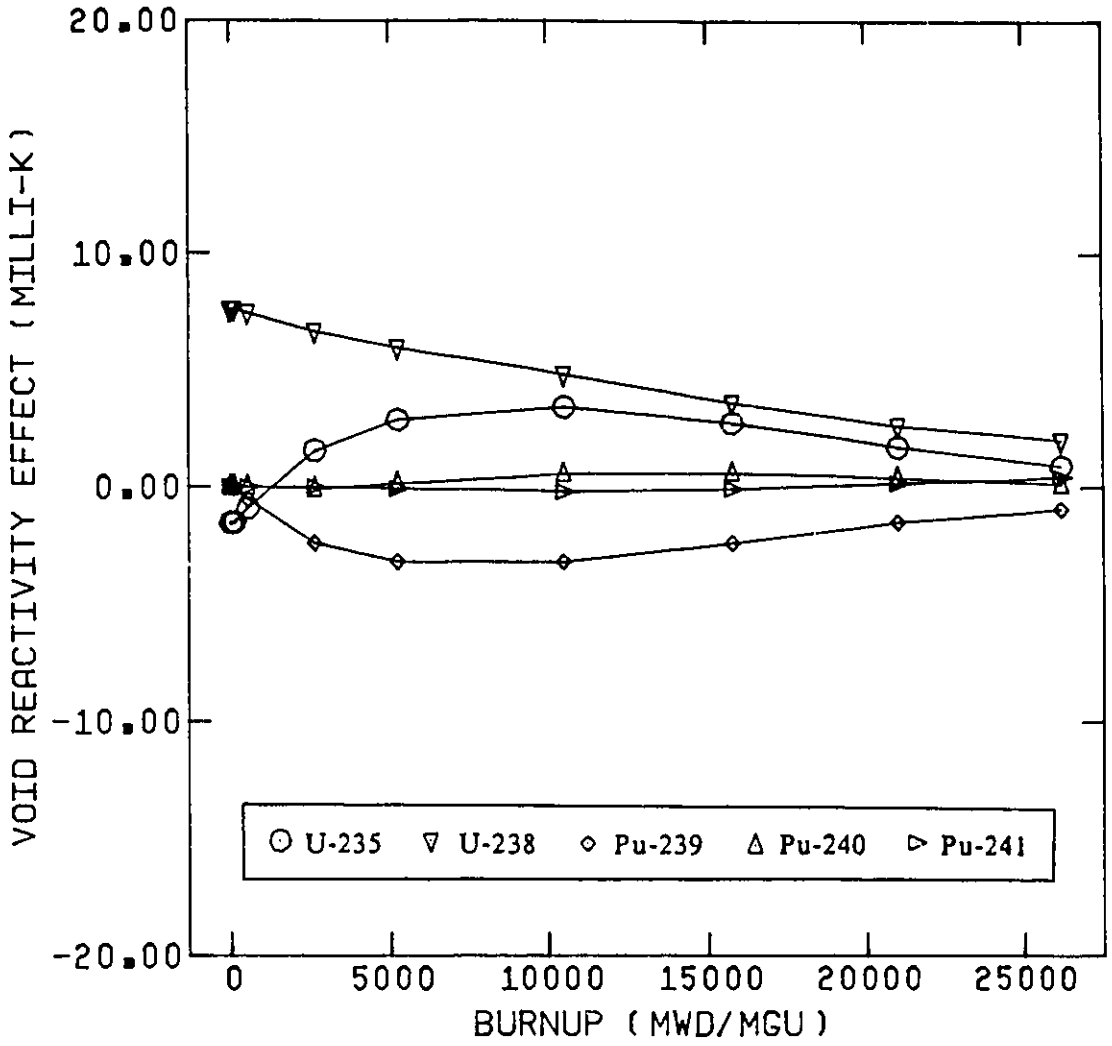

Figure A-14 30(37)-1.3-25-6.4478-CC Total Reactivity Effect

thermal production effect in U-238, is approximately zero. The thermal absorption effect in U-238 is initially positive but becomes negative with increasing fuel burnup. The net effect of the changes in the reaction rates in U-238, is a positive void reactivity contribution which decreases with irradiation.

The contribution to the void reactivity of changes in the reaction rates in U-235 is initially negative, though it quickly becomes positive peaking at approximately 4000 MWd/MgU in the 37 element case and 10000 MWd/MgU in the 30(37) element case (Fig. A-7 and A-14, respectively). Beyond this point the contribution decreases asymptotically towards zero. The thermal production effect, tempered somewhat by the thermal absorption effect, dictates the overall behaviour.

The contribution of Pu-239 is almost the mirror image of the U-235 effect, reflected about the zero void reactivity line. The production effect in Pu-239 is maximized in the harder thermal neutron spectrum in the vicinity of the fuel when the coolant is present. The opposite is true for U-235, and hence the difference in noted response.

The contributions of Pu-240 and Pu-241 are relatively minor in comparison with the U-235, U-238, and Pu-239. The Pu-240 effect is positive resulting from a positive fast absorption effect, and tempered by a negative thermal absorption effect.

It is important to note that the contribution of a particular nuclide to the void reactivity is also dependent on the ring of elements considered. For example, in the 30(37) element case, the U-235 thermal production void reactivity effect per atom of U-235 within the inner ring of fuel elements is positive and monotonically increasing with fuel burnup. In the outer ring, the contribution is initially negative, though also monotonically increasing, becoming positive at a burnup of approximately 15000 MWd/MgU. As the burnup progresses, the concentration of U-235 diminishes, though at a faster rate in the outer ring (higher thermal neutron flux) than in the inner ring. This combination of effects, strongly influenced by the neutronic behaviour of the total dynamic composition of the fuel, results in the complex burnup dependence shown in Fig. A-11, and reflected again in the total U-235 response

shown in Fig. A-14.

This analysis indicates that the 30(37) element design results in a reduction in the contribution to the void reactivity effect of all seven nuclides considered. The most substantial reduction is in the U-238 contribution. This can be attributed to the reduction in the magnitude of the positive fast production and fast absorption effects, resulting from the removal of the central two element rings where the fast flux is at a maximum.

APPENDIX B

DETERMINATION OF THE REQUIRED ENERGY GROUP STRUCTURE

B.1 INTRODUCTION

To determine the required energy group structure for simulating heavy water moderated reactors with enriched fuel, various simulations were conducted using the NATNOM fuel design (standard CANDU-600 fuel bundle) and the 30/37, 1.3 a/o U-235, air core bundle design introduced in Chapter 7 (25 cm LP, 7 cm calandria tube inner radius, 1.71 cm radius central air core surrounded by a zirconium tube of thickness 0.4343 cm).

The study also included an examination of the effect of varying the lattice physics code used in determining lattice cell properties. This allowed for an assessment of acceptable deviations.

B.2 CALCULATIONAL METHODOLOGY

The analysis proceeded as follows:

(i) The computer code, TESHOM (Griffiths, 1978), was used to set up consistent NATNOM and 30/37 models for the WIMS-CRNL (Donnelly, 1986), POWDERPUFS-V (PPV) (Tin and Loken, 1979), and LATREP (Griffiths, 1983) computer codes, which are the basic lattice physics programs in use for CANDU analysis. These codes were then used to determine lattice physics properties for the two fuel types.

(ii) The 18-energy group structure for the various regions in WIMS-CRNL were compressed to 4 groups and 2 groups using the computer code WIMS-SHETAN (Donnelly, 1985). The computer code, WIMS-FMDP (Donnelly and van Dyk, 1983), was used to convert the WIMS energy structure to the modified two group (M-2) format (Eq 8.2.2-1). Lattice cell properties (M-2 format) were extrapolated

directly from the hardcopy output of the PPV and LATREP computer codes.

(iii) A one-quarter reactor face, half axial length reactor core model was devised. This model, and the fuel properties, were input to the computer code MAPDDT (Donnelly, 1982), which, in turn, was used to produce input data sets for the three dimensional, multigroup diffusion-burnup code, 3DDT (Vigil, 1970). This code was used to calculate power distributions and effective multiplication factors for the reactor model with the various input lattice properties.

(iv) Comparisons were made to determine the effect of the energy group structure and lattice physics code employed. Parameters of interest were the effective multiplication factor and power distribution.

B.3 LATTICE PHYSICS CODES

The three lattice physics codes used in the analysis differ in methodology, complexity, and computational cost.

B.3.1 WIMS-CRNL

WIMS-CRNL performs a multigroup transport calculation for a reactor cell in up to 69 groups with full two-dimensional flexibility. The discrete ordinates (DSN) option (Donnelly, 1986) of WIMS-CRNL was used in this analysis. With this option, one-dimensional annular geometry is utilized and clusters of fuel pins are smeared into the appropriate annular geometry. The main transport calculation was performed with 18 neutron energy groups. These were compressed for use in 3DDT. The 18 group structure used in WIMS-CRNL is the default provided by the TESHOM code. This structure was compressed to four groups to provide a single fast group, a single resonant group, and two thermal groups according the division set out by Phillips (1982). A two group structure was also devised with the group division occurring at 0.625 eV (the standard WIMS-CRNL dividing point). The WIMS-CRNL energy group structure

used in the various cases is shown in Table B-1.

B.3.2 LATREP

LATREP utilizes the classical four-factor formulation (Griffiths, 1983). All neutron distributions are calculated using directional current collision probability theory in annular geometry. The group structure is much simpler than in WIMS-CRNL, and various theoretical and numerical approximations and empiricisms are introduced to make the problem more tractible. This code is no longer used extensively.

B.3.3 POWDERPUFS-V

The POWDERPUFS-V code (Tin and Loken, 1979) is the most computationally inexpensive of the three lattice physics codes considered, though it contains more simplifications and makes extensive use of empiricisms to attain this feature. The lattice cell is divided into three regions: fuel, annulus, and moderator. The code utilizes the Westcott cross section convention and employs the conventional four factor formula. The many recipes and empiricisms in the code reduce the flexibility of application. The authors recommend caution in the use of the code to simulate the behaviour of enriched fuels (Tin and Loken, 1979).

B.4 3DDT REACTOR MODEL

The quarter-face, one half axial length 3DDT reactor model is depicted in Figures B-1 and B-2. Lattice cell and reflector properties were obtained from the various lattice cell codes for both fuel types considered. The central adjuster region was simulated by adding an incremental thermal absorption cross section (3×10^{-4} cm^{-1}) to the nominal thermal absorption cross section in the affected lattice cells.

The 3DDT code uses a first order finite difference approximation to the neutron flux spatial derivative. Mesh spacings are as shown in

Neutron Energy (eV)	WIMS-CRNL Energy Group Structure (69 Group)	18 Group Structure	4 Group Structure	2 and M-2 Group Structure
5530 - 1E7	1 - 15	1 - 4	1	1
4.0 - 5530	16 - 27	5 - 8	2	1
0.625 - 4.0	28 - 45	9 - 11	3	1
0.0 - 0.625	46 - 69	12 - 18	4	2

Note: Data given are group identifiers.

Table B-1 Energy Group Structure: WIMS-CRNL Cases

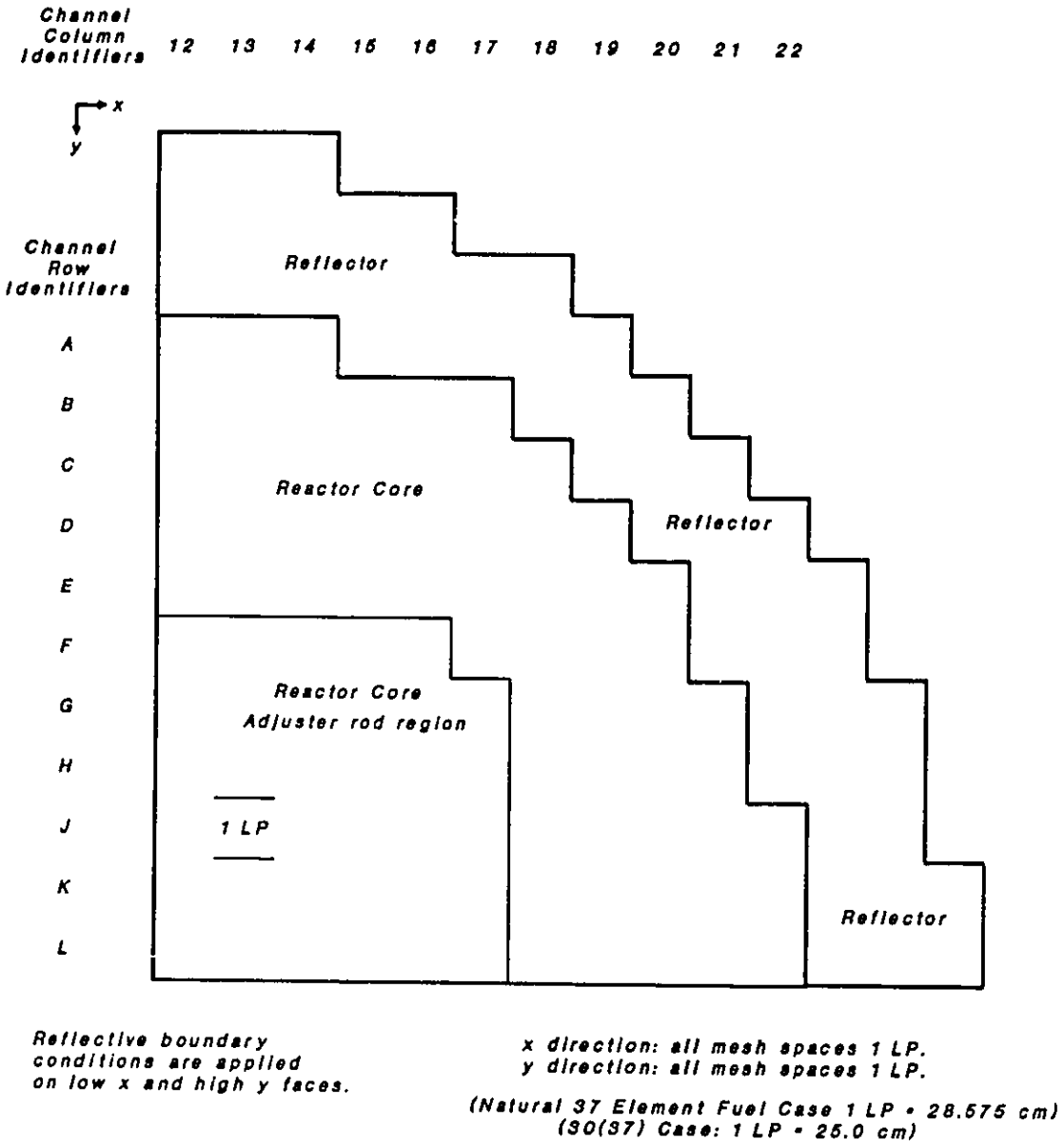

Figure B-1 3DDT Model (x-y View)

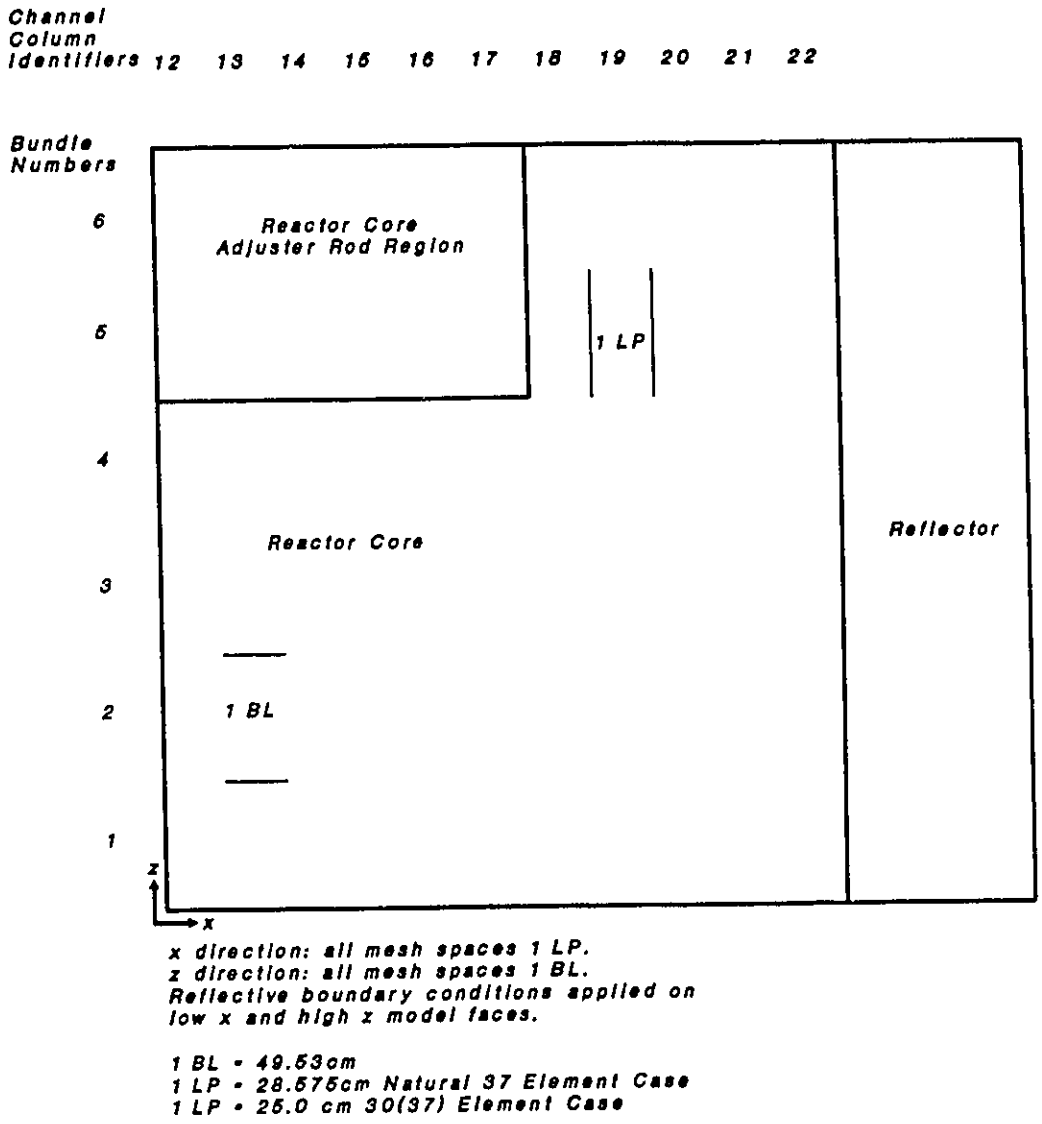

Figure B-2 3DDT Model (x-z View)

Figures B-1 and B-2. In all cases, fresh fuel conditions were assumed.

B.5 RESULTS

B.5.1 Lattice Physics Calculations

Infinite multiplication factors for fresh fuel conditions as determined for the two fuel types with the various lattice physics codes are provided in Table B-2. As can be seen, the infinite multiplication factors for the NATNOM fuel vary within a 5.8 mk range. The enriched 30/37 results are closer, with the WIMS-CRNL and PPV results differing by only 1.1 mk, and all data are within a 2.9 mk range. The change in infinite multiplication factor between the NATNOM and 30/37 fuels ranges from 132.2 mk for the LATREP results to 124.8 mk as calculated using PPV.

B.5.2 Core Physics Calculations

The material properties required for input to the 3DDT core physics code are provided in Tables B-3 to B-6. The data were derived from the lattice physics results as described previously. The data are presented in different forms for different cases, as the 3DDT pre-processor, MAPDDT (Donnelly, 1982), permits the use of two separate input formats for the convenience of the user.

Properties are provided for both the fuel and reflector regions. As noted in Section B.4, the properties for the adjuster region were the same as for the fuel region with the exception being that the thermal absorption cross section in the adjuster region was incremented by 3×10^{-4} cm^{-1} to simulate the effects of the devices.

The effective multiplication factors (k-eff) for the various cases as determined with 3DDT are shown in Table B-7.

In the NATNOM study, the WIMS-CRNL cases yielded lower k-eff values than the PPV code. The LATREP k-eff value was between the other two. This is consistent with the findings in the lattice physics analysis (Table B-2).

Case	Infinite Multiplication Factor		
	WIMS-CRNL	LATREP	PPV
NATNOM	1.12146	1.12314	1.12879
30/37	1.31580	1.31902	1.31391

Table B-2 Infinite Multiplication Factors

Property (cm^{-1})	4 Group Structure				2 Group Structure	
	i=1	i=2	i=3	i=4	i=1	i=2
FUEL REGION						
Σ_f	5.471E-4	1.526E-4	2.553E-4	1.661E-3	3.462E-4	1.661E-3
Σ_a	1.244E-3	2.293E-3	9.326E-4	3.537E-3	1.660E-3	3.537E-3
$\nu\Sigma_f$	1.435E-3	4.003E-4	6.696E-4	4.358E-3	9.081E-4	4.358E-3
Σ_t	2.412E-1	2.753E-1	2.644E-1	3.709E-1	2.584E-1	3.109E-1
Σ_{t1}	2.190E-1	0.0	0.0	0.0	2.480E-1	5.595E-5
Σ_{t2}	2.098E-2	2.527E-1	3.912E-5	0.0	8.753E-3	3.673E-1
Σ_{t3}	2.331E-7	1.991E-2	1.847E-1	5.595E-5	--	--
Σ_{t4}	3.912E-8	4.305E-4	7.874E-2	3.673E-1	--	--
REFLECTOR						
Σ_f	0.0	0.0	0.0	0.0	0.0	0.0
Σ_a	3.614E-6	1.955E-6	1.260E-5	7.589E-5	1.145E-6	7.589E-5
$\nu\Sigma_f$	0.0	0.0	0.0	0.0	0.0	0.0
Σ_t	2.568E-1	2.628E-1	2.717E-1	3.853E-1	2.616E-1	3.853E-1
Σ_{t1}	2.248E-1	0.0	0.0	0.0	2.502E-1	4.548E-5
Σ_{t2}	3.196E-2	2.394E-1	2.109E-5	0.0	1.136E-2	3.852E-1
Σ_{t3}	3.579E-7	2.290E-2	1.831E-1	4.548E-5	--	--
Σ_{t4}	6.018E-8	4.983E-4	8.863E-2	3.852E-1	--	--

Table B-3 NATNOM Fuel Properties: WIMS-CRNL 4 Group and 2 Group Structures

Property (cm^{-1})	4 Group Structure				2 Group Structure	
	i=1	i=2	i=3	i=4	i=1	i=2
FUEL REGION						
Σ_f	4.563E-4	2.841E-4	5.002E-4	3.194E-3	3.873E-4	3.194E-3
Σ_a	1.029E-3	2.760E-3	1.337E-3	5.611E-3	1.803E-3	5.611E-3
$\nu\Sigma_f$	1.197E-3	7.451E-4	1.312E-3	8.378E-3	1.016E-3	8.378E-3
Σ_t	2.206E-1	2.612E-1	2.487E-1	3.472E-1	2.410E-1	3.472E-1
Σ_{i1}	2.003E-1	0.0	0.0	0.0	2.314E-1	9.427E-5
Σ_{i2}	1.929E-2	2.402E-1	4.367E-5	0.0	7.778E-3	3.415E-1
Σ_{i3}	2.142E-7	1.782E-2	1.759E-1	9.427E-5	--	--
Σ_{i4}	3.594E-8	3.840E-4	7.139E-2	3.415E-1	--	--
REFLECTOR						
Σ_f	0.0	0.0	0.0	0.0	0.0	0.0
Σ_a	3.649E-6	1.933E-6	1.259E-5	7.378E-5	1.004E-6	7.378E-5
$\nu\Sigma_f$	0.0	0.0	0.0	0.0	0.0	0.0
Σ_t	2.567E-1	2.628E-1	2.717E-1	3.811E-1	2.614E-1	3.811E-1
Σ_{i1}	2.254E-1	0.0	0.0	0.0	2.506E-1	7.754E-5
Σ_{i2}	3.132E-2	2.399E-1	2.114E-5	0.0	1.089E-2	3.810E-1
Σ_{i3}	3.514E-7	2.242E-2	1.832E-1	7.754E-5	--	--
Σ_{i4}	5.904E-8	4.872E-4	8.847E-2	3.810E-1	--	--

Table B-4 30/37 Fuel Properties: WIMS-CRNL 4 Group and 2 Group Structures

Model	Material	Energy Group i	Material Property (cm^{-1})					
			Σ_f	Σ_a	$\nu\Sigma_f$	Σ_t	Σ_{1i}	Σ_{2i}
NATNOM	Fuel	1	0.0	1.660E-3	0.0	2.58277E-1	2.480E-1	0.0
		2	1.804E-3	3.537E-3	4.733E-3	3.70837E-1	8.617E-3	3.673E-1
	Reflector	1	0.0	1.145E-6	0.0	2.61431E-1	2.502E-1	0.0
		2	0.0	7.589E-5	0.0	3.85280E-1	1.123E-2	3.852E-1
30/37	Fuel	1	0.0	1.803E-3	0.0	2.40850E-1	2.314E-1	0.0
		2	3.478E-3	5.611E-3	9.124E-3	3.47111E-1	7.650E-1	3.415E-1
	Reflector	1	0.0	1.004E-6	0.0	2.61361E-1	2.506E-1	0.0
		2	0.0	7.378E-5	0.0	3.81074E-1	1.076E-2	3.810E-1

Table B-5 NATNOM and 30/37 Material Properties: WIMS-CRNL Modified 2 Group Format

Lattice Physics Code	Model	Material	Material Property						
			D_1 (cm)	D_2 (cm)	Σ_{a1} (cm^{-1})	Σ_{a2} (cm^{-1})	$\nu\Sigma_f$ (cm^{-1})	Σ_m (cm^{-1})	H^* (10^{-11} kWcm^{2}s)
LATREP	NATNOM	Fuel	1.3356	1.2150	9.749E-4	4.828E-3	6.026E-3	8.742E-3	0.3297
		Reflector	1.2739	1.1290	0.0	1.072E-4	0.0	1.077E-2	0.0
	30/37	Fuel	1.4602	1.4560	1.012E-3	8.430E-3	1.256E-2	7.762E-3	0.5204
		Reflector	1.2675	1.2091	0.0	0.1104	0.0	0.1072	0.0
PPV	NATNOM	Fuel	1.2697	0.9374	7.751E-4	3.729E-3	4.651E-3	7.392E-3	0.2543
		Reflector	1.3138	0.8744	0.0	8.420E-5	0.0	1.015E-2	0.0
	30/37	Fuel	1.3587	1.0204	0.8554	5.966E-3	8.869E-3	6.510E-3	0.3701
		Reflector	1.3138	0.8744	0.0	8.420E-5	0.0	1.015E-2	0.0

* The H factor is the bundle power to thermal cell flux ratio.

Table B-6 NATNOM and 30/37 Material Properties: PPV and LATREP

Model	Lattice Physics Code (Group Structure)				
	WIMS-CRNL (4 Group)	WIMS-CRNL (2 Group)	WIMS-CRNL (M-2 Group)	LATREP (M-2 Group)	PPV (M-2 Group)
NATNOM	1.07250	1.07276	1.07084	1.07450	1.07507
30/37	1.26640	1.26698	1.26545	1.27042	1.25951

Note: Data given are effective multiplication factors.

Table B-7 3DDT Results: Effective Multiplication Factors

In the 30/37 cases, the ranking order of the k-eff values was also the same as for the infinite multiplication factor data.

The transformation from the WIMS-CRNL 4-group data to the 2-group representation resulted in a slight increase in k-eff. With the M-2 representation, the k-eff value dropped by 1.4 mk for the NATNOM case and by 0.6 mk for the 30/37 case, in comparison with the 4-group approach.

Note that some of the difference in k-eff between the WIMS-CRNL, LATREP, and PPV cases can be attributed to the simplified treatment of the adjuster region. As the group structure and cross section definitions differ between the codes somewhat, a more rigorously defined adjuster property set consistent with the nominal fuel properties would be expected to reduce the variation between the three codes.

Typical power distributions (horizontally along the reactor centreline at axial plane 3) for the WIMS-CRNL 4 group and M-2 group cases are depicted in Fig. B-3 and B-4. (In all cases the data are normalized to yield a total reactor power of 2000 MW.) Data for the other cases studied are essentially coincident. It can be seen, therefore, that the results are relatively independent of the code or group structure chosen.

B.6 CONCLUSIONS

This analysis has allowed a quantification of the effect of different lattice codes and energy group structures on the effective multiplication factor and reactor power distribution in heavy water moderated CANDU reactors fueled with natural or enriched uranium (1.3 a/o U-235, in this case).

The results indicate that the agreement between lattice codes is not appreciably altered as the fuel enrichment is increased. It was further concluded that, in light of the variations in k-eff that exist between the various codes, the variation resulting from the use of the simplified WIMS-CRNL M-2 representation, as opposed to the more detailed and costly 4-group representation, is acceptably inconsequential. Hence the WIMS-CRNL M-2 representation was chosen for the fuel management studies conducted throughout the remainder of this study. The WIMS-CRNL code (as opposed to PPV

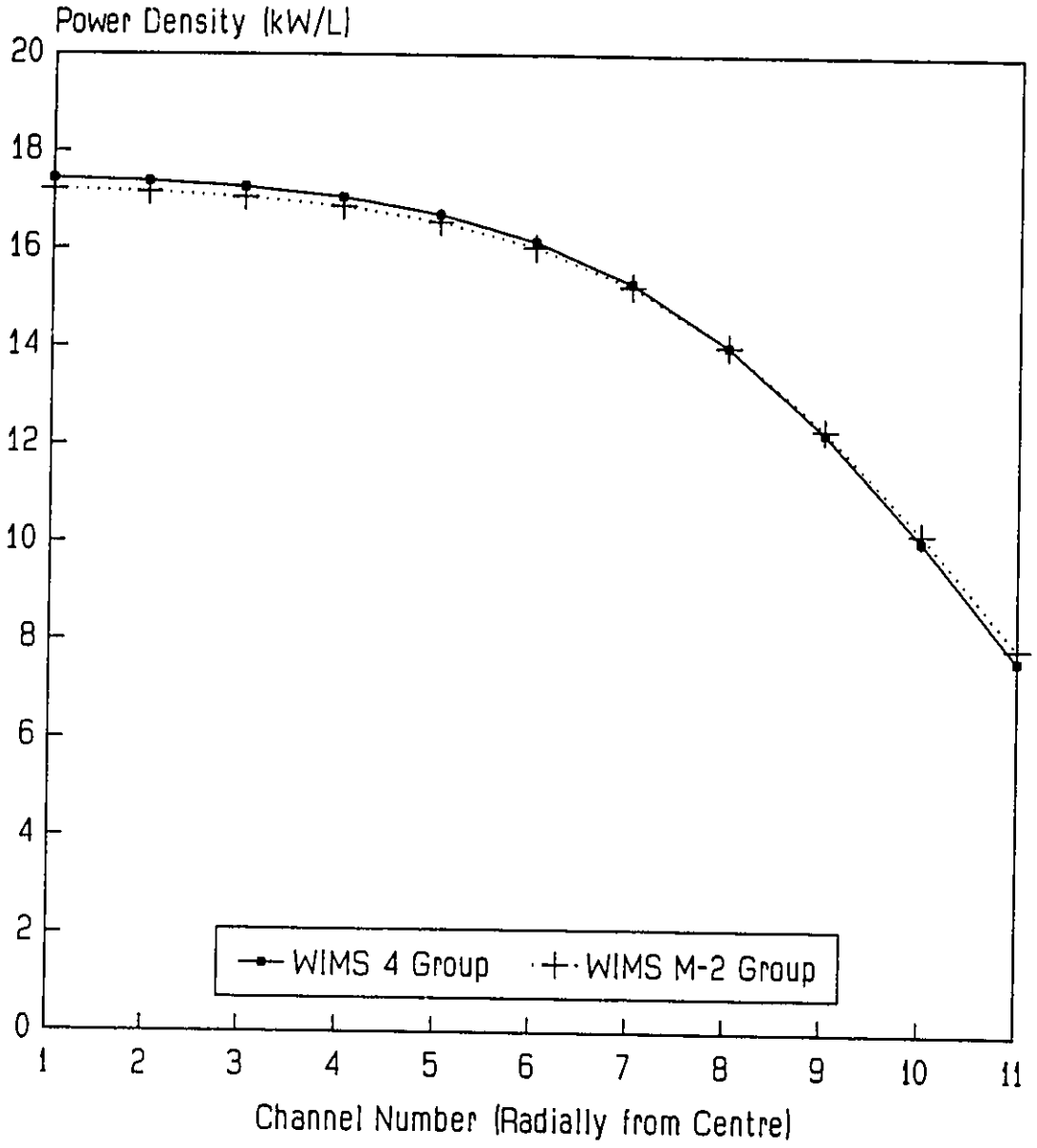

Figure B-3 3DDT Results: Typical Power Distribution (NATNOM)

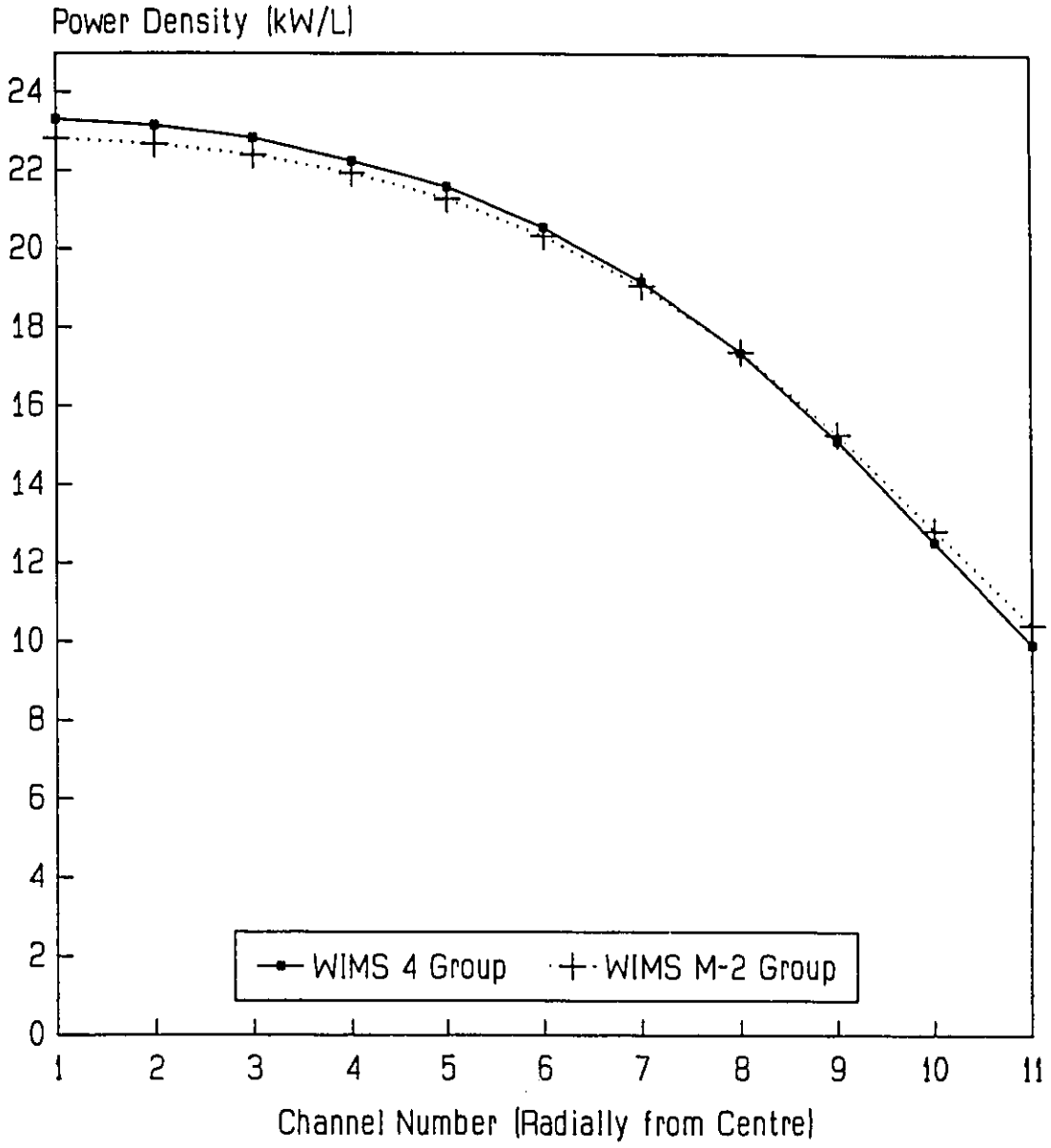

Figure B-4 3DDT Results: Typical Power Distribution (30(37))

or LATREP) was selected because it has greater flexibility, due to the fact that it allows for more detailed lattice models and it avoids many of the empiricisms incorporated into the other codes. As discussed in Chapter 7, parameters such as void reactivity in complex fuel bundles are better quantified with WIMS-CRNL.

APPENDIX C

CALCULATION OF ADJUSTER ROD INCREMENTAL PROPERTIES

C.1 INTRODUCTION

In Chapter 9, the methodology for calculating reactivity device incremental cross sections is outlined. In this appendix, details of the MULTICELL (Dastur and Buss, 1983) simulations performed to determine adjuster rod incremental cross sections, are provided.

C.2 NOMINAL LATTICE COMPONENT PROPERTIES

Fuel, annulus, and moderator properties for input to the MULTICELL code were obtained by using WIMS-SHETAN (Donnelly, 1985) to extract the appropriate data from the WIMS-CRNL (Donnelly, 1986) simulations performed for the various fuel types (Chapter 7).

To best approximate equilibrium conditions, the WIMS-CRNL cross sections were determined at a burnup corresponding to one half of the expected fuel exit burnup (Table C-1). The appropriate WIMS-CRNL Tape 16 data were input to WIMS-SHETAN.

C.3 SIMULATION OF THE FUEL REGION

C.3.1 Geometrical Considerations

The fuel region in the MULTICELL model was taken to extend up to the inside of the pressure tube (inside radius 5.1689 cm). It included all fuel elements and coolant. Fuel region current to flux ratio (CFR) boundary conditions were applied at the pressure tube surface. In the MULTICELL model, the fuel was rectangularized to conserve surface area:

Fuel Type	Burnup (MWd/MgU) at Which Time Integrated Infinite Multiplication Factor = 1.045	Equilibrium Condition Approximated by		
		Days	Burnup (MWd/MgU)	File
NATNOM	6800	100	3251	7
1421NAT	8082	100	3971	5
14211312	23078	300	11916	8
132117153	30661	400	15888	9

Table C-1 WIMS-CRNL Data for Approximation of Equilibrium Conditions

$$2\pi\, 5.1689 = 4\,x \qquad \text{(C.3.1-1)}$$

$$x = 8.1193 \quad \text{cm} \qquad \text{(C.3.1-2)}$$

where x is the length of a side of the rectangularized fuel region.

A source region 10^{-7} cm in width was modelled around the fuel region.

C.3.2 Source Region Properties

From the WIMS-CRNL/WIMS-SHETAN calculations, the average production cross section within the pressure tube radius in the WIMS-CRNL simulations was determined. The effective source region production cross section was then calculated according to Eq 9.4.2-1. Other cross sections for the fuel source region were as for the annulus region (Section C.4).

C.3.3 Fuel Region Boundary Conditions

Fast and thermal current to flux ratio (CFR) boundary conditions were calculated as per Eq 9.4.2-5 and 9.4.2-6. Surface fluxes were obtained from the WIMS-CRNL data for the coolant region between the outer edge of the fuel bundle and the inside of the pressure tube. WIMS-CRNL/WIMS-SHETAN was used to calculate the fuel region average cross sections for input into the CFR equations.

C.3.4 Fuel Region Properties

Fuel region properties were calculated using WIMS-CRNL/WIMS-SHETAN average properties of all materials within the inner radius of the pressure tube. The production cross section was set to zero since the source was modelled separately. A flag in MULTICELL was set to multiply the input fuel region properties by $4/\pi$. (In the model, the fuel region was rectangularized

to conserve surface area).

C.4 FUEL ANNULUS REGION

The fuel annulus region (pressure tube, gas gap, calandria tube) was modelled as a single homogenized region with average properties determined using WIMS-CRNL/WIMS-SHETAN.

The annulus region was modelled as a rectangularized shell around the fuel region. To conserve moderator volume in the model, the annulus was simulated as extending x cm on a side such that:

$$\pi\, 6.5875^2 = x^2$$
$$x = 11.67604 \quad \text{cm} \qquad \text{(C.4-1)}$$

where 6.5875 cm is the outer radius of the calandria tube.

In the model, therefore, the annulus volume per unit axial length is:

$$V_M = 11.67604^2 - 8.1193^2 = 70.40705\ \text{cm}^2 \qquad \text{(C.4-2)}$$

where 8.1193 cm is the length of a side of the rectangularized fuel region. In reality, the annulus region volume per unit axial length is:

$$V_A = \pi (r_2^2 - r_1^2) \qquad \text{(C.4-3)}$$

where r_2 is the outer radius of the calandria tube (6.5875 cm) and r_1 is the inner radius of the pressure tube (5.1689 cm). Hence:

$$V_A = 52.394317\ \text{cm}^2 \qquad \text{(C.4-4)}$$

The WIMS-SHETAN cross sections for the annulus region were multiplied by:

$$V_A / V_M = 0.7441629 \qquad \text{(C.4-5)}$$

to conserve reaction rates in the modelled annulus region.

C.5 MODERATOR REGION

WIMS-SHETAN was used to find average moderator region properties for input to MULTICELL. WIMS-CRNL cross sections were averaged over the region beyond the outside of the calandria tube.

C.6 MATERIAL PROPERTIES FOR NOMINAL LATTICE CELL COMPONENTS

In the WIMS-SHETAN averaging of the WIMS-CRNL results, fuel region properties were calculated by integrating up to region 17 in the NATNOM cases and region 13 in the 14/21 cases. The annulus extended out to region 20 in the NATNOM cases and 16 in the 14/21 cases. The moderator was region 21 in the NATNOM cases and region 17 in the 14/21 cases.

As discussed in Section C.2 and noted in Table C-1, MULTICELL calculations were performed using fuel conditions approximately coinciding with one half of the expected exit burnup. These corresponded to WIMS-CRNL burnup steps 7, 5, 8, and 9 for the NATNOM, 1421NAT, 14211312, and 142117153 cases, respectively. The corresponding files from the WIMS-CRNL generated Tape 16 data were input to WIMS-SHETAN and appropriately averaged (compressed both region-wise and in energy spectrum) for subsequent input to MULTICELL.

Material properties for the nominal lattice cell constituent regions are given in Table C-2.

Fuel region boundary conditions are given in Table C-3.

C.7 NEUTRONIC PROPERTIES FOR ADJUSTER ROD CONSTITUENT MATERIALS

As discussed in Chapter 9, constituent material neutronic cross sections were determined with the WIMS-CRNL code by modelling rings of

Fuel Model Type	Region	Fast Diffusion Coefficient (cm)	Thermal Diffusion Coefficient (cm)	Fast Absorption Cross Section (cm^{-1})	Thermal Absorption Cross Section (cm^{-1})	Production Cross Section (cm^{-1})	Moderation Cross Section (cm^{-1})
NATNOM	Moderator	1.27652	0.87411	2.32612-8	4.55995-5	0.0	1.09875-2
	Fuel Source	4.04777	3.86510	7.04090-4	2.01370-3	1.71721+6	7.10847-5
	Annulus*	4.04777	3.86510	7.04090-4	2.01370-3	0.0	7.10847-5
	Fuel**	1.06488	0.86290	9.50942-3	6.44646-2	0.0	1.75554-3
1421NAT	Moderator	1.27881	0.88000	-1.29419-7	4.48164-5	0.0	1.06020-2
	Fuel Source	12.79836	12.10484	2.43950-4	6.35282-4	1.54280+6	2.61882-5
	Annulus*	12.79836	12.10484	2.43950-4	6.35282-4	0.0	2.61882-5
	Fuel**	1.04731	0.86568	9.72118-3	5.51347-2	0.0	2.19708-3
14211312	Moderator	1.27893	0.88160	-1.47332-7	4.46031-5	0.0	1.04426-2
	Fuel Source	12.80352	12.13662	2.44280-4	6.31911-4	1.80430+6	2.45153-5
	Annulus*	12.80352	12.13662	2.44280-4	6.31911-4	0.0	2.45153-5
	Fuel**	1.05091	0.84434	1.06921-2	6.61579-2	0.0	1.99868-3
142117153	Moderator	1.27898	0.88223	-1.54213-7	4.45208-5	0.0	1.03897-2
	Fuel Source	12.80514	12.17620	2.44374-4	6.30315-4	1.91314+6	2.41107-5
	Annulus*	12.80514	12.17620	2.44374-4	6.30315-5	0.0	2.41107-5
	Fuel**	1.05276	0.83587	1.10265-2	7.07320-2	0.0	1.94837-3

* Cross sections quoted here have been multiplied by 0.7441629 for conservation of reaction rates.
** Cross sections for fuel region are multiplied by $4/\pi$ in the MULTICELL code.

Table C-2 Material Properties for Nominal Lattice Cell Components

Case	Fast Current to Flux Ratio	Thermal Current to Flux Ratio
NATNOM	-3.45426-2	-1.23926-1
1421NAT	-3.46388-2	-1.10677-1
14211312	-3.69930-2	-1.28564-1
142117153	-3.78206-2	-1.35105-1

Table C-3 MULTICELL Fuel Region Boundary Conditions

materials in the appropriate lattice cells. These rings were placed at the radial boundary of the model and were sized such that the ring area equalled the volume of the particular material per unit axial length of a lattice cell with the device. WIMS-SHETAN was used for data compression and extraction.

The cobalt ring inner radius was 16.112 cm in the NATNOM model, and in the 14/21 cases the inner radius was 14.095 cm. This yielded a volume per unit bundle length corresponding to the amount of cobalt in a 6-pin adjuster per unit lattice pitch.

The zirconium ring inner radius was 16.068 cm in the NATNOM case and 14.090 cm in the 14/21 cases. (Recall that in the NATNOM case, the model extended to a radius of 16.12171 cm and in the 14/21 cases, to a radius of 14.10474 cm.)

Sensitivity studies conducted are discussed in Appendix D, Section D.2.1. It was found that the zirconium properties were not sensitive to small variations in ring size. Hence only one set of zirconium cross sections, corresponding to the ring radius from the zone controller zirconium study (Appendix D), were used (radius 16.068 cm in the NATNOM study and 14.051 cm in the 14/21 cases). It was further found that the properties for zirconium and cobalt were not strongly dependent on the fuel irradiation or enrichment. Hence a single set of reactivity device constituent material properties was used for all irradiations in the NATNOM case and a single set (corresponding to the 14211312 case) was used for all fuel enrichments and all irradiations in the 14/21 studies.

C.7.1 Adjuster Rod Guide Tube

The adjuster rod guide tube is Zircaloy-2 with an outside diameter of 8.89 cm and a thickness of 0.127 cm. Circular holes are drilled through the tube in a repeating pattern, removing 40% of the zirconium material.

In the MULTICELL model, the tube was rectangularized, with each side 8.89 cm in length. To conserve total volume, the wall thickness was adjusted to 0.05939 cm. Nominal Zr properties were applied to this region.

C.7.2 Adjuster Rod Central Shaft, Support Tubes, Base Plates

As discussed in Section 9.5.1, the cobalt adjuster bundle has top and bottom bases, a solid central support rod, and two support tubes, all of zirconium. Using a density of 6.55 g/cm^3, each 21.0388 cm adjuster bundle contained 35.817 cm^3 of Zr in addition to the Zr in the sheaths. In the MULTICELL model, this was simulated as a single central solid Zr rectangularized rod, 1.3048 cm on a side.

C.7.3 Adjuster Rod Cobalt Pencil

Adjuster rod cobalt pencils are comprised of 8 cobalt slugs, each 0.6223 cm in diameter and 2.5273 cm in length. The slugs have a density of 8.6 g/cm^3.

The adjuster bundles are 21.0388 cm in length. Consequently, the 8 slugs comprise only 96.1% of the adjuster length. In the MULTICELL model, the cobalt region extended the entire length of the adjuster, and hence it was necessary to multiply the WIMS-CRNL/WIMS-SHETAN cross sections for cobalt by 0.961 for use in the MULTICELL program and in the MULTCFR boundary condition code (Marczak, 1981).

The cobalt region is modelled as a rectangularized rod with a surface area equal to the surface area of a cylindrical rod 0.6223 cm in diameter. The rectangularized region was 0.48875 cm on a side. The cross sections input to MULTICELL for the cobalt region were multiplied by $4/\pi$ in the code to conserve reaction rates (due to the altered region volume).

C.7.4 Adjuster Rod Cobalt Pencil Sheath

The Zr adjuster sheath around each cobalt pencil is 0.8001 cm in diameter, with a 0.0635 cm wall thickness. In the MULTICELL model, the volume of the moderator was conserved. As such, it was necessary to adjust the volume of the sheath region around the cobalt pencils and multiply the cross sections input to MULTICELL by a factor accounting for this difference,

thereby conserving reaction rates.

The adjuster sheaths were rectangularized with a side length of 0.70907 cm. In the model, therefore, it was necessary to multiply the nominal Zr cross sections by 0.5568 to conserve reaction rates in the sheath regions.

Neutronic properties for the cobalt adjuster constituent materials are provided in Table C-4.

C.8 COBALT ADJUSTER ROD BOUNDARY CONDITIONS

The calculation of device boundary conditions was discussed in Section 9.4.2.5.2. Cross sections for cobalt as determined using WIMS-CRNL/WIMS-SHETAN were multiplied by 0.961 (see Section C.7.3) and input into MULTCFR along with the pencil radius and moderator properties (since the moderator was the predominant surrounding medium).

The pertinent MULTCFR input data for the cobalt adjuster cases are given in Table C-5. The calculated boundary conditions are given in Table C-6. These boundary conditions were applied to the rectangularized adjuster pencil surface in the MULTICELL simulations.

C.9 MULTICELL MODEL

The MULTICELL model used in the calculation of the adjuster rod incremental properties took advantage of the natural symmetry of the adjuster/lattice arrangement. The MULTICELL model consisted of one-half lattice pitch by one-half lattice pitch by one-half bundle length (0.5 LP x 0.5 LP x 0.5 BL) cell which included a one-quarter-face fuel assembly and a one-quarter adjuster region, as shown in Figure C-1. Reflective boundary conditions were applied at all faces of the cell.

Mesh spaces used in the model are provided in Table C-7. The mesh spacings in the model were not modified when the adjuster rod was in or out of core. Only the material specifications were altered.

The one-eighth lattice cell MULTICELL model in Figure C-1 allowed for the simulation of 0, 2, 4, and 6 pencil adjusters only. By specifying a

Fuel Model Type	Region	Fast Diffusion Coefficient (cm)	Thermal Diffusion Coefficient (cm)	Fast Absorption Cross Section (cm^{-1})	Thermal Absorption Cross Section (cm^{-1})	Production Cross Section (cm^{-1})	Moderation Cross Section (cm^{-1})
NATNOM	Guide Tube	1.13340	1.08893	2.86865-3	7.31621-3	0.0	4.88739-4
	Central Shaft	1.13340	1.08893	2.86865-3	7.31621-3	0.0	4.88739-4
	Sheath*	2.03551	1.95564	1.59730-3	4.07376-3	0.0	2.72136-4
	Cobalt**	0.34045	0.11544	4.40850-1	2.32195-0	0.0	2.19900-4
14/21	Guide Tube	1.13633	1.08966	2.79404-3	7.16055-3	0.0	4.42912-4
	Central Shaft	1.13633	1.08966	2.79404-3	7.16055-3	0.0	4.42912-4
	Sheath*	2.04077	1.95695	1.55596-3	3.98709-3	0.0	2.46619-4
	Cobalt**	0.34935	0.11804	4.19610-1	2.25843-0	0.0	1.97500-4

* Cobalt adjuster sheath properties quoted here are Zr properties multiplied by 0.5568133 for conservation of reaction rates.

** Cobalt properties quoted here are multiplied by 0.961, and are multiplied internally in MULTICELL by $4/\pi$.

Table C-4 MULTICELL Input Properties for Adjuster Rod Component Materials

Particulars	NATNOM	14/21
Fast Transport Cross Section (cm^{-1})	0.97911	0.95414
Thermal Transport Cross Section (cm^{-1})	2.88761	2.83239
Fast Scattering Cross Section (cm^{-1})	0.53826	0.53453
Thermal Scattering Cross Section (cm^{-1})	0.56567	0.56544
Fast Absorption Cross Section (cm^{-1})	0.44085	0.41961
Slow Absorption Cross Section (cm^{-1})	2.32195	2.25843
Moderation Cross Section (cm^{-1})	0.2199-3	0.1975-3
Moderator Fast Transport Cross Section (cm^{-1})	0.26100	0.26100
Moderator Thermal Transport Cross Section (cm^{-1})	0.38000	0.38000
Region Radius (cm)	0.31115	0.31115

Data from WIMS-CRNL/WIMS-SHETAN cases, with cross sections multiplied by 0.961.

Table C-5 MULTCFR Input Data for the Calculation of Cobalt Pencil Boundary Conditions

Case	Fast Current to Flux Ratio	Thermal Current to Flux Ratio	PES*
NATNOM	-0.0593666	-0.192587	0.500819
1421	-0.0568829	-0.190034	0.493738

* PES = Fraction of neutrons thermalized within the device that are absorbed within the device.

Table C-6 MULTICELL Cobalt Adjuster Boundary Conditions

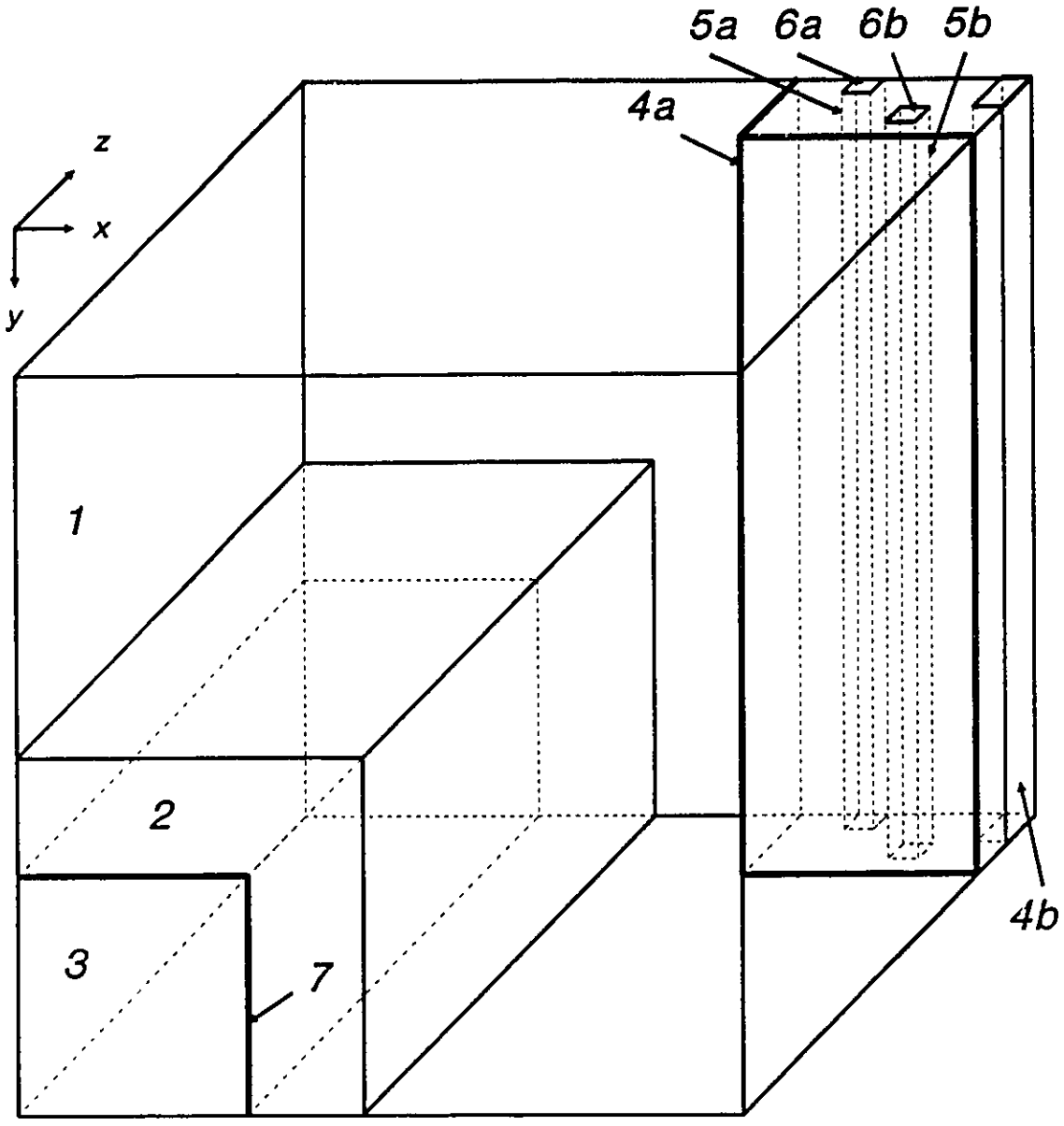

Model Size: 1/2 LP x 1/2 LP x 1/2 BL
Note: Reflective boundary conditions on all faces

Material 1: Moderator
2: Fuel Annulus
3: Fuel Region
4a: Adjuster Rod Guide Tube
4b: Solid Zr Rod
5a,b: Cobalt Pencil Sheath
6a,b: Cobalt Pencil
7: Fuel Source (1E-7cm thick)

Figure C-1 MULTICELL Cobalt Adjuster Model

Mesh Space Number	Mesh Space Size (cm)		
	X	Y	Z
1	0.0	0.0	0.0
2	1.3532134	N	2.0
3	1.3532133	N	2.0
4	1.3532133	N	2.0
5	0.0000001	N	2.0
6	0.8941899	N	2.0
7	0.8841900	N	2.0
8	M	R	2.0
9	M	0.8841900	2.0
10	M	0.8941899	2.0
11	M	0.0000001	2.0
12	0.0593900	1.3532133	P
13	0.7455375	1.3532133	0.0593900
14	0.7455375	1.3532134	1.0
15	0.1001600	0.0	0.8313705
16	0.0100000		0.1001600
17	0.4887500		0.0100000
18	0.0100000		0.4887500
19	0.1001600		0.0100000
20	0.5609300		0.1001600
21	0.1001600		1.1927695
22	0.0100000		0.2978650
23	0.4887500		0.1001600
24	0.0100000		0.0100000
25	0.1001600		0.2443750
26	0.2630650		0.0
27	0.6524000		
28	0.0		

NATNOM: M=1.001120; N=1.3; P=0.320; R=0.64948
14/21: M=0.554245; N=1.0; P=0.555; R=0.66198

Table C-7 MULTICELL Mesh Spacings: Cobalt Adjuster Simulations

cobalt pencil/sheath in materials 5a/6a, a 2 pencil adjuster was simulated. By specifying a cobalt pencil/sheath in materials 5b/6b, a 4 pencil adjuster was simulated. Specifying a cobalt pencil/sheath in materials 5a/6a and 5b/6b, allowed for the simulation of a 6 pencil adjuster.

Simulations were performed with and without the adjuster rods inserted. Cell averaged cross sections were compared and incremental device cross sections applicable over a 1 LP x 1 LP x 1 BL region were determined. Data for the 1, 3, and 5 pencil cases were obtained by linear interpolation of the 0, 2, 4, and 6 pencil cross sections. The incremental properties for the 14/21 cases were found to be relatively insensitive to the fuel enrichment. Hence incremental properties corresponding to the 14211312 cobalt adjuster cases were used for all of the 14/21 cases. The incremental cross sections are listed in Table 9-2.

C.10 INCREMENTAL H AND F FACTORS

From the cell-averaged data provided in the MULTICELL output, it is relatively straight forward to calculate the difference in cross sections to determine the device incremental properties. The FMDP core diffusion code also requires incremental bundle power to cell thermal flux, and incremental fuel to cell thermal flux ratios for each device. These parameters are denoted as incremental H and F factors, respectively. The calculation of these factors is somewhat more involved, requiring additional data post-processing.

C.10.1 Incremental H Factors

A given bundle power, P, is given by:

$$P = H\phi_c = C\nu\Sigma_f\phi_c \qquad \text{(C.10.1-1)}$$

where C is a constant of proportionality and ϕ_c is the cell flux. The first equality is by definition. The second equality is obtained by recognizing

that power is proportional to the fission rate. Hence, the change in H factor when a device is inserted can be related to the change in production cross section via:

$$\Delta H = H \Delta \nu\Sigma_f / \nu\Sigma_f \qquad \text{(C.10.1-2)}$$

Values for the H factor and production cross section for the nominal lattice cells were obtained from the WIMS-FMDP data (see Chapter 8) for the NATNOM and 14/21 fuel types at the irradiations assumed in the MULTICELL cases. These data are provided in Table C-8, and were combined with the corresponding incremental production cross sections to determine the incremental H factors. Prior to the calculation of the H factors, it was concluded that a single set of incremental properties would be sufficient for all of the 14/21 cases. The 14211312 data were chosen as representative.

C.10.2 Incremental F Factors

Incremental fuel to cell thermal flux ratios (F factors) were calculated from the MULTICELL output directly. The program output includes average fuel and cell fluxes. From this, the F factors were determined. The difference in the F factors was calculated to yield incremental values for the NATNOM and 14/21 cases. Again the 14211312 data were used for all 14/21 cases.

Fuel Type	Production Cross Section (cm^{-1})	H Factor ($10^{-11} kWcm^2 s$)
NATNOM	4.9863-3	0.251983
14/21*	7.44516-3	0.283798

* 14211312 data used.

Table C-8 Data Required for Determination of Incremental H Factors

APPENDIX D

CALCULATION OF ZONE CONTROLLER INCREMENTAL PROPERTIES

D.1 INTRODUCTION

In Chapter 9, the methodology for calculating reactivity device incremental cross sections is outlined. In Appendix C, details of the simulation and specification of the fuel, fuel annulus, and moderator regions are provided (see Tables C-2 and C-3). These same nominal lattice cell properties were used in the zone controller MULTICELL (Dastur and Buss, 1983) simulations. The difference in the zone controller simulation cases is that because diffusion theory is valid in light water, it was not necessary to apply boundary conditions on the reactivity device as was required in the cobalt adjuster simulations.

D.2 NEUTRONIC PROPERTIES FOR CONSTITUENT MATERIALS

Neutronic properties for the zone controller constituent materials were obtained using the WIMS-CRNL/WIMS-SHETAN ring-of-material methodology as discussed in Chapter 9 and as utilized for the adjuster rod materials in Appendix C (see Sections 9.4.2.5.1, and C.7).

In the NATNOM analysis, a ring of Zr was modelled as extending from a radius of 16.068 cm to the cell boundary, to obtain Zr properties for input to MULTICELL. Similarly, light water properties were obtained by modelling a ring of H_2O extending to the cell boundary from a radius of 15.555 cm. In the 14/21 cases, the Zr and H_2O rings were modelled as extending to the cell boundary from radii of 14.0514 cm and 13.542 cm, respectively. Ring thicknesses were determined by calculating the amount of the constituent material per affected lattice cell and per unit bundle length and then modelling that amount of material as a ring at the periphery of the lattice

cell.

D.2.1 Sensitivity Studies

Sensitivity studies were conducted which indicated that the constituent material cross sections were not strongly sensitive to the fuel burnup or fuel enrichment.

The sensitivity of the constituent material properties to the ring-of-material thicknesses used in the WIMS-CRNL/WIMS-SHETAN analyses for both the adjuster rod and zone controller components was found to be a function of the material being analyzed. For example, in the NATNOM fresh fuel cases, changing the zirconium ring inner radius from 16.000 cm to 16.107 cm (outer radius 16.12171 cm), caused a 0.3% increase in the zirconium thermal absorption cross section as derived using WIMS-CRNL/WIMS-SHETAN. Changing the inner radius of the H_2O ring from 16.000 cm to 15.555 cm, caused a 0.6% reduction in the light water thermal absorption cross section. Adjusting the cobalt ring inner radius from 16.000 cm to 16.112 cm, caused a 27% increase in the cobalt thermal absorption cross section.

The phenomena can be explained as follows. In the WIMS-SHETAN ring of material calculations, the thermal neutron flux was obtained by grouping the 7 lowest of 18 energy groups used in the WIMS-CRNL simulations (i.e. all groups below 0.625 eV). As the constituent material ring thickness was varied, the neutron spectrum, and hence relative weighting of the multi-group cross sections, changed. The neutron spectrum in the moderator region was affected, which altered the spectrum of the neutrons impinging upon the material ring. Further, as the ring thickness increased, the non-uniform absorption cross section for each of the 7 thermal neutron groups resulted in a spectral hardening effect within the material rings themselves. In the cobalt case for example, the lower energy neutrons were more preferentially absorbed near the surface of the ring, resulting in a reduction in the lower energy neutron flux in the body of the ring (and hence a net increase in the average neutronic energy). The two-group cross sections are flux weighted averages of the multi-group data. Consequently, an increase in the ring

thickness causes a reduction in the thermal absorption cross section for cobalt, water, and zirconium due to the fact that each of the materials has an absorption cross section that decreases with energy over the thermal range. The effect was more pronounced in the cobalt cases because of the very large thermal absorption cross section for that material (as opposed to zirconium or light water). It is noted that the large absorption cross section of cobalt made the MULTICELL simulations less sensitive to a variation in the absorption cross section used in the model. Because of the geometric arrangement and self-shielding effect, a large increase in the input thermal absorption cross section for cobalt, would cause only a relatively small increase in the lattice cell incremental thermal absorption cross section for the Co adjuster.

D.2.2 Constituent Material Properties Used in MULTICELL Simulations

As a result of the sensitivity studies conducted, it was concluded that, as is Appendix C for the cobalt adjuster, only two sets of constituent material properties were required -- one set for the NATNOM cases, and one set for the 14/21 studies. The properties determined with the 14211312 fuel were chosen as representative for all 14/21 zone controller analyses.

Constituent material properties for the zone controllers are provided in Table D-1. It is to be noted that the third material listed is a sheath/helium combination material. It was found that the MULTICELL code did not provide physically acceptable results with a large voided region corresponding to a drained zone controller. To simulate the drained device, therefore, the Zr sheath was homogenized into the entire sheath/void region, necessitating the introduction of a new material with appropriately weighted cross sections.

D.3 MULTICELL MODEL

The MULTICELL model for the zone controller studies is depicted in Figure D-1. As in Appendix C, a one-half lattice pitch by one-half lattice

Fuel Model Type	Region	Fast Diffusion Coefficient (cm)	Thermal Diffusion Coefficient (cm)	Fast Absorption Cross Section (cm^{-1})	Thermal Absorption Cross Section (cm^{-1})	Production Cross Section (cm^{-1})	Moderation Cross Section (cm^{-1})
NATNOM	Sheath	1.13340	1.08893	2.86865-3	7.31621-3	0.0	4.88739-4
	Water	0.69247	0.14737	7.05036-4	1.70534-2	0.0	9.73862-2
	Sheath/Helium*	12.88253	12.37660	2.52383-4	6.43677-4	0.0	4.29991-5
14/21	Sheath	1.13633	1.08966	2.79404-3	7.16055-3	0.0	4.42912-4
	Water	0.71333	0.14853	6.56431-4	1.68927-2	0.0	8.82042-2
	Sheath/Helium*	12.91583	12.38537	2.45819-4	6.29982-4	0.0	3.89672-5

* Zr properties multiplied by 0.0879796 applied over sheath

Table D-I MULTICELL Input Properties for Zone Controller Component Materials

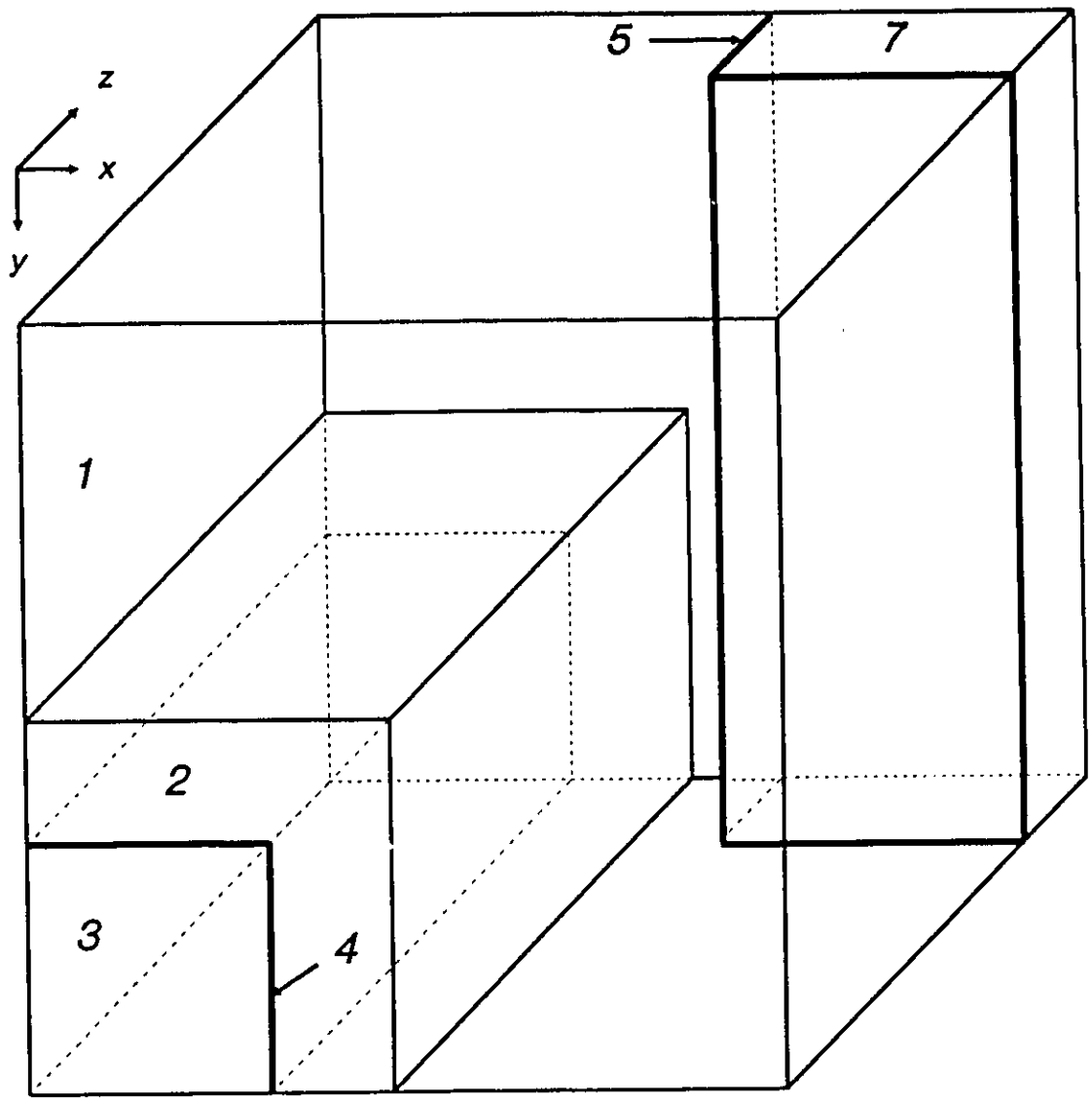

Model Size: 1/2 LP x 1/2 LP x 1/2 BL
Note: Reflective boundary conditions on all faces

Material 1: Moderator
2: Fuel Annulus
3: Fuel Region
4: Fuel Source (1E-7cm thick)
5: Zone Controller Sheath
7: Zone Controller Water (or Air)

Figure D-1 MULTICELL Zone Controller Model

pitch by one-half bundle length model was used. Reflective boundary conditions were applied on all faces of the model. Mesh spacings in the model are provided in Table D-2. Because of the lattice cell size variation between the NATNOM and 14/21 cases, it was necessary to use slightly different mesh sizes in the two models, as indicated in the table.

D.3.1 Nominal Lattice Cell Constituent Materials

The fuel, fuel source, annulus, and moderator region properties and dimensions were as given in Appendix C for the adjuster rod simulations.

D.3.2 Zone Controller Modelling

The zone controller unit is described in Section 9.6.1. Device rectangularization was required for simulation purposes.

D.3.2.1 Zone Controller Water

The water region of the zone controller was reconfigured as a rectangular zone 9.889 cm on a side. The amount of light water in the model therefore matched the volume of light water in the actual zone controller thereby conserving reaction rates. (Recall that the inside radius of the zone controller sheath is 5.715 cm, and that there is a 4.7% reduction in water volume due to structural material enclosed by the sheath.) Only 25% of the zone controller cross sectional area was included in the MULTICELL model.

D.3.2.2 Zone Controller Sheath

The Zircaloy zone controller sheath (inside radius 5.715 cm, wall thickness 0.127 cm) and the Zircaloy structural material (4.7% of the interior volume) were modelled together as a rectangularized annulus 0.233 cm in thickness around the light water region. Conservation of volume (and hence reaction rates) dictated the thickness of the modelled zone controller

Mesh Space Number	Mesh Space Size (cm)		
	X	Y	Z
1	0.0	0.0	0.0
2	1.3532134	N	2.0
3	1.3532133	N	2.0
4	1.3532133	N	2.0
5	0.0000001	N	2.0
6	0.8941899	N	2.0
7	0.8841900	N	2.0
8	M	R	2.0
9	M	0.8841900	2.0
10	M	0.8941899	2.0
11	M	0.0000001	1.0
12	0.2330000	1.3532133	P
13	0.9445000	1.3532133	0.2330000
14	1.0	1.3532134	0.9445000
15	1.0	0.0	1.0
16	1.0		1.0
17	1.0		1.0
18	0.0		1.0
19			0.0

NATNOM: M=0.817995; N=1.3; P=0.5875; R=0.64948
14/21: M=0.371120; N=1.0; P=0.8225; R=0.66198

Table D-2 MULTICELL Mesh Spacings: Zone Controller Simulations

sheath. Standard Zr properties (Section D.2) were applied in this region.

D.3.2.3 Zone Controller Sheath/Helium

To determine incremental cross sections for a drained zone controller (central region filled with He), the zone controller sheath and structural material were homogenized with the helium region to form a single sheath/helium zone in the MULTICELL model. Due to the relatively large macroscopic cross sections of Zircaloy as opposed to the helium gas, the properties for the homogenized zone were obtained by multiplying the Zr properties by:

$$V_S/(V_S + V_H) = 0.08798 \qquad \text{(D.3.2-1)}$$

where V_S is the volume of the sheath and structural material, and V_H is the volume of the helium.

D.4 ZONE CONTROLLER INCREMENTAL PROPERTIES

The incremental properties for the 14/21 zone controller cells were found to be relatively independent of the fuel enrichment. Hence only the incremental cross sections corresponding to the 14211312 fuel type were used in the 14/21 core calculations. Incremental properties for the NATNOM and 14/21 full core fuel management studies are provided in Table 9-3.

APPENDIX E

DATA HANDLING: URANIUM AND SEPARATIVE WORK REQUIREMENTS

E.1 INTRODUCTION

In this appendix, the equations pertaining to uranium and separative work requirements are considered, and appropriate governing equations and conversion factors are derived.

The FMDP core physics simulation code (Wight, Gold, and Marczak, 1981) used in this study provides information on reactor flux and power distributions, fuel burnup, fuel bundles required per full power day (FPD), and effective multiplication factor. For a comparison of reactor burnup and SWU requirements with other published data, the FMDP results must be presented in terms of kgU_{mined}/MW(e)-a and kg SWU/MW(e)-a, respectively.

E.2 Conversion and Fabrication Losses

It is assumed in this analysis, that conversion and fuel fabrication result in uranium losses of 0.5% for each process (Atomic Energy of Canada Limited, 1979a and 1979b). The uranium requirements must therefore be multiplied by 1.005^2 (=1.010) to account for these losses.

E.3 Thermal Burnup to Electrical Energy Conversion Factor

To convert MWd/MgU to kgU/MW(e)-a, a fission power to electrical conversion factor of 0.31 is assumed. The average overall efficiency of CANDU reactors ranges from 29.5% to 31.0% (Hatcher, 1978). New CANDU stations are expected to exceed this efficiency. The 0.31 efficiency factor also allows direct comparison of the results calculated herein with previously published

figures (Section 10.6.8). Hence:

$$x \frac{MWD}{MgU} \equiv 1.1782E6 \; z \frac{kgU(mined)}{x \quad MW(e)\text{-}a} \qquad (E.3\text{-}1)$$

where x is the calculated burnup and z is the amount of uranium mined for each kg of uranium in the fuel. $z=1.005^2$ for natural uranium fuel. For enriched fuel cases, z depends on the enrichment, tails concentration, and conversion and fabrication losses.

E.4 Separative Work Requirements per Unit of Electrical Energy Produced

To calculate kg SWU/MW(e)-a, it is again assumed that the reactor operates with a thermal to electrical conversion efficiency of 0.31. This gives a separative work requirement of:

$$Y = 1.1782E6 \; \frac{z \; kgSWU}{x \; MW(e)\text{-}a} \qquad (E.4\text{-}1)$$

where, in this equation, z is the kg $SWU/kgU_{product}$, and x is the burnup in MWd/MgU. (Note the similarity, yet distinction, between the definition of "z" in Eq E.3-1 and E.4-1.)

E.5 Uranium Requirement Calculations

E.5.1 Direct Production

To produce 1 kg of product with enrichment P w/o U-235 from natural uranium (N w/o U-235) one requires:

$$\frac{M_N}{M_P} = \frac{P\text{-}T}{N\text{-}T} \qquad (E.5\text{-}1)$$

where T is the tailings U-235 concentration (in w/o) and M_N and M_P refer to the mass of natural uranium and product produced respectively (Silvennoinen, 1982). Conversion and fabrication losses are neglected in this equation.

E.5.2 Production Via Dilution with Uranium of Prespecified Enrichment

Often it may not be possible to obtain uranium at the exact U-235 concentration required for particular applications and as a consequence, utilities would be required to dilute quantities at available prespecified enrichments to produce the required product enrichment (P w/o).

Consider, as an example, a general case with the enriched uranium feed available at a concentration of F w/o U-235. This is to be diluted with a dilutant (D w/o U-235) to produce the required product enrichment (P w/o). One obtains:

Conservation of Mass: $$M_F + M_D = M_P \qquad \text{(E.5-2)}$$

Conservation of U-235: $$FM_F + DM_D = PM_P \qquad \text{(E.5-3)}$$

Also, as shown by Silvennoinen (1982) (again, using conservation of mass and U-235), the production of uranium with F w/o U-235 requires:

$$\frac{M_N}{M_F} = \frac{F-T}{N-T} = M_{NF} \qquad \text{(E.5-4)}$$

Similarly to produce the dilutant, with D w/o U-235 requires:

$$\frac{M_N}{M_D} = \frac{D-T}{N-T} = M_{ND} \qquad \text{(E.5-5)}$$

From Eq E.5-2 and E.5-3:

$$\frac{M_F}{M_P} = \frac{P-D}{F-D} = M_{FP} \qquad \text{(E.5-6)}$$

and

$$\frac{M_D}{M_P} = \frac{F-P}{F-D} = M_{DP} \qquad \text{(E.5-7)}$$

Per kg of product:

$$\frac{M_N}{M_P} = M_{NF} M_{FP} + M_{ND} M_{DP} \qquad \text{(E.5-8)}$$

And, hence from Eq E.5-4 through E.5-8:

$$\frac{M_N}{M_P} = \frac{P-T}{N-T} \qquad \text{(E.5-9)}$$

which is exactly the same natural uranium requirement as obtained in Eq E.5-1. Consequently the production of uranium with U-235 concentration, P, requires (P-T)/(N-T) kg of natural uranium per kg product independent of whether the product is produced directly, or from the mixture of uranium with U-235 concentrations of F and D. The amount of separative work required is affected, however (see Section E.6).

Two special dilutant cases deserve particular attention. First, consider the case with D=N. That is, the dilutant is natural uranium. From Eq E.5-5:

$$\frac{M_N}{M_D} = \frac{M_N}{M_N} = \frac{N-T}{N-T} = 1 \qquad \text{(E.5-10)}$$

As expected, the production of 1 kg of natural uranium requires 1 kg of natural uranium, barring production losses.

As a second special case, consider the case with uranium tailings (U-235 concentration, T) used as a dilutant. In this case, Eq E.5-5 yields:

$$\frac{M_N}{M_D} = \frac{M_N}{M_T} = \frac{T-T}{N-T} = 0 \qquad \text{(E.5-11)}$$

That is, no additional natural uranium is required to produce uranium tailings that are already existing at concentration, T. Eq E.5-11 is valid provided that sufficient uranium tailings are available. One must determine whether this is indeed the case.

From Eq E.5-7, the amount of dilutant required is (with D=T):

$$\frac{M_D}{M_P} = \frac{F\text{-}P}{F\text{-}D} = \frac{F\text{-}P}{F\text{-}T} \qquad \text{(E.5-12)}$$

It is necessary to demonstrate that in the production of the more highly enriched uranium (U-235 concentration, F) sufficient tailings are produced to provide the dilution requirements from Eq E.5-12.

Consider, in the production of uranium with U-235 concentration, F, the conservation of mass and U-235:

$$M_F + M_T = M_N \qquad \text{(E.5-13)}$$

$$FM_F + TM_T = NM_N \qquad \text{(E.5-14)}$$

Solving for M_T/M_F yields:

$$\frac{M_T}{M_F} = \frac{F\text{-}N}{N\text{-}T} \qquad \text{(E.5-15)}$$

and hence per kg product (with U-235 concentration, P), the amount of tailings produced in the production of the required amount of uranium with U-235 concentration, F, is given by:

$$\frac{M_T}{M_P} = \frac{M_T}{M_F} * \frac{M_F}{M_P} = \frac{(F\text{-}N)}{(N\text{-}T)} * \frac{(P\text{-}D)}{(F\text{-}D)} \qquad \text{(E.5-16)}$$

where the results from Eq E.5-6 and E.5-15 have been used.

Finally, one must show that (from Eq E.5-12 and E.5-16 with D=T):

$$\frac{(F\text{-}N)}{(N\text{-}T)} * \frac{(P\text{-}T)}{(F\text{-}T)} \geq \frac{(F\text{-}P)}{(F\text{-}T)} \qquad \text{(E.5-17)}$$

or, since all terms are positive:

$$(F-N) * (P-T) \geq (F-P) * (N-T) \qquad \text{(E.5-18)}$$

Because $N \leq P$:

$$(F-N) \geq (F-P) \qquad \text{(E.5-19)}$$

and because $P \geq N$:

$$(P-T) \geq (N-T) \qquad \text{(E.5-20)}$$

Eq E.5-18 and E.5-17 are true. Consequently sufficient tailings are available in the case where D=T.

E.5.3 Uranium Requirements as a Function of Tailings U-235 Concentration

From Eq E.5-1:

$$X \equiv \frac{M_N}{M_P} = \frac{P-T}{N-T} \qquad \text{(E.5-21)}$$

Consider:

$$\frac{dX}{dT} = \frac{P-N}{(N-T)^2} \qquad \text{(E.5-22)}$$

Hence it can be seen that natural uranium requirements as a function of T increase faster as the product enrichment, P, increases. This effect will become evident in Section 10.5.5.

E.6 Separative Work Requirement Calculations

In the separative work calculations performed in this thesis, it was assumed that the gaseous diffusion process was used for uranium enrichment.

Silvennoinen (1982) demonstrated that the separative work requirements per kg of product are given by:

$$\frac{SWU}{M_P} = V(P) - V(T) - \frac{(P-T)}{(N-T)} * (V(N) - V(T)) \qquad (E.6\text{-}1)$$

where

V = the "value function" (defined below),

SWU = the kg of separative work units required,

M_P = the mass of product produced,

P = the U-235 concentration of the product (w/o),

T = the U-235 concentration of the tailings (w/o), and

N = the U-235 concentration of the natural uranium feed (w/o).

The value function for the gaseous diffusion process is given by:

$$V(X) = (2X-100) \ln(X/(100-X)) \qquad (E.6\text{-}2)$$

where X = the U-235 concentration in w/o.

If, as in Section E.5, one considers the production of the product with enrichment, P, from a combination of material with enrichments F>P and D<P, separative work requirements can be calculated for these particular cases.

From Eq E.5-6, E.5-7, and E.6-1 the separative work requirements for the mixture cases are given by:

$$\frac{SWU}{M_P} = M_{FP} * \frac{SWU}{M_F} + M_{DP} * \frac{SWU}{M_D}$$

$$= \frac{(P-D)}{(F-D)} * (V(F) - V(T) - \frac{(F-T)}{(N-T)} * (V(N) - V(T)))$$

$$+ \frac{(F-P)}{(F-D)} * (V(D) - V(T) - \frac{(D-T)}{(N-T)} * (V(N) - V(T))) \qquad \text{(E.6-3)}$$

Two cases are of special interest. First consider the case with D=T. When the dilutant is uranium tailings the second term in Eq E.6-3 becomes zero. This gives:

$$\frac{SWU}{M_P} = \frac{(P-T)}{(F-T)} * (V(F) - V(T) - \frac{(F-T)}{(N-T)} * (V(N) - V(T))) \qquad \text{(E.6-4)}$$

For the case with D=N, the second term also subtracts out leaving:

$$\frac{SWU}{M_P} = \frac{(P-N)}{(F-N)} * (V(F) - V(T) - \frac{(F-T)}{(N-T)} * (V(N) - V(T))) \qquad \text{(E.6-5)}$$

In both cases, the separative work requirements are those associated with the production of sufficient quantities of material with enrichment, F.

E.7 Uranium and Separative Work Requirements for Specific Cases

The enriched fuels considered for this fuel management study are based on the 14/21 fuel bundle design of Chapter 7, with enrichments of 1.3/1.2 and 1.7/1.53 for the inner/outer pencil ring (enrichments quoted are in atom percent U-235). The inner 14 pins were of radius 0.5853 cm. The outer 21 pins were of radius 0.5470 cm. Hence for every kg of fuel produced, it is necessary to produce:

$$(14 * \pi * 0.5853^2 + 21 * \pi * 0.5470^2)^{-1} * (14 * \pi * 0.5853^2) * 1.005^2 = 0.437 \text{ kg}$$

of fuel at the inner ring enrichment, and similarly 0.573 kg of fuel at the

outer ring enrichment. These values include the correction $(1.005)^2$ for conversion and fabrication losses (see Section E.2).

Using the above mass ratios and Eq E.5-1, the amount of natural uranium required to produce a unit of 14/21 fuel can be determined as a function of tailings concentration. This is provided in Table 10-1. In Table 10-2, separative work requirements for the product fuels are calculated in a similar fashion using Eq E.6-2 and E.6-5. (It is noted that these equations require the enrichment to be quoted in weight (or mass) percent rather than atomic percent U-235.)

E.8 Conversion of Burnup per Bundle to Burnup per MgU

The FMDP code output provides average burnup data on a per bundle basis. For data interpretation it is necessary to convert this to Burnup/MgU. For this purpose the following mass data are used:

37 Element fuel: 18.8 kgU/bundle (nominal design)

14/21 Element fuel: 15.388 kgU/bundle.

Hence, to convert MWh/bundle to MWd/MgU:

37 Element fuel: divide by 0.4512

14/21 Element fuel: divide by 0.36912.

APPENDIX F

WIMS-CRNL PROGRAM DESCRIPTION

The WIMS-CRNL computer code (Phillips, 1982; Donnelly, 1986) was derived from the Winfrith Improved Multigroup Scheme (WIMS) program (Askew et al., 1966) created at the United Kingdom Atomic Energy Establishment, Winfrith. WIMS-CRNL performs a multigroup neutron transport theory calculation for a reactor lattice cell, producing flux distributions, eigenvalues, and reaction rates. Much of the original WIMS code has been rewritten by Atomic Energy of Canada Limited staff at the Chalk River Nuclear Laboratories, and consequently the new name, WIMS-CRNL, has been adopted for this version of the code.

The code is structured to utilize up to 69 neutron energy groups. For most applications, the expense of using 69 groups cannot be justified and hence the code allows for user flexibility in specifying the number of energy groups. Various aspects of the WIMS-CRNL code are described below.

F.1 SPECTROX Calculation

A special procedure has been incorporated into the code for group condensation (Askew et al., 1966). The spectrum determination for the group condensation is accomplished through the SPECTROX chain in WIMS-CRNL. A detailed flux spectrum in the full 69 groups of the library is obtained for each of the principal regions of the lattice which are coupled through collision probability expressions and then condensed as required. For a fuel bundle arrangement, the regions are the bulk moderator, the fuel, fuel sheath, and coolant annuli of an average fuel element.

Following the SPECTROX routine, a more accurate spatial solution is

obtained using the condensed energy structure. Several solution options are provided (Donnelly, 1986). For the purposes of this discussion, only the two options utilized in this work are considered, viz, the DSN and PIJ options (Donnelly, 1986).

F.2 DSN Calculation

The DSN option provides a discrete ordinates solution to the neutron transport equation (Askew and Brissenden, 1963). In this approach, the Boltzmann equation is solved for a number of discrete directions, to each of which is associated a weighting value. Each of these weightings represents a segment or area on the unit directional sphere. In WIMS-CRNL, one-dimensional annular geometry is utilized. Fuel clusters are homogenized into annular rings using the fine structure determined for the "average pin" in the SPECTROX calculation. The S_4 approximation (Stammler and Abbate, 1983) is generally adopted.

F.3 PIJ Calculation

The PIJ option (Anderson, 1973) is the most detailed and most expensive solution scheme available in WIMS-CRNL. This two dimensional collision probability routine allows for specific representation of individual rods in cluster geometry with internal subdivision of the rods if required. The two dimensional collision probability solution within the fuel/coolant region is normally coupled to a one-dimensional solution in the region beyond to reduce computational costs.

F.4 Leakage Routines

The code incorporates a number of methods to modify the infinite lattice results obtained from the main transport calculation to include the effects of leakage from a finite reactor (Askew et al., 1966). These

calculations employ the same energy group structure as the main transport routine. Using the modified flux distribution, integrated reaction rates are calculated, and parameters such as k-eff (production rate / loss rate) and the system reactivity are determined.

F.5 Burnup Calculation

Fuel burnup can be simulated between successive main transport calculations. Reaction rates for all isotopes in the fuel are calculated, and updated constituent materials are determined. Several burnup steps are generally taken. The cell flux distribution is only modified following the next main transport calculation. Burnup can occur in the neutron spectrum with input neutronic buckling, or in the critical spectrum where the buckling (or leakage) is adjusted to achieve a critical reactor cell.

F.6 WIMS-CRNL Energy Group Structure

In all analyses included in this thesis, the 69 energy groups in WIMS-CRNL were condensed to 18 energy groups for the main transport calculations. This group structure is the default provided by the TESHOM computer code (Griffiths, 1978), which is used to set up complex lattice models for input to various lattice physics codes. The group structure is shown in Table 6-2. All neutrons with energy less than 0.625 eV are considered thermal neutrons.

BIBLIOGRAPHY

Ahn, D.H., and Levine, S.H., "Automatic Optimized Reload and Depletion Methods for a Pressurized Water Reactor", Nuclear Technology, 71, pp 535-547, 1985.

Akebi, M., and Fujiki, I., "Development of Plutonium Fuel Utilization in a Fugen Type HWR", Nuclear Power Experience, Vienna: International Atomic Energy Agency, 3, pp 687-698, 1983.

Akhtar, P., and Trojan, O.A., "Load Following Capability of CANDU Reactors", Trans. Am. Nucl. Soc., 14, p 753, 1971.

Akhtar, P., and Trojan, O.A., "Spatial Power Oscillations in CANDU", Physics in Canada, 31, Congress Issue, 1975.

Akhtar, P., and Trojan, O.A., "Xenon Induced Power Oscillations in CANDU", Trans. Am. Nucl. Soc., 23, p 596, 1976.

Akhtar, P., and Trojan, O.A., "Xenon Override Capability in Pickering A Reactors", Proceedings of Can. Nucl. Assoc., 17th Annual International Conference, Montreal, 77-CNA-600, p 83, 1977.

Anderson, D.W., The WIMS 'E' Module W-PIJ A Two Dimensional Collision Probability Code With General Boundary Conditions, AEEW-R 862, Winfrith: United Kingdom Atomic Energy Authority, 1973.

Andrews, M.G., and Lobre, J.A., "Examining Fuel Behaviour in Longer Operating Cycles", Nuclear Engineering International, 30(413), pp 42-43, 1988.

Archinoff, G.H., The Low Enriched Uranium Fuel Cycle in Ontario: A Resource Utilization Study, D&D-79011, Toronto: Ontario Hydro, 1979.

Archinoff, G.H., Future Fuel Cycles: A Resource Utilization and Economic Assessment, D&D-80007, Toronto: Ontario Hydro, 1980.

Askew, J.R., and Brissendin, R.J., Some Improvements in the Discrete Ordinate Method of B.G. Carlson for Solving the Neutron Transport Equation, AEEW-R161, Winfrith: United Kingdom Atomic Energy Authority, 1963.

Askew, J.R., et al., "A General Description of the Lattice Code WIMS", The Journal of the British Nuclear Energy Society, 5(4), pp 564-585, 1966.

Atomic Energy Control Board, "Reactor Operating Licence No. 8/86, Bruce NGS-B Units 5, 6, 7", File 26-1-14-1-6, J.H. Jennekens, July 2, 1986.

Atomic Energy of Canada Limited, The Canadian Nuclear Power Program, AECL-4767, Chalk River: Atomic Energy of Canada Limited, 1974.

Atomic Energy of Canada Limited, Data Base for a CANDU-PHW Operating on a Once-Through Natural Uranium Cycle, AECL-6593, INFCE/WG 8/CAN/DOC 2, Chalk River: Atomic Energy of Canada Limited, 1979a.

Atomic Energy of Canada Limited, Data Base for a CANDU-PHW Operating on a Once-Through Slightly Enriched Uranium Cycle, AECL-6594, INFCE/WG 8/CAN/DOC 3, Chalk River: Atomic Energy of Canada Limited, 1979b.

Atomic Energy of Canada Limited, CANDU Nuclear Power System, TDSI-105, Mississauga: Atomic Energy of Canada Limited, 1981.

Badruzzaman, A., "Ecomonic Potential of Annular Fuel in PWRs", Trans. Am. Nucl. Soc., 34, pp 384-385, 1980.

Bagnal, C.W., et al., Feasibility of HWR Evolutionary Designs for Developing Nuclear Programs, CEND-392, Windsor, Conn: Combustion Engineering, Inc., 1981.

Bailey, H.S., and Lu, Y.S., "Nuclear Performance of LMFBRs Designed to Preclude Energetic HCDAs", Trans. Am. Nucl. Soc., 26, pp 557-558, 1977.

Bairot, H., "High Burnup: Status and Expectations", Nuclear Power Experience, Vol. 3, Nuclear Fuel Cycle, Vienna: International Atomic Energy Agency, pp 635-660, 1983.

Barns, G.M., Private Communication, Canadian General Electric Unpublished Report, 1979.

Barre, B., et al., "Development Trends for Future French Pressurized Water Reactors", Nuclear Technology, 80(1), p 11, 1988.

Barthold, W.P., and Beitel, J.C., "Performance Characteristics of Homogeneous vs Heterogeneous LMFBRs", Nuclear Technology, 44(1), pp 45-60, 1979.

Bartholomew, R.W., et al., Ontario Hydro CANDU Operating Experience, NGD-9 (1987), Toronto: Ontario Hydro, 1988.

Becker, E.W., et al., "Uranium Enrichment by Separation Nozzle Process", Trans. Am. Nucl. Soc., 22, pp 313-314, 1975.

Becker, E.W., et al., "Uranium Enrichment by the Separation Nozzle Method Within the Framework of German/Brazilian Cooperation", Nuclear Technology, 52(1), pp 57-65, 1981.

Benedict, M., "Enrichment: A Critical Status Report", Trans. Am. Nucl. Soc., 25, pp 44-56, 1977.

Benoist, P., "Streaming Effects and Collision Probabilities in Lattices", Nuclear Science and Engineering, 34, p 285, 1968.

Best, F.R., and Driscoll, M.J., "Prospects for the Recovery of Uranium from Seawater", Nuclear Technology, 73(1), pp 55-68, 1986.

Blahnik, C., Uranium Enrichment (A Strategy Analysis Overview), D&D-79247, 1, Toronto: Ontario Hydro, 1979.

Boczar, P.G., and van Dyk, M.T., Improved Locations of Reactivity Devices in Future CANDU Reactors Fuelled with Natural Uranium or Enriched Fuels, AECL-9194, Chalk River: Atomic Energy of Canada Limited, 1986.

Bonalumi, R.A., and Lau, J.H.K., Preliminary Assessment of the Low-Enriched Uranium Cycle in Bruce NGS-B, D&D-79399, Toronto: Ontario Hydro, 1979.

Bonalumi, R.A., et al., "Design Criteria and Analysis for a Cirene Reactor Core", Trans. Am. Nucl. Soc., 23, pp 61-62, 1976.

Boulton, J., Ed., Management of Radioactive Fuel Wastes: The Canadian Disposal Program, AECL-6314, Pinawa: Atomic Energy of Canada Limited, 1978.

Brogli, R.H., et al., Research and Development Efforts for the Light Water High Conversion Reactor", Nuclear Technology, 80(1), p 61, 1988.

Carle, R., "The Future for Nuclear Power", Energy: Needs and Expectations, London: World Energy Conference, pp 272-284, 1987.

Cartwright, H., "Commercial SGHWR", Steam Generating and Other Heavy Water Reactors, London: British Nuclear Energy Society, 1968.

Chan, P.S.W., Private Communication, Atomic Energy of Canada Limited Unpublished Report, 1979.

Chan, P.S.W., and Dastur, A.R., "Checkerboard Fuelling -- The Key to Advanced Fuel Cycles in Existing CANDU Reactors", Sixth Annual Canadian Nuclear Society Conference Summaries, ISSN-0227-0129, 1985.

Chow, H.C., Private Communication, Atomic Energy of Canada Limited, 1984.

Chow, H.C., and Roshd, M.H., SHETAN -- A Three Dimensional Integral Transport Code for Reactor Analysis, AECL-6878, Mississauga: Atomic Energy of Canada Limited, 1980.

Clarke, F.J., and Main, F.K., "Selection and Evaluation of Nuclear Fuel Cycle Strategies", Nuclear Power Experience, Volume 3, Nuclear Fuel Cycle, Vienna: International Atomic Energy Agency, 1983.

Coates, J.H., et al., "Status of the Chemical Exchange Enrichment Process (CHEMEX)", Nuclear Power Experience, Volume 3, Nuclear Fuel Cycle, Vienna: International Atomic Energy Agency, 1983.

Coates, J.H., et al., "France Makes Steady Progress With Lasers", Nuclear Engineering International, 33(409), pp 30-33, 1988.

Coleman, T.A., et al., "Improved Uranium Utilization in Pressurized Water Reactors", Trans. Am. Nucl. Soc., 39, p 133, 1981.

Critoph, E., The Thorium Fuel Cycle in Water-Moderated Reactor Systems, AECL-5705, Chalk River: Atomic Energy of Canada Limited, 1977.

Critoph, E., et al., Prospects for Self-Sufficient Equilibrium Thorium Cycles in CANDU Reactors, AECL-5501, Chalk River: Atomic Energy of Canada Limited, 1976.

Crocker, V.S., and Roberts, P.F., "UK Laser Isotope Separation", Atom, No. 363, 1987.

Cruickshank, A., Editor, 1989 World Nuclear Industry Handbook, Sutton, UK: Reed Business Publishing, 1988.

Dalton, K., Private Communication, Atomic Energy of Canada Limited, 1984.

Dastur, A.R., Private Communication, Atomic Energy of Canada Limited, 1984.

Dastur, A.R., Private Communication, Atomic Energy of Canada Limited, 1988.

Dastur, A.R., and Buss, D.B., MULTICELL - A 3-D Program for the Simulation of Reactivity Devices in CANDU Reactors, AECL-7544, Mississauga: Atomic Energy of Canada Limited, 1983.

Dastur, A.R., Marczak, J.V., Piva, F., and Donnelly, J.V., Private Communication, Atomic Energy of Canada Limited Unpublished Report, 1979.

Department of Energy, Mines and Resources, Canada, Energy in Canada, Ottawa: Minister of Supply and Services, Canada, 1987.

Dickson, P.W., Jr., and Arnold, W.H., "Design of the Heterogeneous Core of the Clinch River Breeder Plant", Nuclear Power Experience, Vol 5, Vienna: International Atomic Energy Agency, 1983.

Donnelly, J., "Opening Address", Canadian Nuclear Association Twenty-First Annual International Conference, Vol 2, Conference Summaries, 1981.

Donnelly, J.V., Private Communication, Atomic Energy of Canada Limited Unpublished Report, 1982.

Donnelly, J.V., Private Communication, Atomic Energy of Canada Limited, 1984.

Donnelly, J.V., Private Communication, Atomic Energy of Canada Limited Unpublished Report, 1985.

Donnelly, J.V., WIMS-CRNL A User's Manual for the Chalk River Version of WIMS, AECL-8955, Chalk River: Atomic Energy of Canada Limited, 1986.

Donnelly, J.V., and van Dyk, M.T., Private Communication, Atomic Energy of Canada Limited Unpublished Report, 1983.

Duderstadt J.J., and Hamilton, L.J., Nuclear Reactor Analysis, Toronto: John Wiley & Sons, Inc., 1976.

Dyne, P.J., Waste Management in Canadian Nuclear Programs, AECL-5249, Pinawa: Atomic Energy of Canada Limited, 1975.

Edlund, M.C., "On High Conversion LWRs", Nuclear Technology, 80(1), p 9, 1988.

Edwards, T.T., and Wilcox, P., "Achieving an Ever-Improving Centrifuge Performance", Nuclear Engineering International, 33(409), pp 33-36, 1988.

Forsen, H.K., et al., "Prospects for Uranium Laser Isotope Separation", Trans. Am. Nucl. Soc., 22, pp 312-313, 1975.

Foster, J.S., "Summary and Conclusions", Energy: Needs and Expectations, London: World Energy Conference, pp 13-21, 1987.

Fraser, J.S., et al., A Review of Prospects for an Accelerator Breeder, AECL-7260, Chalk River: Atomic Energy of Canada Limited, 1981.

French, P.M., and Jones, R.T., Private Communication, Atomic Energy of Canada Limited Unpublished Report, 1976.

Frescura, G.M., and Wight, A.L., "CANDU-PHW Fuel Management", Operational Physics of Power Reactors, IAEA-SMR-68/II, Trieste: International Centre for Theoretical Physics, 1982.

Gacesa, M., et al., CANDU Fuel Design: Current Concepts, AECL-MISC-250, Chalk River: Atomic Energy of Canada Limited, 1983.

Garland, W., Private Communication, McMaster University, 1985.

Garvey, P.M., Physics Characteristics of CANDU Cores With Advanced Fuel Cycles, AECL-8703, Chalk River: Atomic Energy of Canada Limited, 1985.

Geston, D.K., "Gas Centrifuge Uranium Enrichment Program in the United States of America", Nuclear Power Experience, Volume 3, Nuclear Fuel Cycle, Vienna: International Atomic Energy Agency, pp 481-489, 1983.

Gordon, C.W., and Harms, A.A., "The Basic Characteristics of an Efficient Fusion Breeder", Atomkernenergie, 29, p 213, 1977.

Griffiths, J., TESHOM: A User Manual, AECL-6355, Chalk River: Atomic Energy of Canada Limited, 1978.

Groeneveld, D.C., and Goel, K.C., Private Communication, Atomic Energy of Canada Limited Unpublished Report, 1978.

Harms, A.A., Introduction of Fusion Energy, Hamilton: McMaster University, 1983.

Harms, A.A., Principles of Nuclear Science and Engineering, Toronto: John Wiley & Sons Inc., 1987.

Harms, A.A., and Haefele, W., "Nuclear Synergism: An Emerging Framework for Energy Systems", American Scientist, 69, 1981.

Harms, A.A., and Hartmann, W.J., "Spent Nuclear Fuel Re-enrichment Without Reprocessing", Annals of Nuclear Energy, 5, p 213, 1978.

Harms, A.A., and Heindler, M., Nuclear Energy Synergetics, New York: Plenum Press, 1982.

Hart, R.G., Sources, Availability and Costs of Future Energy, AECL-5816, Pinawa: Atomic Energy of Canada Limited, 1977.

Hastings, I.J., and MacDonald, R.D., "High Burnup Performance of Annular UO_2 Fuel With Interpellet Graphite Discs", Journal of Nuclear Materials, 126(2), 1984.

Hastings, I.J., et al., "Canadian High Burnup Fuel Experience", Sixth Annual Canadian Nuclear Society Conference Summaries, ISSN-0227-0129, 1985.

Hatcher, S.R., Nuclear Power in Canada: Status and Prospects, AECL-6173, Ottawa: Atomic Energy of Canada Limited, 1978.

Hatcher, S.R., Prospects for Future CANDU Fuel Cycles, AECL-6334, Pinawa: Atomic Energy of Canada Limited, 1979.

Hatton, G.C., and Barns, G.M., Private Communication, Canadian General Electric Unpublished Report, 1980.

Hawley, N.J., Fuel Cycles: A Bibliography of AECL Publications, AECL-6425 Rev 1, Pinawa: Atomic Energy of Canada Limited, 1983.

Henry, A.F., Nuclear Reactor Analysis, Cambridge Mass.: The MIT Press, 1975.

Hicks, D., et al., "Nuclear Design of SGHWRs", Steam Generating and Other Heavy Water Reactors, London: British Nuclear Energy Society, 1968.

Hittner, D., et al., "Preliminary Results of the Feasibility Study on the Convertible Spectral Shift Reactor Concept", Nuclear Technology, 80, p 181, 1988.

Holdren, J.P., "Nuclear Power and Nuclear Weapons: The Connection is Dangerous", Nuclear Energy, Nuclear Weapons Proliferation and the Arms Race, New York: American Association of Physics Teachers, pp 13-27, 1982.

International Atomic Energy Agency, Advanced Fuel Cycle and Reactor Concepts, Report of INFCE Working Group 8, Vienna, 1980.

International Atomic Energy Agency, International Nuclear Fuel Cycle Evaluation, Summary Volume, Vienna, 1980a.

Jenkins, D.A., Private Communication, Atomic Energy of Canada Limited Unpublished Report, 1984.

Jenkins, D.A., Private Communication, Atomic Energy of Canada Limited, 1985.

Kato, H., et al., "Core Management Analysis of the FUGEN Heavy Water Moderated, Plutonium Uranium Mixed Oxide Reactor", Nuclear Science and Engineering, 87(4), pp 361-380, 1984.

Keller, H.W., and Shank, R.C., "Providing Fuel and Core Designs for the 1990s", Nuclear Engineering International, 32(400), pp 50-53, 1987.

Killmar, W., et al., "Arguing the Case for Shorter Cycles", Nuclear Engineering International, 33(413), pp 30-34, 1988.

Knox, R., "Safeguards for CANDU Reactors: Advancing the Art", Nuclear Engineering International, 29(359), 1984.

Krafft, P., "Research and Development: Medium Term Prospects", Energy: Needs and Expectations, London: World Energy Conference, 1987.

Kratzer, M.B., "Historical Overview of International Safeguards", Nuclear Power Experience, Volume 5, Advanced Systems and International Cooperation, Vienna: International Atomic Energy Agency, pp 273-292, 1983.

Krishnan, M., Physics Review Letters, 16(1), January 1981.

Kriysinski, T.L., et al., "Improving Uranium Utilization in LWRs", Nuclear Engineering International, 31(389), pp 37-41, 1986.

Kugler, G., Private Communication, Atomic Energy of Canada Limited Unpublished Report, 1975.

Kugler, G., Distinctive Safety Aspects of the CANDU-PHW Reactor Design, AECL-6789, Mississauga: Atomic Energy of Canada Limited, 1980.

Kushneriuk, S.A., Neutron Capture by Long Cylindrical Bodies Surrounded by Predominantly Scattering Media, AECL-462, Chalk River: Atomic Energy of Canada Limited, 1957, Reprinted 1959.

Lamarsh, J.R., Introduction of Nuclear Engineering, Reading: Addison-Wesley Publishing Company, 1977.

Lang, P.M., et al., "Improvements in LWR Fuel Utilization", Nuclear Power Experience, Volume 3, Nuclear Fuel Cycle, pp 621-633, Vienna: International Atomic Energy Agency, 1983.

Lee, K.H., "Energy and the Quality of Life", Canadian Nuclear Association Twenty-First Annual International Conference, Volume 2, Conference Summaries, 1981.

Levine, S.H., "In-Core Fuel Management for the Course on Operational Physics of Power Reactors", Operational Physics of Power Reactors, IAEA-SMR-68/II, Trieste: International Centre for Theoretical Physics, 1982.

Lewis, W.B., Outlook for Heavy Water Reactors, AECL-2947, Chalk River: Atomic Energy of Canada Limited, 1967.

Lewis, W.B., Canada, the Quality of Life, and Nuclear Energy, AECL-3683, Chalk River: Atomic Energy of Canada Limited, 1970.

Lewis, W.B., Nuclear Energy and the Quality of Life, AECL-4380, Chalk River: Atomic Energy of Canada Limited, 1972.

Lidsky, L.M., "Fission-Fusion Systems: Hybrid, Symbiotic, and Augean", Nuclear Fusion, 15, p 151, 1975.

Lone, M.A., Proceedings of the Fourth International Symposium on Neutron Capture Gamma-Ray Spectroscopy and Related Topics, Grenoble, France: Inst. du Physics, September, 1981.

Lone, M.A., and Bartholomew, G.A., "Zr-90 Studies With Thermal Neutrons", Third International Symposium on Neutron Capture Gamma-Ray Spectroscopy and Related Topics, BNL, USA, September 18-20, 1978.

Macdonald, I.P.L., "Enhancement of Critical Heat Flux in CANDU 37-Element Bundles", Sixth Annual Canadian Nuclear Society Conference Summaries, ISSN 0227-0129, Ottawa, 1985.

MacEwan, J.R., et al., "CANDU Fuel: Past, Present and Future", Nuclear Power Experience, Volume 3, Nuclear Fuel Cycle, Vienna: International Atomic Energy Agency, pp 527-540, 1983.

Marczak, J.V., Private Communication, Atomic Energy of Canada Limited Unpublished Report, 1981.

Marinelli, V., "Critical Heat Flux: A Review of Recent Publications", Nuclear Technology, 34(2), 1977.

Markl, H., "Advanced Technologies on Pressurized Water Reactors and Fuel Cycles", Trans. Am. Nucl. Soc., 42, pp 15-17, 1982.

McMillan, R.N., et al., The Physics and Control of the Steam Generating Heavy Water Reactor, TRG Report 1343(R), Risley: United Kingdom Atomic Energy Authority, 1968.

Melvin, J.G., Energy and the Value Society, Chalk River: Atomic Energy of Canada Limited, 1979.

Milgram, M.S., Once-Through Thorium Cycles in CANDU Reactors, AECL-7516, Chalk River: Atomic Energy of Canada Limited, 1982.

Mooradian, A.J., and Runnalls, O.J., CANDU - Economic Alternative to the Fast Breeders, AECL-4916, Chalk River: Atomic Energy of Canada Limited, 1974.

Moore, R.V., and Holmes, J.E., "The SGHWR System", Steam Generating and Other Heavy Water Reactors, London: British Nuclear Energy Society, 1968.

Mughabghab, S., and Garber, D., Neutron Cross Sections, Volume 1, BNL-325, Brookhaven: National Neutron Cross Section Centre, Brookhaven National Laboratory, 1973.

Nuclear Canada, XXV(3), March, 1986.

Nuclear News, "World List of Nuclear Power Plants", 31(10), pp 69-88, 1988.

NUKEM, "The Nuclear Power Plant Capacity of the Western World", Special Report, Germany, March, 1988.

O'Dell, F.P., et al., "Fuel Management in SGHWRs", Steam Generating and Other Heavy Water Reactors, London: British Nuclear Energy Society, 1968.

Office of Technology Assessment, Nuclear Power in an Age of Uncertainty, Washington: US Congress, 1984.

Orpen, V.C., Private Communication, Atomic Energy of Canada Limited, 1984.

Palmer, G., and Bolef, D., "Laser Isotope Separation: The Plutonium Connection", Bulletin of the Atomic Scientists, 40(3), 1984.

Pasanen, A.A., "Fundamentals of CANDU Reactor Nuclear Design", in Operational Physics of Power Reactors, IAEA-SMR-68/II, Trieste: International Centre for Theoretical Physics, 1982.

Phillips, G.J., WIMS-CRNL A User's Manual for the Chalk River Version of WIMS, AECL-7432, Chalk River: Atomic Energy of Canada Limited, 1982.

Robertson, J.A., Research and Development for Canadian Nuclear Power, AECL-5314, Ottawa: Atomic Energy of Canada Limited, 1976.

Roshd, M.H., "The Physics of CANDU Reactor Design", Trans. Am. Nucl. Soc., 23, p 513, 1976.

Roshd, M.H., and Chow, H.C., GETRANS - A Two Dimensional Integral Transport Code, AECL-6359, Mississauga: Atomic Energy of Canada Limited, 1978.

Roshd, M.H., et al., "Nuclear Fuel Bundle Design With Reduced Void Effect", Trans. Am. Nucl. Soc., 26, p 457, 1977.

Rouben, B., Private Communication, Atomic Energy of Canada Limited, 1981.

Rozon, D., et al., "The Application of Generalized Perturbation Theory and Mathematical Programming to Equilibrium Refuelling Studies of a CANDU Reactor", Nuclear Science and Engineering, 78(3), pp 211-226, 1981.

Seko, M., et al., "Uranium Isotope Enrichment by Chemical Method", Nuclear Technology, 50(2), pp 178-186, 1980.

Sewell, P.G., and Haberman, N., "AVLIS Programme Powers Ahead in the United States", Nuclear Engineering International, 33(411), 1988.

Shapiro, N.L., and Jesick, J.F., Conceptual Design of a Large Heavy Water Reactor for U.S. Siting, CEND-379, Volume 1, Windsor Connecticut: Combustion Engineering, Inc., 1979.

Shiba, K., et al., "Heavy Water Critical Experiments for FUGEN (I) Void Reactivity in Plutonium Lattice", Trans. Am. Nucl. Soc., 21, p 467, 1975.

Sider, F.M., and Matzie, R.A., "Plutonium Fuel Cycles in the Spectral Shift Controlled Reactor", Nuclear Technology, 47(3), p 444, 1980.

Sider, F.M., et al., "An Improved Once Through Fuel Cycle for Pressurized Water Reactors", Trans. Am. Nucl. Soc., 34, p 382, 1980.

Silvennoinen, P., Reactor Core Fuel Management, New York: Pergamon Press, 1976.

Silvennoinen, P., Nuclear Fuel Cycle Optimization, New York: Pergamon Press, 1982.

Slater, J.B., "Potential of Advanced Fuel Cycles in CANDU Reactors", Nuclear Energy, 20(5), pp 421-429, 1981.

Slater, J.B., Economic Potential of Advanced Fuel Cycles in CANDU, AECL-7753, Chalk River: Atomic Energy of Canada Limited, 1982.

Spinrad, B.I., "Nuclear Power and Nuclear Weapons: The Connection in Tenuous", Nuclear Energy, Nuclear Weapons Proliferation and the Arms Race, New York: American Association of Physics Teachers, pp 1-12, 1982.

Stammler, R.J., and Abbate, M.J., Methods of Steady-State Reactor Physics in Nuclear Design, London: Academic Press, 1983.

Stewart, H.B., Transitional Energy Policy, 1980-2030, Toronto: Pergamon Press Inc., 1981.

Steyn, J., "Why did the U.S. Choose AVLIS", Nuclear Engineering International, 30(373), p 13, 1985.

Takeda, K., "Asahi Chemical Succeeds in 3 per cent Enrichment", Nuclear Engineering International, 33(409), pp 26-27, 1988.

Tammemagi, H.Y., Geologic Disposal of Radioactive Wastes - The Canadian Development Program, AECL-5392, Pinawa: Atomic Energy of Canada Limited, 1976.

Thompson, T.J., and Beckerley, J.G., Ed., The Technology of Nuclear Reactor Safety, Volume 1, Chapter 11, Cambridge: The MIT Press, 1964.

Till, C., "Non-Conventional Core Designs for Liquid Metal Fast Breeder Reactors", Nuclear Technology, 44(1), p 9, 1979.

Tin, E.S.Y., Private Communication, Atomic Energy of Canada Limited Unpublished Report, 1981.

Tin, E.S.Y., and Loken, P.C., Private Communication, Atomic Energy of Canada Limited Unpublished Report, 1979.

Townes, B.M., Private Communication, Atomic Energy of Canada Limited Unpublished Report, 1982.

Townes, B.M., Private Communication, Atomic Energy of Canada Limited, 1984.

Trojan, O.A., and Dastur, A.R., "Boosters vs Absorbers for Xenon Override in Large CANDU Reactors: The Reactor Physics Aspects", Proceedings of the Canadian Nuclear Association 13th Annual International Conference, Toronto, CN 155N 0068-8517, 73-CNA-500, 1973.

Tursky, R.B., et al., "Sensitivity of Sodium Void Reactivity to Changes in Basic Design Conditions of Oxide LMFBRs", Trans. Am. Nucl. Soc., 26, pp 457-458, 1977.

Tzanos, C.P., "Enrichment Zoning and Control Rod Programming for Reactivity and Power Shape Control", Nuclear Technology, 41(2), pp 195-206, 1978.

Untermyer, S., "More on Positive Reactivity", Letter to the Editor, Nuclear News, 29(10), 1986.

van Dyk, M.T., Private Communication, Atomic Energy of Canada Limited Unpublished Report, 1983.

Varley, J., Ed., "Reactor Information - Section 2: Technical Data", Nuclear Engineering International, 30(372), pp 42-45, 1985.

Varley, J., Ed., "Small LMR Cuts Costs and Boosts Safety", Nuclear Engineering International, 32(400), pp 19-22, 1987a.

Varley, J., Ed., "The World's Nuclear Fuel Cycle Facilities", Nuclear Engineering International, 32(401), pp 47-48, 1987b.

Varley, J., Ed., "Japan Forges Ahead on Four Fronts", Nuclear Engineering International, 33(409), pp 26-29, 1988.

Vigil, J.C., 3DDT, A Three-Dimensional Multigroup Diffusion-Burnup Program, LA-4396, Los Alamos: Los Alamos Scientific Laboratory, 1970.

Villani, S., "The CIRENE Reactor Concept", Steam Generating and Other Heavy Water Reactors, London: British Nuclear Energy Society, 1968.

Vitti, J.A., et al., "Nuclear Design and Economic Comparison of a Conventional and Bullseye Liquid Metal Fast Breeder Reactor Core", Nuclear Technology, 44(1), p 10, 1979.

Voigt, W.R., et al., "Uranium Enrichment", Nuclear Power Experience, Volume 3, Nuclear Fuel Cycle, Vienna: International Atomic Energy Agency, pp 41-58, 1983.

Wahba, N.N., and Lorenc, J.A., Private Communication, Ontario Hydro Unpublished Report, 1984.

Walker, F.W., et al., Chart of the Nuclides, Twelfth Edition (Revised), San Jose: General Electric Company, 1977.

Wall, I., and Fenech, H., "The Application of Dynamic Programming to Fuel Management Optimization", Nuclear Science and Engineering, 22, pp 285-297, 1965.

Weinberg, A.M., "A Second Nuclear Era", Trans. Am. Nucl. Soc., 47, p 286, 1984.

Westcott, C.H., Effective Cross section Values for Well-Moderated Thermal Reactor Spectra, AECL-1101, Chalk River: Atomic Energy of Canada Limited, 1960, Reprinted 1970.

Wight, A.L., Ontario Hydro Reactor Fuelling Simulation Program - OHRFSP, D&D-86000, Toronto: Ontario Hydro, 1987.

Wight, A.L., and Girouard, P., "Optimum Burnup Distribution in a Continuously Fuelled Reactor", Nuclear Science and Engineering, 68(1), pp 61-72, 1978.

Wight, A.L., and Sibley, R., Private Communication, Atomic Energy of Canada Limited Unpublished Report, 1977.

Wight, A.L., Gold, M., and Marczak, J.V., Private Communication, Atomic Energy of Canada Limited Unpublished Report, 1979.

Willrich, M., Ed., International Safeguards and Nuclear Industry, Baltimore: John Hopkins University Press, 1973.

Wolf, W.H., and Blumenthal, A.E., "Litigation, Legislation and Lasers: The Enrichment Year in Review", Nuclear Engineering International, 32(401), pp 42-44, 1987.

Younis, et al., "Fuel Management with Enriched Uranium Fuel in CANDU Reactors Using the Checkerboard Fuel Management Scheme", Canadian Nuclear Society, International Conference on CANDU Fuel, Chalk River, 1986.

Zraket, C.A., "Current Evolution and Future Trends in Technology", Energy: Needs and Expectations, London: World Energy Conference, pp 141-152, 1987.